A Petrological Study of Mafic Hypabyssal and Ultramafic Plutonic Rocks of the Cuillin Igneous Complex, Isle of Skye, Scotland.

A thesis submitted for the degree of Doctor of Philosophy

by

Russell Van Claydon, B.Sc. (Wales).
University of Glasgow.

ProQuest LLC.
789 East Eisenhower Parkway
P.O. Box 1346
Ann Arbor, MI 48106 – 1346

For Karen

Always and Forever

Acknowledgements

I am deeply indebted to Dr. Brian Bell for suggesting and allowing me to proceed with this study with academic freedom but who was always willing to give his time freely to appraise progress and suggest possible avenues of research. I also gratefully acknowledge the assistance of Dr. George Bowes who wrote many computer programs on my behalf and provided much needed tuition in their implementation and other aspects of computing. For instruction on the use of the electron probe micro-analyser, my sincere thanks go to Dr. Peter Hill and other members of the probe unit at the Grant Institute of Geology, University of Edinburgh.

The central Cuillin of Skye were rendered more accessible by the Junior mountaineering club of Scotland (J.M.C.S.) who kindly allowed me the use of the Coruisk memorial hut and I therefore wish to thank them, and in particular Mr. Dick Edie, the hut custodian, for providing comfortable accomodation in this wild but beautiful part of Skye.

I also wish to thank Mr. Murdoch Mcleod, Mr. Peter Wallace, Mr. John Gilleece and Mr. Dougie Turner for their assistance in the preparation of thin sections and samples and assistance in analytical procedures.

For assistance in formatting and printing the main body of the text I am indebted to Mr and Mrs and particularly Kenny Page of Microstaff Ltd.

For no particular reason other than for his support above and beyond the call of duty, my warmest and sincere thanks go to Mr S. Kean.

Finally I gratefully acknowledge financial assistance from the N.E.R.C..

Contents

List of Figures

ABSTRACT

The Lower Tertiary Cuillin Central Igneous Complex of Skye was mapped by Harker between 1895 and 1900. He concluded that the ultrabasic and basic rocks were formed from repeated injections of heterogeneous magma which initially was ultrabasic and became progressively more evolved with time. It was not until the late 1950's and early 60's that the complex was again investigated, when a number of researchers proposed that many of the different rock types of the complex could be related by differentiation processes which were almost exclusively envisaged to be gravity settling of early cumulus phases accompanying crystal-liquid fractionation.

The object of the present investigation was two-fold, namely to characterize the geochemistry of some of the myriad of mafic minor intrusions which transect and are associated with the plutonic rocks of the complex, and, secondly to remap the ultrabasic rocks (mainly peridotites)which cropout in An Garbh-choire and its environs within the Southern Cuillin. In the latter, particular emphasis has been placed on lithological and structural relationships within the peridotites to ascertain the processes involved in their genesis and what inferences may be drawn in the broader context of the evolution of the complex as a whole.

Most notable of the minor intrusions is a suite of basic cone-sheets which are broadly arcuate in plan and which appear to dip to a common focal point coincident with the centre of the complex, at an approximate depth of 4km. Cross cutting field relationships confirm that the cone-sheets were emplaced in a protracted, progressive event over a period of time, rather than in separate isolated events as proposed by previous workers. This is supported by major, trace and rare-earth-element geochemical evidence which fails to distinguish any significant criteria for variation of the parental magma type with time. It is shown that the parental magma to the cone-sheets is indistinguishable, albeit more evolved, from the previously identified Preshal Mhor Type (Esson et al 1975) which

tholeiitic in nature. Although geochemical modelling has shown that much of the intra-suite variation displayed by the cone-sheets may be produced by redistribution of the observed phenocryst assemblage of principally plagioclase, with minor amounts of olivine, the well constrained trends of the suite to more evolved representatives requires the involvement of a phase whose Ca/Al ratio exceeds unity. It is proposed, on the basis of major, trace and rare earth element data, that the occult phase is a (monoclinic) calcium-rich pyroxene. Modelling of crystal-liquid fractionation utilising these three phases produces predicted magma compositions which are in close agreement to those actually observed. Therefore, it is concluded that crystal-liquid fractionation, involving plagioclase, pyroxene and minor olivine, in the calculated proportions 55:35:10 was the dominant process involved in the evolution of the suite. Some samples show plagioclase phenocrysts present in quantities greater than is called for by the 3-phase cotectic signature displayed by the normative geochemistry of the suite. Mechanisms for this selective fractionation are discussed and it is tentatively suggested that gravity settling of the dense pyroxene and concomitant flotation of the less dense feldspar occurred. As this mechanism can be shown not to have occurred in-situ a storage-processing reservoir must have existed at a relatively shallow but greater depth.

A comparative geochemical study of certain so-called Intrusive Tholeiite Sheets (Hutchison 1964, 1966) was also undertaken. Data reported here indicate certain geochemical similarities between the Intrusive Tholeiite Sheets and the Cone-sheets. However, no simple evolutionary model could be constructed which explains the geochemical evolution of these sheets. This, in part may be due to the advanced state of secondary alteration within most of the material analysed.

In contrast to the liquid compositions generally preserved within the cone-sheets, the peridotites of An Garbh-choire are considered to represent the solid residuum of extreme crystal-liquid fractionation. They do, however, preserve evidence for both-syn and post-cumulus processes. Within the peridotites six zones have been identified, which range

from almost pure dunites, at the lowest exposed level (Zone 1), with occasional seams of Al-rich spinel, to feldspathic peridotites and allivalites within the structurally higher zones (Zones 5 and 6). Zone 2 is believed to represent a marginal facies to the series and pre-dates Zones 1 and 3. Zone 3 appears to be conformable upon Zone 1. Olivine, towards the base of Zone 1, is the most forsteritic (Fo_{94}) reported from the Cuillin Complex, to date. Although spinel seams are present within Zone 3, they are less common, laterally less persistent and less planar in form than those of Zone 1, whilst individual spinels are richer in chrome at the expense of aluminium. From the conflicting orientation of spinel seams and feldspar veins within Zone 3 it is concluded that post cumulus compaction, expelling trapped intercumulus melt, was the cause of the subhorizontal fabric observed in the field and that this process played an important role in the formation of Zone 4, which consists of highly brecciated lithologies. The higher structural levels of the peridotite display evidence of a significantly more porous cumulus framework which facilitated the growth of unusual intergrowths between cumulus olivine and intercumulus feldspar. These features take the form of either hemi-spherical dendritic growths of bladed to acicular olivines within radiating rays of intercumulus feldspar, or as generally planar horizons, a few tens of centimetres thick displaying the same relationships between the olivine and plagioclase as the radiating structures, but with random orientations. It is proposed that these features owe their origin to the mixing and subsequent quenching of the olivines when peridotite magma and a more feldspathic melt, either a discrete batch or an expressed intercumulus melt, were juxtaposed. Certainly, within the higher zones of the Peridotite Series, evidence for a feldspathic magma is compelling, with feldspathic peridotite bands up to two metres in thickness not infrequently found within, and broadly coincident with, the overall structure and fabric of the peridotite.

An interesting and unusual occurrence of large pyroxene aggregates is documented. These generally occur within the more feldspathic peridotite and feldspathic peridotite-allivalite xenoliths. These aggregates may possibly have formed during attempted re-

equilibration between intercumulus melt and/or sub-liquidus olivine and pyroxene of the more feldspathic rocks when subjected to elevated temperatures by either foundering into or upon being juxtaposed against the peridotite magma.

Although the peridotites do become more feldspathic with increasing structural height and mineral compositions less primitive it is generally concluded that this is the result of post-cumulus processes, in particular magma-mixing, rather than crystal-liquid fractionation.

Part 1

The cone-sheets and tholeiitic sheets of the Cuillin Complex

Easterly view of Blaven (top left) and Sgurr na Stri (centre) of the Black Cuillin of Skye. These mountains are formed from basic and ultrabasic rocks which, in part, exhibit igneous layering. The prominent fabric dipping to the left (north) at about 30' on the flanks of Sgurr na Stri is predominantly due to the occurrence of numerous fine to medium grained basic cone-sheets which were intruded approximately parallel to a pre-existing primary igneous fabric. Beyond Blaven, the pale coloured rounded hills of the Red Cuillin are visible. These hills are granitic in composition and truncate the earlier basic and ultrabasic Black Cuillin.

1.1 Introduction

1.1.1 Situation and topography

The Black Cuillin of central Skye represents the most northerly of the four Lower Tertiary, predominantly basic/ultrabasic, igneous central complexes of the Inner Hebrides off the west coast of Scotland (Fig.1.1). An original circular to elliptical plan is inferred for the complex, which has been modified by the later emplacement of granitic rocks which represent three younger centres, namely the Srath na Creitheach, Western Red Hills and Eastern Red Hills Centres (Fig.1.2). In contrast to these younger silicic centres, the Cuillin Complex is composed predominantly of basic and ultrabasic rocks which, in part, exhibit igneous layering. The most striking feature of this mountainous area is the Cuillin ridge, which runs from Sgurr nan Gillean in the north to Gars-bheinn in the south, and is concave towards the east, with individual peaks along its length attaining heights of just under 1000m O.D. The precipitous and irregular topography of the main ridge is due to the inweathering and outweathering of the many minor intrusions which transect the complex. Whilst the greater part of the complex is confined to the west of a line running north-south through Glen Sligachan to Camasunary Bay, the major rock units may be correlated with those forming the Garbh-bheinn - Blaven ridge occurring to the east of this line (Fig.1.3). Within the area bounded by the main ridge to the west and Glen Sligachan, three drainage areas have developed (Fig.1.3): Harta Corrie to the north, which drains northwards into Glen Sligachan; Coir'-Uisg which drains south east into Loch Coruisk; and Srath nan Creitheach to the west of Blaven which drains south. Exposure throughout the area is excellent, with the exception of some of the low ground in Srath nan Creitheach which is covered by thick accumulations of peat, and the area around Camasunary which marks a "25-Foot" (10m) raised beach level.

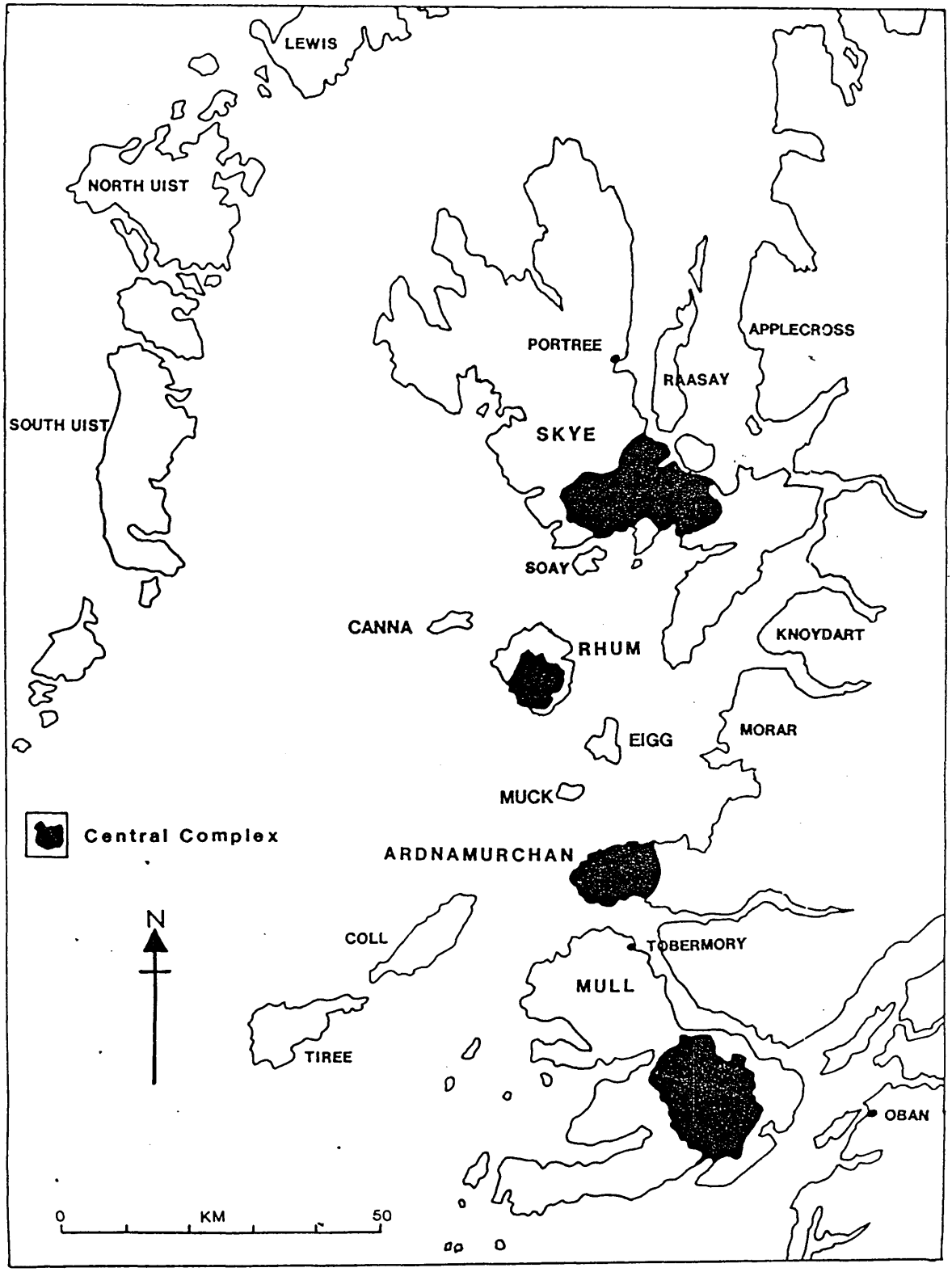

Fig. 1.1. Distribution of Lower Tertiary, predominantly basic/ultrabasic central complexes of the west of Scotland.

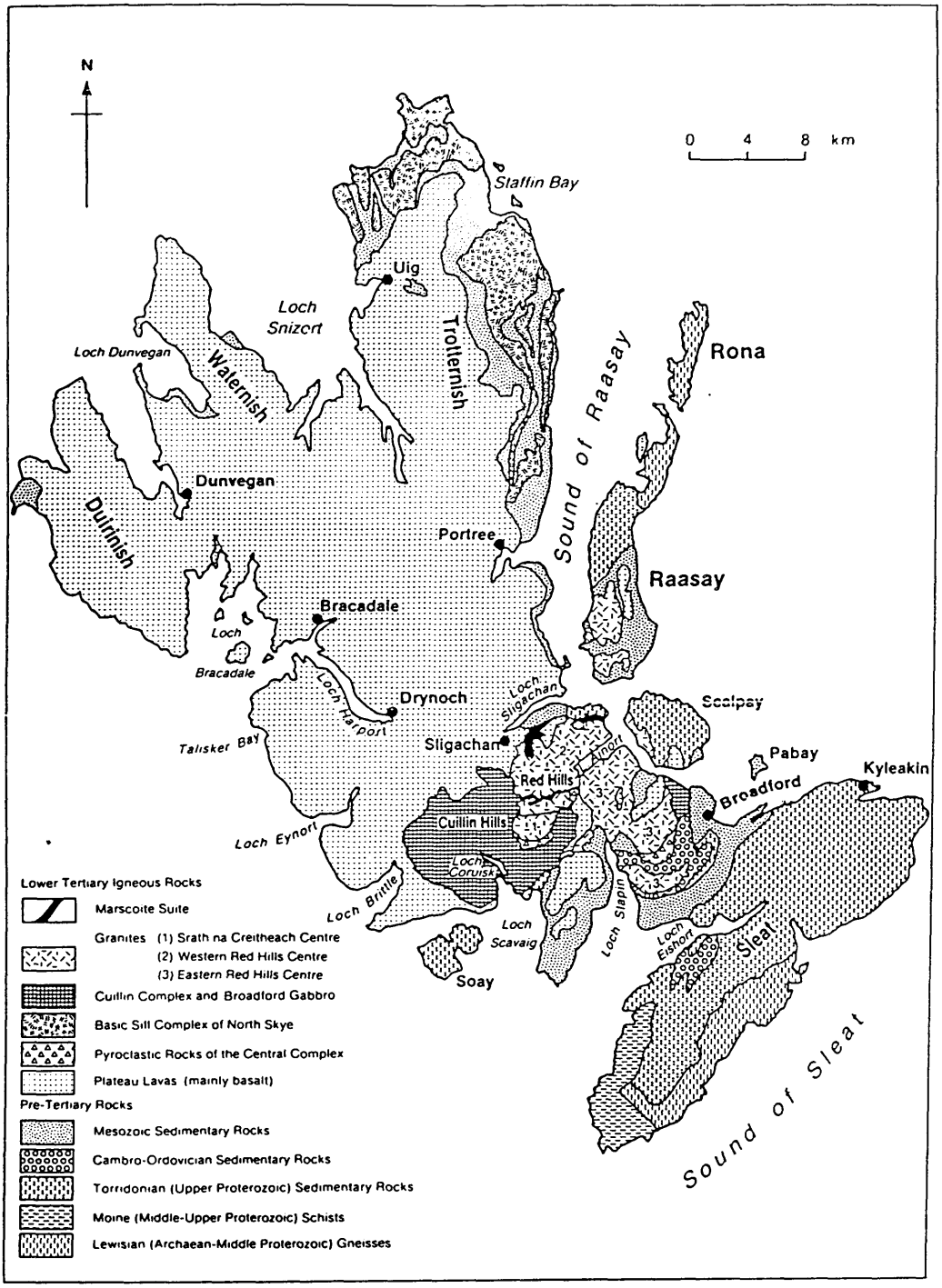

Fig. 1.2. Simplified geology of the Isle of Skye, Scotland (from Bell & Harris, 1986).

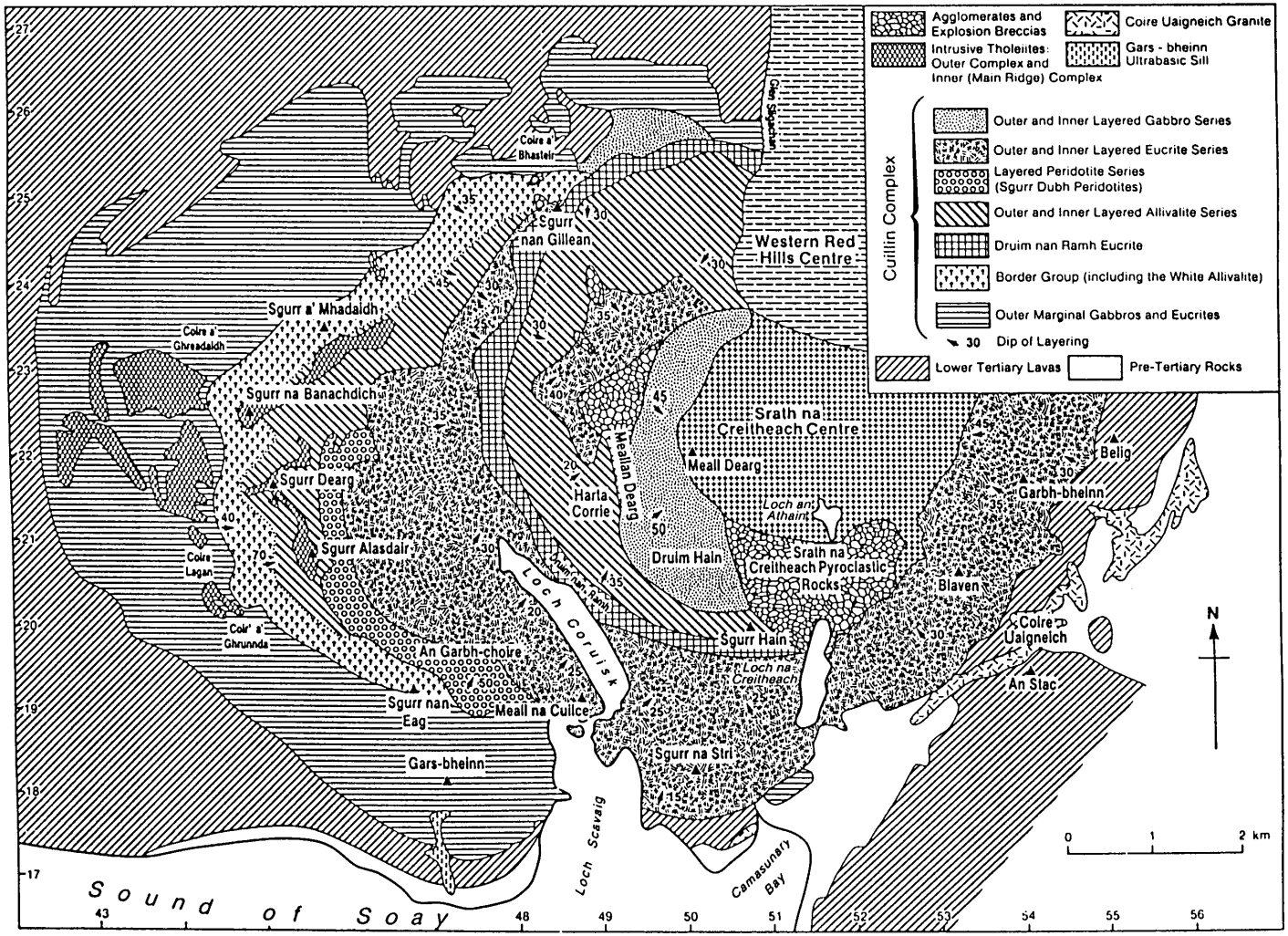

Fig. 1.3. Geology of the Cuillin Igneous Complex, Isle of Skye, Scotland (from Bell and Harris 1986).

1.1.2 Geological setting of the Cuillin Complex

A comprehensive account of the geology of Skye has been given by B.R.Bell & Harris (1986) and detailed accounts of the Cuiliin Complex by J.D. Bell (1976) and Wadsworth (1982). Therefore, the major rock-types of the complex and their disposition will only be described briefly.

In common with all the Early Tertiary central complexes of Scotland, with the exception of that occurring on Rhum, the intrusive centres post-date the lava flows with which they may be spatially associated. On Skye, alkalic and tholeiitic basaltic lavas were erupted on to a peneplained late Cretaceous land surface.

Significantly, on the southern margin of the Cuillin Complex, south of Sgurr na Stri (Fig.1.4), lavas are separated from Torridonian (Upper Proterozoic) sandstones and arkoses by the Coire Uaigneich Granite, this being the only intrusion of truly granitic composition associated with the complex. Dickin and Exley (1981) proposed that this granite was formed by the mixing of two discrete magmas: one being an acid differentiate of the basic Cuillin magma and the other a partial melt of Torridonian sedimentary rock.

Within the complex itself, basic and ultrabasic rocks form an arcuate pattern which is truncated by the granites of the Srath na Creitheach and Western Red Hills Centres (Fig.1.3). In general, successively younger members of the complex are found to occur progressively towards the centre, although there is evidence of differential movements within the complex (Carr 1952). The complex may be conveniently subdivided into an Outer and an Inner Layered Series (OLS and ILS, respectively), separated by the Druim nan Ramh Eucrite and bounded to the west by outer marginal gabbros and eucrites which are themselves intruded by tholeiitic basaltic sheets (Hutchison 1966). A Border Group to the OLS was identified by Zinovieff (1958) and studied in detail by Hutchison (1964), who reported a fine-grained xenolithic outer margin which grades into a coarse-grained unlayered troctolite which can be traced for a distance of over 5km along strike. The OLS consists of peridotites, troctolites, eucrites and gabbros which locally exhibit igneous layering that dips towards a focal point below Meall Dearg at a depth of approximately 3km. The layered peridotites within the OLS grade from olivine-rich adcumulates (Section 2.1.1)

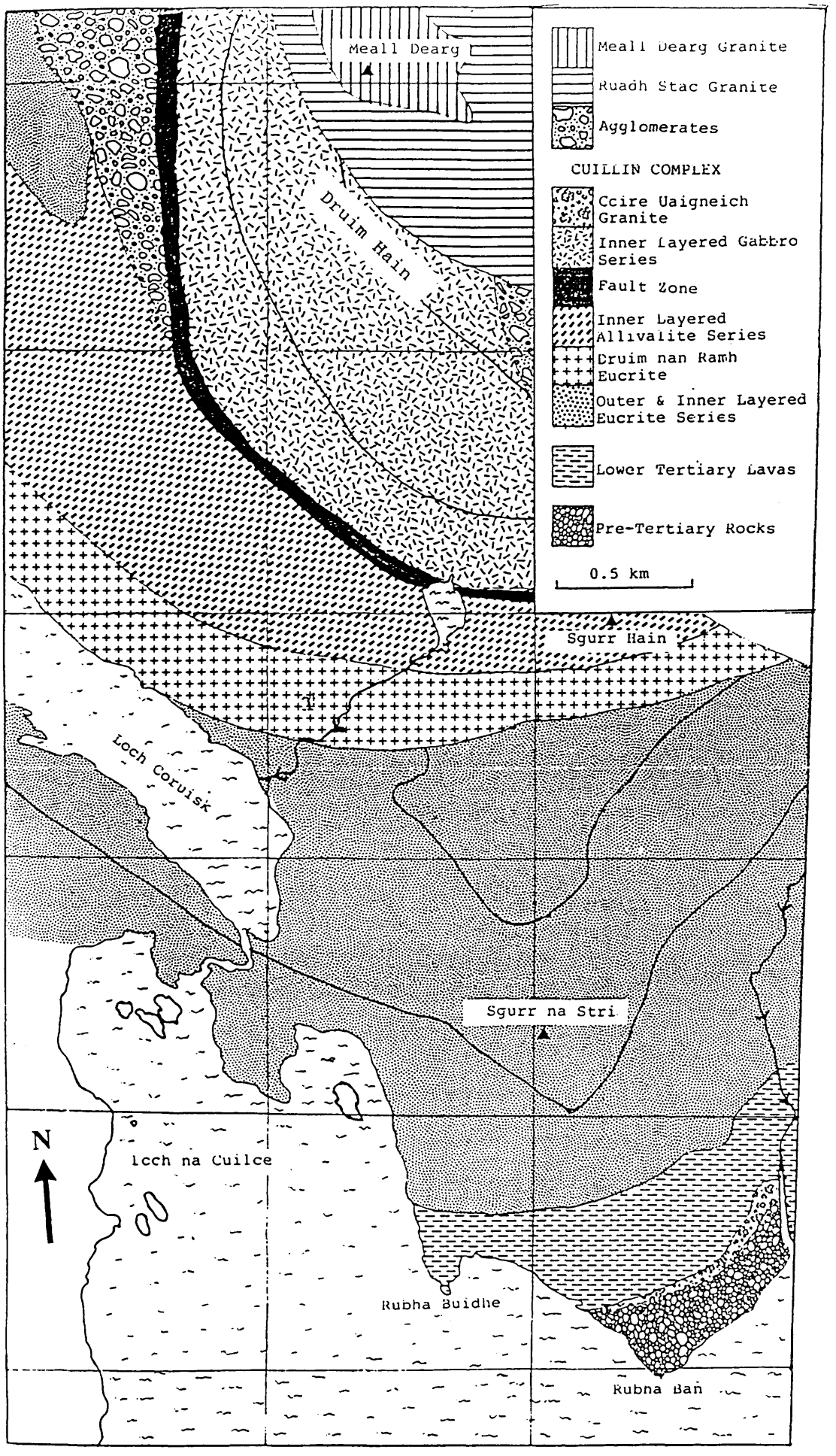

Fig. 1.4. Geology of the Sgurr na Stri-Meall Dearg area of the Black Cuillin of Skye, Scotland.

at the base into olivine-feldspar adcumulates further up the succession. Within the lower part of this series occur thin seams of cumulus chromite. Truncating the rocks of the OLS is the Druim nan Ramh Eucrite, a course-grained unlayered rock (Carr 1952), which Zinovieff (1958) suggested was a ring-dyke since rocks of the ILS could be correlated with those of the OLS. Alternatively, this eucrite may represent a marginal group of rocks to the ILS, equivalent to the Border group of the OLS and thus may signify the beginning of a second phase of activity within the complex. Similarly, the ILS comprises layered allivalites, eucrites and gabbros dipping towards the same focal point indentified for the OLS.

The formation of the Skye Central Complex was followed by the emplacement of a suite of minor intrusions, the so-called cone-sheets. These inclined sheets, which are arcuate in plan apparently dip to a common focal point coincident with the centre of the complex. Unlike the major lithological units of the complex, which the cone-sheets bisect, these minor intrusions are believed to preserve, in their geochemistry, the composition of their parental magmas. Cone-sheet suites are a common occurrence of the central complexes of the British Tertiary Volcanic Province (BTVP) and although not exclusively found within the BTVP accounts of similar occurrences are rare.

1.1.3 Objectives of research

Previous ideas and models on the evolution of layered igneous central complexes within the British Tertiary Volcanic Province (BTVP) rely heavily on those developed for the Skaergaard intrusion of East Greenland. The disposition, mineralogy and chemistry of the layered rocks of this intrusion accord well with those predicted by the model which suggests that these rocks have formed by a process of closed system crystal-liquid fractionation (Wager & Deer 1939; McBirney & Noyes 1979). However detailed investigations of the central complexes within the BTVP, notably those of the Skye and Rhum centres, suggest that more elaborate dynamic models of volcanic plumbing need to be developed. It has been proposed on the basis of the obvious cyclicity of layered cumulates within the Rhum Centre (Brown 1956), that the magma chamber behaved as an open system with respect to parental magma replenishment and eruption of derivative

fractionated basaltic magma. The geochemical consequences of such a model have been investigated by O'Hara (1977) and O'Hara and Mathews (1981). This model may itself be simplistic in the light of recent observations, which suggests that some individual layers within the layered series were intruded as discrete sills which then fractionated and caused partial melting of their roof rocks (Morse 1986; Bedard et al. 1988).

The cyclic nature of many layered complexes is one facet of an open magma chamber model. One purpose of this research is to describe and characterize the petrography and geochemistry of certain minor intrusions which represent trapped magma batches from a presumed open system central Skye magma chamber, and to ascertain how much of the chemical and mineralogical variation within this suite of related intrusions can be ascribed to the processes of fractional crystallization in an open system enviroment. The chamber is presumed to be open not only to the inflow and outflow of parental and derivative magmas, respectively, but also open with respect to chemical exchange and re-equilibration and contamination/assimilation of its country-rocks, with possible mixing of derived magmas.

Implicit in this discussion is that the samples chosen represent liquid compositions and, therefore, that the data set allows the evolution of these liquids to be documented.

1.1.4 History of research

1.1.4.1 Cuillin Central Complex

Detailed accounts of previous investigations into the Cuillin Complex have been presented by Carr (1952), Weedon (1956), Zinovieff (1958) and Brown (1982). Consequently, only a very brief summary of the early work will be given here.

Macculloch (1819) first described the igneous rocks of the Cuillins in his "Description of the Western Isles". In 1829 Von Oeynhausen and Von Dechen investigated the gabbro-basalt boundary but said little about the rocks inside it. However, in 1845 Forbes suggested that the gabbro was younger than the basalts and expressed the view that the gabbro mass is sheet like in form, to be reiterated later by Geikie (1888) and Harker (1904). The first detailed account of any of the basic rocks was by Geikie and Teall (1894). Geikie, in his book "Ancient volcanoes of Great Britain" (1897), ascribed the layering present within

some of the gabbros to the streaking out of a heterogeneous magma. In 1904 Harker published his classic Skye memoir "The Tertiary Igneous rocks of Skye". He recognised that there had been several intrusive episodes and that the central complex arose from the intrusion of a series of already differentiated magmas with high surface tensions. Following a visit to Skye to study the peridotite dykes, Bowen published his monumental book "The evolution of the Igneous rocks" (1928), emphasising the importance of fractionation processes. These processes were subsequently applied, with success, to account for much of the layering within the Skaergaard intrusion of East Greenland (Wager & Deer 1939). Subsequently, Stewart and Wager (1947) identified the presence of phase layering within the layered gabbros of the Druim Hain area of the Cuillin Hills on Skye. This observation instigated a detailed re-investigation of the Cuillin Complex, which was began by Carr (1952) in the Sgurr na Stri area, and who concluded, after observing banding and cryptic variation within the gabbros, that the bulk of the rocks of this area had been formed by crystal accumulation from a fractionating basic magma. He was able to divide the gabbros into three zones on field and petrographic grounds and showed that the younger Druim nan Ramh Eucrite (Fig.1.4) (his "invading eucrite") was of more than one episode. To the north of the eucrites he mapped a belt of disturbance with numerous dykes, crushed eucrites and a zone of mylonite, which separated a further sequence of layered gabbros. These, he concluded, were an uplifted part of the same layered series mapped to the south, exterior to the Druim nan Ramh Eucrite.

Whereas Harker (1904) had said that the gabbros post-date the agglomerates of the area, Carr (1952) was able to demonstrate the reverse. Subsequently, Weedon (1956) showed that the gabbro zones defined by Carr were traceable to the west and could be correlated with gabbros on the concave side of the peridotites (Fig.1.3). These he termed the Inner Layered Gabbros, in order to distinguish them from those occurring to the west of the peridotites, which he termed the Outer Layered Gabbros. In addition, Weedon was able to demonstrate that the Outer Layered Gabbros pre-dated the peridotites and Inner Layered Gabbros. The peridotites, he suggested, formed a layered intrusion and divided them into two groups on the basis of their cumulus assemblages. Zinovieff (1958), working further to

the north, recognised and defined a Border Group to the Outer Layered Gabbros and divided the layered series into two, separated by a ring-dyke (part of Carr's "invading eucrite") which was intruded, he concluded, as a crystal mush. Zinovieff related the peridotites, eucrites and allivalites to one fractionating parent magma which he suggested was similar to the Porphyritic Central Type of Mull (Section 1.2.1).

The fractional crystallization of a single parental magma to produce the Cuillin layered intrusion was questioned by Walker (1975), although he did not question a cumulus origin for the generation of the igneous lamination. Walker proposed that many of the BTVP central complexes may be, as Harker originally suggested, a confluent cone-sheet complex, citing multiple intrusion as evidence.

The magma chamber in which the Cuillin cumulates were formed is inferred to have been funnel shaped (Hutchison 1968; Hutchison and Bevan 1977). This has raised doubts regarding the possibility of accomodating a sufficient volume of basic magma in order to produce the 6km of observed cumulates in one or two main magmatic events. However, the evidence for differential movements within the Complex implies the existence of a subjacent magma body which may have acted as a storage reservoir, allowing replenishment of the higher chamber by magma which had itself been cooling and fractionating within the lower chamber (Wadsworth 1982).

1.1.4.2 Cone-sheets

The first mention and description of the Skye cone-sheets in the literature is to be found in the "Tertiary Igneous Rocks of Skye" (Harker 1904). By careful mapping, Harker was able to demonstrate the arcuate form and common focal point beneath Meall Dearg of a suite of so-called inclined basic sheets at the southern end of Glen Sligachan (Fig.1.4). Although only one chemical analysis of an inclined sheet was reported (Table 1.1) it indicated their tholeiitic nature.

	A	B	C	D
SiO_2	47.64	46.80	52.50	49.80
TiO_2	1.27	0.80	1.00	1.37
Al_2O_3	14.15	18.60	13.50	15.70
Fe_2O_3	5.18	1.40	9.50*	1.50
FeO	7.96	7.70		8.90
MgO	7.38	10.90	8.50	7.30
CaO	11.71	10.60	12.00	10.80
MnO	0.33	0.10	-	0.20
Na_2O	2.38	2.70	2.00	3.00
K_2O	0.71	0.30	1.00	0.20
P_2O_5	0.09	0.04	-	0.15
H_2O^+	1.44	-	-	-
H_2O^-	0.19	-	-	-
Cr_2O_3	0.01	0.04	-	-
V_2O_5	0.06	-	-	-
NiO	tr			
CoO	tr			
Total	100.53	100.00	100.00	98.62

Table 1.1 Comparison of suggested parent magmas of the Tertiary central complexes of Scotland

*= Fe reported as total iron.

A: Cone-sheet, Skye (Harker 1904).

B: Hypothetical Rhum parent magma (Brown 1956).

C: Hypothetical Ardnamurchan parent magma (Gribble 1974).

D: Cone-sheet, Ardnamurchan (Holland and Brown 1972).

Harker identified four main petrographic types:

1. Olivine-free non-porphyritic dolerite:

   These comprise of labradorite and very pale-brown augite in ophitic to sub-ophitic texture, with abundant opaque minerals, mainly magnetite but with some ilmenite, both as grains and skeletal growths. Within this group Harker recognised two variations on the above; firstly a group which showed a slightly later, coarser generation of feldspar moulded on the augite and, secondly, a variety possessing large rounded feldspars which he concluded to be a xenocrystic phase. Apatite is only sparingly present.

2. Porphyritic olivine-free dolerite:

   The most prevalent type noted by Harker, which contain abundant phenocrysts of labradorite, often showing a glomeroporphyritic texture and containing glass inclusions.

3. Porphyritic olivine dolerite:

   Contains micro-phenocrysts of olivine represented by green-green/yellow pleochroic pseudomorphs, in addition to plagioclase feldspar phenocrysts.

4. Olivine dolerite:

   Similar to Type 3 but aphyric and more basic, containing abundant groundmass olivine and bytownite showing obvious zoning. The olivine is represented by pseudomorphs of green serpentine with pilitic hornblende. Sparingly present are a few needles of apatite.

Harker (1904) regarded these sheets to be the product of a single intrusive event and speculated that, as the sheets die out downwards, they were probably fed by dyke-like feeders.

With the publication of the Mull memoir (Bailey et al. 1924), the term cone-sheet superseded that of Harker's "inclined basic sheets", and for this particular igneous centre the authors were able to identify more than one phase of cone-sheet emplacement. Multiple cone-sheet

emplacement events were tentatively suggested for the Skye centre by Carr (1952), who noted metamorphosed remnants of cone-sheets enclosed within the gabbros of the Camasunary area. This observation was confirmed by Almond (1960) who concluded that there had been at least two phases of cone-sheet emplacement; the later one, occurred after the emplacement of the Cuillin Complex and the Coire Uaigneich Granite, but prior to the emplacement of the later granitic centres, and was more dominant.

Zinovieff (1958), was able to identify at least three phases of cone-sheet emplacement and suggested that there might have been a slight shift in the focus of each phase after observing two discrete orientations in the western cliffs of Sgurr an Feadhain. According to Zinovieff, each phase can be characterized by the following criteria:

1st phase: Characterized by their large size and commonly displaying differentiation within the thickness of a single cone-sheet. Representatives of this first phase of activity are only present within the Outer unlayered gabbros and eucrites.

2nd phase: This phase is also confined to the Outer Unlayered Gabbros. These cone-sheets are porphyritic with phenocrysts of calcic bytownite. Zinovieff suggested that these sheets may have formed from the same magma as that which formed the layered rocks of the complex.

3rd phase: Comprise of non-porphyritic types, generally fine-grained sheets which possess thick chilled margins.

In the only other recent petrographic and geochemical study of cone-sheets within the BTVP, Holland & Brown (1972) demonstrated the tholeiitic nature of the basic Ardnamurchan examples, which range from olivine to quartz tholeiite. They compared the identified tholeiitic and the alkalic Hebridean trends with the corresponding Hawaiian geochemical trends and suggested that the transitional nature of the former is probably related to derivation from an alkali olivine basalt magma rather than from an olivine tholeiite magma, as in Hawaii.

1.1.5 Mechanisms of emplacement

Anderson (1936), in a general study of the dynamics of formation of ring structures, concluded that cone-sheets were the result of increased pressure in a magma chamber, in order to account for the observed uplift of the overlying central area, which he calculated to be 1100m for the Ardnamurchan centre. A decrease in the magma pressure, he proposed, would account for the formation of ring-dykes. The formation of cone-sheets was re-addressed by Phillips (1974) who showed that retrograde boiling of a magma with subsequent hydraulic fracturing were possible means of generating the stress trajectories required for their formation.

The structural aspects and mechanisms of emplacement of the cone-sheets have not been studied in any detail here, as this study is more concerned with their petrological and geochemical aspects.

1.2 Igneous Concepts

1.2.1 Concept of magma-type

The publication of the Geological Survey of Scotland memoir describing the Lower Tertiary igneous geology of Mull (Bailey et al. 1924), introduced the concept of magma-type. In this classic volume, the classification scheme adopted was based on magma compositions. Samples with similar compositions were grouped into magma-types, nine of which were recognised. Those which appeared to be genetically related were further grouped into magma-series. The so-called Normal Mull Magma Series comprises: the Plateau Magma-Type (PMT) of (magnesian) olivine-rich basalts; the Non-porphyritic Central Magma-Type (NPCMT) of (magnesian) olivine-poor or olivine-free basalts; the Intermediate to Sub-acidic Magma-Type; and, the Acid Magma-Type. The authors believed that the Plateau Magma-Type held a parental status and that the more evolved magma-types could be derived from it by fractionation processes. However, it was recognised by Bailey et al. (1924), that the presence of SiO_2-undersaturated zeolites within the Plateau Magma-Type and interstitial silicic glass within the Non-porphyritic Central Magma-Type were evidence against the latter being derived from the former. Therefore, assimilation of sialic crust was proposed to account for the observed interstitial silica glass of the NPCMT. Bowen (1928) argued that, on the basis of graphical analysis of the available whole rock geochemical data, it was highly improbable that the determined chemical trend could be accounted for by crustal assimilation alone, and proposed, with recourse to experimental studies, that crystallization of olivine and plagioclase from the Plateau Magma-Type, with separation of the olivine such that it was unable to react with the cooling magma, could produce the observed compositional relationships.

Washington (1922) noted that lavas closely resembling the Mull Non-porphyritic Central Magma-Type are predominant throughout the major plateau basalt regions of the world and, therefore, from their enormous worldwide distribution and remarkable uniformity of composition could be regarded as representative of undifferentiated primary basic magma.

Kennedy (1930) reversed the status of the two Mull magma-types and proposed that it was the Non-porphyritic Central Magma-Type which had evolved by early separation and concentration of olivine and calcic plagioclase to the Plateau Magma-Type. Subsequently, Kennedy revised his suggestion and regarded both as independent parental liquids with the Plateau Magma-Type, which he renamed olivine basalt, and the Non-porphyritic Central Magma-Type, renamed tholeiite, fractionating to feldspathoidal and silicic residues, respectively (Kennedy 1933). Tilley (1950), after much work on Hawaiian volcanism, renamed the olivine basalt as alkali olivine basalt.

A more realistic definition of magma-type, in the light of previous studies, depends upon recognising rocks which represent related liquids and can be demonstrated to exhibit an evolutionary trend. If well-defined groups are identified then the differences between these groups, which are not explicable in terms of low-pressure crystal-liquid fractionation might be ascribed to processes operating in the upper mantle. For example, the lavas of north Skye (Table 1.2) have been divided into three distinct groups (Thompson et al. 1972; Mattey et al. 1977): (i) a transitional series, with respect to their position relative to the critical plane of silica saturation within the basalt tetrahedron of Yoder and Tilley (1962), which Thompson terms the Skye Main Lava Series (SMLS); (ii) the second group, the so-called Preshal Mhor (PM) Type, comprising distinctly tholeiitic basalts similar in composition to Mid ocean Ridge basalts (MORB), with extremely low concentrations of large-ion lithophile (LIL) elements and showing depletion of light rare earth elements (LREE) relative to heavy rare earth elements (HREE) on Masuda-Coryell plots; (iii) the third type, the Fairy Bridge (FB) basalts, which were identified by Mattey et al. (1977) in a study of the regional dyke swarm of Skye and have been defined as possessing a major element composition similar to members of the SMLS, and incompatible trace-elements mostly intermediate between the SMLS and the PM tholeiites, with a flat chondrite-normalised REE pattern.

	SMLS					Preshal Mhor						Fairy Bridge				
Sample	947	906	956	931	980	S017	S021	1031	H037B	H110	A048	1061	H060	1043	H002	H325
SiO_2	46.34	44.61	47.82	46.86	51.09	48.04	44.28	45.45	46.98	46.37	49.92	45.80	47.48	46.06	46.46	47.79
TiO_2	1.68	2.51	1.39	3.34	1.92	0.70	0.53	0.93	0.71	0.95	0.89	1.04	1.20	1.44	1.77	1.87
Al_2O_3	15.73	15.82	15.46	15.68	16.32	16.35	19.05	15.84	15.46	15.78	16.69	16.43	15.96	16.30	16.44	13.86
Fe_2O_3	1.50	1.50	1.50	4.30	2.00	1.50	1.50	1.50	1.50	1.50	1.50	1.50	1.50	1.50	2.00	1.50
FeO	9.24	12.53	10.15	9.68	8.10	7.55	6.28	9.47	7.61	8.75	8.38	8.42	10.29	10.50	11.12	12.11
MnO	0.17	0.20	0.22	0.20	0.21	0.15	0.12	0.17	0.16	0.18	0.16	0.14	0.19	0.16	0.18	0.23
MgO	7.96	8.49	6.89	4.31	4.35	8.34	8.87	9.10	11.83	8.60	7.95	7.95	7.67	7.56	6.80	5.56
CaO	9.32	8.67	10.13	6.66	5.78	12.22	13.26	12.79	11.77	12.81	12.63	9.51	9.64	9.07	8.12	9.67
Na_2O	2.94	3.39	2.97	4.75	4.21	1.84	1.44	1.71	1.62	1.85	2.16	2.72	3.38	3.11	3.45	3.11
K_2O	0.65	0.18	0.58	0.77	2.51	0.24	0.11	0.13	0.11	0.09	0.28	0.36	0.45	0.61	0.57	0.65
P_2O_5	0.25	0.25	0.22	0.47	0.73	0.09	0.08	0.09	0.05	0.06	0.11	0.16	0.12	0.12	0.25	0.23
H_2O^+	2.85	2.60	1.92	2.12	2.06	-	-	-	-	-	-	4.64	1.85	2.52	1.58	2.45
Total	98.63	100.75	99.25	99.14	99.28	97.02	95.52	97.18	97.80	96.94	100.67	99.67	99.73	98.95	98.74	99.03
Trace elements (ppm)																
Rb	10	3	9	10	n.d	5	1	0	1	1	6	0	4	9	6	8
Ba	225	n.d	n.d	123	n.d	n.d	n.d	n.d	n.d	n.d	n.d	n.d	n.d	n.d	n.d	n.d
Sr	582	449	418	659	n.d	113	113	101	99	111	110	287	476	570	511	267
Nb	4	10	7	40	n.d	2	4	6	4	4	6	7	4	6	6	7
Zr	131	157	108	253	n.d	36	23	45	32	46	43	69	70	74	81	94
Y	24	31	27	40	n.d	19	12	19	13	23	28	27	27	31	25	33

Table 1.2 Representative analyses of previously identified magma types of Skye; The Skye Main Lava Series (SMLS), the Preshal Mhor and Fairy Bridge magma types (Mattey et al. 1977).

1.2.2 Magmas of the Central Complexes

The determination of the parental magma(s) from which the central complexes crystallized is hampered by their accepted cumulative origin and thus they are unlikely to represent the liquid compositions from which they formed. Thus the exact nature of the parental magmas of the central complexes within the BTVP remains controversial. Brown (1956), first estimated the composition of the Rhum layered peridotites and troctolites parent magma from the composition of interstitial areas in orthocumulates within the layered series as being broadly tholeiitic (Table 1.1). This suggestion was supported by Wadsworth (1961), but subsequently, Esson et al. (1975) have shown that Brown's postulated composition has transitional-alkalic characteristics, this being consistent with the observation that orthopyroxene is rare within the Rhum layered rocks. Donaldson (1975) and Gibb (1976) proposed an ultrabasic parent for the Rhum rocks whilst Henderson and Gijbels (1976) showed that the layered series displays a LREE enrichment and thus they favoured an alkalic magma produced from limited partial melting of the mantle source region. Kitchen (1985), on the basis of alkalic segregations and veins within the peridotites, proposed a transitional to mildly alkalic parent magma, showing affinities with the SMLS magma-type. However, an analysis of a rare chilled margin to one peridotite layer within the Eastern Layered Series indicates that the parental magma was that of an ultrabasic tholeiite, with olivine crystals in suspension. (Greenwood et al. 1990)

The fine-grained margins of some of the large unlayered doleritic intrusions associated with the Ardnamurchan Complex were analysed by Gribble (1974). He argued that as crystal-liquid separation could not be identified as having occurred, the composition was that of the original parental magma. The results of this analysis (Table 3.2) occupy the same field on a MgO-SiO_2 plot as the Ardnamurchan cone-sheets (Holland and Brown 1972), the most magnesian of which has a composition which clearly identifies it as a member of the PM Magma-Type.

Zinovieff (1958) related the Cuillin peridotites, eucrites and allivalites to one fractionating basaltic magma which he concluded was similar to the Porphyritic Central Magma-Type of Mull, but depleted in titanium. Wager & Brown (1968) repeated the suggestion for a basaltic parent, whilst Hutchison (1968) and Hutchison & Bevan (1977) appealed to a gradual progression from early ultrabasic to later basic magmas, all of tholeiitic affinities, on the grounds that a basaltic magma was incapable of producing the thickness of ultrabasic rocks observed. This suggestion was repeated by Walker (1975) and supported by Gibb (1976) and Donaldson (1977). Gibb (1968) examined the peridotite dykes of south Skye, and concluded that they were emplaced as an olivine charged eucritic magma, co-magmatic with the layered peridotites of the Cuillin Complex.

1.2.3 Processes causing chemical variation within igneous rocks, including evidence from the British Tertiary Volcanic Province.

1.2.3.1 Hydrothermal Alteration

It is essential, before any meaningful discussion of the chemical petrology of the BTVP, to ascertain the extent of the hydrothermal alteration which has affected rocks of the Province to a greater or lesser extent.

Bailey et al. (1924) showed that a "zone of pneumatolysis" extended to about 5km from the central complex on Mull and similar zones have since been recognised around other central complexes within the Province (Moorbath & Thompson 1980). Within this zone the alteration is characterized by a greenschist-facies metamorphic mineral assemblage with the breakdown of calcic plagioclase to albite and clinozoisite and actinolite, and the oxidation of Fe-Ti oxides. Also recognised within the Skye, Mull and Antrim basalts are flat-lying zones of zeolitization, each zone characterised by a distinct mineral assemblage. These zones cross-cut the lava stratigraphy and are attributed to hydrothermal burial metamorphism (King 1977). Within the basic rocks cut by these zones, olivine, where present, is pseudomorphed to varying degrees by serpentine, iddingsite and Fe-Ti oxides; interstitial glass is replaced by zeolites causing corrosion of surrounding plagioclase, whilst pyroxene usually remains apparently unaffected.

Tilley and Muir (1962) pointed out that all previously published average chemical compositions of mafic rocks from the BTVP were based largely upon analyses of rocks considerably affected by hydrothermal alteration. They suggested that the affect of this metamorphism was to increase H_2O^+ and Fe_2O_3 concentrations and therefore increase Si-saturation. After demonstrating that a hydrothermally-metamorphosed basalt was Hy-normative whilst its remnant unaltered pyroxene was Ne-normative, they proposed that prior to metamorphism the Plateau magma-types were all Ne-normative. However, Ridley (1973) demonstrated that fresh basalts could range in SiO_2 from Ne-normative to Hy-normative whilst preserving intrinsic features of alkali basalts, such as groundmass olivine. Similarly, Thompson et al. (1972) demonstrated a strong correlation between SiO_2 saturation and immobile trace-element concentrations for the plateau lavas of northern Skye.

1.2.3.2 Partial melting

Initial chemical characteristics are imparted to a magma at its site of generation, where a number of variables control the composition of the melt produced:

i) Composition of the source material and the ratio of the minerals within it.

ii) Relative concentration of volatile components.

iii) Confining pressure.

iv) Degree and type of partial melting episode.

Obviously the composition of the source material and the ratio of minerals comprising it is of paramount importance in determining the composition of any liquid produced during a melting episode. For melts produced within the upper mantle, believed to be the site of generation for ocean floor and terrestrial flood basalts, only a limited range of liquids can be produced still in equilibrium with the source mineral assemblage. From experimental and field evidence the "fertile" upper mantle (ie. an assemblage which is still capable of producing a basic magma upon partial melting) is believed to consist of an aluminous lherzolite (olivine, orthopyroxene, clinopyroxene and one of three possible alumina-rich

phases: garnet, spinel or plagioclase feldspar, depending on the confining pressure). However, olivine and orthopyroxene are considered to be so abundant in the source that, during partial melting, these phases will be the last and penultimate phases to be consumed, respectively, and, therefore, almost all of the melting episode is characterised by the production of liquids in equilibrium with olivine and orthopyroxene.

Experimental data show that the CO_2/H_2O ratio may, in addition to lowering the solidus temperature, have an important influence on the composition of melts generated (Wyllie 1979). A high partial pressure of H_2O is believed to contribute to the generation of Si-saturated liquids whilst a high CO_2 partial pressure favours the production of melts critically undersaturated with respect to silica.

The phase equilibria of a mantle assemblage is dependent on pressure. Notably, the liquidus field of olivine decreases with increasing pressure whilst that of clinopyroxene increases with increasing pressure. Consequently, liquids generated become richer in the chemical components of olivine and depleted in those of clinopyroxene with increasing pressure. The confining pressure will also affect the solubility of volatiles leading to the effects noted above.

Whilst the major element chemistry of a melt produced may not vary much with limited degrees of partial melting, the trace element chemistry is strongly controlled by the amount of melt produced. All elements incompatible with respect to mantle minerals will be strongly partitioned into any melt formed, and will be rapidly depleted in the residuum. Consequently, for small degrees of partial melting their concentration will be much greater in the melt than for larger degrees of melting, where they will be relatively diluted.

The composition of the melt produced is also controlled by the type of melting operating. During equilibrium partial melting the bulk composition of the system remains constant until the melt is separated from the residuum, unlike perfect fractional partial melting, where each drop of liquid is, in theory, removed from the system as soon as it forms. This has important consequences for the incompatible elements which are rapidly removed in the early melt fractions and therefore rapidly depleted in the residuum. The compatible elements, however, are enriched in the residuum. Equilibrium and fractional partial melting are

idealized cases and in reality some combination of these processes is expected to occur. More realistic melting processes have been formulated and during accumulated fractional partial melting liquid fractions are mixed prior to eruption, the principle effect being on the minor and trace element chemistry of the erupted liquids.

Dynamic melting (Langmuir et al. 1977) assumes that throughout the partial melting process a certain percentage of the melt remains trapped between the residual crystals. The trend followed by the major elements lies between that of equilibrium and fractional partial melting. Trace element behaviour however is different to that expected from either of the two simpler models. The most notable affect during dynamic melting is the ability of this process to produce melts of different composition which have different degrees of LREE enrichment and crossing REE patterns from a homogenous source (Wood 1979).

The equations which govern the behaviour of trace-elements during the different types of partial-melting processes are given in Appendix III.

1.2.3.3 Fractional crystallization

Bowen (1928) recognised the importance of fractional crystallization and for the last 60 years this process has been regarded as being fundamental in producing the diversity observed within igneous rocks. The essential feature of this process is that early formed minerals crystallizing from a complex melt are of a different composition to the melt itself and therefore if a means exists to separate these minerals from the melt such that they are isolated and cannot react with the residual liquid, the composition of the liquid will change (evolve). As the composition of the liquid changes, the composition of the crystallizing phase may also change and/or new phases may join in the fractionating process. Alternatively, an early fractionating phase may cease to crystallize and undergo a reaction with the liquid as in the classic reaction of: olivine + liquid = orthopyroxene, shown by tholeiitic magmas.

One important mechanism for isolating crystals from a magma is generally considered to be that of gravitational settling of the crystals; the crystals being denser than the magma and consequently sinking under their own weight. This process of crystallization accompanied by gravity settling has been invoked to explain the cryptic and phase layering observed

within many layered intrusions, especially those of mafic-ultramafic composition. However, over the last 10 years the dominance of gravitational settling in crystal-liquid fractionation has been questioned. Plagioclase is often part of the cumulus phase assemblage within mafic layered intrusions and it has been demonstrated in general (Campbell et al. 1978), and for the particular case of the Skaergaard intrusion (McBirney & Noyes 1979), that the liquids from which the plagioclase crystallized would have been more dense than the crystals and consequently the buoyant plagioclase should have risen through the melt. The presence of volatiles may however decrease the yield strength of a magma allowing the plagioclase to sink; alternatively, it has been suggested that the feldspar may settle by being incorparated into glomeroporphyritic aggregates along with other denser phases such that the overall density of the aggregate is greater than that of the melt (Campbell et al. 1978). This mechanism fails to account for the examples where feldspar alone is the cumulus phase and consequently in-situ crystallization has been invoked (McBirney & Noyes, 1979) as a possible mechanism.

As a consequence of the failure of gravitational settling to account for all features of differentiated layered intrusions Sparks et al. (1984), after experimenting with aqueous solutions, have proposed that it is almost inevitable that a reservoir of magma may develop compositional and thermal gradients. They suggest that discrete compositional layers may form from a single homogenous body of magma by the selective removal of heavy or light components into a crystal, resulting in a locally lighter or denser fluid, respectively, a process they term convective fractionation. McBirney & Noyes (1979) suggested that if crystallization overtakes the homogenisation process caused by mixing of layers when their densities are equal then the discrete compositional layers may be frozen into the rock. This proposal may account for certain of the layering phenomena observed in the field.

1.2.3.4 Magma mixing

Magma mixing as a process of differentiation was once thought to be responsible for the production of rocks transitional between acid and basic extremes but was discarded as a major process when compositional and mineralogical variation within the suggested magma series proved to be too complex to be explained in terms of a limited number of end members. The process of mixing has, however, been used to explain localised occurrences where complete homogenization of two end members has not occurred, the resultant rock thus retaining textural, mineralogical and chemical evidence for its generation. Textural evidence for mixing is often lacking in many examples postulated to represent such a process. However, on Skye, textural, mineralogical and chemical evidence supports the derivation of the hybrid rock type colloquially called marscoite by the mixing of 65% of ferrodioritic magma with 35% of porphyritic felsite magma (Wager et al. 1965), both of which are individually preserved locally.

Mixing has been proposed on phase equilibria and chemical grounds to be an important process in the evolution of MORB (Dungan & Rhodes 1978; Rhodes et al. 1979; Walker et al. 1979). Unlike marscoite, however, the mixing is believed to occur between consanguineous evolved and primitive magmas.

1.2.3.5 Flow differentiation

Bowen (1928), whilst studying many of the ultrabasic dykes of Skye, observed that:

i) The central parts of the dykes contained more olivine than the margins;

ii) Offshoots from the dykes were generally of a doleritic nature;

iii) Considerable variation existed within individual dykes.

He concluded from these observations that the ultrabasic dykes of southern Skye were composite intrusions formed by the early intrusion of an olivine-poor basic magma which, whilst still hot, acted as a lubricant to the subsequent intrusion of an olivine-phyric magma along the centre of the dyke. He considered that the intrusion of the latter magma was not possible without the lubricating basic magma due to the advanced state of crystallization of the olivine-phyric magma. Gibb (1968), studying the same suite of dykes, came to the

conclusion that the variation in olivine crystals across the dyke was the result of flow differentiation, a mechanism of differentiation proposed by Bhattacharji et al. (1964) to account for the central picritic zone of the feeder dyke of the Muskox Igneous Complex, Canada. Essentially, the velocity profile across a liquid exhibiting laminar flow within a conduit is parabolic (Starkey 1962), there existing a boundary layer where the velocity is zero and consequently entrained particles (crystals) will migrate axially to where the velocity is at a maximum. Alternatively, it is possible to envisage a magma flowing past a cooling surface where crystals nucleate and grow but where the magma continues to flow impoverished in the crystallizing components.

1.2.4 Primary magmas

After Bowen (1928) established the belief in the basic composition of primary magmas and dispelled the concept of picritic liquids, the following 50 years of petrogenetic thought were dominated by the "recognition" of so-called primary magmas. The chemistry of these magmas, thought to be unaltered from their site of genesis, has subsequently been used to characterize the composition of the mantle and its evolution. Various compositions from the voluminous terrestrial flood basalts and Mid Ocean Ridge Basalts (MORB) have variously been cited as examples (Green & Ringwood 1967; Carmichael et al. 1974). It was generally considered that the apparent uniform composition of these rocks could not be due to the "random" processes of differentiation, and that if they were the products of fractional crystallization, then the composition of the erupted basalts should plot along the appropriate cotectic boundaries. In consequence O' Hara (1965) interpreted the cotectic nature of many basalts as being the result of modification of the parental magma(s) by crystal-liquid separation at shallow levels within the crust. He suggested that the only partial melts of substantial volume which could be generated from within the upper mantle would be picritic and it was these liquids that, by fractionating large volumes of olivine, were parental to the observed erupted basalts. The recognition of picritic and ultrabasic magmas and the scarcity of erupted examples has been explained on the basis of their pronounced high densities (Sparks et al. 1980; Huppert and Sparks 1980).

Cox (1980) has shown that the uniformity of composition of flood basalts is illusory and that terrestrial flood basalts do show a wide range of compositions and, more importantly, this range is scattered along the low pressure cotectic surfaces, as called for by low pressure fractional crystallization.

The use of trace elements in igneous petrology has perpetuated the arguments for the primary nature of some erupted basalts, with varying amounts of partial melting of a heterogeneous mantle being invoked to explain variations in incompatible-elements within basalts of similar major-element chemistry. It is widely believed by many (See Basaltic Volcanism Study Project 1981), that rocks showing large increases in the concentration of incompatible-elements could only be explained by limited partial-melting of a fertile source

(any previous melting episode having depleted the source mantle in these elements) and/or extreme fractional crystallization. Another widely held view was that ratios of incompatible-elements were insensitive to fractionation processes It was claimed that variations in the ratios of incompatible-elements and isotopes could be used to characterize discrete source regions, the effects of contamination and the possible mixing of magmas. However, to substantially increase incompatible trace-element concentrations during crystallization requires considerable amounts of closed system fractional crystallization, thereby reducing the amount of magma into which these elements are concentrated; however, this amount of crystallization also effects the major-element chemistry and changes the liquid composition far beyond that of basalt.

Contamination of magmas provides a means of altering liquid compositions, the compositions, however, are strictly controlled by the pertinent phase equilibria and energy content of the liquid (O'Hara 1980). Obvious field and isotopic evidence from both ophiolites and terrestrial rocks support this as a major process involved in the evolution of certain magmas.

1.3 Cone-sheets of the Southern Cuillin Complex

1.3.1 Field relationships

Detailed mapping of minor intrusions within the Cuillin Complex has illustrated the concentric disposition of the cone-sheets and although not perfect or complete on a regional scale has allowed extrapolation of their dips to define a focus below Meall Dearg, at an approximate depth of 3km (Harker 1904). This focus is approximately coincident with that of the central complex itself, after allowing for later modification by the intrusion of the granitic Srath na Creitheach and Western Red Hills centres. Observed individual cone-sheets vary in thickness from a few centimetres (Fig.1.5) to more than three metres (Fig.1.6). However, the majority are between 0.5 and 1m thick. Whilst the sheets may maintain a reasonably constant thickness and attitude, at least on a local scale, over a larger area a single sheet may thicken and thin considerably, bifurcate and vary in attitude leading to multiple intrusion and anastomosing forms. Without exception, all sheets are chilled against their host rocks with the development of a marginal fine-grained to glassy chill, usually around 1cm thick, which is gradational on a doleritic centre, although basaltic and gabbroic textures may be developed in the thinner and thicker sheets, respectively.

The sheets of the outer (southern) portion of the complex have dips of around 30^{o}, cutting Torridonian (Upper Proterozoic) sedimentary rocks and basaltic lavas (Fig.1.4), whilst those further to the north, dipping at steeper angles ($60\text{-}75^{o}$), intrude various units of the Inner and Outer Layered Series. It is interesting to note that where a fabric is developed within the units of the central complex, the cone-sheets are generally parallel to this fabric. Xenoliths within the sheets are generally scarce but where they do occur are of the same lithology as the local wallrock.

The frequency of cone-sheet distribution along the traverse is not regular. The southern end of the sampling traverse undertaken (see Section 1.3.2), from the tip of the Sgurr na Stri peninsula to south of Druim Hain, shows a high concentration of cone-sheets with many examples of multiple intrusion, or with only thin screens of country-rocks between individual sheets. In contrast, the area to the north, from Sgurr Hain to Meall Dearg is only sparsely intruded.

Fig.1.5. Gently inclined cone-sheet occurring on the flanks of Sgurr na Stri. Where individual sheets are in contact, they are invariably chilled against each other suggesting a protracted emplacement event. The upper narrower sheet in the figure converges upon the lower sheet but retains its identity along strike [G.R.5010 1908].

Fig.1.6. The majority of cone-sheets occurring within the Black Cuillin of Skye vary in thickness from 10cm to 100cm. Occasionally, however, they may attain thicknesses in excess of three metres. The pale coloured veins which pre-date the emplacement of the sheet are related to the Corrie Uaigneich Granite, believed to be an acid differentiate of the Cuillin layered intrusion. [G.R.5049 1847].

The total cumulative thickness of all cone-sheets along the traverse, and hence, potentially the total uplift produced by their emplacement, is in the order of approximately 100m.

1.3.2 Sampling procedure

The mountainous and often precipitous nature of the study area limited the choice of where systamatic sampling could be undertaken. It was therefore decided that for the purpose of this study, samples would be collected along a traverse from Rubha Ban on the southern tip of the Sgurr na Stri peninsula to Druim Hain (Fig.1.4), a distance of approximately 5km.

The limitations imposed by the nature of the topography did not, however, restrict a full representative suite of samples from being collected along the traverse, as access to all parts was possible without significant deviation from the line which was radial to the central complex and therefore traversed many of the major units of the Cuillin-Intrusion.

All cone-sheets which were visually free from alteration were sampled, resulting in some ninety specimens being collected and subsequently analysed. These are reported in Appendix IV (sample identifiers bearing the prefix CS). All major oxide analyses reported are in wt% whilst, trace element analyses are given in ppm.

1.3.3 Petrography and mineral chemistry

1.3.3.1 Introduction

All specimens examined show the ubiquitous alteration imposed by the hydrothermal convective cell associated with the Skye Centre (Taylor & Forester 1971; Forester & Taylor 1977; Ferry 1985, Ferry et al. 1987). At its most extreme, adjacent to microfractures, this is manifested by the almost complete alteration of the primary mineralogy to a matted assemblage of chlorite with minor pyrite, amphibole and only poorly preserved plagioclase phenocrysts displaying advanced alteration to epidote and sericite. However, at best, the alteration is evident only from the chloritization of the mesostasis and it is therefore possible by the careful selection of samples to elucidate the primary mineralogical and textural features of the rocks.

The rocks are of a simple basaltic mineralogy with aphyric and feldspar-phyric types being equally represented, although the frequency of phenocrysts varies markedly. Even the most aphyric looking rock may, with careful examination and the cutting of numerous sections yield the odd phenocryst testifying to the absence of superheated liquids during the emplacement of the cone-sheets. In all but a few of the porphyritic types the phenocryst assemblage comprises of bytownite, whilst in the remainder, plagioclase along with a small percentage of tentatively identified olivine occurs. The groundmass shows a variety of textures, from sub-ophitic (Fig.1.7) to intersertal or intergranular and is composed of a high-calcium augite, labradorite laths, Fe-Ti oxides, and interstitial glass now altered to chlorite. Rare apatite is present in a few samples.

1.3.3.2 Pyroxene

Selected pyroxene analyses are presented in Table 1.3, total iron having been divided between ferrous and ferric iron by the method of Finger (1972) and the distribution of elements between the Z and M positions is in accordance with the method outlined by Hess (1949). Pyroxene phenocrysts have not been observed in any of the rocks although this phase constitutes a major proportion of the groundmass. It occurs as either poikilitic plates sub-ophitically enclosing laths of plagioclase feldspar or as small, less than 0.25mm, equant subhedral grains.

Variation of Ca, Mg, Fe.

Within all analysed rocks only a single pale brown Ca-rich clinopyroxene has been identified, as predicted by the work of Coombes (1963), and these are plotted in the conventional Di-Hd-En-Fs quadrilateral (Fig.1.8) utilizing the atomic Ca, Mg, Fe (Fe = $Fe^{2+} + Fe^{3+} + Mn$) proportions.

The pyroxene is a calcium-rich augite (classification of Poldevaart and Hess 1951) and within any one single sheet generally shows only limited compositional range. This range is, however, extended to $Wo_{36}En_{50}Fs_{14}$ - $Wo_{42}En_{20}Fs_{38}$ when pyroxenes from all sheets are considered. The combined data from all sheets forms a scattered trend characterized by slight depletion in Ca with a concomitant increase in Fe. A comparison (Fig.1.9) of the

Sample	CS19/1	CS19/3	CS11/6	CS28/2	CS28/5	CS26/6	CS24/2	CS22/1	CS23/1
SiO_2	48.77	47.63	50.26	51.84	49.57	49.38	48.90	50.03	50.96
TiO_2	1.03	1.28	0.72	0.50	0.84	1.05	0.98	0.80	0.60
Al_2O_3	4.06	6.46	4.37	2.33	4.53	3.24	3.80	5.53	1.75
Cr_2O_3	0.05	0.13	0.04	-	0.02	0.01	0.01	0.50	0.01
Fe_2O_3	5.94	3.45	2.71	3.24	4.02	3.07	3.06	1.81	2.37
FeO	5.46	5.56	5.37	5.97	4.46	10.94	11.71	4.37	10.25
MnO	0.25	0.18	0.19	0.23	0.18	0.34	0.38	0.13	0.38
MgO	13.57	13.07	15.34	16.39	14.61	12.57	12.25	15.36	15.05
CaO	19.94	21.48	20.63	20.14	21.70	19.18	18.45	21.38	17.72
Na_2O	0.82	0.33	0.30	0.26	0.33	0.37	0.38	0.27	0.28
Total	100.04	99.65	99.99	100.99	100.33	100.14	99.92	100.18	99.37
FeO*	10.78	8.66	7.80	8.86	8.10	13.68	14.48	6.02	12.39
				Atomic % (Mn included with Fe)					
Ca	42.14	46.17	42.84	40.30	44.79	39.89	36.26	44.99	36.35
Mg	39.91	39.11	44.30	45.61	41.95	36.35	39.27	44.99	43.56
Fe	17.95	14.72	12.86	14.09	13.26	23.76	24.47	10.02	20.29
				Formula (based on 6 oxygens)					
Si	1.853	1.798	1.870	1.916	1.851	1.871	1.871	1.844	1.932
Al	.147	.202	.130	.084	.149	.129	.129	.156	.068
Fe+++	-	-	-	-	-	-	-	-	-
Al	.035	.086	.062	.018	.051	.015	.042	.084	.010
Fe+++	.167	.097	.075	.089	.112	.087	.087	.050	.067
Fe++	.171	.174	.166	.183	.138	.346	.372	.134	.323
Ti	.030	.037	.021	.014	.024	.030	.028	.022	.017
Mn	.009	.006	.006	.008	.006	.011	.012	.004	.012
Mg	.769	.736	.851	.903	.813	.710	.698	.844	.859
Ca	.812	.869	.823	.798	.868	.779	.756	.844	.720
Na	.061	.025	.022	.019	.024	.027	.028	.019	.021
Cr	.002	.004	.002	.001	.001	.001	-	.014	-
Total	4.056	4.034	4.028	4.033	4.037	4.006	4.023	4.015	4.029
M	2.056	2.034	2.028	2.033	2.037	2.066	2.023	2.015	2.024
% Al in Z	7.35	10.10	6.50	4.20	7.45	4.80	6.45	7.80	3.40

Table 1.3 Representative analyses of clinopyroxene from the Cuillin Complex cone-sheets. Total iron was determined as FeO^* and subsequently partitioned between ferrous and ferric iron by the method of Finger (1972).

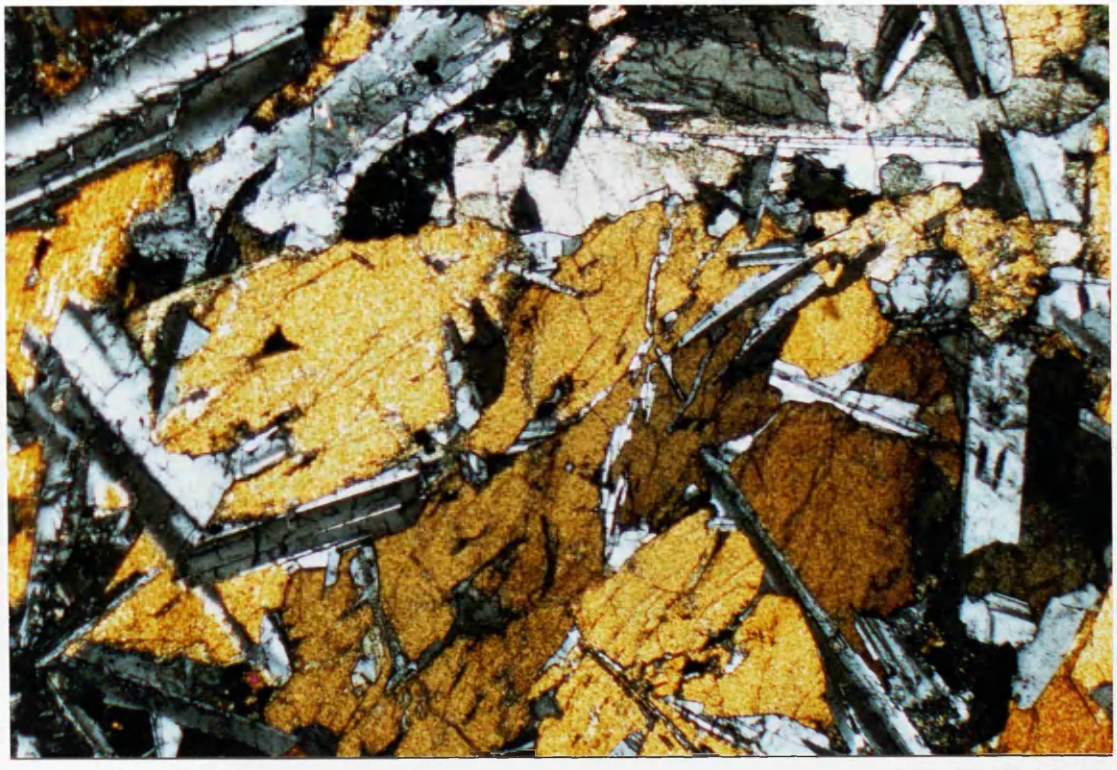

Fig.1.7. Sub-ophitic texture developed within cone-sheet. Field of view c.3 x 2mm. Crossed polars. Sample CS024.

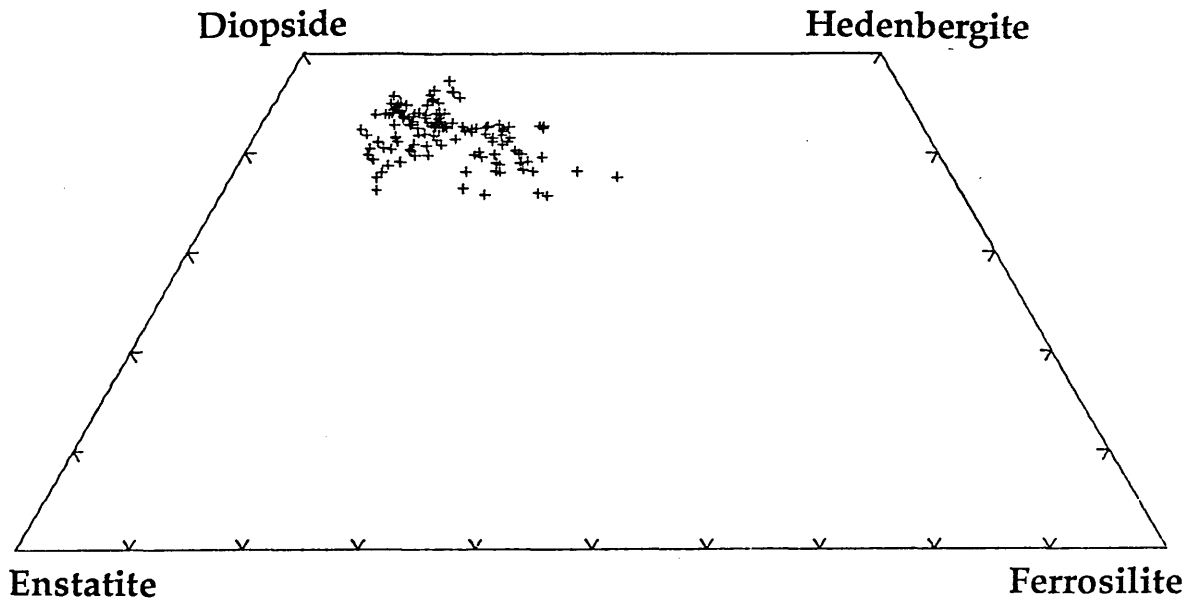

Fig. 1.8. Pyroxenes from the cone -sheet suite plotted in the pyroxene quadrilateral Di-En-Fs-Hd.

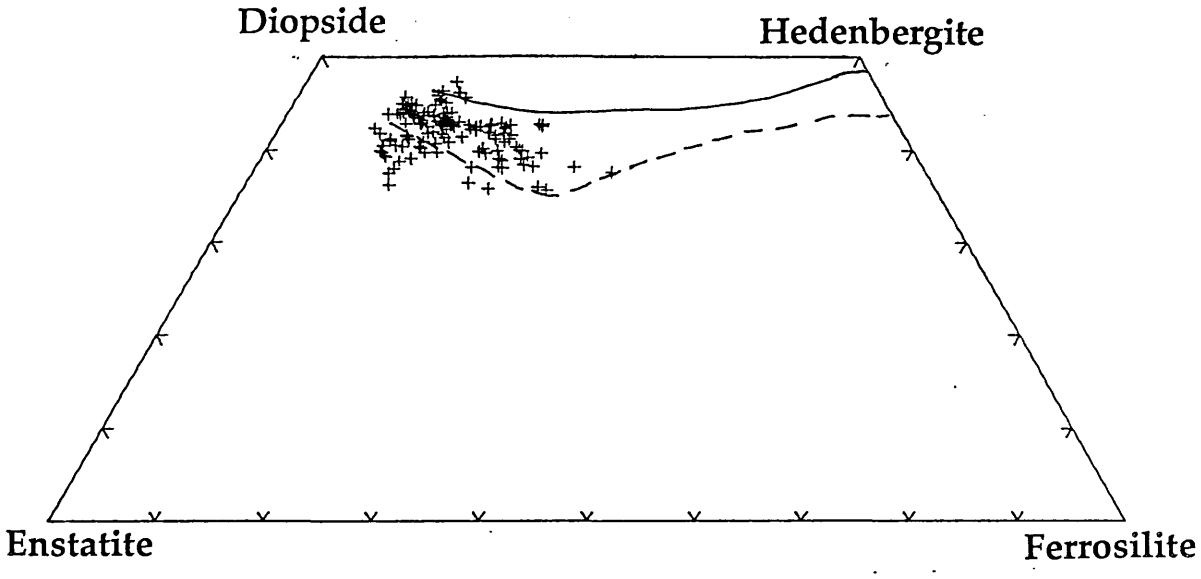

Fig. 1.9. Comparison of clinopyroxenes occurring within the cone-sheets with the trends of those from the Shiant Isles sill (—) (Gibb, 1973) and the Skaergaard intrusion (---) (after Brown and Vincent 1957, 1963), representing alkalic and tholeiitic trends, respectively.

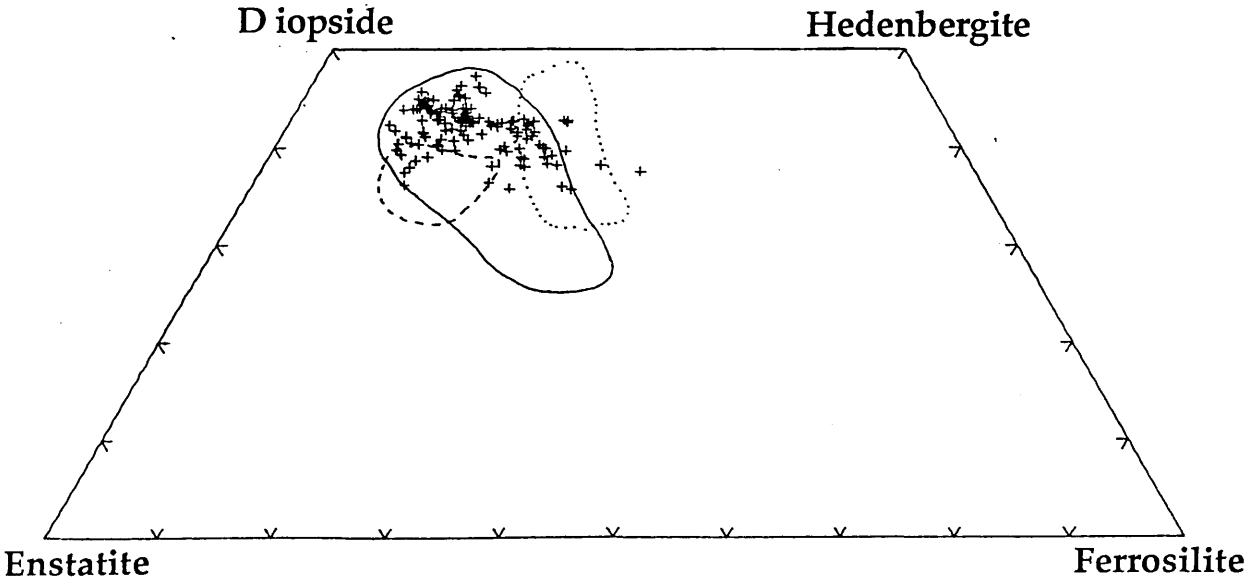

Fig. 1.10. Comparison of pyroxenes from the Skye cone-sheet suite (+) with those from the Preshal Mhor basalts (◇), Fairy Bridge basalts (∴) and the SMLS (◁▷), (data other than cone-sheets from Mattey 1980).

pyroxenes with those from the Skaergaard intrusion (taken as the classic fractionation trend representing tholeiitic intrusions) and pyroxenes from the Shiant Isles sill (taken as representative of pyroxenes from alkalic intrusions) shows that those from the Skye cone-sheets broadly follow the tholeiitic Skaergaard trend. However, the Skye cone-sheets show a slightly higher Ca content at a given Mg/Mg+Fe value (fractionation index). This may potentially be accounted for by the more calcic nature of the parent magma. The majority of pyroxenes do, however, fall within the compositional area (Fig.1.10) defined for Preshal Mhor pyroxenes (Mattey 1980).

The most striking feature of the pyroxene analyses (Table 1.3) is the high ferric-ferrous iron ratio which may attain values of ~1, although commonly is around 0.5. This high ratio may be caused by a high oxygen fugacity (fo_2) and changes in temperature at the time of crystallization (Thornber et al. 1980). Alternatively, Thornber et al. report that the addition of the oxides K, Na, Si, Al, Ca (in decreasing order of significance), may affect an increase in fO_2. However, the low concentrations of alkalis within the cone-sheets suggest that the high ferric-ferrous ratio was not caused by an excessive concentration of these oxides and it is therefore suggested that the high ratio is the result of a high fO_2 at the time of crystallization, possibly through a high PH_2O, with subsequent diffusion of H_2 out of the system. Such high values of PH_2O might be attributed to high-temperature rock-water interactions during protracted groundwater circulation (Forester & Taylor 1977).

Variation of Al, Ti, Cr and Mn

Pyroxenes from the Skye cone-sheets are characterized by having relatively low concentrations of TiO_2 (~0.3 - 1.3 %) and Al_2O_3 concentrations typically within the range of 2 - 5 %. These values are comparable to those found within pyroxenes from the Preshal Mhor basalts (Mattey 1980), with the TiO_2 content being significantly lower than those found within pyroxenes from the Fairy Bridge and SMLS basalts (Mattey 1980).

In Fig.1.11, ions per formula unit (IPFU) are plotted for Si against Al (recalculated on the basis of 6 oxygens) and clearly shows that in nearly all the analyses Al is present in sufficient quantities to satisfy the remaining tetrahedral sites after allocation of Si.

Le Bas (1962) has suggested that the amount of Al and Ti entering clinopyroxenes is

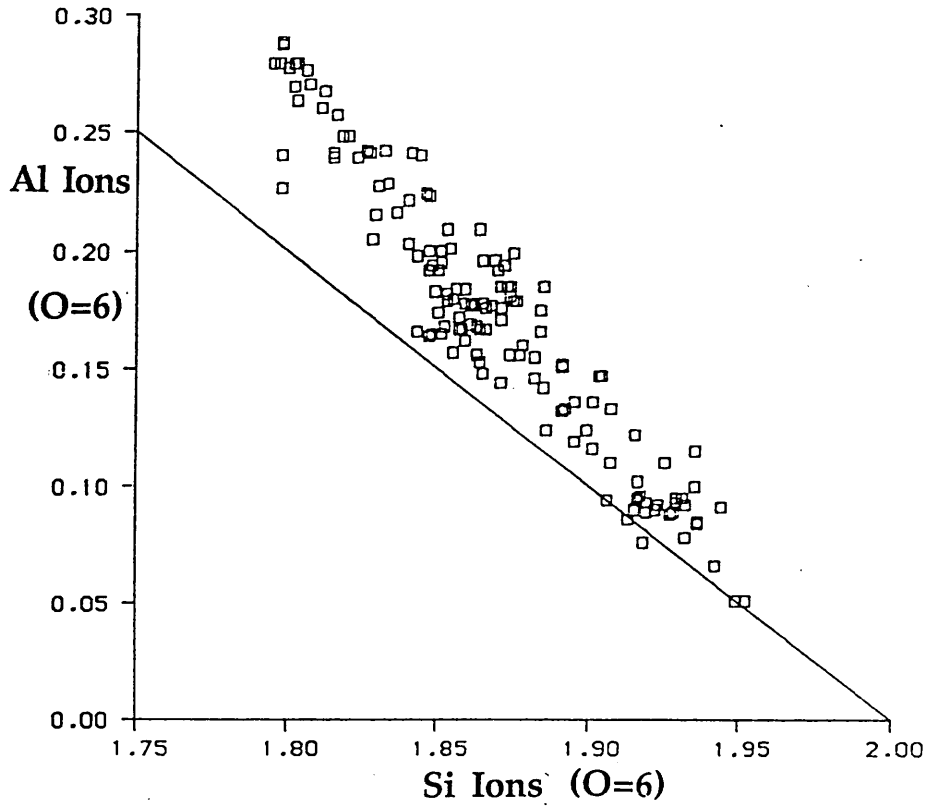

Fig. 1.11. Variation of Al with Si (on the basis of 6 oxygens) for clinpyroxenes of the Skye cone-sheets. The line Si+Al=2 represents tetrahedrally co-ordinated ions within the pyroxene structure and as illustrated, in the majority of the cone-sheet samples there is sufficient aluminium to fill the remaining sites after the allocation of silica.

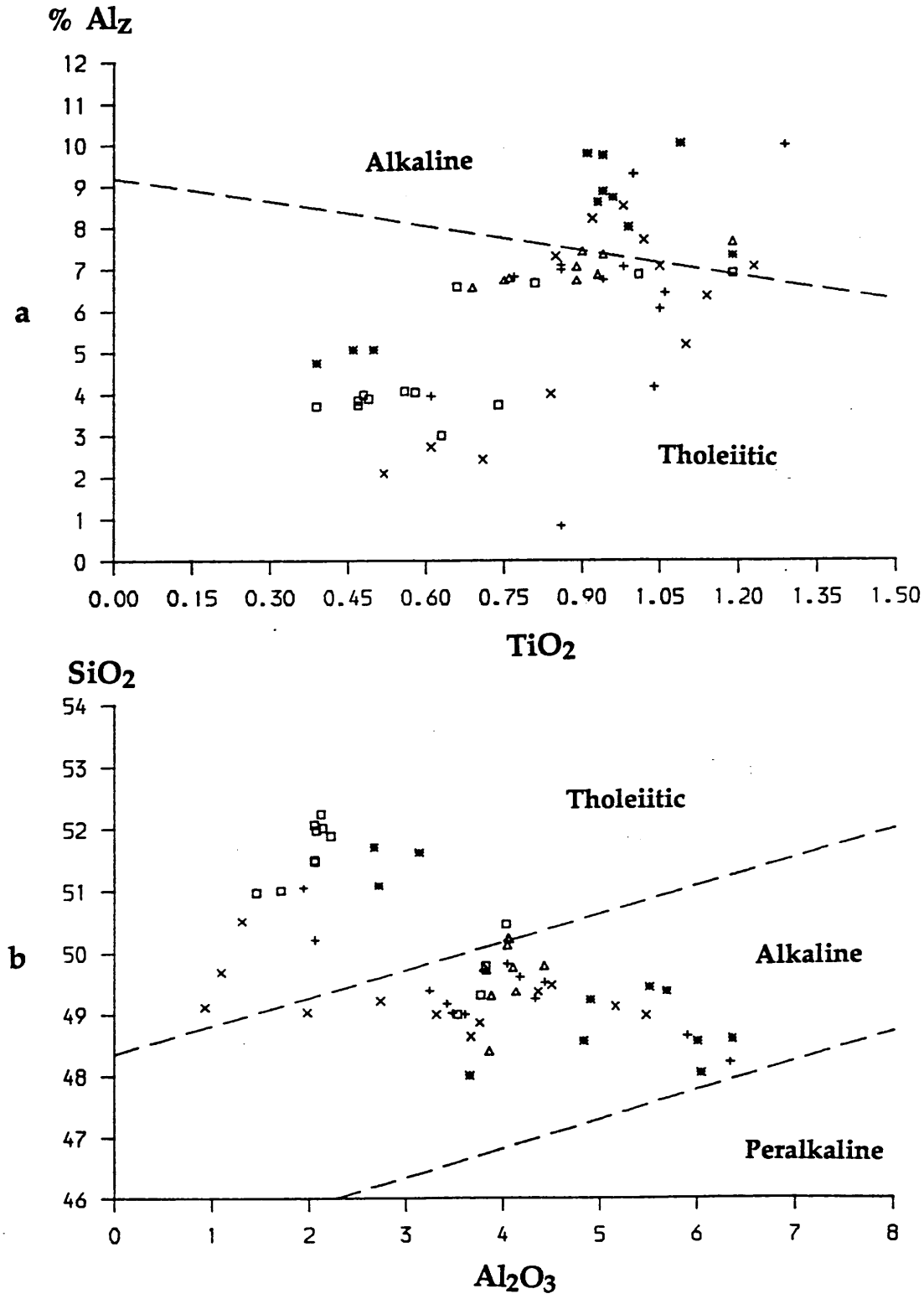

Fig. 1.12. Plots illustrating that the fields defined by Le Bas (1962) are not suitable for characterization of magma type on the basis of a) Al_Z v TiO_2 and b) SiO_2 v Al_2O_3 content of clinopyroxenes.
(□) = CS014, (+) = CS026, (*) = CS036, (△) = CS044, (x) = CS070.

dependent on the alkalinity of the parent magma and consequently Al and Ti contents of pyroxenes can be used to characterize the original parental magma.

In Fig.1.12a and b tetrahedrally-coordinated Al is plotted against percentage weight of TiO_2, and percentage weight SiO_2 is plotted against percentage weight of Al_2O_3, respectively. The analyses are approximately equally divided between the tholeiitic and alkaline fields as defined by Le Bas (1962), with pyroxenes from a single rock occupying both fields supporting the findings of Barberi (1971) that the Al and Ti content of clinopyroxenes cannot be regarded as diagnostic of the parental magma. Coish and Taylor (1979) have demonstrated that the amount of Al and Ti entering pyroxene increases with cooling rate. However, Mattey (1980) has shown it is possible to distinguish FB clinopyroxenes from those in the SMLS and PM on the basis of Al and Ti. Fig.1.13 shows the fields outlined by Mattey for FB, PM and SMLS with the results obtained from the Skye cone-sheet pyroxenes. Al/Ti (on the basis of 6 oxygens) ratios of the pyroxenes from cone-sheets are generally in excess of 8, similar to those of the tholeiitic PM magma type and the SMLS. The relatively low proportion of tetrahedrally coordinated Al to total Al suggests that the dominant substitution occurring within pyroxenes of the cone-sheets is $2Al^{3+} <=> M^{2+} + Si^{4+}$.

The variations of Ti, Mn, Cr and Al (as number of cations on basis of 6 oxygens) with respect to Mg number (MgO/MgO+FeO) are illustrated in Figs.1.14a,b. The data shows no systematic variations in Al at Mg numbers greater than approximately 0.75 (Fig.1.14a). However, below this value Al_y decreases rapidly; probably as a result of lower Al activities induced by fractionation, whilst Al_z shows a more subdued decrease possibly due to the SiO_2 activity remaining low. The abundance of Cr in the Skye cone-sheet pyroxenes is seen to fall very rapidly from ~0.015 ions per formula unit (IPFU) at a Mg number of ~0.84 to the limits of detection of the electronprobe, ~0.001 IPFU, at Mg numbers of <0.68 (Fig.1.14b). This high concentration of Cr in the more magnesian pyroxenes may be explained by the reaction relationship between clinopyroxene and spinel proposed by Irvine (1967). The onset of pyroxene crystallization would inhibit further crystallization of spinel and thus any Cr remaining in the melt would be strongly partitioned into the early formed clinopyroxene.

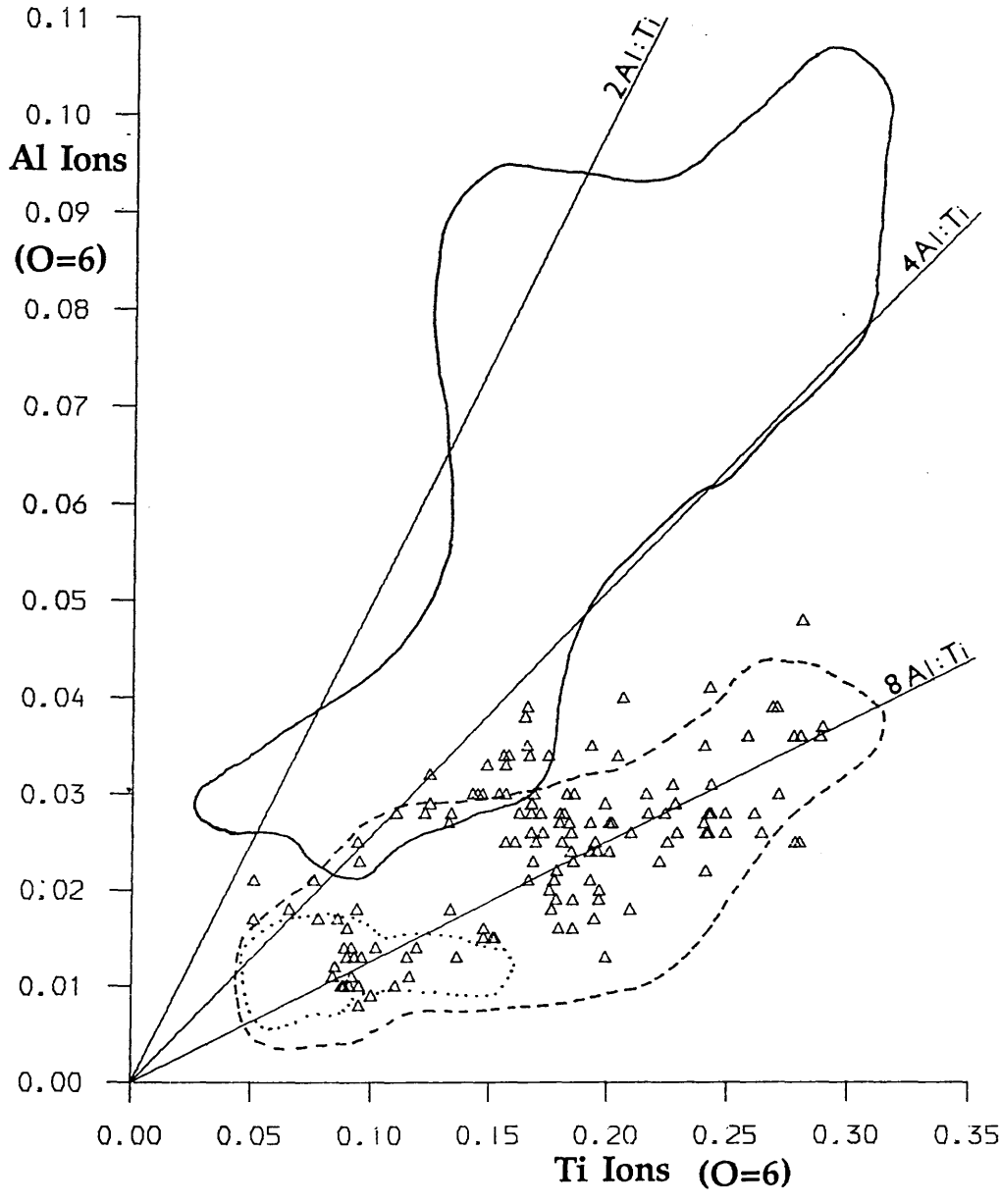

Fig. 1.13. Comparison of the variation of Ti and Al (on the basis of 6 oxygens) within pyroxenes of the Skye cone-sheets suite with those of the Preshal Mhor, Fairy Bridge and Skye Main Lava Series magma types (⬭) = FB magma-Type. (⊂⊃) = PM Magma-Type. (⁘) = SMLS Magma-Type (after Mattey 1980).

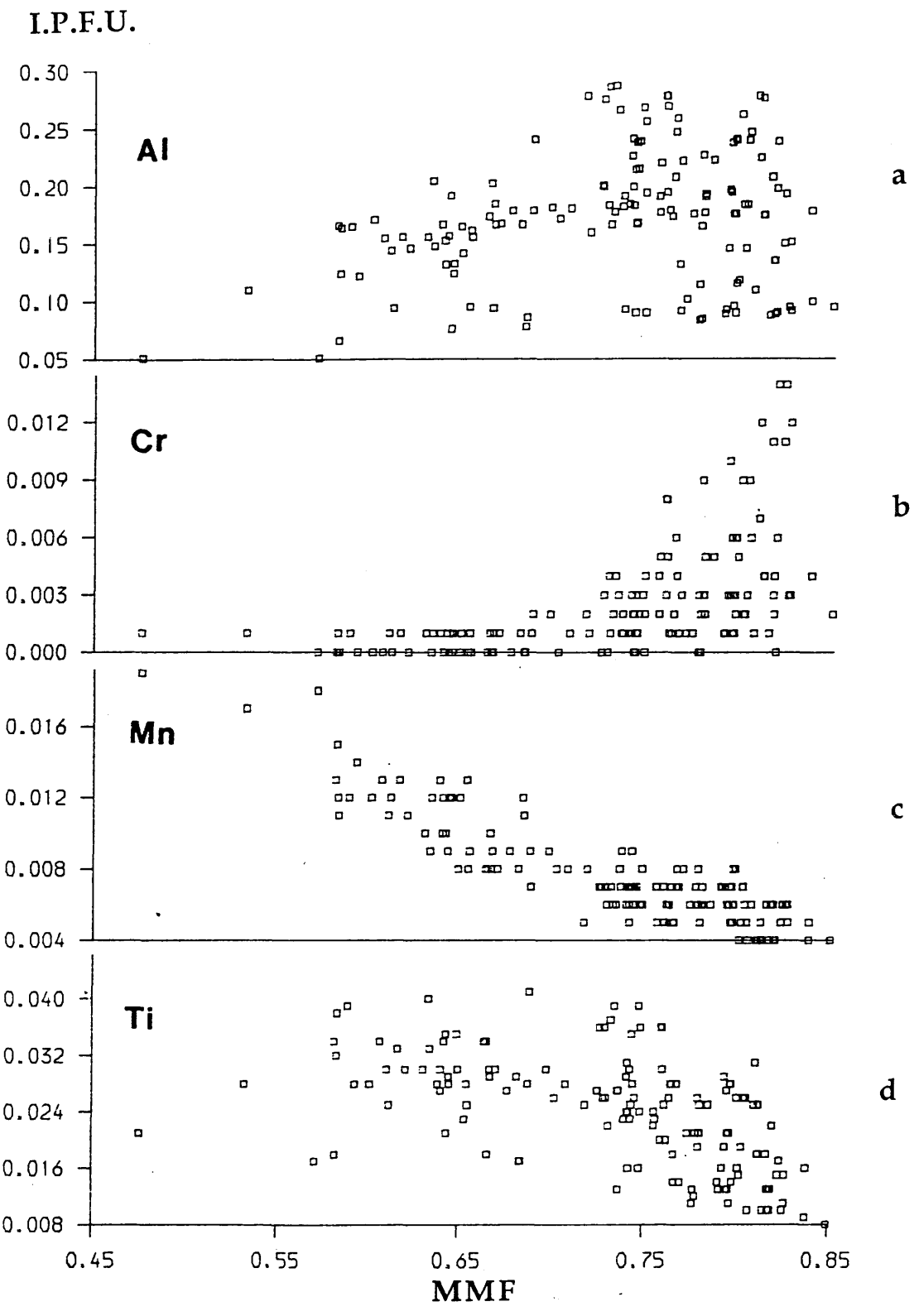

Fig. 1.14. Variation of Al, Cr, Mn and Ti (on the basis of 6 oxygens) within pyroxenes of the Skye cone-sheets. I.P.F.U. = Ions per formula unit. MMF=Mg/Mg+Fe*. ($Fe^{*}=Fe^{2+}+Fe^{3+}$).

In contrast to the behaviour of Al in the pyroxenes, Mn shows a well correlated linear increase with increased fractionation (Fig.1.14c) from ~0.005 IPFU to 0.022 IPFU at Mg numbers of ~0.84 and ~0.35, respectively. Ti also increases with increased fractionation from 0.01 IPFU to 0.39 IPFU, at fractionation indices of ~0.83 and ~0.57 respectively. However, unlike the behaviour of Mn, a considerable spread of the data occurs (Fig.1.14d).

1.3.3.3 Plagioclase

Plagioclase is commonly the only phenocryst phase and may account for up to 30% volume of the rock. Selected representative analyses of plagioclase phenocrysts are given in Table 1.4. Crystals may attain lengths of up to 4mm, although 2mm is the norm and show both simple and polysynthetic twinning. It is possible to identify two distinct populations of phenocrysts. The volumetrically less significant comprise of subhedral to euhedral crystals up to 2mm in length (Type I, Fig.1.15), whilst the second type (Type II) comprise invariably anhedral, partly resorbed crystals (Fig.1.16), and attain lengths up to 4mm. Both types may concentrically contain small round inclusions (Fig.1.17a,b) of glass, which may be regularly or randomly disposed throughout the phenocrysts and which are now altered to chlorite, indicative of rapid crystal growth. Both types may also be criss-crossed by a series of microfractures, although this appears to be more common in the latter type which occasionally displays albitized reaction rims.

Electron probe micro-analyses show only slight chemical differences between the two types of phenocrysts observed optically. Both show normal growth zoning, although the generally larger, partly resorbed anhedral Type II phenocrysts have extremely calcic cores, usually in excess of An_{85}, whilst the smaller euhedral Type I phenocrysts have core compositions of around An_{70}, at a host rock F/F + M of 0.6. Both Type I and II crystals have rim compositions around An_{55} and an orthoclase component of less than 0.3. Fig.1.18 illustrates that whilst the An content of the Type I cores generally decreases with increasing fractionation (F/F + M), Type II retain their high calcic cores regardless of host rock F/F + M value. This observation supports the interpretation that the Type II crystals are in some way xenocrystic, possibly cognate in that they crystallized earlier in the history of the cone-sheet magma.

	CS19/2 P	CS28/1 P	CS69/9 P	CS19/5 X	CS16/4 X	CS26/1 X
SiO_2	50.13	51.67	49.70	46.87	45.49	45.78
Al_2O_3	29.99	29.32	30.75	33.43	33.71	33.87
CaO	14.98	13.42	14.83	17.90	18.13	18.22
Na_2O	3.29	3.89	3.19	1.64	1.26	1.35
K_2O	0.09	0.08	0.06	0.05	0.02	0.01
TiO_2	0.06	0.06	0.04	0.01	0.01	0.02
FeO	0.72	0.76	0.65	0.48	0.42	0.41
MgO	0.30	0.14	0.22	0.19	0.15	0.21
Total	99.91	99.33	99.46	100.57	99.22	99.90
An	71.17	65.28	71.71	85.50	88.70	88.15
Ab	28.30	34.25	27.93	14.19	11.18	11.79
Or	0.53	0.47	0.36	0.31	0.12	0.06

	CS26/6 G	CS26/8 G	CS14/2 G	CS14/5 G	CS70/2 G	CS36/12 G
SiO_2	52.16	55.06	52.33	53.02	51.49	50.12
Al_2O_3	29.55	27.83	28.64	29.04	29.48	30.06
CaO	13.52	10.85	12.63	12.54	13.41	14.67
Na_2O	3.89	5.44	4.59	4.83	4.15	3.16
K_2O	0.06	0.11	0.09	0.07	0.06	0.05
TiO_2	0.07	0.09	0.08	0.07	0.07	0.05
FeO	0.94	0.89	0.92	1.04	0.80	0.88
MgO	0.18	0.11	0.13	0.18	0.15	0.31
Total	100.37	100.38	99.41	100.79	99.61	99.30
An	65.53	52.12	60.04	58.67	63.90	71.72
Ab	34.12	47.26	39.46	40.92	35.77	28.00
Or	0.35	0.62	0.50	0.41	0.33	0.28

Table 1.4 Representative analyses of feldspars from the Cuillin complex cone-sheet suite. P=phenocryst, X=xenocryst, G=groundmass crystal.

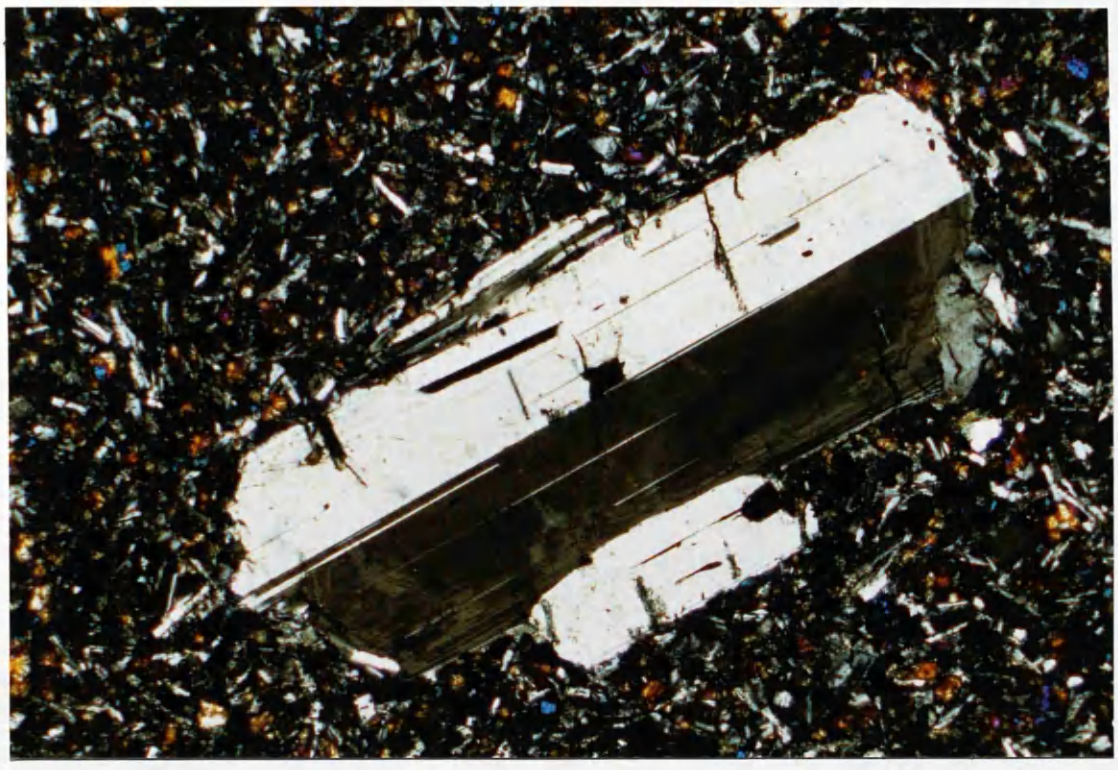

Fig.1.15. Normally zoned euhedral plagioclase phenocryst (An_{75}) in granular groundmass of cone-sheet. Field of view c. 3 x 2mm. Crossed polars. Sample CS060.

Fig.1.16. Corroded/resorbed plagioclse (An_{86}) phenocrysts within granular groundmass of cone-sheet. Field of view c.3 x 2mm. Crossed polars. Sample CS022.

a

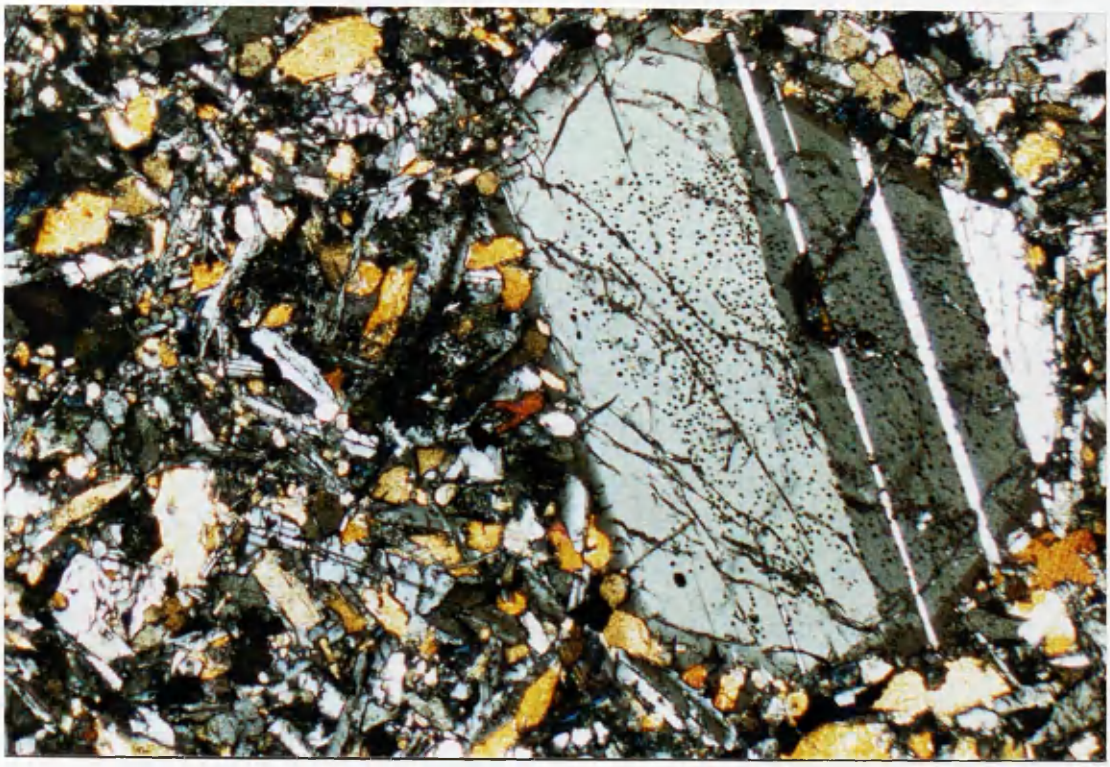

b

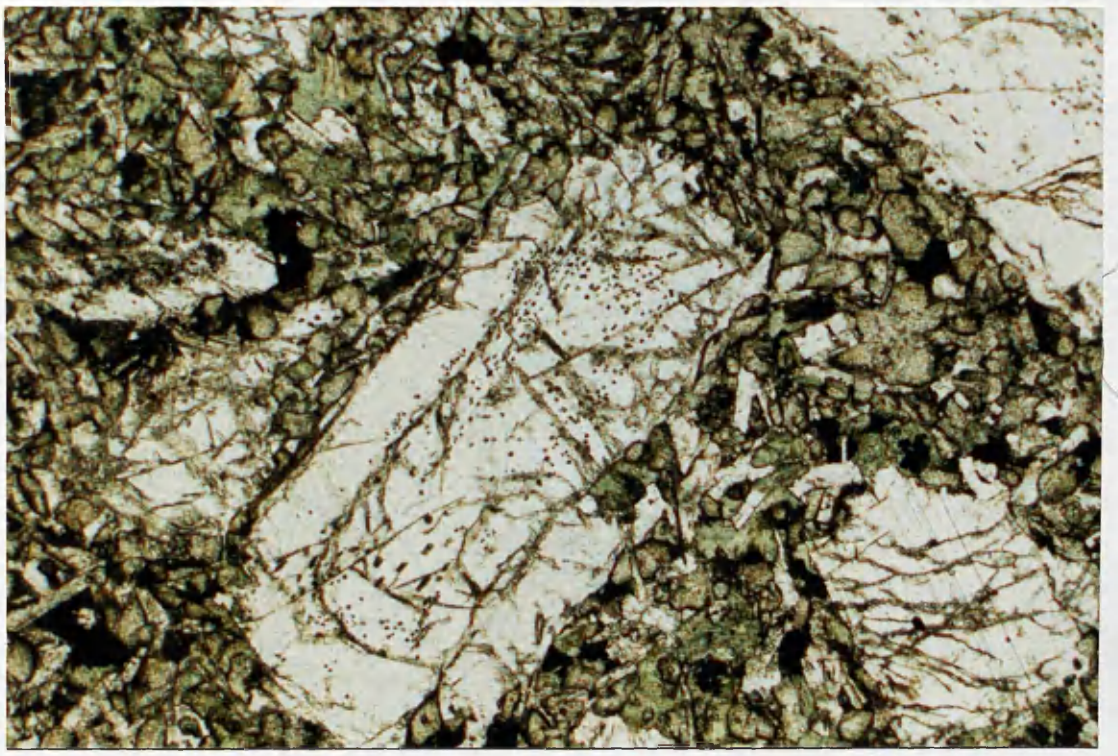

Fig.1.17. Euhedral plagioclase (An_{70}) phenocrysts with inclusions in granular groundmass. Inclusions may either be a) randomly or b) regularly distributed throughout phenocrysts. Field of view c.3 x 2mm. Sample CS053.

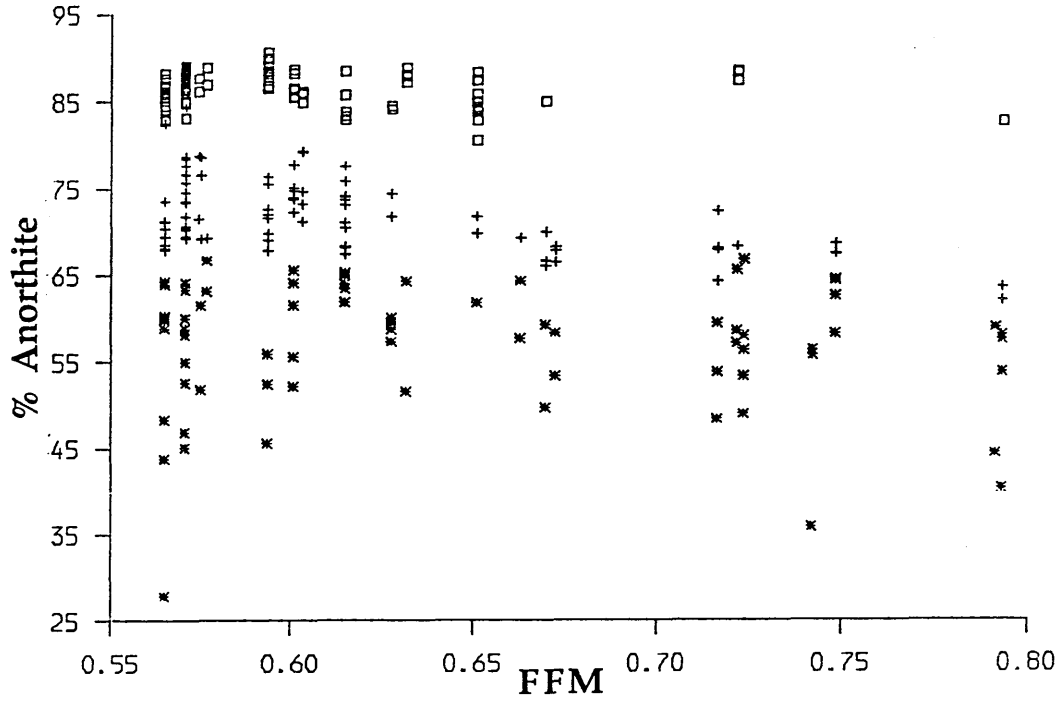

Fig. 1.18. Variation of anorthite content of plagioclase with fractionation within the cone-sheets. (▫) = Type II, (+) = Type I, (*) = groundmass crystal.

1.3.3.4 Olivine

Olivine phenocrysts have only tentatively been identified from its alteration products iddingsite and serpentine. Where present they are of a small size, <0.5mm and account for less than 8% of any one sample.

1.3.3.5 Opaque minerals

The only opaque mineral identified in any of the samples is an optically homogenous titanomagnetite and representative analyses are given in Table 1.5. This phase accounts for less than 5% of any one sample.

1.3.4 Normative mineralogy

Tilley and Muir (1962) suggested that hydrothermal alteration was responsible for increasing the H_2O^+ and Fe_2O_3 concentrations in the BTVP basalts, thus increasing Si-saturation (Section 1.2.3.1). However, Fig.1.19 reveals that no systematic correlation exists between these variables and therefore it is considered here that discussion of their normative components is meaningful and is of significance during magmatic evolution. In total, the oxides of ten major elements: Si, Al, Ti, Fe, Mg, Ca, Na, K, Mn, P, were analysed for by X-ray fluorescence spectrometry (XRFS). Total iron was recorded as Fe_2O_3. Subsequent determination of Fe^{2+} (Whipple 1974) gave an averaged ferric-ferrous ratio of ~0.2 (Appendix I). Coombes (1963) has suggested that the Fe_2O_3 contents of basalts should be reduced to allow for post-crystallization oxidation and consequently the determined ferric-ferrous ratio has been reduced to 0.15 as suggested by Brooks (1976). This reduction has little effect on the iron-magnesium ratio but causes changes of a few percent in the normative ferromagesium minerals. An increase in the Fe_2O_3/FeO ratio will allow more magnetite to form thus liberating increasing amounts of silica which is then available for converting nepheline to albite, olivine to hypersthene and eventually may lead to free quartz.

Apart from the correlation between high alkalis and the most southerly cone-sheets (Section 1.3.5.1) no systematic variation exists between composition and position along the traverse.

	CS11/1	CS23/2	CS38/1	CS50/1	CS49/3	CS53/2
TiO_2	18.75	16.94	21.43	25.30	16.97	24.24
MgO	0.05	0.20	0.04	0.07	0.05	0.05
Cr_2O_3	0.12	0.21	0.12	0.09	0.14	0.11
Al_2O_3	1.89	2.70	1.32	1.19	0.62	1.21
MnO	2.10	1.71	1.76	1.24	1.76	2.33
FeO^*	68.06	69.38	69.14	66.52	74.86	65.17
SiO_2	0.28	0.82	0.24	0.18	0.35	0.28
Total	91.25	92.96	94.05	94.59	94.75	93.39

Table 1.5 Representative analyses of opaque minerals in the Cuillin cone-sheets. FeO^* = Total iron determined as FeO.

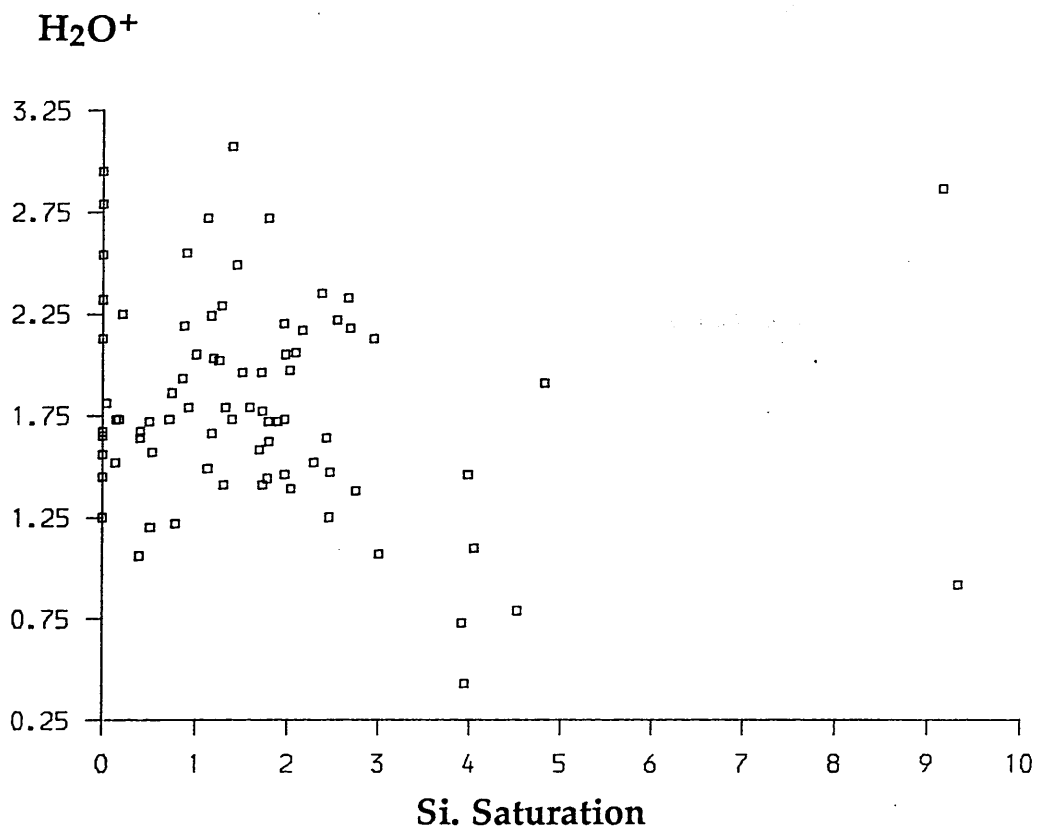

Fig. 1.19. H_2O^+ v Silica saturation (normative quartz + quartz from recasting hypersthene to olivine + quartz).

With the Fe_2O_3/FeO ratio set at 0.15, all samples are just saturated with respect to silica, the saturation ranging from ~0-5% (Fig.1.20).

Chemically, all analyses plot within the tholeiitic field on a total alkali v silica plot (Fig.1.21) as defined by Macdonald and Katsura (1964), which is in agreement with their petrographic classification. All but three specimens contain both normative ol and hy (5-18% and 4-20%, respectively) and consequently plot within the ol-tholeiite field (Fig.1.22) of Yoder and Tilley (1962).

Approximately 80% of the normative mineralogy can be accommodated within the generalized basalt tetrahedron (Yoder and Tilley 1962) and the samples satisfy the criteria suggested by Cox et al. (1979, p232); in that, projection of basalts should be restricted to those that have:

i) normative pl > An_{50}

ii) $FeO^*/FeO^* + MgO < 0.70$ (where FeO^* = total iron)

iii) $K_2O < 1\%$

iv) qtz parameter < 10%

Therefore, the prediction that these rocks should be cotectic with respect to pl-ol-cpx (Figs.1.23 1.24) in the approximate proportions 55:10:35 can be accepted with some degree of confidence. This, however, is contrary to the observed phenocryst assemblage which contains only plagioclase and possibly a small proportion of olivine (Section 1.3.3.4). Table 1.6 illustrates the principal normative variation shown by the Skye cone-sheets. Normative feldspar for the more primitive aphyric samples is predicted to be around An_{70} which is in close agreement with the majority of the Type I phenocrysts determined (Section 1.3.3.3).

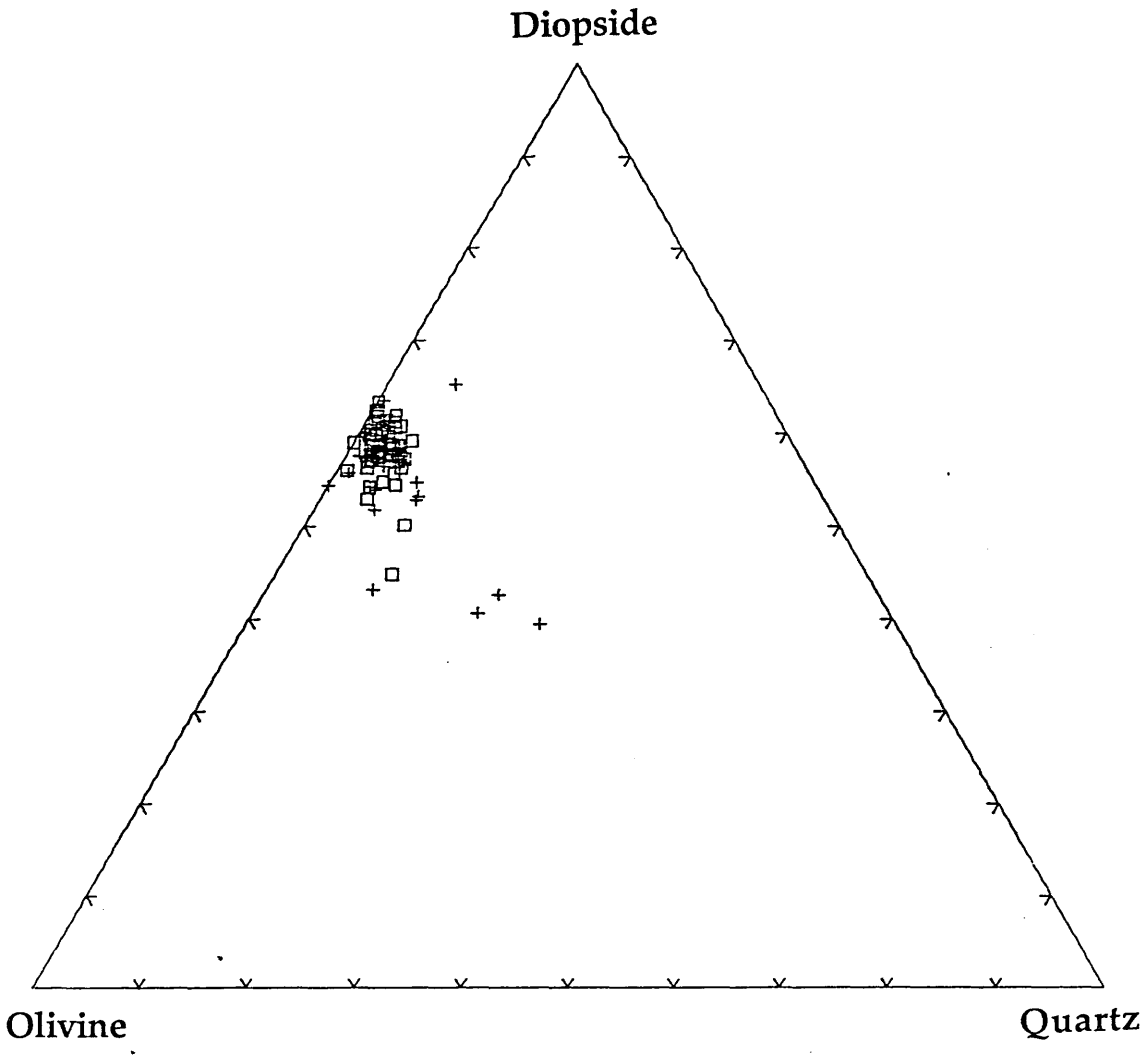

Fig. 1.20. Silica saturation of cone-sheets plotted in the system ol-di-qtz of the basalt tetrahedron (Yoder and Tilley 1962). (▫)= aphyric samples (less than 5% v/v phenocrysts), (+) = porphyritic samples (greater than 5% v/v phenocrysts).

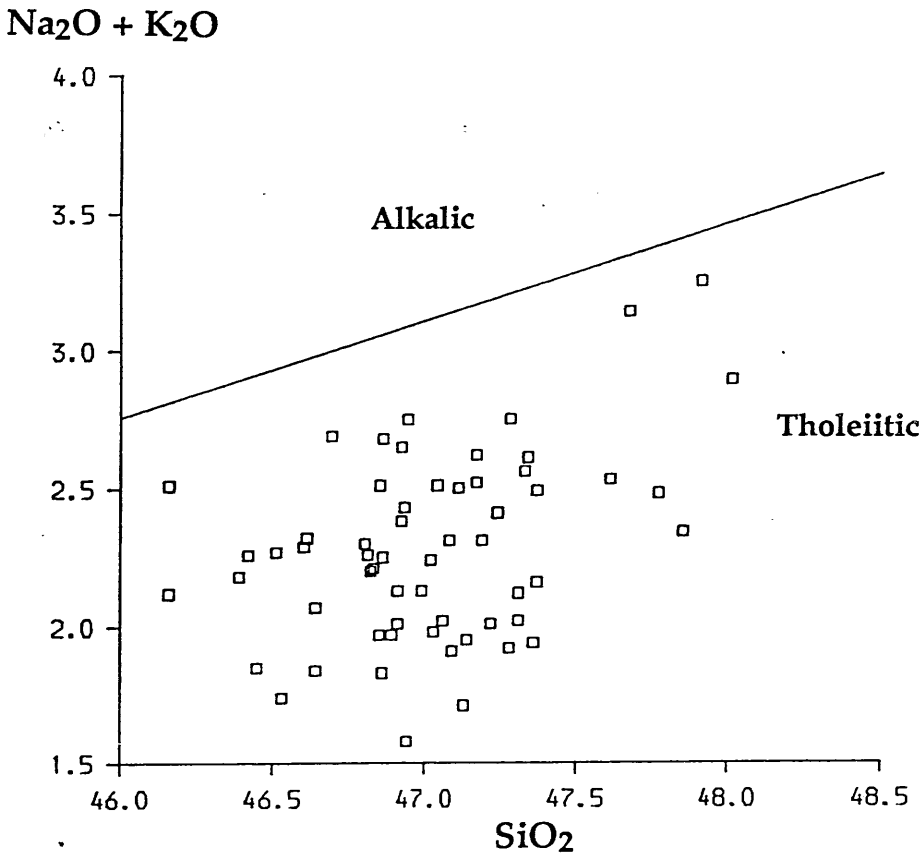

Fig. 1.21. Total alkali v silica diagram for Skye cone-sheets. All samples plot within the field for tholeiites as defined by Macdonald and Katsura (1964).

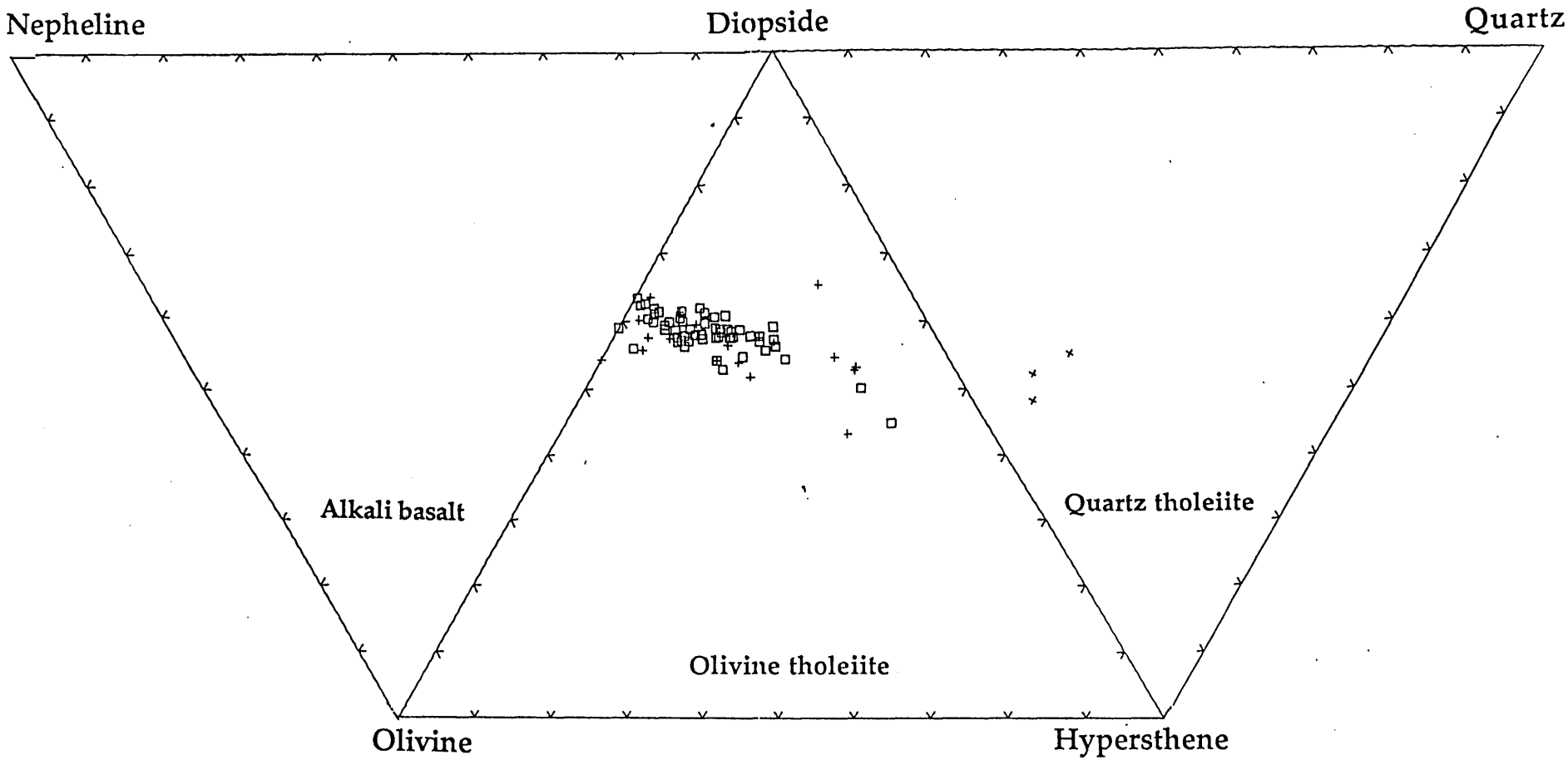

Fig. 1.22. Variation of Skye cone-sheets within the normative basalt tetrahedron. All samples plot within the field of olivine tholeiites except three highly feldspar phyric samples. (□)= aphryric samples (< 5% phenocrysts), (+) = porphyritic samples (> 5% phenocrysts).

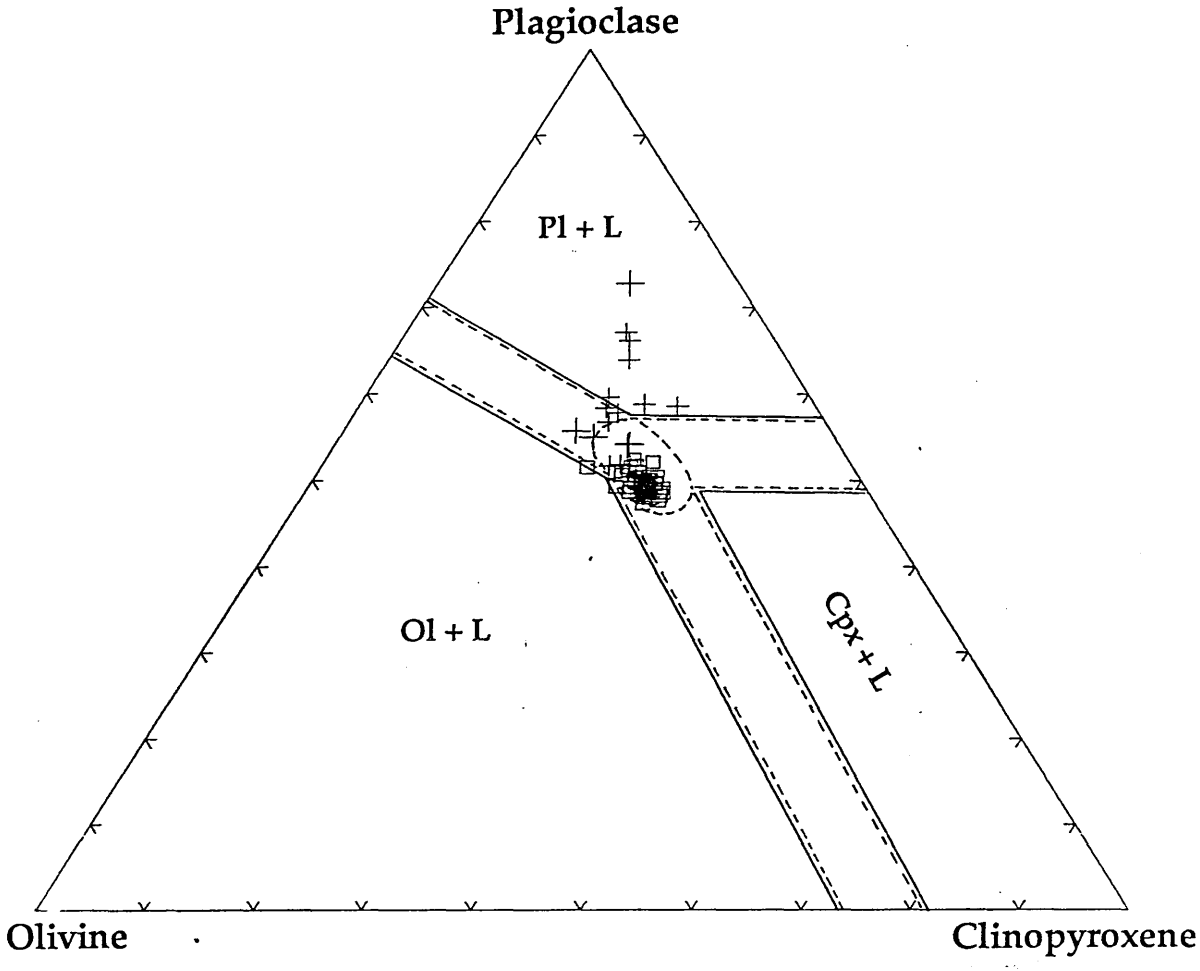

Fig. 1.23. Variation of cone-sheets within the normative basalt system ol-pl-cpx projected from SiO_2. (≡) = Area in which basalts can be expected to equilibrate with ol + pl, pl+cpx and ol+cpx.(:) = Area in which plotted compositions would be expected to show cotectic behaviour with respect to ol+pl+cpx. Symbols as in Fig. 1.20. (After Cox et al. 1979 p232)

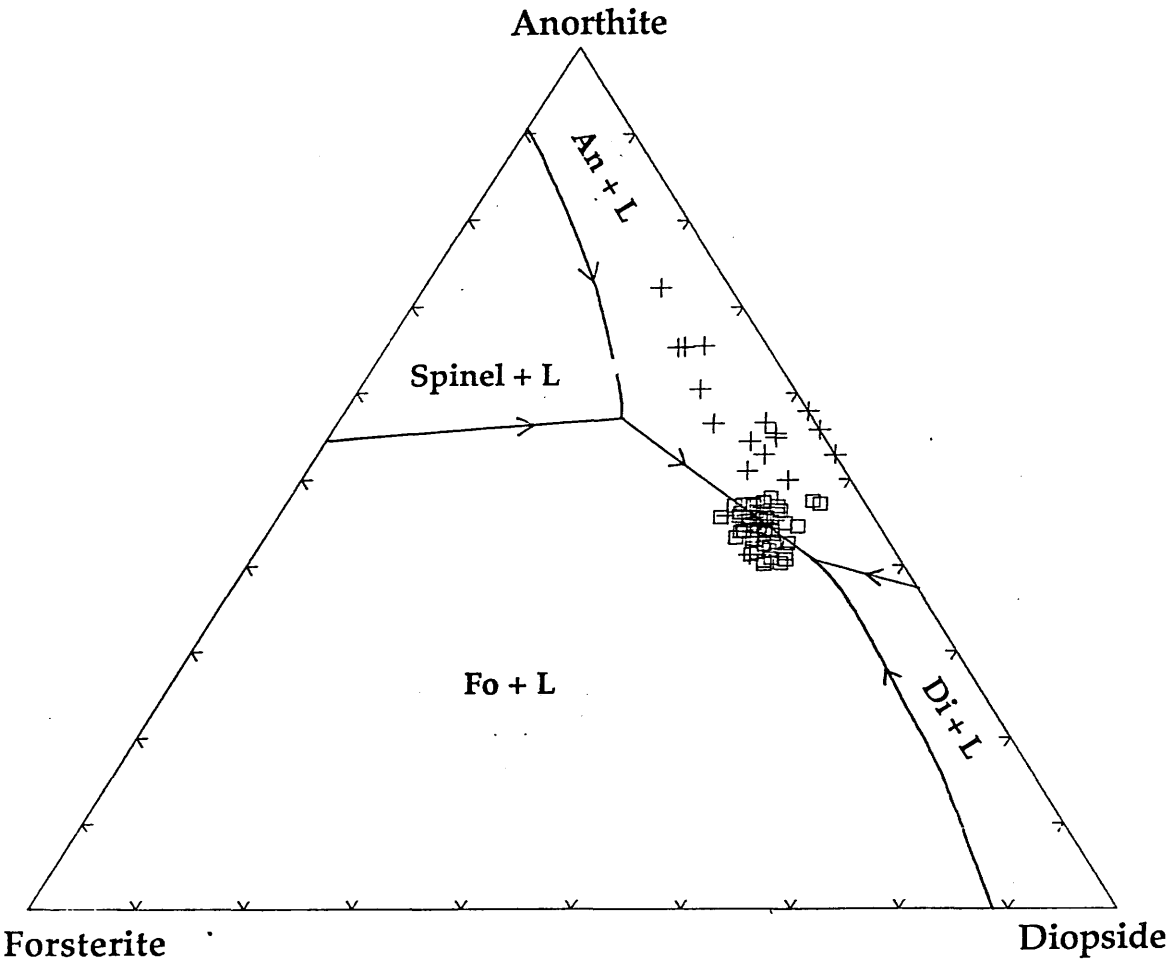

Fig.1.24. Liquidus projection for the system Fo-Di-An at 1 atmosphere pressure (after Osborn & Tait, 1952). Symbols as in Fig.1.23.

Sample		CS022	CS023
Qtz		-	-
Or		0.71	3.13
Ab		15.65	23.02
An		30.69	19.40
Di	Wo	14.34	9.87
Di	En	7.87	3.38
Di	Fs	5.94	6.76
Hy	En	2.13	6.38
Hy	Fs	1.61	12.75
Ol	Fo	8.23	1.71
Ol	Fa	6.85	3.78
Mt		2.23	3.51
Il		1.71	4.25
Ap		0.17	0.57
Ne		-	-

Table 1.6 Normative variation displayed by the cone-sheets of the Cuillin complex.

1.3.5 Major element geochemistry

1.3.5.1 Introduction

In addition to the alteration imposed by the Skye hydrothermal system (Section 1.2.3.1), cone-sheets towards the southern tip of the Sgurr na Stri peninsula show pronounced alteration (Fig.1.25). Compositionally, these sheets are enriched in large ion lithophile (LIL) elements. Notably, those sheets occuring within c.50m of the observed Coire Uaigneich Granite contact show high concentrations of K_2O, P_2O_5, SiO_2, Ba and Sr and low concentrations of CaO, with respect to the cone-sheets further north. In addition, TiO_2, Na_2O, Zr, La, Rb and Th show high and MgO low concentrations, but still within the range of the values displayed by the whole suite (Table.1.7). It therefore seems probable that the most southerly cone-sheets have been subjected to alkali metasomatism emanating from the Coire Uaigneich Granite during and subsequent to its emplacement. Due to this mineralogical and chemical alteration, samples CS001 and CS002 will be omitted from the data set in subsequent presentation and discussion of the suite.

Occurring towards the base of the cone-sheet complex on the southern tip of the Sgur na Stri penninsular are two "sills". These sheets are each approximately 2m thick and are inclined at similar angles and in the same direction as adjacent sheets. The two sills, originally described by Harker (1904) and Carr (1952), are considerably coarser than any of the cone-sheets, possess chilled contacts with the lavas, and are highly feldspar-phyric, containing up to 40% sub-euhedral phenocrysts which attain sizes of 4mm and are zoned from An_{86} to An_{71} at their rims. They also contain abundant groundmass feldspar laths of An_{60-50}, a brown Ca-rich pyroxene which is generally interstitial, although a crude sub-ophitic texture may be developed, and minor amounts of Fe-Ti oxides. Both sheets are olivine free. Carr (1952) did not wish to correlate the sheets with the cone-sheets, instead suggesting that both were probably related to porphyritic basalt sills on the Island of Soay, 4.5 km to the south-west (Harker 1904). However, due the protracted emplacement of cone-sheets it is possible that the two sheets are in some way related to the suite of cone-sheets. This hypothesis is supported upon comparison of their whole rock geochemistry with that of the typical cone-sheets. Major element analyses of the two sheets (Table.1.8) reflect the

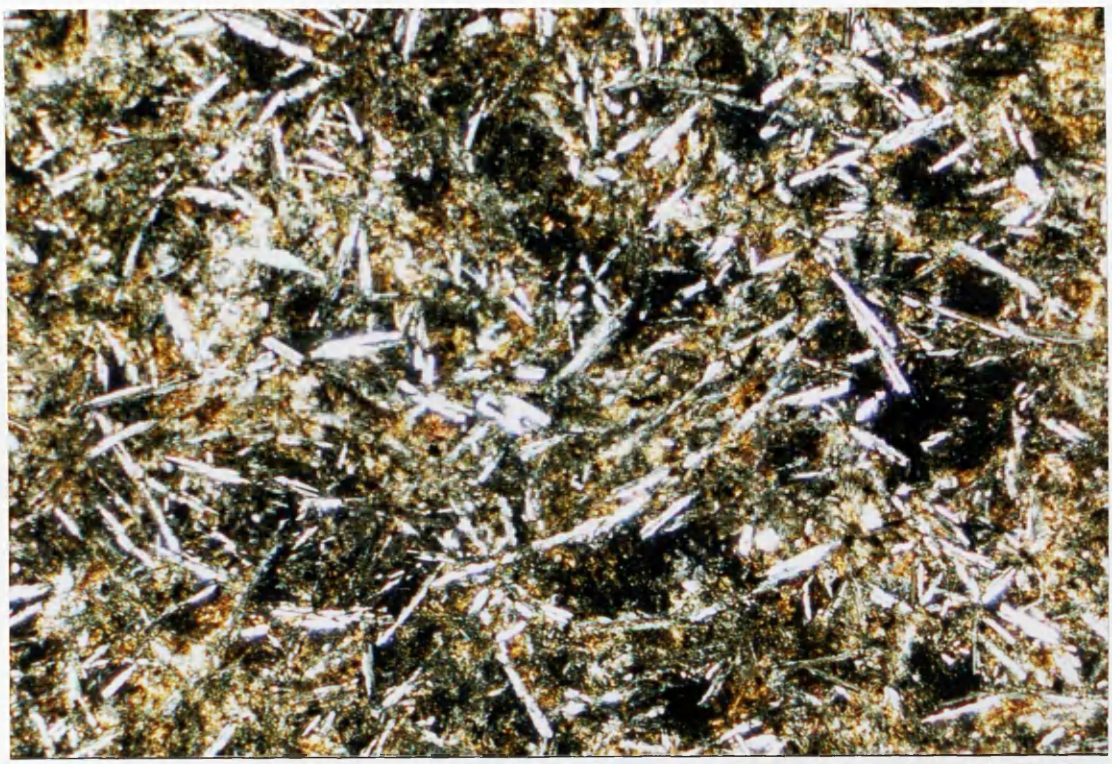

Fig.1.25. Alteration of cone-sheet adjacent to the Coire Uaigneich Granite. Clinopyroxene has been altered to a matted assemblage of chlorite, whilst acicular plagioclase shows only slight development of sericite, principally around crystal edges. Field of view c.3 x 2mm. Crossed polars. Sample CS001.

			All other aphyric samples			
Sample	CS001	CS002	min.	max	mean	std. dev.
SiO_2	49.80	50.94	46.16	48.01	47.07	0.38
Al_2O_3	14.53	13.53	12.16	14.62	13.59	0.47
TiO_2	1.49	1.89	0.90	2.24	1.22	0.25
Fe_2O_3	1.86	1.91	1.54	2.42	1.83	0.19
FeO	12.40	12.73	10.27	16.13	12.23	1.26
MgO	5.93	5.29	4.90	8.73	7.66	0.78
CaO	9.40	9.62	8.99	13.38	12.33	0.84
MnO	0.19	0.19	0.17	0.26	0.21	0.02
Na_2O	2.49	2.17	1.39	2.80	2.06	0.33
K_2O	1.43	0.77	0.05	0.53	0.21	0.11
P_2O_5	0.27	0.18	0.06	0.24	0.09	0.03
H_2O^+	0.73	0.92				
Total	100.52	100.14				
Ba	600	151	48	171	95.00	24.79
Sr	399	368	118	154	136.33	9.69
Zr	138	128	54	156	71.51	20.07
La	15	12	0	9	1.78	-
Rb	79	39	5	18	9.18	2.98
Th	6	1	0	5	1.29	-
Y	32	30	21	52	26.50	5.20

Table 1.7 Comparrison of samples CS001 and CS002 with statistical data from all other remaining aphyric cone-sheets, shows enrichment in large ion lithophile elements as expected if metasomatized by Coire Uaigneich Granite.

accumulation of feldspar, particularly the data on alumina, which exceeds 23 wt.% and their low ferro-magnesian element concentrations. Significantly, high-Ca low-alkali characteristics of the cone-sheets are still reflected by the recast data. The immobile trace-elements considered incompatible with a crystallizing assemblage of olivine, clinopyroxene and feldspar suggest a reasonably primitive status if the sheets are indeed cogenetic with the cone-sheets. Obviously, the high proportion of feldspar phenocrysts precludes the analysis from representing a liquid composition; however, due to their suggested primitive nature (compared with other members of the cone-sheet suite) and their possible spatial importance towards the base of the cone-sheet complex, the analysis has been recast into a liquid composition (Table 1.8) allowing for 40% feldspar accumulation. The resultant "liquid" composition is comparable to other previously identified primitive samples within the suite.

Implicit within the recalculation of the analysis to a liquid composition are the following assumptions;

1 that a liquid of this composition did exist but was subsequently modified by the addition of feldspar phenocrysts by some means.
2 that whilst trace-element concentrations will have been modified, the ratio of certain incompatible elements which are excluded from plagioclase during its crystallization reflect original or only slightly modified ratios.

As can be seen from Table 1.8, even with the removal of 40% feldspar, the sheet is still enriched in the feldspar components suggesting that, contrary to modal analysis, insufficient feldspar has been allowed for in recasting to a liquid composition. If these two sheets do represent primitive members of the cone-sheet suite, then substantial phenocryst accumulation/fractionation must have occurred, for not only are they significantly enriched in feldspar phenocrysts but they also lack olivine, which is occasionally seen in other primitive members of the suite.

	CS006 as analysed	CS006 recast	CS022	CS006/2 phenocryst
SiO_2	46.26	47.60	46.85	45.68
Al_2O_3	23.21	16.75	14.42	33.58
TiO_2	0.46	0.78	0.90	-
FeO	5.60	9.18	10.27	0.44
Fe_2O_3	0.84	1.42	1.54	-
MgO	4.77	7.95	8.73	0.23
CaO	15.34	14.02	13.20	17.79
Na_2O	1.60	1.78	1.85	1.38
K_2O	0.17	0.28	0.12	0.01
MnO	0.10	0.16	0.17	-
P_2O_5	0.05	0.08	0.07	-
Total	98.40	100.00	98.12	99.11
FFM	.5745	.5714	.5750	.6567

Table 1.8 Comparison of the highly feldspar phyric lower "sill" (CS006) towards the base of the cone-sheet complex, recast into a liquid composition by the removal of 40% feldspar phenocrysts (composition given above), with the least evolved sample (CS022) from the cone-sheet suite.
FFM= $FeO+Fe_2O_3/FeO+Fe_2O_3+MgO$

1.3.5.2 Major element characteristics

The cone-sheets are characterized by relatively high concentrations of CaO (~9-13%) and low concentrations of alkalis, Na (~1.4-2.8), K (~0.05-0.53) and show a typical tholeiitic differentiation trend on an AMF diagram (Fig.1.26). Major element variation diagrams are presented (Figs.1.27 a-j), utilizing the ratio $FeO^*/FeO^* + MgO$ (where FeO^* = total iron) as a fractionation index, for all samples.

The most primitive sample (that having the lowest F/F + M ratio) contains 8.73 wt. % MgO at an F/F + M value of 0.575, the composition then becoming more evolved until at F/F + M = 0.791 the MgO content has fallen to 4.90 wt. %.

It is clear from Figs.1.27 a-j, that the observed chemical trends must require the fractionation of a Mg rich phase (confirming the identification of a small percentage of olivine phenocrysts; Section 1.3.3.4). The geochemical trends displayed by the suite are generally well correlated. However, some scatter of the data is evident. Phenocryst subtraction vectors for olivine and plagioclase are superimposed on the variation diagrams and assess the effect of olivine and plagioclase phenocryst subtraction (or addition with arrows operating in opposite sense). The plots clearly show that whilst the scatter about the trend may be caused by plagioclase phenocryst accumulation the trend itself cannot be explained in terms of plagioclase and olivine fractionation alone. Fig.1.28 shows the ratio CaO/Al_2O_3 plotted against the differentiation index and it is clear from these data that fractionation of a phase with Ca > Al is required, the most obvious being a calcic pyroxene, as suggested by the normative phase diagrams (Fig.1.23 & 1.24) and trace element data (Section 1.3.6).

The need to postulate such a phase which is not seen in the fractionating assemblage is not uncommon (For example see basaltic volcanism study project). Cox and Mitchell (1988) have suggested that selective crystal settling was an important fractionation process in the differentiation of the magmas which gave rise to the Deccan Trap basalts. These authors found that aphyric and highly feldspar-phyric samples occupied only slightly overlapping compositional space in terms of their FeO and MgO contents and on the basis of density calculations concluded that the less dense aphyric trend had lost all of its crystalizing

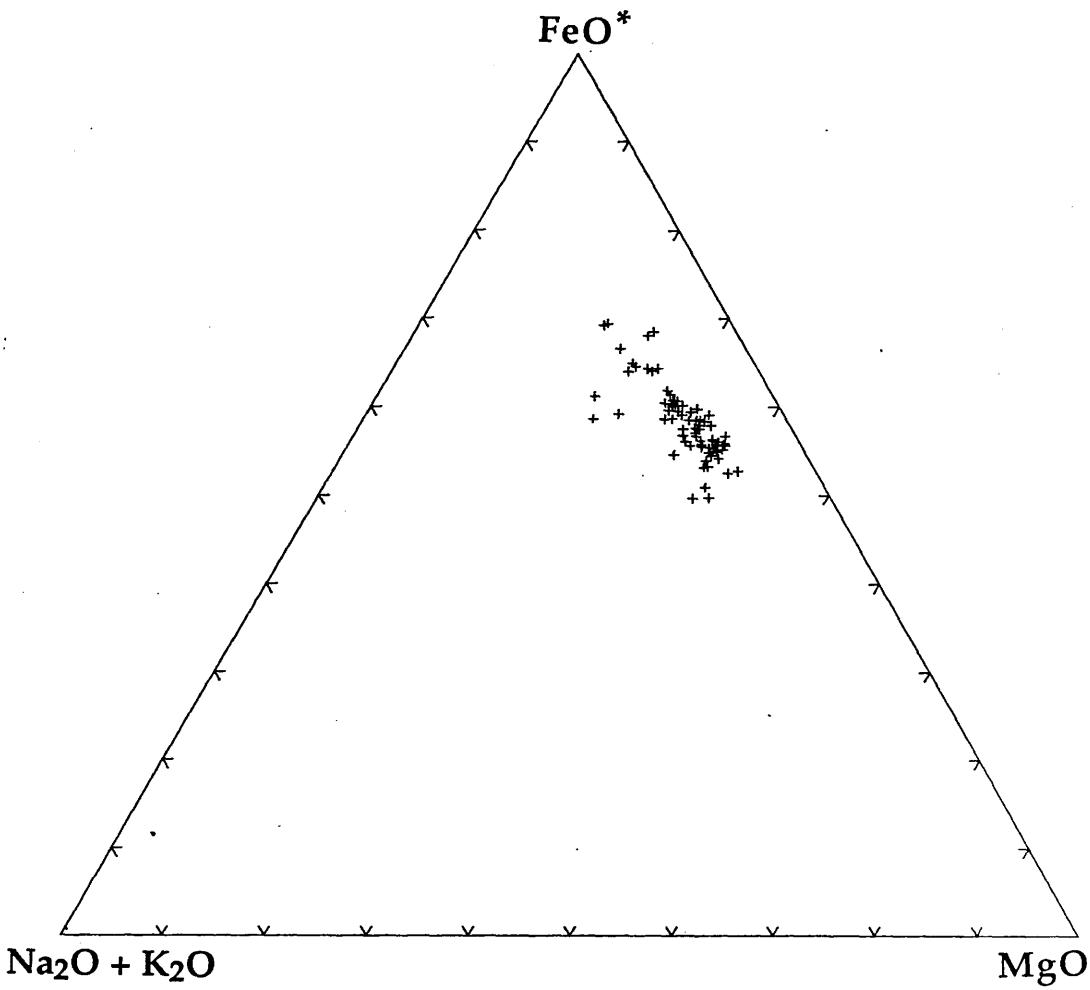

Fig. 1.26. AFM diagram illustrating the typical tholeiitic enrichment trend of iron within the cone-sheets of the Çuillin complex.

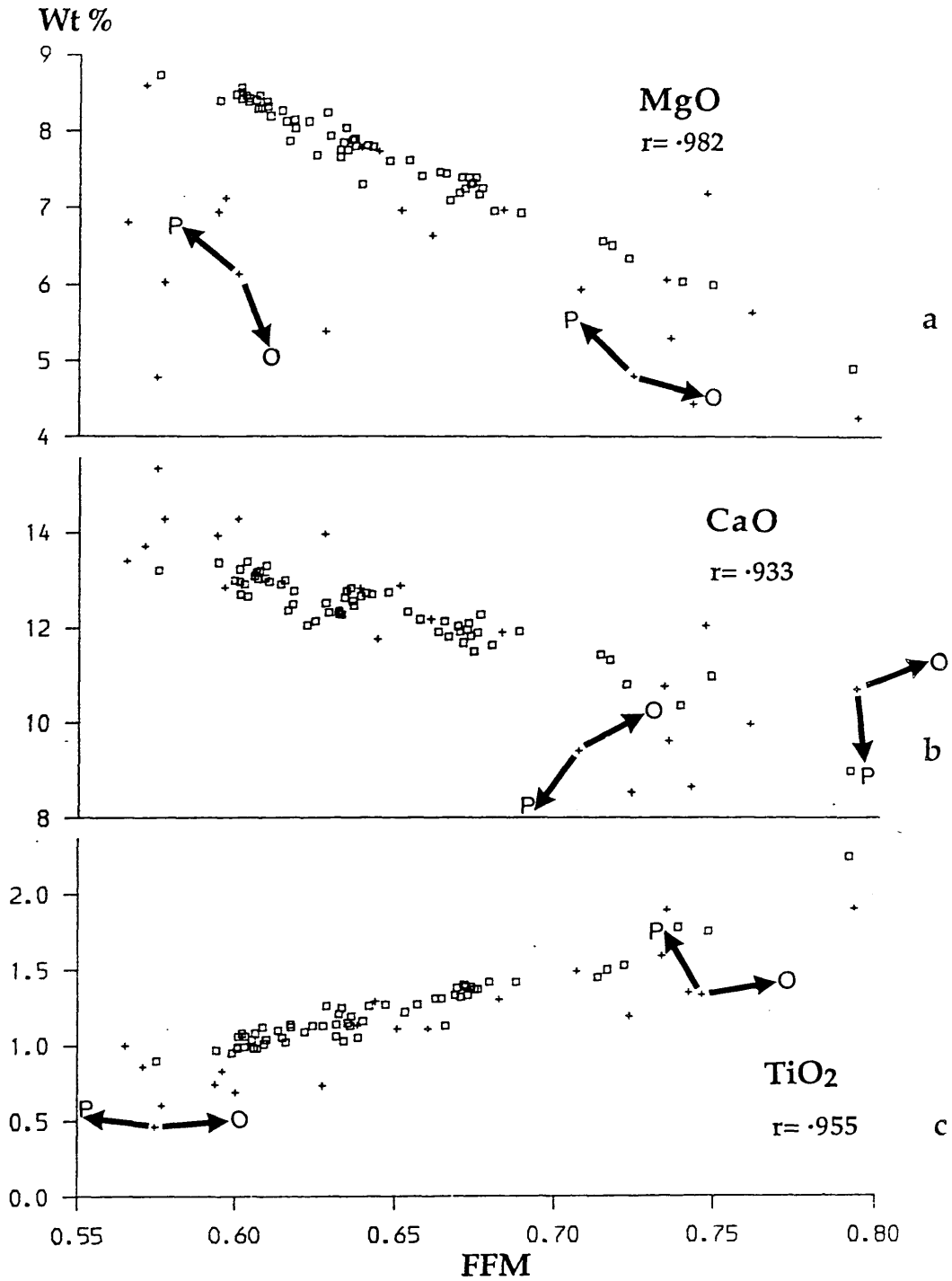

Fig. 1.27. Major element variation (wt.%) displayed by the cone-sheets of the Cuillin complex. (□) = aphyric samples (less than 5% phenocrysts), (+) = porphyritic samples (greater than 5% phenocrysts). FFM = $FeO + Fe_2O_3 / FeO + Fe_2O_3 + MgO$. $FeO^* = FeO + Fe_2O_3$. r = correlation coefficient for all aphyric samples. Arrows illustrate the effect of removal of plagioclase (P) and olivine (O) from selected porphyritic samples.

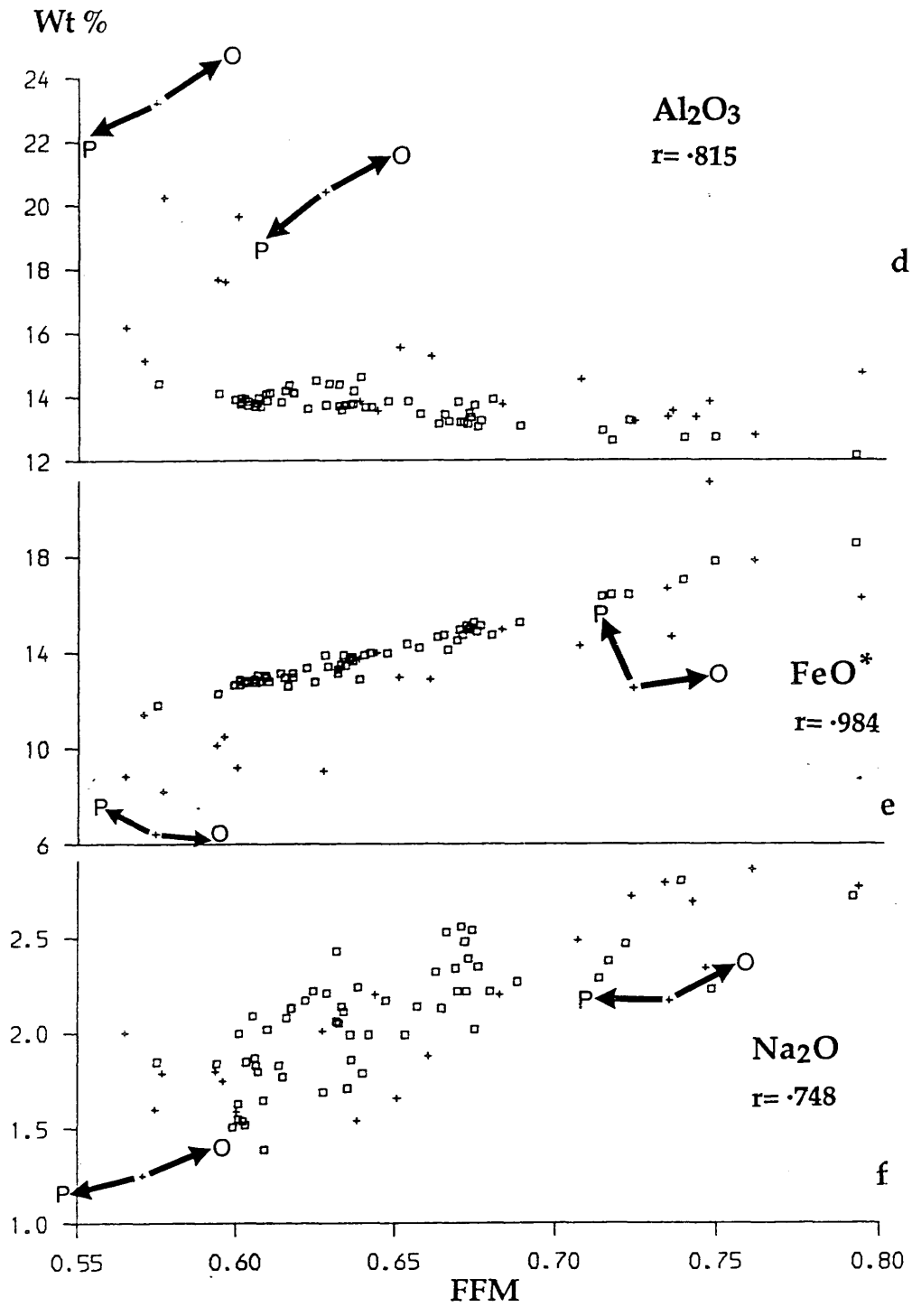

Fig. 1.27. Major element variation (wt.%) displayed by the cone-sheets of the Cuillin complex. (□) = aphyric samples (less than 5% phenocrysts), (+) = porphyritic samples (greater than 5% phenocrysts). FFM = $FeO + Fe_2O_3 / FeO + Fe_2O_3 + MgO$. $FeO^* = FeO + Fe_2O_3$. r = correlation coefficient for all aphyric samples. Arrows illustrate the effect of removal of plagioclase (P) and olivine (O) from selected porphyritic samples.

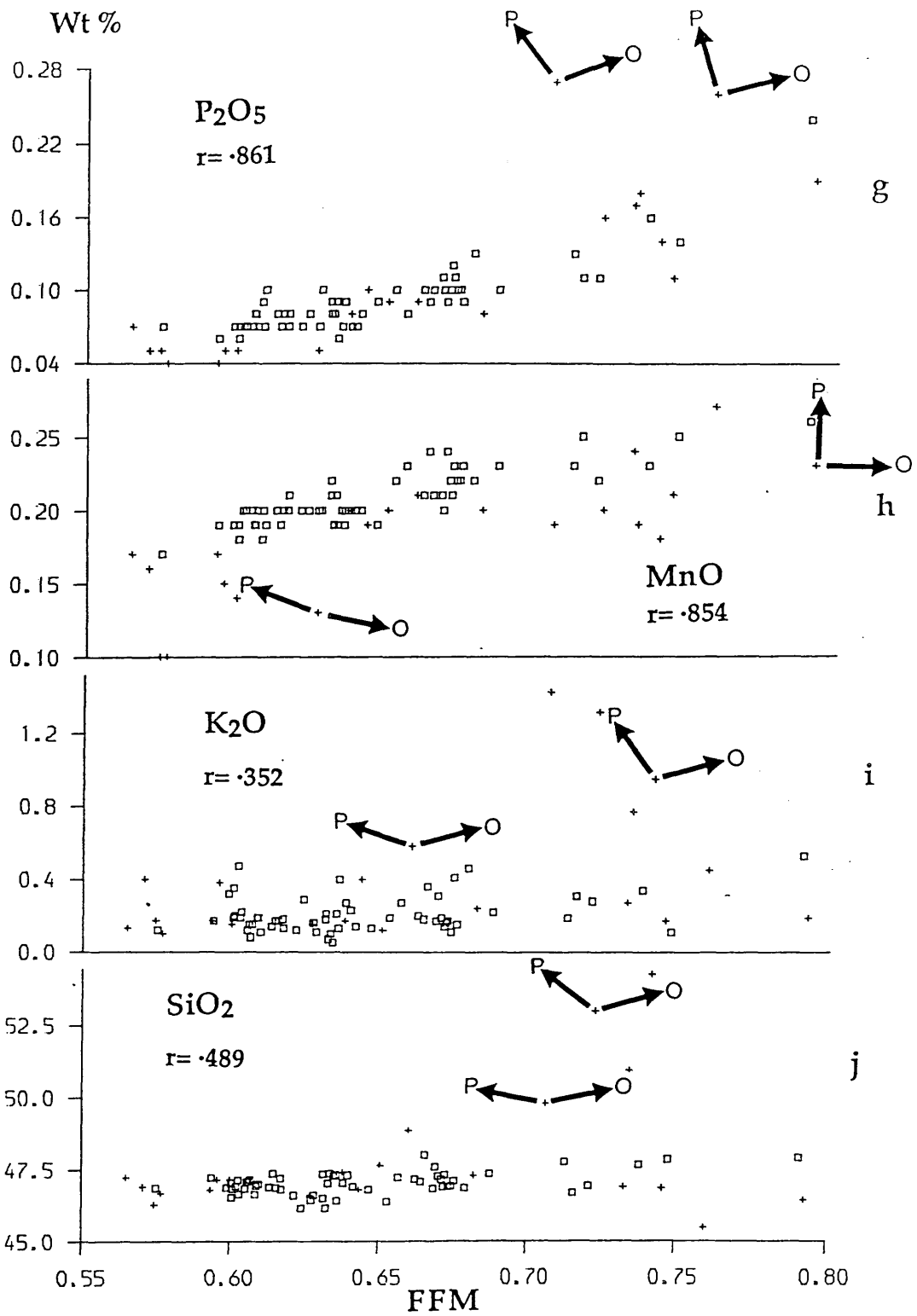

Fig. 1.27. Major element variation (wt.%) displayed by the cone-sheets of the Cuillin complex. (¤) = aphyric samples (less than 5% phenocrysts), (+) = porphyritic samples (greater than 5% phenocrysts). FFM = $FeO + Fe_2O_3 / FeO + Fe_2O_3 + MgO$. r = correlation coefficient for all aphyric samples. Arrows illustrate the effect of removal of plagioclase (P) and olivine (O) from selected porphyritic samples.

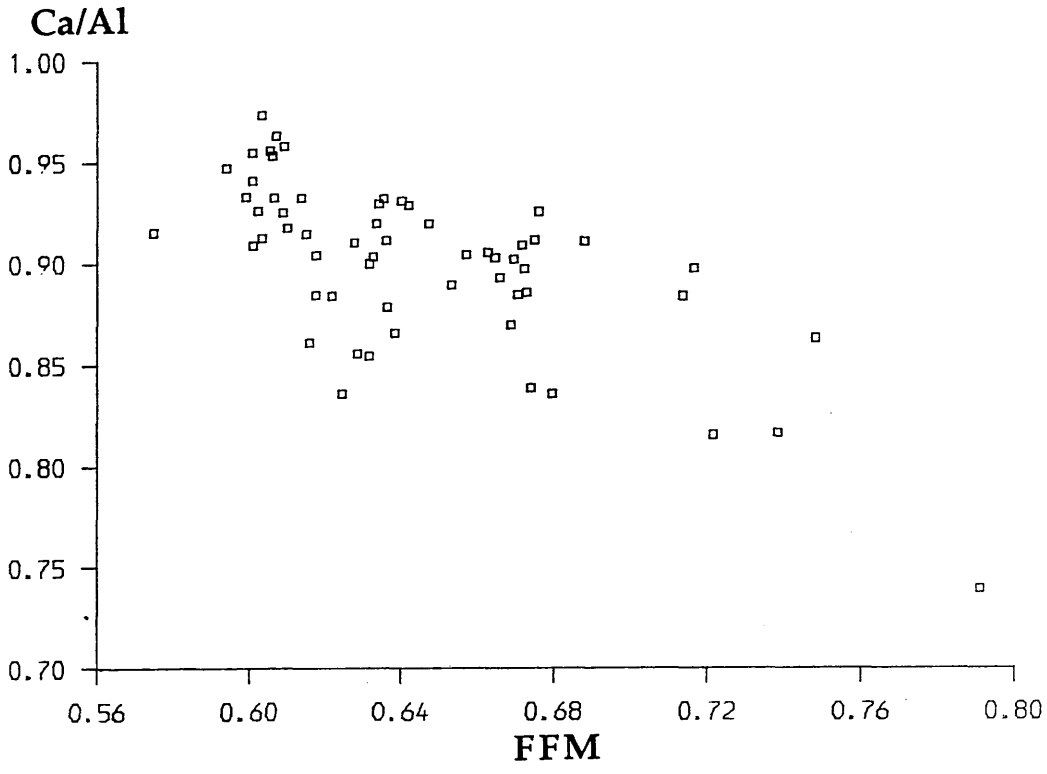

Fig. 1.28. Variation of Ca/Al with fractionation, FFM, within the cone-sheet suite (FFM = $FeO + Fe_2O_3 / FeO + Fe_2O_3 + MgO$).

phases whilst the denser porphyritic trend had selectively lost their ferro-magnesian phases, but retained their less dense feldspar phenocrysts.

Two variants of the selective fractionation process may be envisaged:

A) A liquid crystallizes several phases, e.g. ol, px and pl. The olivine and pyroxene sink within the liquid whilst plagioclase, having a lower density, remains in situ.

B) Plagioclase crystals within a crystallizing liquid float upwards to produce plagioclase crystal enrichment in the upper part of the magma chamber.

The variables governing this type of behaviour are the differential density between crystals and melt, the size of the crystals and the rheology of the melt.

The so-called Cpx paradox has been investigated by Francis (1986), who concluded that the requirement to incorporate clinopyroxene as part of the fractionating assemblage to explain the decrease in Ca over and above that removed by plagioclase fractionation may be illusionary. He has shown that the difference in compositional trends produced by perfect equilibrium and perfect fractional crystalization of olivine, assuming a range of parental magmas, can, under less imaginative schemes, require the presence of clinopyroxene to explain the trends (Fig.1.29). However, the limited role played by olivine in the evolution of the cone-sheets (Section 1.3.3.4) suggests that such a mechanism is not applicable and thus the paradox remains. Experimental studies of basaltic systems at 1 atm. (Dungan & Rhodes 1978; Walker et al 1979) show that clinopyroxene crystallizes at a considerably lower temperature than either olivine or plagioclase and is therefore less likely to have a major influence in basaltic crystal-liquid fractionation schemes unless stable conditions persist to allow cotectic olivine-plagioclase crystallization to intersect the olivine-plagioclase-clinopyroxene cotectic. Repeated replenishment of the magma chamber will continually "pull" the liquid composition back into the olivine or plagioclase liquidus field whilst crystallization will tend to reverse this trend. The loci of the liquid compositions will only be linear if replenishment occurs prior to the onset of crystallization. If crystallization is proceeding during the replenishment (the most geologically reasonable case) then the loci of liquids produced will depend on the relevent phase equilibria.

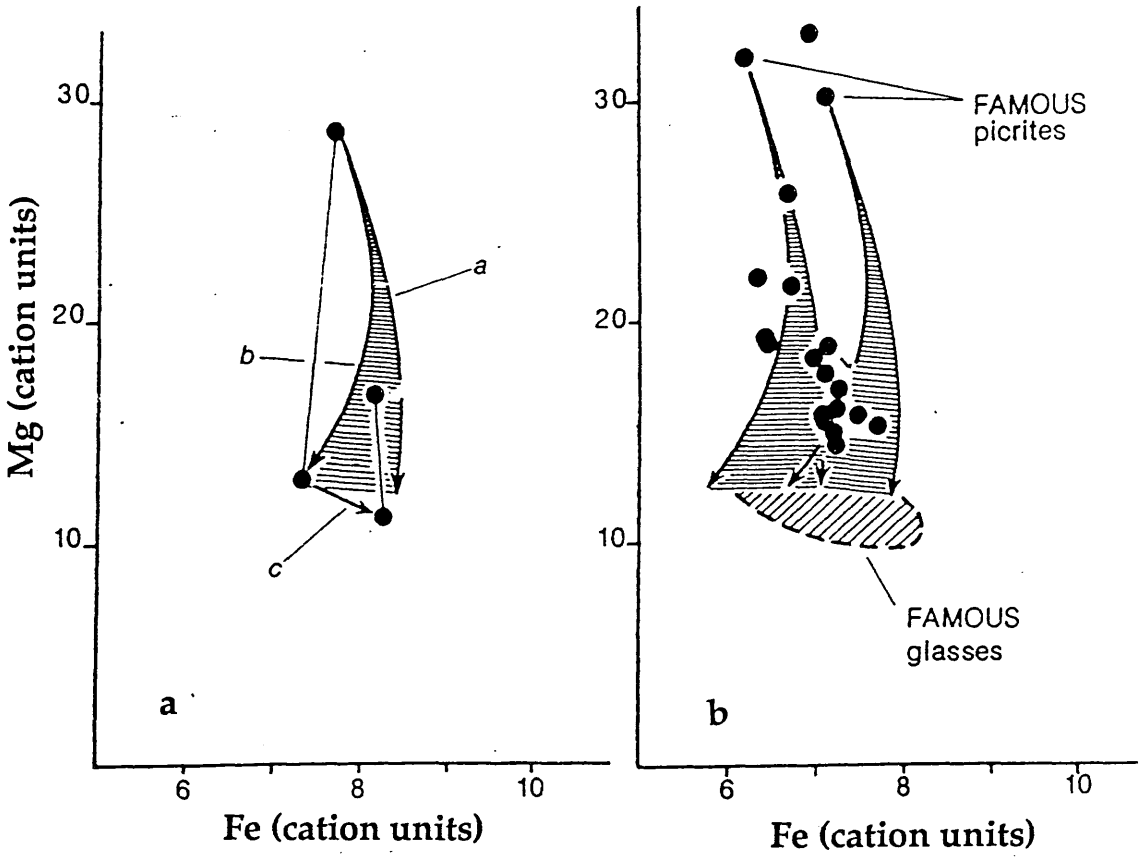

Fig. 1.29. A) Mg-Fe plot (cation units) indicating calculated crystal fractionation paths. Trend a represents the path of a primitive lava (Mg wt %=21.94) undergoing perfect fractional crystallization. Trend b represents a perfect equilibrium olivine crystallization path. Both the low Mg ends of each trend terminate at the point of plagioclase saturation. Trend c represents the crystal fractionation path for ol+pl+cpx.

B) Mg-Fe plot (cation units) illustrating composition of MORB (Famous) picrite lavas. The heavy arrows indicate the fractional and equilibrium olivine crystallization paths (as in A) and again terminate at the plagioclase saturation point. Note the correspondence between the plagioclase saturation points at the ends of the fractionation arrows and the diagonally shaded fields of analysed glass compositions. (after Francis 1986).

Walker et al (1979) have shown that for the reverse case, where an evolved MORB, presumably related to an olivine and/or plagioclase saturated parent, crystallizes clinopyroxene before either of these two phases, mixing of the primitive magma and an evolved cogenetic magma may be resposible for the anomalous composition. Fig.1.30 shows the phase relationships elucidated by Walker et al (1979) and their possible bearing on clinopyroxene crystallization. The phase boundaries separating the liquid fields of olivine (+ plagioclase), high-Ca pyroxene (+ plagioclase) and low-Ca pyroxene (+ plagioclase) were constructed from electron probe analyses of experimental glasses, equilibrated with these three silicate phases. In Fig 1.30, considering a primitive sample (P), this evolves by ol (+pl) fractionation along the solid arrow until the liquid composition intersects the liquidus field of Cpx. The liquids then continue evolving along the solid arrow by crystal-liquid fractionation of ol+cpx (+pl). The composition (X) studied by Walker et al. (1979), which plots in the high-Ca pyroxene field, cannot be produced by a simple crystal-liquid fractionation scheme. The authors proposed that mixing of liquids at various stages of evolution along the ol+cpx (+pl) cotectic was responsible for this anomalous composition.

To return to the original problem of explaining the lack of cpx phenocrysts, it is possible to postulate mixing of liquids saturated with respect to ol+cpx (+pl) with primitive liquids saturated in only one phase (dotted line of Fig.1.30). If the mechanism of crystal-liquid fractionation (by any means) is efficient, the mixed magmas would retain the cryptic signature of cpx fractionation (ie. reduction in the Ca/Al ratio) but without the phenocryst evidence.

Fig. 1.31 shows data for the Skye cone-sheets recast (method in footnote to Fig.1.31) into the parameters utilised by Walker et al. and plotted on the relevent diagram. In all but a few specimens, the analyses plot within the field of ol (+pl), and thus the Skye data are consistent with the above scenario.

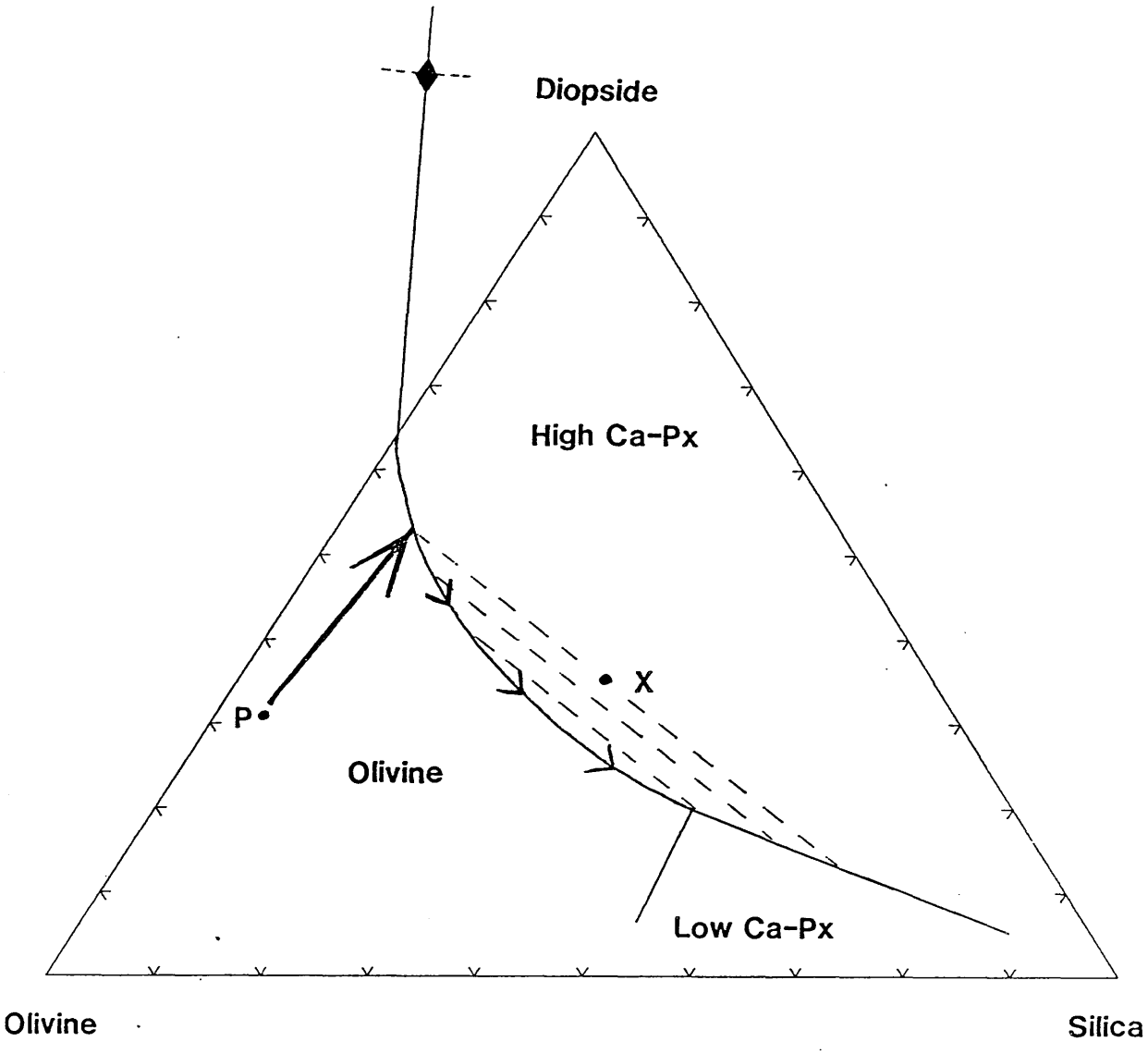

Fig. 1.30. Projected plagioclase saturated liquidus (1 atm.) on olivine-diopside-silica. Diamond symbol is approximate location of thermal divide seperating tholeiitic from alkalic basalt evolution. Fractionation of ol (+pl) from liquid P will produce liquids which will plot along the heavy arrow until the composition intersects the olivine + high Ca-Px (+pl) cotectic where upon liquids will evolve along the light arrow. The primitive sample P cannot produce composition X as a residual liquid by crystal-liquid fractionation alone. The liquid can, however, be produced by mixing of various liquids along the fractionation curve (dashed lines).

Plagioclase=$Al_2O_3+Na_2O+K_2O$

Diopside=$CaO+Al_2O_3+Na_2O+K_2O$

Olivine=$(FeO+MgO+MnO+2Fe_2O_3 +FeO+MgO+MnO+2Fe_2O_3)/2$

Silica=$SiO_2-(FeO+MgO+MnO+2Fe_2O_3+Al_2O_3+11Na_2O+11K_2O+3CaO)/2$

All parameters derived from molecular proportions. After Walker et al. 1979.

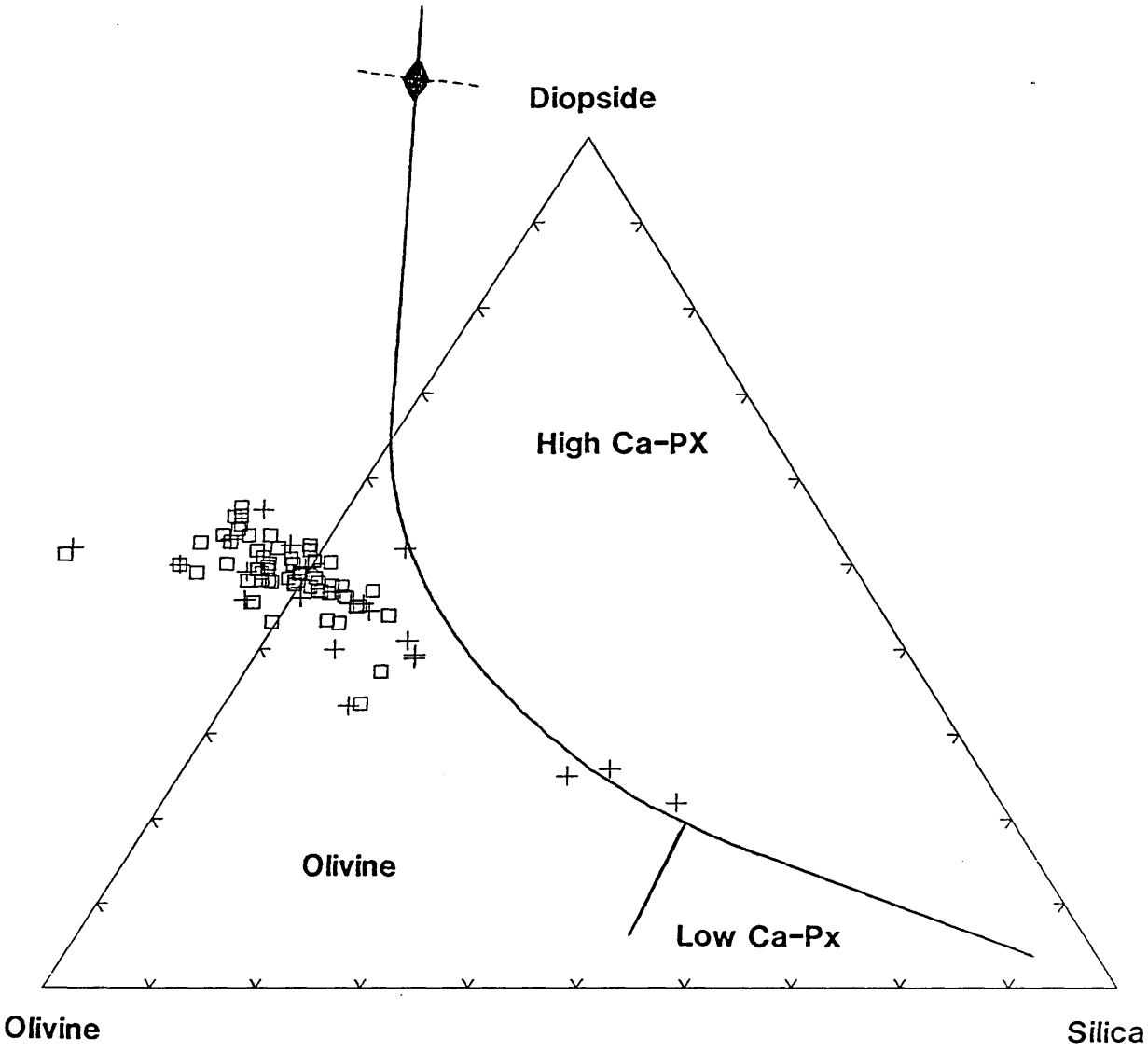

Fig. 1.31. Skye cone-sheet analyses plotted within the plagioclase saturated liquidus on olivine-diopside-silica (Walker et al. 1979). Mixing of liquids evolving along the ol+high Ca-Px (+Pl) cotectic with primitive liquids may produce liquids saturated in only one phase but retaining the cryptic signature of previous cpx fractionation. (□) = aphyric samples (< 5% phenocrysts). (+) = porphyritic samples (> 5% phenocrysts).

1.3.6 Trace element geochemistry

1.3.6.1 Introduction

Concentrations of Ba, Cr, Cu, Ni, Pb, V, Zn, Zr, Sc, Y, Sr, Rb and Nb were determined by XRFS for all samples, (Appendix IV) whilst selected samples representing the compositional range displayed by the suite were analysed for rare earth elements (REE) by induction coupled plasma spectrometry (ICPS) (See Appendix II for experimental method and Appendix V for results). Hydrothermal alteration (Section 1.2.3.1) has led to the development of minor amounts of pyrite, as evidenced by high S contents in some samples, for example CS021, CS032 and CS040, with 8039, 1399 and 1311 ppm, respectively. These, therefore, have been omitted from the data set.

Variation in transition elements

The concentration of the elements Ni, Cr, V and Zn show well defined differentiation trends when plotted against the fractionation index F/F+M (Fig.1.32). The depletion in Ni, from 106ppm to 35ppm at fractionation indices of 0.5750 and 0.7910, respectively, is consistent with olivine fractionation, whilst the depletion in Cr may be explained by fractionation of Cr spinel or clinopyroxene: two phases which have not been identified as forming phenocryst phases. However, the rapid fall in the Cr content of clinopyroxenes (Section 1.3.3.2) and the need to postulate clinopyroxene as a fractionating phase (Section 1.4.2) suggests that the Cr content of the cone-sheets is controlled by pyroxene fractionation. V shows enrichment factors of $\sim$2 and Zn $\sim$1.6. Both V and Sc are expected to partition into pyroxene and should therefore be indicators of clinopyroxene fractionation. The increase of V and the almost constant concentration of Sc (30ppm), however, suggests that the distribution coefficients between clinopyroxene and silicate melt are <1 and close to unity for these elements, respectively.

Variation in large ion lithophile (LIL) elements

Any systematic variation shown by the elements La, Nb, Th, and U is poorly constrained (Fig.1.32) with many of the samples containing Th, La, and U below the limits of detection of the XRFS. Those samples containing measurable amounts of La (4-9ppm), Th (1-5ppm), Nb (2-6ppm), Pb (0-10ppm) and U (1-2ppm) show a broad scatter of the data with no

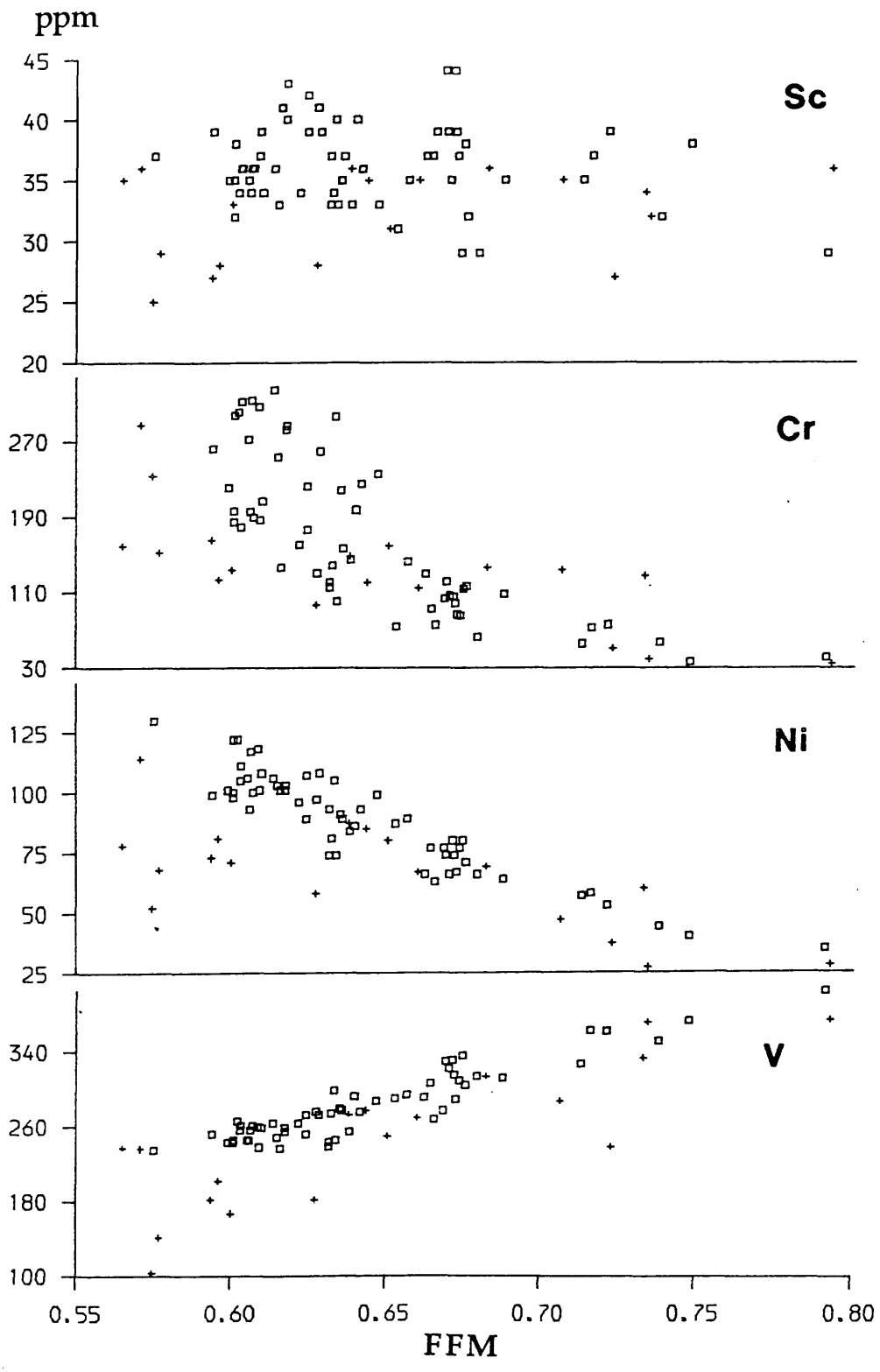

Fig. 1.32. Trace element variation within Skye cone-sheets. (□) = aphyric samples (<5% phenocrysts). (+) = porphyritic samples (>5% phenocrysts).
FFM = $FeO + Fe_2O_3 / FeO + Fe_2O_3 + MgO$.

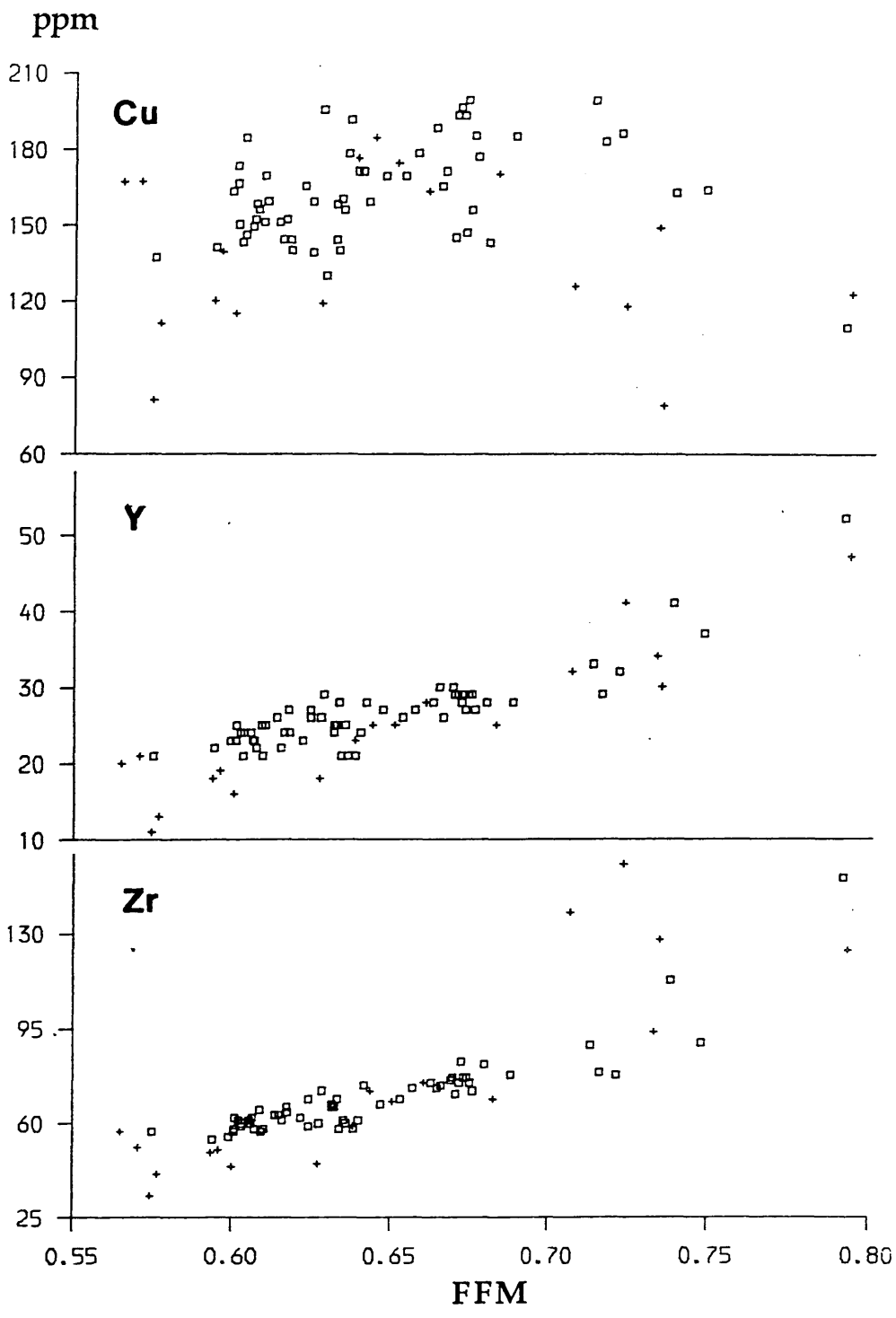

Fig. 1.32. Trace element variation within Skye cone-sheets. (▫) = aphyric samples (<5% phenocrysts). (+) = porphyritic samples (>5% phenocrysts).
FFM = $FeO + Fe_2O_3 / FeO + Fe_2O_3 + MgO$.

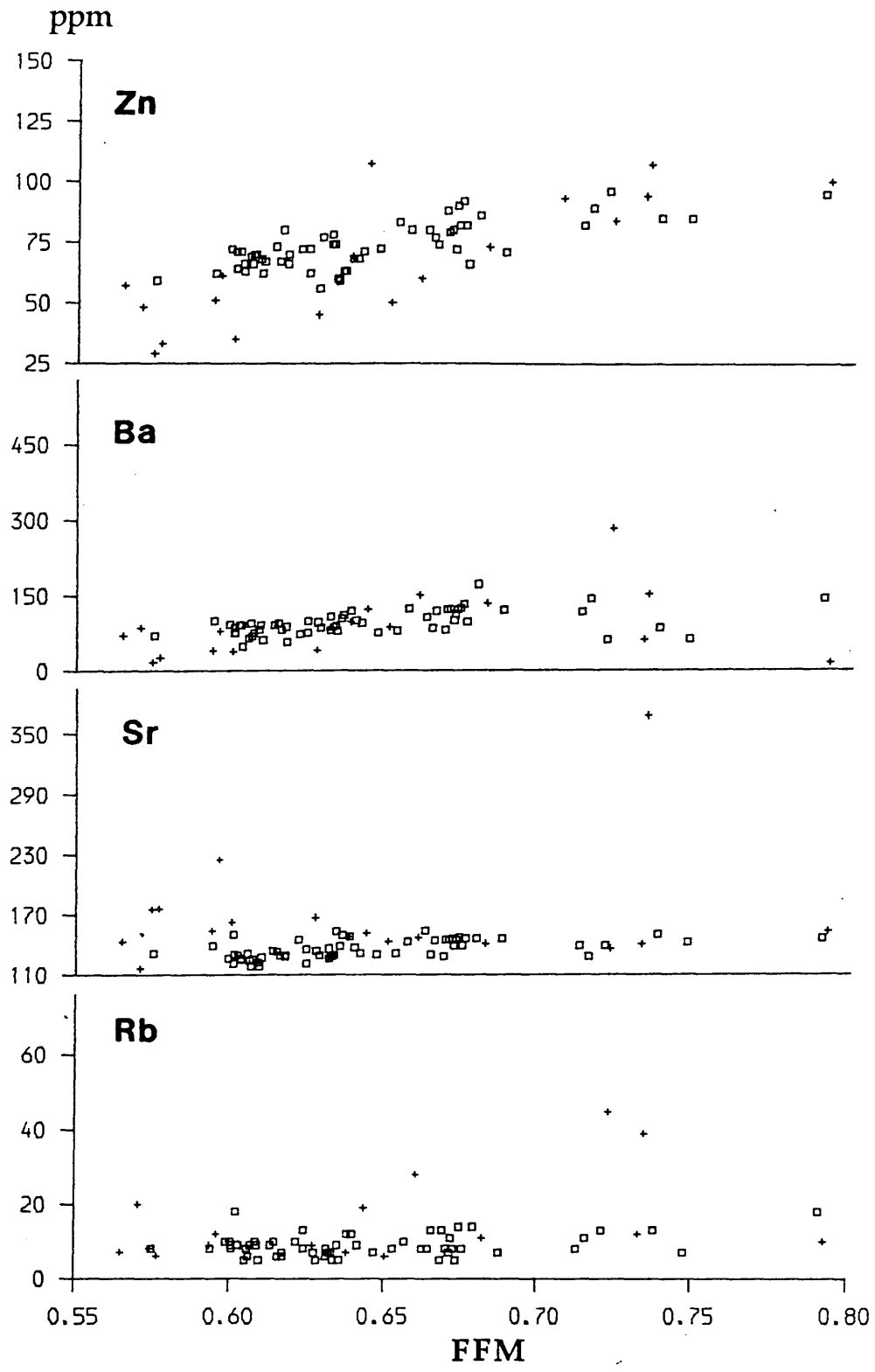

Fig. 1.32. Trace element variation within Skye cone-sheets. (▫) = aphyric samples (<5% phenocrysts). (+) = porphyritic samples (>5% phenocrysts).
FFM = $FeO + Fe_2O_3 / FeO + Fe_2O_3 + MgO$.

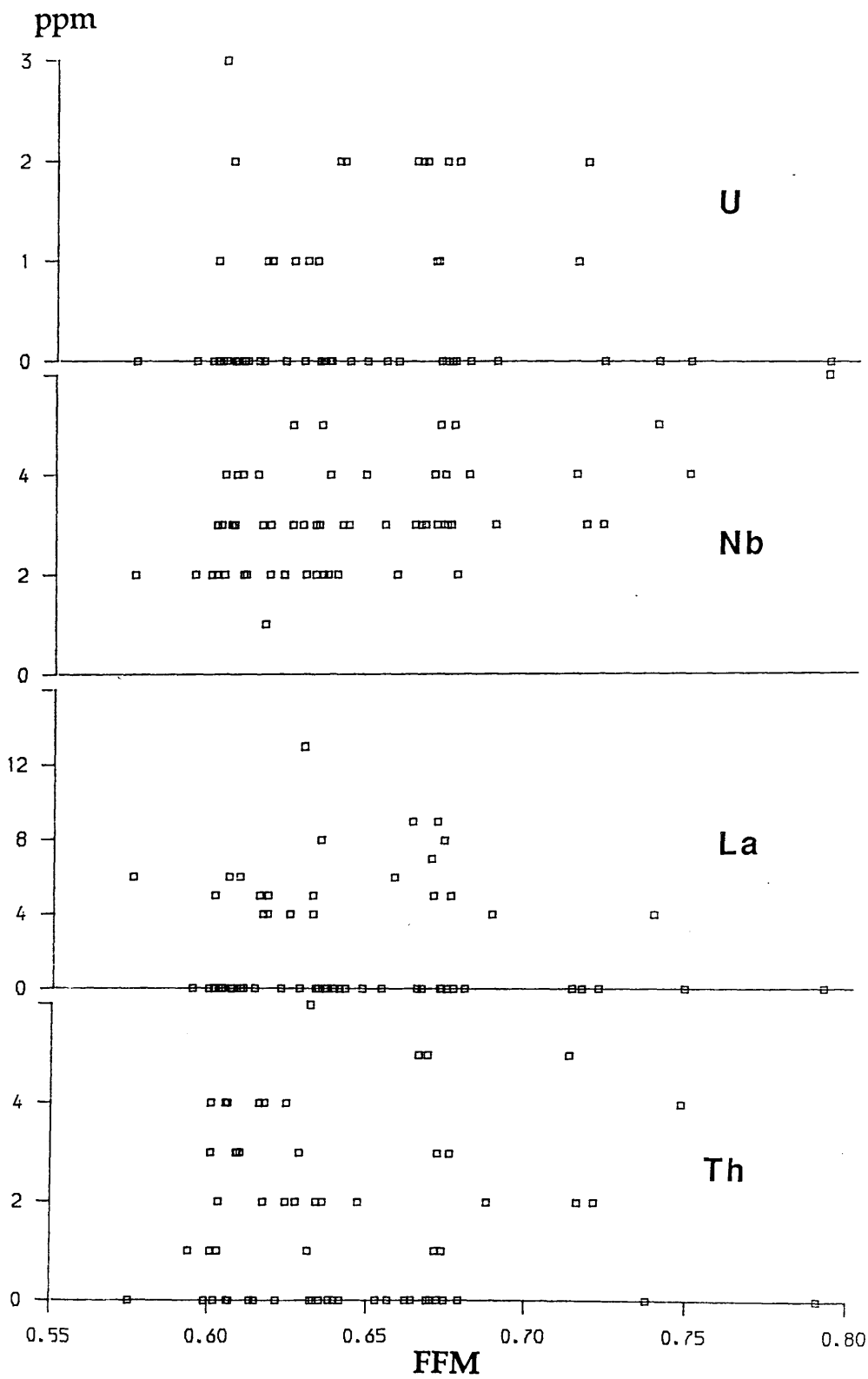

Fig. 1.32. Trace element variation within Skye cone-sheets. (□) = aphyric samples (<5% phenocrysts). (+) = porphyritic samples (>5% phenocrysts).
FFM = $FeO + Fe_2O_3 / FeO + Fe_2O_3 + MgO$.

correlation with differentiation, and therefore the data are consistent with the hypothesis that these elements were rendered mobile during the alteration process. Ba, Sr and to some extent Rb concentrations do show slight increases with differentiation although the correlation is poor. Again, the susceptible nature of these elements to alteration processes is probably responsible for the observed poor correlations. Y and Zr are considered immobile (Pearce & Cann 1973) during alteration, this being substantiated for the Skye cone-sheets by the well-correlated trends displayed (Figs.1.32). As expected, Y and Zr increase with differentiation from ~50 to ~120ppm, and ~20 to ~40ppm, respectively. Mattey et.al (1977) have demonstrated that it is possible to distinguish between the SMLS and the PM lavas and dykes on the basis of their Ti/Zr and Y/Zr ratios. These elements are excluded from a crystallizing assemblage of olivine, clinopyroxene and plagioclase and consequently their ratios remain unchanged and therefore reflect initial differences between the identified magma types. The SMLS has Y/Zr ratios of <0.3 and Ti/Zr ratios of ~90, whilst rocks of the PM type have Y/Zr and Ti/Zr ratios of >0.3 and ~90-120, respectively (Fig.1.33). A comparison of the Skye cone-sheets with these previously identified magma types (Fig.1.34) shows little difference between the cone-sheets and the PM magma type, with respect to their Ti/Zr and Y/Zr ratios.

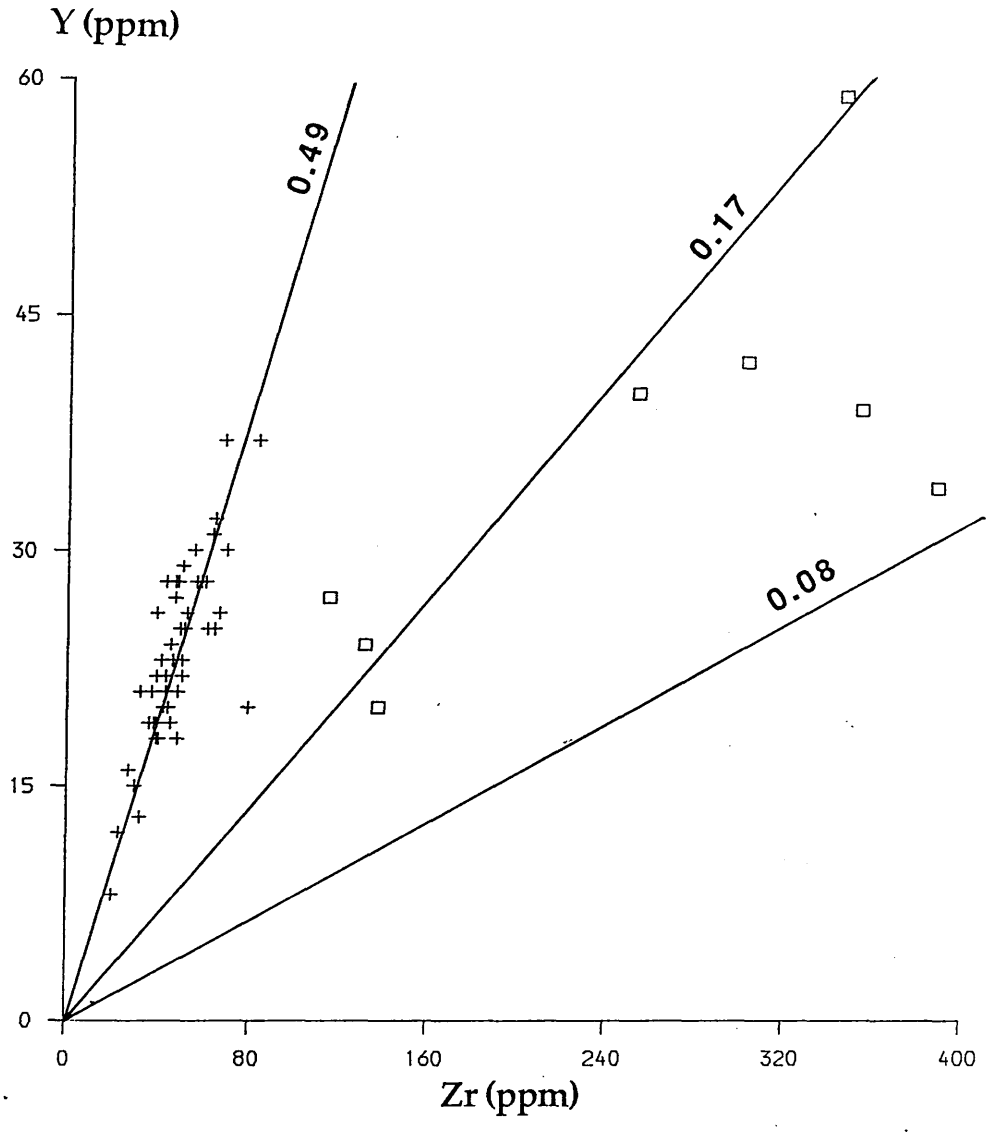

Fig 1.33. Variation of Y and Zr within lavas of the Preshal Mhor (+) and Skye Main Lava Series (◻) of Skye. Members of the PM series generally have Y/Zr ratios of >0.3 whilst members of the SMLS have ratios of <0.3.

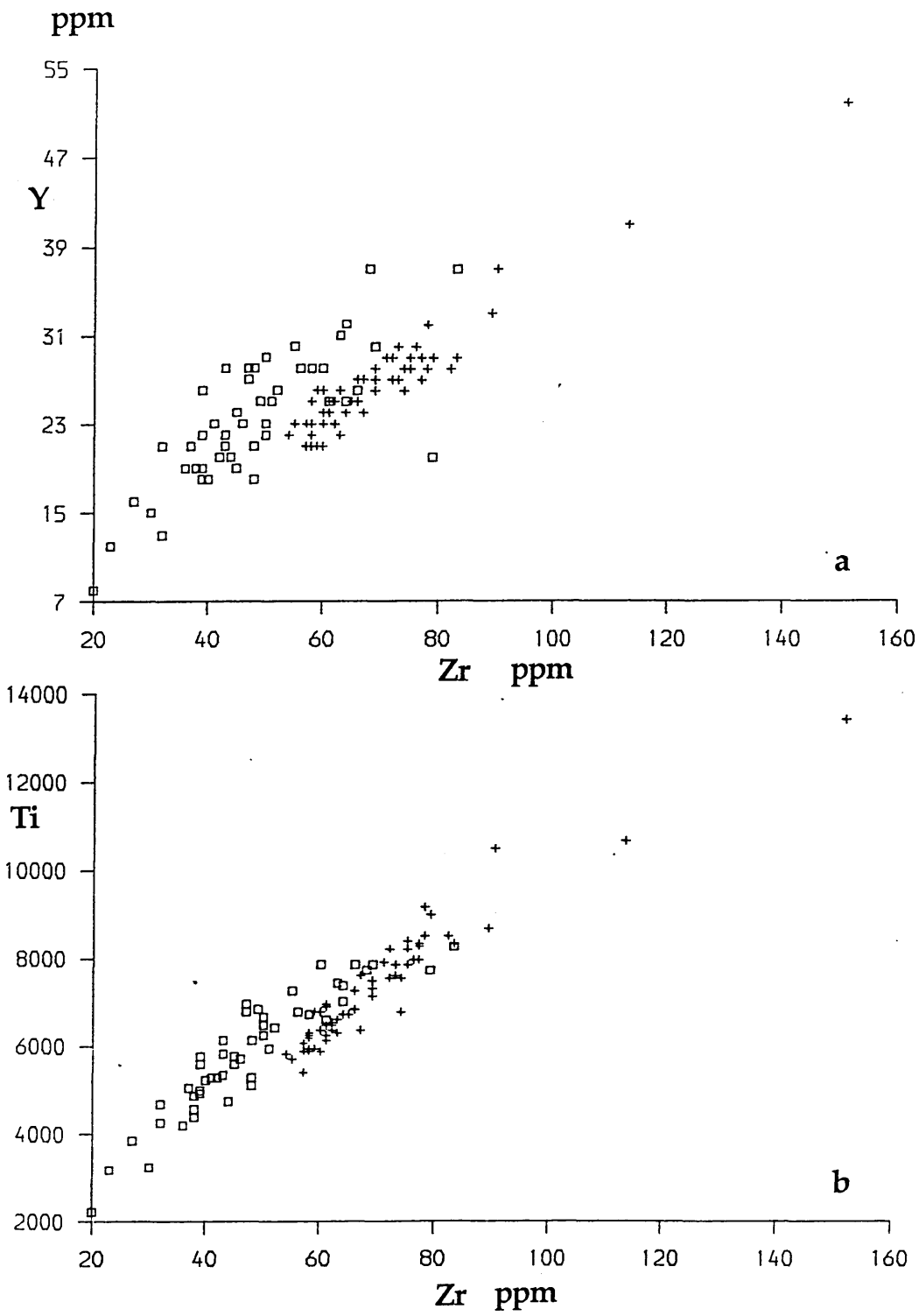

Fig.1.34. Variation of a) Y v Zr and b) Ti v Zr within Skye cone-sheets (+), and Preshal Mhor basalts (□) (Preshal Mhor data from Mattey et al. 1977).

1.3.7 Rare Earth Elements

1.3.7.1 Mobility of the Rare Earth Elements

The susceptibility of the rare earth elements (REE) to mobility during alteration processes is dependent on a number of factors (Humphries 1984):

i) The initial abundance of REE in the unaltered rock;

ii) The mineral phases in which the elements are concentrated and the susceptibility of these phases to alteration;

iii) The concentration of the REE in any fluid and their partitioning between the fluid and the mineral phases;

iv) The ability of secondary minerals formed during the alteration process to accommodate the REE liberated by the breakdown of the primary mineralogy.

Partition coefficients for REE between a silicate melt and the common rock-forming minerals are generally very low, indicating that the REE have a preference to remain in the melt during crystallization, or to enter a melt during partial melting events. However, an exception to this behaviour is the REE affinities for clinopyroxene, an important major phase in many igneous rocks. Partition coefficients for light (low z) rare earth elememnts (LREE) between clinopyroxene and silicate melt are of the order of $\sim$0.3, whilst for the heavy (high z) rare earth elements (HREE) the partition coefficients are $\sim$1.0. Consequently, as clinopyroxene shows a preference for HREE relative to LREE, the ratio of LREE/HREE in the melt will increase with pyroxene fractionation.

Generally, the behaviour of REE during crystallization of a basic magma is very much dependent upon the late-stage accessory minerals, such as apatite, zircon and sphene, which may crystallize. These accessory minerals have partition coefficients generally a few orders of magnitude greater than those of the common rock-forming minerals, and will therefore contain the bulk of the REE within the rock. Thus, the post-crystallization behaviour of these minor phases generally governs any subsequent REE mobility.

Clinopyroxene within the Skye cone-sheets is an important phase, with a modal abundance of $\sim$40%, and therefore alteration of this phase would have a profound effect on

subsequent REE patterns. However, petrographic examination (Section 1.3.3) reveals little or no alteration of pyroxene. The texture of the rock may also affect the stability of the REE. Within the cone-sheets, the pyroxene typically, sub-ophitically to ophitically, encloses the feldspar and being resistant to alteration effectively armours the feldspar against alteration. Thus, any modification of REE concentrations and relative abundances will have resulted from alteration of late-stage accessory minerals. Of these minerals only apatite has been identified. It is only rarely present, and only in small quantities, and like the clinopyroxene shows no alteration. Interstitial glass on the other hand can be volumetrically significant (up to 15%) and is invariably altered to a chloritic assemblage. Menzies et al. (1979) have demonstrated that the greenschist alteration of a glassy tholeiite has no effect on the REE profiles; this has been ascribed to stabilization of the REE by secondary minerals, particularly chlorite (Luddon & Thompson 1979). Nesbitt (1979), however, has shown that samples of a granodiorite became more enriched in LREE with increasing alteration. After normalization of his data to TiO_2, agreed to be immobile, Nesbitt concludes that the HREE show depletion whilst the LREE are enriched relative to the fresh rock.

In a study of the lavas occurring on the Isle of Mull, Humphries et al. (1978) demonstrated that no change in the REE concentrations and the ratios of incompatible trace elements had occurred, even in the most altered samples. It would appear, then, that should REE profiles have undergone subsequent change, it may be restricted to those having a high proportion of chlorite representing original interstitial glass. Consequently, REE analyses were determined for selected samples that contained only minor chlorite and which spanned the observed differentiation trend shown by the suite.

1.3.7.2 REE profiles

The range of REE concentrations, normalized to those found in chondrites (Nakamura 1974), displayed by the Skye cone-sheets is shown in Fig.1.35a. Individual REE profiles are generally characteristically flat with $(Ce/Yb)_N$ ratios ranging from $\sim$0.8 to 1.2. This pattern distinguishes the cone-sheets from either the SMLS, with its LREE enriched patterns and the FB magma type which displays slight LREE enriched patterns (Fig.1.35b). Within the PM magma type, Mattey (1980) has indentified 2 sub-types on the basis of REE profiles. His

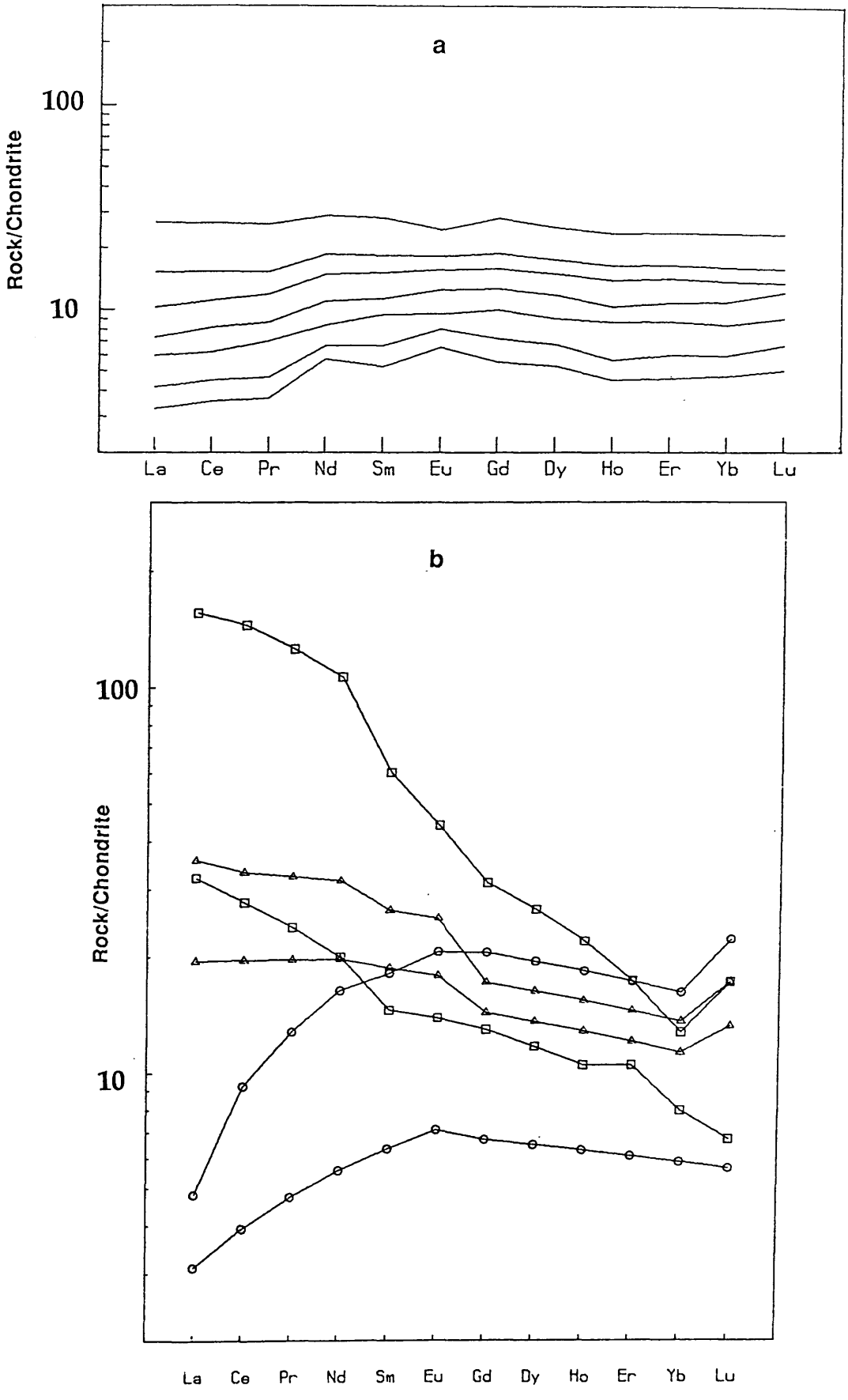

Fig. 1.35. Range of REE concentrations (chondrite normalized) found within a) the Skye cone-sheets and b) previously identified magma types.
(□) = SMLS, (△) = FB, (O) = PM.

sub-type 1 shows parallel patterns with a slight positive Eu anomaly and $(Ce/Yb)_N$ ratios of $\sim$0.9. The second sub-type also shows parallel patterns but dislays no Eu anomaly and a significantly greater degree of LREE depletion, with $(Ce/Yb)_N$ ratios of $\sim$0.5. These differing patterns can be equated with those found in MORB. Sub-type-I is similar to the pattern displayed by Type I MORB, whilst sub-type II is characteristic of Type II MORB. Within the Skye cone-sheets, REE concentrations vary by a factor of approximately 3 (Ce $\sim$2.9, Yb $\sim$2.8). The most primitive sample (CS022), has $(Ce/Yb)_N$ ratio of 0.8, with normalized concentrations of around 0.9. As expected, concentrations increase in more evolved members of the suite; the most evolved sample (CS023) having normalized concentrations of approximately 28. Concomitant with the increase in concentration of the REE is the flattening of the profiles, the evolved members having $(Ce/Yb)_N$ of $\sim$1.1. Of the twenty one samples analysed for REE, the 2 least evolved (in terms of their REE concentrations) (CS006 & CS009) display a small positive Eu anomaly, of Eu/Eu^* = 1.1 & 1.2, respectively, where Eu^* is the normalized concentration calculated by interpolating between Sm and Gd. As Eu can exist as either the divalent or the trivalent ion, depending upon oxygen fugacity, then in most silicate liquids there will exist an appreciable Eu^{2+}/Eu^{3+} ratio and if plagioclase is crystallizing it will be capable of incorporating Eu^{2+}, due to its similar ionic size with Ca and Sr, whilst discriminating against Eu^{3+}. Consequently, Eu may be used as an indicator of plagioclase fractionation/accumulation. Petrographically, samples CS006 and CS009 contain a high proportion of plagioclase phenocrysts (40% and 38%, respectively) which readily explains the positve Eu anomalies. In contrast, the two most evolved members of the suite (CS023 & CS080) display a slight negative Eu anomaly (Eu/Eu^* = 0.88 & 0.94, respectively) indicative of plagioclase removal (Fig.1.36).

It would appear that the REE profiles displayed by the Skye cone-sheets are a hybrid of Mattey's two subtypes, having the flat pattern of Sub-type 1, but without the positive Eu anomaly.

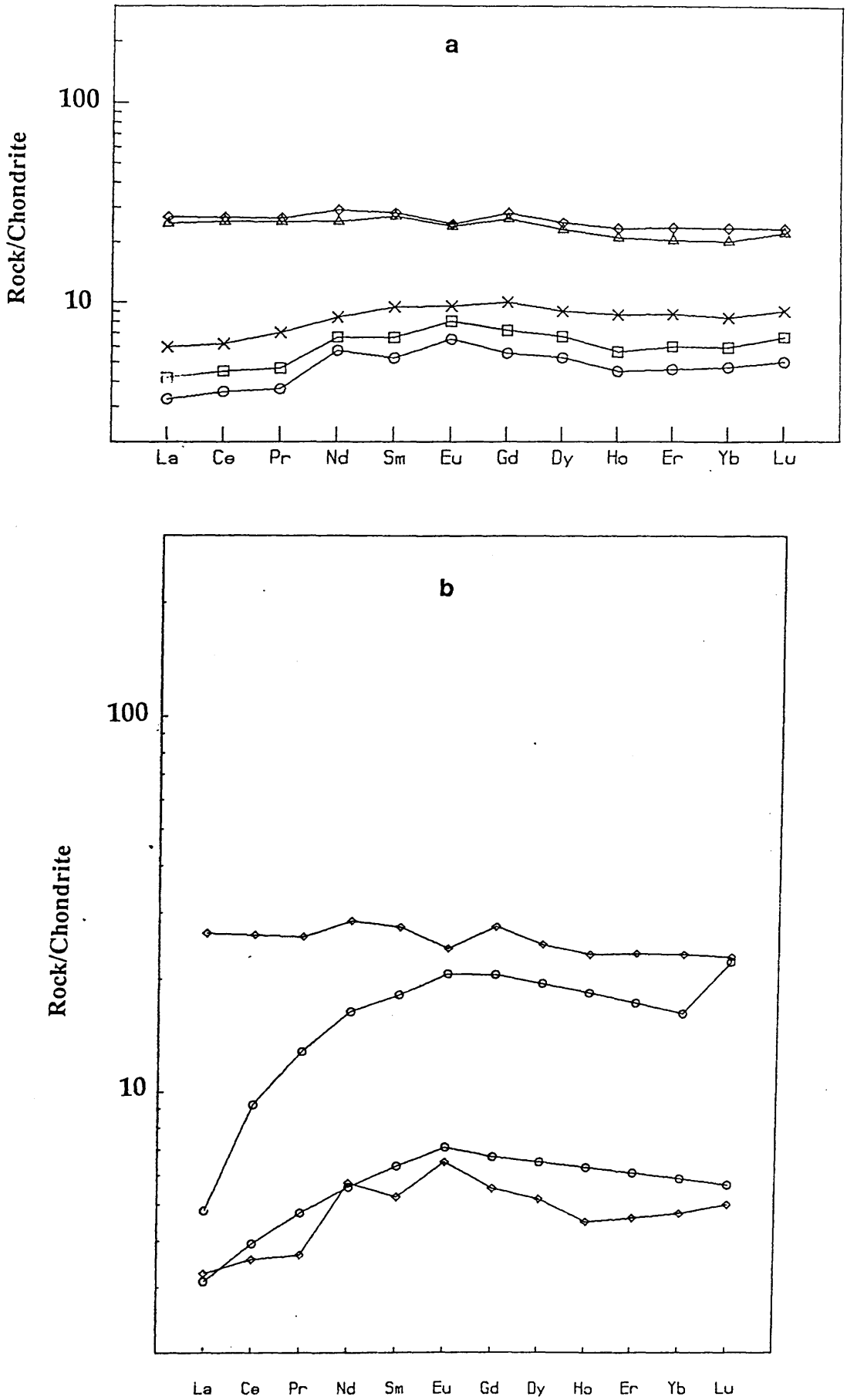

Fig. 1.36. REE profiles of selected Skye cone-sheets and sills to a) illustrate the range and profile displayed by the suite and b) compare the observed range within the cone-sheets (□) with those from the Preshal Mhor basalts (o) (after Mattey 1980).

1.4 Petrological Models

1.4.1 Introduction

The purpose of this section is to identify the proccess(es) which have affected the chemical composition of the cone-sheets and given rise to the observed chemical trends within the suite. Having identified the controls over intra-suite variation, the relationship of the cone-sheet parental magma to previously identified Skye magma types will be addressed.

1.4.2 Intra-suite Variation

In Section 1.3.5.2 it was demonstrated (Fig.1.27) that the scatter of data about the trends shown by the major elements is probably due to the redistribution of plagioclase phenocrysts. Conclusions drawn from the normative mineralogy and, more importantly, the major and trace element data, suggests that the trends themselves can be generated by fractionating an assemblage comprising plagioclase, olivine and pyroxene (mineral/melt and calculated bulk distribution coefficients shown in Table 1.9). Attempts to model such a process, however, require that the composition of the fractionating mineral phases be known.

The composition of the olivine is determined from the empirical equations derived by Roeder and Emslie. (1970). Their experimental results (Fig.1.37) suggest that an olivine having a forsteritic content of Fo_{85} would be in equilibrium with the most primitive of the Skye cone-sheets and this is in accord with that actually observed within the PM basalts of similar major element composition (Mattey et al. 1977). Therefore, appropriate olivine compositions may be obtained from the data of Mattey et al. (1977). They concluded that the intra-suite variation shown by the PM basalts could be generated by fractionating olivine, plagioclase and pyroxene, in the proportion 29:70:1, and consequently the composition of the pyroxene he identified as being a phenocrystic phase has been used in the modelling. A cursory glance at the major-element variation diagrams reveals that the trend lines are linear, with no inflection points which would indicate changes in the fractionating phases.

In determining the fractionation path taken by the suite it is possible to model fractionation steps from the most primitive to the most evolved ie. A to B, B to C, C to D, etc. or to model from the most primitive in each step ie. A to B, A to C, A to D, etc. The first method suffers

Element	olivine	Cpx	Plagioclase	D^B
Ni	16.3000	2.7500	0.0500	2.6200
Cr	1.9200	11.5000	0.0600	4.2500
Ti[1]	0.0370	0.2000	0.0380	0.0946
Y[2]	0.0100	0.2000	0.0600	0.1040
Zr	0.0300	0.2800	0.0800	0.1450
Ce[3]	0.0069	0.1500	0.1200	0.1192
Nd[3]	0.0066	0.3100	0.0810	0.1537
Sm[3]	0.0066	0.5000	0.0670	0.2125
Eu[3]	0.0068	0.5100	0.3400	0.3662
Gd[3]	0.0077	0.6100	0.0630	0.2489
Yb[3]	0.0140	0.6200	0.0670	0.2552
Rb	0.0200	0.0300	0.0900	0.0620
Sr	0.0140	0.1100	2.1000	1.1949
V[1]	0.0880	0.7400	0.1000	0.3228
Ba	0.0190	0.0200	0.3800	0.2179
Sc	0.1900	2.6700	0.0300	0.9700

Table 1.9 Mineral/melt and bulk distribution (D^B) coefficients used in trace element modelling. Bulk distribution coefficients calculated for a fractionating assemblage comprising olivine, plagioclase and clinopyroxene in the relative proportions 10:55:35, respectively.

Source of data Z: McBirney 1984.
Z^1: data from Bryan et al. 1979.
Z^2: Data from Thompson et al. 1980.
Z^3: data from Arth et al. 1975.

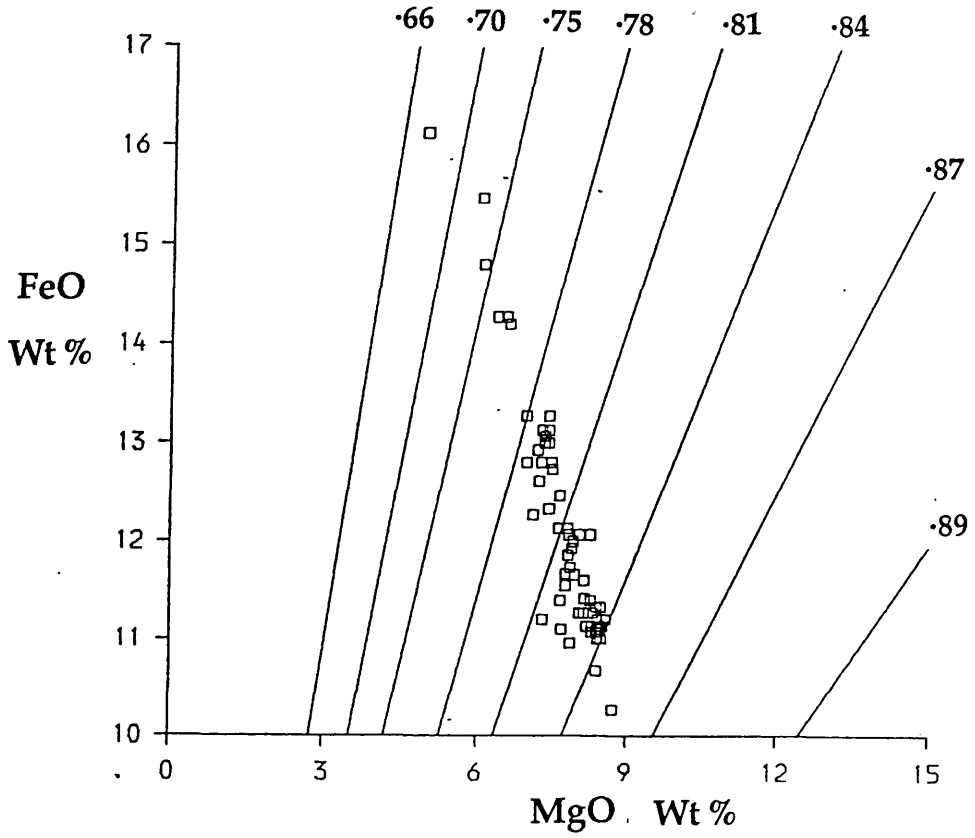

Fig. 1.37. Variation of FeO with MgO in in silicate melt, contoured for Fo content of olivines in equillibrium with that melt (after Roeder & Emslie 1970).

from the effect that the accumulated errors are larger, but it does offer the versatility of accommodating new phases should the need arise. Table 1.10 documents the compositions of the fractionating phases used in the modelling, whilst Table 1.11 displays the results of the least squares modelling method (Wright & Docherty 1970).

The solutions to this type of calculation are generally considered potentially valid if the sum of the oxide residuals are close to or less than unity (Wright & Docherty 1974). The residuals (Table 1.11) are sufficiently low to justify confidence in the proposed model that the major element geochemical trends of the suite have been produced by approximately 60% crystal-liquid fractionation of an assemblage comprising plagioclase, pyroxene and olivine in the relative proportions 55:35:10. The above fractional crystallization model can be independently tested by noting the behaviour of the trace-elements for which mineral/melt distribution coefficients are known (Table 1.9). The behaviour predicted by the model for the trace-elements and the actual trends shown by the suite are illustrated on Fig.1.38. As can readily be seen from the plots, correlation between the trends of predicted and actual behaviour are generally very good. The elements may broadly be subdivided into two groups on the basis of the relative behaviour between actual and predicted trends.

Actual trends displayed by the chalcophile elements: Ni, Cr, V, and to a certain extent Sc and Cu, show excellent fractionation trends relative to those predicted. The Ni, Cr and V trends are tightly constrained about the predicted trends. However, Cu, and particularly Sc, display considerable scatter about the predicted trends. For the most evolved sample (CS023) a large discrepancy exists between predicted and actual ppm values of 225, 37, and 110, 29, respectively. For Cu this discrepency is greater than for any other sample, whilst for Sc it is comparable to other large discrepencies displayed by the trend. Certainly, for Cu there is the suggestion that a depletion in concentration may have occurred. Two possible processes that could account for this are the fractionation of Fe-Ti oxides, or the redistribution of the element by hydrothermal processes. If the former has occurred then one would expect to see sympathetic behaviour of all the chalcophile elements, and particularly a marked depletion in the major element trends of FeO and TiO_2. This is clearly

	olivine*	feldspar	pyroxene*
SiO_2	40.44	46.00	50.03
Al_2O_3	-	33.93	5.53
CaO	0.44	17.95	21.38
TiO_2	-	-	0.08
FeO	13.20	0.49	6.02
MgO	47.09	0.15	15.36
Na_2O	-	1.27	0.27
K_2O	-	0.01	-
MnO	0.29	-	0.13
Total	100.56	99.80	99.39

Table1.10 Major element compositions of fractionating phases used in the least squares modelling process. (* from Mattey 1980).

Sample	FFM	Sr^2	F
022	.5750		1.000
015	.5990	.103	.907
024	.6007	.086	.902
027	.6069	.012	.891
059	.6063	.042	.879
028	.6148	.034	.874
081	.6158	.237	.869
089	.6174	.046	.861
088	.6284	.154	.819
017	.6339	.089	.818
016	.6315	.423	.812
029	.6530	.278	.754
063	.6568	.187	.748
007	.6719	.112	.707
060	.6692	.253	.704
057	.6756	.123	.702
058	.6877	.165	.679
068	.7131	.292	.623
035	.7213	.265	.606
031	.7381	1.315	.573
050	.7478	.296	.561
023	.7910	4.820	.430

Table 1.11 Results of least squares mixing calculation (Wright et al. 1970), modelling the evolution of the Skye cone-sheets in terms of crystal-liquid fractionation.

FFM=$FeO+Fe_2O_3/FeO+Fe_2O_3+MgO$

F=weight fraction of melt remaining.

Sr^2= Sum of the squares of the residuals.

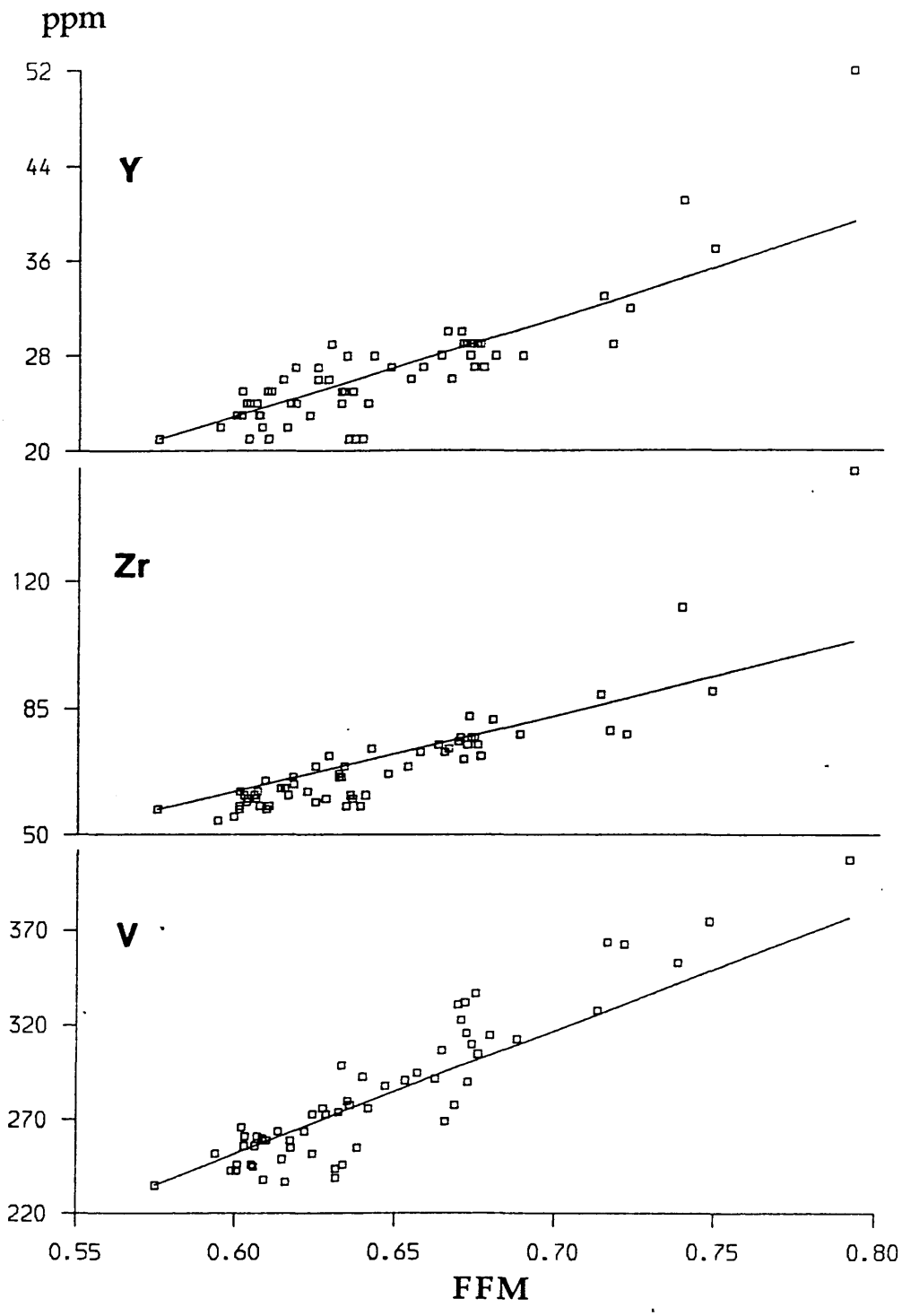

Fig. 1.38. Comparison of analysed cone-sheet data (□) with that predicted from the crystal fractionation model. FFM = $FeO + Fe_2O_3 / FeO + Fe_2O_3 + MgO$.

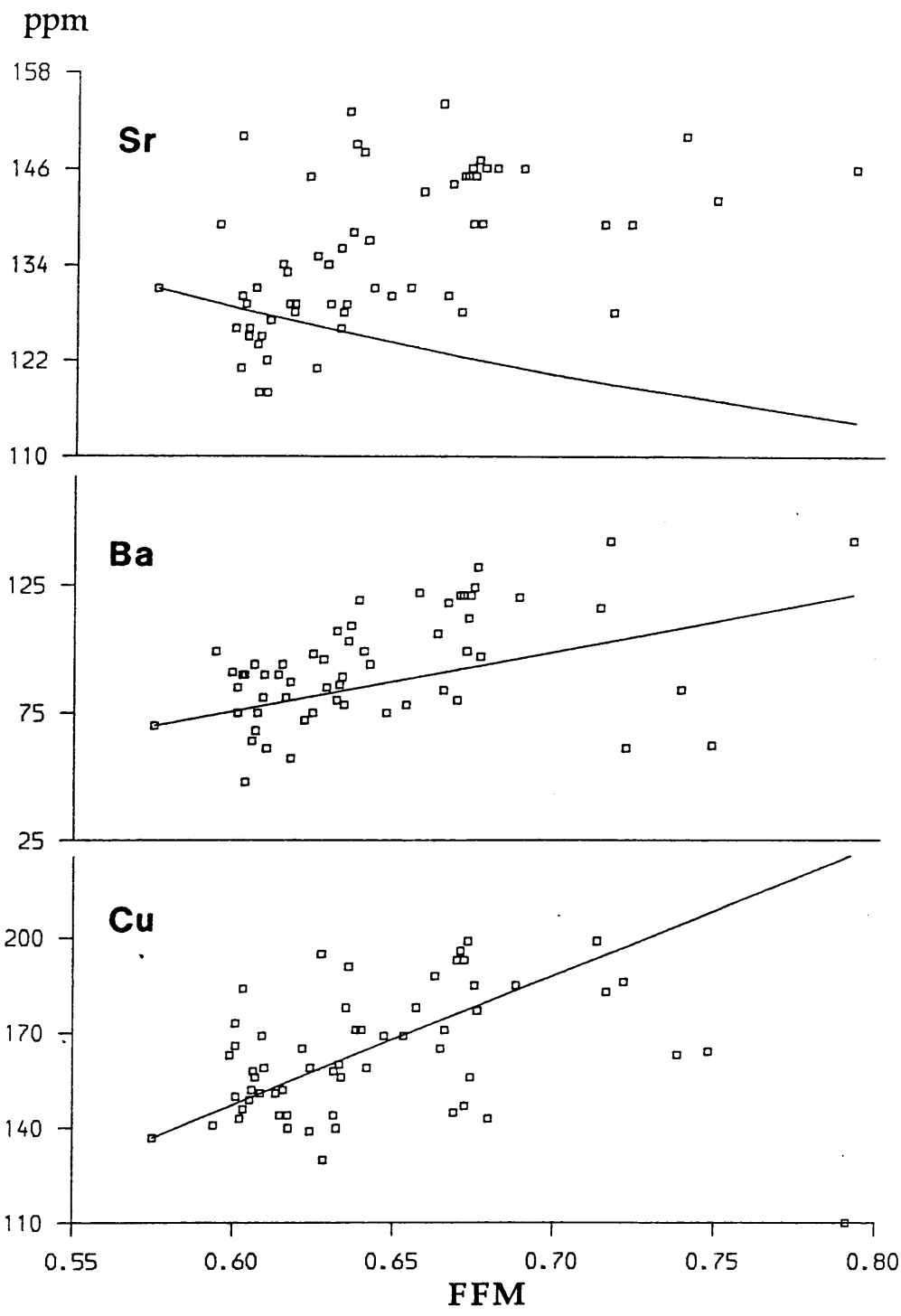

Fig. 1.38. Comparison of analysed cone-sheet data (▫) with that predicted from the crystal fractionation model. FFM = $FeO + Fe_2O_3 / FeO + Fe_2O_3 + MgO$.

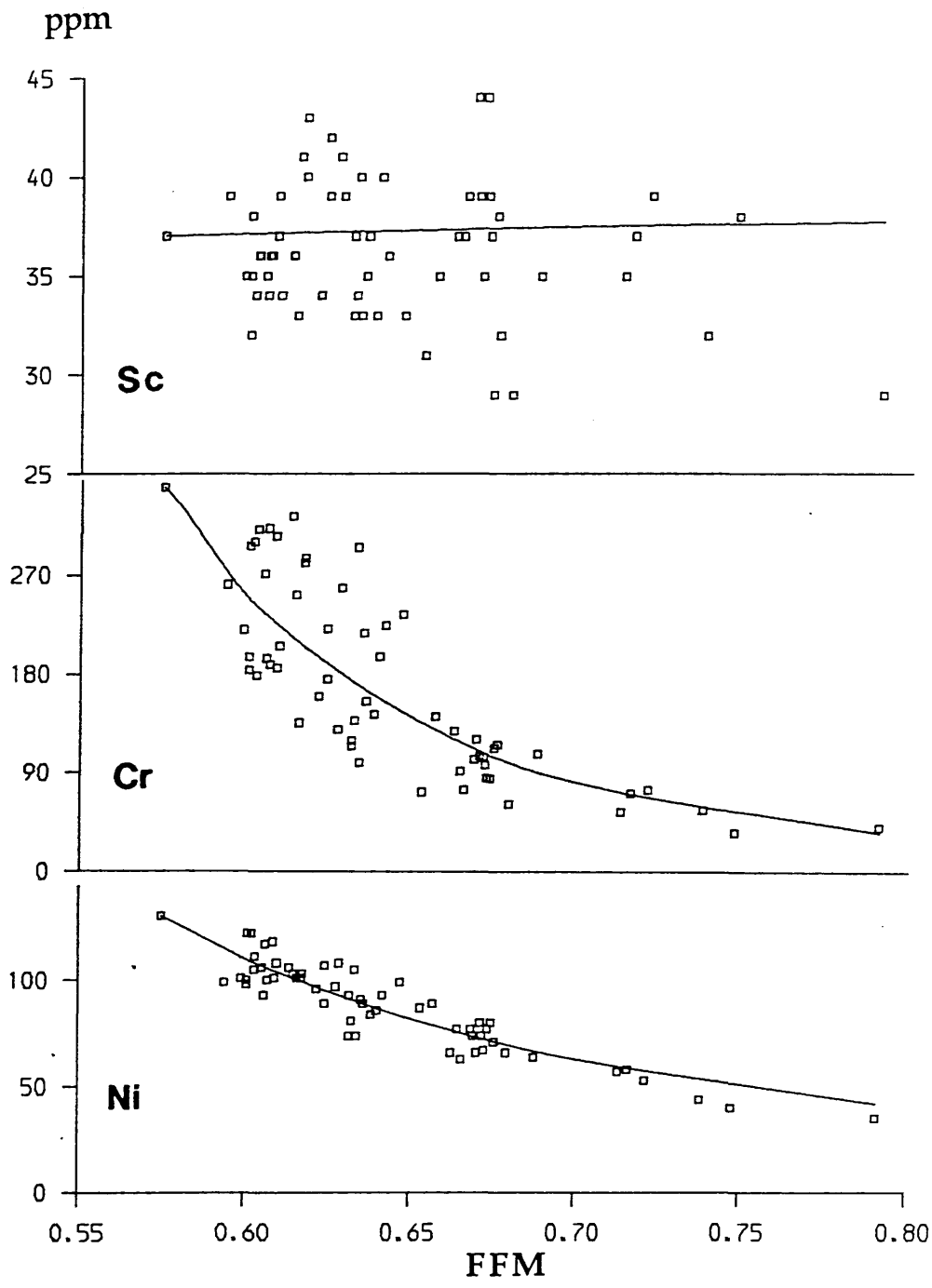

Fig. 1.38. Comparison of analysed cone-sheet data (▫) with that predicted from the crystal fractionation model. FFM = $FeO + Fe_2O_3 / FeO + Fe_2O_3 + MgO$.

not the case (Fig.1.27 e,c) and therefore it must be concluded that selective hydrothermal redistribution is the cause of the anomaly. Sc differentiation is practically insignificant, with concentrations of around 36ppm shown throughout the suite, however, considerable scatter exists with samples of similar FFM value displaying Sc concentrations of between 28 to 44ppm. The bulk distribution coefficient for Sc between a silicate melt and the gabbroic fractionating assemblage is close to unity and therefore the element shows no preference for either the liquid or the solid. Consequently, the fractionation trend is not constrained to the extent of that shown by elements having bulk distribution coefficients which depart significantly from unity. The incompatible elements Y, Zr and the REE (Ce, Eu, Gd & Yb chosen to represent the range of behaviour shown by the REE) display the behaviour of the second identified group. Predicted and actual trends are very well correlated throughout most of the differentiation trend, however, the two trends diverge for more evolved members of the suite, with actual concentrations more enriched than is called for by the model. The behaviour shown by the two groups is said to be decoupled: with respect to the major elements the trace elements require differing amounts of crystallization to explain their abundances. Amounts of crystallization necessary to explain the observed concentrations are dependent upon the bulk distribution coefficients (Table. 1.12); those elements which have high coefficients require less crystallization than those with lower coefficients.

For the Skye cone-sheets, the incompatible elements Y, Zr and the REE (D_b=0.104-.36) require 65-75% closed system fractional crystallization to explain their distribution, whilst the compatible elements Ni and Cr (D_b= 4.25 and 2.62, respectively) only require in the region of 40-50% crystallization. These values are correspondingly higher and lower than the 60% crystallization predicted by the least squares modelling of the major elements.

This type of behaviour is indicative of magmas derived from a fractionating open-system magma chamber undergoing periodic replenishment and tapping (O' Hara 1977; O' Hara and Mathews 1981). Periodically replenished, periodically tapped continuously fractionated (RTF) magma chambers have the ability to decouple trace elements on the basis of their distribution coefficients. In effect, the compatible elements are continuously

Element	C_o	C_l	D_B	F
Cr	350	41	4.25	.45
Ni	130	35	2.62	.44
V	235	408	.3228	.44
Zr	57	151	.145	.32
Y	21	52	.1040	.36
Eu	9.50	24.25	.3662	.25
Yb	8.36	23.36	.2552	.26
Gd	9.93	27.68	.2489	.26
Ce	8.99	26.27	.1197	.29

Table 1.12 Trace element concentrations of primitive and evolved samples with their bulk distribution coefficients and the amount of closed system fractionation crystallization necessary to explain the abundances.

C_o= Conecentration in primitive sample.

C_l= Concentration in evolved sample.

D_B=Bulk distribution coefficient.

F=amount of liquid remaining after crystallization.

being removed from the magma by crystallization whilst the excluded (incompatible) elements become concentrated within the melt. O' Hara and Mathews (1981) concluded that the composition of the magma residing in a chamber undergoing this process would approach a steady state provided that the amount and composition of the parental magma in each cycle was held constant, as was the ratio of the magma crystallizing to that escaping from the chamber. The concentration of an element in the steady state liquid is given by the equation (O' Hara and Mathews 1981):

$$C_l = C_o \frac{*\,(x+y)(1-x)^{D-1}}{1-(1-x-y)(1-x)^{D-1}}$$

Where C_l = concentration in the steady state liquid

C_o = concentration in parental magma

D = Bulk distribution coefficient

x = mass fraction of magma removed by fractionation

y = mass fraction of magma erupted

The number of cycles, where 1 cycle is the fractionation and eruption of a mass of the chamber followed by the introduction of more parental magma which subsequently mixes with the residual liquid in the chamber, required to produce the steady state composition is dependent upon the distribution coefficients of the element under consideration, and the parameters x and y. Cox (1988) has shown that when x, y and the mass (z) of parental magma, relative to the original size of the chamber added in each cycle, are held constant at values of 0.3, 0.2 and 1 respectively, the steady state liquid may be produced after only a limited number of cycles (Fig.1.39a). Furthermore Cox (1988) has explored the process when using the parameters randomized within given bounds to simulate natural processes more realistically (Fig.1.39b). Under these conditions a quasi-steady state situation is reached where after a number of cycles the concentration of elements within the liquid vary randomly about the steady state value.

Considering Fig.1.40, PAR is the path of Rayleigh crystal fractionation from the parent (P). S is the steady state liquid produced from the ideal fractionation curve. The discrepancy between the two curves AR and AS represents the decoupling described above, where the

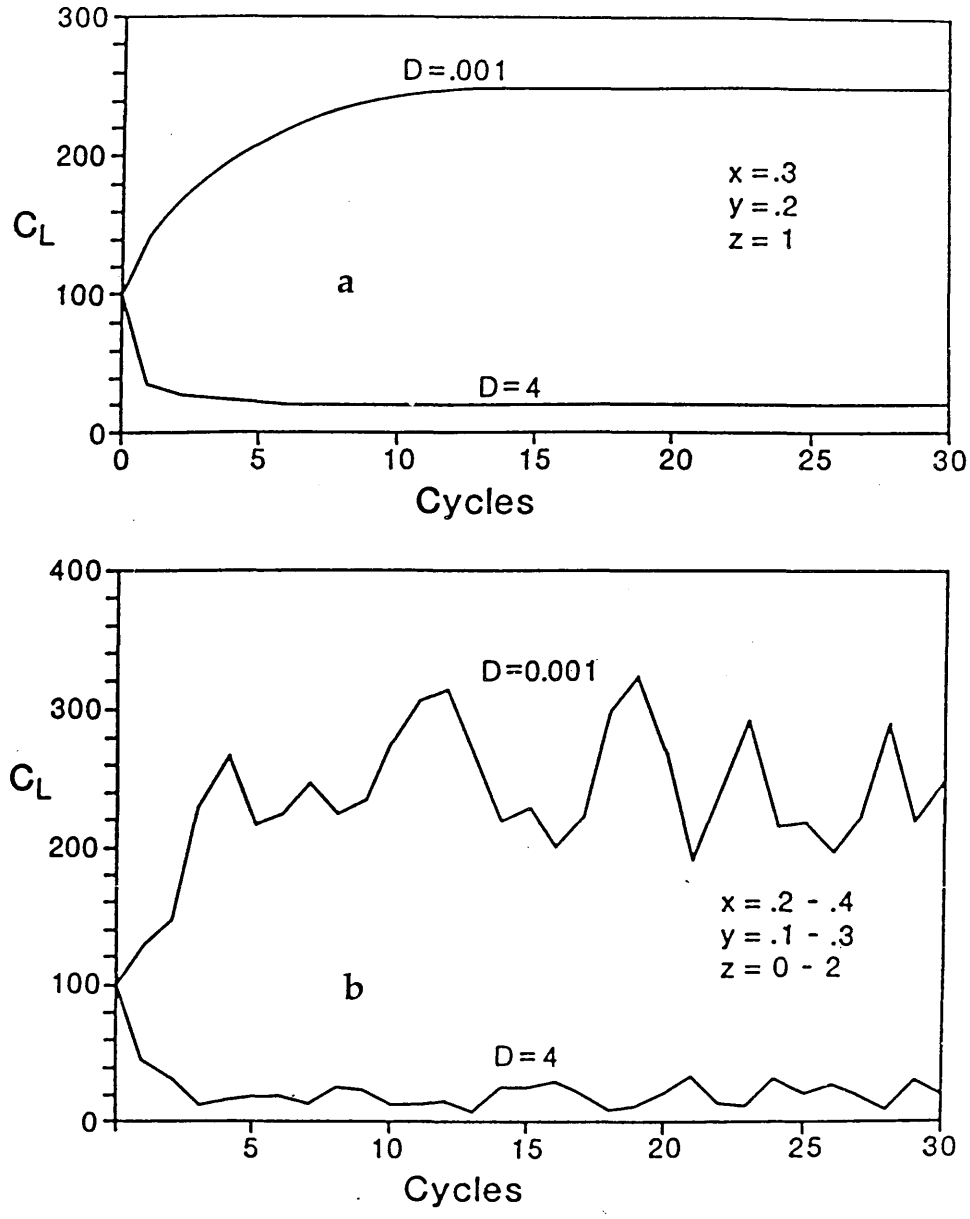

Fig. 1.39. Trace element concentrations plotted against number of cycles of mixing, fractionation and eruption for a highly incompatible element (D=0.001) and a compatible element (D=4) with a) constant input parameters and b) with parameters randomized within the limits shown.

C_l= concentration of element in the liquid

x= mass fraction of magma removed by fractionation in each cycle

y= mass fraction of magma removed by eruption in each cycle

z= mass fraction of magma relative to to original mass of magma added in each cycle. After Cox 1988.

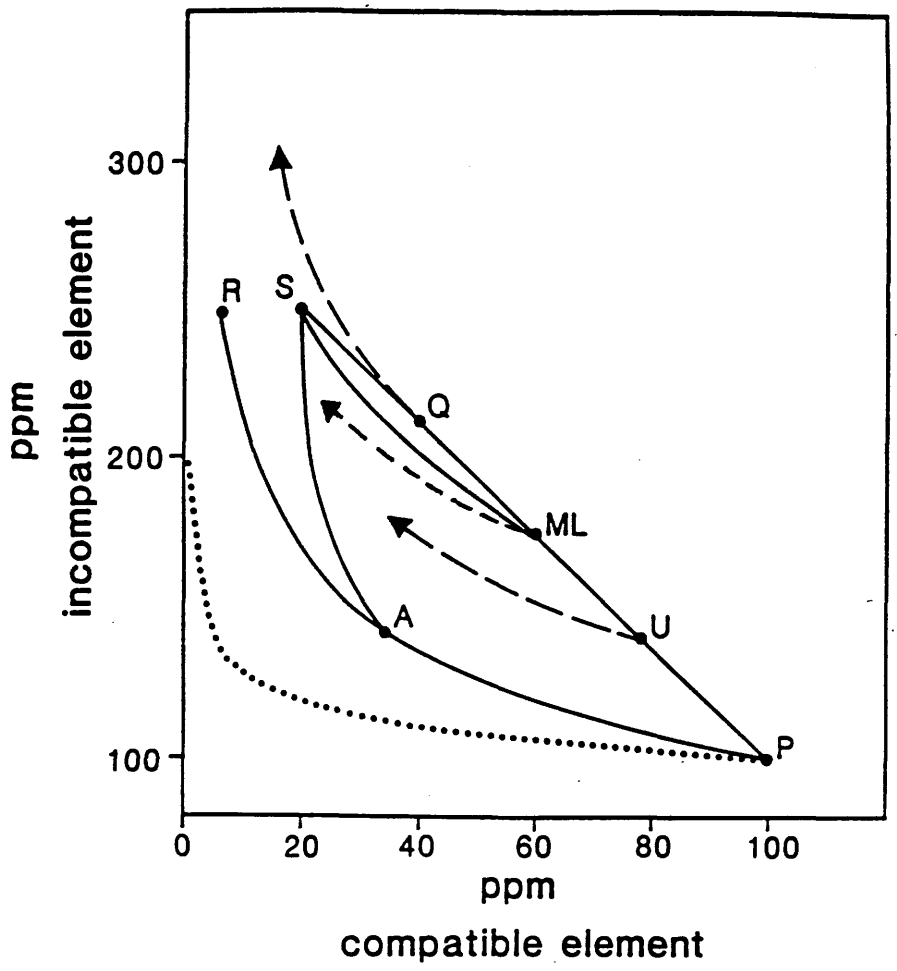

Fig. 1.40. Concentration of an incompatible element versus a compatible element to illustrate the process of decoupling and resultant scattering of data when plotted on a two element variation diagram. The parent magma is represented by point P and with closed system Rayleigh fractionation evolves along the curve PAR. With fractionation and eruption, the steady state liquid (S) is reached by path PAS. The derived steady state liquid may then mix with more parental material (P) to produce liquids plotting between S and P (ie. ML). Fractionation then takes the liquid back to S via the curved path ML-S. However, under randomized conditions, the resultant mixed magma may plot anywhere upon the line P-S depending on the mass of parental to steady state magma. With a large influx of parental magma, liquid composition U may be produced whilst a smaller input would result in liquid Q. Each of these will fractionate along the appropriate Rayleigh curve (broken lines with arrows) to form a variety of possible differentiates which in time could mix back towards P during replenishment to fractionate again, thus producing a considerable scatter of liquid compositions (after Cox 1988).

compatible element is less depleted than the incompatible one. If, however, replenishment of the chamber occurs then the resultant mixed magma will plot somewhere along the line SP (the exact position dependant on the ratio of parental to residual magma). Mixed magma MLwill then again approach the steady state composition along the curve ML-S, or if no further tapping or replenishment occurs, will follow the the Rayleigh fractionation curve (broken arrow). Thus, liquids are produced with differing ratios of incompatible to compatible elements. This explains another aspect of the decoupling of elements due to RTF processes in that poor correlations are observed on plots of elements with differing bulk distribution coefficients. If RTF chambers do operate then the assignment of parent-daughter status may not be meaningful. On major element plots the recognition of such parent-daughter pairs may be obvious. However, on consideration of the trace elements it may not be possible to correlate these with the parent-daughter pairs previously identified on the basis of the major elements, as the trace element abundances are derived from a combination of fractionation and mixing.

1.4.3 Petrogenesis

As the cone-sheets exhibit geochemical characteristics which suggest that they crystallized from parental magmas of the Preshal Mhor magma type,but which precludes any of them from representing magmas of a primary status, only a brief discussion of the petrogenesis of the cone-sheets relative to the other recognised magma types of Skye will be presented.

Thompson et al. (1972) demonstrated that the majority of the preserved lavas were compositionally transitional in nature, ranging from Hy to Ne normative, and that the former contained less TiO_2 and P_2O_5 but more K_2O than the latter. These they termed the Skye Main Lava Series (SMLS); whilst the remainder were identified as low alkali tholeiitic basalts. Due to the SMLS basalts straddling the low pressure thermal divide near the critical plane of si-saturation of Yoder & Tilley (1962), the authors concluded that the variation within the series was caused by high pressure upper mantle processes and that due to their unusual incompatible element patterns, a K-rich mantle phase, tentatively identified as phlogopite, was involved in their genesis.

Subsequently, Mattey et al. (1977) identified that the low alkali tholeiites accounted for much of the hypabyssal suite occurring on Skye and these they termed the Preshal Mhor type (PM) whilst also identifying a suite of some 30 samples whose characteristics precluded them from either the SMLS or the PM types and consequently proposed that these crystallized from a third magma type which they named the Fairy Bridge (FB) type.

Whilst the SMLS and PM magma types were well defined in compositional space, the distinction between these two types and the FB type was less clear, as the latter possesses major element characteristics similar to the SMLS whilst their incompatible element concentrations were intermediate between the SMLS and the PM tholeiites. Mattey et al. (1977) discounted the possibilty of the FB type as being a low pressure derivative of the PM type on the basis of the mostly flat REE patterns displayed by the suite which could not be generated by crystal-liquid processes involving olivine and plagioclase (the phenocryst assemblage observed within the SMLS and PM basalts). Therefore, Mattey (1980) following Thompson et al. (1972,) and Thompson (1974), related the three magma types to a single progressive melting event which was initiated by partial melting of an incompatible-element depleted spinel lherzolite source containing olivine, plagioclase, orthopyroxene, up to 20% clinopyroxene, spinel and minor garnet and a K-rich phase (either phlogopite or an amphibole, to explain the rising K/Na ratio in Hy normative relative to Ne normative SMLS basalts) at c.60km depth. Initial melting (c.3-5%) of this source produced the Ne normative representatives of the SMLS whilst a further 5-7% melting led to the development of the Hy normative basalts. Following this and with further melting up to 12-14%, the FB magma type was generated. The melting episode culminated with c.18-20% melting of the source during which time all the Ca-rich pyroxene was consumed, leaving a harzburgite residuum and producing the PM magma type, which is believed to have been associated with the emplacement of the Cuillin Igneous Complex (Mattey et al. 1977).

Within this framework, the Skye cone-sheets are believed to preserve liquid compositions of evolved differentiation products of the PM Magma Type. It is possible that the liquids were present as a residual melt which was intruded after the formation of the central complex.

1.5 Intrusive Tholeiites

1.5.1 Introduction

Harker (1904), interpreted a series of fine-grained basaltic sheets occurring within the gabbros of the western Cuillin Hills as being remnants of lavas. He proposed that these lavas had foundered into, and consequently had been almost completely fused by, the magma which crystallized to form the gabbros of the central complex. Subsequently, Hutchison (1966), supported the view of Bailey (1952) that these rocks had formed from the normal crystallization of a tholeiitic magma. On remapping the area, Hutchison (1966) was able to divide the sheets into an Outer Complex and a Main Ridge Complex (Fig.1.41). Members of the Outer Complex are exposed predominantly within Coire na Banachdich and on the spurs of Sgurr nan Gobhar (630m.O.D.) and Sgurr Dearg (986m.O.D.) and are confined to the outer unlayered gabbros. Further, but poorly exposed, examples occur on the low grassy slopes below Coire na Banachdich (Fig.1.41). The Main Ridge Complex, as the name implies, is distributed along and on the eastern (concave) side of the main Cuillin ridge and is emplaced into units of the Outer Unlayered Series.

1.5.2 Field Relationships

Samples of the intrusive tholeiites were collected and analysed from both the Outer and Main Ridge complexes. In addition, further examples were observed distributed along the main ridge in the southern Cuillin Hills (Map 1) and a comprehensive suite was collected and analysed. These latter sheets, although occurring along the main ridge, have been emplaced into the outer unlayered gabbro (Gars-bheinn Gabbro) and therefore contrary to their distribution should, if somewhat pedantically, be classified as members of the Outer Complex.

The sheets generally have irregular contacts with the country rock and where it is possible to determine, are sub-horizontal, or dip eastwards at angles up to c.50^{O}. In one case (Fig.1.42), microscopic examination of a sample (IT02) suggests that for this sheet the contacts may be tectonic rather than intrusive, for along the contact with the Outer Layered Allivalites a thin band of pseudotachylite, containing angular fragments of feldspar and

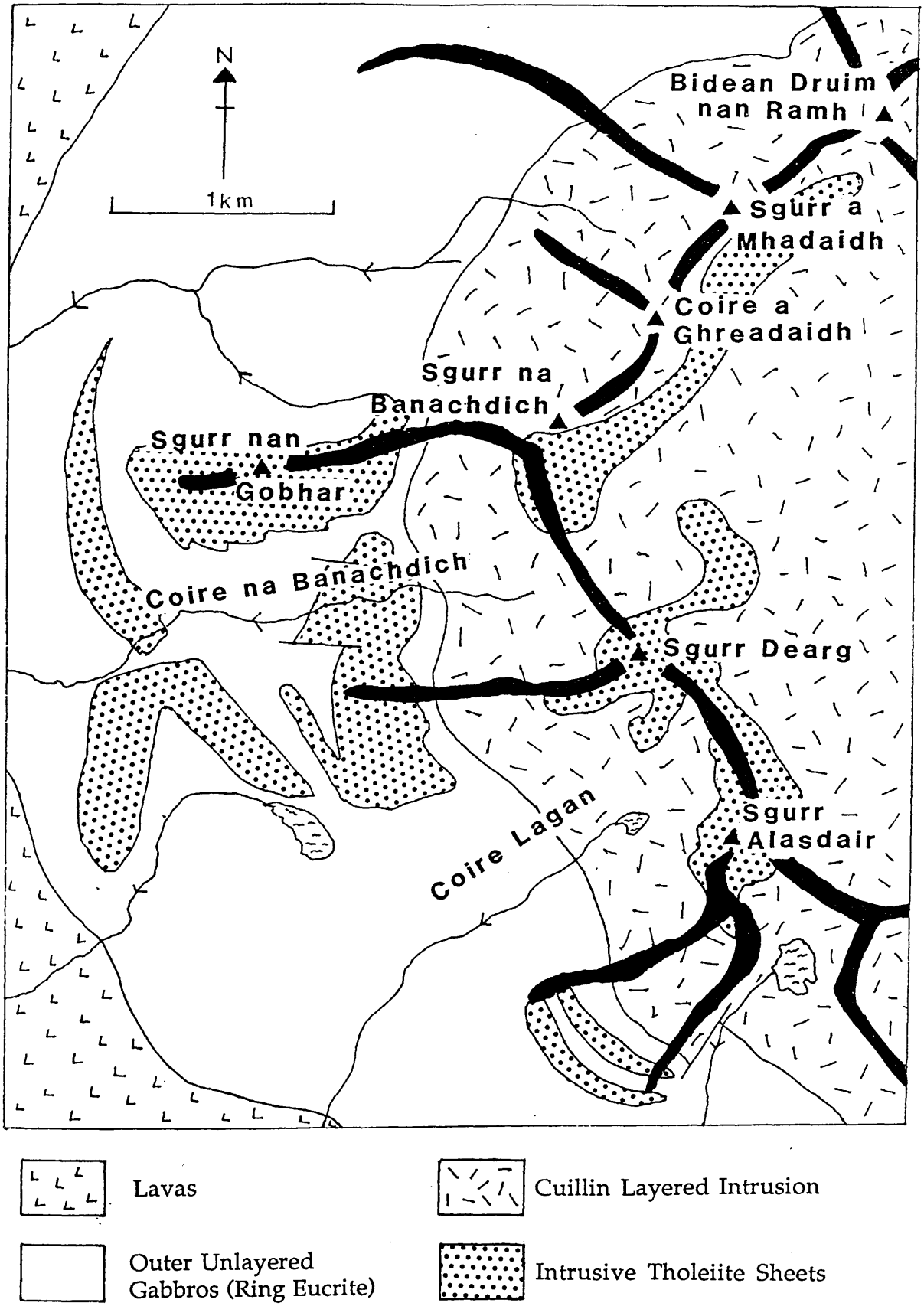

Fig.1.41. Distribution of Tholeiite sheets within the western Black Cuillin of Skye.

Fig.1.42. Contact between an intrusive tholeiite sheet (below) and unlayered gabbro. Many of the contacts of the sheets are believed to be intrusive, however, comminutation of the minerals within this sheet adjacent to the upper contact and the occasional vein of pseudotachilyte suggest this contact to be tectonic [G.R.4337 2259]. Crossed polars.

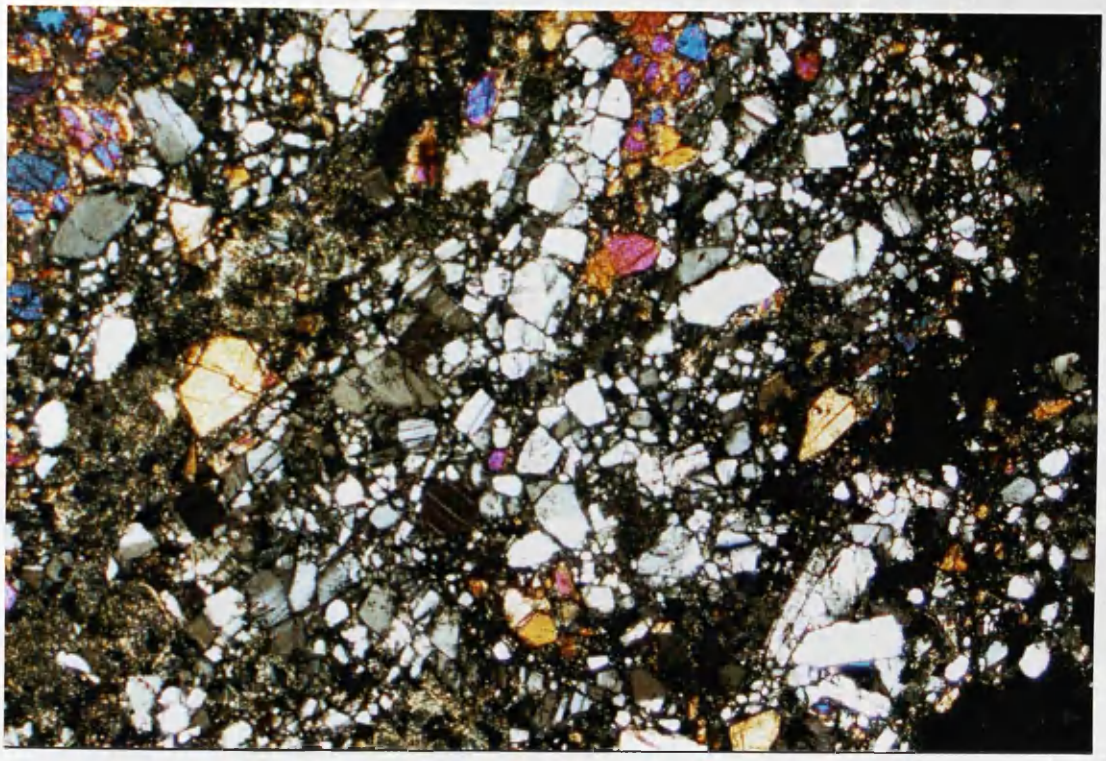

Fig.1.43. Angular fragments of feldspar and clinopyroxene within an intrusive tholeiite sheet adjacent to the contact with the unlayered gabbro. Field of view c.3 x 2mm. Crossed polars. Sample IT02.

pyroxene, is developed (Fig.1.43b), with comminution of the mineral grains increasing towards the contact. Individual sheets range in thickness from c.1m. to several metres, although the thicker sheets may represent coalesced thinner sheets, as chilled contacts are not readily observed and in some cases coalescing and anastamosing geometries may be readily demonstrated. In the field, the sheets may easily be identified as they are generally finer grained than their host rocks and weather with a grey-green coloration, although the finer grained examples are considerably darker. The majority of the sheets also have a fractured blocky appearence due the numerous thin secondary hydrothermal (c1mm.) veins which criss-cross typical exposures. It is probable that these veins, composed principally of quartz, calcite, chlorite and epidote are responsible for the severe alteration seen in many of the sheets. Amygdales of quartz, chorite and hydrous silicates are common, rendering it neccessary to choose samples for analysis with great care.

1.5.3 Petrography and mineral chemistry

In thin section the alteration of the intrusive tholeiites suggested by field observations is confirmed with the majority of specimens displaying varying degrees of replacement of the primary mineralogy. Olivine, where present, is generally completely pseudomorphed by serpentine, whilst the mesostasis of all samples has been altered to chlorite. In those specimens displaying a high degree of alteration, chlorite along with a little fibrous amphibole partly replaces pyroxene whilst the plagioclase may show the development of sericite and/or epidote. Amygdales are common and are principally of chlorite, however, quartz and hydrated silicate occur. Quartz also commonly occurs as an interstitial phase within the groundmass and is not restricted to those specimens lacking olivine. Frequently quartz crystals unconnected in the plane of a thin section are in optical continuity, suggesting that the quartz was introduced at a later stage.

A primary ophitic texture is preserved in most specimens, although in the finer grained varieties the texture is granular. All sheets are porphyritic with resect to olivine, clinopyroxene and feldspar in the approximate proportions .1:.6:.3, the phenocrysts usually occuring as aggregates in a glomeroporphyritic texture (Fig.1.44). Occasional needles of apatite are to be found occurring within the feldspar.

Fig.1.44. Glomeroporphyritic cluster of plagioclase (An_{75}) laths and clinopyroxene within granular groundmass of plagioclase (An_{54}), clinopyroxene and magnetite of an intrusive tholeiite sheet. Field of view c.3 x 2mm. Crossed polars. Sample IT06.

1.5.3.1 Pyroxene

As in the cone-sheets (Section 1.3) only a single Ca-rich pyroxene has been observed. It is pale-brown, is often schillerized, and typically ophitically encloses plagioclase laths. Equant subhedral-euhedral phenocrysts of the augite occur principally within the glomeroporphyritic aggregates of feldspar where they may attain sizes up to 0.75mm. Representative electron probe analyses of the pyroxenes are presented in Table 1.13 and are plotted in the conventional Di-Hd-En-Fs quadralateral in Fig.1.45.

1.5.3.2 Feldspar

Groundmass feldspar occurs as subhedral laths showing polysynthetic twinning and normal growth zoning with cores of An_{60-50} and rims of An_{50-40}. Occasionally a crude trachytic texture is developed, with tabular/accicular feldspar showing a preferential alignment. Euhedral-subhedral phenocrysts of plagioclase occur in all samples analysed, frequently as glomeroporphyritic aggregates. Individual phenocrysts range in size from approximatly 0.3 to 1.5mm. Two populations of phenocrysts have been identified on the basis of zoning, determined by electron probe analysis. Those phenocrysts having core compositions less than An_{58} display normal zoning down to $An_{52-48,}$ whilst those with core compositions greater than An_{70} display normal zoning down to around this value, where upon a reverse zone up to An_{70} exists. Following the reversal, normal zoning again follows down to the rim. Fig.1.46 illustrates the core-rim relationships of selected phenocrysts showing this feature and Table 1.14 lists selected electron probe analyses.

1.5.4 Major element whole rock geochemistry

Table 1.15 lists representative analyses of members of the Intrusive Tholeiite sheets whilst Fig.1.47 illustrates their tholeiitic nature in a total alkali-silica plot. Fig.1.48 show that silica saturation ranges from c.2% to c.18%. Similar to the Skye cone-sheets, the tholeiite sheets range from olivine to quartz tholeiites (Fig.1.49) and plot within the region of the ol-pl-cpx cotectic on a corresponding normative diagram (Fig.1.50) (Cox et al. 1979). Major element variations are shown in Fig.1.51, plotted against $FeO+Fe_2O_3$ / $FeO+Fe_2O_3+MgO$ (FFM) as an index of fractionation and to facilitate direct comparison with the suite of cone-sheets.

Sample	IT09/2	IT09/3	IT06/2	IT15/1	IT08/1	IT16/3
SiO_2	51.36	51.57	51.81	49.67	51.83	48.73
Al_2O_3	2.92	3.12	1.81	3.55	3.16	3.96
TiO_2	0.54	0.54	0.46	1.24	0.61	0.95
FeO	5.77	5.21	8.26	7.91	7.77	9.30
Fe_2O_3	1.29	1.95	1.79	3.75	0.77	3.72
Cr_2O_3	0.59	0.64	0.04	0.13	0.12	0.01
MnO	0.18	0.17	0.28	0.29	0.22	0.29
Na_2O	0.31	0.57	0.22	0.62	0.24	0.43
MgO	16.13	16.47	16.33	14.47	15.33	12.86
CaO	20.09	20.08	18.48	18.44	18.69	19.20
Total	99.18	100.32	99.62	100.07	101.84	99.45
FeO^*	6.93	6.87	9.86	11.26	8.44	12.66
			Atomic % (Mn included with Fe)			
Ca	41.89	41.53	37.78	38.91	38.95	40.88
Mg	46.81	47.37	46.47	42.52	47.33	38.08
Fe	11.30	11.11	15.75	18.57	13.72	21.04
			Formula (on the basis of 6 oxygens)			
Si	1.911	1.904	1.935	1.872	1.914	1.864
Al	.089	.096	.065	.128	.086	.136
Z						
Al	.039	.040	.021	0.30	.053	.042
Mg	.895	.898	.909	.813	.904	.733
Fe^{+++}	.036	.054	.050	.105	.241	.295
Fe^{++}	.179	.160	.257	.247	.021	.106
Na	.022	.025	.016	.045	.017	.032
Cr	.017	.016	.001	.004	.003	-
Ti	.015	.015	.013	.035	.017	.027
Mn	.006	.005	.009	.009	.007	.009
Ca	.801	.804	.739	.744	.744	.787
M	2.010	2.017	2.015	2.032	2.007	2.031
% Al in Z	4.45	4.80	3.25	6.40	4.30	6.80

Table 1.13 Representative analyses of pyroxenes of the Intrusive Tholeiite suite. Total iron was determined as FeO^* and subsequently partitioned between ferrous and ferric iron by the method of Finger (1972)

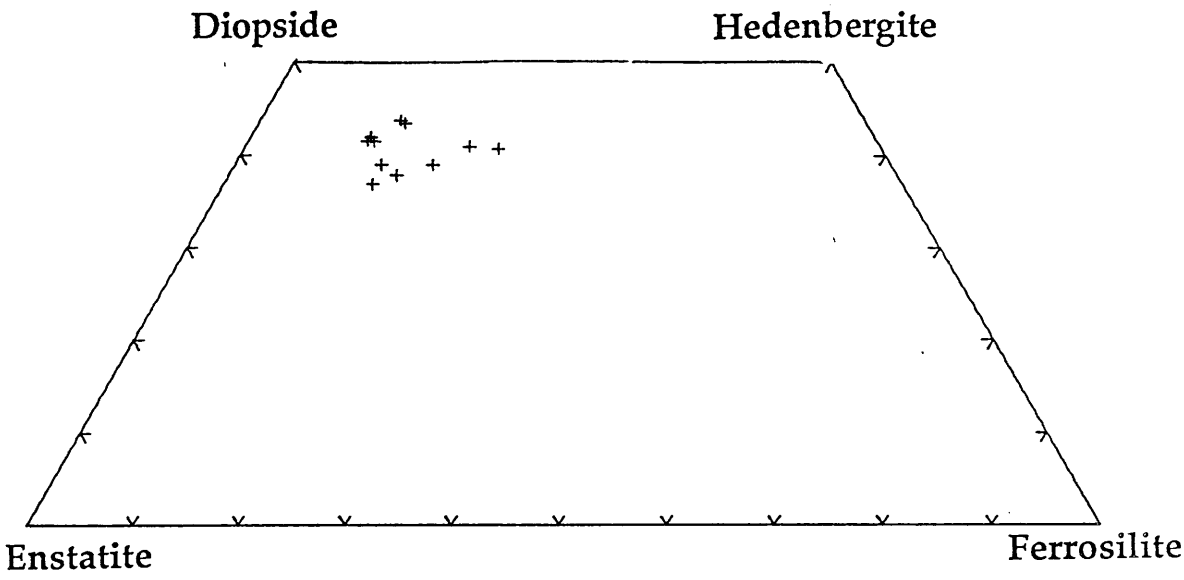

Fig.1.45. Clinopyroxenes from the Intrusive Tholeiite suite plotted in the Di-Hd-En-Fs quadrilateral.

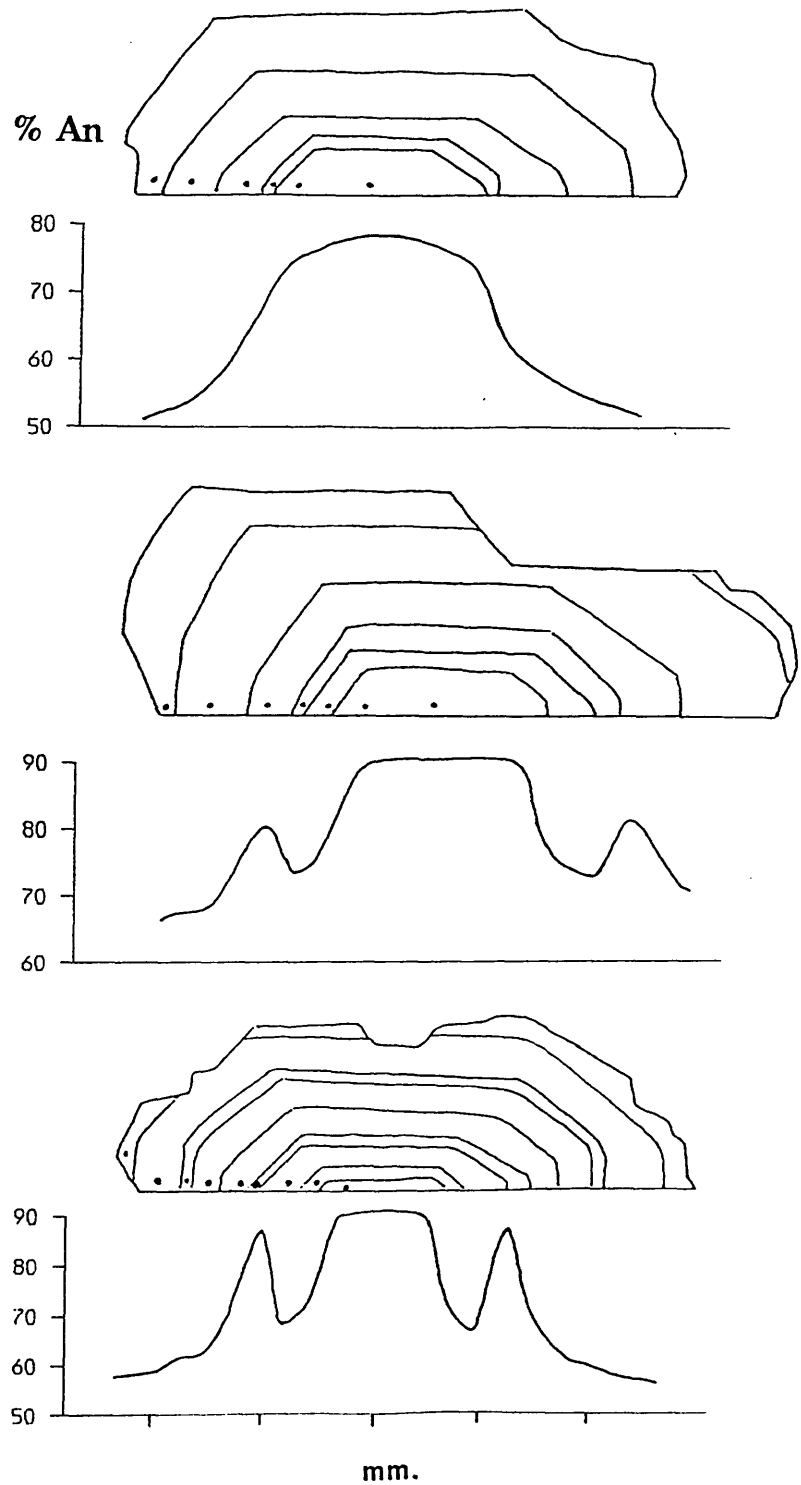

Fig.1.46. Anorthite content of plagioclase phenocrysts from the Intrusive Tholeiite sheets as determined by electron probe micro-analyser.

Sample	IT10/1 G	IT15/2 G	IT08/1 G	IT10/1 PC	IT10/1 PR	IT09/1 PC	IT09/1 PR	IT10/A PR	IT10/B PC
SiO_2	54.15	52.93	54.61	49.89	54.15	49.25	54.31	51.65	47.40
Al_2O_3	28.15	26.36	27.69	30.95	28.15	31.59	27.74	29.39	32.27
K_2O	0.14	0.26	0.24	0.10	0.14	0.14	0.38	0.16	0.09
Na_2O	5.08	6.43	5.07	2.89	5.08	2.73	5.06	4.03	2.28
CaO	11.31	8.99	11.14	14.94	11.31	15.09	11.04	13.06	16.05
MgO	0.19	0.04	0.15	0.14	0.19	0.21	0.17	0.07	0.09
BaO	-	-	-	-	-	-	-	-	-
FeO*	0.85	0.53	0.91	0.62	0.85	0.62	1.01	0.72	0.65
Total	99.87	99.56	99.81	100.61	99.81	99.63	99.71	99.08	98.83
				Atomic %					
An	54.71	42.93	54.09	73.67	54.71	74.70	53.45	63.57	79.13
Ab	44.49	55.59	44.51	25.76	44.49	24.40	44.34	35.54	20.33
Or	0.80	1.48	1.40	0.58	0.08	0.85	2.21	0.89	0.54
				Formula (on the basis of 32 oxygens)					
Si	9.834	10.287	9.919	9.170	9.834	9.053	9.889	9.500	8.823
Al	6.026	5.624	5.930	6.705	6.026	6.845	5.995	6.372	7.082
K	.032	.060	.056	.023	.032	.034	.089	.036	.022
Na	1.790	2.257	1.785	1.029	1.79	.972	1.787	1.439	.822
Ca	2.201	1.743	2.169	2.943	2.201	2.971	2.154	2.574	3.200
Mg	.052	.011	.040	.037	.052	.057	.045	.019	.024
Ba	-	-	-	-	-	-	-	-	-
Fe	.129	.080	.138	.095	.129	.095	.153	.111	.085
Total	20.064	20.062	20.037	20.002	20.064	20.027	20.112	20.051	20.058

Table 1.14 Representative analyses of feldspars from the Intrusive Tholeiite suite. G=groundmass crystal, PC= phenocryst core, PR= phenocryst rim.

Sample	IT002	IT003	IT006	IT010	IT015
SiO_2	48.96	52.82	46.31	50.64	51.00
Al_2O_3	15.44	13.96	15.21	14.26	12.88
TiO_2	0.72	1.06	0.88	0.98	2.26
Fe_2O_3	1.39	1.63	1.54	1.53	2.10
FeO	9.24	10.88	10.28	10.22	13.91
MgO	7.99	5.74	9.14	7.34	4.26
CaO	11.89	9.70	12.68	11.57	8.48
Na_2O	2.26	2.77	1.49	2.28	3.09
K_2O	0.31	0.58	0.54	0.38	1.35
MnO	0.14	0.21	0.20	0.21	0.23
P_2O_5	0.06	0.10	0.07	0.09	0.33
H_2O^+	1.65	0.84	1.89	0.25	0.21
Total	100.05	100.29	100.23	99.75	100.10
Trace elements (ppm)					
Ba	78	244	82	257	623
Cr	296	45	387	245	71
Cu	101	145	137	114	237
La	0	19	0	11	33
Ni	93	50	143	73	26
Nb	2	2	2	3	7
Pb	4	8	4	10	9
Rb	13	14	15	15	30
Sc	38	35	33	41	38
Sr	134	215	107	234	281
Th	0	4	4	3	5
U	0	0	2	0	0
V	193	265	223	241	393
Y	19	29	21	24	50
Zn	58	73	61	85	110
Zr	55	96	53	76	225
Y/Zr	0.35	0.30	0.40	0.32	0.22

Table 1.15 Representative analyses of members of the Intrusive Tholeiite suite. All iron was determined as Fe_2O_3 and subsequently partitioned to give $Fe_2O_3/FeO = 0.15$.

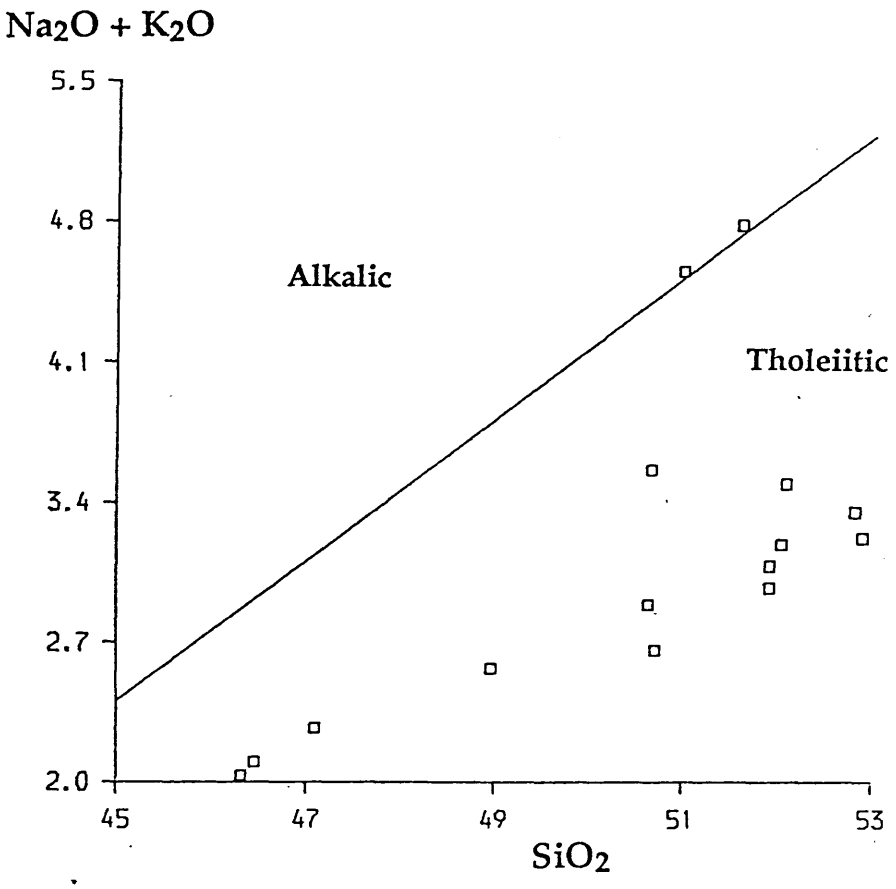

Fig. 1.47. Total alkalis v SiO_2 for Intrusive Tholeiites. Fields for alkalic and tholeiitic basalts are those defined by Macdonald and Katsura (1964).

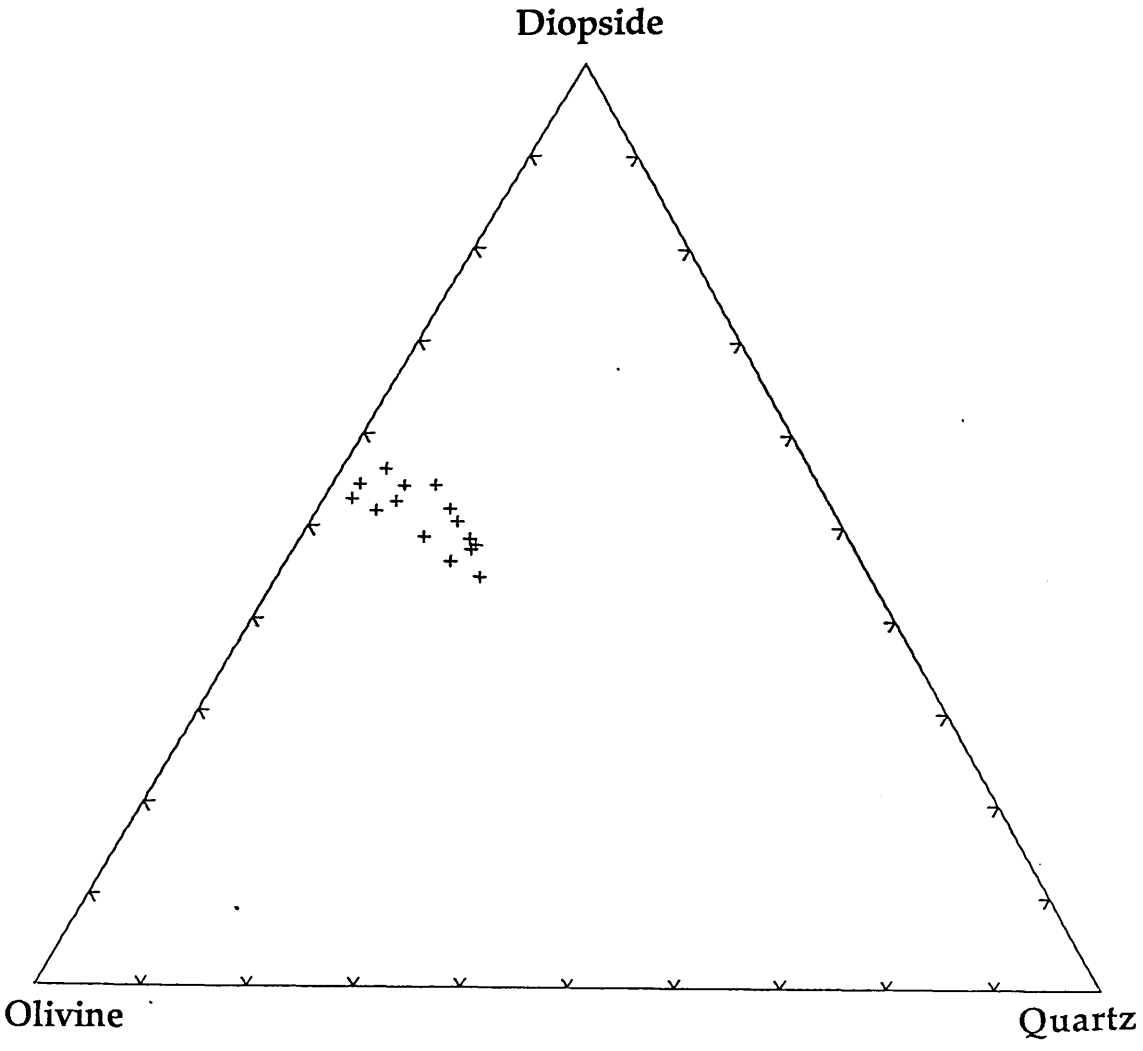

Fig. 1.48. Plot of Ol-Di-Qtz to illustrate the silica saturation of Intrusive Tholeiites. (Quartz is normative quartz + quartz made over from recasting hypersthene to olivine + quartz).

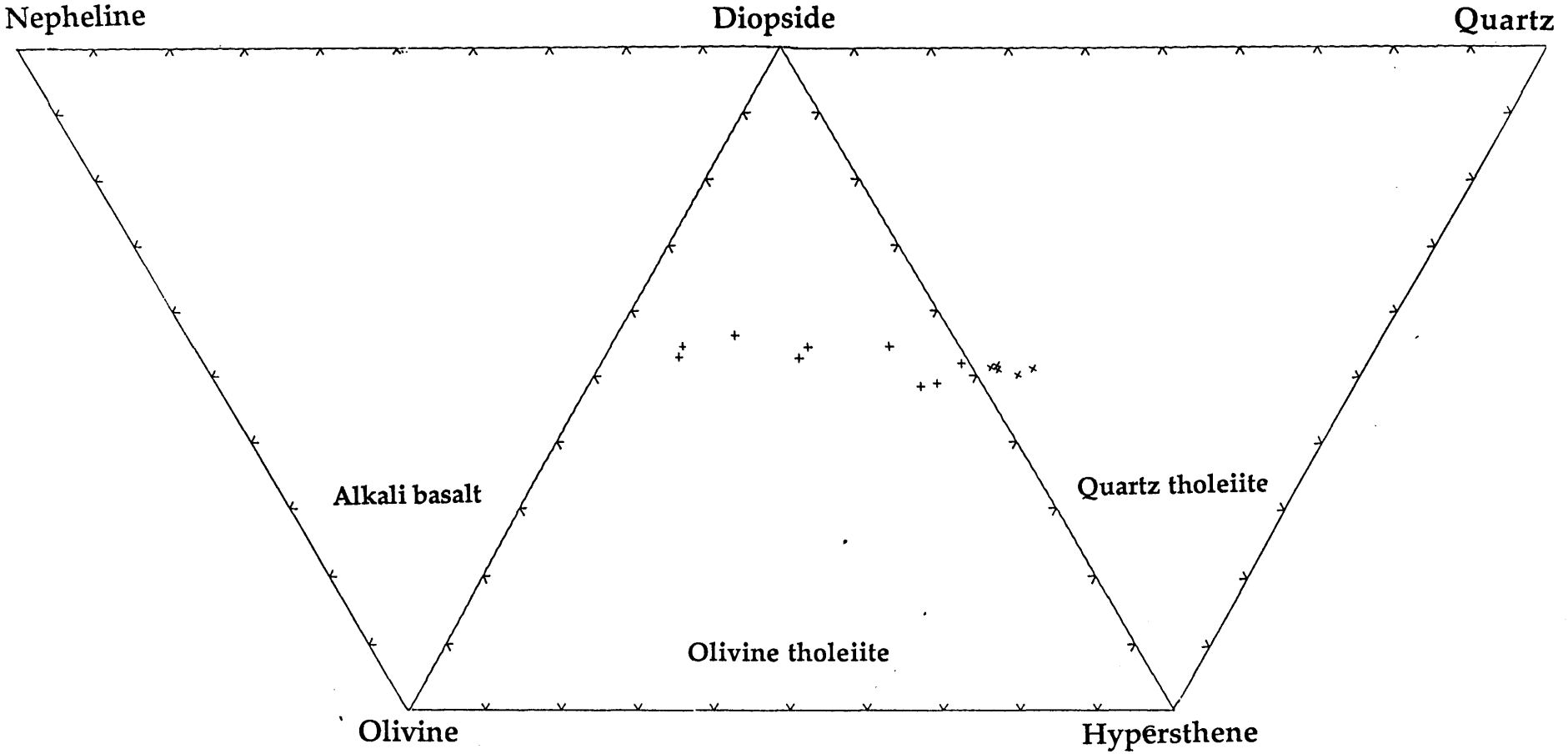

Fig.1.49. Variation of the Intrusive Tholeiites within the normative basalt tetrahedron.

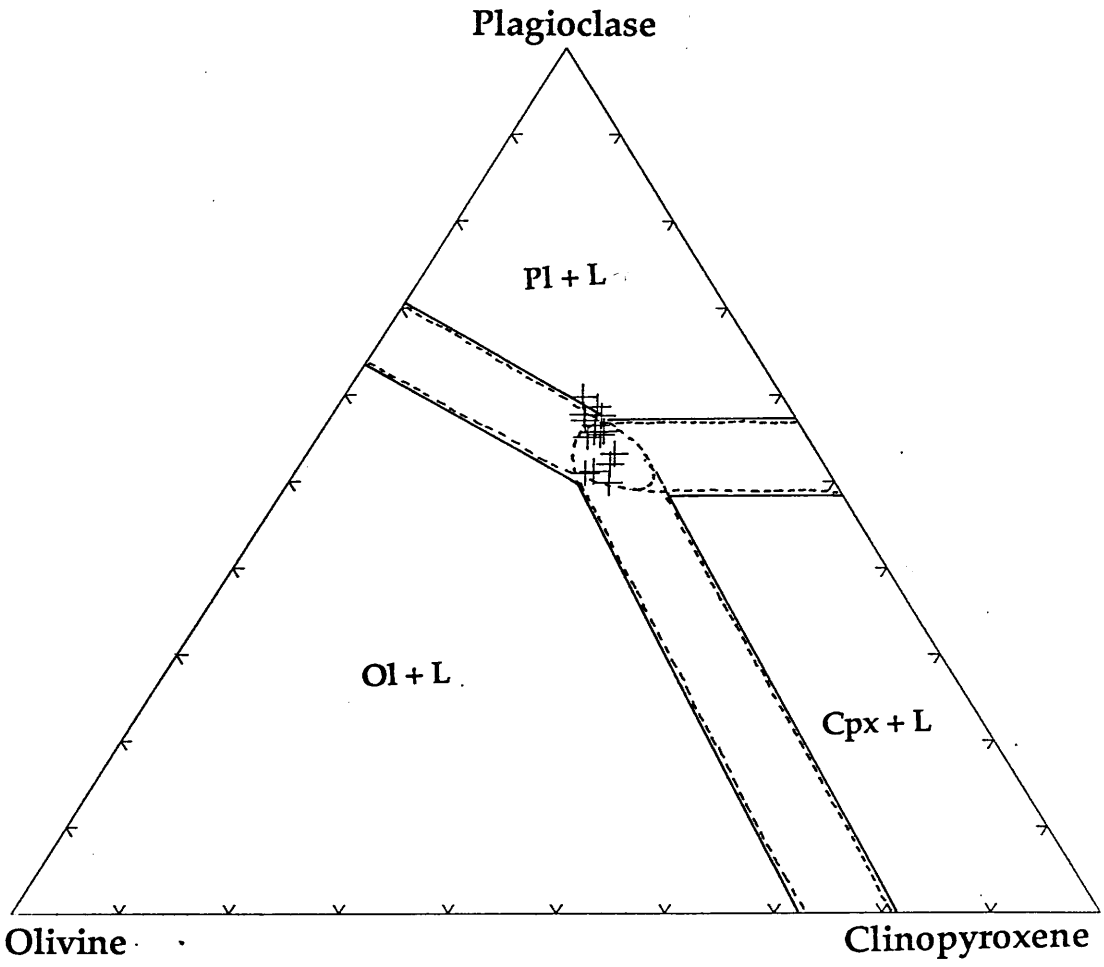

Fig.1.50. Variation of the Intrusive Tholeiite sheets within the normative basalt system ol-pl-cpx, projected from silica. (≡≡) = area in which basalts can be expected to equilibrate with ol + pl, pl + cpx and ol + cpx. (<>) = area in which plotted compositions would be expected to show cotectic behaviour with respect to ol + pl + cpx (after Cox et al, 1979).

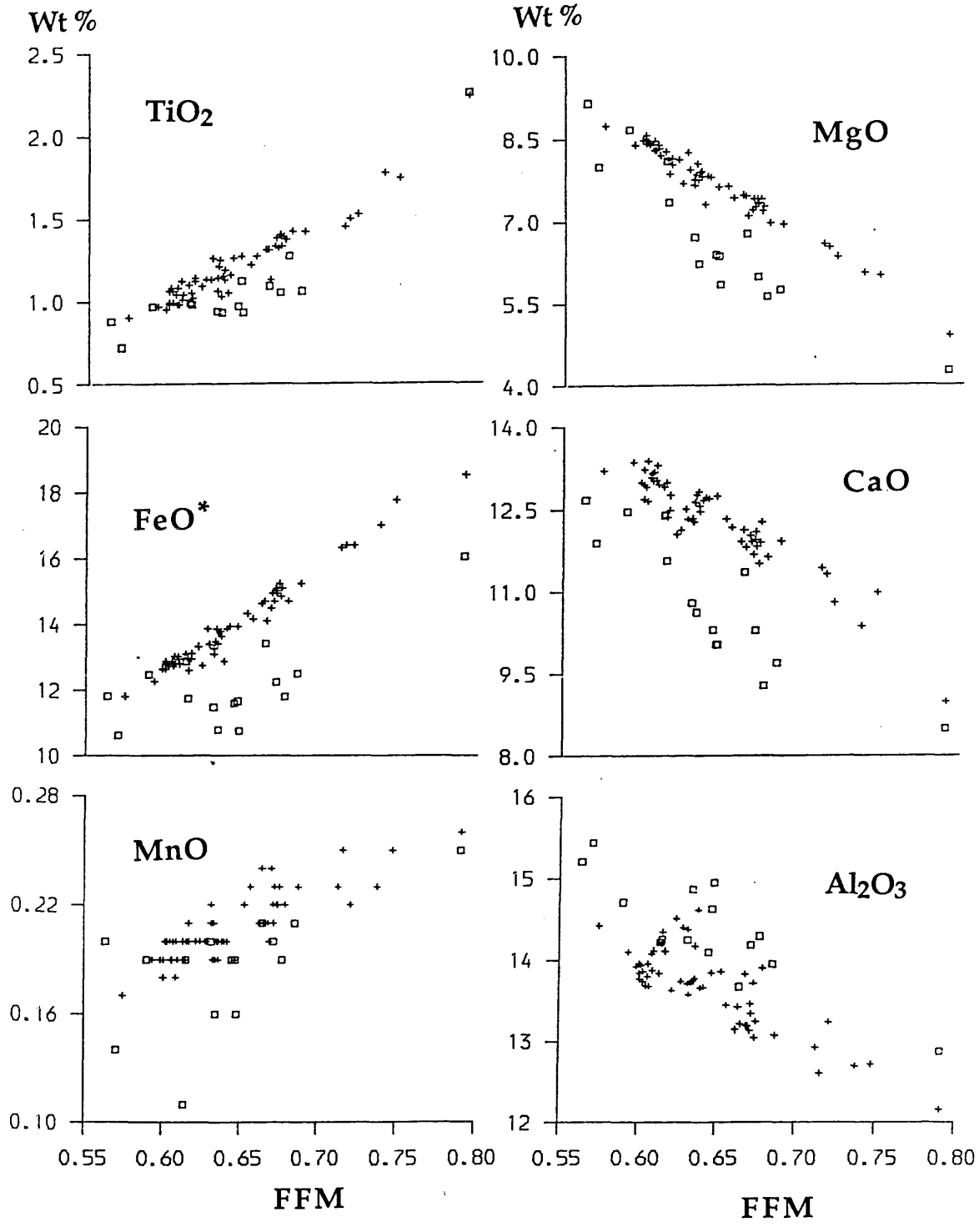

Fig. 1.51. Major element comparison of Intrusive Tholeiites (▫) and cone-sheets (+). FFM = $FeO + Fe_2O_3 / (FeO + Fe_2O_3 + MgO)$. $FeO^* = FeO + Fe_2O_3$.

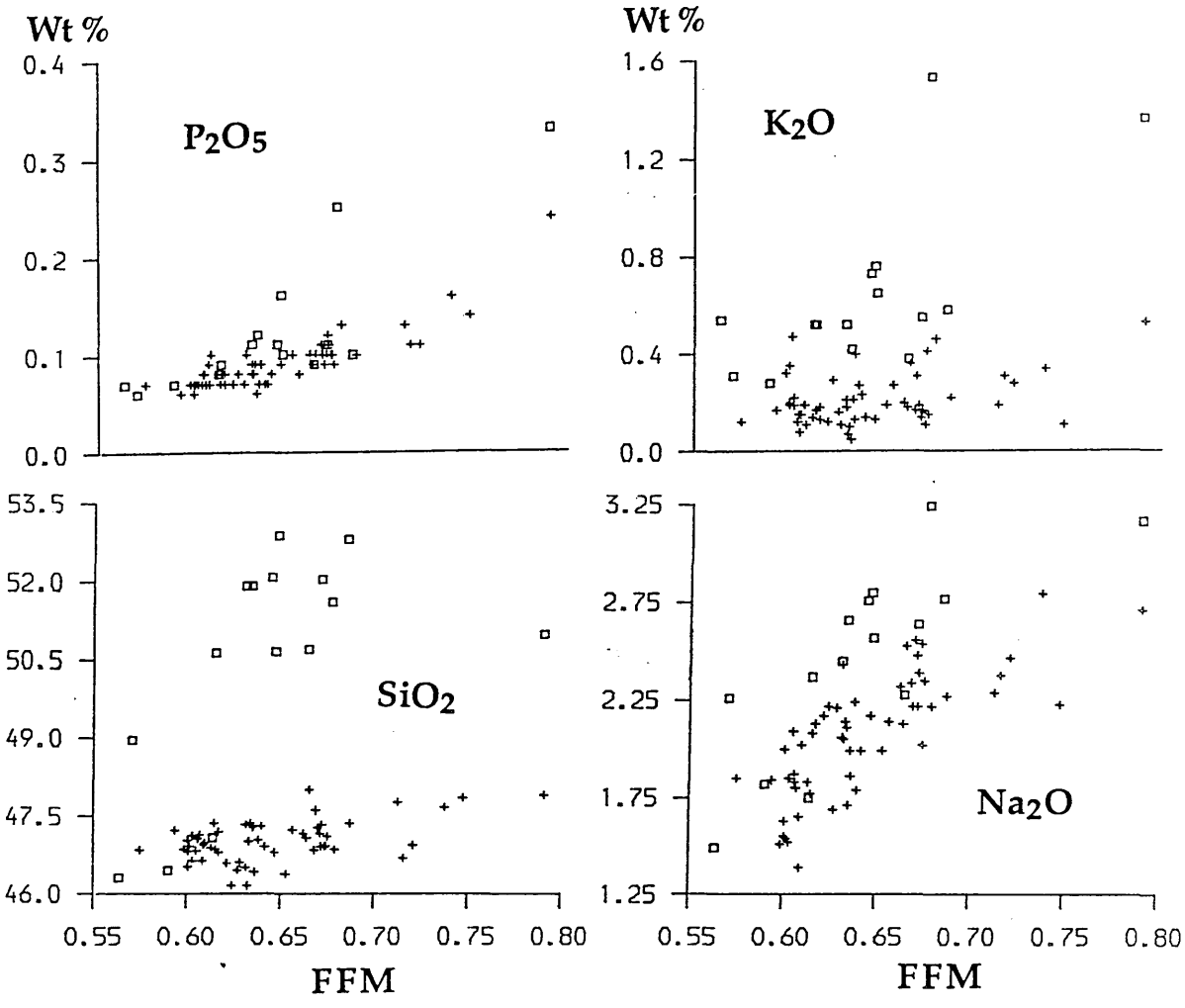

Fig. 1.51. Major element comparison of Intrusive Tholeiites (□) and cone-sheets (+). FFM = $FeO + Fe_2O_3 / (FeO + Fe_2O_3 + MgO)$.

The most primitive sample analysed has an FFM value of 0.5639, whilst the most evolved member of the suite analysed has a corresponding value of 0.7906. These values encompassing those determined by Hutchison (1966). The FFM values are comparable to those found within the cone-sheets, i.e. 0.5750 to 0.7910, however, the intrusive tholeiites are more evolved in terms of their major element chemistry, with CaO and MgO depleted, whilst Na_2O and P_2O_5 are enriched relative to the concentrations found within the cone-sheets at a given FFM. These observations are significant as all major element trends show a small but consistent discrepancy with those of the cone-sheets.

1.5.5 Trace element whole rock geochemistry

The systematic differences displayed by the major elements of the intrusive tholeiites when compared with members of the cone-sheet suite are also shown when comparisons are made of the trace-elements from the two suites (Fig.1.52). LIL elements ie. Zr, Ba, Rb and Sr are enriched relative to cone-sheets at a given FFM, whilst Ni and V show a slight depletion. The elements Y, Cr, Zn, and Sc display similar concentrations between the two groupings. Intrusive tholeiites generally have Y/Zr ratios of the order of $\sim$0.15 and Ti/Zr ratios of $\sim$45, which compares with 0.35 and 90 for Y/Zr and Ti/Zr, respectively, in the cone-sheets (Fig.1.53a,b).

Y and Zr are both incompatible with the crystallizing phases in the two suites and consequently are concentrated within the melt and as their distribution coefficients are similar, the ratio Y/Zr may be considered to act as a potential signature of the parent magma.

The convergence of the major element trends of the cone-sheets and the intrusive tholeiites at an FFM value of c.0.575, raises the possibility that the two suites had a common parent and they subsequently evolved along seperate paths due to differing low pressure processes. This possibility gains credence upon considering the common late-stage emplacement of the two suites, and, more significantly, their trace element trends which also converge at an FFM value of 0.575. It is also significant that no sample from either suite has been identified with a more primitive FFM value. Whilst the magma which gave rise to these two suites could not be assigned a primary status, the data considered so far

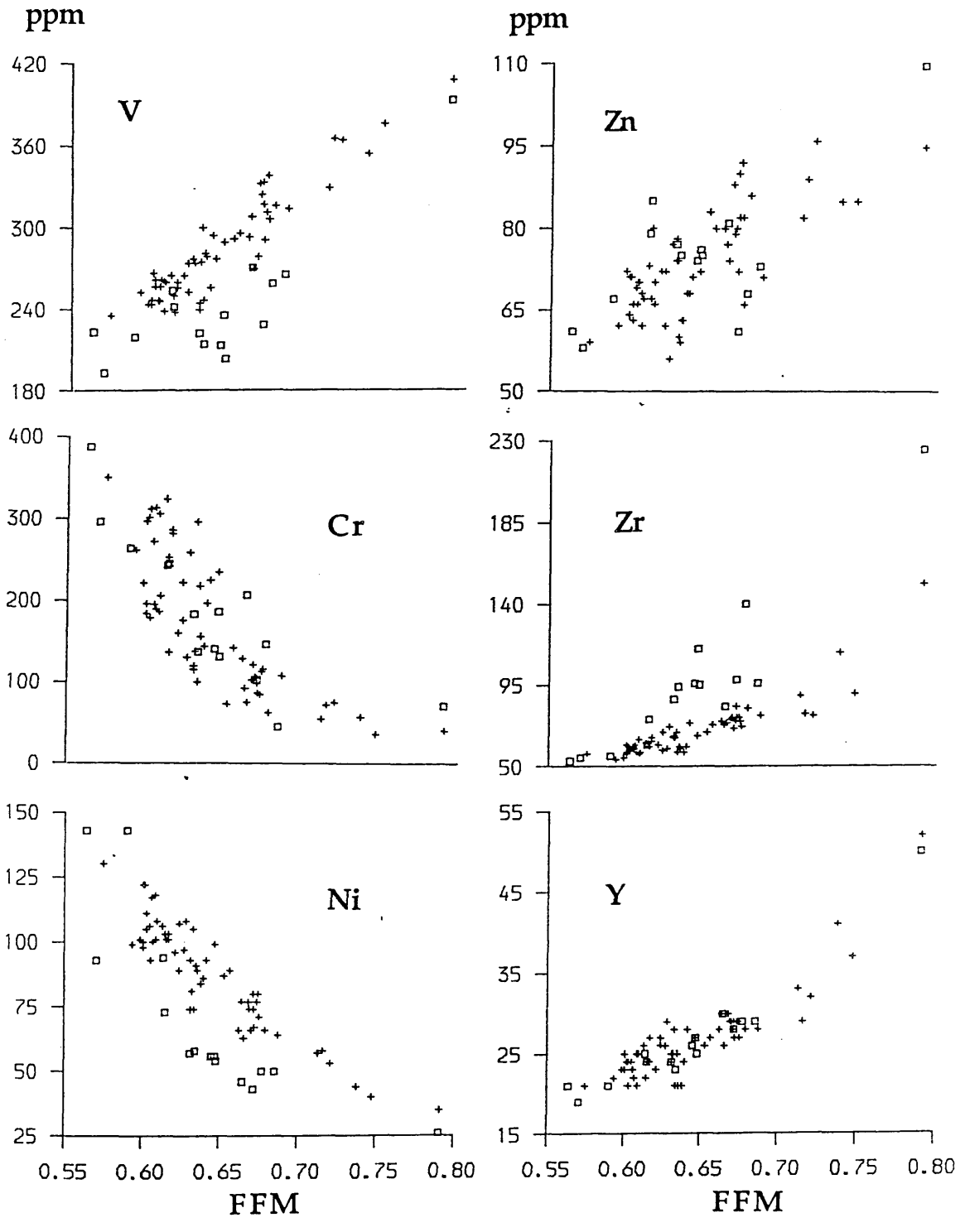

Fig. 1.52. Trace element comparison of Intrusive Tholeiites (▪) and cone-sheets (+).
FFM = $FeO + Fe_2O_3 /(FeO + Fe_2O_3 + MgO)$.

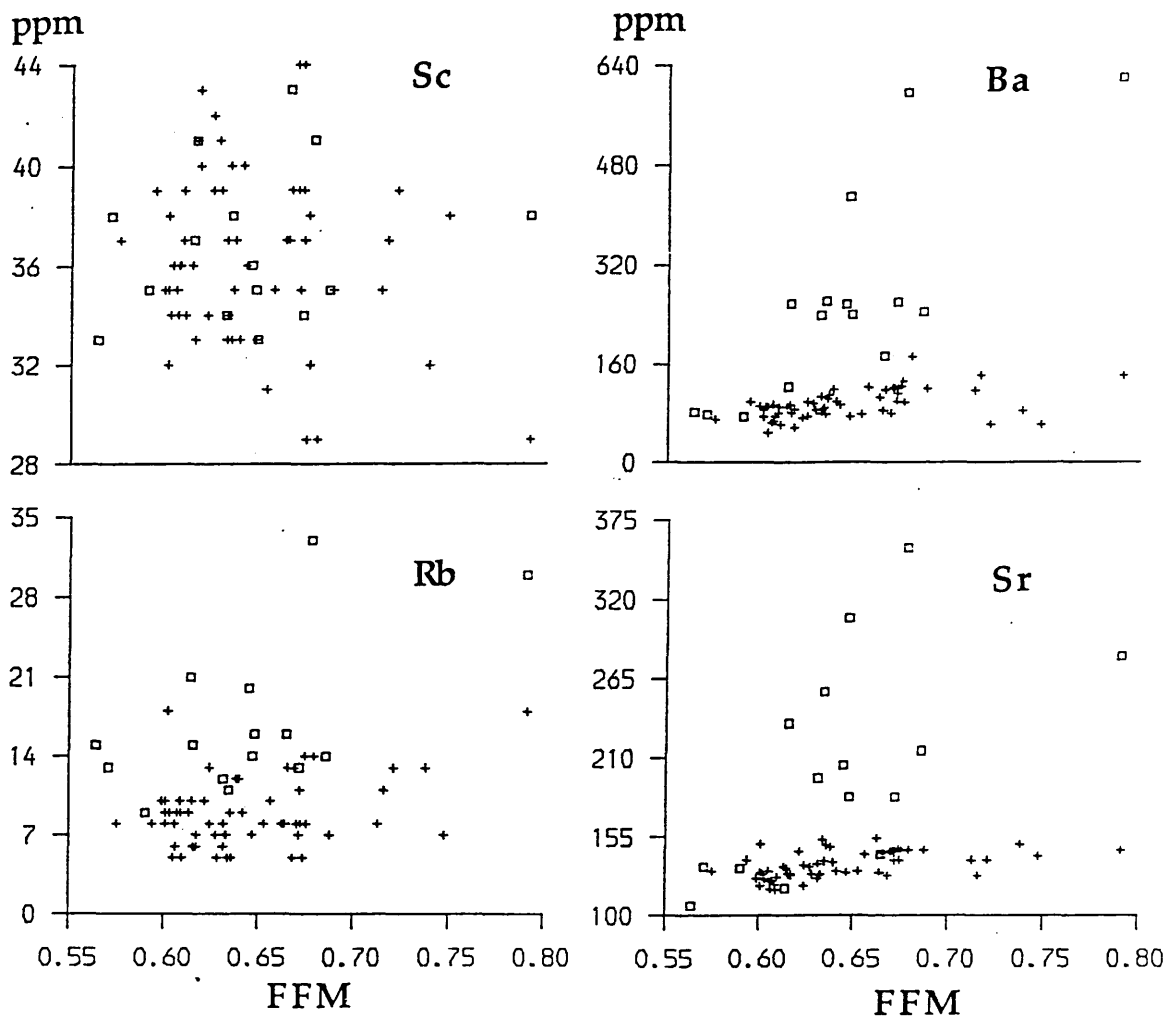

Fig. 1.52. Trace element comparison of Intrusive Tholeiites (¤) and cone-sheets (+).
FFM = $FeO + Fe_2O_3 /(FeO + Fe_2O_3 + MgO)$.

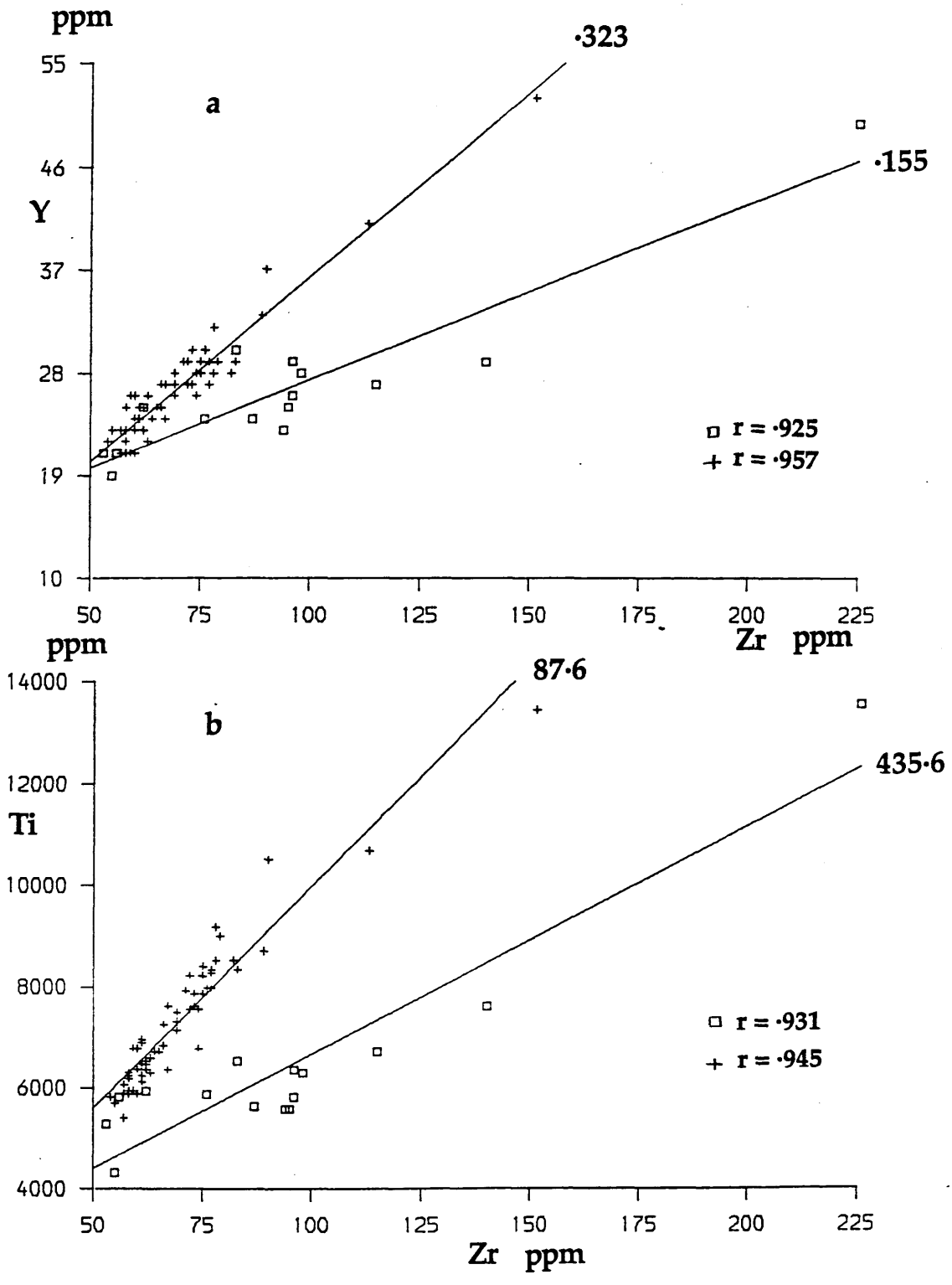

Fig. 1.53. Variation of (a) Y and b) Ti with Zr in both the cone-sheet (+) and the Intrusive tholeiite suites (□). r = correlation coefficient.

are consistent with the parental magmas being derived from a common reservoir, which had the composition of the most primitive sample analysed.

1.5.6 Rare Earth Elements

Rare earth element (REE) concentrations in four intrusive tholeiite sheets were determined by ICPS (Fig.1.54a), the samples having been chosen to represent the range of FFM values displayed by the suite. The LREE for the suite, as a whole, show concentrations which vary by approximately a factor of 10 (Ce ~10.4) whilst the HREE vary by a factor of 2.5 (Yb ~2.4). The most primitive sample, (IT06), with an FFM value of 0.5639, is anomalous in that it shows LREE depletion $(Ce/Yb)_N$ = 0.86. The remaining samples, IT17, IT03 and IT15, with FFM values of 0.6315, 0.6855 and 0.7906 respectively, display increasing LREE enrichment with $(Ce/Yb)_N$ increasing from 2.96 to 3.63. A small negative Eu anomaly is evident within all samples, with (Eu/Eu^*) increasing from 0.97 to 0.84 throughout the suite. This observation is consistent with plagioclase forming part of the fractionating assemblage. The REE concentrations of the most primitive sample are comparable with those from the most primitive cone-sheet (CS022) at a similar FFM value, strengthening the premise that the two suites share a common parentage. A comparison between the REE profiles of the tholeiite sheets with the most primitive of the cone-sheet suite reveal them to be of similar shape (Fig.1.54b) and with similar concentrations of the REE, strengthening the premise that the two suite had a common parentage, but were subsequently isolated and evolved along different paths. More evolved samples of the cone-sheets retain their flat REE pattern and consequently cross-cut those of the more evolved tholeiitic sheets (Fig.1.54c), a phenomonem which could not arise had they followed identical low-pressure evolutionary paths.

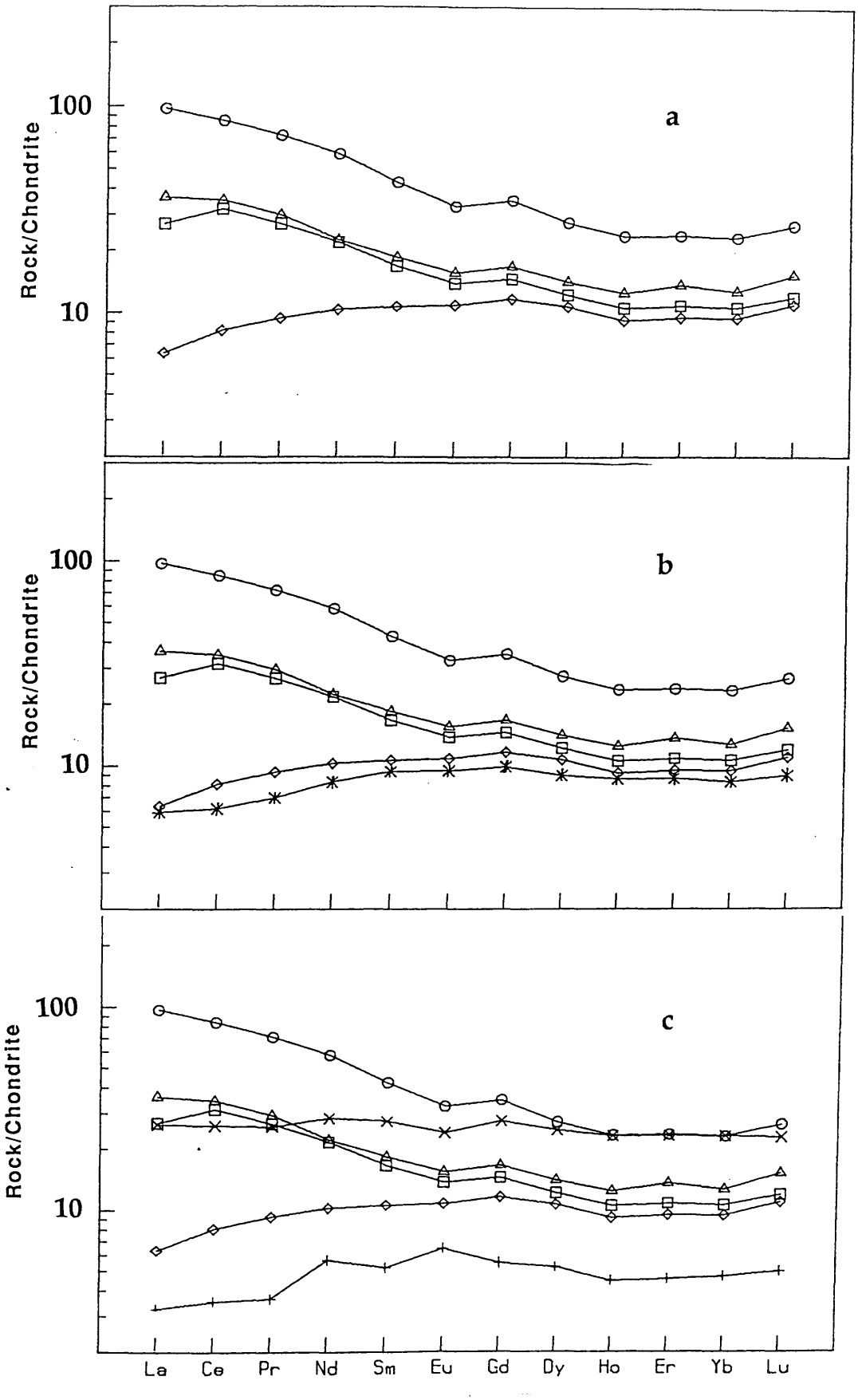

Fig. 1.54. REE profiles for a) intrusive tholeiites and b) a comparison of these with the most primitive and c) the most evolved of the cone-sheet samples.(*) = CS0022 , (x) = CS023, (+) = CS006, (o) = IT15, (△) = IT13, (□) = IT17, (◇) = IT06.

1.5.7 Petrogenesis

Numerical modelling, utilizing the determined REE concentrations of the intrusive tholeiites has failed to produce satisfactory solutions for all conceived types of crystallization of any geological reasonable assemblage compatible with the petrographic features of the suite. A dominant role of clinopyroxene in the crystallization history is suggested by the slight increase in concentrations of the HREE compared to the LREE. However, the amount of crystallization neccesary to produce the observed range of HREE fails to produce the concentrations of the LREE observed within the suite. It must therefore be concluded that the LREE enrichment shown by the suite might in fact be due to hydrothermal alteration/ metasomatism by a LREE enriched fluid.

Part 2

The Cuillin Peridotite Series

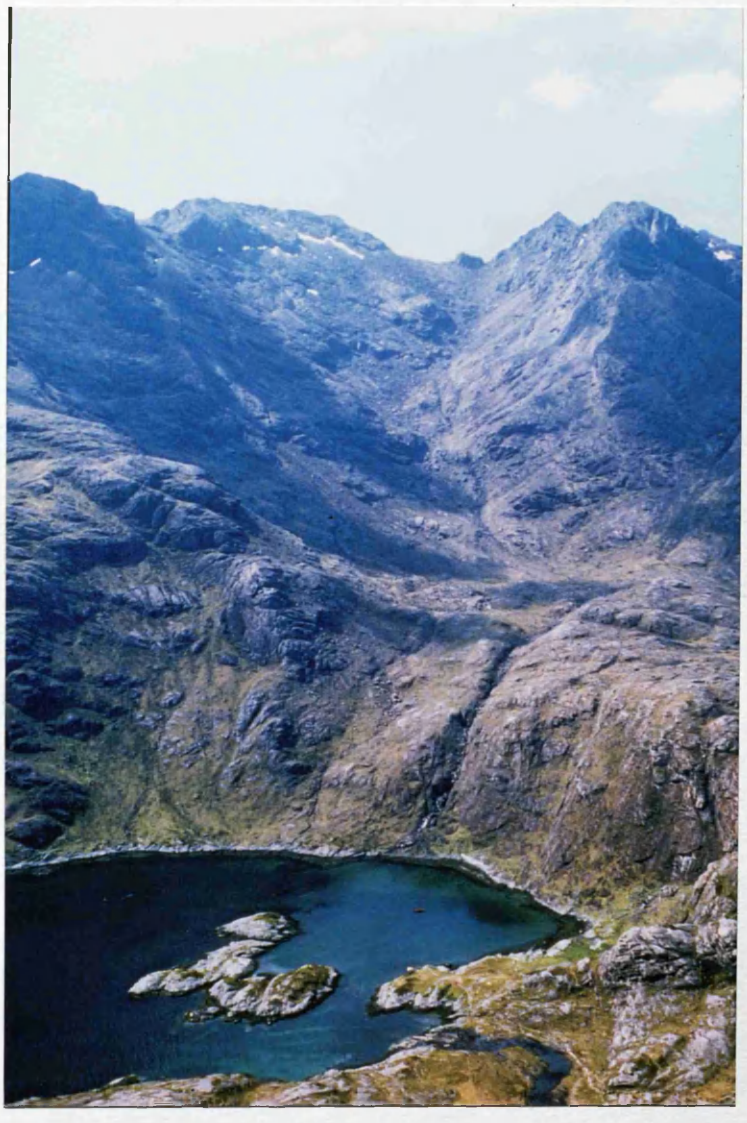

An Garbh-choire of the southern Cuillin Hills of Skye seen from the summit of Sgurr na Stri. Forming much of the floor of the corrie are ultrabasic rocks of the Peridotite Series. These extend upto and over the Cuillin main ridge between the summits of Sgurr nan Eag (774m) on the left (south) and Sgurr Dubh an Da Bheinn (938m) on the right (north). The Gars-bheinn Gabbro cropsout on the hummocky ground (centre left) whilst the Outer Allivalite Series cropsout and forms much of the steep slabby ground beyond. To the north of the corrie, the Outer Layered Eucrite Series forms the steeper ground of the Dubh's, Sgurr Dubh an Da Bheinn, Sgurr Dubh Mor (944m) and Sgurr Dubh Beag (733m). The pale coloured rocks (centre right) are the heterogeneous, generally feldspathic gabbros of Meall na Cuilce.

2.1 Introduction

The ultrabasic rocks which floor An-Garbh corrie in the Southern Cuillin (Fig.2.1) were first investigated by Harker (1904), who concluded that they were laccolitic in form, and had contacts with the surrounding gabbros generally dipping at shallow angles towards the north-east. The most detailed study, to date, of these rocks was made by Weedon (1956), who was able to divide the rocks into three "Zones" on the basis of the principal rock types present (Fig.2.2). Rocks occuring low down in the corrie constituted his Zone 1 and comprise dunites and peridotites, whilst rocks of Zone 2, occuring structurally higher in the corrie, comprise feldspathic peridotites and allivalites. Zone 3 rocks consist of brecciation and seggregation veins within Zones 1 and 2.

Following the work of Wager and Deer (1939) on the Skaergaard intrusion of east Greenland, Weedon (1956) related the ultrabasics to a single fractionating magma which gave rise to the lowest observed cumulates of Zone 1 and, with increased crystallization of intercumulus feldspar, the feldspathic peridotites of Zone 2. When feldspar joined olivine as the cumulus phase the allivalites of Zone 2 were precipitated, which, following Wager and Brown (1968), Hutchison and Bevan (1977) relate to the Allivalite series to the north and consequently refer to them as the inner allivalites. Since the work of Hutchison & Bevan (1977) further studies of the Skye layered intrusion all but ceased and attention focussed on the Rhum intrusion.

Over the last ten years the validity of crystal settling as a viable explanation for all examples of layering observed in layered intrusions has been called into question (Section 1.2.3.3) In particular, studies on Rhum have indicated that the cyclic peridotite-troctolite layering seen may not be due to periodic replenishment of the magma chamber by the influx of fresh parental magma (Brown 1956). It has been proposed (Butcher et al. 1985; Bedard et al. 1988) that the layering may alternatively be explained by the injection of picritic magma as sills, emplaced into partly crystallized troctolite.

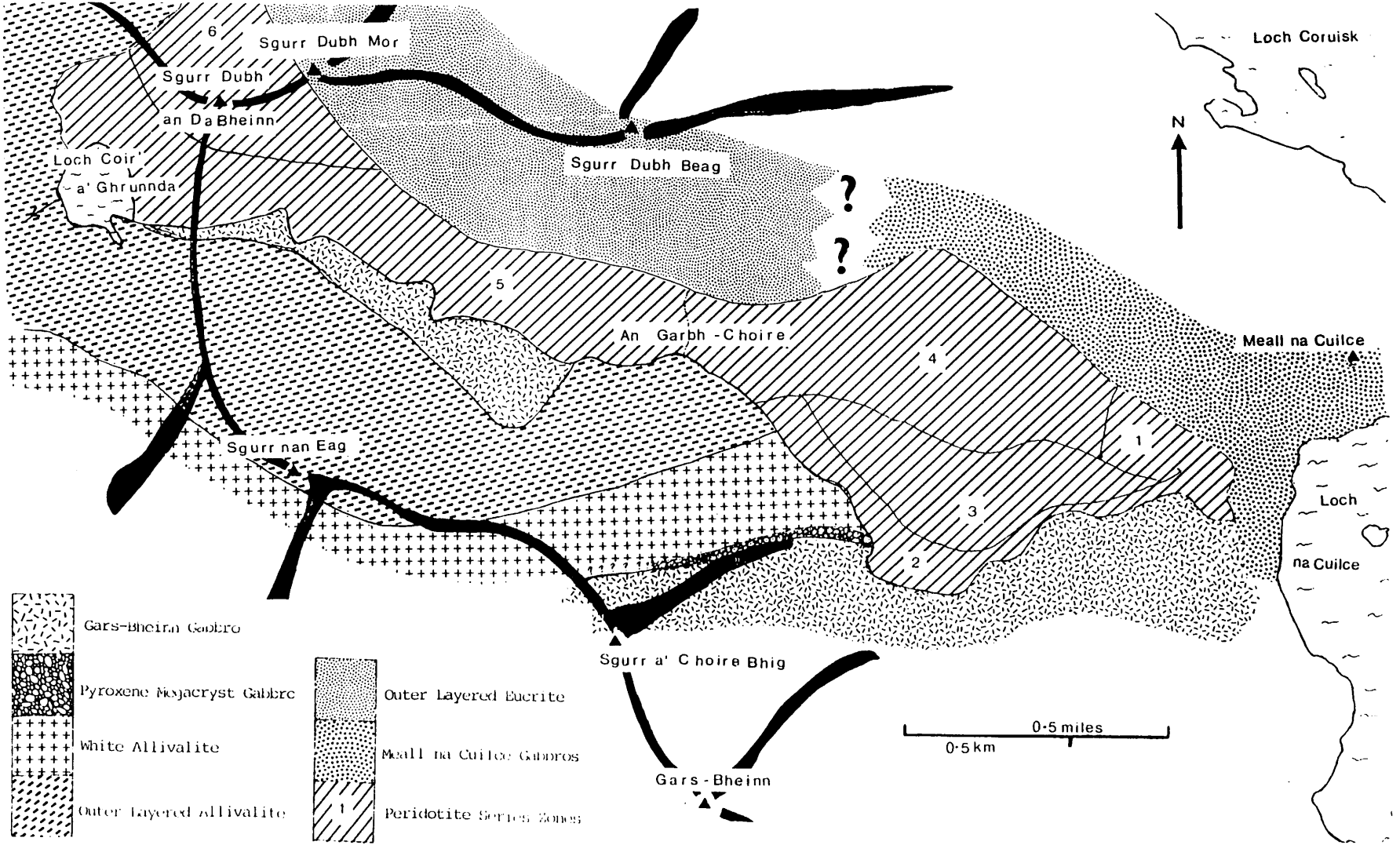

Fig. 2.1. Simplified geological map of the southern Cuillin of Skye, Scotland.

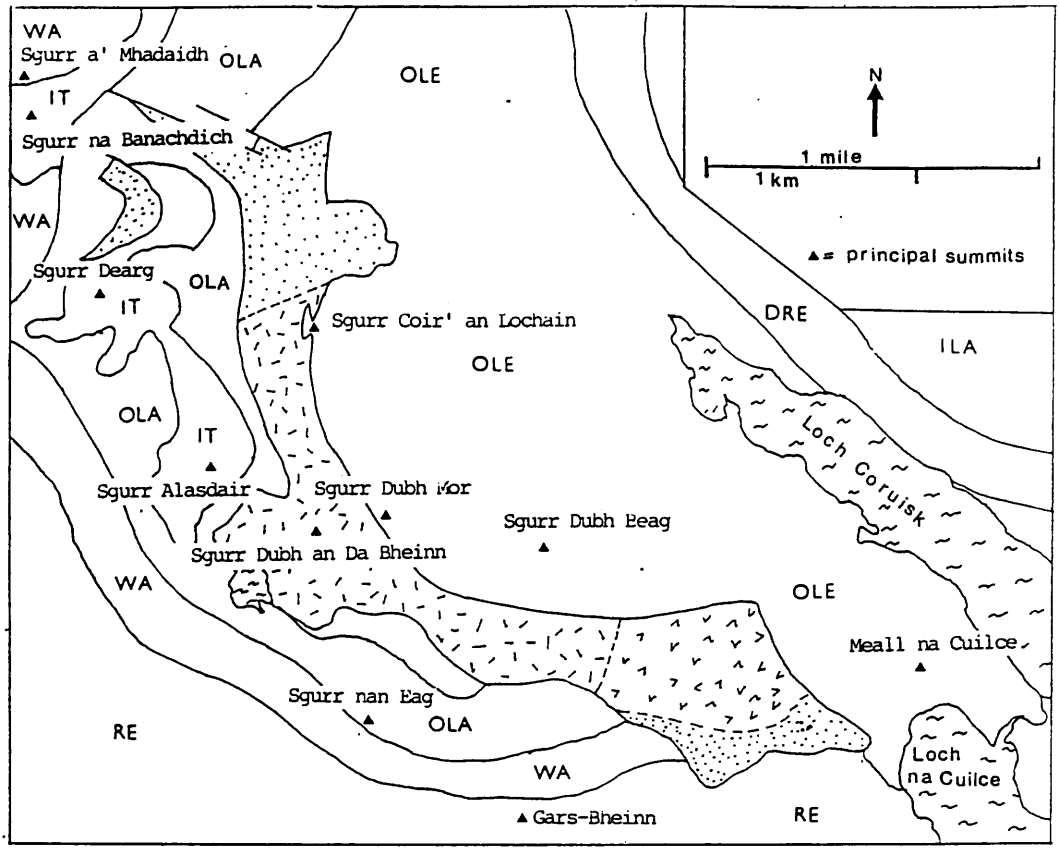

IT	Intusive Tholeiite Suite	DRE	Druim nan Ramh Eucrite
RE	Ring Eucrite (including Gars-Bheinn Gabbro)	ILA	Inner Layered Allivalite
WA	White Allivalite		
OLA	Outer Layered Allivalite	Zone 3	Peridotite Series
OLE	Outer Layered Eucrite	Zone 2	
		Zone 1	

Fig. 2.2. Simplified geological map of the southern Cuillin of Skye illustrating the three peridotite zones identified by Weedon (1956).

Following preliminary observations of the Skye peridotites and in the light of recent advances in knowledge obtained from the work on Rhum, it was apparent that previously proposed models for the evolution of the Skye peridotites were simplistic and furthermore could not explain all of the observations. Consequently it was believed that a re-investigation of these rocks was warranted.

Whilst Weedon's work (1956, 1965) provides a first order classification for the Skye peridotites it became apparent that further advances would require a more tightly constrained lithological and structural framework upon which to "hang" observations. Unlike the Rhum peridotites, with their "layer cake" stratigraphy, those occurring on Skye are less amenable to study and consequently considerable time and energy was expended in trying to erect a meaningful framework of zones/units (Section 2.3.3 & Fig. 2.2a).

2.1.1 Cumulate theory

Cumulate theory has been developed from observations on layered igneous intrusions, where it is recognised that the lower structural levels contain minerals of presumed high temperature crystallization, whilst at higher structural levels the minerals are of a progressively lower temperature type. This relationship, supported by textural features, has led to the view that discrete crystals are capable of separating out of a magma due to their greater density and accumulating on the floor of a magma chamber. Such crystals are termed the cumulus crystals to distinguish them from the so-called intercumulus crystals which crystallized from liquid trapped within the accumulating crystal pile (Wager et al. 1960). Various types of cumulates have been recognised on the basis of their morphology and the relationship of cumulus crystals to intercumulus crystals (Fig.2.3).

Some definitions are as follows:

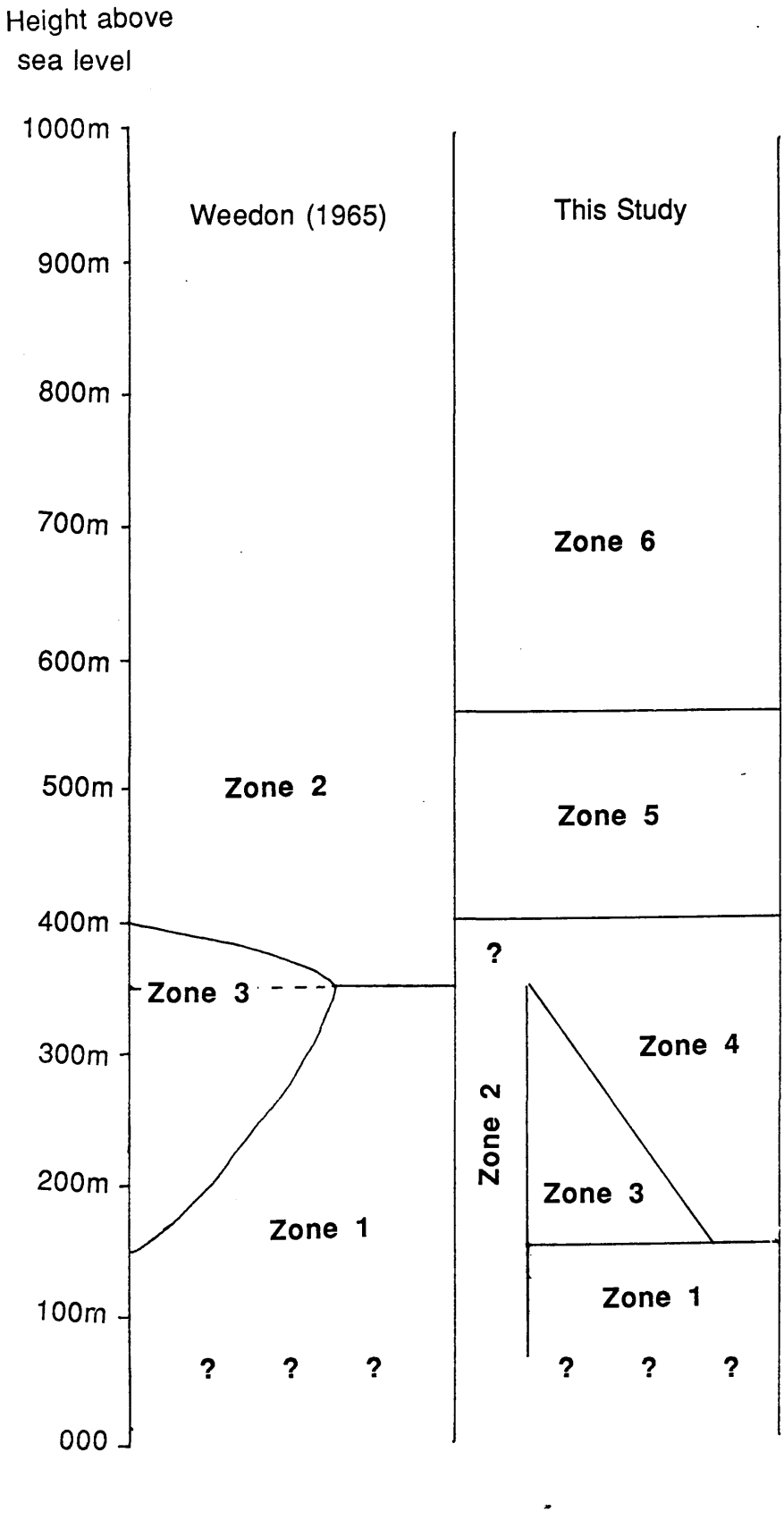

Fig 2.2a Correlation between Peridotite Zones identified in this study with those of Weedon (1965).

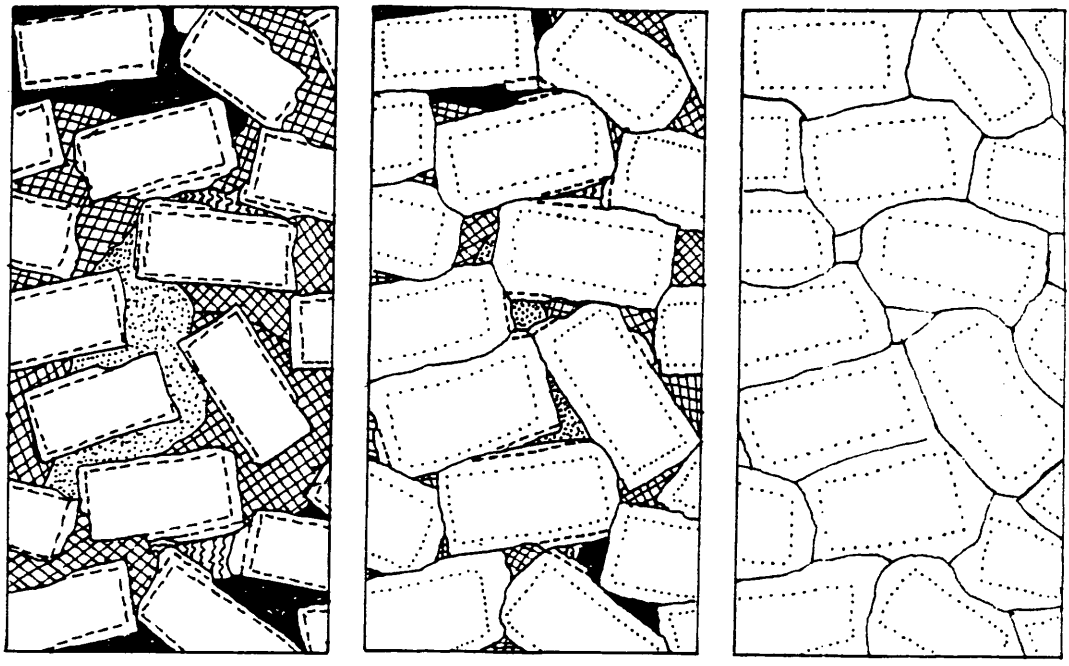

PLAGIOCLASE
Boundary of the cumulus crystals diagrammatically shown by the innermost rectangle. The limits of medium and low temperature zones, where develcped shown outside the cumulus crystal boundary.

PLAGIOCLASE
Boundary of the cumulus crystals shown by the dotted line. Outside is adcumulate growth of plagiocalse of similar compcsition. In places beyond the broken lines, lower temperature zones are shown.

PLAGIOCLASE
The cumulus part of the crystal is shown within the dotted line. This has been enlarged by g rowth of more plagioclase of the same composition, which fills the interstices.

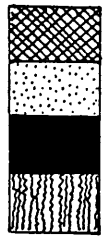

Pyroxene

Olivine

Iron Ore

Poikilitic crystals, zoned but not shown

Quartz and orthoclase, locally the final residuum.

Fig. 2.3. Diagrammatic representation of plagioclase cumulates formed from a gabbroic magma. A) Extreme plagioclase orthocumulate, B) Plagioclase mesocumulate, C) Extreme plagioclase adcumulate. (After Wager et al. 1960)

Orthocumulates. The intercumulus melt crystallizes successively lower temperature zones around the primary cumulus phase(s) and new mineral phase(s).

Adcumulates. Studies have shown that in some rocks the simple idea of an intercumulus melt crystallizing around the cumulus crystals is not tenable and that a mechanism which facilitated the enlargement of the cumulus crystals at the same temperature of their formation needed to be postulated. Hess (1939) suggested that this mechanism was one of diffusion, with components required by the growing cumulus crystals diffusing through the intercumulus liquid from the overlying magma to the growing crystals in the top layers of the cumulate pile, accompanied by diffusion of unwanted components away from the growing crystals. Hess suggested that certain compositional changes could be correlated with the rate of accumulation of the cumulate pile. Slow accumulation would facilitate diffusion and consequently the crystallization of mineral overgrowths with almost the same composition as that of the cumulus minerals. In the limiting case, this would produce a monomineralic rock. If, however, accumulation was rapid, diffusion of material would be inhibited and consequently intercumulus liquid would crystallize to produce an orthocumulate. Wager et al. (1960) have suggested that the term adcumulate be reserved for rocks with interstitial material representing less than 5% of original trapped melt. For cumulates showing characteristics between ortho and adcumulates the term mesocumulate is used.

Crescumulate. Harker (1908) described an occurrence of layering on Rhum characterised by skeletal and dendritic olivines which range in size up to 2m which he named harrisite. Wager and Brown (1968) consider this rock to be an example of a crescumulate formed by the rapid upward growth of olivine into overlying magma from cumulus olivine nuclei at the top of the cumulate pile. Donaldson (1982), whilst agreeing to this mechanism of growth for the majority of examples, describes atypical types which he concludes to be a differentiate of upward moving intercumulus melt expelled by compaction from the cumulate pile.

2.1.2 Nomenclature

As the ultrabasic rocks of the Peridotite Series of the Southern Cuillin show every gradation, at least on a local scale, between dunite and anorthosite, it is neccessary to define a suitable working nomenclature. Dunite is clearly defined as a rock made up entirely of olivine crystals, with only 3-4% of other interstitial material. It is used in this account as such but is taken to include also cumulus spinel. Brown (1956) suggested that the term peridotite may be used as a general term to include ultrabasic rocks containing feldspar and pyroxene, on the grounds that feldspar free rocks are sufficiently well defined. Therefore, the term is adopted here to include all olivine-dominated rocks in which olivine +/- spinel is the only cumulus phase and interstitial material accounts for 4-20% of the mode. The term feldspathic peridotite (Weedon 1956) is used for rocks containing cumulus olivine +/- spinel but with greater than 20% interstitial material. For ultrabasic rocks containing a greater proportion of interstitial feldspar and pyroxene, Harker (1904) used the term troctolite. In this account the term is reserved for rocks containing cumulus olivine + feldspar +/- spinel, with the feldspar accounting for less than 50% of the cumulus minerals. Harker (1908) defined the term allivalite for ultrabasic rocks occurring on Rhum where (calcic) plagioclase is present in quantities greater than olivine. Brown (1956) has

subsequently shown that the feldspar in these rocks is a cumulus phase and therefore the term is reserved in this account for rocks in which olivine + feldspar +/- spinel are cumulative and where the feldspar accounts for greater than 50% of the cumulus phases.

In Summary:

Dunite	practically pure olivine +/- spinel with <3-4% of intercumulus material.
Peridotite	cumulative olivine +/- spinel with intercumulus material <20%.
Feldspathic peridotite	cumulative olivine +/- spinel with >20% intercumulus material.
Troctolite	cumulative olivine + feldspar +/- spinel (feldspar <50% of cumulative minerals).
Allivalite	cumulative olivine + feldspar +/- spinel (feldspar >50% of cumulative minerals).

2.2 Contact rocks to the Peridotite Series

2.2.1 Nature of the northern margin around Meall na Cuilce

From the western shores of Loch na Cuilce to the rock step (Map 1), approximately halfway up An Garbh-choire (c.1250m.) the northern contact of the peridotite with the adjacent younger gabbros is poorly constrained. This is due to both poor exposure and the number and frequency of peridotite xenoliths occurring within the adjacent gabbros.

Although not mapped in any detail, the gabbros of Meall na Cuilce are heterogeneous in terms of both composition and texture, with two principal types readily identifiable in the field. The first, a dark, medium-grained pyroxene-rich gabbro, which exhibits rhythmic layering due to the concentration of pyroxene into thin (c.2cm) bands (Fig.2.4), is in sharp contact with the second, a more feldspathic variety. These two gabbros are disposed in at least 3 complete alternating units which dip at c.40^{o} towards the north-east. Peridotite xenoliths up to 1.5m in size are common throughout both gabbros, their frequency however decreasing towards the north-east, away from the main peridotite outcrop. South of the summit of Meall na Cuilce, the xenoliths are concentrated into a narrow zone (c.2m) which forms a well defined horizon which may be traced laterally for c.100m in either direction. Towards the ultrabasic tongue which crops out in the vicinity of the Allt Beag, the frequency of blocks increases, passing from the gabbros with occasional xenoliths (Fig.2.5a), through the well defined horizon and, prior to entering the main peridotite body, through a zone of peridotite heavily veined by gabbro (Fig.2.5b). The xenoliths are invariably angular and where a fabric is developed within them, by alignment of olivine +/- spinel +/- plagioclase, it is often parallel to that occurring within the adjacent peridotite. This observation coupled with the fact that the variation in xenolith lithology, texture and fabric frequently matches that within the adjacent peridotite, i.e. spinel seams/blebs in the east to feldspathic peridotite below the rock step suggests that the blocks are locally derived. (Weedon (1956), however, reports peridotite xenoliths occurring within gabbros up to 2km to the east). Occasionally stringers of peridotite extend from the xenoliths and are accompanied by curvature of any fabric present, suggesting that the peridotite was still relatively ductile during the emplacement of the gabbros. Immediately below the northern end of the rock

Fig.2.4. Rhythmic modal layering of feldspar-rich and clinopyroxene-rich bands developed within the gabbros of the Meall na Cuilce area [G.R. 4843 1988].

a

b

Fig.2.5. The northerly inner contact between Zone 4 peridotites and the younger Outer Layered Eucrite Series is poorly constrained. Considerable veining and isolation of peridotite blocks has occurred. The frequency of peridotite blocks increases rapidly southwards ranging from a) isolated xenoliths of peridotite within the eucrite [G.R.4824 2001].to b) interdigitating peridotite and eucrite (b). [G.R.4760 2009].

step a very coarse-grained, sometimes pegmatitic, facies of the Outer Layered Eucrite interdigitates with the peridotite parallel to the contact. Unfortunately, the contact between the eucrite and the Meall na Cuilce gabbros (Weedon 1956) is not seen due to poor exposure. No xenoliths of either peridotite or the Meall na Cuilce gabbros have been seen within the eucrite occurring in the upper part of the corrie.

2.2.2 Contact rocks of the southern margin

The rocks with which the peridotite is in contact along its southern margin in the southern Cuillin may broadly be divided into four types (Fig.2.1): i) the Gars-bheinn Gabbro (Weedon 1956); ii) a coarse-grained pyroxene-rich gabbro; iii) a feldspathic allivalite, and iv) a more mafic allivalite which appears to be gradational upon the feldspathic allivalite. The contacts of these four lithologies trend NE-SW and are therefore truncated by the peridotite which trends E-W in this region. As the contact is generally marked by a line of cliffs and steep ground it has not been possible to trace any of these gabbros along strike for any great distance, however, the exposure is such that it provides an excellent section through the marginal rock types.

2.2.2.1 The Gars-bheinn Gabbro

The Gars-bheinn gabbro crops out on the summit of that name and may be traced northwards to where it is truncated by the Peridotite Series (Fig.2.1). It cropsout on much of the rising ground between the shores of Loch Scavaig in the east, to the north-east spur of Sgurr a' Choire Bhig in the west. Close to the peridotite, the feldspars within the gabbro suffer varying degrees of clouding (Fig.2.6) which allowed Weedon (1956) to differentiate the gabbro into two sub-types. The boundary between these two types is highly irregular and gradational over a large distance and, therefore, for the purpose of this study, they have been mapped as a single unit. The gabbro, devoid of any internal structure, is fine grained, smooth weathering and, on fresh surfaces, possesses a strong green coloration. Some variation in the grain size is apparent throughout the outcrop but it is never coarse and these departures from the norm are of limited lateral extent.

Within the upper part of An Garbh-choire occurs a rock with similar characteristics to the Gars-bheinn Gabbro and was consequently mapped as such by the author. Petrographic examination has supported this assumption, although it is slightly more feldspathic. Mineral compositions, particularly those of the feldspars, fall within the range determined for the main outcrop to the east.

Petrography and mineral chemistry

In thin section the texture of the gabbro varies between sub-ophitic to granular, in which the dominant mineral is subhedral to euhedral lath-shaped plagioclase which may account for up to 60% of the mode. Individual laths may attain lengths of up to 2mm, although 0.5-1mm is the norm. Slight normal zoning is detected from cores which may be as calcic as An_{72}, but are usually around An_{65} (Table 2.1). Interstitial areas composed of either an alkali feldspar or, more commonly, oligoclase (An_{20}) and/or cryptocrystalline material may be present. Both clinopyroxene and orthopyroxene are present (Table 2.2), the former, reddish brown in colour may, on occasion, ophitically enclose small plagioclase laths, but more commonly occurs as small equant, subhedral intergranular grains around 0.5-1mm in size. The orthopyroxene is pale brown, interstitial and subhedral but is present in only minor quantities. The presence of olivine is variable but is nowhere an important phase (<2%), where present it is usually pseudomorphed by antigorite.

2.2.2.2 Pyroxene Rich Gabbro

Adjacent to the western side of the bulk of the Gars-bheinn Gabbro, running up and along the north-east spur of Sgurr a' Choire Bhig, is exposed a narrow outcrop of a dark weathering coarse grained gabbro. It is characterized by the apparent random distribution of large black pyroxenes up to 2cm in size, which, being resistant to weathering stand proud of the surface (Fig.2.7). The gabbro is only 10m in width and quite distinctive, however, no comparable lithology has been observed along the main ridge and consequently its relationship to the adjacent gabbros can only be speculated upon. It has sharp sub-vertical

Sample	248/1	248/3	248/c	287/a	287/c	248/b	287/b	248/4
SiO_2	53.21	53.08	52.04	50.46	52.34	51.87	51.80	52.76
Al_2O_3	28.77	28.77	29.72	31.17	29.88	29.84	30.44	28.94
K_2O	0.20	0.25	0.30	0.17	0.19	0.21	0.26	0.25
Na_2O	2.39	4.14	3.81	3.10	3.87	3.84	3.60	4.19
CaO	12.29	12.44	13.39	14.48	12.70	13.81	13.40	12.63
MgO	0.03	0.04	0.03	0.03	0.03	0.04	0.04	0.04
BaO	-	-	-	-	0.01	-	-	-
FeO^*	0.58	0.61	0.41	0.58	0.67	0.50	0.40	0.53
Total	99.47	99.33	99.70	99.99	99.94	100.11	99.94	99.34
				Atomic %				
An	60.04	61.47	64.89	71.34	66.24	65.71	66.24	61.55
Ab	38.78	37.06	33.40	27.68	32.26	33.09	32.26	36.99
Or	1.18	1.46	1.71	0.98	1.50	1.20	1.50	1.46
				Formula (based on 32 oxygens)				
Si	9.708	9.700	9.502	9.216	9.216	9.426	9.427	9.649
Al	6.188	6.198	6.399	6.712	6.712	6.437	6.531	6.241
K	.047	.058	.069	.039	.039	.049	.059	.059
Na	1.552	1.468	1.348	1.099	1.099	1.354	1.272	1.488
Ca	4.403	2.435	2.619	2.833	2.833	2.869	2.612	2.476
Mg	.012	.012	.008	.009	.009	.011	.011	.010
Ba	-	-	-	-	-	-	-	-
Fe	.088	.093	.063	.089	.089	.091	.061	.081

Table 2.1 Representative analyses of feldspar within the Gars-bheinn Gabbro. FeO^* = total iron determined as FeO.

Sample	287/d	287/b	248/4	248/g	287/f	248/b	248/a
SiO_2	54.68	53.53	51.77	52.85	53.26	52.71	53.07
MgO	27.34	23.55	15.79	24.27	15.19	17.05	23.94
CaO	2.14	2.02	19.52	1.96	22.36	18.50	1.86
FeO	12.84	18.99	7.21	16.96	6.53	6.53	17.91
Fe_2O_3	1.76	0.14	1.92	1.52	0.36	1.35	1.16
Al_2O_3	1.24	0.97	1.88	1.44	1.26	1.74	1.09
MnO	0.31	0.42	0.28	0.46	0.21	0.26	0.48
TiO_2	0.21	0.23	0.27	0.31	0.15	0.27	0.24
Cr_2O_3	0.11	0.04	0.35	0.01	0.32	0.25	0.01
Na_2O	0.20	0.05	0.32	0.06	0.29	0.27	0.04
Total	100.83	99.94	99.31	99.84	99.93	99.93	99.80
FeO^*	14.43	19.20	8.96	18.31	6.85	8.84	18.99
			Atomic % (Mn included with Fe)				
Ca	4.41	4.05	40.05	3.87	45.63	37.46	3.71
Mg	73.61	65.47	45.12	67.05	43.11	48.08	66.10
Fe	22.25	30.48	14.83	29.07	11.27	14.47	30.19
			Formula (on the basis of 6 oxygens)				
Si	1.958	1.973	1.939	1.948	1.971	1.942	1.960
Mg	1.459	1.293	.882	1.333	.838	.937	1.318
Ca	.082	.080	.783	.077	.887	.730	.074
Fe^{+++}	.047	.004	.054	.042	.010	.037	.032
Fe^{++}	.387	.585	.225	.521	.202	.235	.552
Al	.052	.042	.083	.063	.055	.086	.047
Mn	.009	.013	.009	.014	.007	.008	.015
Ti	.006	.006	.008	.008	.004	.008	.007
Cr	.003	.001	.010	-	.009	.009	-
Na	.014	.003	.023	.004	.021	.019	.003
Total	4.017	3.987	4.016	4.010	4.004	4.012	4.008

Table 2.2 Representative analysis of pyroxenes of the Gars-bheinn Gabbro. Total iron was determined as FeO^* and subsequently partitioned between ferrous and ferric iron by the method of Finger (1972).

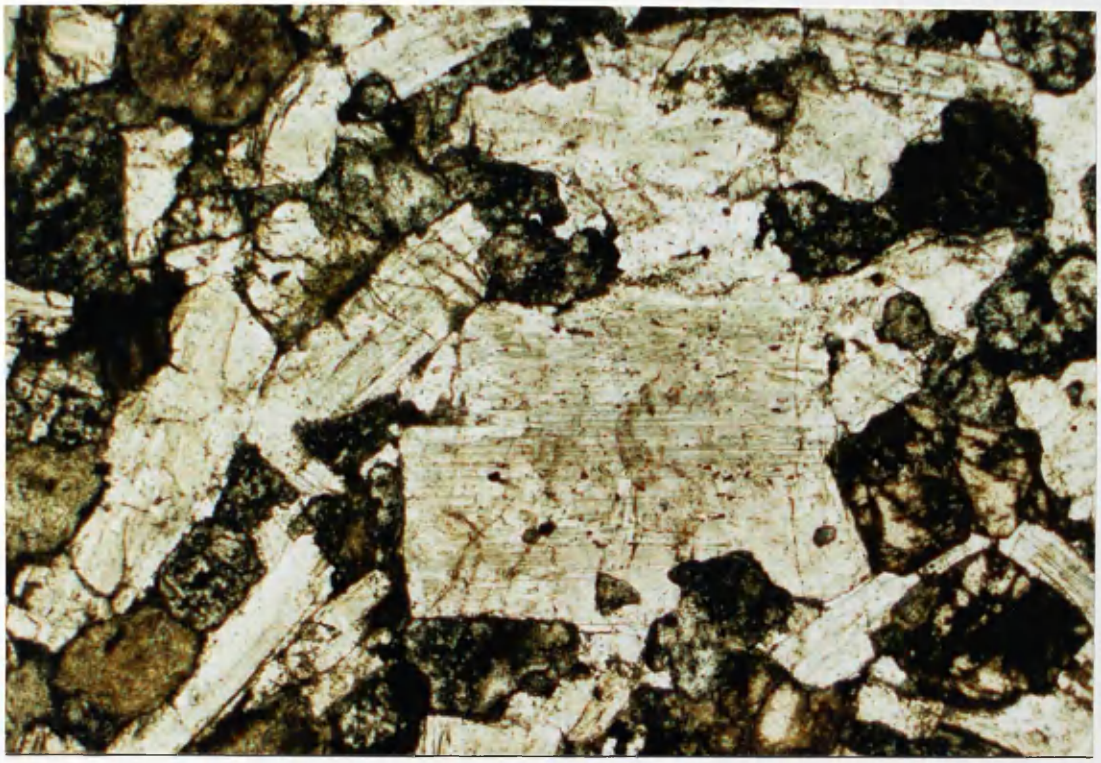

Fig.2.6. Euhedral tabular plagioclase (An_{70}) of the Gars-bheinn gabbro, many of which display clouding due to reheating, presumably as a result of the emplacement of the Peridotite Series. Field of view c.3 x 2mm. Plane polarized light. Sample AG287.

Fig.2.7. Randomly distributed pyroxene aggregates occurring within the Pyroxene Gabbro. [G.R.4728 1938].

contacts with both the adjacent Gars-bheinn Gabbro to the east and feldspathic allivalite (Section 2.2.2.3) to the west. As is common to all the gabbro occurring along the southern flank of the Peridotite Series, no appreciable variation in grain size on approaching the contacts has been detected.

Petrography and mineral chemistry

Apart from the apparent random presence of the large pyroxene aggregates, the pyroxene gabbro is similar petrographically to the Allivalite Series (Section 2.2.2.4). Feldspar is the dominant phase, with the majority of crystals being tabular and euhedral, with lengths up to 3mm. Also present, however, are smaller angular fragments c.1mm in size. Compositionally (Table 2.3), the feldspar is comparable to that of the Allivalite Series. Olivine is subordinate in quantity to the feldspar and occurs mainly as anhedral interstitial grains (c.1-2mm) and has compositions of Fo_{81-83} (Table 2.3). The pyroxene, which may form large aggregates, ranges from a pale grey to a dark brown augite (Table 2.4) and frequently contains angular fragments of feldspar and occasionally displays simple twinning and a blebby exsolution. In contrast, the smaller interstitial pyroxenes are invariably paler and show none of these features.

2.2.2.3 The Feldspathic Allivalite

Where An Garbh-coire begins to narrow, some 500m east of the rock step, a rocky spur descends from Sgurr a' Choire Bhig towards An Garbh-coire. This spur intersects the peridotite approximately 200m NW of the stream that drains Coire Beag. Under favourable lighting conditions a sharp lithological contact can be seen following the crest of the spur as it is approached from the east. The contact, which as far as can be ascertained, is vertical, separates the Pyroxene-rich Gabbro to the east from the Feldspathic Allivalite to the west.

The Feldspathic Allivalite is structureless and on weathered surfaces is whitish grey due to the very high proportion of plagioclase within it. In hand specimen it is coarse grained and appears to be composed essentially of two minerals, plagioclase and pyroxene, both of which are around 6mm in size, although occasionally pegmatitic facies exist where the crystal size increases to around 1cm. On traversing a couple of hundred metres north-west

	Olivines			Feldspars				
Sample	312/a	312/b	312/c	Sample 312/ac	312/ar	312bc	312/br	312/e
SiO_2	39.42	39.64	39.10	SiO_2 46.55	46.83	47.64	46.97	47.49
MgO	42.81	43.38	42.53	Al_2O_3 34.12	34.20	33.59	33.42	34.20
FeO*	17.09	16.43	17.10	CaO 16.75	16.90	15.70	16.05	16.57
MnO	0.27	0.28	0.25	Na_2O 1.89	1.84	2.45	2.32	1.96
NiO	0.17	0.16	0.17	K_2O 0.02	0.02	0.03	0.06	0.03
CaO	0.05	0.04	0.05	BaO -	-	-	-	-
Al_2O_3	0.05	0.05	0.05	FeO* 0.33	0.46	0.53	0.53	0.39
				MgO 0.04	0.17	0.05	0.13	0.06
Total	99.84	99.98	99.25					
				Total 99.70	100.42	100.21	99.49	100.70
	Atomic %					Atomic %		
Fo	81.54	82.84	81.58					
Fa	18.46	17.16	18.42	An 82.96	83.57	77.86	79.69	82.24
				Ab 16.94	16.31	21.99	19.93	17.61
	Formula (on the basis of 4 oxygens)			Or 0.10	0.12	0.15	0.38	0.15
Si	1.000	1.005	1.000			Formula (on the basis of f 32 oxygens)		
Mg	1.621	1.641	1.621	Si 8.582	8.567	8.743	8.693	8.656
Fe	.367	.340	.366	Al 7.416	7.378	7.259	7.270	7.351
Mn	.005	.006	.005	Ca 3.310	3.352	3.087	3.183	3.236
Ca	.001	.002	.001	Na .676	.654	.872	.796	.693
Al	.002	.002	.002	K .004	.005	.006	.015	.006
Ni	.003	.003	.003	Ba -	-	-	-	-
				Fe .015	.070	.081	.082	.059
Total	2.999	2.999	2.998	Mg .012	.047	.014	.037	.019
				Total 20.015	20.073	20.064	20.076	20.020

Table 2.3 Representative olivine and feldspar analyses of the Pyroxene-rich Gabbro. FeO* = Total iron determined as FeO.

Sample	312/a	312/b	312/c	312/d	312/e
SiO_2	52.51	52.09	52.38	52.36	53.28
CaO	20.39	21.81	22.21	22.15	21.29
MgO	17.17	16.08	15.97	16.05	17.47
FeO	4.87	4.04	4.17	3.66	3.95
Fe_2O_3	0.63	1.12	1.30	1.51	1.08
TiO_2	0.23	0.19	0.21	0.21	0.16
Cr_2O_3	0.44	0.53	0.50	0.57	0.31
MnO	0.14	0.17	0.15	0.17	0.13
Al_2O_3	2.59	2.50	2.57	2.44	2.41
Na_2O	0.27	0.35	0.34	0.35	0.29
Total	99.16	98.78	99.68	99.74	100.37
FeO^*	5.42	5.06	5.35	5.01	4.92
	Atomic % (Mn included with Fe)				
Ca	43.71	45.23	45.37	46.04	49.10
Mg	47.64	46.38	45.89	45.68	43.00
Fe	8.64	8.39	8.74	8.28	7.90
	Formula (on the basis of 6 oxygens)				
Si	1.935	1.934	1.931	1.935	1.943
Ca	.865	.868	.877	.889	.950
Mg	.943	.890	.887	.882	.832
Fe^{++}	.150	.125	.128	.113	.120
Fe^{+++}	.017	.031	.036	.042	.029
Ti	.006	.005	.006	.006	.004
Cr	.013	.016	.015	.017	.009
Mn	.004	.005	.005	.005	.004
Al	.112	.109	.112	.107	.104
Na	.019	.025	.024	.025	.018
Total	4.064	4.008	4.021	4.021	4.013

Table 2.4 Representative analyses of pyroxenes from the Pyroxene-rich Gabbro. Total iron was determined as FeO^* and then subsequently partitioned between ferrous and ferric iron by the method of Finger (1972).

across the strike, the allivalite gradually becomes richer in pyroxene at the expense of both plagioclase and rare olivine. After a further 200m, the olivine component increases significantly and is distictive enough to be mapped as a separate unit, the Allivalite Series (Section 2.2.2.4), albeit with gradational contacts.

Petrography and mineral chemistry

Plagioclase is the dominant mineral within the Feldspathic Allivalite, approximately 60% by mode, and occurs as euhedral laths showing both simple and polysynthetic twinning. Core compositions are around $An_{85\text{-}90}$ and normal zoning gives rim compositions of An_{76} (Table 2.5). The majority of the pyroxene is a chromium-rich augite (Table 2.6), of which the larger grains ophitically enclose a few of the smaller feldspar laths; the majority of the pyroxene, however, occurs as anhedral interstitial grains along with a small amount of orthopyroxene, a pale green magnesian hypersthene ($Mg/Mg+Fe^{2+}+Fe^{3+}+Mn = 0.69$). As noted in the field, the modal proportions of plagioclase, olivine and pyroxene vary significantly throughout the outcrop. In the east, where in contact with the Pyroxene-rich Gabbro (Section 2.2.2.2), plagioclase accounts for c.70% of the mode, with 20% olivine and 10% pyroxene, whilst further west the Feldspathic Allivalite becomes less feldspathic. On traversing west, the pyroxene content increases significantly to c.40%, principally at the expense of olivine (5%) and plagioclase (50%). Accompanying the modal variation is a systematic change in mineral chemistry, particularly of the olivines (Table 2.5), which in the eastern lower part of the unit have compositions of Fo_{85}. This decreases to c.Fo_{75} upon ascending the unit, with a concomitant decrease in NiO, from 0.26 to 0.13 (wt%) at the top of the unit. These changes are complemented by variation in the clinopyroxene from $(Ca_{.43}Mg_{.50}Fe_{.07})_2Si_2O_6$ to $(Ca_{.44}Mg_{.44}Fe_{.12})_2Si_2O_6$, with a significant decrease in Cr_2O_3 (Table 2.6). In contrast to the compositional-spatial behaviour of the olivine and pyroxene, the composition of the plagioclase remains relatively constant.

Feldspars

Sample	190B/D	190B/E	240/C	240/A
SiO_2	46.36	46.44	46.75	47.01
Al_2O_3	33.78	33.46	34.01	33.66
CaO	17.72	17.66	17.88	17.36
Na_2O	1.42	1.63	1.23	1.47
K_2O	0.01	0.02	0.02	0.03
BaO	-	-	-	-
FeO^*	0.47	0.45	0.50	0.51
MgO	0.04	0.05	-	0.02
Total	99.80	99.71	100.39	100.06
	Atomic %			
An	87.24	85.55	87.96	86.00
Ab	12.69	14.30	11.78	13.44
Or	0.07	0.15	0.26	0.56
	Formula (on the basis of 32oxygens)			
Si	8.562	8.588	8.575	8.698
Al	7.354	7.296	7.339	7.235
Ca	3.506	3.499	3.540	3.392
Na	.510	.585	.437	.530
K	.003	.006	.010	.022
Ba	-	-	-	-
FeO^*	.073	.070	.077	.078
Mg	.010	.014	-	.002
Total	20.018	20.058	19.978	19.957

Olivines

Sample	190B/E	190B/B	240/B	240/C
SiO_2	39.60	39.87	38.89	37.44
MgO	45.33	45.69	39.94	36.65
FeO^*	14.52	14.05	20.43	25.18
NiO	0.26	0.27	0.20	0.13
MnO	0.31	0.28	0.43	0.44
Al_2O_3	0.08	0.03	0.05	0.06
Total	100.15	100.21	99.99	99.97
	Atomic %			
Fo	84.78	85.29	77.69	71.90
Fa	15.22	14.71	22.31	28.10
	Formula (on the basis of 4 oxygens)			
Si	.993	.994	1.003	.995
Mg	1.693	1.705	1.536	1.433
Fe	.304	.294	.441	.560
Ni	.005	.005	.004	.003
Mn	.007	.006	.009	.010
Al	.002	-	.001	.002
Total	3.005	3.005	2.995	3.005

Table 2.5 Representative analyses of feldspars and olivines of the Feldspathic Allivalite. Total iron was determined as FeO^*.

Sample	190B/1	190B/B	190B/5	190B/C	240/B	240/D	240/C
SiO_2	52.08	51.64	52.20	52.33	50.92	52.15	52.81
CaO	21.60	22.01	20.25	21.63	20.66	21.94	1.80
MgO	17.26	16.94	18.03	17.49	15.35	15.85	25.52
FeO	2.90	2.41	3.74	2.91	7.01	4.79	15.49
Fe_2O_3	0.79	1.52	1.23	1.65	1.92	2.03	1.48
Al_2O_3	2.67	3.13	2.28	2.55	2.54	2.49	1.20
Cr_2O_3	1.10	1.32	0.47	0.66	0.12	0.15	-
TiO_2	0.29	0.45	0.52	0.39	0.90	0.46	0.51
MnO	0.12	0.10	0.13	0.13	0.27	0.21	0.39
Na_2O	0.23	0.24	0.20	0.23	0.29	0.30	0.51
Total	99.04	99.96	99.05	99.97	99.98	100.37	100.05
FeO^*	3.62	3.78	4.83	4.14	8.76	6.61	16.81
			Atomic % (Mn included with Fe)				
Ca	44.52	45.30	41.15	43.87	41.61	44.48	3.61
Mg	49.48	48.49	50.98	49.38	43.82	44.69	69.54
Fe	6.00	6.21	7.87	6.75	14.57	10.83	26.85
			Formula (on the basis of 6 oxygens)				
Si	1.919	1.901	1.925	1.923	1.911	1.923	1.949
Ca	.853	.868	.800	.851	.811	.867	.072
Mg	.948	.929	.991	.958	.854	.871	1.388
Fe^{++}	.089	.074	.115	.089	.219	.147	.481
Fe^{+++}	.022	.042	.034	.045	.054	.056	.041
Al	.116	.131	.099	.105	.112	.007	.012
Cr	.032	.038	.014	.019	-	.004	-
Ti	.008	.009	.014	.016	.021	.021	.004
Mn	.004	.003	.004	.004	.009	.007	.012
Na	.016	.017	.014	.016	.021	.021	.004
Total	4.007	4.012	4.010	4.021	4.016	4.017	4.010

Table 2.6 Representative analyses of pyroxenes from the Feldspathic Allivalite. Total iron was determined as FeO^* and subsequently partitioned between ferrous and ferric iron by the method of Finger (1972).

2.2.2.4 The Allivalite Series

The Outer Layered Allivalite Series, like the Border Group (Zinovieff 1958) was first identified in the northern Cuillin, and similarly forms an arcuate band which may be traced south to Coir' a' Ghrunnda. Both field and mineralogical data from the present study suggest that the "allivalite" truncated by the Peridotite Series in An Garbh-coire may be correlated with the Allivalite Series to the north and west (Fig.2.1). These rocks have an estimated thickness of 1800m and have been subdivided into five units (Zinovieff 1958). The lowest unit (Unit 1) is a feldspar-olivine cumulate, whilst each of the remaining upper four units consist of a feldspar-augite cumulate base, which grades up into a feldspar-olivine cumulate top. The Allivalite Series mapped in An Garbh-choire has an approximate thickness of 500m and its mineralogical features are broadly similar to those described above.

Petrography and mineral chemistry

Petrographically, the Allivalite Series is very similar to the underlying Feldspathic Allivalite (Section 2.2.2.3), with comparable variation in modal proportions and mineral chemistry, with plagioclase showing only limited compositional variation, An_{85-81} at its base to An_{80-75} in its upper part (Table 2.7), forsterite contents of olivines decreasing from Fo_{82} to Fo_{73} (Table 2.7) up the sequence, and slight compositional variation in pyroxenes from $(Ca_{.42}Mg_{.48}Fe_{.10})_2Si_2O_6$ to $(Ca_{.40}Mg_{.45}Fe_{.15})_2Si_2O_6$, which is accompanied by significant increases in MnO and TiO_2 and depletion in Cr_2O_3 (Table 2.8). It is worthy to note, however, that this series is richer in orthopyroxene, which becomes prevalent up the sequence and is nearly always associated with subhedral-anhedral olivine.

Feldspars

Sample	241/A	241/3	241/H	297/A	297/C
SiO_2	47.96	47.73	47.16	46.39	48.46
Al_2O_3	32.91	34.04	33.69	33.55	32.15
CaO	16.64	17.22	17.37	17.68	16.08
Na_2O	2.18	1.74	1.63	1.44	2.31
K_2O	0.01	0.05	0.02	0.08	0.11
BaO	-	-	-	0.02	0.01
MgO	0.09	0.04	0.03	0.03	0.05
FeO^*	0.35	0.37	0.41	0.53	0.57
Total	100.14	101.19	100.31	99.72	99.74
			Atomic %		
An	80.76	84.34	85.34	86.80	78.88
Ab	19.17	15.38	14.51	12.75	20.47
Or	0.07	0.28	0.15	0.45	0.65
			Formula (on the basis of 32 oxygens)		
Si	8.795	8.668	8.630	8.581	8.919
Al	7.115	7.289	7.312	7.318	6.975
Ca	3.270	3.351	3.405	3.505	3.171
Na	.776	.611	.579	.515	.823
K	.003	.011	.006	.018	.026
Ba	-	-	-	.001	-
Mg	.024	.010	.010	.002	.005
Fe	.054	.056	.063	.083	.088
Total	20.037	19.996	20.005	20.023	20.007

Olivines

Sample	241/A	241/D	297/CC	297/RC	297/1
SiO_2	39.44	39.76	38.02	37.84	38.29
MgO	43.58	43.41	36.96	36.62	37.42
FeO^*	16.38	16.38	24.30	26.64	24.75
NiO	0.24	0.24	0.27	.24	0.21
MnO	0.25	0.24	0.40	0.40	0.40
Al_2O_3	0.03	0.03	0.07	0.05	0.05
CaO	0.01	0.02	0.03	0.04	0.03
Total	99.93	100.08	100.05	99.83	101.15
			Atomic %		
Fo	82.26	82.60	73.06	72.59	72.91
Fa	17.74	17.40	26.94	27.41	27.09
			Formula (on the basis of 4 oxygens)		
Si	.996	1.002	1.001	.999	.997
Mg	1.641	1.638	1.448	1.441	1.451
Fe	.354	.345	.534	.544	.539
Ni	.005	.005	.006	.005	.004
Mn	.006	.006	.008	.009	.009
Al	.001	-	.002	.002	.002
Ca	-	.001	.001	.001	-
Total	3.003	2.997	3.000	3.001	3.002

Table 2.7 Representative analyses of olivines and feldspars from the Allivalite Series. Total iron was determined as FeO^*.

Sample	241/E	241/1	241/D	241/2	297/H	297/I	297/B	297/F
SiO_2	51.50	52.13	51.42	50.96	51.98	51.87	51.48	54.17
TiO_2	0.49	0.59	0.35	0.76	0.73	0.53	0.58	0.38
Al_2O_3	3.29	2.54	3.25	2.49	2.32	2.35	2.29	1.19
Cr_2O_3	0.82	0.76	1.19	0.76	0.24	0.27	0.22	0.08
Fe_2O_3	1.95	2.68	1.85	2.56	0.48	0.32	1.91	0.22
FeO	3.71	4.91	3.15	3.09	8.22	6.77	7.63	15.92
MnO	0.17	0.23	0.14	0.18	0.32	0.19	0.22	0.33
MgO	15.93	19.77	15.78	16.27	15.79	15.19	16.67	26.47
CaO	21.90	16.48	22.44	21.52	19.45	22.05	18.32	1.23
Na_2O	0.36	0.29	0.32	0.38	0.26	0.27	0.22	0.02
Total	100.12	100.38	99.89	98.97	99.79	99.81	99.54	100.01
FeO^*	5.48	7.33	4.76	5.39	8.63	7.69	9.34	16.11
				Atomic % (Mn included with Fe)				
Ca	45.19	33.04	46.52	44.38	40.25	44.65	37.44	2.43
Mg	45.72	55.12	45.53	46.65	45.45	46.28	47.34	72.35
Fe	9.09	11.83	7.95	8.97	14.30	12.67	15.22	25.22
				Formula (based on 6 oxygens)				
Si	1.898	1.904	1.900	1.903	1.932	1.931	1.921	1.962
Al	.143	.109	.137	.110	.102	.103	.101	.051
Fe^{+++}	.054	.073	.050	.071	.013	.028	.053	.006
Fe^{++}	.114	.149	.097	.096	.255	.210	.237	.482
Ti	.014	.016	.009	.021	.020	.015	.016	.010
Mn	.005	.007	.005	.006	.007	.006	.007	.010
Mg	.875	1.076	.871	.905	.874	.825	.927	1.429
Ca	.865	.645	.890	.861	.774	.863	.733	.048
Na	.026	.021	.023	.027	.019	.020	.016	.002
Cr	.024	.022	.035	.022	.007	.008	.006	.002
Total	4.018	4.022	4.017	4.022	4.003	4.009	4.017	4.002

Table 2.8 Representative analyses of pyroxenes of the Allivalite Series. All iron was determined as FeO^* and was subsequently partitioned between ferrous and ferric iron by the method of Finger (1972).

2.2.3 Discussion

Following the recognition of a Border Group to the layered intrusion in the Northern Cuillin by Zinovieff (1958), Hutchison (1964) was able to confirm its existence in the west. Due to its distinctive appearance and composite form, Hutchison was able to trace the group as far as Coir' a' Ghrunnda in the south-west. The Border Group comprises a fine grained tholeiite with xenoliths of Outer Unlayered Gabbro (Ring Eucrite of Hutchison 1964) along its outer margin and passes inwards to a coarse grained unlayered allivalite (The "White Allivalite" of Hutchison 1964), the thickness of which varies between 200m in the west and 600m in the north. Its outer contact with the Outer Unlayered Gabbro is sub-vertical and, therefore, as the inner margin dips inwards at approximately 60^{o}, the White Allivalite must thin upwards and outwards. During this study the White Allivalite has been traced eastwards from Coir' a' Ghrunnda, where it forms the third "boiler plate" slab of this spectacular rocky corrie (Fig.2.8), towards the summits of Sgurr nan Eag and Sgurr a' Choire Bhig. Unfortunately, due to the precipitous topography it has not been possible to traverse the full length of the contacts, however, it is believed that the White Allivalite crosses the main Cuillin ridge at the col between Sgurr nan Eag and Sgurr a' Choire Bhig. It therefore seems probable that the Feldspathic Allivalite mapped in An Garbh-coire is the easterly continuation of the White Allivalite, a proposal generally supported by both field observations and textural/mineralogical studies.

Following the work of Weedon (1956), Wager & Brown (1968) concluded that the allivalites and the peridotites of An Garbh-choire were of the same series, with the latter forming the basal part of the former. This conclusion was generally supported by Hutchison and Bevan (1977), who correlated the Unit 1 allivalite with allivalites occurring within rocks formerly assigned to the Peridotites Series. These proposals were largely based on the field relationships for the Southern Cuillin as deduced by Weedon (1956). He, however, erroneously assigned all rocks occurring to the south and in contact with the Peridotite Series to the Outer Unlayered Gabbros (Ring Eucrite) and which therefore did form an integral component of the basic layered complex. Hutchison and Bevan (1977) suggested, principally from evidence in Coireachan Ruadha, that the peridotites and dunites of the

Fig.2.8. Coir' a' Ghrunnda. The White Allivalite of the Border Group forms the prominent pale band extending across the view overlying the Outer Unlayered Gabbro and overlain by the Allivalite Series.

Peridotite Series are no more than the basal part of the Allivalite Series which is banked up upon the Border Group (Fig.2.9) and that the crescentic outcrop of peridotite occurring on Sron Bhuidhe is the result of downfaulting of a central block, negating Harker's (1904) hypothesis that the outcrop is a sill emplaced into the Allivalite Series.

The identification of the Allivalite Series in An Garbh-hoire, and its relationship to the peridotites, precludes the latter from being the basal part of the Allivalite Series, as suggested by Hutchison and Bevan (1977), as the peridotites clearly truncate both the Border Group and the Allivalite Series. Consequently, the origin of the peridotite outcrop on Sron Bhuidhe is here once again reverted to a sill origin, as originally proposed by Harker (1904).

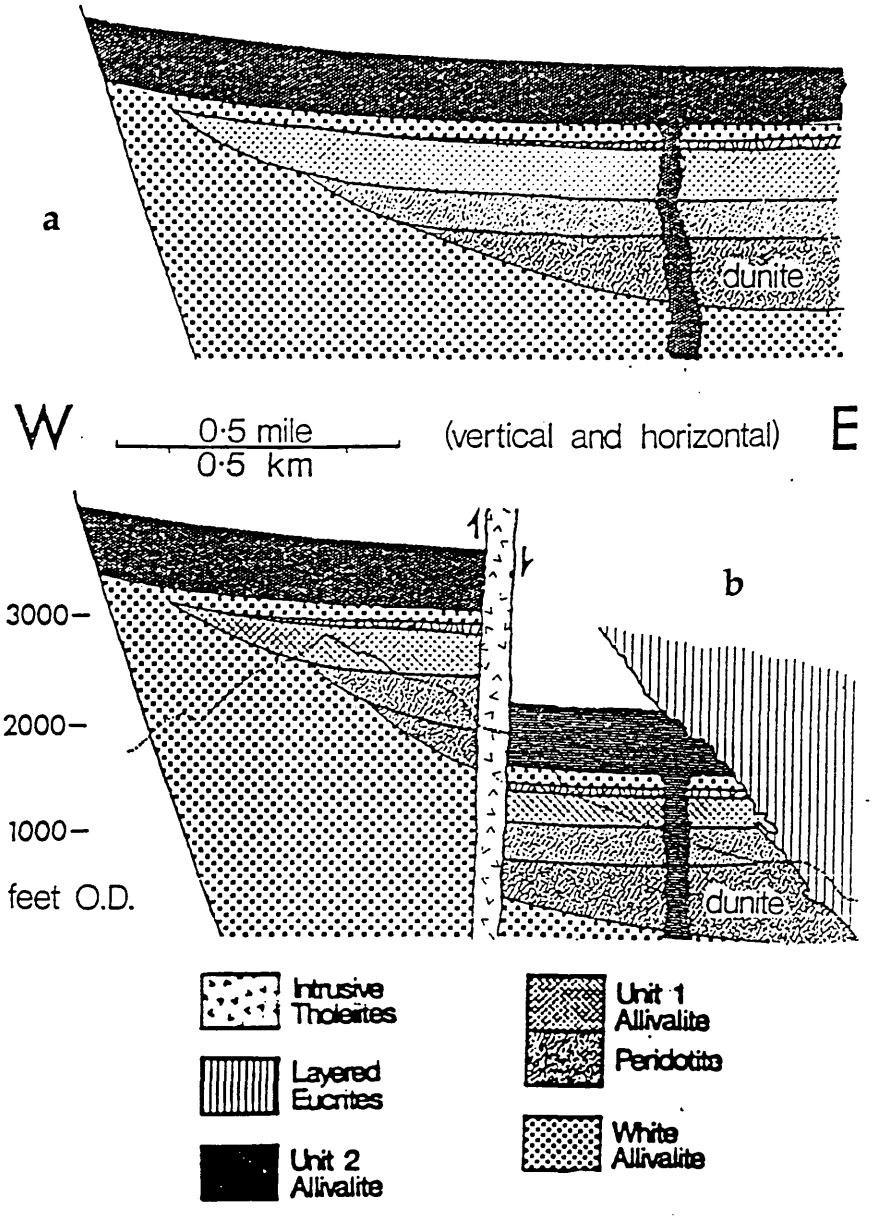

Fig. 2.9. Proposed formation of the Cuillin Central Igneous complex (a) and faulting model to account for the distribution of the principal rock types in Coireachan Ruadha. (After Hutchison and Bevan 1977).

a) Development of funnel shaped intrusion, bounded by marginal "White Allivalite". The lower lithologies comprise dunite and peridotites of the Peridotite Series which pass up into The Allivalite Series.

b) Subsequent to the formation of the layered complex the intrusion is cut by the emplacement of the Outer Layered Eucrite Series. Finally, accompanying intrusion of the Tholeiitic volcanic breccia, rocks to the east are downthrown relative to those occurring to the west of the breccia.

Present day topography shown by dotted line.

2.3 The Peridotite Series

2.3.1 Field relationships

Rocks assigned to the Peridotite Series are exposed in an arcuate band in the Southern Cuillin (Map 1). The outcrop is principally confined to the north and east of the main Cuillin ridge. In addition, the upper part of Coir' a' Ghrunnda is floored by peridotite. The main arcuate exposure extends from just above the shores of Loch Scavaig in the east to the headwaters of Loch Coruisk in Coir'-Uisg in the north, a distance of approximately 5km. Exposure is excellent throughout the outcrop, with the exception of its northern termination, where the ground is boulder strewn, and in the east, above the Allt a' Chaoich where thick accumulations of peat occur. The southern contact between the peridotite and the outer gabbros is easily identified due to the intense brick-red coloration of the weathered peridotite. Where contacts are not exposed they may be mapped to within approximately 5m. Such precision is unobtainable for the northern inner contact with the layered gabbros of Meall na Cuilce in the east where, in the hummocky ground above the Allt a' Chaoich, a large number of blocks of peridotite are enclosed within the eucrite. Exposure here varies from irregular veins of eucrite cutting the peridotite to eucrite with occasional peridotite xenoliths (see Section 2.3.3.4 and Fig.2.5, 2.30, and 2.31) of the rock step no xenoliths are present and it is possible to map a sharp, clearly defined boundary.

The lowest exposure of peridotite occurs as a small tongue extending down the Allt Beag, the small stream to the south of the Allt a' Chaoich, towards Loch Scavaig in the east. This narrow tongue broadens significantly on the poorly exposed ground above (c.230m O.D.). The outcrop follows An Garbh-choire and narrows to approximately 500m, with the formation of a rock step at about 370m O.D. This marked narrowing of the peridotite is the result of the encroachment of the more resistant surrounding gabbros and eucrites. Above the rock step, both the inner and outer contacts are sharp, the inner (northern) contact here totally devoid of xenoliths. A relatively constant width is maintained by the peridotite as the exposure continues towards the main ridge. However, just below the ridge, at c740m O.D., the outer contact trends south-west to cross the ridge on the northern shoulder of Sgurr nan Eag (924m O.D.), whilst the inner contact maintains its north-westerly trend to cross the

ridge between the peaks of Sgurr Dubh an Da Bheinn (938m O.D.) and Sgurr Dubh Mor (944m O.D.). The southern contact descends into Coir' a' Ghrunnda, crosses Loch Coir' a' Ghrunnda and climbs the north-westerlly slopes of the corrie to recross the main ridge to the south-east of Sgurr Alasdair (992m O.D.). Both contacts then gradually swing to a more northerly trend, maintaining a constant width of approximately 500m, before terminating in Coir'-Uisg. The nature of the termination is uncertain due to the poor exposure here, however, evidence from mapping suggests that the contacts may be faulted against the Outer Layered Allivalite Series (Map 1).

A further isolated exposure of peridotite occurs forming the easterly cliffs of Sron Bhuidhe to the east of the main ridge, overlooking the main peridotite outcrop. This small crescentic exposure was considered by Hutchison and Bevan (1977) to have originally been part of the main Peridotite Series, but was subsequently faulted into its present position. One further outcrop of peridotite, to be found to the south-west of the main ridge, is the peridotite forming the small knoll of An Sguman (246m O.D.). This outcrop is seen to have been intruded into the plateau lavas (Map 1) and Outer Unlayered Gabbros.

Weedon (1956) suggested that the outer contacts of the Peridotite Series with the surrounding gabbros are considerably steeper than the northerly 30^{o} dip envisaged by Harker (1904). Whilst locally the contacts are vertical, the Gars-bheinn Gabbro is exposed in small bluffs within the main body of the peridotite in the vicinity of the Allt Beag, which suggests that the overall dip of the contact is of the order of 45^{o} towards the north-west (Fig.2.10). The inner contact with the Outer Layered Eucrite Series has also been found to be steeper than envisaged in earlier work, with dips or around 80^{o} towards the north-west.

The outer gabbros were divided by Weedon into two sub-types; the Gars-bheinn and the Clouded Feldspar Gabbro. The clouding of the feldspar, he surmised, was due to the exsolution of iron oxides during the reheating of the gabbro by the emplacement of the peridotite.

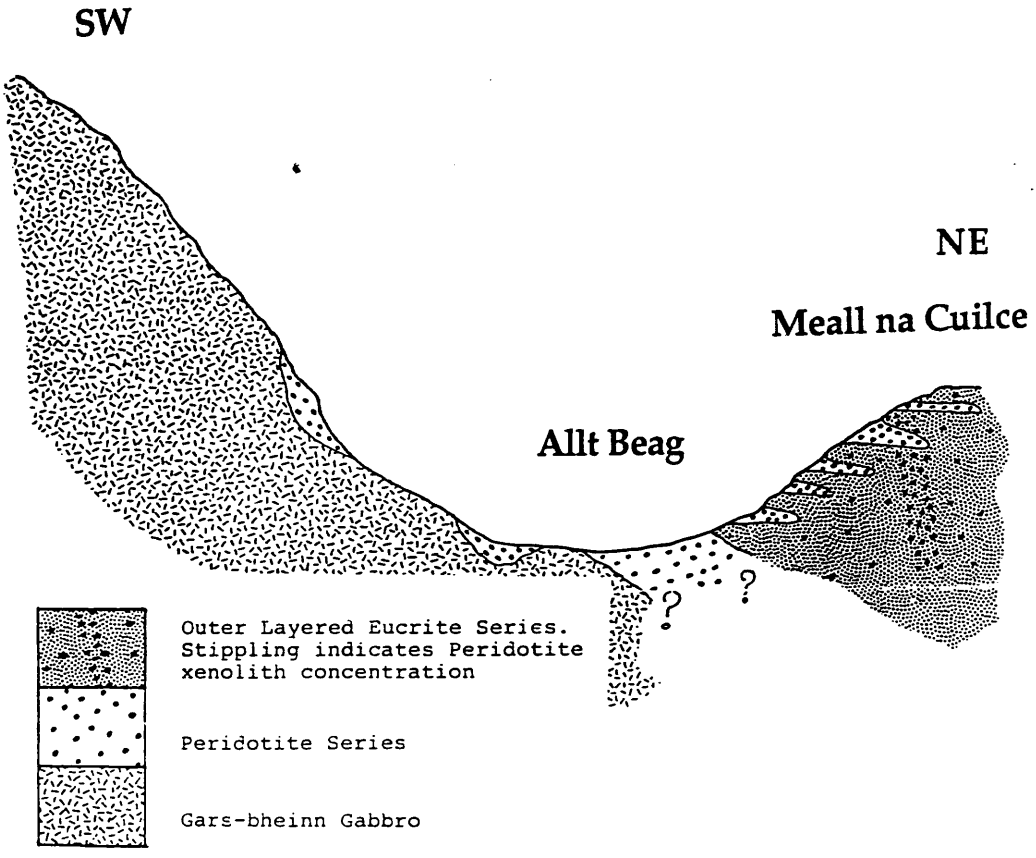

Fig. 2.10. Suggested field relationships of the peridotite series (Zone 1) with the (older) Gars-bheinn Gabbro and the (younger) Outer Layered Eucrite Series.

The most striking feature of the Peridotite Series is the lithological heterogeneity they show in outcrop. Whilst Weedon's classification (1956) provides a first order approximation to the disposition of the observed lithologies, with dunites giving way to troctolites as the succession is ascended, much inter-digitation of the dunites and troctolites with allivalite and feldspathic peridotite is observed.

The overall structure of the mass was determined by Weedon (1956) on the basis of phase layering. However, such layering is scarce throughout the succession and at best can only be described as being patchily developed. Where it does occur, it is of limited lateral extent, which unfortunately does not allow direct correlation with adjacent exposures, whose layering may show conflicting attitudes. Within the peridotites in the Allt Beag area (Zone 1), such a problem does not exist. Here, the occurrence of several thin (<2cm) seams of chromite dipping at c.70^{o} towards the north-east, can be traced for approximately 100m and which allow the attitude and local succession to be determined. The rocks occurring in this area are principally dunites, which locally may pass laterally into peridotites. Coincident with the attitude of the chromite seams, a lineation fabric has developed by the alignment of olivine crystals on (010) and (001). This fabric generally parallels the contact of the peridotites with the gabbros to the south.

2.3.2 Structure

The overall internal structure of the Peridotite Series may be discerned from the presence of phase layering which, although not ubiquitous, is widely developed. Within the area of the ultrabasic tongue of the Allt Beag, the principal lithology is dunite, with occasional phase layering displayed by the two cumulus minerals olivine and spinel (Section 2.3.5).

Structurally higher within the peridotites there exist horizons where feldspar joins olivine and spinel in the cumulus assemblage and in these areas phase layering comprises thin alternations of troctolite and peridotite.

The most notable feature of the flat ground in An Garbh-choire, below the rock step, is the extent to which brecciation has occurred (Fig.2.11). This area of disruption appears to occupy all the poorly exposed low ground but dies out rapidly on approaching and ascending the well exposed rising ground to the south. Where disruption of the peridotite is

Fig.2.11. Type II brecciation within Zone 4 peridotites. The dominant lithologies are allivalitic xenoliths enclosed within a peridotite matrix. The dark angular inclusions occurring within the xenoliths (top right) are of pyroxene (Section 2.3.5.3.). Length of hammer shaft c.70cm.

minimal, layering is seen to be concordant to that occurring within and around the ultrabasic tongue, with dips between c.30-70^{O} towards the NNW, and strike approximately parallel to the margins of the mass.

The only significant departure of the orientation of the layering to that described above is to be found in a relatively narrow band which may be traced from the high ground above and south of the Allt Beag area, to just below the rock step, a distance of approximately 1km. Within the band, wispy inter-digitating layers of peridotite, feldspathic peridotite and troctolite occur. These layers are of the order of a few centimetres to a few tens of centimetres thick (Fig.2.12). However, individual layers are impersistent and thicken and thin continuously, and may even pinch out over a metre or so along strike, parallel to the contact of the Peridotite Series. Layering within the band is vertical and, where it can be determined, is concordant to the margins of the band. It is uncertain whether the band extends as far south as the contact of the peridotites with the Gars-bheinn Gabbro but steep dips observed in isolated exposures and occasional lineation fabrics which extend right up to the contact suggests this to be the case. If this is so, then the band has a thickness which varies from a few metres in the east to c.150m as it is traced towards the rock step in the west. However uncertain the relationship of the band to the margins of the peridotites, there is no doubt that this unit represents an important discordance within the structurally lowest peridotites, a conclusion which is supported by mineral chemistry data (Section 2.3.3).

Immediately above the rock step, peridotite-troctolite layering becomes prevalent (Fig.2.13), with dips approximating those seen lower in the sequence. Particularly well developed modal and phase layering is exposed along a narrow knoll trending parallel to the contacts just above the confluence of two streams (G.R. 4697 1995) in the upper part of the corrie. At this locality, narrow bands of peridotite are gradational upon troctolite bands of similar thickness (Fig.2.14). Within this exposure some of the peridotite bands are characterized by a lace-like texture (Fig.2.15) which re-appears higher in the corrie (Section 2.3.3.5). The most obvious layering above the rock step, however, is one of generally thin, sharp, clearly defined layers of allivalite, similar to much of the material in the Zone of Brecciation.

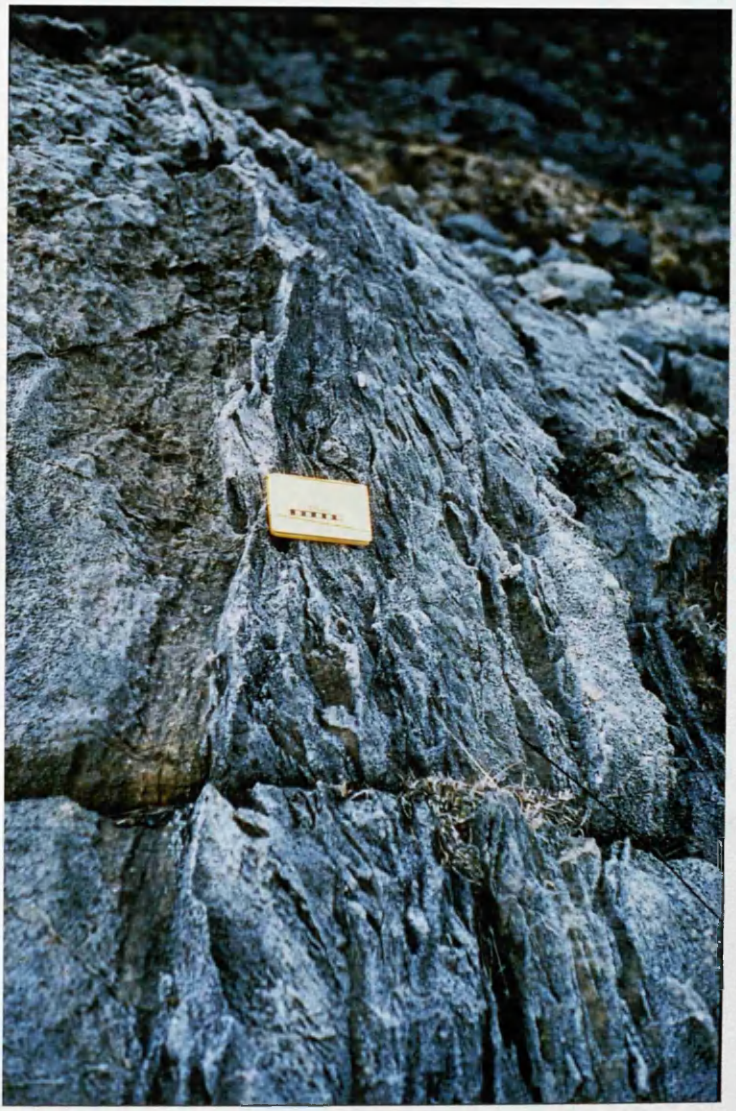

Fig.2.12. Zone 2 peridotites are characterized by impersistent, undulatory, interdigitating, wispy bands of peridotite, feldspathic peridotite and troctolite [G.R.4771 1950].

Fig.2.13. Vertical phase layering comprising olivine cumulate (peridotite) and olivine + plagioclase cumulate (troctolite) occurring within Zone 5 [G.R.4524 2026]. Length of hammer shaft c. 60cm.

Fig.2.14. Gradational cyclic phase layering within Zone 5. Steeply northerly dipping peridotites (olivine cumulate) are gradationally overlain by troctolite (olivine + plagioclase cumulate). These in turn are overlain by peridotite [G.R.4636 2002].

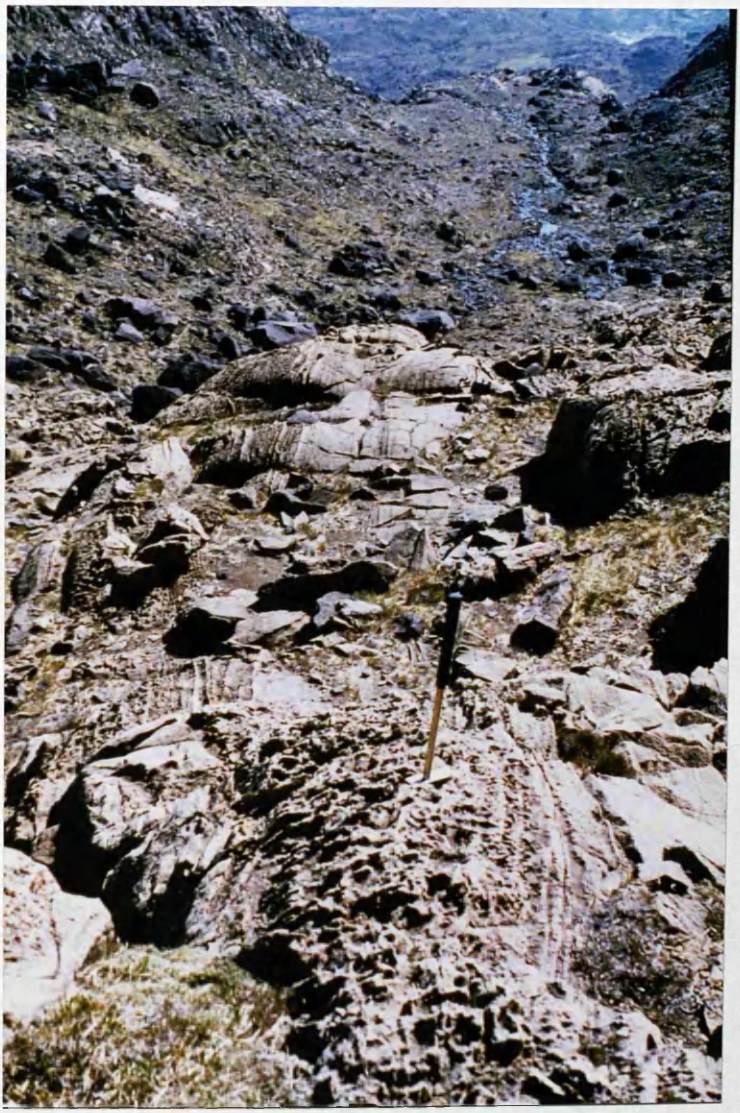

Fig.2.15. Sub-vertical lace-textured peridotite band within massive peridotite and allivalite of Zone 5 [G.R.4622 2005]. Length of hammer shaft c. 60cm.

The structure of the boulder strewn upper part of the corrie may most easily be deduced by extrapolation of that observed in Choir a' Ghrunnda. Within this corrie, an almost complete sequence of the Upper Peridotites, with an estimated thickness of 500 metres is exposed. Occurring within this sequence is a prominent two metre thick allivalitic band which acts as a useful marker horizon from which the overall structure may be elucidated (cf. Hutchison & Bevan 1977). The band is exposed on the west side of the main ridge just below and to the south of Caisteal a' Garbh-choire (Fig.2.16), approximately 5 metres below the ridge. It may then be traced north-westwards to about 30m above the lochan, from which it ascends to the rear (northern) wall of the corrie and crosses the ridge to the south-east of Sgurr Alasdair. Exposure is then lost on the poorly exposed ground to the north of the ridge. This distinctive band has a broad plunging synclinal geometry, the axis of which dips north-east at about 50^{o}. The dominant lithology below this horizon is peridotite, with thin feldspathic peridotite or allivalite bands. The more feldspathic bands are irregular, may pinch out laterally, or either be truncated by the peridotite or asymptotic towards it (Fig.2.17). In contrast, any fabric within the peridotite is usually regular and persistent. The structurally higher levels above the allivalitic band are characterized by feldspathic peridotite and allivalite (Fig.2.18), with much of the upper sequence containing xenoliths of either peridotite and/or allivalite (Fig.2.19). Whilst a small proportion of the xenoliths range in size up to c.50cm, the majority are less than 10cm and are usually well rounded. It seems likely that the xenoliths are of local origin, as they may be correlated with adjacent lithologies. However, the presence of a coarse-grained, open textured, feldspathic type is more problematic, for a similar lithology is not found within the Peridotite Series. Mineralogically and texturally, these examples are comparable to the White Allivalite (Section 2.2.2.3) of the Border Group, which crops out approximately 500m to the south. This unit, however, is separated from the Peridotite Series in Choir' a' Ghrunnda by the less feldspathic Allivalite Series (section 2.2.2.4). The only locality where peridotite is in contact with such a feldspathic rock occurs approximately 2km to the east, where the Peridotite Series truncates members of the Border Group (Fig.2.1). The field evidence suggests that

Fig.2.16. Casteal a' Garbh choire and Loch coir' a' Ghrunnda. The southern (outer) contact of the Peridotite Series with the Gars-bheinn Gabbro runs approximately vertically at the right hand side of the figure. The structure of the peridotites of this area is deduced from the feldspathic bands which may be seen dipping at about 40' to the left (north-west). The junction between Zone 5 and the overlying Zone 6 runs through the notch in the ridge to the left (north) of the casteal.

Fig.2.17. Feldspathic veins and pods within peridotites of Zone 5. The veins are generally concordant to any fabric which may occur within the peridotite. [G.R.4530 2028]. Length of hammer shaft c. 40cm.

Fig.2.18. Zone 6 of the peridotite series comprises alternating peridotite and feldspathic peridotite bands. The contact between the Peridotite Series and the overlying darker Outer Layered Eucrite Series may readily be seen to the right of the col between Sgurr Dubh Mor and Sgurr Dubh an Da Bheinn.

Fig.2.19. Angular, feldspathic, blebby xenoliths within peridotites of Zone 5. [G.R.4549 2025]. Length of hammer shaft c.60cm.

the Peridotite Series gradually oversteps the Border Group in the region of Choir' a' Ghrunnda, thus preventing incorporation of the feldspathic allivalite as xenoliths until a later stage in the development of the peridotites.

It has proved impractical to map individual lithologies due to the heterogeneity displayed by much of the peridotite, particularly the laterally impersistent modal/phase layered bands. The only significant lithological variation which appears to be continuous and may be mapped with certainty is the peridotite-allivalite alternations. On this basis and the evidence of brecciation, and a possible discontinuity within the structurally lower peridotites, six zones have been identified and may be defined as follows.

The structurally lowest Zone (1) is essentialy that of Weedon (1956 & 1965) and comprises dunites and peridotites. It is uncertain how this zone relates both spatially and temporally to the Marginal Band (Zone 2). Certainly, the two zones are distinct with the Marginal Band more evolved (cumulus olivine + feldspar +/- spinel). It is possible that the marginal zone may represent a Border Group to the Zone 1 peridotites (Fig.2.20). Zone 3 comprises those rocks which cropout on the rising ground to the south of An Garbh-choire between the brecciated peridotite and allivalite of Zone 4 occupying the flat ground of the Corrie in the north and the whispy banded Zone 2 peridotites in the south. The contact relationship of this zone with Zone 2 is unclear, however, the northerly contact with Zone 4 is gradational over a short distance. Zones 1-4 all appear to be truncated by zone 5 which commences at the rock barrier. The rock step forms not only a topographic feature but also a structural discontinuity the nature of which remains enigmatic due to the convergence of Zones 3 and 4 below the step and the termination of Zone 4 at or just above the barrier. Phase and modal layering within Zone 5, above the barrier, coincident with that observed in zones 1, 2 and 3, is generally gradational in nature and particularly well displayed within the lower part of the upper corrie. However, discrete allivalitic bands up to c.1m in thickness may also be seen in this area (Section 2.3.4). Within the higher part of Zone 5 the dominant lithology is peridotite, although irregular patches of feldspathic peridotite do occur and contain unusual textural features produced by the intergrowth of intercumulus feldspar with cumulus olivine. The contact of Zone 5 with Zone 6 occurs approximately along the base of the summit cliffs

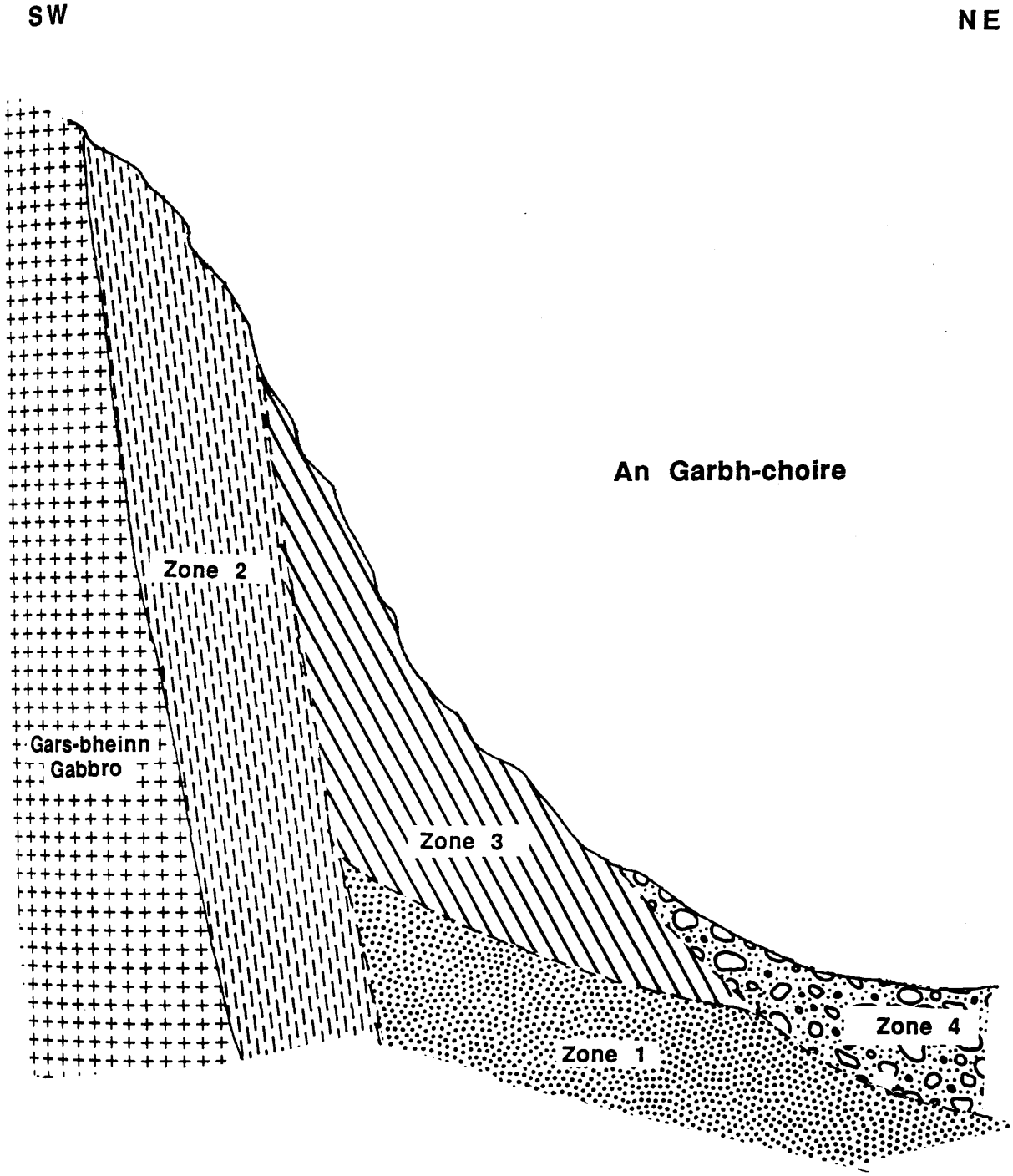

Fig.2.20 Schematic diagram illustrating the relationships between the Gars-bheinn Gabbro and Zones 1, 2, 3 & 4 of the Peridotite Series within the lower part of An Garbh-choire.

of Sgurr Dubh an Da Bheinn and Sgurr Dubh Mhor (Fig.2.20) towards the northerly contact of the Peridotite Series with the Outer Layered Eucrite series. Rocks of Zone 6 are characteristically more feldspathic and contain alternating bands of peridotite and allivalite both of which are notably richer in pyroxene than seen elsewhere within the series. The field characteristics of this zone have much in common with the Outer Layered Allivalite series occurring to the south, but contains numerous xenoliths generally of the order of a few tens of centimetres in size composed of a variety of ultrabasic lithologies (Fig.2.21).

2.3.3 Peridotite Zones

2.3.3.1 Zone 1

Zone 1 comprises those rocks occurring within the ultrabasic tongue which crops out in the area around the Allt Beag and extends from the eastern extremity of the exposures of ultrabasic rocks, about 35m above Loch Scavaig, westwards for about 375m. Rocks within this zone are principally dunites which weather to a smooth reddish-brown surface and are believed to represent the structurally lowest exposed part of the Peridotite Series. The lower part of this zone is thoroughly dunitic with olivine accounting for 85-90% of the mode, spinel 8-10% and plagioclase 2-4%. Phase layering is absent within the lowest part of the zone. However, a lineation fabric due to the alignment of olivines is evident throughout much of the exposure, to a greater or lesser extent. This fabric generally parallels the margins of the dunites with the enclosing gabbros. Slightly higher in the sequence, phase layering is developed due to the occurrence of thin seams of spinel (Fig.2.22) (Section 2.3.4.1). Pyroxene is all but absent from the zone and plagioclase is insignificant, only occurring occasionally as small (c.0.5mm) interstitial plates, the composition of which varies from An_{85-90} to An_{81-87} (Table 2.9) on ascending the sequence. The most obvious mineralogical variation throughout the zone is the change in the colour of the spinels (Section 2.3.4.1), from reddish-brown at the base of the zone through to black, almost opaque, octahedra at the top. The olivines are commonly 1-2mm in diameter, sub-hedral, and are tightly packed together, the contact between individual crystals straight or simply curved, parallel to (110) and inter-crystal contacts of c.120^{O} parallel to (001). Olivine

Fig.2.21. Angular peridotite and allivalite xenoliths within feldspathic peridotite of Zone 6.

Fig.2.22. Sub-vertical spinel seams within dunites of Zone 1. These seams may be traced for approximately 100m along strike without significant deviation and enable the structure of the otherwise structureless dunites to be elucidated. [G.R.4787 1967].

crystals may contain spinel inclusions up to 0.5mm. Clearly distinguishable from the spinels are trains of minute inclusions, which are present within most crystals. The composition of these inclusions remains unknown. Occasionally, these trains may be traced into adjacent olivines or, rarely, into intercumulus plagioclase. Poorly developed cleavage is occasionally seen parallel to (010) and (100). Over the 150m thickness of this zone, there is a decrease from Fo_{94} adjacent to the spinel seams to Fo_{88} at the apparent top of the sequence. The olivines from the base of the zone, adjacent to the spinel seams, are the most forsteritic reported from the Cuillin Complex to date (Table 2.9). It is interesting to note that there is no detectable variation in both the major and minor element composition of the olivines across the spinel seams.

2.3.3.2 Zone 2

Zone 2 is probably the most poorly defined zone in terms of both its extent and its structural relationships with adjacent zones. Lithologically, it comprises impersistent, wispy bands of troctolite and feldspathic peridotite although, locally, small pods (c.20cm) of peridotite and dunite may be present. These irregular, sub-vertical bands (Fig.2.23) are generally of the order of 10cm in thickness, but thicken and thin along strike, frequently with individual bands pinching out. At its eastern end, the zone is approximately 2-3 metres in width and separates the dunites of Zone 1 from the Gars-bheinn Gabbro (Section 2.2.2.1). In common with much of the zone, a strong, well developed lineation fabric is evident due to the alignment of olivine and, where present, plagioclase. Further west, the zone appears to widen significantly, such that in its middle reaches it attains a thickness of approximately 170 metres. However, exposure in this region is discontinuous and the foregoing assumption is based on the observation that many of the small exposures in this area possess similar sub-vertical bands, whilst peridotite adjacent to the gabbros to the south displays a lineation fabric. The lineation fabric, particularly well developed in the east, extends a few metres into the zone. Where the peridotite is in contact with the White Allivalite and Outer Allivalite Series, it is observed locally that the peridotite invades the feldspathic rocks with small irregular apophyses which may extend up to a few tens of centimetres. These apophyses may isolate xenoliths of the feldspathic rocks (Fig.2.24).

	Feldspars			
Sample	AG1/1	AG5/8	AG1/3	AG5/1
SiO_2	46.71	46.42	46.58	47.65
Al_2O_3	33.92	33.78	33.57	33.00
CaO	17.66	18.00	18.2	16.74
MgO	0.03	0.03	0.02	0.04
FeO^*	0.16	0.30	0.18	0.19
BaO	0.01	0.02	0.01	-
Na_2O	1.43	1.21	1.39	2.16
K_2O	0.01	0.01	0.02	0.04
Total	99.93	9.77	99.97	99.82
	Atomic %			
An	87.16	89.43	87.81	80.92
Ab	12.79	10.49	12.08	18.86
Or	0.05	0.07	0.10	0.22
	Formula (on the basis of 32 oxygens)			
Si	8.595	8.530	8.588	8.767
Al	7.358	7.317	7.296	7.157
Ca	3.481	3.690	3.597	3.299
Mg	.009	.008	.007	.012
Fe	.025	.045	.028	.030
Ba	-	.002	-	-
Na	.511	.433	.495	.769
K	.002	.003	.004	.009
Total	19.981	20.028	20.015	20.043

	Olivines						
Sample	AG5/3	AG1/2	AG1/1	AG5/4	AG2/3	AG2/5	AG2/4
SiO_2	40.44	41.58	41.23	40.53	41.07	41.36	41.02
Al_2O_3	0.05	0.02	0.02	0.01	0.10	0.02	0.03
CaO	0.09	0.07	0.10	0.06	0.05	0.07	0.08
MgO	48.27	50.07	50.01	47.43	52.04	52.07	52.19
FeO^*	10.27	7.65	7.6	11.19	6.07	5.99	6.17
MnO	0.18	0.24	0.18	0.19	0.14	0.13	0.13
NiO	0.42	0.34	0.33	0.39	0.33	0.33	0.33
Total	99.72	99.97	99.57	99.80	99.80	99.97	99.95
	Atomic %						
Fo	89.33	92.12	92.16	88.29	93.85	93.93	93.77
Fa	10.67	7.88	7.84	11.71	6.15	6.07	6.23
	Formula (on the basis of 4oxygens)						
Si	.998	1.009	1.005	1.003	.993	.998	.991
Al	.001	-	.001	-	.003	.001	-
Ca	.002	.002	.003	.002	.001	.002	.002
Mg	1.775	1.812	1.821	1.749	1.876	1.872	1.880
Fe	.212	.155	.155	.232	.123	.121	.125
Mn	.004	.005	.004	.004	.003	.003	.003
Ni	.008	.007	.006	.008	.006	.006	.006
Total	3.000	2.990	2.995	2.998	3.005	3.003	3.007

Table 2.9 Representative olivine and feldspar analyses of Zone 1 of the Peridotite Series. Total iron was determined as FeO^*.

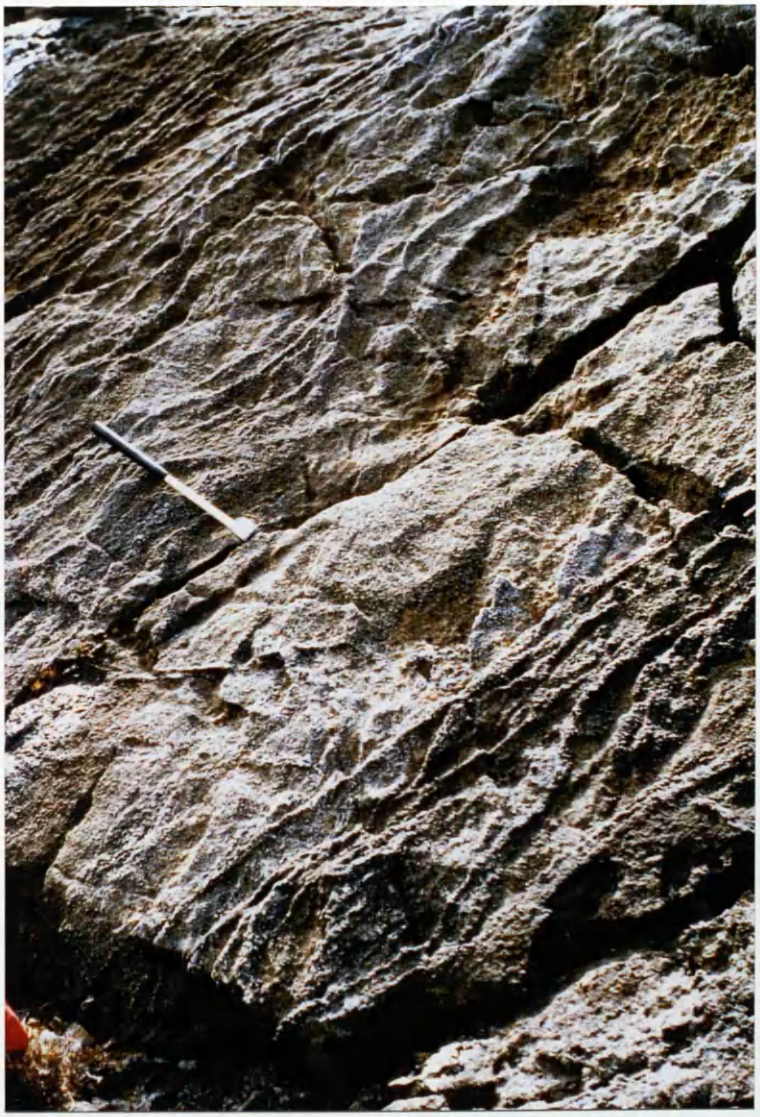

Fig.2.23. Wispy, impersistent, coarse feldspathic peridotite, peridotite and troctolite bands of Zone 2. (G.R. 4784 1947). Length of hammer shaft c. 60cm.

Petrographically, the most notable feature is the presence of colourless granular material which may take the form of individual isolated anhedral grains less than 2mm in size enclosed within any of the silicate phases but more commonly are aggregated into narrow (<1mm) veinlets. These veins may either be seen bisecting olivine, plagioclase or pyroxene crystals or may be found rimming subhedral olivine or clinpyroxene. Occasionally olivine crystals may be wholly or partly replaced by this granular material (Fig.2.25) whilst clinopyroxene may be rimmed by hornblende. Electron probe studies have revealed that the granular material is mainly composed of orthopyroxene (Table. 2.10) with subordinate amounts of olivine and plagioclase. Whilst the size of the granular orthopyroxene remains constant, the plagioclase may exhibit a range of sizes. Strongly pleochroic (colourless-dark brown) biotite may also be seen within the veins or as discrete clusters often associated with black spinel (Fig.2.26). Of note is the infrequent occurrence of dusty intergranular quartz showing undulatory extinction (Fig.2.27). The nature of the westerly termination of the zone is uncertain due to poor exposure, however, it appears that the zone begins to narrow as it is encroached upon by Zone 3 and Zone 4 peridotites, approximately 100 metres before the rock barrier. Throughout much of the central and westerly exposure the rock is coarse and weathers to give a rough clinkery surface due to the high proportion of large (c.5cm) angular clots of intercumulus plagioclase which stand proud of the weathered surface (Fig.2.28). Contacts between individual troctolite and peridotite bands may be gradational or sharp.

Although significant lithological variation across the zone is apparent, this is generally not reflected in mineral compositions, which appear to be independent of host lithology. A small decrease in the forsterite content of olivine has, however, been detected across the width of the outcrop (Table 2.11). Towards the peridotite-gabbro contact to the south, olivines are at their most primitive, Fo_{89-90}. This value decreases slightly to Fo_{86-88} and is accompanied by a decrease in NiO (0.37-0.32 wt. %) further up the zone. Cumulus plagioclase within the troctolite-allivalite bands is euhedral (An_{89-90}) and shows no zoning, whilst intercumulus feldspar varies between An_{89} and An_{86} (Table 2.11). Within the peridotite bands olivine accounts for 75-80% of the mode, intercumulus plagioclase for

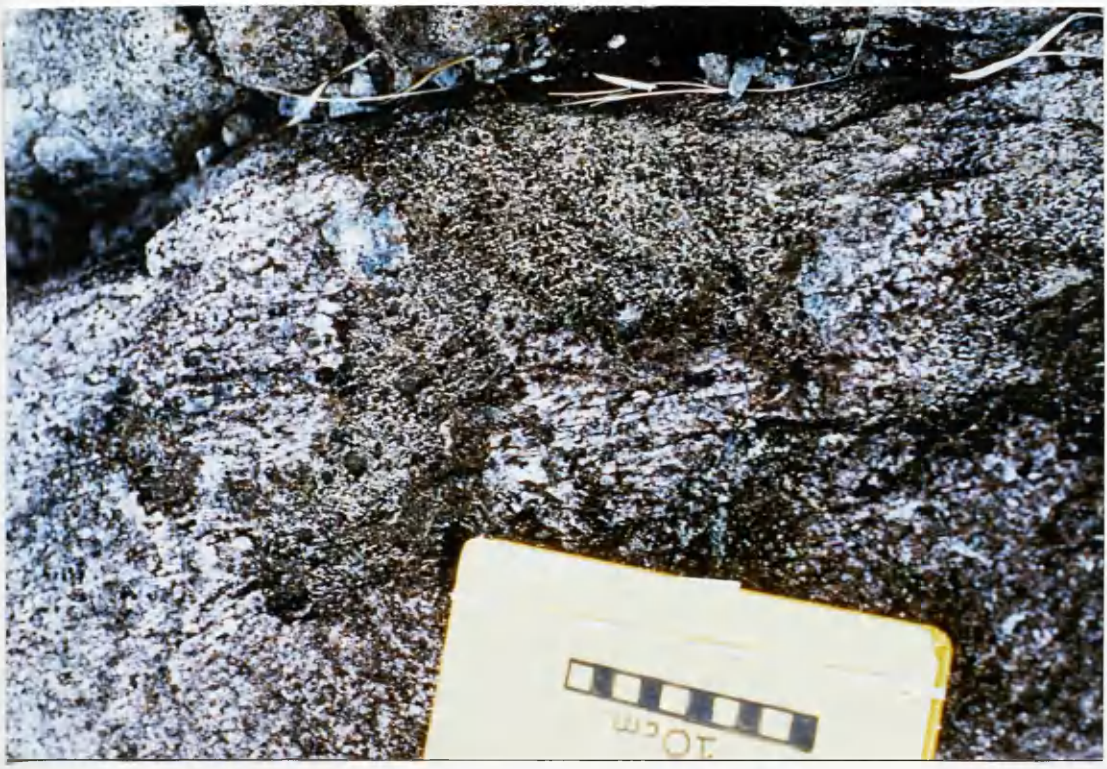

Fig.2.24. Irregular, apparently corrosive contact between peridotite and the White Allivalite. The localized sub-horizontal fabric of the White Allivalite is preserved locally within presumed detached blocks. [G.R. 4715 1954].

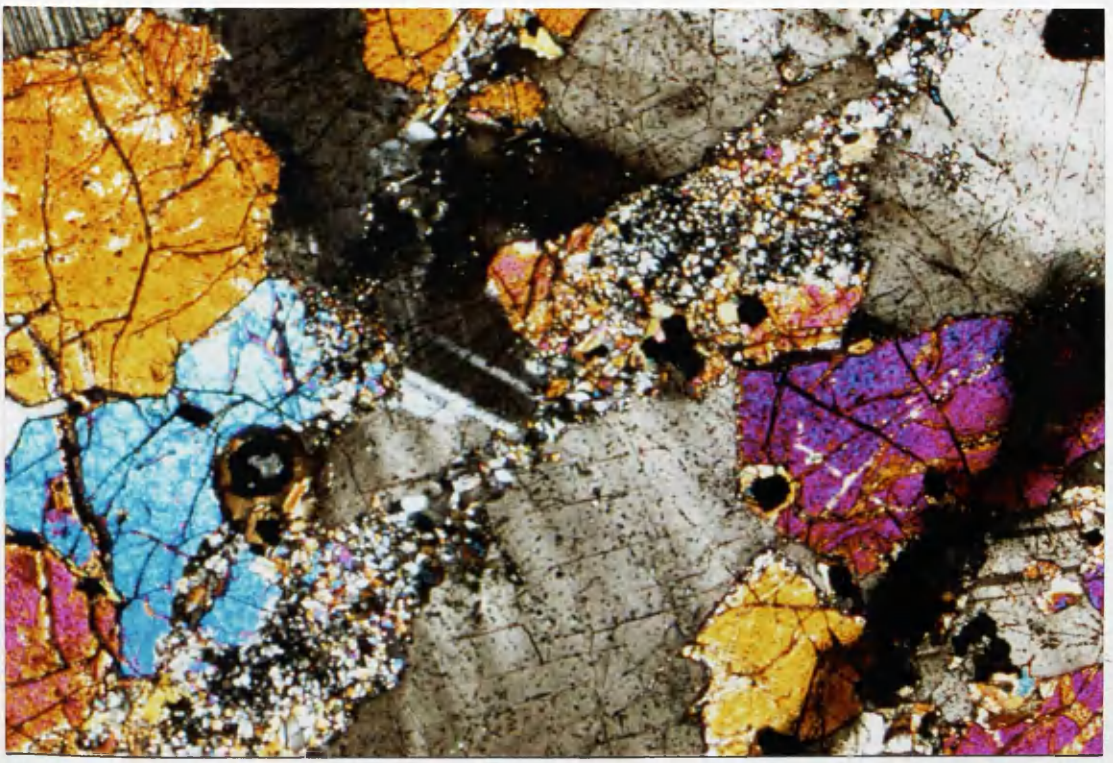

Fig.2.25. Granular vein comprising olivine, orthopyroxene, clinopyroxene and plagioclase within Zone 2 adjacent to the Gars-bheinn Gabbro. The vein can be seen cutting and partly replacing olivine which is characteristically anhedral within the lower part of the zone. Field of view c.3 x 2mm.Crossed polars. Sample AG291A.

Sample	291B/1	291A/2	291B/3	178/1	181A/2	181A/6	181A/1	192/2
SiO_2	54.03	52.51	54.89	48.83	51.98	50.85	51.31	51.08
TiO_2	0.52	0.64	0.40	2.35	0.61	1.00	0.93	1.46
Al_2O_3	1.48	2.96	1.45	4.38	2.90	3.79	3.46	2.73
Cr_2O_3	0.47	0.85	0.30	1.06	1.40	1.31	0.92	-
Fe_2O_3	1.45	0.71	2.43	2.71	0.77	0.99	0.58	1.71
FeO	6.65	3.51	6.62	1.75	2.80	2.67	3.13	2.83
MnO	0.23	0.13	0.27	0.14	0.14	0.11	0.09	0.09
MgO	31.77	15.73	32.56	15.66	16.34	15.92	16.31	18.00
CaO	1.09	23.14	0.74	22.26	22.74	22.45	21.99	19.78
Na_2O	0.03	0.44	0.02	0.47	0.32	0.38	0.37	0.44
Total	98.72	100.62	99.43	99.47	99.66	99.56	99.48	99.04
FeO^*	9.10	4.13	8.80	4.15	3.50	3.57	3.65	4.35
				Atomic % (Mn included with Fe)				
Ca	2.09	47.88	1.40	46.96	47.08	47.31	46.19	40.97
Mg	84.06	45.24	85.29	45.95	47.08	46.67	47.68	51.86
Fe	13.85	6.88	13.32	7.09	5.84	6.03	6.13	7.17
				Formula (based on 6 oxygens)				
Si	1.925	1.916	1.935	1.818	1.910	1.874	1.888	1.887
Al	.062	.127	.006	.192	.126	.165	.150	.119
Fe+++	.072	.019	.064	.075	.021	.027	.016	.047
Fe++	.197	.107	.194	.054	.086	.082	.096	.087
Ti	.014	.017	.011	.066	.017	.028	.026	.040
Mn	.007	.004	.008	.005	.004	.003	.003	.003
Mg	1.687	.855	1.710	.868	.895	.875	.895	.991
Ca	.042	.905	.028	.887	.895	.887	.867	.783
Na	.002	.031	.001	.034	.023	.027	.026	.031
Cr	.013	.024	.008	.027	.031	.041	.038	.027
Total	4.023	4.005	3.966	4.026	4.008	4.009	4.005	4.015

Table 2.10 Representative analyses of pyroxenes from Zone 2 of the Peridotite Series. All iron was determined as FeO^* and subsequently partitioned between ferrous and ferric iron by the method of Finger (1972). Samples 291A and 291B are from peridotite adjacent to the contact with the Gars-bheinn Gabbro.

Fig.2.26. Granular vein of Zone 2 adjacent to anhedral olivines containing small inclusions of orthopyroxene. Within and adjacent to to the granular material, biotite is frequently associated with opaque anhedral spinels. Field of view c.3 x 2mm. Plane polarized light. Sample AG291B.

Fig.2.27. Intergranular quartz containing inclusions showing undulatory extinction adjacent to granular vein within Zone 2 of the peridotite series. Field of view c. 3 x 2 mm. Crossed polars. Sample AG328A.

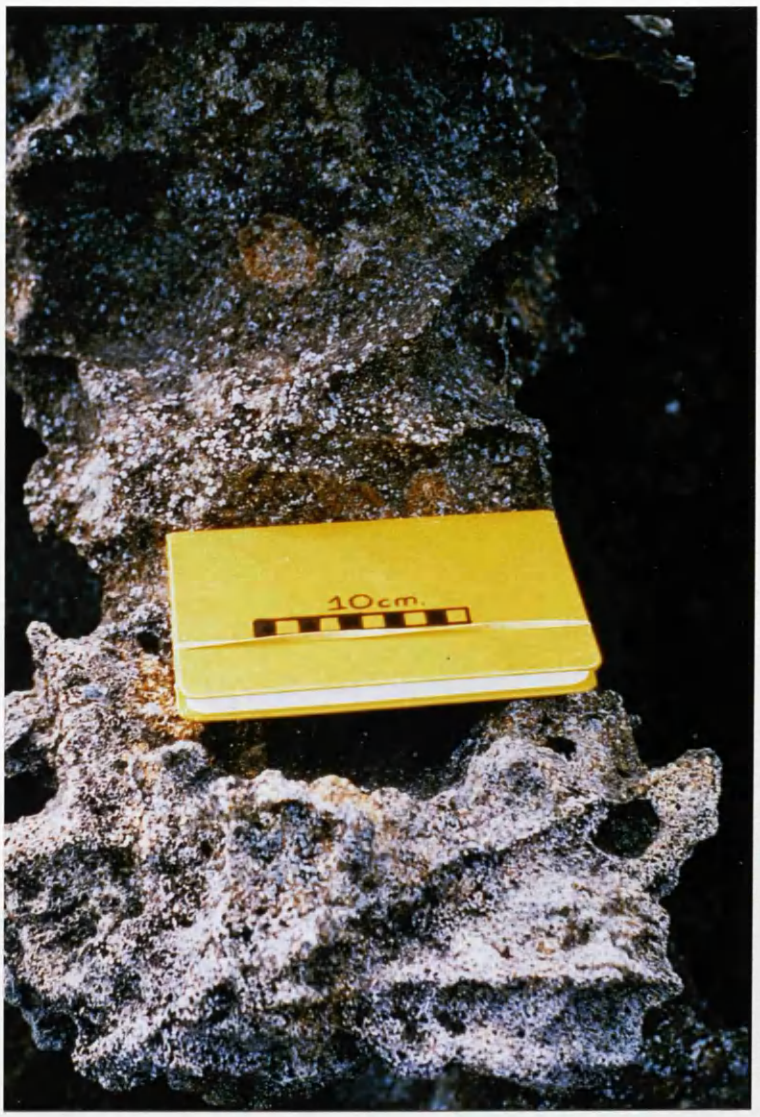

Fig.2.28. Zone 2 feldspathic peridotite. Throughout much of the zone, large aggregates of feldspar occur. Petrographic studies have shown that, in all examined sections, the feldspar is intercumulus.

Feldspars

Sample	181C/2	181A/1	192/2	178/1	181B/3
SiO_2	46.11	45.78	45.62	46.95	46.01
Al_2O_3	33.88	34.67	34.05	33.51	34.09
CaO	18.03	18.37	18.33	16.66	18.03
Na_2O	1.32	1.09	1.19	2.18	1.50
K_2O	0.04	0.10	0.04	0.04	0.01
BaO	-	-	-	-	-
FeO^*	0.30	0.26	0.29	0.24	0.03
MgO	0.19	0.01	0.03	0.03	0.26
Total	99.87	100.28	99.55	99.61	99.93
			Atomic %		
An	88.10	90.19	89.24	80.67	86.36
Ab	11.68	9.73	10.51	19.08	13.57
Or	0.22	0.07	0.25	0.24	0.07
			Formula (on the basis of 32 oxygens)		
Si	8.514	8.427	8.544	8.659	8.547
Al	7.376	7.522	7.358	7.291	7.360
Ca	3.568	3.623	3.555	3.306	3.538
Na	.476	.391	.519	.782	.556
K	.009	.003	.010	.010	.003
Ba	-	-	-	-	-
Fe	.047	.041	.048	.036	.040
Mg	.052	.003	.007	.007	.007
Total	20.042	20.010	20.041	20.091	20.051

Olivines

Sample	181C/2	178/2	181B/3	181B/6	181A/3	178/6
SiO_2	40.32	39.64	40.26	40.42	40.38	39.98
MgO	48.38	45.91	47.90	47.71	47.79	46.89
FeO^*	10.71	13.54	11.22	11.07	11.26	12.15
MnO	0.16	0.24	0.18	0.16	0.19	0.20
NiO	0.37	0.36	0.36	0.36	0.35	0.33
CaO	0.04	0.07	0.02	0.04	0.04	0.03
Al_2O_3	0.02	0.05	0.03	0.04	0.03	0.02
Total	100.00	99.81	99.87	99.80	100.04	99.60
			Atomic %			
Fo	88.94	85.79	88.38	8.48	88.30	87.31
Fa	11.06	14.21	11.62	11.52	11.70	12.69
			Formula (on the basis of 4 oxygens)			
Si	.994	.993	.995	1.000	.997	.996
Mg	1.778	1.714	1.765	1.758	1.759	1.741
Fe	.221	.284	.232	.229	.233	.253
Mn	.004	.005	.004	.003	.004	.004
Ni	.007	.007	.007	.007	.007	.007
Ca	-	.002	-	.001	.001	-
Al	.001	.001	-	.001	-	-
Total	3.005	3.006	3.003	2.999	3.001	3.001

Table 2.11 Representative analyses of olivines and feldspars from Zone 2 of the Peridotite Series. All iron determined as FeO^*

c.15-20%, and spinel for up to 5%, pyroxene being absent. The troctolite-allivalite bands are still dominated by olivine (60-75%), which is accompanied by approximately 15-35% cumulus plagioclase. The presence of a pale grey/green intercumulus pyroxene is extremely variable but is never present in quantities greater than c.5%. It is generally absent from the peridotite bands.

2.3.3.3 Zone 3

Rocks ascribed to Zone 3 are lithologically the most homogenous. They lack any phase or modal layering and, apart from an occasional faint alignment of olivine, any internal fabric. They are best observed to the south of where the Allt Beag broadens into the flat ground at the eastern end of An Garbh-choire. Here, a complete sequence is exposed, with peridotite giving way to feldspathic peridotite up the succession. Where present, the layering produced by the alignment of olivine dips at a shallow angle, c.20-30^{O}, towards the north-east. Occcasionally occurring, particularly within the lower parts of the zone, are impersistent undulatory spinel seams which generally dip at c. 50-70^{O} towards the north-east and are discordant to any fabric within the host rock. They also appear to predate the development of the most obvious fabric of the host rock which comprises subhorizontal intercumulus feldspathic veins (Fig.2.29a,b).

The northerly contact is sharp and is easily defined by the presence of the steeply dipping allivalite/troctolite bands of Zone 2. However, the southerly contact is less clearly defined and appears to be gradational over a short distance, of the order of two metres, with Weedon's (1956) Zone of Brecciation (Zone-4 of this study, see below). On approaching the Zone of Brecciation, faint, irregular feldspathic veins intrude the peridotites of Zone 3 and become more numerous to the north, often forming an anastomosing network which appears to originate from the brecciated peridotite. As in the previously described zones, systematic variation in the composition of the olivines has been detected, with samples from the lowest horizons the most primitive (Table 2.12). Olivines from the base of the zone have forsterite contents of Fo_{91}, decreasing to $Fo_{87\text{-}88}$ on ascending the sequence, with a concomitant decrease in NiO content from 0.42-0.37 wt %. Plagioclase is present only as an intercumulus phase (Table 2.12), which becomes volumetrically more significant up the sequence.

a

b

Fig.2.29. Spinel seams occurring within the higher parts of Zone 1 and the lower parts of Zone 3 are often impersistent and undulatory in form. Whilst their attitude is generally concordant with those occurring lower in Zone 1, they are frequently cut by sub-horizontal feldspathic veins (a) which form the dominant fabric within the peridotites of Zone 3 (b) [G.R.4872 1960].

Feldspars						
Sample	175/1	175/2	173/1	173/2	158/2	158/3
SiO_2	47.93	47.95	46.45	46.39	47.64	46.54
Al_2O_3	32.75	32.69	33.81	34.06	32.99	33.54
CaO	16.88	17.01	17.75	17.86	17.43	17.75
Na_2O	1.98	1.97	1.54	1.41	1.73	1.52
K_2O	0.01	0.03	0.01	0.03	0.03	0.04
BaO	-	-	-	0.01	-	-
FeO*	0.23	0.26	0.19	0.14	0.26	0.22
MgO	0.03	0.09	0.04	0.03	0.06	0.07
Total	99.81	100.00	99.79	99.93	100.14	99.68
			Atomic %			
An	82.40	82.52	86.39	87.34	84.62	86.36
Ab	17.55	17.33	13.54	12.51	15.18	13.39
Or	0.05	0.15	0.07	0.15	0.20	0.25
			Formula (on the basis of 32 oxygens)			
Si	8.813	8.808	8.572	8.547	8.747	8.599
Al	7.099	7.079	7.355	7.396	7.140	7.305
Ca	3.325	3.348	3.509	3.525	3.429	3.514
Na	.708	.703	.550	.505	.615	.545
K	.002	.006	.003	.006	.008	.010
Ba	-	-	-	-	-	-
Fe	.036	.040	.029	.022	.040	.034
Mg	.008	.024	.010	.007	.016	.018
Total	19.991	20.008	20.028	20.008	19.995	20.025

Olivines						
Sample	173/1	173/2	175/3	175/4	158/3	158/4
SiO_2	40.91	40.86	40.43	40.13	40.50	40.20
MgO	47.67	47.51	50.17	50.04	49.99	49.51
FeO*	11.48	11.24	8.42	8.58	9.54	9.52
MnO	0.21	0.21	0.15	0.15	0.15	0.15
NiO	0.40	0.41	0.41	0.42	0.39	0.37
CaO	0.05	0.04	0.06	0.08	0.04	0.04
Al_2O_3	0.03	0.01	0.02	0.03	0.04	0.06
Total	100.75	100.28	99.66	99.43	100.65	99.85
			Atomic %			
Fo	88.07	88.30	91.37	91.20	90.21	90.25
Fa	11.93	11.70	8.63	8.80	9.79	9.75
			Formula (on the basis of 4 oxygens)			
Si	1.004	1.006	.991	.987	.992	.988
Mg	1.743	1.743	1.832	1.835	1.807	1.814
Fe	.236	.231	.175	.177	.196	.196
Mn	.004	.004	.003	.003	.003	.003
Ni	.008	.008	.008	.008	.008	.007
Ca	.001	.001	.002	.002	.001	.001
Al	-	-	.001	-	.001	.002
Total	2.996	2.993	3.012	3.012	3.008	3.011

Table 2.12 Representative analyses of olivines and feldspars from Zone 3 of the Peridotite Series. Total iron was determined as FeO*.

2.3.3.4 Zone 4

The rocks which crop out on the flat floor of the lower corrie, up to and including the rock step, constitute Zone 4. These comprise a heterogeneous, brecciated assemblage consisting of a variety of ultrabasic lithologies, all of which have been observed within the undisrupted part of the ultrabasic mass, although it is significant that the volume of allivalite far exceeds that found throughout the remainder of the mass. Low down in the corrie, the peridotites have been intruded by gabbro, which may, with some certainty, be correlated with that occurring to the north on Meall na Cuilce (Section 2.2.1) and the Gars-bheinn Gabbro (Section 2.2.2.1). These gabbros, whilst forming veins within the peridotite, appear to originate from pods of the gabbro within the peridotite. However, the emplacement of these pods and veins is not thought to be the cause of the brecciation of Zone 4 for two principal reasons:

1) The veins are restricted to the easterly end of the zone of brecciation;
2) Where present, they remain coherent and may only be traced into the peridotite for short distances.

The brecciation may usefully be divided into two-types: I) blocks of peridotite enclosed within a matrix of feldspathic peridotite/allivalite (Fig.2.30); and, II) pods of allivalite surrounded by peridotite (Fig.2.31). However, the two types may be gradational upon each other. Generally, type I brecciation is prevalent within the eastern part of the zone, whilst Type II is particularly well displayed in the west, below the rock barrier. Here, large pods of allivalite enclosed within peridotite frequently display a strong, well developed, lineation fabric caused by the alignment of cumulus plagioclase (Fig.2.32a,b) on (010) and (100). Often this fabric retains its orientation between isolated pods of allivalite and occasional isolated fold-like structures may be seen (Fig.2.32a,b) which bear no relationship to fabric within the peridotite. Any fabric developed within the allivalite pods may either terminate at the allivalite-peridotite contacts or be asymptotic towards it. Occasionally, a marginal facies between allivalite and peridotite is developed whereby a honeycomb texture is imparted to the rock by large olivines, up to 1cm in length, seperated by thin "walls" of intercumulus feldspar.

Fig.2.30. Type I brecciation within Zone 4 is common within the eastern part of the zone. The brecciation agent is believed to have been expelled intercumulus feldspathic melt, which isolated peridotite xenoliths showing consistent fabric orientations [G.R.47691976]. Length of hammer shaft c. 40cm.

Fig.2.31. Type II brecciation within Zone 4. Troctolite and allivalite xenoliths have been intruded and isolated by peridotite. Brecciation throughout the zone is variable with individual xenoliths varying in size from a few centimetres to a large rafts several metres in size. Length of hammer shaft c.40cm.

a

b

Fig.2.32. Small scale flow structures developed within a) feldspathic peridotite and b) allivalite caused by alignment of cumulus minerals. [G.R. 4605 2015].

Weedon (1956) concluded that much of the brecciation of syn-cumulus material was due to back-veining from an overlying magma or intercumulus liquid within an upper layer of crystal mush. Whilst olivine compositions between peridotite and matrix and allivalite pods are comparable, usually around $Fo_{85\text{-}86.5}$, the composition of intercumulus plagioclase within the allivalite is greater, extending to less calcic compositions. Frequently, within the allivalites of both the Zone of Brecciation (Zone 4) and the structurally higher Zone 5 (see below), reverse zoning of the cumulus feldspar has been detected, which is absent from adjacent peridotites. Consequently, whilst the expression of intercumulus liquid may be responsible for some of the brecciation seen in the field, particularly within the eastern parts of the zone, it cannot account for the most obvious allivalite/peridotite assemblages.

The complicated field relationships between peridotite and allivalite/troctolite were not generated during a single brecciation event (Fig.2.33). If it is assumed that brecciation occurred when magma interacted with solid rock, then at least three seperate events need to be and can be demonstrated. However, it is tentatively suggested that one progressive event integrates the field evidence more satisfactorily and will be discussed further in Section 2.3.6.

2.3.3.5 Zone 5

Immeadiately above the rock step, the zone of brecciation (Zone 4) is in contact with the gabbros occurring along the southern contact of the peridotite but rapidly dies out to be replaced by peridotite-troctolite-allivalite bands which may be traversed across strike to the northern contact of the peridotite with the Outer Layered Eucrite Series. Within this zone, the overall dominant structure seen is one of layering produced by occasional horizons of troctolite/allivalite occurring conformably within peridotite/feldspathic peridotite. The layering dips steeply towards the north-east, parallel to the axis of An Garbh-coire. Much of the small scale layering is gradational. However, throughout the exposure, massive layers of allivalite, seldom thicker than a metre, are seen, their contacts with the surrounding peridotites being generally sharp and their attitude conformable with the gradational small scale layering.

Fig.2.33. Foliated allivalite, passing locally into xenolithic horizons containing peridotite xenoliths, discordantly intruded by peridotite. Length of hammer shaft 60cm.

Occurring near the southern contact of the peridotite with the gabbros in the upper part of the corrie, is a series of terraces within the peridotite. On these terraces certain textural features are seen which comprise large radiating and dendritic growths of inter-cumulus plagioclase enclosing cumulus olivine (Fig.2.34). This texture has been observed on both vertical and horizontal surfaces and it is therefore concluded that in 3-dimensions, they possess a crude hemi-spherical geometry.

These structures, which are found within typical peridotite/feldspathic peridotite, comprise orientated rays of inter-cumulus bytownite (An_{84-86}) (Table 2.13) which, due to differential weathering stand proud on weathered surfaces. Individual examples of these structures vary in size from c.15cm to c.1.5m. It is observed that the structures constantly radiate away from the margins of the peridotite. The amount of plagioclase within the structures, seen in the field, is exaggerated due to the differential weathering and this becomes clear on petrographic examination. Whilst the percentage of feldspar varies, it is never present in quantities greater than c.15%. The plagioclase is unzoned and frequently, although unconnected in the plane of a thin section, is in optical continuity throughout a large portion of a given thin section (Fig.2.35). Enclosed by and occurring between the rays of feldspar are euhedral olivines (Fo_{88}) (Table 2.13) which form the bulk of the rock (upto 85% by volume) and frequently posess an accicular to bladed habit indicative of rapid growth. Similar to the feldspar, the olivine is unzoned. The majority of olivines are around 0.25mm in size but occasionally may attain sizes up to 1mm; all olivines generally show a preferred orientation, (001) orthogonal to the ray direction in which they are enclosed. Small, opaque spinels (Table 2.13) are disseminated throught the rock, although there is a suggestion that they may be concentrated within the poikilitic feldspar rather than occurring as inclusions within the olivines. They are small, up to 0.1mm, and generally square in cross section. Those occurring within the olivines are depleted in Mg, Fe and Al, with respect to those enclosed by plagioclase.

Although the hemi-spherulitic structures are only found within a relatively small area of the Peridotite Series, similar textural relationships between olivine and plagioclse are developed within planar layers of certain layered peridotites, both in the middle part of the upper corrie

Fig.2.34. Dendritic crystallization of intercumulus plagioclase (An_{86}) around bladed cumulus olivine ($Fo_{87.6}$) crystals to form braid structures within Zone 5. The structures vary in size from c. 15cm to 200cm and invariably are orientated away from the southern margin of the peridotite, near to which they occur. For explanation see text. [G.R.4562 2022].

Spinels

Sample	SPPL/1	SPPL/2	SPOL/1	SPOL/2
SiO_2	0.03	0.42	0.08	0.07
MgO	9.86	10.01	7.14	7.15
Al_2O_3	17.46	17.86	15.48	15.66
Cr_2O_3	37.44	37.52	36.43	37.39
Fe_2O_3	12.85	11.53	14.68	13.80
FeO	19.82	20.22	23.28	23.55
TiO_2	1.26	1.20	0.99	1.06
NiO	0.22	0.26	0.22	0.24
MnO	0.43	0.41	0.44	0.49
Total	99.37	99.45	98.74	99.41
FeO^*	31.32	30.63	35.17	35.93
		Formula (O=32)		
Si	.008	.111	.024	.018
Mg	3.965	3.984	2.987	2.962
Al	5.550	5.624	5.124	5.133
Cr	7.982	7.921	8.085	8.221
Fe^{+++}	2.504	2.240	2.960	2.760
Fe^{++}	4.296	4.360	5.216	5.240
Ti	.255	.240	.210	.222
Ni	.048	.056	.049	.053
Mn	.098	.093	.104	.115
Total	24.706	24.629	24.759	24.724

Feldspars

Sample	320/2	320/3	320/4	320/6
SiO_2	45.73	46.13	45.57	45.92
MgO	0.17	0.21	0.06	0.06
Al_2O_3	34.29	34.17	34.78	34.24
CaO	17.67	17.41	17.85	17.24
Na_2O	1.64	1.58	1.55	1.71
K_2O	0.02	0.01	0.03	0.03
BaO	0.01	-	.02	-
FeO^*	0.34	0.37	0.28	0.28
Total	99.88	99.88	100.15	99..47
		Atomic %		
An	85.48	85.79	86.23	84.66
Ab	14.37	14.14	13.57	15.17
Or	0.15	0.07	0.20	0.17
		Formula (O=32)		
Si	8.450	8.508	8.399	8.501
Mg	.047	.058	.014	.015
Al	7.469	7.429	7.557	7.473
Ca	3.498	3.440	3.526	3.420
Na	.588	.567	.555	.613
K	.006	.003	.008	.007
Ba	.001	-	.002	-
Fe	.053	.057	.043	.043
Total	20.113	20.062	20.104	20.073

Olivines

Sample	320/1	320/2
SiO2	39.78	39.86
MgO	47.58	47.58
FeO^*	12.02	12.02
NiO	0.34	0.30
MnO	0.19	0.20
Al_2O_3	0.02	0.03
CaO	0.05	0.07
Total	99.98	100.05
	Atomic %	
Fo	87.57	87.61
Fa	12.43	12.39
	Formula (O=4)	
Si	.998	.989
Mg	1.761	1.760
Fe	.250	.249
Ni	.007	.006
Mn	.004	.004
Al	-	-
Ca	.001	.002
Total	99.98	100.05

Table 2.13 Representative mineral analyses of spinels, olivines and feldspars occurring within the braid textured peridotite. Total iron was determined as FeO^* and subsequently partitioned between ferrous and ferric iron for the spinel analyses by the method of Finger (1972).

Fig.2.35. Section cut orthogonal to plagioclase ray (lower left) of Zone 5 dendritic/braid structure. Much of the intercumulus feldspar is in optical continuity and encloses olivines which are characteristically bladed and elongated parallel to the c axis. Field of view c.3 x 2mm. Crossed polars. Sample AG320.

and within Coir' a' Ghrunnda. At these localities, poikilitic feldspar encloses olivine with the same textural and mineralogical characteristics as in the spherulitic structures, but with random orientation which, on weathered surfaces, imparts a "lace" structure to the rock (Fig.2.36). In Coir' a' Grunnda, structure less "normal" peridotite of Zone 5 underlies, and has a gradational contact with, the overlying lace peridotite (Fig.2.37). Within the upper part of An Garbh-choire, the peridotite forms a small ridge which trends approximately parallel to the strike of the observed layering and is notable for the coarse sub-vertical layers of lace peridotite it contains (Fig.2.15) which are disposed between layers of allivalite. The thickness of individual layers of lace peridotite varies between c.30cm to in excess of 150cm. Where the tops of layers are exposed, they are sharp and planar. Occasionally, the lace structure may be interupted by one or more thin (a few centimetres) layers/seams of peridotite, where, the textural relationships between the feldspar and olivine described above are not developed.

The form of the dendritic/braid structures and their texture bears some resemblance to the cres-cumulate "harrisite" documented from the Rhum Central Complex in that both comprise braid-like growth of minerals. The harrisite of Rhum is however, considered to be a primary texture developed by the rapid, unhindered, growth of olivine from the top of the cumulate pile into an overlying saturated magma (Wager et al. 1960), whereas that occurring on Skye developed by, and within, the "intercumulus" material and is constrained and was possibly facilitated by the characteristic bladed habit of the cumulus olivine crystals. Peridotite occurring in the upper part of Zone 5 in which the textures are developed is believed to have had a high initial porosity, as deduced from the high proportion of intercumulus material locally preserved and the euhedral form of the cumulus phases (Fig.2.38). It is believed that this high porosity was critical to braid growth in that it allowed considerable amounts of melt to be trapped within the cumulate pile and/or allowed subsequent migration of melt with ease. The similar relationships of cumulus to intercumulus material developed within the hemi-spherical structures and the planar layers

Fig.2.36. Lace textured peridotites of Zone 5. Randomly orientated bladed olivine crystals ($Fo_{87.6}$) are enclosed by intercumulus plagioclase (An_{86}). The amount of intercumulus feldspar is much exaggerated due to preferential weathering of the cumulus olivine [G.R.4555 2019].

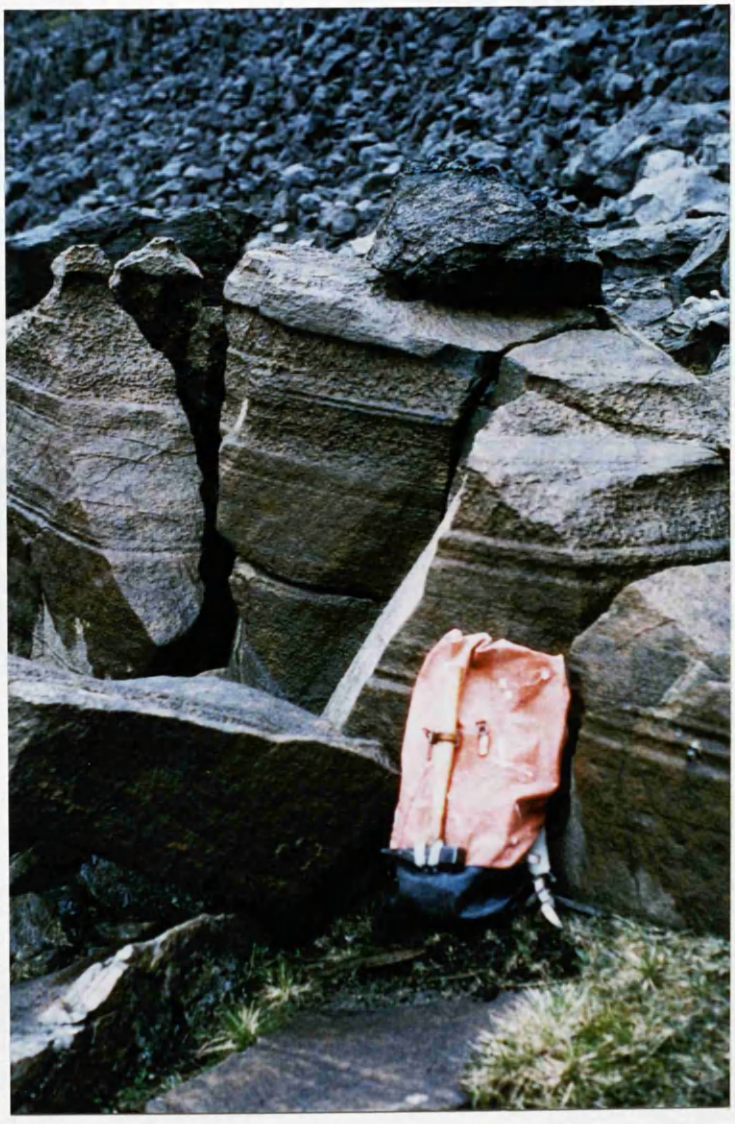

Fig.2.37. Zone 5 peridotites of Coir' a' Ghrunnda. The fabric displayed by the peridotites consists of alternating flat lying or gently inclined planar layers of massive unstructured and lace textured peridotite. Exposures may be traced intermittently and correlated across much of the corrie [G.R.4528 2031].

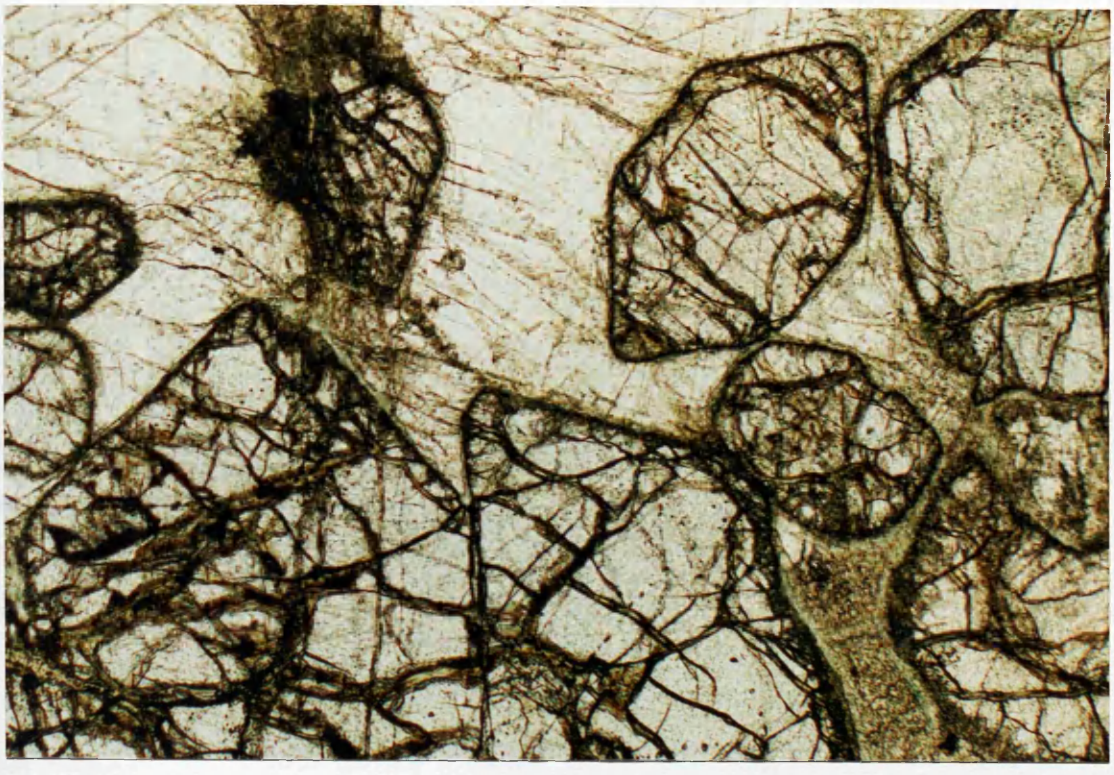

Fig.2.38. Euhedral olivines (Fo_{88}) of Zone 5, enclosed within intercumulus plagioclase (An_{89-86}) which, volumetrically, forms an important component throughout much of the zone. Field of view c.3 x 2mm. Plane polarized light. Sample AG192.

of the lace peridotite and the occasional gradational nature of the contact between peridotite and overlying allivalite suggest similar dynamic and crystallization processes were responsible for their occurrence.

Three processes can readily be envisaged, each having its merits to account for the features:

1) Expulsion of intercumulus melt.

2) Convective fractionation.

3) Magma mixing/interaction.

Common to all is the rapid crystallization of the cumulus olivine and intercumulus plagioclase, which records the flux of feldspathic melt through the cumulate pile and which may be promoted by a) rapid cooling; b) a change in PH_2O, or, c) a change in composition of the melt.

Donaldson et al. (1973) have described braid-like growths of intercumulus feldspar similar to the Skye examples from Rhum and suggests that a hydrous magma may have been responsible for their growth on the evidence of hydrous mineral present within the intercumulus material. It is difficult, however, to reconcile such a proposal with the Skye examples as evidence for a hydrous feldspathic magma is lacking.

As stated above, it is believed that the peridotites of Zone 5 had a high initial porosity. Subsequent compaction and expulsion of intercumulus melt may locally cause rotation of the cumulus olivines entrained within the fluid (Fig.2.39a). Whilst such a process could explain the planar lace textured layers, deviatoric compaction or compaction of the cumulate pile in which isolated pockets of intercumulus melt are trapped has to be invoked to explain the braided hemi-spherical structures. If the above process occurred it is not clear how supersaturated crystallization could have been initiated when prior to expulsion of pore melt crystallization was proceeding normally. It is possible that intercumulus melt was displaced into a cooler environment, thus promoting rapid crystallization.

However, it is difficult to envisage a high temperature gradient over the small distances involved. Rapid crystallization of olivine will locally deplete the magma in the heavier mafic components, thus releasing a buoyant feldspathic melt which may convect vigorously

Fig.2.39. Suggested mechanisms by which the dendritic (a-c) and lace textures (d) of Zone 5 may have developed.

a) Compaction.
Rapid crystallization of cumulus olivine which accumulated by gravity settling to produce a porous cumulus crystal framework (a) which, under the influence of the overlying weight of crystals and/or deviatoric stress compacts, expelling trapped intercumulus melt (b). The expelled intercumulus melt facilitates rotation of the cumulus olivines normal to the greatest flux whilst crystallizing around the rotated olivines to produce the characteristic intergrowth of olivine and plagioclase.

b) Convective Fractionation.
Rapid crystallization of cumulus olivine with associated vigorous convective fractionation allows rotation of cumulus olivines within strems of greatest flux. Insert shows crystallization of cumulus olivine crystals accompanied by diffusion of material required by growing crystals (heavy arrows) and liberation of lighter depleted intercumulus melt (light arrows).

c) Magma mixing.
Injection and infiltration of lighter felsic magma through porous cumulate pile.

d) Hybridization
Juxtaposition of cooler lighter felsic magma against hotter olivine cumulates (unshaded crystals) and intercumulus melt. Limited mixing promotes quench crystallization of characteristic bladed/accicular olivines (shaded crystals) and intercumulus feldspar in a narrow zone of hybridization.

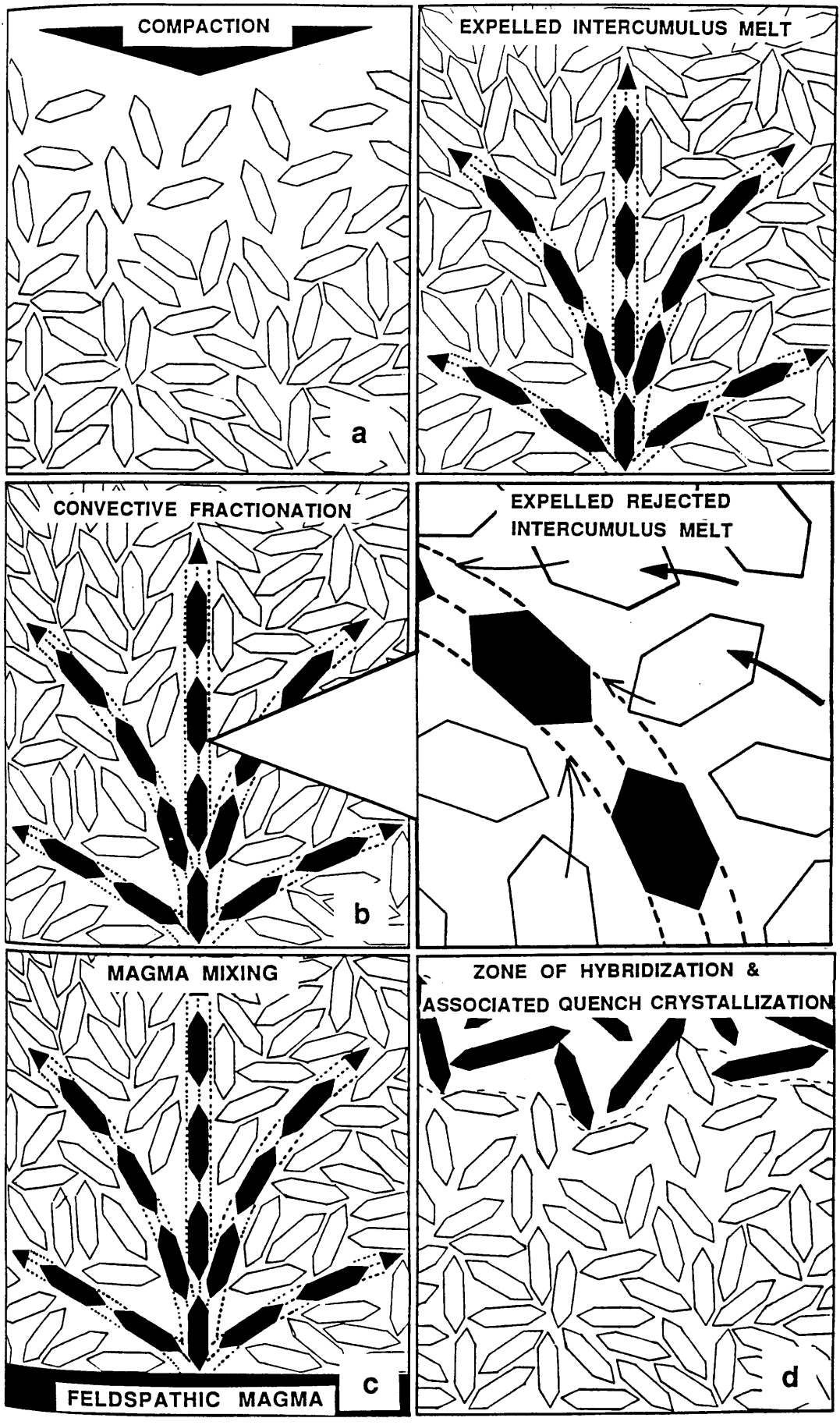
COMPACTION
a
EXPELLED INTERCUMULUS MELT
CONVECTIVE FRACTIONATION
b
EXPELLED REJECTED
INTERCUMULUS MELT
MAGMA MIXING
FELDSPATHIC MAGMA
c
ZONE OF HYBRIDIZATION &
ASSOCIATED QUENCH CRYSTALLIZATION
d

Fig. 2.39.

through the cumulate mush, again entraining cumulus olivines where the flux is greatest (Fig.2.39b). As in the compaction model, it is difficult to envisage supersaturation of this light lower temperature melt as it convects away from the crystal-liquid interface. The introduction of a discrete feldspathic magma through the cumulate pile (Fig.2.39c) alleviates the problems associated with the two previous models as a higher temperature melt may be invoked which becomes supersaturated within the cooler environment of the cumulate pile through which it percolates. Melt escaping into the magma reservoir may then mix with the magma already in residence or may form discreet compositional horizons within it. A variant of the third model involves the juxtaposition of a feldspathic magma adjacent to a crystallizing peridotite layer (Fig.2.39d). Percolation/mixing of the felsic melt with the more mafic melt may induce rapid crystallization of olivine within the peridotite layer by either changing the composition of the melt or by a decrease in the temperature caused by mixing of the two melts. Essentially, the lace peridotite could then crystallize within the top of the peridotite layer or within a hybrid zone between the two melts. This mechanism would explain the presence of the lower gradational contacts of the peridotite and allivalite (Section 2.3.4). However, for many of the examples of lace peridotite occurring low within Coir' a' Ghrunnda, discrete feldspathic horizons are absent. Similarly, such a model fails to account for the hemi-spherical/braid textures unless they are initiated and influenced by the injection of underlying allivalite, as in Fig.2.39(C), and thus represent isolated pools of the hybrid magma. Certainly, field evidence suggests that a felsic melt from whatever source played an important post-cumulus role, forming both impersistent veins within the cumulate pile and discrete massive bands within the body of the cumulate pile. The volume of the feldspathic material within the upper part of Zones 5 and 6 strongly suggests a non inter-cumulus origin and which may have promoted much of the reverse zoning detected within many of the allivalitic bands.

Further into the upper part of An Garbh-choire and higher within the sequence, the peridotite becomes structureless with the exception of impersistent, faint feldspathic peridotite layers. There is no evidence of either the hemi-spherical/spherical or lace peridotite observed lower in the sequence.

Olivine compositions throughout the zone are variable, ranging from Fo_{84} to Fo_{87} (Table 2.14), but it has proved impossible to relate this variation to stratigraphic or structural position within the peridotite, although, generally, the more forsteritic olivines are to be found towards the southern, lower margin of the mass. Similarly, the NiO contents of the olivines do not appear to vary in any systematic way with concentrations varying between 0.3 and 0.4 wt. %. Pyroxene (Table 2.15), a green chromian augite, is present in minor amounts up to 15% and always as an intercumulus phase. No evident correlation has been observed between the pyroxene and the amounts or composition of the plagioclase present.

Occurring about 20 m to the south-east and approximately 10m below Caisteal a' Garbh-choire is to be found a localised, thin (c.40cm) band of allivalite which may be traced laterally for c.5m. It is approximately concordant with the deduced structure of the peridotite within this area and is worthy of note for its contact relationships with the surrounding peridotite. Olivine compositions within the band are around Fo_{86} with NiO contents of 0.26 wt.%, whilst within the underlying and overlying peridotite the olivine has a forsterite composition of Fo_{88} and NiO contents of around 0.31wt.%. The upper contact of the allivalite band with the overlying peridotite is sharp and planar in form, whilst the lower contact, although also sharp, is highly irregular with finger like protrusions of peridotite extending into the overlying allivalite (Fig.2.40). Due to sampling difficulties, it has not proved possible to extract a sample across the protrusions for further detailed analysis, however, similar features have been observed occurring in the Rhum Layered (Brown 1956). In a recent study of these features, Butcher et al. (1985) proposed the term finger structures and described their characteristics, briefly summarised below:

A) Finger structures only develop where peridotite is overlain by allivalite.

B) Fingers form only along abrupt contacts and not gradational contacts.

C) Only the upper surface of peridotite layers develop finger structures, the lower surface being characteristically flat.

D) Fingers are found in a variety of environments but only in the lower contact of allivalite which is underlain by peridotite.

Feldspars

Sample	244/I2	245/I3	245/C3	245A/C2	295/2	255/2	254/1
SiO_2	48.40	49.07	47.55	46.60	46.52	47.46	47.82
Al_2O_3	32.59	31.88	32.64	33.06	33.40	32.89	33.12
CaO	16.09	15.39	17.38	17.69	17.53	17.05	16.10
Na_2O	2.41	2.89	1.70	1.61	1.77	1.85	2.46
K_2O	0.04	0.05	0.07	0.04	0.08	0.04	0.01
BaO	0.03	-	-	-	-	-	-
FeO*	0.30	0.30	0.50	0.50	0.47	0.27	0.19
MgO	0.04	0.05	0.07	0.07	0.05	0.03	0.08
Total	99.87	99.66	99.91	99.57	99.82	99.59	99.78
			Atomic %				
An	78.49	74.43	84.61	85.69	84.16	83.60	78.27
Ab	21.26	25.30	14.97	14.09	15.40	16.20	21.66
Or	0.25	0.27	0.42	0.22	0.44	0.20	0.07
			Formula (on the basis of 32 oxygens)				
Si	8.883	9.015	8.763	8.628	8.598	8.761	8.809
Al	7.052	6.906	7.090	7.228	7.278	7.149	7.136
Ca	3.146	3.030	3.432	3.515	3.471	3.374	3.184
Na	.857	1.030	.607	.578	.635	.654	.881
K	.010	.011	.017	.009	.018	.008	.003
Ba	-	.002	-	-	-	-	-
Fe	.046	.047	.076	.075	.073	.041	.028
Mg	.012	.013	.019	.019	.015	.008	.023
Total	20.024	19.024	20.004	20.052	20.088	19.995	20.064

Olivines

Sample	244/2	245/1	245/3	245A/1	245A/3	295/3	254/4
SiO_2	40.30	40.07	40.72	40.00	39.93	39.51	40.46
MgO	47.02	47.57	46.90	46.19	45.97	45.28	48.42
FeO*	11.71	11.33	11.39	13.11	13.45	14.61	9.67
MnO	0.20	0.19	0.18	0.22	0.22	0.31	0.14
NiO	0.38	0.31	0.30	0.23	0.26	0.26	0.44
CaO	0.05	0.03	0.06	0.06	0.05	0.09	0.06
Al_2O_3	0.09	0.04	0.02	0.05	0.07	0.05	0.02
Total	99.74	100.17	99.57	99.87	99.95	100.12	99.21
				Atomic %			
Fo	87.74	88.19	88.01	86.24	85.89	84.66	89.92
Fa	12.26	11.81	11.99	13.76	14.11	15.34	10.08
				Fomula (on the basis of 4 oxygens)			
Si	1.000	1.003	1.009	.998	.997	.992	1.001
Mg	1.739	1.747	1.733	1.717	1.711	1.694	1.785
Fe	.243	.234	.236	.274	.281	.307	.200
Mn	.004	.004	.004	.005	.005	.006	.003
Ni	.008	.006	.006	.005	.005	.006	.009
Ca	.001	-	.002	.002	.001	.002	.002
Al	.003	.001	-	.001	.002	.002	-
Total	2.998	2.995	2.990	3.002	3.002	3.008	3.000

Table 2.14 Representative analyses of feldspars and olivines occurring within Zone 5 of the Peridotite Series.

Fig.2.40. Finger structures developed within 40 cm. allivalite band of Zone 5 [G.R.4552 2019].

E) Structures at any given locality are often remarkably consistent, generally being parallel-sided or tapering protrusions with circular cross-sections.

F) Peridotite occurring in the fingers is modally and texturally similar to the underlying peridotite which may range from feldspathic peridotite to dunitic peridotite.

G) Finger structures cross-cut slumped allivalite and therefore post date slumping events.

H) The mineral chemistry between fingers and overlying allivalite are essentially the same in composition except for plagioclase which is more Na-rich in the fingers.

The authors discussed three possible mechanisms for the origin of the structures;

1) Allivalite was deposited on an irregular peridotite floor.

2) Finger structures represnt the response of peridotite to vertical loading by allivalite, analagous to load structures which may develop in some sedimentary sequences due to the gravitational unstable arrangement of dense material overlying less dense material.

3) The finger structures formed by selective metasomatic replacement of pre-existing allivalite by secondary peridotite within the crystal pile.

Butcher et al. (1985) discounted mechanism 1, as transgressive relationships suggested that the fingers formed after deposition of the allivalite. Mechanism 2 was also rejected as the structures are found at contacts with a normal density gradient i.e. dense peridotite overlain by less dense allivalite, as suggested by present day rock densities, and that allivalite adjacent to the finger structures is apparently undeformed. It was therefore concluded that the origin of the finger structure was best explained by selective metasomatic relacement.

In a subsequent study Morse et al. (1987) eliminated metasomatism as a credible mechanism for finger formation on the grounds that a three phase saturated melt (ol+pl+cpx) does not have the thermal capacity to dissolve a higher temperature allivalite cumulate. Consequently the authors suggested that the finger structures formed by dissolution of allivalite by a hot mafic magma emplaced into the largely solidified allivalite. In this model a rapidly cooling mafic magma is emplaced into allivalite which causes melt corrosion of the allivalitic roof whilst crystallizing olivine within the mafic magma. The

release of a light fluid from the melt surrounding the growing olivine crystals allows the latent heat of crystallization to be transferred by compositional convection (Sparks et al. 1984) to the site of assimilation. Eventually, the mafic magma super-cools sufficiently to metastably nucleate pyroxene which, along with the olivine, grows in the dissolution spaces (fingers). It is assumed that components of the digested troctolite (allivalite) are flushed out of the fingers by convective flow. A summary of the mechanism and phase equilibria of such a process is shown in Fig. 2.41 and Fig. 2.42 respectively.

The implication of the finger structures and their formation is that many if not all of the allivalite layers had already largely crystallized prior to the emplacement of the peridotite which was intruded as sill like bodies and which in conjunction with detailed field mapping evidence reported by Beddard et al. (1988), negates the hypothesis that each peridotite-allivalite cyclic unit represents closed system fractionation as originally proposed by Brown (1956).

Although the finger structures found below Caisteal a' Garbh-Coire are the best developed within the peridotite series, incipient finger structures may be found at many of the allivalite-peridotite contacts and even within allivalite blocks in the brecciated Zone (Fig.2.43). They appear, in general, however, to be less widespread and less well developed than their counterparts occurring on Rhum.

Commencing approximately at the same structural level as the above allivalite band and extending some 30m up the succession the peridotite is xenolithic (Fig.2.44). Initially xenoliths are small (c.<15cm), sub-rounded to angular and are composed of coarse allivalite mineralogically similar to both the Feldspathic Allivalite (White Allivalite; Section 2.2.2.3) and the allivalitic bands occurring within the Peridotite Series.

2.3.3.6 Zone 6

Immediately beyond and to the north of Caisteal a' Garbh-choire, the main ridge steepens to form the shoulder of Sgurr Dubh an Da Bheinn and whilst the rock which crops out here forms part of the Peridotite Series, it is lithologically and structurally more varied. Essentially, there exists a bimodal distribution of peridotite and troctolite arranged in alternating horizons, up to 18m thick, on a broad scale but each containing thin (<1m),

Fig. 2.41. Mechanism of finger growth produced when hot ultrabasic liquid is emplaced into nearly solidified troctolite. Crystallization of olivine at the base of the ultrabasic sill l iberates light fluid which is convected away from the growing basal layer (magnified view in lower circle). This convection maintains the top of the hot mafic liquid at high temperature to permit melting of the overlying troctolite (shown in temperature diagram to right). When the convectional stirring becomes weak, supercooling within the fingers allows metastable growth of pyroxene (dashed curve cpx). Extraction of heat causing growth of olivine occurs by conduction through the substrate and by convection above. The thermal maximum at the top of the dunite cumulate arises from the local maximum of latent heat released.(After Morse et al. 1987).

Fig. 2.42. Phase equilibria explanation of formation of finger structures. A) The ternary system forsterite-diopside-anorthite (Osborn and Tait 1952). The mafic liquid L_d produces pure olivine cumulates (D^{cum}) and drives the liquid composition towards the plagioclase saturated liquid L_t), capable of producing troctolite (T^{cum}). The hot liquid l_d has the capacity to dissolve either troctolite cumulate or a hypothetical plagioclase cumulate (Pl^{cum}) but L_t does not since it is already saturated with both olivine and plagioclase. Therefore the locus of candidate liquids for dissolution of troctolite run from L_d toward (but not to) L_t. A sufficiently supercooled daughter of liquid L_d, fractionating olivine may encounter the metastable pyroxene liquidus at L_s (A & B) before reaching the stable plagioclase saturated condition, thus having the capacity to to dissolve plagioclase whilst crystallizing pyroxene. The arrows L_p and L_{px} are trajectories away from the wehrlitic peridotite and pyroxene respectively. B) a T-X section along the line T^{cum}-G is shown to illustrate the location of the metastable saturated surfaces (S-cool) relative to the equilibrium (EQM) liquidus (after Morse et al. 1987).

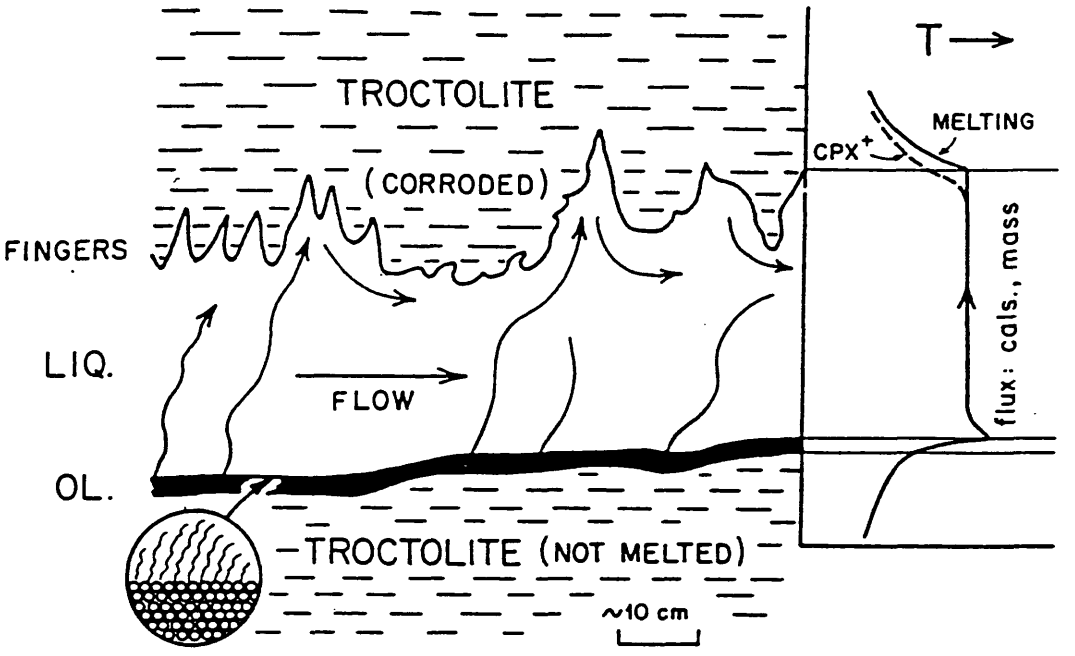

Fig. 2.41.

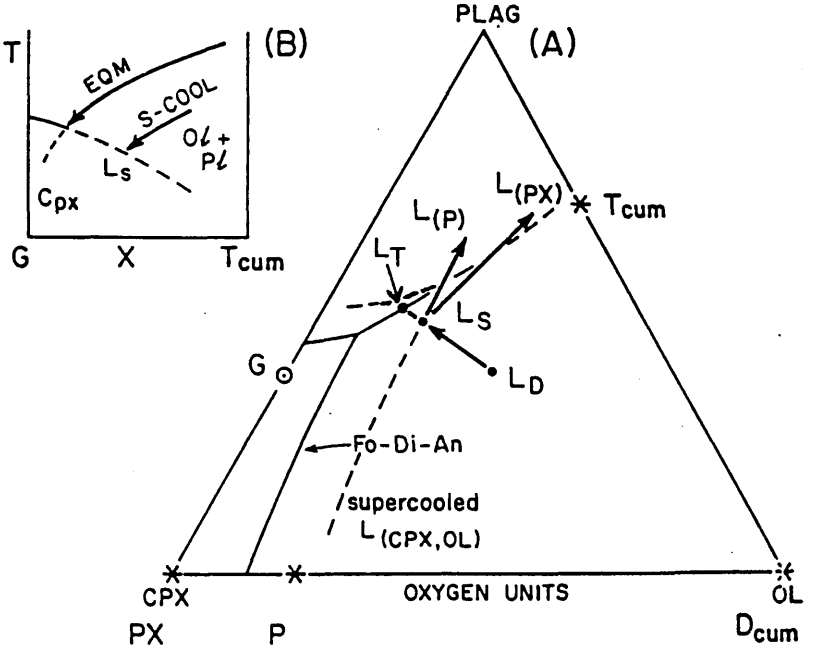

Fig. 2.42.

Fig.2.43. Incipient finger structures developed within the base of a feldspathic xenolith occurring within Zone 4.

Fig.2.44. Feldspathic angular xenoliths occurring within feldspathic peridotite towards the base of Zone 6 of the Peridotite Series. [G.R. 4545 2031].

laterally impersistant bands of each other. Occurring within each lithology, but more noticable within the peridotite, are thin wispy bands of coarse intercumulus/cumulus feldspar (Fig.2.45) whose orientation may either be parallel or orthogonal to the layers in which thay occur. Throughout this area, xenoliths are much in evidence. The dominant type is allivalitic, as seen lower in the series, although both feldspathic and dunitic peridotite types are present in the more feldspathic bands. Associated with the more feldspathic nature of the Peridotite Series on the flanks of Sgurr Dubh an Da Bheinn is an increase in the pyroxene content, which may locally comprise c.20% of the mode.

The variation in lithology throughout the zone is reflected in the mineral chemistry (Tables 2.16 and 2.17) which and are more varied than those occurring within Zone 5 and only partly reflect host lithology. Feldspars are generally more calcic (An_{85-90}) within the feldspathic lithologies than those of the peridotite (An_{80-85}). The forsterite content of olivines varies between Fo_{80} and Fo_{88} and is independent of host lithology. In commom with Zone 5, discrete 1-2m thick allivalitic bands are again present (Section 2.3.4), their orientation broadly conformable with the structure of the peridotite.

2.3.4 Peridotite-allivalite contacts

Occurring within Zones 5 and 6 are discrete allivalitic bands which usually are between 1 and 2 metres in thickness and whose attitude is broadly concordant with the structure of, and any fabric occurring within, the adjacent peridotites. The bands frequently show a preferrred orientation of cumulus tabular feldspars throughout their thickness parallel to the orientation of the bands themselves. Without exception their upper contacts with peridotite are sharp and planar whilst their lower contacts may be either sharp or gradational. Where gradational, a texture, not unlike the lace textured peridotite, desribed in Section 2.3.3.5, is observed (Fig.2.46) and may be developed over a thickness of up to c. 60cm. The sharp upper contacts and those lower contacts not displaying the lace texture possess a strong planar fabric imparted to the rock by a preferred alignment of tabular feldspars (Fig.2.47).

Many of the cumulus feldspars within the allivalitic bands along and adjacent to the contact with the peridotite frequently show reverse zoning. Cores are of the order of An_{85-87} whilst rim compositions are in the region of An_{81-83}, however, concentric zones as calcic as An_{90}

Fig.2.45. Wispy feldspathic veins within peridotite and feldspathic peridotite of zone 6. The orientation of these veins is highly irregular and may range from horizontal to vertical within peridotite bands which themselves dip at shallow angles (c.30') towards the north.

Feldspars

Sample	277/5	143P/1	249/1	143F/C1	143F/C2	143P/3	277/1
SiO_2	46.11	47.04	47.11	45.90	45.52	46.82	46.27
Al_2O_3	34.12	32.94	33.62	33.88	34.47	33.30	34.12
CaO	18.27	17.37	17.36	17.97	18.66	17.89	18.12
Na_2O	1.27	1.66	1.61	1.36	1.05	1.48	1.28
K_2O	0.07	0.03	0.04	0.05	0.04	0.03	0.04
BaO	0.02	0.01	-	0.03	-	-	-
FeO*	0.39	0.32	0.38	0.51	0.41	0.35	0.39
MgO	0.07	0.02	0.01	0.06	0.04	0.02	0.07
Total	100.32	99.39	100.13	99.76	100.19	99.89	100.29
			Atomic %				
An	88.46	85.08	85.43	87.68	90.58	86.89	88.36
Ab	11.15	14.75	14.35	12.00	9.20	12.94	11.35
Or	0.39	0.17	0.22	0.32	0.22	0.17	0.30
			Formula (on the basis of 32 oxygens)				
Si	8.488	8.707	8.613	8.498	8.381	8.624	8.509
Al	7.405	7.189	7.348	7.395	7.525	7.255	7.398
Ca	3.603	3.444	3.400	3.564	3.683	3.545	3.574
Na	.454	.597	.571	.488	.374	.528	.459
K	.016	.007	.009	.013	.009	.007	.012
Ba	.001	-	-	.002	-	-	-
Fe	.060	.050	.058	.079	.064	.052	.060
Mg	.018	.005	.003	.016	.012	.006	.015
Total	20.045	19.999	20.002	20.055	20.048	20.017	20.027

Olivines

Sample	277/D	249/1	143F/1	143F/2	143P/1	143P/2
SiO_2	40.18	39.40	39.97	39.81	39.72	39.64
MgO	47.93	42.03	46.79	46.45	46.42	46.68
FeO*	11.40	18.07	12.88	12.78	12.84	12.79
MnO	0.18	0.31	0.21	0.18	0.22	0.22
NiO	0.29	0.31	0.27	0.26	0.35	0.31
CaO	0.04	0.03	0.06	0.08	0.04	0.08
Al_2O_3	0.05	0.05	0.03	0.05	0.02	0.06
Total	100.07	100.18	100.21	99.61	99.61	99.78
Fo	88.21	80.55	86.61	86.63	86.54	86.68
Fa	11.79	19.45	13.39	13.37	13.46	13.32
			Formula (on the basis of 4 oxygens)			
Si	.993	1.003	.993	.995	.994	.990
Mg	1.765	1.594	1.733	1.730	1.730	1.737
Fe	.236	.385	.268	.267	.269	.267
Mn	.004	.007	.005	.004	.004	.005
Ni	.006	.006	.005	.005	.007	.006
Ca	.001	.001	.002	.002	.001	.002
Al	.001	.001	-	.001	-	.002
Total	3.006	2.997	3.006	3.004	3.006	3.009

Table 2.16 Representative analyses of feldspars and olivines occurring within Zone 6 of the Peridotite Series. Total iron was determined as FeO*

Sample	143P/3	277/1	143F/2	249/4	249/C	249/6	249/E	277/2	277/3
SiO_2	52.05	51.88	51.70	54.43	52.68	52.84	53.50	51.29	51.73
CaO	20.73	21.55	21.19	1.58	19.24	17.35	2.19	21.62	22.94
MgO	17.38	17.52	17.15	27.97	16.89	18.05	27.53	17.33	16.64
FeO	3.94	2.46	3.33	12.94	3.68	7.72	11.79	2.56	2.02
Fe_2O_3	0.73	1.68	1.36	0.67	0.43	1.06	1.44	1.80	1.97
MnO	0.21	0.20	0.21	0.37	0.23	0.22	0.39	0.17	0.16
Al_2O_3	2.71	2.78	3.01	1.33	2.39	2.19	1.15	3.19	2.84
TiO_2	1.35	0.61	0.53	0.45	0.30	0.35	0.28	0.60	0.64
Cr_2O_3	0.92	1.07	1.21	0.09	0.52	0.29	0.09	1.47	1.68
Na_2O	0.38	0.23	0.22	0.06	0.31	0.25	0.03	0.28	0.27
Total	101.51	99.98	99.91	99.89	99.82	100.32	98.39	100.32	100.49
FeO^*	4.58	3.96	4.56	13.53	7.20	8.64	13.09	4.10	3.77
					Atomic %				
Ca	42.59	43.83	43.48	3.09	39.63	35.14	4.31	44.06	46.68
Mg	49.68	49.59	48.91	75.76	48.41	50.85	75.06	49.09	47.10
Fe	7.73	6.58	7.61	21.15	11.96	14.01	20.63	6.85	6.22
					Formula (on the basis of 6 oxygens)				
Si	1.898	1.901	1.898	1.955	1.940	1.938	1.954	1.880	1.894
Ca	.810	.846	.834	.061	.759	.682	.086	.849	.900
Mg	.945	.957	.938	1.497	.927	.987	1.499	.946	.908
Fe^{++}	.020	.075	.102	.388	.210	.236	.359	.070	.060
Fe^{+++}	.012	.046	.037	.018	.012	.029	.039	.055	.055
Mn	.007	.006	.006	.011	.007	.007	.012	.006	.005
Al	.116	.120	.130	.056	.104	.095	.049	.138	.123
Ti	.037	.017	.015	.012	.008	.010	.008	.017	.017
Cr	.026	.031	.035	.002	.015	.008	.003	.042	.037
Na	.027	.016	.016	.004	.022	.018	.002	.020	.019
Total	3.898	4.015	4.011	4.004	4.004	4.010	4.011	4.023	4.018

Table 2.17 Representative analyses of pyroxenes occurring within Zone 6 of the Peridotite Series. All iron was determined as FeO^* and was subsequently partitioned between ferrous and ferric iron by the method of Finger (1972).

Fig.2.46. A 2m. thick allivalitic band occurring within Zone 6. The band, in common with many such examples, displays a sharp, planar upper contact with peridotite. The lower contact however, is gradational with the development of a marginal lace textured horizon. [G.R. 4541 2043].

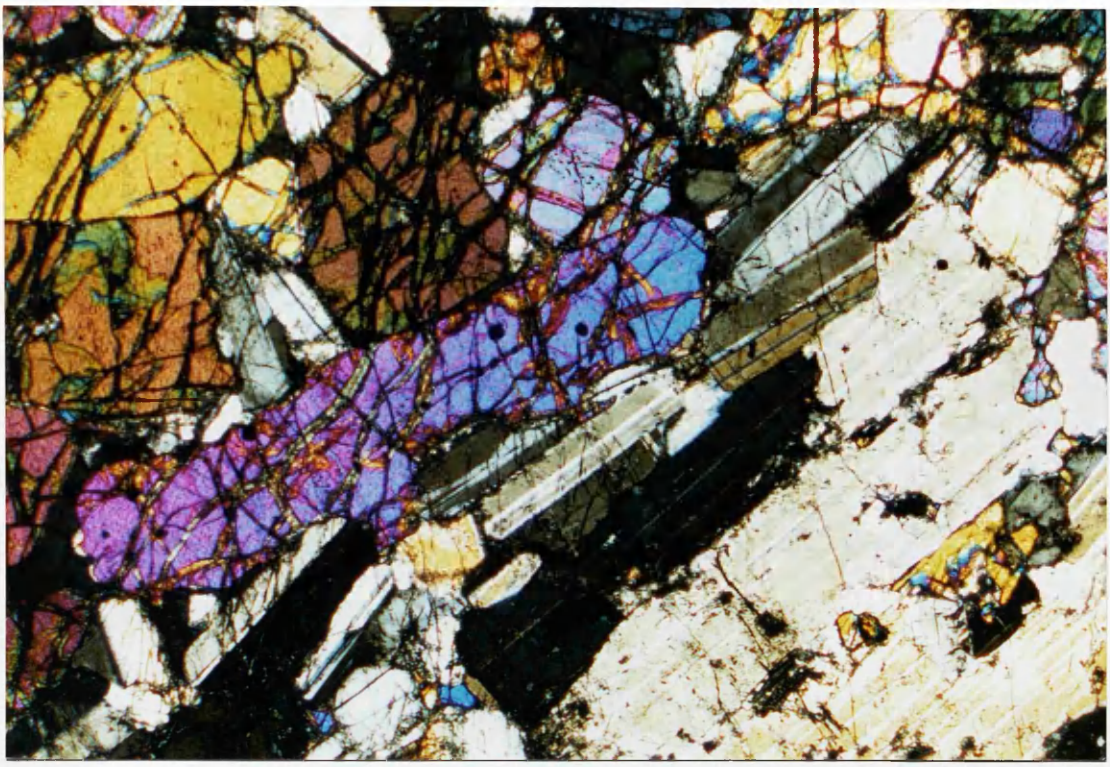

Fig.2.47. Contact between allivalite band showing preferred orientation of cumulus tabular feldspar (An_{86-81}) and peridotite comprising cumulus olivine (Fo_{88}). Occasionally the olivines adjacent to the contact show bladed habits orientated parallel to the contact. Field of view c. 3 x 2 mm. Crossed polars. Sample AG317.

have been detected. Intercumulus feldspars within the peridotite and marginal lace bands have compositions of An_{85}. In contrast olivines from both the allivalitic bands and the peridotite bands display similar compositions in terms of their major element chemistry c.$Fo_{86.5\text{-}87.5}$, with no detectable zonation. NiO contents are however constantly lower (Table 2.18) in the olivines of the allivalitic bands (c.0.25-0.27 wt. % NiO) compared with those from the peridotite (c.0.31-0.35 wt %).

2.3.5 Mineralogy of the Peridotite Series.

2.3.5.1 Characteristics and parageneses of spinels in the Peridotite Series

Within the ultrabasic rocks of the Peridotite Series, spinel occurs in two different parageneses. It may be disseminated throughout the rock or may be concentrated into thin seams. Spinels of the former category may be further subdivided into those occurring within cumulus silicate minerals as inclusions or those within intercumulus minerals.

Seams

The seams into which spinel may be concentrated never exceed 2cm in thickness and are commonly less than 1cm. These seams are restricted to the eastern part of the outcrop and particularly to the ultrabasic tongue of the Allt Beag (Zone 1), extending towards Loch Scavaig. Within this tongue, half a dozen or so thin seams, never separated by more than c60cm., may be observed dipping steeply, at approximately 75^{O}, towards the NNW (Fig. 2.48). These may be traced laterally without significant deviation for approximately 100m. Above the tongue, within structurally higher units of the peridotite series, only laterally impersistent, undulatory seams are seen, occasionally more pod like. Worthy of note is the occurrence, within the brecciated zone (Zone 4) of a xenolith measuring c100cm x 40cm comprising numerous spinel seams (Fig.2.49), the frequency of which is considerably higher than the seams seen in situ within the structurally lower dunites of Zone 1 (Section 2.3.3.1). Within the marginal peridotites, spinel seams are rare and where they do occur are irregular and impersistent and are often observed along the contact between peridotite and more feldspathic rocks (Fig.2.50, 2.51). Spinels of the persistent seams and their immediate environs within the Allt Beag ultrabasic tongue are a translucent reddish brown-

Feldspars

Sample	143P/1	143P/3	143F/1	143F/2	143P/2	143F/4
SiO_2	47.04	45.90	45.52	46.82	46.60	46.31
Al_2O_3	32.94	33.88	34.47	33.30	33.24	33.34
CaO	17.37	17.97	18.66	17.89	17.38	17.90
Na_2O	1.66	1.36	1.05	1.48	1.62	1.39
K_2O	0.03	0.05	0.04	0.03	0.04	0.05
BaO	0.01	0.03	-	-	0.03	-
FeO*	0.32	0.51	0.41	0.35	0.31	0.43
MgO	0.02	0.06	0.04	0.02	0.07	0.07
Total	99.39	99.76	100.19	99.89	99.29	99.49
	Atomic %					
An	85.08	87.68	90.58	86.89	85.39	87.41
Ab	14.75	12.00	9.20	12.94	14.39	12.29
Or	0.17	0.32	0.22	0.17	0.22	0.30
	Formula (on the basis of 32 oxygens)					
Si	8.707	8.498	8.381	8.624	8.641	8.586
Al	7.189	7.395	7.525	7.255	7.267	7.288
Ca	3.444	3.564	3.683	3.545	3.454	3.555
Na	.597	.488	.374	.528	.582	.500
K	.007	.013	.009	.007	.009	0.12
Ba	-	.002	-	-	.002	-
Fe	.050	.079	.064	.052	.047	.067
Mg	.005	.016	.012	.006	.018	.018
Total	19.999	20.055	20.048	20.017	20.020	20.026

Olivines

Sample	143F/1	143F/2	143P/1	143P/2	143P/3	143F/3
SiO_2	39.97	39.81	39.72	39.64	39.41	39.56
MgO	46.79	46.45	46.42	46.68	46.63	46.14
FeO*	12.88	12.78	12.84	12.79	12.92	12.86
MnO	0.21	0.18	0.22	0.22	0.22	0.22
NiO	0.27	0.26	0.35	0.31	0.33	0.27
CaO	0.06	0.08	0.04	0.08	0.07	0.05
Al_2O_3	0.03	0.05	0.02	0.06	0.03	0.02
Total	100.07	100.18	100.21	99.61	99.61	99.78
Fo	86.61	86.63	86.54	86.68	86.54	86.68
Fa	13.39	13.37	13.46	13.32	13.46	13.32
	Formula (on the basis of 4 oxygens)					
Si	.993	.995	.994	.990	.987	.994
Mg	1.733	1.730	1.730	1.737	1.740	1.728
Fe	.268	.267	.269	.267	.271	.270
Mn	.005	.004	.004	.005	.005	.005
Ni	.005	.005	.007	.006	.007	.005
Ca	.002	.002	.001	.002	.002	.001
Al	-	.001	-	.002	.001	-
Total	3.006	3.004	3.006	3.009	3.013	2.998

Table 2.18 Representative analyses of feldspars and olivines from allivalitic bands and adjacent peridotite of zone 6. Upper case P and F of the sample identifier refer to peridotite and allivalite respectively.

Fig.2.48. Sub-vertical spinel seams within Zone 1 dunites. Spinel seams occurring low within the zone are persistent and generally planar whilst structurally higher within the zone and subsequent zones they are impersistant and undulatory in form.

Fig.2.49. High concentrations of spinel seams within dunite xenolith of Zone 4. Length of hammer shaft c. 40cm.

Fig.2.50. Spinel seam developed within Zone 2 peridotite adjacent to contact with the Allivalite Series. Spinel seams of all but the lowest exposed parts of Zone 1 are undulatory and impersistent in occurrence with maximum development adjacent to contacts with feldspathic material [G.R. 4687 1975].

Fig.2.51. Within the higher parts of the Peridotite Series, impersistent spinel veins/pods are frequently developed at contacts between peridotite and more feldspathic material.The above example occurrs at the contact of the Peridotite Series with the White Allivalite. [G.R. 4713 1953].

brown and attain sizes up to c.1mm, although 0.5mm is the norm. These crystals are generally significantly larger than those dispersed in the rock adjacent. The spinels of the seams are generally well formed octahedra and exhibit a close packing with only an insignificant proportion of interstitial feldspar (Fig.2.52). Individual seams have a planar lower surface, whilst the upper surface may be irregular and somewhat gradational (Fig.2.53). Electron probe analyses (Table 2.19) reveal these to be a chrome-spinel of fairly uniform composition:

$(Mg_{.87}Fe^{2+}_{.13})(Cr_{.31}Al_{1.61}Fe^{3+}_{.08})O_4$ to $(Mg_{.80}Fe^{2+}_{.20})(Cr_{.36}Al_{1.52}Fe^{3+}_{.12})O_4$

between seams and with no significant compositional zoning to either individual spinels or to the seams themselves. In contrast to the lower seams, the impersistent, structurally higher, seams/pods display a significantly more loosely packed structure, with considerably greater amounts of interstitial material (Fig.2.54) which, like the lower seams, is feldspar, but in addition contains small (c. 50 microns) olivines dispersed throughout. Individual spinels are again of fairly uniform composition:

$(Mg_{.65}Fe^{2+}_{.35})(Cr_{.63}Al_{1.19}Fe^{3+}_{.18})O_4$ to $(Mg_{.65}Fe^{2+}_{.35})(Cr_{.59}Al_{.24}Fe^{3+}_{.17})O_4$

but richer in Cr and Fe and poorer in Mg and Al. They are also darker in colour, many being essentially opaque, and frequently display hollow cores and embayments associated with corrosion/resorbtion (Fig.2.54). The dominant mineral occurring within the cores and embayments is feldspar; occasionally poikilitically enclosed feldspar is in optical continuity with that surrounding the spinel. Rare small olivines have also been identified within the cores.

Dispersed Spinels

Isolated, dispersed spinels are found throughout the Peridotite Series. They range up to 1mm in size and are always opaque, except in the immediate environs of the lower seams. These spinels may occur as inclusions within silicate cumulus phases or within intercumulus minerals, with significant compositional differences and trends accompanying

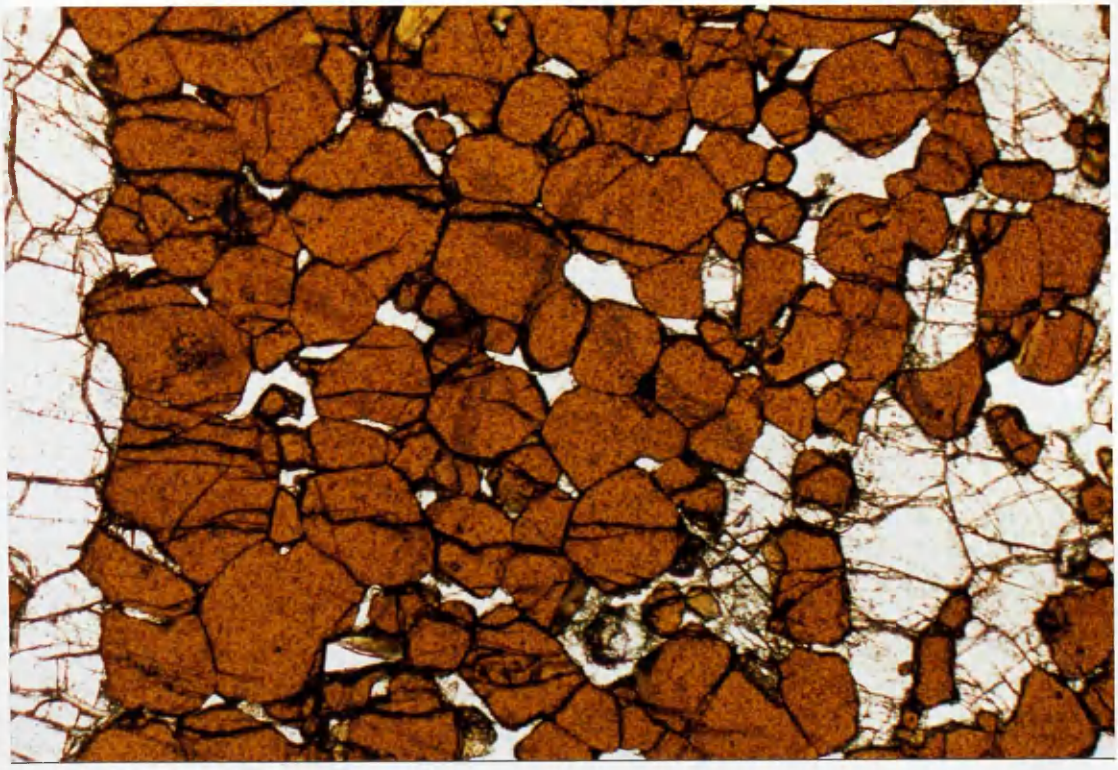

Fig. 2.52. Reddish brown spinels of the lower seams of Zone 1. These lower seams display none of the corrosion/resorbtion features associated with seams higher in the series (fig. 2.54.). Interstitial material is also much less in evidence.
Field of view c.3 x 2mm. Plane polarized light. Sample AG002.

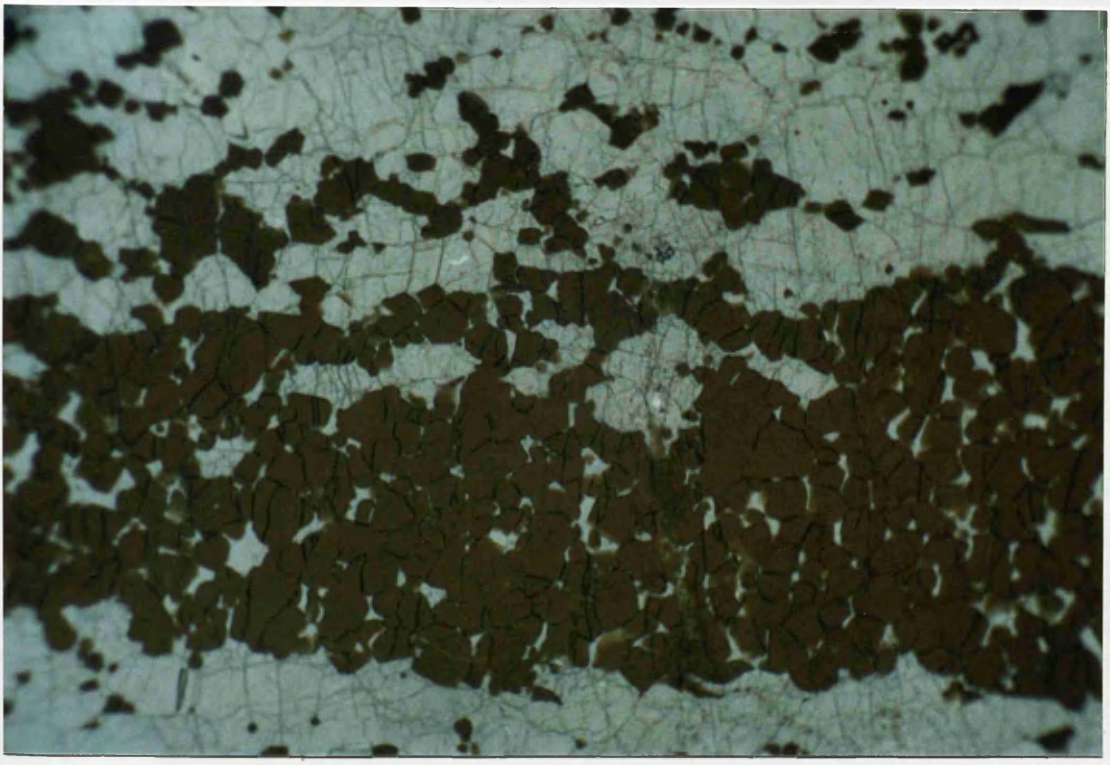

Fig.2.53. Spinel seam within the lower dunites of Zone 1. Seams frequently show sharp lower and gradational upper contacts with dunite. Field of view c.8 x 6mm.
Sample AG002.

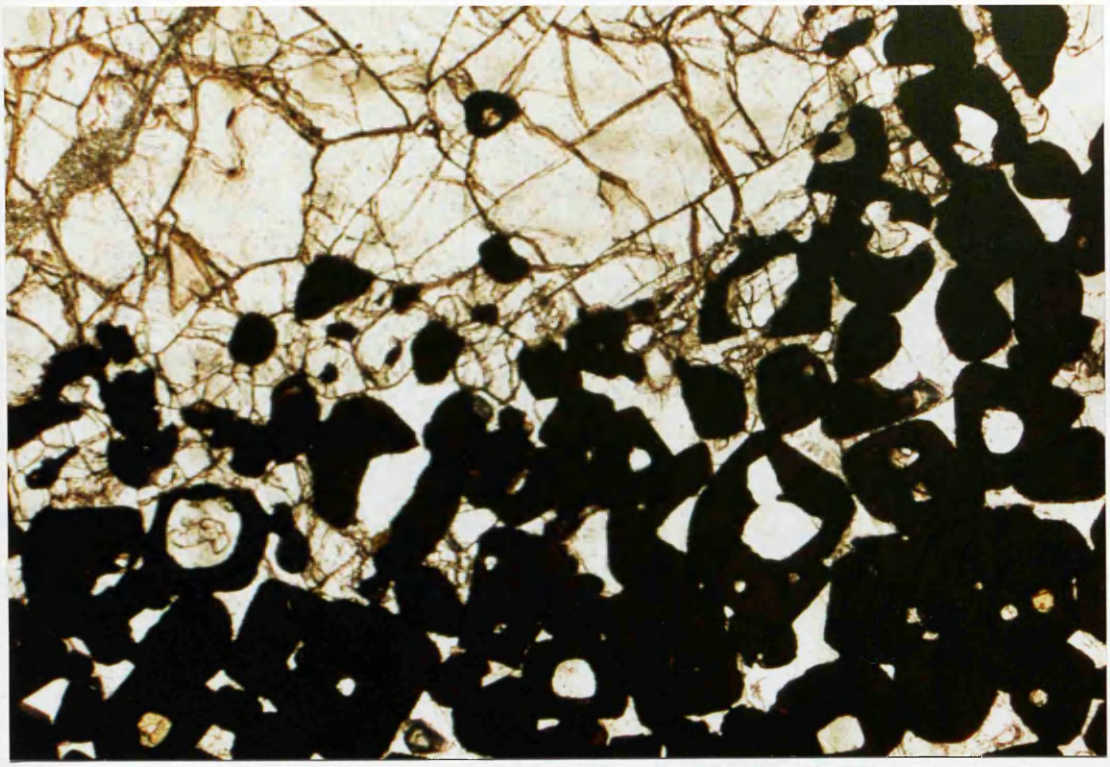

Fig.2.54. Top of spinel seam occurring high within Zone 1. The band is immediately overlain by dunite (Fo_{88}) with rare intercumulus plagioclase (An_{88}). Within the seam however, interstitial plagioclase (An_{88}) is common. Many of the spinels within the seam display corrosion/resorbtion features and hollow cores. Associated with these features is plentiful plagioclase and small olivine crystals. The spinels occurring within the upper part of Zone 1 and higher within the Peridotite Series are anhedral and opaque which contrasts with those occurring lower within Zone 1 (Fig. 2.52.). Field of view c. 3 x 2 mm. Plane polarized light. Sample AG005.

each distribution. Those occurring as inclusions, principally within cumulus olivine, but occasionally in cumulus feldspar, are notably richer in Cr and Fe and deficient in Al and Mg, with respect to those occurring in seams, and are richer in Al , Cr and Mg and deficient in Fe compared to those spinels occurring within intercumulus minerals (Table 2.19).

Discussion

Extensive solid-solution exists within naturally occurring spinels (Haggerty 1976), consequently, all spinel analyses reported here are plotted onto the basal plane of the spinel prism (Fig.2.55) which documents the change in $Fe^{2+}/(Fe^{2+}+Mg)$ relative to $Cr/(Cr+Al)$, whilst Fig.2.56 displays the variation in $Fe^{2+}/(Fe^{2+}+Mg)$ relative to $Fe^{3+}/(Fe^{3+}+Cr+Al)$. Spinels from the seams and those occurring as inclusions within cumulus silicate minerals define a trend of decreasing Al/Cr ratio with little change in Fe^{3+}. These spinels have only a minor Fe^{3+} component, which increases slightly with decreasing Al/Cr. In contrast, intercumulus spinels are characterized by fairly uniform Cr/Al and Fe^{2+}/Mg ratios but show considerable variation in their $Fe^{3+}/(Fe^{3+}+Cr+Al)$ ratio, where Ti correlates with Fe^{3+}. These two trends are easily distinguished on a triangular plot of their tri valent cations (Fig.2.57) and on the inter-element plots of Fig.2.58a,b.

The compositional trends observed above have also been identified within the Eastern Layered Series of the Rhum Central Complex by Henderson (1975), who concluded that the spectrum of compositions define two diverging trends. Henderson (1975) postulated that the Cr-rich spinels found as inclusions within the cumulus minerals represent the composition of the initial spinel which crystallized and that their inclusion into early cumulus phases prevented them reacting with the magma. From this initial composition the two diverging trends were produced dependent upon the enviroment of the spinel. Henderson (1975) proposed that the trend of increasing Al resulted from the reaction of cumulus chromite with olivine and plagioclase, or a melt rich in the plagioclase component, whereas spinels which were able to react with trapped intercumulus melt over a considerable temperature interval were made over to a more Fe^{3+}-rich composition and it is these spinels that define the increasing Fe^{3+} trend.

Sample	AG2	AG5	AG157	AG173	AG249B	AG244
Lithology	Dun	Dun	Per	Tro	F/Per	Per
Type	S	S	S	Pl	Pl	Ol
SiO_2	-	0.01	0.02	0.02	0.03	0.04
TiO_2	0.21	0.48	0.23	1.36	3.95	1.46
Al_2O_3	51.64	33.78	52.13	17.94	6.66	16.55
Cr_2O_3	14.80	26.64	14.26	39.80	20.47	39.65
FeO_3	3.72	8.48	4.37	10.48	34.99	10.83
MgO	22.03	14.40	21.58	9.53	3.86	7.80
FeO	6.11	14.49	7.21	20.64	29.70	23.09
NiO	-	0.51	n.d	0.44	-	0.42
Total	98.57	99.17	100.02	100.77	100.10	100.43
FeO^*	9.44	22.13	11.16	30.11	61.14	32.86

Formula (on the basis of 32 oxygens)

Si	-	.002	.004	.004	.011	.012
Ti	.033	.088	.037	.269	.956	.297
Al	12.991	9.598	13.011	5.584	2.525	5.267
Cr	2.496	5.075	2.386	8.307	5.208	8.462
Fe^{3+}	.592	1.504	.688	4.416	7.064	5.040
Mg	7.006	5.173	6.809	3.749	1.849	3.140
Fe^{2+}	1.080	2.856	1.264	2.016	7.488	2.128
Mn	.011	.077	.029	.125	.120	.136
Ni	-	.009	-	.094	-	.092
Total	24.209	24.382	24.228	24.564	24.574	25.221

Table 2.19 Representative analyses of spinels occurring in the Peridotite Series. Dun=Dunite,Per=peridotite, F/per=feldspathic peridotite, Tro=troctolite. Type; S=spinel fom seam,Pl=inclusion in plagioclase, Ol=inclusion in olivine. Total iron was determined as FeO^* and subsequently partitioned between ferrous and ferric iron by the method of Finger (1972).

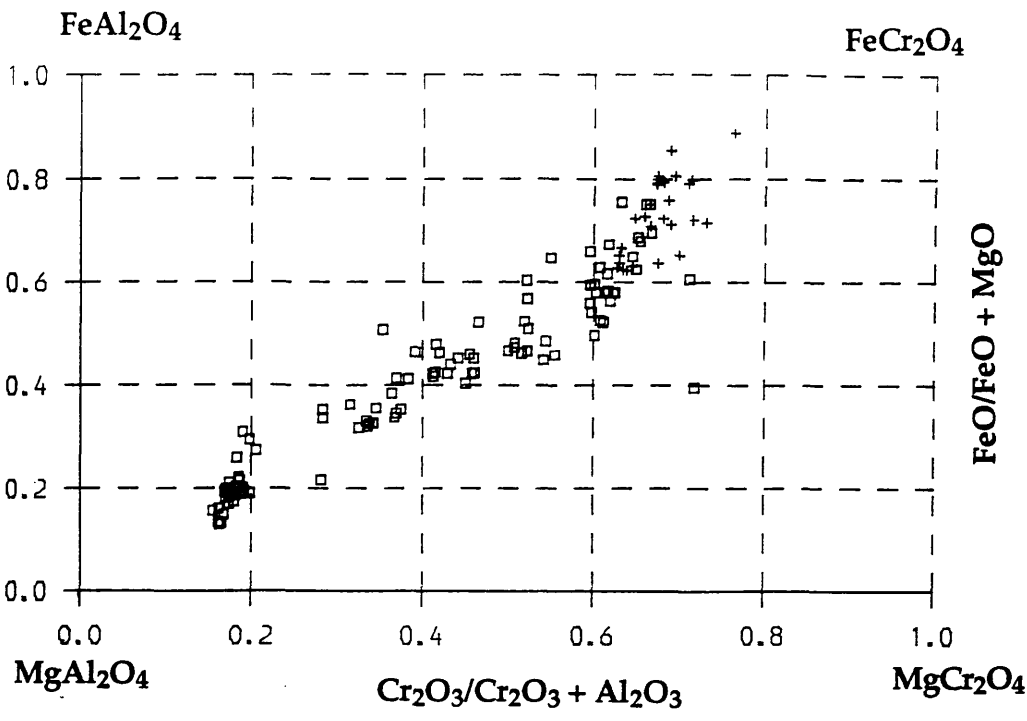

Fig. 2.55. Variation of FeO/FeO+MgO v Cr_2O_3/+Cr_2O_3+Al_2O_3 within spinels from the Peridotite Series. (□) = Cumulus spinels, (+) = intercumulus spinels.

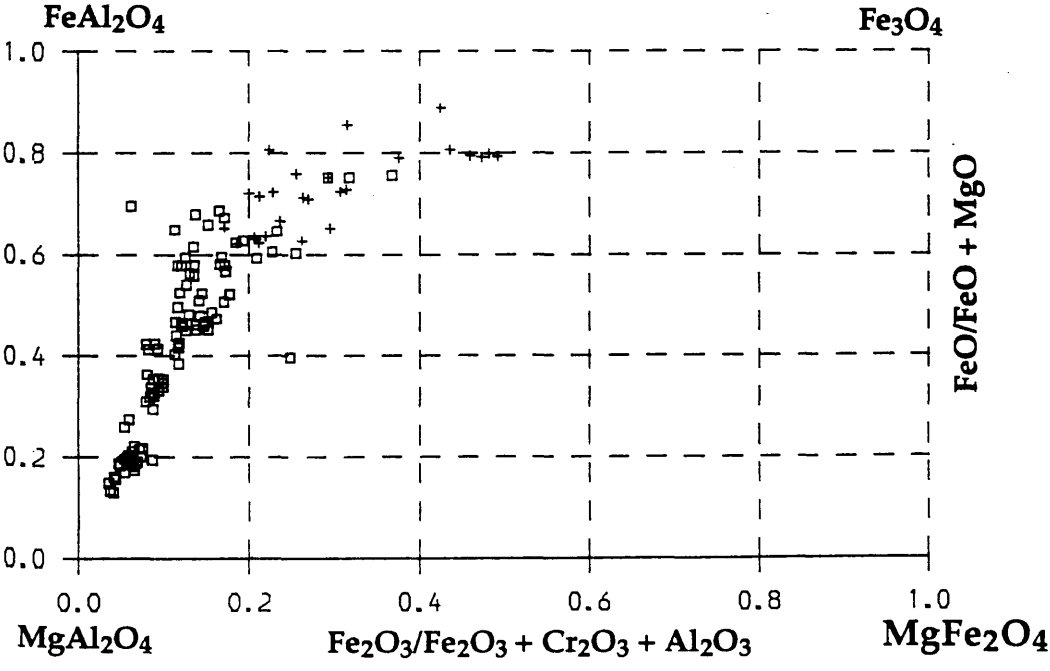

Fig. 2.56. Variation of FeO/FeO+MgO v Fe_2O_3/Fe_2O_3+Cr_2O_3+Al_2O_3 within spinels from the Peridotite Series. (□) = Cumulus spinels, (+) = intercumulus spinels.

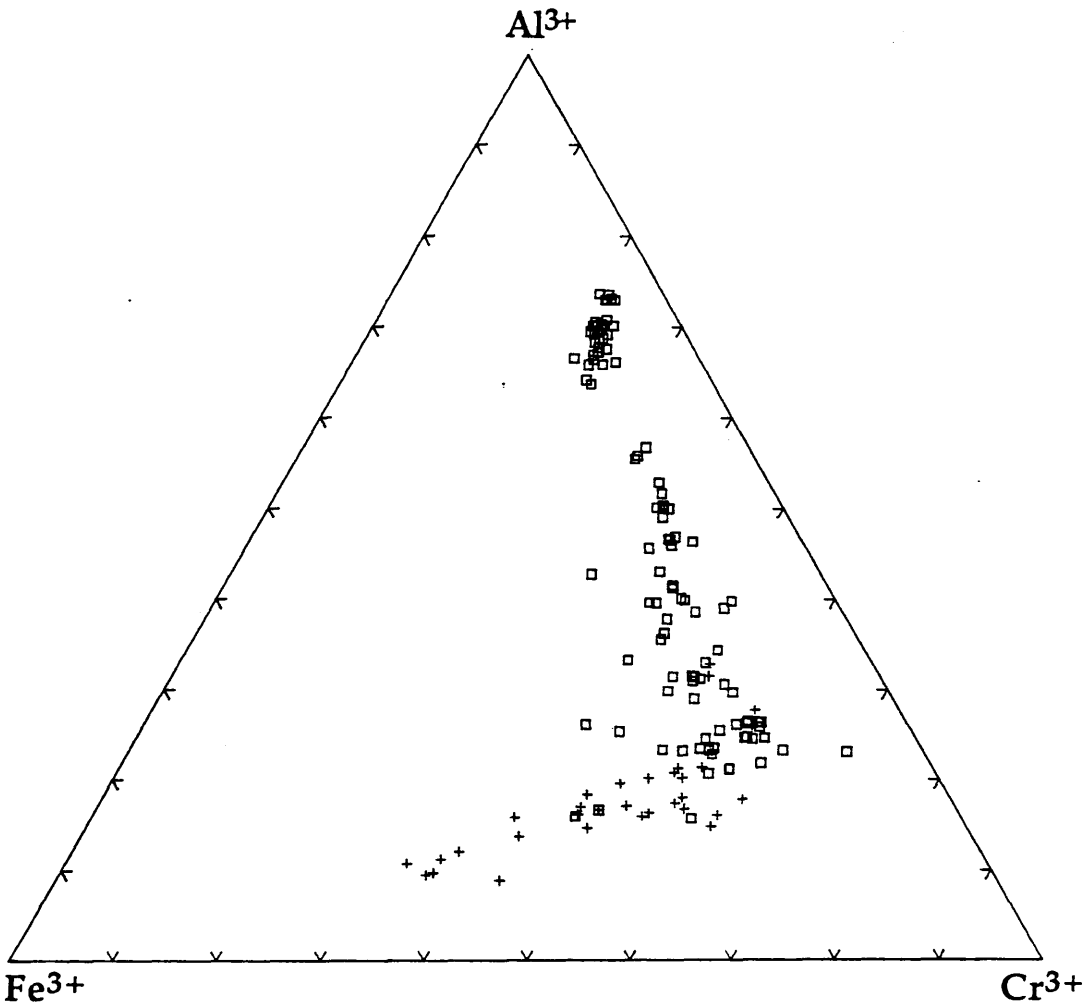

Fig. 2.57. Variation of the trivalent cations, Al^{3+}, Fe^{3+} and Cr^{3+}, within spinels of the Peridotite Series. (□) = Cumulus spinels, (+) = intercumulus spinels.

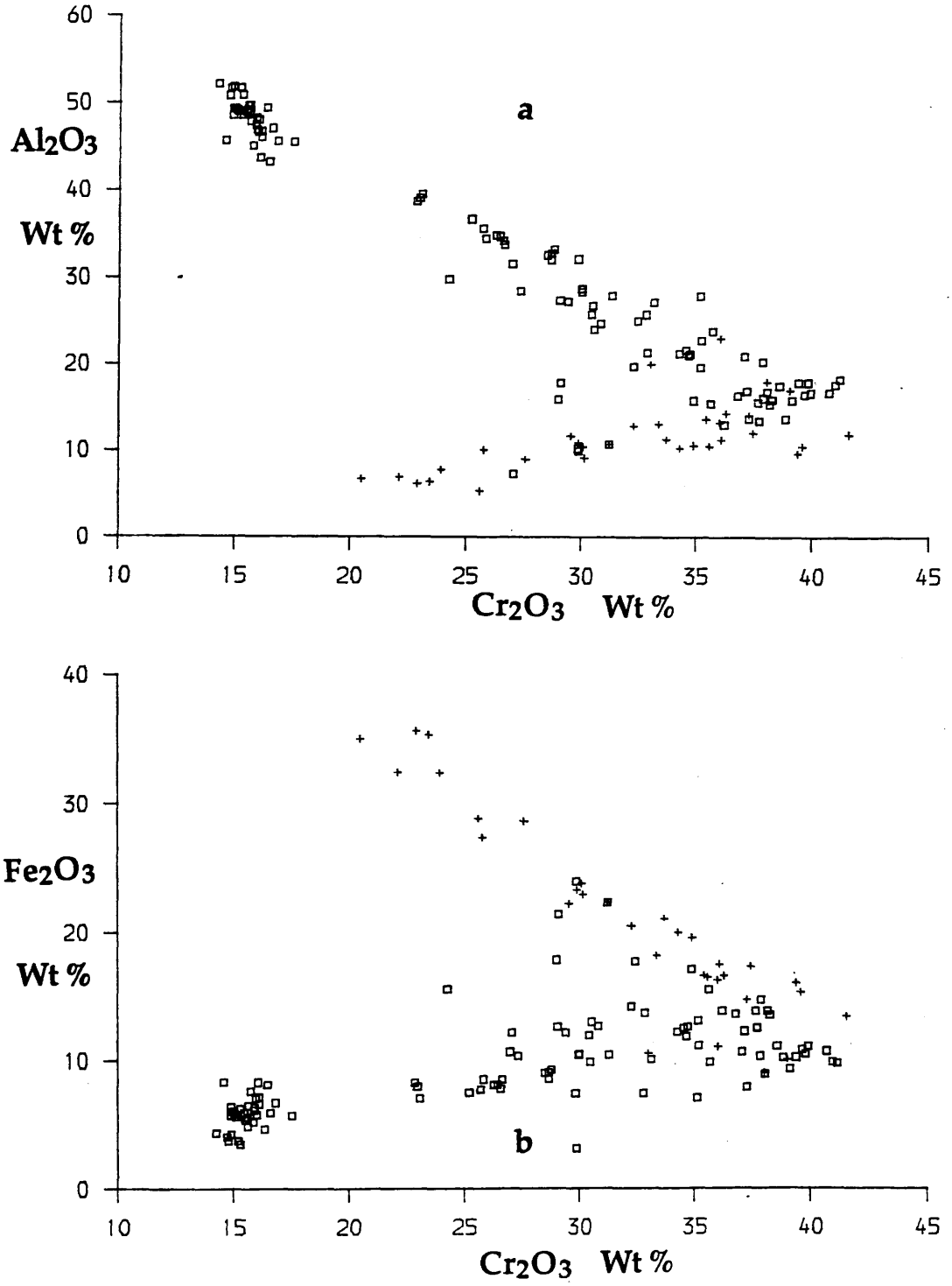

Fig. 2.58. Variation of a) Al_2O_3 and b) Fe_2O_3 with Cr_2O_3 within spinels of the Peridotite Series. (+) = spinels occurring within intercumulus phases. (□) = Cumulus spinels and inclusions occurring within cumulus silicate phases.

Current theories pertinent to the compositional variation of spinels within ultrabasic rocks fall within two main categories. The first of these is that the composition of the spinel is determined during the initial crystallization (cumulus) stage and that any compositional changes are caused by variations in the chemical and/or physical parameters of the parent magma. In contrast, the second category assumes that initial spinels crystallize with a fairly uniform composition which is modified by either post-cumulus or sub-solidus reaction with adjacent silicates and/or inter-cumulus liquid. Experimental data (Ulmer 1969) on systems crystallizing a spinel phase show that a higher fO_2 results in both spinel and silicates becoming more Mg-rich. Muan (1957) has shown that, within the system FeO-Fe_2O_3-Al_2O_3-SiO_2, decreasing fO_2 causes an increase in the Al content of the crystallizing spinel. These results are in conflict with those implied from the spinels of the Peridotite Series, where a sympathetic trend of decreasing Mg and Al is observed (Fig.2.59). However, Hill and Roeder (1974), found that decreasing fO_2 is accompanied by an increase in both Mg/Mg+Fe and Al, the reverse of that observed from simple synthetic systems.

Whilst the spinels which occur as inclusions within the silicate phases above Zone 1 of the Skye peridotites are generally the most chrome-rich, it is suggested here that the initial spinels to crystalize were enriched in Al relative to Cr, and it is these spinels which define the Al-rich end of the Al-Cr trend. Based on the observed sharply defined bases and the gradational tops to the spinel seams it is suggested that the seams were formed by crystal settling during periods of cessation of olivine crystallization. This proposal is supported by the evidence that the most aluminous spinels, both within and dispersed around the seams are associated with the most forsteritic olivine (cf. Henderson & Suddaby 1981) which presumably crystallized at the highest temperature. These spinels also have the highest MgO and lowest TiO_2 concentrations, consistent with a high temperature, magmatic origin. It may be argued that the aluminous spinels are the result of extensive reaction with the melt but it is believed that this was prevented by rapid isolation of the crystals by cumulus olivine in the majority of the lower seams. However, spinels of the structurally higher seams do

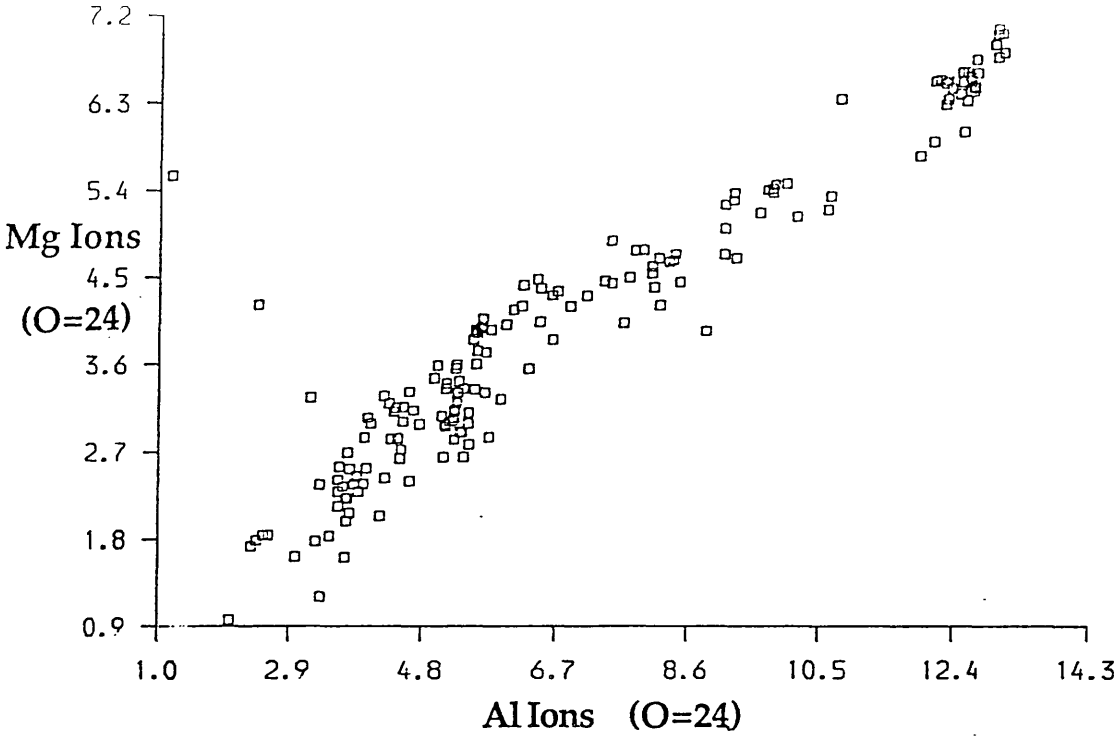

Fig. 2.59. Variation of Mg and Al (on the basis of 32 oxygens) within spinels of the Peridotite Series.

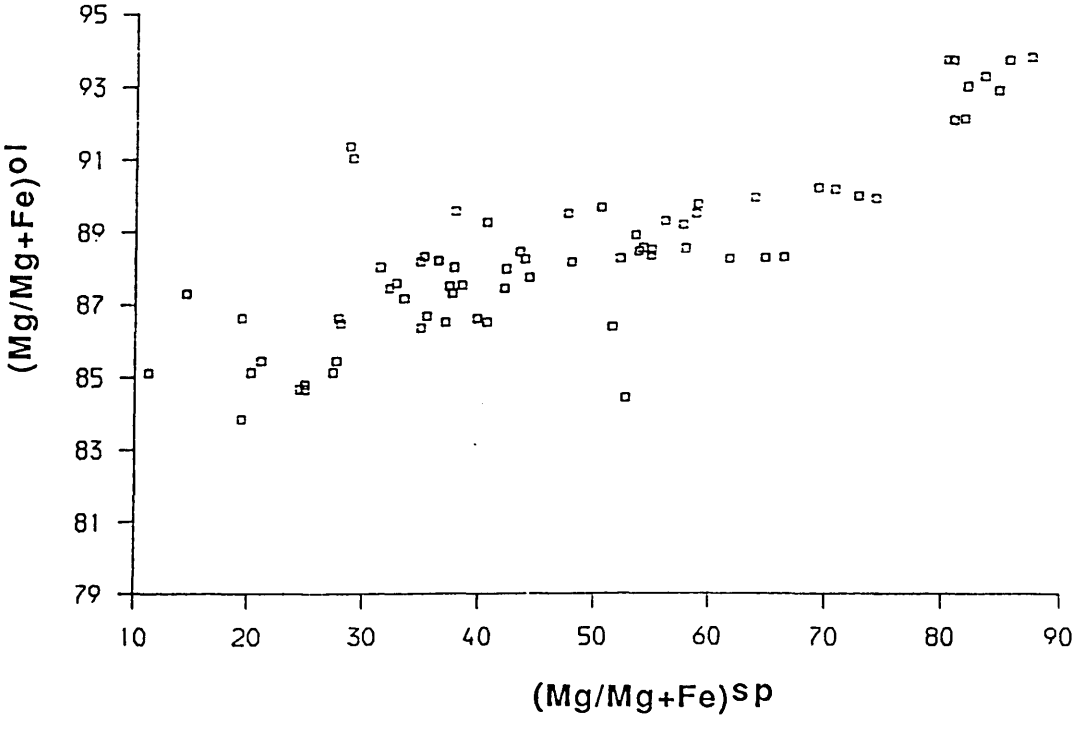

Fig. 2.60. Variation of forsterite content of olivines with Mg number of associated spinels within the Peridotite Series.

show reaction features and their compositions are notably enriched in chromium relative to aluminium. It is proposed that these loosely packed seams favoured reaction between spinel and melt. Reaction of the spinels with the silicate melt resulted in a series of cation exchanges.

Initialy this involved the single cation substitutions:

$Fe^{2+} <=> Mg^{2+}$

$Cr^{3+} <=> Al^{3+}$

$Fe^{3+} <=> Cr^{3+} \& Al^{3+}$

Extensive late stage reaction, where possible, resulted in the enrichment of Ti, probably by the coupled substitution of:

$Ti^{4+} + Fe^{2+} <=> Cr^{3+} + Al^{3+}$

Fig.2.60 documents the sympathetic variation of the magnesium number (Mg# = $Mg/Mg+Fe^{2+}$) of the spinels with that of associated olivines. Spinels having the highest Mg# (Mg# = c85) are associated with the most magnesian olivines (Fo_{90-94}), whilst rocks which contain olivine of less than Fo_{88} have spinels with Mg# between 10 and 40. There is a suggestion from Fig.2.61 that there is little variation in spinel Mg# for rocks containing olivine in the region Fo_{88-90}. This inflexion in the correlation between forsterite compositions of olivines and the Mg# of associated spinels, appears to coincide with the appearence of cumulus plagioclase crystallization.

Previous studies on spinel occurrences have emphasized the reduction in Al/Cr of crystallizing spinels with increased fractionation (Evans & Moore 1968; Henderson 1975; Hamlyn & Keays 1979; Fisk & Bence 1980; Henderson et al. 1981; Agata 1988). Aluminous spinels are often assigned to a high pressure origin (Irvine 1967; Fisk & Bence 1980; Dick & Bullen 1984).

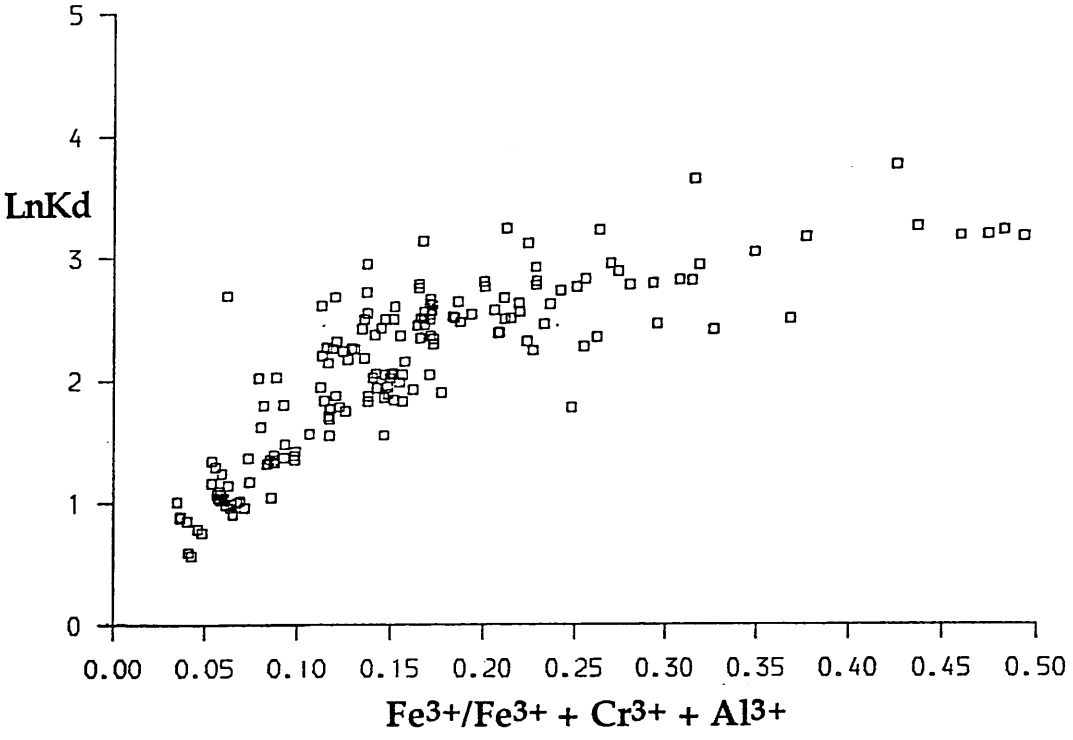

Fig. 2.61. variation of LnKd with $Fe^{3+}/ Fe^{3+}+Cr^{3+}+Al^{3+}$ (on the basis of 24 oxygens) for spinels of the peridotite series.

$$LnKd = \left[\frac{(X)^{Mg}}{(X)^{Fe}}\right]^{Ol} \times \left[\frac{(X)^{Fe}}{(X)^{Mg}}\right]^{Sp}$$

Where $(X)^{Mg}$ = Mg/Mg+Fe and $(X)^{Fe}$ = Fe/Mg+Fe.

Utilising the olivine-spinel geothermometer reavaluated by Roeder et al (1979):

$$T(K) = \frac{A3480 + B1018 - C1720 + 2400}{A2.23 + B2.56 - C3.08 - 1.47 + \ln K_d}$$

where

$$A = \frac{Cr^{3+}}{Cr^{3+} + Fe^{3+} + Al^{3+}} \qquad B = \frac{Al^{3+}}{Cr^{3+} + Fe^{3+} + Al^{3+}} \qquad C = \frac{Fe^{3+}}{Cr^{3+} + Fe^{3+} + Al^{3+}}$$

and

$$K_d = \left[\frac{X^{mg}}{X^{Fe}}\right]^{ol} \cdot \left[\frac{X^{Fe}}{X^{mg}}\right]^{sp}$$

where

$$X_{mg} = \frac{Mg}{Mg + Fe} \qquad X_{Fe} = \frac{Fe}{Mg + Fe}$$

There exists considerable variation in the $Fe^{3+}/(Fe^{3+} + Al^{3+} + Cr^{3+})$ ratio of all analysed spinels with respect to $\ln K_d$ (Fig.2.61), however, with C=0.1 (approximate mean of aluminous spinels of the seams and Zone 1 dunites), the calculated temperatures of spinel-olivine equilibration, derived from the above equation range between c.500^{o}C and c.1500^{o}C (Fig.2.62a) whilst with C=0.2 (approximate mean of remaining samples) temperatures vary from 400^{o}C to 1400^{o}C (Fig.2.62b). Consequently, the lower temperatures of the more chrome rich spinels are believed to represent sub-solidus re-equilibration temperatures. Roeder et al. (1979) have demonstrated that possible Mg/(Mg+Fe) re-equilibration may occur, with olivine undergoing an increase in Mg/Mg+Fe at the expense of that in spinel. Nevertheless, the above results support the premise that the aluminous spinels do in fact represent magmatic compositions.

From synthetic systems, peritectic reactions may be predicted and have been inferred (Irvine 1967), whereby, spinel may crystallize with either olivine or feldspar but should cease crystallization once both of these minerals start to crystallize. However, evidence from spinels documented in this study and those occurring on Rhum (Henderson & Suddaby 1971) show post-cumulus reactions that modify the initial spinel compositions. These reactions involve several cation exchanges and suggest extensive solid-solution exists between Al, Cr, Fe, Mg and Ti. These wide ranging limits of solid-solution preclude the

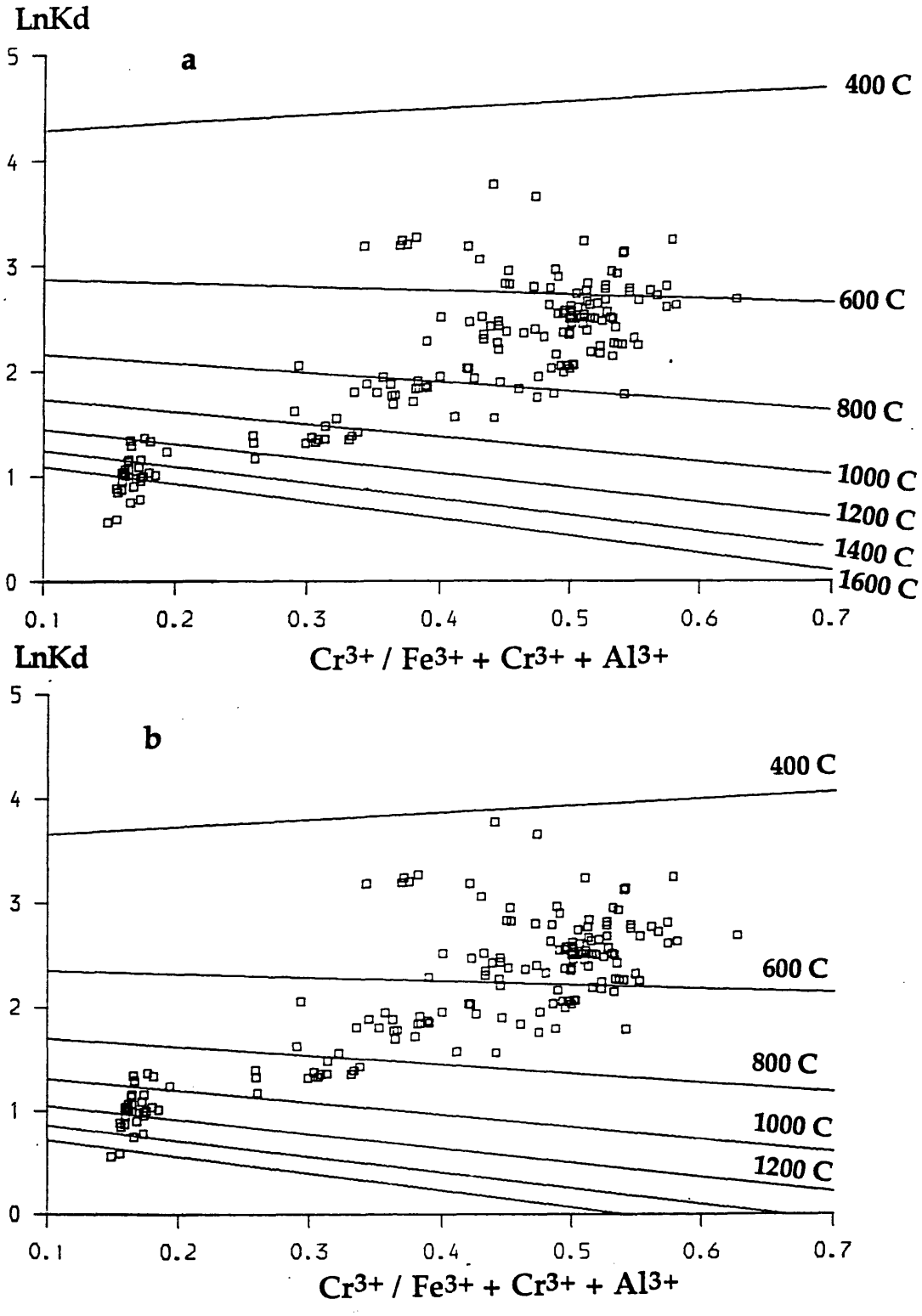

Fig. 2.62. Variation of LnKd with $Cr^{3+} / Fe^{3+}+Cr^{3+}+Al^{3+}$ for all spinels occurring within the peridotite series. The plots are contoured for temperature (Roeder et al. 1979) with (a) $Fe^{3+}/ Fe^{3+}+Cr^{3+}+Al^{3+} = 0.1$

(b) $Fe^{3+}/ Fe^{3+}+Cr^{3+}+Al^{3+} = 0.2$

possibility that spinel will cease to crystallize from a cooling ultrabasic system by a simple peritectic reaction as would be expected from a simple synthetic system. Instead, the spinel exchanges cations with the melt along a reaction line which may involve spinel, olivine and feldspar, resulting in a gradually less aluminous spinel as plagioclase crystallizes:

Al spinel + melt = Cr spinel + plagioclase

For spinels documented here, the semi-quantitative equation:

$$4(Mg,Fe)(Fe_{.1}Cr_{.3}Al_{1.6})O_4 + Ca_2Si_5O_{12} = 2CaAl_2Si_2O_8 + (Mg,Fe)_2SiO_4 + 2(Mg,Fe)(Fe_{.2}Cr_{.6}Al_{1.2})O_4$$

Al-spinel melt feldspar olivine Cr-spinel

shows reasonably good agreement with the compositions noted from the lower and higher seams. The equation is essentially the reverse of that proposed by Henderson (1975) to account for the Cr-Al trend of Rhum spinels, however, it is believed that it is equally applicable to the Al-Cr trend observed in spinels of the Skye peridotites. In addition, it explains the increased interstitial feldspar associated with the seams, the small interstitial olivines and the decrease in Al and the concomitant increase in Cr of the spinels as feldspar crystallizes. Typically the most chrome-rich spinels are associated with rocks containing cumulus plagioclase.

This increase in Cr and decrease in Al of the spinels as feldspar crystallizes is what one would intuitively expect and suggests that the Cr content of the spinels is governed principally by the preference of Al for plagioclase and the fact that the Cr is stabilized in the octahedral site of the spinel by a high octahedral site preference energy, a feature not shared by Al. As can be seen from Fig.2.57, there exists a few spinels occurring as inclusions which plot along the Fe-enrichment trend of intercumulus spinels. It is suggested that these anomalous compositions were either relatively late in the crystallization history and were consequently affected by similar conditions giving rise to the Fe^{3+} trend before being armoured by a silicate phase, or alternatively, the spinel may not have been totally enclosed by the silicate phase in three-dimensions or was subsequently exposed to the melt by fracturing of the silicate phase.

2.3.5.2 Olivine

Olivine is the dominant mineral occurring throughout the Peridotite Series and along with spinel (section 2.3.5.1) was an early phase in the crystallization history. Those olivines occurring within Zone 1 may contain small trains of minute inclusions (Fig.2.63), the composition of which remains unknown. Many of the olivines of this zone display broad lamellae (Fig.2.63) which generally may only be detected when the crystal is close to extinction and it is believed that such structures result from strain (Hess 1938). Individual crystals usually display well defined margins which are straight. Olivines of structurally higher zones are often remarkably euhedral (Fig.2.38) and range in size up to approximately 10mm.

When trace element data of olivines from all zones is considered together (Fig.2.64) some generalizations, which may have possible bearing on the evolution and form of emplacement of the Peridotite Series, may be made. The most primitive olivines (Fo_{92-94}) are those occurring within the structurally lowest exposed dunites of Zone 1. Olivines become less forsteritic on ascending the peridotite, albeit with considerable overlap, with the most evolved olivines (Fo_{84-88}) occurring within Zone 6, the structurally highest zone. Zone 3 olivines are generally more primitive than those of the marginal zone 2 which have little compositional differences to differentiate them from those of the bulk of Zone 5.

Due to the similar ionic radius and the same ionic charge of the nickel cation with that of the magnesium ion, nickel may substitute for magnesium within the crystal lattice of olivine. The high distribution coefficient of Ni in olivine (D = c.16) predicts that the nickel content of a magma, fractionating olivine, will fall rapidly with continued olivine crystallization in a closed system and consequently olivines of a more evolved nature should contain lesser amounts of nickel. Fig.2.64 illustrates that whilst Zone 1 olivines are the most forsteritic, particularlly those adjacent to the spinel seams, their nickel contents may be lower than those from other zones. Roeder et al. (1979) have demonstrated experimentally that re-equilibration of magnesium may occur between olivine and spinel, with olivine experiencing an increase in

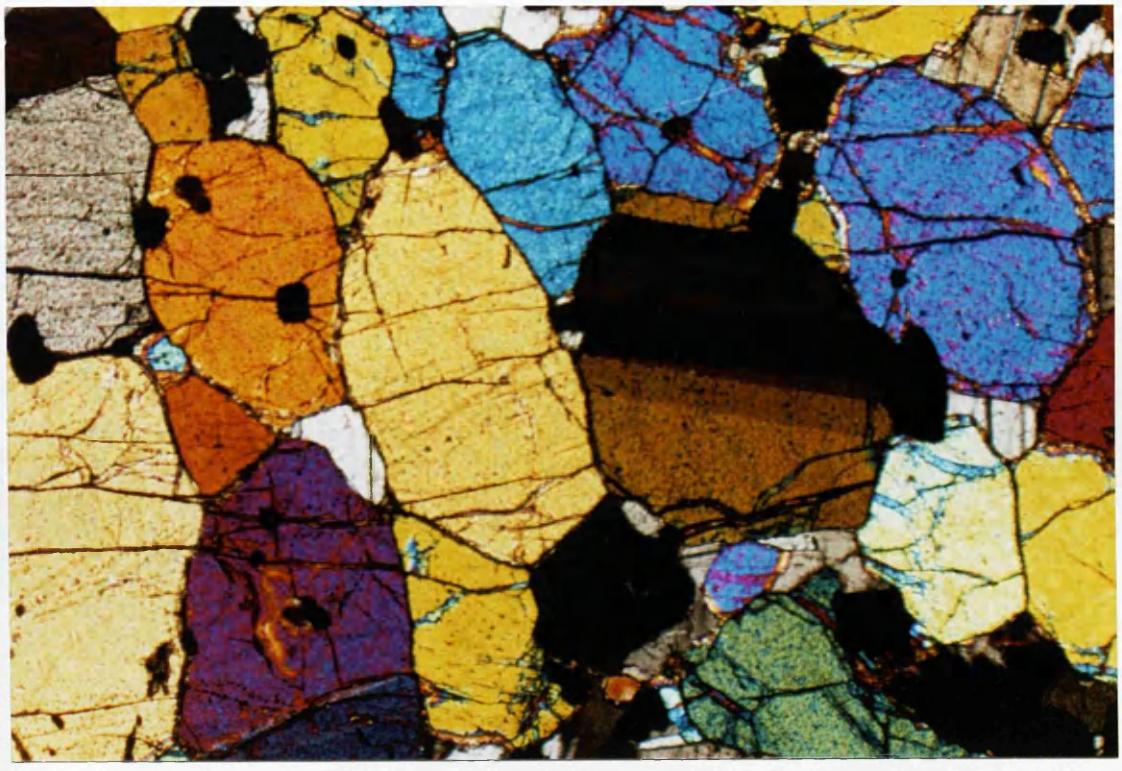

Fig. 2.63. Zone 1 dunite with only minor intercumulus material, which is invariably plagioclase (An_{89}). The olivines occasionally show translation lamellae. Field of view c.3 x 2mm. Crossed polars. Sample AG002.

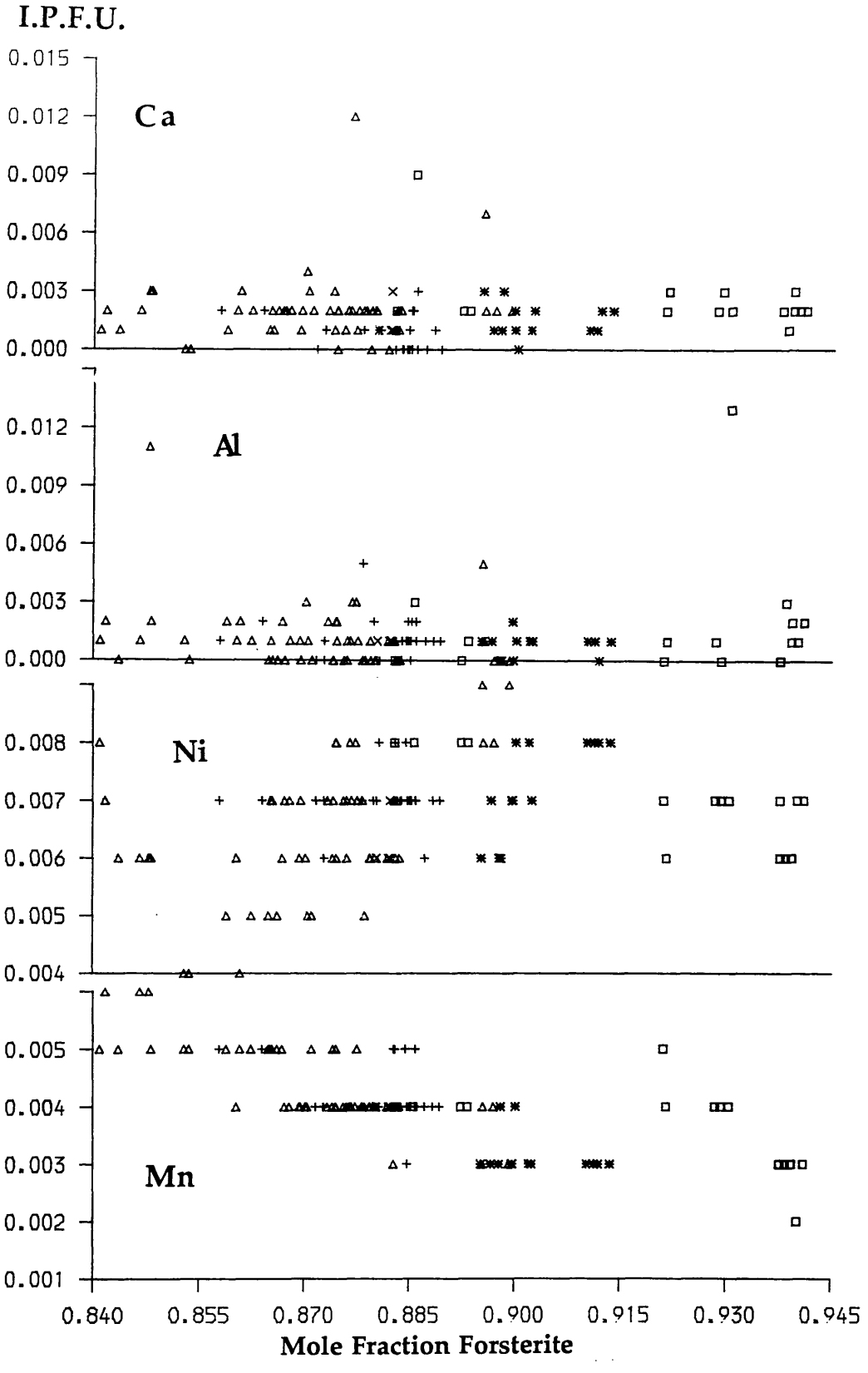

Fig. 2.64. Trace element variation of Ca, Al, Ni and Mn (on the basis of 4 oxygens) with forsterite content of host olivines from the Peridotite Series.
(□) = Zone 1. (+) = Zone 2. (*) = Zone 3. (△) = Zone 5. (x) = Zone 6.

magnesium derived from associated spinel. Should such a process be applicable to to Zone 1 olivines, then prior to re-equilibration they would have been less forsteritic although still deficient in nickel, unless similar re-equilibration of nickel has also occurred, if derived from the same magma which gave rise to subsequent zones.

It was principally the observation of decreasing forsterite content of the olivines allied with the generally more feldspathic nature of the peridotite on ascending the series that led Weedon (1956) to conclude that the Peridotite Series was the product of a single fractionating magma. Whilst the data obtained during the present study does not in general conflict with this view, enough data has been analysed to show that in detail considerable complexities exist which require an explanation to reconcile field observations and major and trace element distributions.

2.3.5.3 Pyroxene

Throughout the Peridotite Series, pyroxene is never present as a cumulus phase, occurring only as an interstitial phase in variable, but minor, amounts. Within the dunites and peridotites of Zone 1 pyroxene is absent. However, immediately above the Allt Beag ultrabasic tongue (Zone 1), minor amounts of clinopyroxene are present, generally increasing with structural height within the series. As an interstitial phase, pyroxene is present in amounts of generally less than 5%. This figure is only exceeded in the allivalitic bands (Section 2.3.4) and the troctolite bands occurring on the summit ridge of Sgurr dubh an Da Bheinn (938 O.D.), where up to 20% of the rock may comprise pyroxene. The pyroxene is invariably clinopyroxene, with the exception of that occurring in the structurally highest levels on Sgurr dubh an Da Bhienn, where minor amounts of orthopyroxene accompany clinopyroxene.

Clinopyroxenes throughout the sequenece are generally green/brown and may poikilitically enclose all cumulus phases. All analyses are plotted in Fig.2.65 and representative analyses are presented in Table 2.20, from which it can be seen that the clinopyroxene is a Cr-rich augite, with limited compositional variation, $(Ca_{.36}Mg_{.54}Fe_{.10})_2Si_2O_6$-$(Ca_{.47}Mg_{.46}Fe_{.07})_2Si_2O_6$), whilst orthopyroxene is a pale-green bronzite (Mg/Mg+Fe+Mn = 0.75).

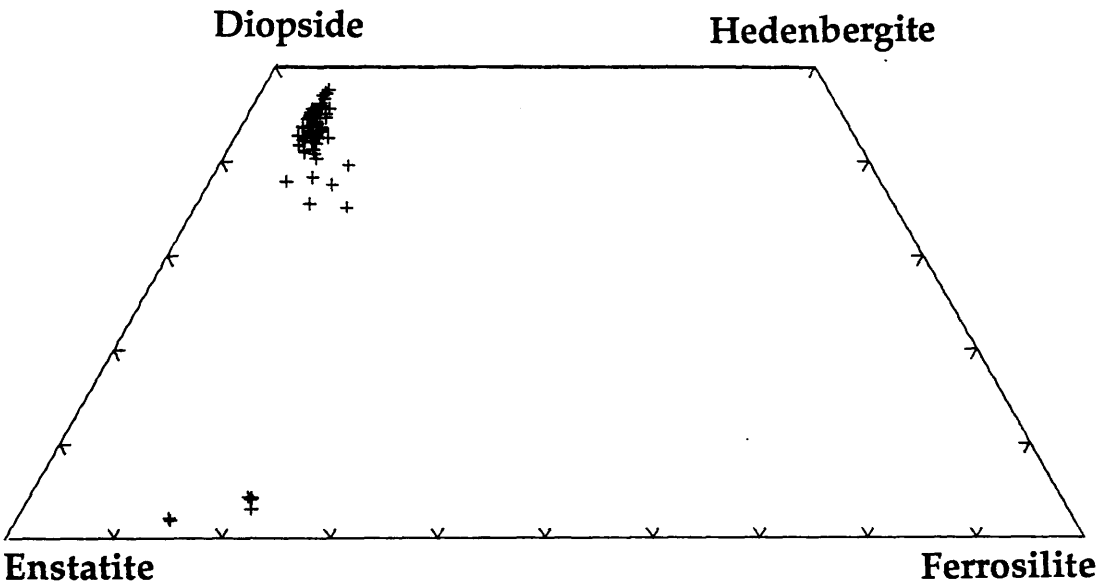

Fig.2.65. Pyroxenes of the Peridotite Series plotted in the Di-Hd-En-Fs pyroxene quadrilateral, illustrating the general lack of major element variation which exists between the monoclinic pyroxenes of the Peridotite Series.

Sample	AG143P	AG143F	AG245	AG245A	AG295	AG266B	AG249/G	AG249/D
Lithology	Per	F/Per	Per	All	Per	All	All	All
SiO_2	52.05	51.70	52.18	51.91	52.04	52.43	54.38	54.43
TiO_2	1.35	0.53	0.35	1.18	0.97	0.46	0.22	0.45
Al_2O_3	2.71	3.01	2.76	2.84	2.42	2.90	1.11	1.33
Cr_2O_3	0.92	1.21	1.19	0.71	0.86	0.92	0.09	0.09
Fe_2O_3	0.73	1.36	1.28	0.92	2.02	0.51	1.21	0.67
MgO	17.38	17.15	17.88	16.81	19.27	16.62	27.81	27.97
MnO	0.21	0.21	0.09	0.16	0.25	0.17	0.37	0.37
CaO	20.73	21.19	20.79	21.80	17.62	21.77	2.26	1.58
FeO	0.73	1.36	2.75	3.64	4.54	3.49	12.05	12.94
Na_2O	0.38	0.22	0.29	0.31	0.30	0.41	0.06	0.06
Total	100.40	99.91	99.56	100.28	100.29	99.68	99.56	99.89
FeO^*	4.58	4.56	3.90	40.45	6.32	3.96	12.91	13.53
				Atomic% (Mn included with Fe)				
Ca	42.59	43.48	42.61	44.67	35.57	45.26	4.43	3.09
Mg	49.68	48.91	50.97	47.96	54.07	48.07	75.38	75.76
Fe	7.73	7.61	6.42	7.37	10.36	6.67	20.19	21.15
				Formula (on the basis of 6 oxygens)				
Si	1.898	1.898	1.912	1.899	1.901	1.922	1.964	1.955
Al	.102	.102	.088	.101	.099	.078	.036	.045
Al	.014	.028	.031	.021	.005	.047	.011	.011
Ti	.037	.015	.010	.032	.027	.013	.005	.012
Cr	.026	.035	.034	.021	.025	.027	..003	.002
Fe3+	.020	.037	.035	.025	.055	.014	.026	.018
Mg	.945	.938	.976	.917	1.049	.908	1.497	1.497
Mn	.007	.006	.003	.005	.008	.005	.011	.011
Ca	.810	.834	.816	.854	.690	.855	.088	.061
Fe^{2+}	.120	.102	.084	.111	.138	.107	.353	.388
Na	.027	.016	.021	.022	.021	.029	.004	.004
Total	4.006	4.011	4.010	4.008	4.018	4.005	3.998	4.004

Table 2.20 Representative analyses of pyroxenes from the Peridotite Series. Per=peridotite, All=allivalite, F/perid=feldspathic peridotite. Total iron was determined as FeO^* and subsequently partitioned between ferrous and ferric iron by the method of Finger (1972).

With the exception of Zone 6, the limited major element compositional range (MMF = 0.85-0.90) broadly correlates with the variation of olivine forsterite contents from respective zones Fig.2.66). The minor elements Al and Cr, although not tightly constrained, decrease with decreasing MMF whilst the increase in Mn is slightly better correlated (Fig.2.66). Ti shows ambivalent behaviour, with concentrations ranging from c. 0.01 to 0.05 Ions per formula unit at a given value of MMF.

The compositional range of pyroxenes from Zone 6 is considerably greater (MMF = 0.79-0.89) than that displayed throughout the remainder of the series (Fig.2.66) and is commensurate with the variety and variation of ultrabasic lithologies observed.

Occurring sparodically throughout Zone 5 are atypical exposures in which large (c.2cm) aggregates of a dark green/black pyroxene form a prominent component of the rock (usually a feldspathic peridotite) and which weather proud on weathered surfaces (Figs.2.67, 2.68) similar to the Pyroxene-rich Gabbro (Section 2.2.2.2). The occurrence of the pyroxenes is unusual not only for their presence, being rare throughout the remainder of the Peridotite Series, but also as the field evidence suggests that the pyroxenes are of a secondary origin. With the exception of the pyroxenes, themselves, the rocks in which they occur are indistinguishable from surrounding pyroxene-free lithologies. Although the pyroxenes and their distribution have not been studied in detail a clue to their origin and distribution may be deduced from a locality approximately 10m above the rock barrier along the southern contact of the Peridotite Series with the Outer Allivalite Series. At this locality, irregular xenoliths/pods of feldspathic peridotite, up to a few metres in size, are enclosed within similar but slightly more feldspathic peridotite and occasionally "normal" peridotite.. All the xenoliths display the pyroxenes and indeed in some cases the presence of xenoliths may only be inferred from the distribution of the pyroxenes (Fig.2.68), such is the similarity between xenoliths and matrix. The pyroxenes, however, may not neccesarily be confined to xenoliths and narrow pyroxene-rich bands may be traced uninterupted through both matrix and xenolith (Fig.2.67). Elsewhere, within the Peridotite Series, xenoliths of similar composition enclosed within similar matrices may not show the feature described above. Within the brecciated Zone 4, allivalitic xenoliths frequently display the pyroxenes. Similarly,

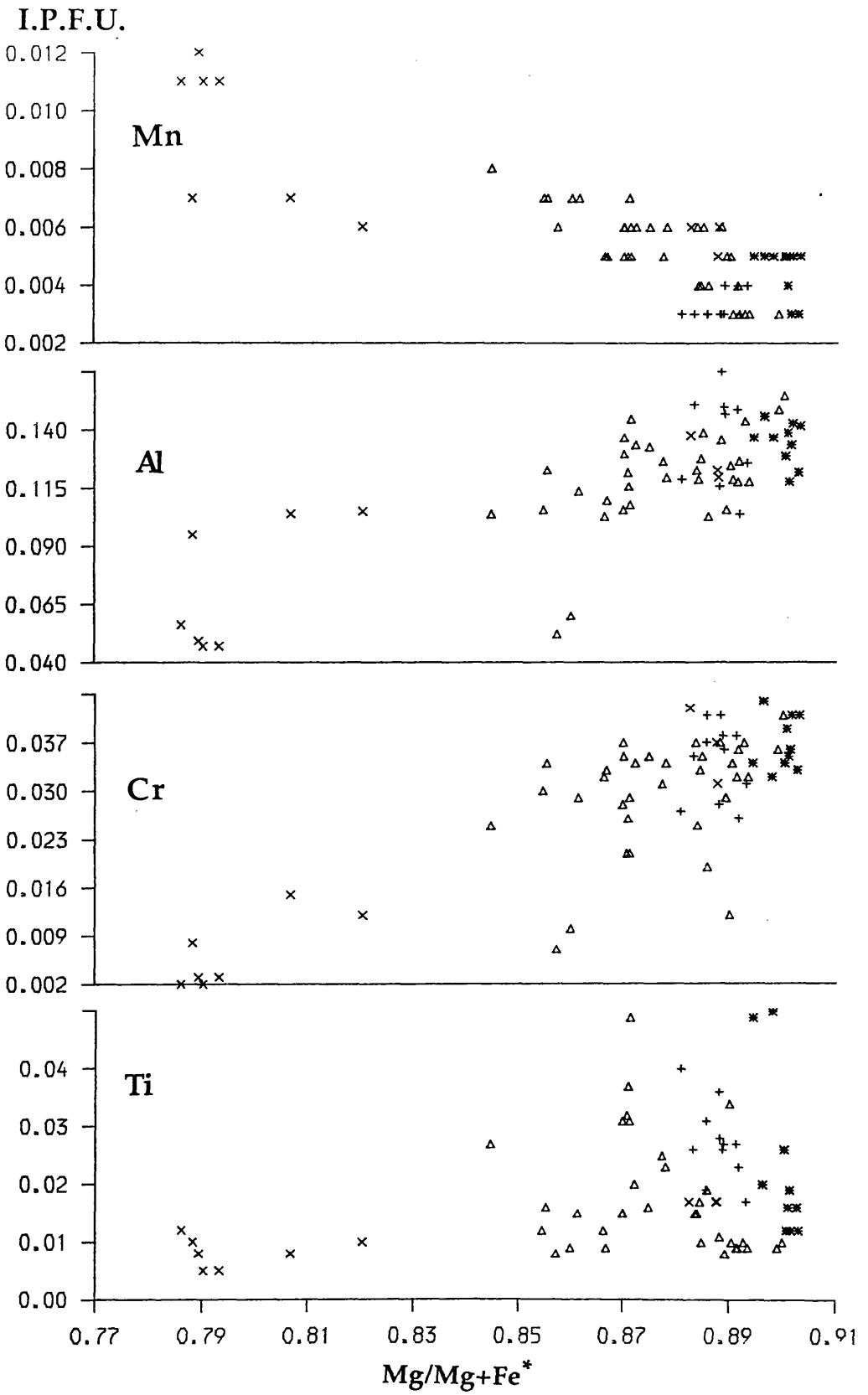

Fig. 2.66. Trace element variation of Mn, Al, Cr and Ti (on the basis of 6 oxygens) with MMF ($Mg/Mg+Fe^{2+}+Fe^{3+}$) of pyroxenes from the Peridotite Series. (+) = Zone 2. (*) = Zone 3. (△) = Zone 5. (x) = Zone 6. I.P.F.U. = Ions per formula unit.

Fig.2.67. Randomly orientated angular aggregates of pyroxene weathering proud of feldspathic peridotite. A band of the pyroxenes may be seen (top right) traversing both matrix (feldspathic peridotite) and xenolith (allivalite). [G.R. 4666 1989].

Fig.2.68. Coarse randomly orientated pyroxene aggregates adjacent to the southern contact of the Peridotite Series with the Outer Allivalite series. The pyroxenes highlight the otherwise diffuse margins of a rounded xenolith of feldspathic peridotite surrounded by a more feldspathic matrix. [G.R. 4666 1990].

within the less accessible Coir' an Lochain (Zone 6), large lithologically homogenous feldspathic peridotite exposures occur in which pyroxene aggregates feature prominently. Occasionally the presence and distribution of the pyroxenes appears to be controlled by thin, impersistent secondary veins, although this correlation is extremely tenuous as in many of the examples such a relationship cannot be demonstrated.

Three thin-sections were prepared to study the nature of these atypical pyroxenes and were taken from samples collected at the locality above the rock barrier. The first section (AG316) was taken from a sample approximately 3m into the peridotite. The second (AG315) was collected from within 50cm of the contact whilst the third (AG314) was collected from within the Outer Allivalite Series adjacent to the pyroxene-bearing peridotite. Away from the peridotite-allivalite contact the allivalite shows few remarkable petrographic features. All phase are generally fresh, with clinopyroxene, a pale brown augite (Table 2.21) poikilitically enclosing tabular, euhedral cumulus feldspar (An_{70-84}) which attains sizes up to 4mm, although 1-2mm is the norm. Anhedral to subhedral olivine (Fo_{76-77}) is to be found interstitial to the feldspar along with infrequent orthopyroxene. Occasionally, the clinopyroxene may show a minor development of blebby exsolution of orthopyroxene, this however being rare. The character of the pyroxenes changes on approaching the peridotite and in particular the areas where the pyroxene aggregates occur. The exsolution becomes more prevalent (Fig.2.69) and adjacent feldspar may display corrosive contacts with the pyroxene (Fig.2.70). Where the aggregates are well developed they form the dominant phase and may contain angular fragments of both olivine and feldspar (Fig.2.71), the pyroxene appearing to be assimilating the olivine which shows irregular rims of orthopyroxene (Table 2.21). The pyroxenes themselves show irregular exsolution of both orthopyroxene and a sub-calcic augite (Table 2.21). Where the agrregates are dominant it is difficult to reconcile their presence simply to the crystallization of intercumulus melt, as two dimensional studies suggest that the cumulate pile in which the pyroxene crystallized would have possesed an improbably large porosity. It therefore seems probable that the pyroxene aggregates have a late-post crystallization paragenesis.

Fig.2.69. Blebby exsolution of hypersthene within clinopyroxene aggregates occurring within allivalite adjacent to Zone 5. Field of view c. 1.2 x 1mm. Crossed polars. Sample AG315.

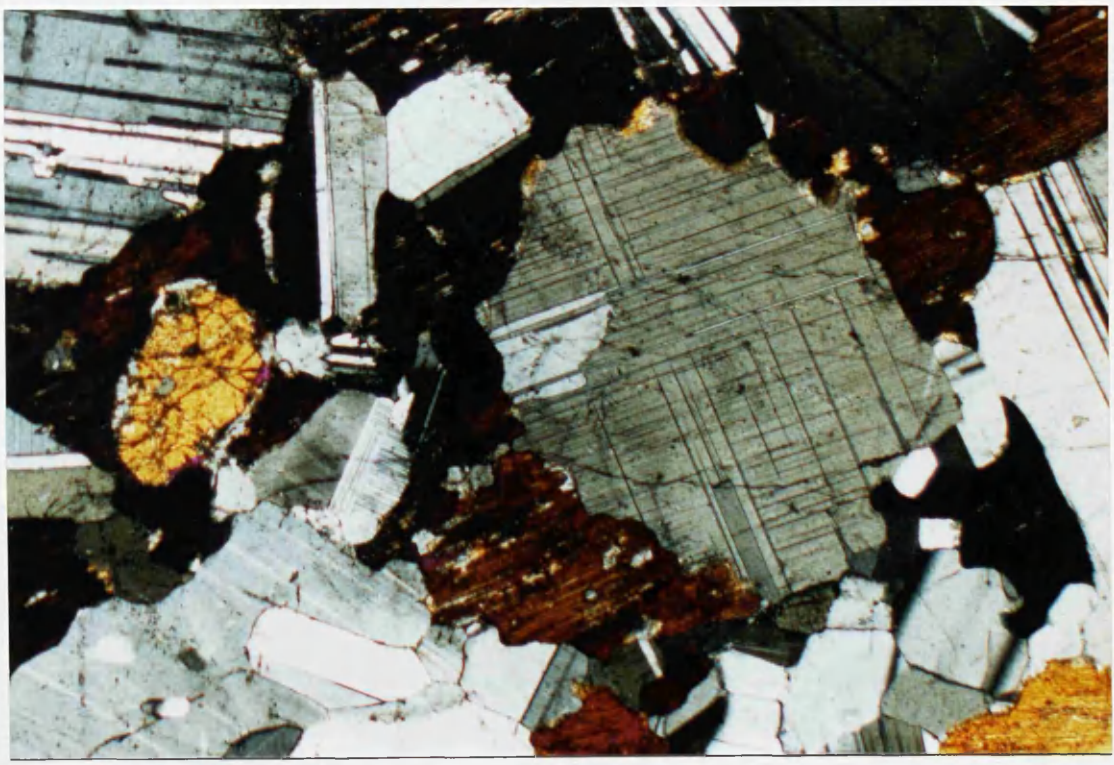

Fig.2.70. Corrosive contacts between feldspar and clinopyroxene, displaying blebby exsolution of orthopyroxene and sub-calcic augite. Field of view c.3 x 2 mm. Crossed polars. Sample AG315.

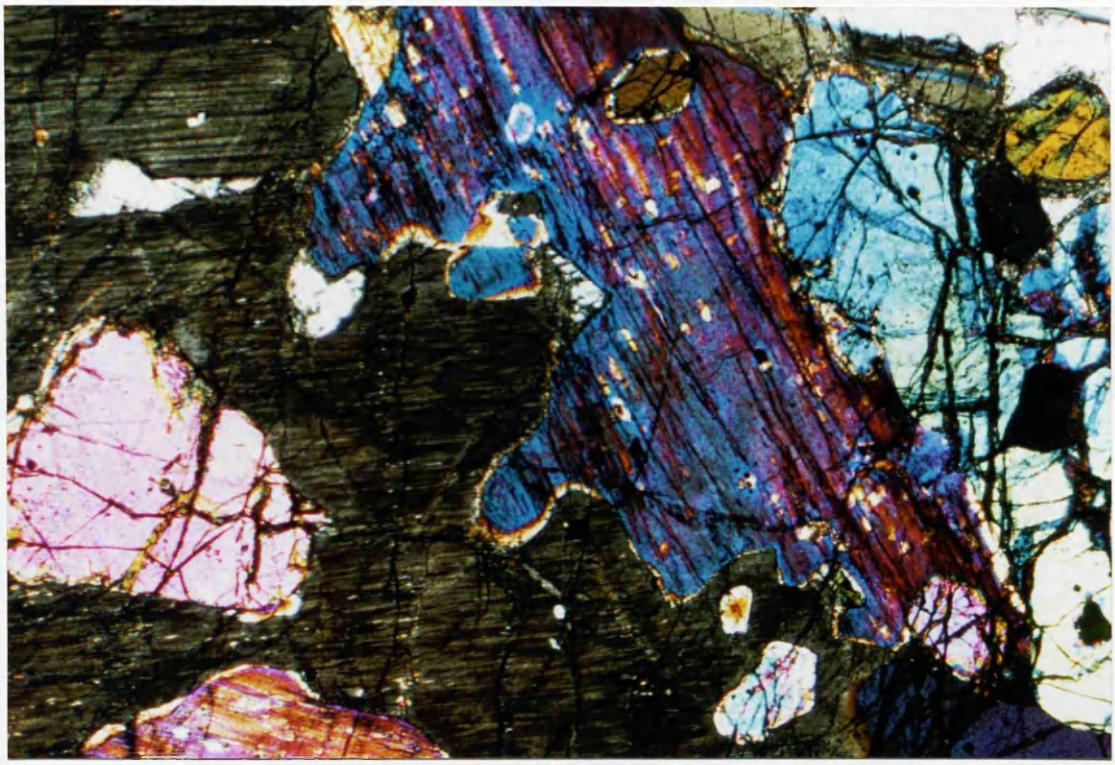

FIG.2.71. Angular fragments of feldspar and olivine within pyroxene aggregates of Zone 5. A thin intermittent rim of orthopyroxene is visible along the contact of the two pyroxenes occupying most of the field of view and around part of the angular olivine fragment (left). Field of view c.3 x 2 mm. Crossed polars. Sample AG316.

Sample	314/2	314/6	315/2	315/3	315/6	315/8	315/7	316/2	316/5	316/10	316/11
SiO_2	54.39	52.21	56.88	56.02	55.68	51.68	54.56	51.57	54.60	52.25	53.55
TiO_2	0.51	0.89	0.07	0.19	0.25	0.31	0.31	0.98	0.17	0.49	0.33
Al_2O_3	1.13	2.33	1.65	1.33	1.15	3.36	4.58	2.56	1.59	2.83	2.74
Cr_2O_3	0.05	0.15	-	0.14	0.09	1.11	0.13	0.18	0.25	0.74	0.50
MnO	0.31	0.15	0.18	0.29	0.32	0.21	0.29	0.18	0.25	0.19	0.21
MgO	27.72	15.78	22.50	29.01	30.22	15.74	22.16	16.42	29.96	20.54	25.64
CaO	1.51	22.08	11.06	1.65	0.98	20.97	10.98	21.47	2.10	15.39	25.64
Na_2O	0.02	0.26	0.22	0.04	0.02	0.41	0.70	0.42	0.09	0.33	0.17
FeO^*	13.72	6.17	5.29	11.86	11.76	6.23	5.51	5.55	10.59	7.04	9.95
Total	100.07	100.02	99.83	100.53	99.22	100.02	99.22	99.87	100.08	100.03	100.87

Atomic % (Mn included with Fe)

Ca	2.51	45.64	23.73	3.18	1.87	43.76	24.57	44.02	4.02	31.01	14.72
Mg	76.47	44.83	67.13	78.38	80.13	45.72	65.98	46.82	79.74	57.59	69.79
Fe	21.02	10.08	9.14	18.44	18.00	10.52	9.45	9.16	16.24	11.40	15.49

Formula (on the basis of 6 oxygens)

Si	1.956	1.924	2.044	1.977	1.964	1.904	1.956	1.905	1.934	1.905	1.913
Ti	.014	.025	.002	.005	.007	.009	.008	.027	.005	.013	.009
Al	.048	.101	.070	.055	.048	.146	.197	.112	.071	.121	.115
Cr	.001	.004	-	.004	.003	.036	.004	.014	.019	.021	.014
Mn	.009	.005	.005	.009	.010	.007	.009	.006	.007	.006	.006
Mg	1.486	.867	1.205	1.526	1.589	.865	1.152	.850	1.572	1.116	1.365
Ca	.058	.872	.426	.062	.037	.828	.429	.850	.088	.601	.288
Na	.001	.018	.015	.003	.001	.029	.049	.030	.006	.023	.012
Fe	.432	.190	.159	.350	.347	.192	.156	.171	.316	.215	.297
	4.005	4.006	4.006	3.991	4.006	4.016	3.960	3.955	4.018	4.021	4.019

Table 2.21 Representative analyses of pyroxenes from an area within Zone 5 displaying coarse pyroxene aggregates. Total iron was determined as FeO^*.

The compositions, as determined by electron probe microanalyser (Table 2.21) of some of the rims occurring around the olivines fall between the Ca-rich and Ca-poor categories (Fig.2.72) and it is suggested that these are not in equilibrium with the present assemblage. It is tentatively suggested that these are the transient expression of the assimilation and conversion of olivine to clinopyroxene. This process however would require the addition of Ca which may have been supplied from the feldspars as evidenced by their corroded contacts adjacent to the pyroxene. That the occurrence of the aggregates almost invariably occurs within xenoliths or rocks adjacent to the peridotite, it is proposed that the aggregates are the result of attempted re-equilibration initiated by the reheating of intercumulus material within xenoliths foundering into the peridotite magma or by the juxtoposition of magma and suitable protoliths.

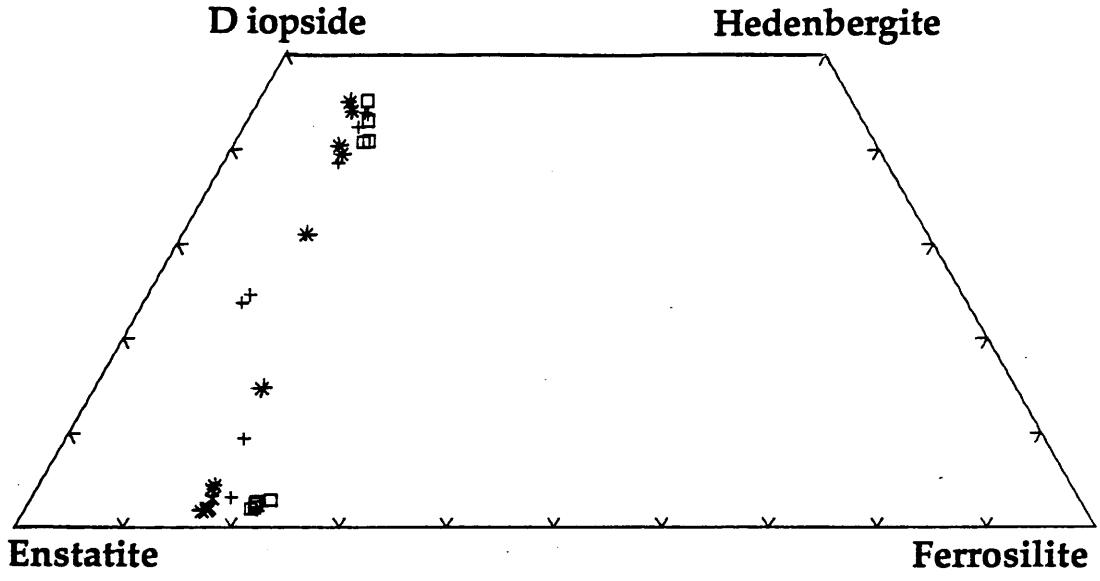

Fig.2.72. Pyroxenes from, and around the area of the pyroxene aggregates. (▫) = samples from within the Allivalite (AG314). (+) = samples from near the contact of the peridotite with the allivalite (AG315). (*) = samples from xenoliths within the peridotite (AG316). See text for explanation.

2.4 Discussion and Synthesis

As alluded to in Section 2.3.1, although the Peridotite Series shows a general mineralogical trend, albeit erratically, of becoming more feldspathic with stratigraphic height, in detail the disposition of the variable lithologies is complex. It is believed that this trend is not due to to the simple evolutionary processes of in-situ differentiation/fractionation. Their disposition and the apparent interaction of the magmas which gave rise to their present distribution allow a speculative integrated history of emplacement-crystallization to be proposed. Paramount within this discussion is the importance of post cumulus processes.

The earliest visible history of the peridotite begins with the formation of Zone 1 dunites, whose basal olivine compositions are Fo_{94} and which become slightly less forsteritic (Fo_{88}) with increasing stratigraphic height. Accompanying the olivine as the earliest phase to crystallize from the parent magma are spinels which may be found either within intercumulus feldspar or as inclusions within cumulus olivine. During cessation of olivine crystallization spinels were concentrated into thin seams, whose sharp lower contacts and gradational upper contacts with surrounding dunite suggest probable gravity settling.

The sub-vertical orientation of the whispy bands of Zone 2 preclude gravity settling as a viable mechanism to account for their disposition if it is accepted that they have undergone little or no post crystallization faulting/tilting, for which there is no evidence. Consequently, their orientation parallel to the southern margin of the peridotite mass suggests some form of in-situ crystallization in the manner proposed by McBirney & Noyes (1979), whereby crystallization proceeds as an advancing front parallel to the cooling surface, the southern margin, which at the time of emplacement of the peridotite was coherent. The presence of the pyroxene aggregates adjacent to the peridotite suggests, however, that the margin may not have been completely solid, or at least, was still at a sufficiently high enough temperature to be significantly affected by the heat from the peridotite. The role of a fluid phase cannot be dismissed, particularly as this would aid diffusion and recrystallization. The minor amounts of biotite, the granulation and conversion of olivine to orthopyroxene accompanied by free quartz may testify to a limited role played by a free fluid phase at or soon after emplacement.

Unlike Zone 2, Zone 3 appears to be conformable upon Zone 1 and the forsteritic content of olivines within the zone continue decreasing from c.Fo_{90}, as detected at the top of Zone 1 to c.Fo_{88} at the top of Zone 3.

The most notable fabric of Zone 3 rocks is the subhorizontal to shallowly dipping planar veinlets of intercumulus feldspar (Fig.2.29). The orientation of this fabric is oblique to the rare laterally restricted spinel seams of the zone (Fig.2.29). Furthermore, it can be shown from cross-cutting relationships (Fig.2.29) that the formation of the feldspar veinlets post dates that of the spinel seams. Consequently, dismissing the possibility of tilting of the cumulate pile having occurred between their formation , the feldspar veinlets and/or the spinel seams must have formed oblique to the horizontal. The orientation of the spinel seams is approximately coincident with that observed for the persistent seams of Zone 1 (Section 2.3.5.1) and therefore accepting these as having formed with their present attitude it seems possible that a similar original attitude of the seams of Zone 3 is preserved. It then follows that the feldspar veinlets owe their origin to the expulsion of trapped intercumulus melt due to compaction of the cumulate pile by the overlying weight of of cumulus minerals.

During the terminal stages of the formation of Zone 1 and throughout the formation of Zone 3, a significant proportion of the peridotite, as preserved, underwent intense brecciation. From the present day distribution it is deduced that the brecciation (i.e. Zone 4 rocks) was confined to a saucer-shaped volume coincident with the lower part of the corrie and rapidly diminished in intensity both laterally and with stratigraphic height. As proposed in Section 2.3.3.4, it is believed that the brecciation may be sub-divided into two types, that caused by the foundering of ultrabasic blocks into the body of the magma and that which owes its origin to the expulsion of intercumulus melt from a cumulate pile of high porosity. Whether the latter process was initiated by loading of the cumulates by unusually rapid crystallization and settling of olivine/spinel or as a direct result of the load imposed by the foundering ultrabasic blocks is not clear. The source of the blocks is uncertain and most ultrabasic lithologies which predate the peridotite have been tentatively identified, however, all contacts of the peridotite with these older rocks are generally planar, at least over a few tens of centimeters or so, and no evidence of stopping has been observed. The presence of the

large pyroxene aggregates and the coincidence of any fabric within the blocks with that of enclosing peridotite again suggests that the initial source of the xenoliths may have been plastic at the time of formation of the breccia and that brecciation may have been initiated by turbulent mixing of a feldspathic magma with the peridotite magma. Alternatively, the rock step area, at approximately mid height within the corrie may have some significance, as brecciation, which is intense below it, ceases at this locality and it may therefore represent a palaeo scarp within the magma chamber.

Following cessation of the brecciation event(s), rocks of Zones 5 and 6 were formed. Initially, crystallization appears to have occurred in a quiescent environment, as evidenced by the preservation of phase layering and the lace structures which reflect the importance of a feldspathic melt higher within the sequence.

Prior to the complete crystallization of the peridotite magma, at least within the lower zones, the influx of the parental magma to the Outer Layered Eucrite Series caused further brecciation and locally incorporated peridotite blocks as xenoliths.

References

REFERENCES

Agata, T. 1988 Chrome spinels from the Oura layered igneous complex, Central Japan.
Lithos v21 p97-108

Almond, D.C. 1960 The Tertiary igneous geology of Strathaird, Skye.
D. Phil. thesis Univ. Durham

Anderson, E.M. 1936 Dynamics of formation of cone-sheets, ring dykes and cauldron subsidence.
Proc. Royal Soc. Edinb. v61 p128-157

Arth, J.G., Gilbert, N. & Hanson, N. 1975 Geochemistry and origin of the early Pre-Cambrian crust of northwestern Minnesota.
Geochim. Cosmochim. Acta. v39 p325-362

Bailey, E.B. 1952 So-called amygdaloidal gabbro, Skye.
Geol. Mag. v89 p369-375

Bailey, E.B., Clough, C.T., Wright, W.B., Richey, J.E. & Wilson, G.V. 1924
Tertiary and post Tertiary geology of Mull, Loch Aline and Oban
Memm. Geol. Surv. Scotland

Barberi, F. 1971 Nature of the clinopyroxene and iron enrichment in alkalic and transitional basaltic magmas.
Cont. Min. & Pet. v33 p93-107

Basalt Volcanism study project. 1981 Basalt volcanism on the terrestrial planets.
Pergamon Press. New York.

Bedard, J.H., Sparks, R.S.J., Renner, R., Cheadle, M.J. & Hallworth, M.A. 1988
Peridotite sills and metasomatic gabbros in the Eastern layered series of the Rhum complex.
Jour. Geol. Soc. Lond. v145 p207-224

Bell, B.R. & Harris, J.W. 1986 An excursion guide to the geology of the Isle of Skye.
Geol. Soc. Glasgow.

Bell, J.D. 1976 The Tertiary intrusive complex on the Isle of Skye.
Proc. Geol. Ass. v87 p247-271

Bhattacharji, S.& Smith, C.H. 1964 Flow differentiation.
Science, N.Y. v145 p150-153

Bowen, N.L. 1928 The Evolution of the Igneous Rocks.
Princetown Univ. Press, Princetown, N.J.

Brooks, C.K. 1976 The Fe_2O_3/FeO ratio of basalt analyses: An appeal for a standardized procedure.
Bull. Geol. Soc. Denmark. v25 p117-120

Brown, G.M. 1956 The layered ultrabasic rocks of Rhum, Inner Hebrides.
Phil. Trans. Royal Soc. Lond. A240 p1-53

Brown, G.M. 1982 The British Tertiary Province,Introduction to Pt. 7; An appraisal of the Igneous history.
In "Igneous Rocks of the British Isle" p345-350 Ed. Sutherland, D.S.

Brown, G.M. & Vincent, E.A. 1957 Pyroxenes from the early and middle stages of fractionation of the Skaergaard intrusion, East Greenland.
Min. Mag. v31 p511-543

Brown, G.M. & Vincent, E.A. 1963 Pyroxenes from the late stages of fractionation of the Skaergaard Intrusion, East Greenland.
Jour. Pet. v4 p175-197

Bryan, W.B., Thompson, G. & Michael, P.J. 1979 Compositional variation in a steady-state zoned magma chamber: Mid-Atlantic ridge at $36^{o}50'N$.
Tectonophysics v55 p63-85

Butcher, A.R., Young, I.M. & Faithfull. J.W. 1985 Finger structures in the Rhum complex.
Geol. Mag. v122 p491-502

Campbell, I.H., Roeder, P.L. & Dixon, J.M. 1978 Plagioclase buoyancy in basaltic liquid as determined with a centrifuge furnace.
Cont. Min. & Pet. v67 p369-377

Campbell, I.S.E., Turner, F.J. & Verhoogen, J. 1974 Igneous Petrology.
McGraw Hill, New York

Carr, J.M. 1952 An Investigation of the Sgurr na Stri-Druim Hain sector of the basic igneous complex of the Cuillin Hills, Isle of Skye.
D. Phil. thesis Univ. Oxford

Coish, R.A. & Taylor, L.A. 1979 The effects of cooling rate on texture and pyroxene chemistry in DSDP Leg 34 basalt: A microprobe study.
E.P.S.L. v42 p389-398

Coombes, D.S. 1963 Trends and affinities of basaltic magmas and pyroxenes as illustrated on the diopside-olivine-silica diagram.
Min. Soc. Amm. Sp. Paper 1 p227-250

Cox, K.G. 1980 A model for flood basalt vulcanism.
Jour. Pet. v21 p629-650

Cox, K.G. 1988 Numerical modelling of a randomized RTF magma chamber: A comparison with continental flood basalt sequences.
Jour. Pet. v29 p681-697

Cox, K.G., Bell, J.D. & Pankhurst, R.J. 1979 The interpretation of the Igneous rocks.
George, Allen & Unwin, London.

Cox, K.G. & Mitchell, C. 1988 Importance of crystal settling in the differentiation of Deccan Trap basaltic magmas.
Nature v333 p447-449

Dick, H.J.B. & Bullen, T. 1984 Chromian spinel as a petrogenetic indicator in abyssal and alpine-type peridotites and spatially associated lavas.
Cont. Min. & Pet. v86 p54-76

Dickin, A.P. & Exley, R.A. 1981 Isotopic and geochemical evidence for magma mixing in the petrogenesis of the Coire Uaigeich granophyre, Isle of Skye, North West Scotland.
Cont. Min. & Pet. v76 p98-108

Donaldson, C.H. 1975 Ultrabasic breccias in layered intrusions- The Rhum Complex.
Jour. Geol. v83 p33-45

Donaldson, C.H. 1977 Petrology of Anorthite-bearing gabbroic Anorthosite dykes in Northwest Skye.
Jour. Pet. v18 p595-620

Donaldson, C.H. 1982 Origin of the Rhum Harrisite by segregation of Intercumulus liquid.
Min. Mag. v45 p201-209

Donaldson, C.H., Drever, H.I. & Johnston, R. 1973 Crystallization of poikilo-spherulitic feldspar in a Rhum peridotite.
Nature Phys. Sci. v243 p69-70

Dungan, M.A. & Rhodes, J.M. 1978 Residual glasses and melt inclusions in basalts from DSDP legs 45 & 46: Evidence for magma mixing.
Cont. Min. & Pet. v67 p417-431

Esson, J., Dunham, A.C. & Thompson, R.N. 1975 Low alkali, high calcium olivine tholeiite lavas from the Isle of Skye, Scotland.
Jour. Pet. v16 p488-497

Evans, B.W. & Moore, J.G. 1968 Mineralogy as a function of depth in the pre-historic Makaopuhi tholeiitic lava lake, Hawaii.
Cont. Min. & Pet. v17 p85-115

Ferry, J.M. 1985 Hydrothermal alteration of Tertiary igneous rocks from the Isle of Skye, Northwest Scotland. 1. Gabbros.
Cont. Min. & Pet. v91 p264-282

Ferry, J.M., Mutti, L.J. & Zuccala, G.J. 1987 Contact metamorphism/hydrothermal alteration of Tertiary basalts from the Isle of Skye, Northwest Scotland.
Cont. Min. & Pet. v95 p166-181

Finger, L.W. 1972 The uncertainty in the calculated ferric iron content of a microprobe analysis.
Carnegie inst. Wash. Year bk.71 p600-603

Fisk, M.R. & Bence, A.E. 1980 Experimental crystallization of chrome spinel in FAMOUS basalt 527-1-1.
E.P.S.L. v48 p111-123

Forbes, J.D. 1845 Notes on the topography and geology of the Cuchullin Hills in Skye, and on the traces of ancient glaciers which they present.
Edinb. New Phil. Jour. v40 p76-99

Forester, R.W. & Taylor, H.P. Jr. 1977 $^{18}O/^{16}O$, D/H & $^{13}C/^{12}C$ studies of the Tertiary Igneous Complex of Skye, Scotland.
Amer. Jour. Sci. v277 p136-177

Francis, D. 1986 The pyroxene paradox in MORB glasses - a signature of picritic parental magmas?.
Nature v319 p586-589

Geikie, A. 1888 The history of volcanic history during the Tertiary period in the British Isles.
Trans. Royal Soc. Edinb. v35 p21-184

Geikie, A. 1897 The ancient volcanoes of Great Britain. Vol 2.
Macmillan, London.

Geikie, A. & Teall, J.J.H. 1894 On the banded structure of some Tertiary gabbros in the Isle of Skye.
Quart. Jour. Geol. Soc. Lond. v1 p212-229

Gibb, F.G.F. 1968 Flow differentiation in the xenolithic ultrabasic dykes of the Cuillins and the Straithaird peninsula. Isle of Skye, Scotland.
Jour. Pet. v9 p411-443

Gibb, F.G.F. 1973 The zoned clinopyroxenes of the Shiant Isles sill, Scotland.
Jour. Pet. v14 p203-230

Gibb, F.G.F. 1976 Ultrabasic rocks of Rhum and Skye: The nature of the parent magma.
Jour. Geol. Soc. Lond. v132 p209-222

Green, D.H. & Ringwood, A.E. 1967 The genesis of basalt magmas.
Cont. Min.& Pet. v15 p103-190

Greenwood, R.C., Donaldson, C.H. & Emeleus, C.H. 1990 The contact zone of the Rhum ultrabasic intrusion: Evidence of peridotite formation from magnesian magmas.
Jour. Geol. Soc. Lond. v147 p209-212

Gribble, C.D. 1974 The dolerites of Ardnamurchan.
Scott. Jour. Geol. v10 p203-230

Haggerty, S.E. 1976 Ch. 8 Opaque minerals oxides in terrestrial igneous rocks.
Oxide Minerals: Min. Soc. Amm. Short course notes.

Hamlyn, P.R. & Keays, R.R. 1979 Origin of chromite compositional variation in the Panton sill, Western Australia.
Cont. Min. & Pet. v69 p75-82

Harker, A. 1904 The Tertiary Igneous rocks of Skye.
Memm. Geol. Surv.

Harker, A. 1908 The geology of the small Isles of Inverness-shire.
Mem. Geol. Surv. Scotland. 1-210

Harvey, P.K. 1989 Automated X-ray fluorescence in geochemical exploration.
In "X-ray fluorescence analysis in the geological sciences" Ed. Ahmedali.
Geol. Ass. Canada. Short Course Vol 7.

Henderson, P. 1975 Reaction trends shown by chrome-spinels of the Rhum layered Intrusion.
Geochim. Cosmochim. Acta. v39 p1035-1044

Henderson, P. & Gijbels, R. 1976 Trace element indicators of the genesis of of the Rhum layered Intrusion. Inner Hebrides.
Scott. Jour. geol. v12 p325-333

Henderson, P & Suddaby, P. 1971 The nature and origin of the chrome-spinel of the Rhum layered Intrusion.
Cont. Min. & Pet. v33 p21-31

Henderson, P & Wood, R.J. 1981 Reaction relationships of chrome-spinels in igneous rocks - Further evidence from the layered intrusions of Rhum and Mull, Inner Hebrides, Scotland.
Cont. Min. & Pet. v78 p225-229

Hess, H.H. 1938 Primary banding in Norite and Gabbro.
Trans. Amer. G eophys. Union. Pt1 p264-267

Hess, H.H 1939 Extreme fractional crystallization of a basaltic magma. The Stillwater Igneous Complex.
Trans. Amer. Geophys. Union. Pt3 p431-432

Hess, H.H. 1949 Chemical composition and optical properties of common clinopyroxenes.
Pt. 1 Amm. Min. v34 p621-666

Hill, R. & Roeder, P. 1974 The crystallization of spinel from basaltic liquid as a function of oxygen fugacity.
Jour. Geol. v82 p709-729

Holland, J.G. & Brown, G.M. 1972 Hebridean tholeiitic magmas: A geochemical study of the Ardnamurchan cone-sheets.
Cont. Min. & Pet. v37 p139-160

Humphries, S.E. 1984 The mobilty of the rare earth elements in the crust
Chapter 9 p317-342 in "Rare earth element geochemistry" Ed. Henderson, P.

Humphries, S.E., Morrison, M.A. & Thompson, R.N. 1978 Influence of rock crystallization history upon subsequent lanthanide mobility during hydrothermal alteration of basalt.
Chem. Geol. v23 p125-137

Huppert, H.E. & Sparks, R.S.J. 1980 The fluid dynamics of a basaltic magma chamber replenished by influx of hot, dense ultrabasic magma.
Cont. Min. & Pet. v75 p279-289

Hutchison, R. 1964 The Tertiary basic Igneous rocks of the Western Cuillins, Isle of Skye.
D. Phil. thesis Univ. Glasgow.

Hutchison, R. 1966 Intrusive tholeiites of the Western Cuillins , Isle of Skye.
Geol. Mag. v103 p352-363

Hutchison, R. 1968 Origin of the White Allivalite, Western Cuillin-Isle of Skye.
Geol. Mag. v105 p338-347

Hutchison, R. & Bevan, J.C. 1977 The Cuillin layered Igneous complex-evidence for multiple intrusion and former presence of a picritic liquid.
Scott. Jour. Geol. v13 p197-210

Irvine, T.N. 1967 Chromian spinel as a petrographic indicator. Pt. 2 Petrologic applications.
Can. Jour. Earth Sci. v4 p71-103

Kennedy, W.Q. 1930 The parent magma of the British Tertiary Province.
Summ. Prog. Pt.2 Memm. Geol. Surv.

Kennedy, W.Q. 1933 Trends of differentiation in basic magmas.
Amm. Jour. Sci. v25 p239-256

King, P. 1977 The secondary minerals of the Tertiary lavas of northern and central Skye - zeolite zonation patterns, their origin and formation.
D. Phil. thesis Univ. Aberdeen

Kitchen, D.E. 1985 The parental magma on Rhum: Evidence from alkaline segregations and veins in the peridotites from Salisbury's dam.
Geol. Mag. v122 p529-537

Langmuir, C.H., Bender, J.F., Bence, A.E., Hanson, G.N. & Taylor, S.R. 1977 Petrogenesis of basalts from the FAMOUS area; Mid Atlantic ridge.
E.P.S.L. v36 p133-156

Le Bas, M.J. 1962 The role of aluminium in igneous clinopyroxenes with relation to their parentage.
Amm. Jour. Sci. v260 p267-288

Luddon, J.N. & Thompson, G. 1979 An evaluation of the behaviour of rare earth elements during weathering of sea floor basalts.
Nature v274 p147-149

Macculloch, J. 1819 A description of the western Islands of Scotland.
London.

Macdonald, G.A. & Katsura, T. 1964 Chemical composition of Hawaiian lavas.
Jour. Pet. v5 p82-133

Mattey, D.P. 1980 The petrology of high calcium low-alkali tholeiitic dykes from the Isle of Skye regional swarm.
Univ. London Ph.D. thesis.

Mattey, D.P., Gibson, I.L., Mariner, G.F. & Thompson, R.N. 1977 The diagnostic geochemistry, relative abundance and spatial distribution of high calcium, low alkali olivine tholeiite dykes in the lower Tertiary regional swarm of the Isle of Skye, northwest Scotland.
Min. Mag. v41 p273-285

McBirney, A.R. 1984 Igneous Petrology
Freeman, Cooper & Co.

McBirney, A.R. & Noyes, R.M. 1979 Crystallization and layering of the Skaergaard intrusion.
Jour. Pet. v20 p487-554

Menzies, M., Seyfied, W. & Blanchard, D. 1979 Experimental evidence of rare earth immobility in greenstones.
Nature v282 p398-399

Moorbath, S. & Thompson, R.N. 1980 Strontium isotope geochemistry and petrogenesis of the early Tertiary lava pile of the island of Skye, Scotland, and other basic rocks of the British Tertiary province: An example of magma-crust interaction.
Jour. Pet. v21 p295-321

Morse, S.A. 1986 A magmatic heat pump
Nature v324 p658-660

Morse, S.A., Owens, B.E. & Butcher, A.R. 1987 Origin of Finger structures in the Rhum complex: Phase equilibrium and heat effects.
Geol. Mag. v124 p205-210

Muan, A. 1957 Phase equilibrium relationships at liquidus temperatures in the system $FeO-Fe_2O_3-Al_2O_3-SiO_2$
Jour. Amm. Ceram. Soc. v40 p420-431

Nakamura, N. 1974 Determination of REE, Ba, Fe, Mg, Na and K in carbonaceous and ordinary chondrites.
Geochim. Cosmochim Acta. v38 p757-775

Nesbitt, H.W. 1979 Mobility and fractionation of rare earth elements during weathering of a granodiorite.
Nature v279 p206-210

O'Hara, M.J. 1965 Primary magmas and the origin of basalts.
Scott. Jour. Geol. v1 p19-140

O'Hara, M.J. 1977 Geochemical evolution during fractional crystalization of a periodically refilled magma chamber.
Nature v266 p503-507

OHara, M.J. 1980 Non-linear nature of the unavoidable long-lived isotopic, trace and major element contamination of a developing magma chamber.
Phil. Trans. Royal Soc. Lond. A297 p215-227

O'Hara, M.J. & Mathews, R.E. 1981 Geochemical evolution in an advancing, periodically replenished, periodically tapped, continuously fractionated magma chamber.
Jour. Geol. Soc. Lond. v138 p237-277

Osborn, E.F. & Tait, D.B. 1952 The system diopside-forsterite-anorthite.,
Amm. Jour. Sci. Bowen volume p413-433

Pearce, J.A. & Cann, J.R. 1973 Tectonic setting of basic volcanic rocks determined using trace element analysis.
E.P.S.L. v19 p290-300

Phillips, W.J. 1974 The dynamic emplacement of cone-sheets.
Tectonophysics v24 p69-84

Poldervaart, A. & Hess, H.H 1951 Pyroxenes in the crystallization of basaltic magma.
Jour. Geol. V59 p472-489

Rhodes, J.M., Dungan, M.A., Blanchard, D.P. & Long, P.E. 1979 Magma mixing at mid ocean ridges: Evidence from basalt drilled near 22°N. on the Mid-Atlantic ridge.
Tectonophysics v55 p35-61

Ridley, W.I. 1973 The petrology of volcanic rocks from the small Isles of Invernessshire.
Rep. Inst. Geol. Sci. No 73/10

Roeder, P.L., Campbell, I.H. & Jamieson, H.E. 1979 A re-evaluation of the olivine-spinel geothermometer.
Cont. Min. Pet. v68 p325-334

Roeder, P.L. & Emslie, R.F. 1970 Olivine-liquid equilibrium.
Cont. Min. Pet. v29 p275-289

Sparks, R.S.J., Huppert, H.E. & Turner, J.S. 1984 The fluid dynamics of evolving magma chambers.
Phil. Trans. Royal Soc. Lond. A310 p511-534

Sparks, R.S.J. Meyer, P. & Sigurdsson, H. 1980 Density variation amonst MORB: I mplications for magma mixing and the scarcity of primary Lavas.
E.P.S.L. v46 p419-430

Starkey, T.V. 1962 Principles governing the viscous flow of suspensoids.
Brit. Jour. Appl. Physics v13 p182

Stewart, F.H. & Wager, L.R. 1947 Gravity stratification in the Cuillin gabbro of Skye.
Geol. Mag. v84 p374

Taylor, H.R. Jr. & Forester, R.W. . 1971 Low O^{18} igneous rocks from the intrusive complexes of Skye, Mull and Ardnamurchan, western Scotland.
Jour. Pet. v12 p465-497

Thompson, R.N. 1974 Primary basalts and magma genesis, Isle of Skye, North-west Scotland.
Cont. Min. Pet. v45 p317-341

Thompson, R.N., Esson, J. & Dunham, A.C. 1972 Major element chemical variation in the Eocene lavas of the Isle of Skye, Scotland.
Jour. Pet. v13 p219-253

Thompson, R.N., Gibson, I.L., Marriner, G.F., Mattey, D.P. & Morrison, A.M. 1980 Trace-element evidence of multistage mantle fusion and polybaric fractional crystalization in the palaeocene lavas of Skye, NW Scotland.
Jour. Pet. v21 p265-293

Thornber, C.R., Roeder, P.L. & Forester, J.R. 1980 The effect of composition on the ferric-ferrous ratio in basaltic liquids at atmospheric pressure.
Geochim. Cosmochim. Acta. v44 p525-532

Tilley, C.E. 1950 Some aspects of magmatic evolution.
Quart. Jour. Geol. Soc. Lond. v106 p37-61

Tilley, C.E. & Muir, I.D. 1962 The Hebridean Plateau Magma-Type.
Trans. Geol. Soc. Edinb. v19 p208-215

Ulmer, G.C. 1969 Experimental investigations of chromite spinels.
Econ. Geol. Mon. v4 p114-131

Von Oeynhausen, C. & Von Dechen, H. 1829 Die Insel Skye.
Karstens Archiv fur Min. v1 p56-104

Wadsworth, W.J. 1961 The layered ultrabasic rocks of SW Rhum.
Phil. Trans. Royal Soc. B244 p21-64

Wadsworth, W.J. 1982 The major basic Intrusions p415-425 Pt 7
In "Igneous rocks of the British Isles" Ed. Sutherland, D.S.

Wager, L.R. & Brown, G.M. 1968 Layered Igneous rocks.
Oliver & Boyd. Edinbugh

Wager, L.R., Brown, G.M. & Wadsworth, W.J. 1960 Types of Igneous cumulates.
Jour. Pet. v1 p73-85

Wager, L.R. & Deer, W. 1939 The petrology of the Skaergaard intrusion, Kangerdlugssuag, East Greenland.
Medd. om Gronland v105 p1-352

Wager, L.R., Vincent, W.A., Brown, G.M. & Bell, J.D. 1965 Marscoite and related rocks from the Western Red Hills complex, Isle of Skye.
Phil. Trans. Royal Soc. Lond. A257 p273-307

Walker, G.P.L. 1975 A new concept of the evolution of the British Tertiary intrusive centres.
Jour. Geol. Soc. Lond. v131 p131-141

Walker, D., Shibata, T. & Delong, S.E. 1979 Abysal Tholeiites from the Oceanogrpher Fracture zone, ii. Phase equilibria and mixing.
Cont. Min. Pet. v70 p111-125

Washington, H.S. 1922 Deccan traps and other plateau basalts.
Bull. Geol. Soc. Amm. v33 p765-804

Weedon, D.S. 1956 Studies concerning the Tertiary Igneous rocks of the southern Cuillins, Isle of Skye.
D. Phil. thesis Univ. Oxford

Weedon, D.S. 1961 Basic Igneous rocks of the Southern Cuillin, Isle of Skye.
Trans. Geol. Soc. Glas. v24 p190-212

Weedon, D.S. 1965 The layered ultrabasic rocks of Sgurr Dubh, Isle of Skye.
Scott. Jour. Geol. v1 p41-68

Whipple, E.R. 1974 A study of Wilson's determination of ferrous iron in silicates.
Chem. Geol. v14 p223-238

Wood, B.J. & Fraser, D.G. 1977 Elementary thermodynamics for geologists.
Oxford Uni. Press.

Wood, D.A. 1979 Dynamic partial melting: its application to the petrogenesis of basalts erupted in Iceland, the Isle of Skye (Scotland) and the Troodos Massif (Cyprus).
Geochim. Cosmochim. Acta. v43 p1031-1046

Wright, T.L. & Docherty, P.C. 1970 A linear programming and least squares computer method for solving petrologic mixing problems.
Geol. Soc. Amm. Bull. v81 p1995-2008

Wright, T.L. & Docherty, P.C. 1974 Presentation and interpretation of chemical data for Igneous rocks.
Cont. Min. Pet. v48 p233-248

Wyllie, P.J. 1979 Petrogenesis and the physics of the earth.
In "The Evolution of the Igneous Rocks: Fiftieth anniversary perspectives" p483-520
Princetown: Princetown Uni. press

Yoder, H.S. & Tilley, C.E. 1962 Origin of basalt magmas: An experimental study of natural and synthetic rock systems.
Jour. Pet. v3 p342-532

Zinovieff, P. 1958 The basic layered intrusion and the associated igneous rocks of the central and eastern Cuillin hills, Isle of Skye.
D. Phil. thesis Univ. Oxford

Appendices

App. I Determination of ferrous iron.

App. II Preparation of samples for ICP analysis.

App. III Equations governing the behaviour of trace elements during crystallization and melting.

App. IV Whole rock major and trace element analytical results.

App. V Whole rock rare earth element analytical reults.

App. VI Mineral chemistry.

Appendix I

Determination of Ferrous Iron

The method to determine the ferrous iron content of the cone-sheets is essentially that reported by Whipple (1974).

Reagents

Metavanadate 0.05N
Ferrous Ammonium Sulphate 0.55N
Acid mixture; 40ml. sulphuric and 40ml. phosforic acid
Boric acid solution 5%
Standard Potassium dichromate solution 0.05N
Barium diphenylamine sulphanate indicator 0.04%
Hydrofluoric acid 40%

Method

10ml. of metavanadate was pipetted into 125ml. plastic bottles to which was added 0.2000 g+/- 0.0002g of powdered (<200 mesh) sample with two bottles run as blanks. To each sample was added 8 +/- 1ml. of conc. hydrofluoric acid and then left to stand for 48 hours. 60ml. of the Boric acid solution was then added and the solutions left to stand overnight to facilitate dissolution of any precipertate. The contents of the bottles were then transferred to a series of clean 600ml. beakers, the bottles being rinsed out with a further 120ml. of the boric acid which was then added to the beakers. 10ml. of ferrous ammonium sulphate was pipetted into each beaker just prior to titration and well stirred. 2ml. of the indicator barium diphenylamine sulphanate was added and then the solutions were titrated with standard potassium dichromate using a micro burette. When the violet colour of the indicator which was produced by the addition of titrant only just dissapeared, 5ml. of the acid mixture was added to the solution. The solution was then stirred well and the titration continued slowly until the grey-green colour just turned violet, the final end point.

The % of FeO in the samples is then given by the equation;

$$FeO = \frac{\text{ml. } K_2Cr_2O_7 \text{ (sample)} - \text{ml. } K_2Cr_2O_7 \text{ (blank)} \times N\ (K_2Cr_2O_7) \times 7.185}{\text{sample weight in grams}}$$

However, Whipple (1974) suggests the following correction factors depending on the length of time the samples stand in the hydrofluoric acid;

For samples standing for 2 days multiply by 1.004

For samples standing for 7 days multiply by 1.006

Results

Sample No.	Total iron as $Fe_2O_3^*$	Wt. % FeO	Fe_2O_3/FeO
CS036	11.07	9.69	0.14
CS044	8.76	7.43	0.18
CS019	12.33	9.38	0.31
CS048	11.85	8.69	0.36
CS022	11.42	9.12	0.25
CS041	13.41	9.69	0.38
CS021	13.07	9.91	0.32
CS017	12.99	10.23	0.26
CS040	14.19	10.41	0.36
CS032	14.41	11.20	0.28
CS006	6.26	3.51	0.78

$Fe_2O_3^*$ as determined by XRF analysis.

Appendix II

Preparation of samples prior to induction coupled plasma spectrometry analysis (ICPS)

0.5g of sample powder were weighed into PTFE beakers to which were added 4mls. of $HClO_4$ and 15mls. of HF acid. This was evaporated to dryness and when cool, 5mls. of concentrated HCl was added and the crucible half filled with distilled warm water. The soloution was then filtered (no. 42 filter paper), rinsing with distilled water, and the filtrate collected in a 100ml. beaker. The filter paper was ignited in a platinum crucible, placed in a furnace at 800 C for 30 minutes. When cool 1.5g. of lithium metaborate was mixed with the residue. The mixture was then ignited at 1000^{o} C in a furnace. When cool the cake was digested with c. 5mls. of distilled water and 3ml. of concentrated HCl, warming carefully. The solution was then added to to the filtrate which was then made up to c.100mls. with distilled water.

Ion exchange columns were prepared by shaking 40g. of Bio-rad AG-50W-X8 resin (H^{+} form, 200-400 mesh) with 50 mls. of water and pouring the slurry into the column. After compaction this gave a resin height of c.10cm. When the resin had settled the acidity of the column was adjusted by passing 250mls. of 1.00 N HCl through the column, taking care to ensure that the resin was always covered by c. 5cm. of liquid.

The solutions were then loaded into the columns and after passing through, the columns were eluted with 500mls. of 1.75N HCl. This portion was then discarded. The REE were then eluted with 600mls. of 4.00N HCl, collecting the elutrant through a no.42 filter paper. This portion was then evaporated down to c. 15mls. when 10mls. of concentrated HNO_3 were added, transferred to a 50ml. beaker and then evaporated to dryness. When dry, the beaker was allowed to cool prior to covering with plastic film. Immeadiately prior to analysis, the evaporated salts were dissolved in 5.00mls. of 2N HNO_3. With each group of 9 samples, a blank, a standard and a duplicate were run.

Notes

It is important to ensure that the PTFE beakers and all glassware used is scrupulously clean. This is achieved by soaking all apparatus in a 2% solution of Decon overnight. Apparatus is then rised and left filled with de-ionised water overnight.

Appendix III

Equations governing the behaviour of trace elements during crystallization and melting

1) The distribution coefficient (K) for an element X between silicate melt and crystal species Z is given by the equation;

$$K_d = \frac{\text{concentration of X in species Z}}{\text{concentration of X in melt}}$$

2) For a multiphse assemblage, the bulk distribution coefficient (D) is given by the equation;

$$D = \sum_{i=1}^{N} (M \, x.K_{di})$$

Where N = The number of solid phases
M = The mass fraction of phase i
K_d = The distribution coefficient of the element between the ith solid phase and the liquid

3) A general equation for equillibrium melting and crystallization (Wood and Fraser 1977) is given by;

$$\frac{C_l}{C_o} = \frac{1}{F+D-FD}$$

Where C_l = The concentration of the trace element in the liquid
C_o = The concentration of the trace element in the initial source
F = The mass fraction of liquid
D = The bulk distribution coefficient of the trace element concerned

4) For perfect fractional partial melting the concentration of the trace element in the melt is given by;

$$\frac{C_l}{C_o} = \frac{(1-F)^{(1/D-1)}}{D}$$

5) For incremental partial melting (Wood 1979) the average concentration of the trace element in the melt is given by

$$\frac{(C_l)_R}{C_o} = \frac{(C_s)_{R-1}/C_o}{1+D_R(1-l)}$$

Where R = The number of the melting increment
C_s = The concentration of the trace element in the residue
l = The mass fraction of the liquid generated in each melting increment
D = The bulk distribution coefficient for the Rth melting increment

6) An equation for dynamic melting (incremental melting modified to take into account an irremovable amount of liquid trapped within the source undergoing melting. Langmuir et al. 1977);

$$\frac{(C_l)_R}{C_o} = \frac{(C_s)_{R-1}/C_o}{(Q+l) + D_R(1-(Q+l)}$$

Where Q = The mass fraction of liquid remaining in the residue
C_s = The concentration of the trace element in the residue

7) Fractional crystallization (Cox et al. 1979);

$$\frac{C_l}{C_o} = F^{(D-1)}$$

Appendix IV

Whole Rock Analytical Results

Analyses determined by X.R.F spectrometry. Major element oxide analyses are reported in weight percent whilst trace element data is reorted in parts per million (ppm). For review of techniques and discussion on analytical precision see Harvey (1989).

Sample identifiers CS and IT refer to cone-sheets and intrusive tholeiite sheets respectively.

Explanation of terms appearing in the results tables.

FFM = FeO^*/FeO^*+MgO. Where $FeO^* = FeO+Fe_2O_3$

$Fe_2O_3^*$ = Total iron was determined as Fe_2O_3 and subsequently partitioned between ferrous and ferric iron to give $Fe_2O_3/FeO=0.15$ (Brooks 1976).

% Pheno. = Volume % phenocrysts present. Determined by point counting (n=2000).

A.I. = Alteration Index. = $\frac{\text{secondary minerals} \times 100}{\text{secondary minerals} + \text{primary minerals}}$

REE = Rare earth elements determined (Appendix V).

Min Chem. = Mineral chemistry determined (Appendix VI).

n.d. = Not determined

Alk = Na_2O+K_2O

Sample	CS001	CS002	CS003	CS006	CS007	CS008	CS009	CS010	CS011	CS012	CS013	CS014N
SiO_2	49.80	50.94	48.85	46.26	46.92	47.15	46.66	46.92	46.79	46.80	47.15	46.45
Al_2O_3	14.53	13.53	15.27	23.21	13.47	17.60	20.23	13.72	17.66	13.55	19.62	13.74
TiO_2	1.49	1.89	1.11	0.46	1.39	0.83	0.60	1.39	0.74	1.29	0.69	1.13
FeO	12.40	12.73	11.20	5.60	13.00	9.13	7.13	13.27	8.80	12.13	8.00	12.07
Fe_2O_3	1.86	1.91	1.68	0.84	1.95	1.37	1.07	1.99	1.32	1.82	1.20	1.81
MgO	5.93	5.29	6.63	4.77	7.30	7.12	6.02	7.39	6.93	7.73	6.13	8.24
CaO	9.40	9.62	12.17	15.34	12.09	12.84	14.27	11.51	13.92	11.76	14.28	12.51
Na_2O	2.49	2.17	1.88	1.60	2.22	1.75	1.79	2.54	1.80	2.20	1.59	1.69
K_2O	1.43	0.77	0.58	0.17	0.16	0.38	0.10	0.11	0.17	0.40	0.15	0.16
MnO	0.19	0.19	0.21	0.10	0.21	0.15	0.10	0.22	0.17	0.19	0.14	0.20
P_2O_5	0.27	0.18	0.09	0.05	0.12	0.05	0.04	0.10	0.04	0.10	0.05	0.07
H_2O^+	0.73	0.92	0.43	1.52	1.41	2.17	2.19	1.67	1.73	2.55	1.39	2.35
Total	100.49	100.13	100.10	99.91	100.22	100.53	100.20	100.30	100.07	100.53	100.38	100.42
FFM	.7063	.7346	.6602	.5745	.6719	.5959	.5767	.5935	.6435	.6001	.6275	.6315
$Fe_2O_3^*$	13.77	14.16	12.47	6.26	14.47	10.16	7.95	14.72	9.81	13.52	8.88	13.41
Alk	3.92	2.94	2.46	1.77	2.38	2.13	1.89	2.65	1.97	2.60	1.74	1.85
% Pheno	5	4	6	1	<1	16	<1	n.d	32	n.d	29	42
A.I.	88	81	76	1	10	4	3	n.d	8	14	18	17
R.E.E.	n.d	n.d	n.d	*	*	n.d	*	n.d	n.d	n.d	n.d	n.d
Min chem.	n.d	n.d	n.d	*	*	n.d	*	n.d	*	n.d	n.d	n.d

Trace Elements (ppm)

Ba	600	151	149	16	112	79	25	124	40	121	37	96
Cr	133	39	114	233	98	123	152	85	165	120	133	130
Cu	126	79	163	81	147	139	111	156	120	184	115	195
La	15	12	4	0	0	5	0	0	0	0	5	0
Ni	47	27	67	52	74	81	68	77	73	85	71	97
Nb	5	5	4	1	4	0	2	3	3	4	0	3
Pb	5	11	5	7	10	4	6	5	6	3	7	6
Rb	79	39	28	8	11	12	6	5	9	19	10	7
Sc	35	32	35	25	39	28	29	29	27	35	33	41
Sr	399	368	147	175	139	225	176	147	154	151	162	134
Th	6	1	0	1	3	0	0	1	0	2	0	2
U	1	0	0	0	2	0	2	0	0	0	0	0
V	288	373	270	103	316	202	141	310	182	278	167	276
Y	32	30	28	11	29	19	13	29	18	25	16	26
Zn	93	107	60	29	90	61	33	92	51	107	35	56
Zr	138	128	75	33	83	50	41	77	49	72	44	60
Y/Zr	.23	.23	.37	.33	.35	.38	.32	.38	.37	.35	.36	.43

Sample	CS014	CS015	CS016	CS017	CS018	CS019	CS020	CS021	CS022	CS023	CS024	CS025
SiO_2	46.31	46.86	47.34	47.37	46.89	47.13	48.01	46.16	46.85	47.91	47.03	46.94
Al_2O_3	14.30	13.92	13.71	13.72	13.35	13.74	13.22	13.58	14.42	12.16	13.77	13.88
TiO_2	1.09	0.95	1.06	1.03	1.59	0.99	1.13	1.21	0.90	2.24	0.98	1.01
FeO	11.67	11.00	11.40	11.67	14.47	11.07	12.27	11.73	10.27	16.13	11.00	11.27
Fe_2O_3	1.75	1.65	1.71	1.75	2.13	1.66	1.84	1.76	1.54	2.42	1.65	1.69
MgO	8.13	8.47	7.65	7.75	6.06	8.38	7.09	7.84	8.73	4.90	8.41	8.32
CaO	12.01	12.99	12.34	12.76	10.76	13.38	11.81	12.27	13.20	8.99	12.96	13.30
Na_2O	1.94	1.51	2.43	2.11	2.79	1.52	2.53	2.05	1.85	2.72	1.63	1.39
K_2O	0.31	0.32	0.18	0.05	0.27	0.19	0.36	0.07	0.12	0.53	0.35	0.19
MnO	0.18	0.19	0.21	0.19	0.24	0.20	0.21	0.19	0.17	0.26	0.19	0.20
P_2O_5	0.13	0.07	0.08	0.06	0.17	0.07	0.10	0.08	0.07	0.24	0.06	0.07
H_2O^+	2.71	2.22	2.25	1.96	1.57	2.18	1.93	3.07	2.05	1.91	2.06	2.13
Total	100.10	99.76	99.94	100.00	100.28	100.52	100.50	100.01	110.17	100.42	100.09	100.39
FFM	.6315	.5990	.6315	.6339	.7330	.6030	.6656	.6324	.5750	.7910	.6007	.6090
$Fe_2O_3^*$	12.99	12.26	12.69	12.99	16.07	12.33	13.66	13.07	11.42	17.96	12.25	12.53
Alk	2.25	1.83	2.61	2.16	3.06	1.71	2.89	2.12	1.97	3.25	1.98	1.58
% Pheno	4	<1	2	5	n.d	<1	n.d	n.d	1	4	3	n.d
A.I.	6	26	13	13	n.d	11	n.d	n.d	19	13	11	n.d
R.E.E.	n.d	*	*	n.d	n.d	*	n.d	n.d	*	*	*	n.d
Min chem.*		n.d	*	n.d	n.d	*	n.d	n.d	*	*	*	n.d
Trace Elements (ppm)												
Ba	92	91	107	78	61	90	118	86	70	142	85	90
Cr	124	221	115	100	127	179	75	138	350	41	184	186
Cu	177	163	144	156	149	184	171	140	137	110	173	169
La	0	0	5	8	0	0	0	0	6	0	0	0
Ni	106	101	74	74	60	105	63	81	130	35	98	101
Nb	3	2	3	2	6	2	3	3	2	6	2	2
Pb	7	5	5	5	10	6	7	3	6	6	5	4
Rb	14	10	6	5	12	9	13	7	8	18	10	9
Sc	30	35	33	33	34	36	39	34	37	29	32	39
Sr	165	126	136	153	140	125	144	128	131	146	150	118
Th	2	0	1	2	2	1	5	0	0	0	3	3
U	0	0	1	0	0	3	2	0	0	0	0	0
V	270	243	244	246	334	256	269	274	235	408	243	238
Y	24	23	24	21	34	21	26	25	21	52	23	21
Zn	57	72	74	59	94	66	74	74	59	95	71	62
Zr	53	55	67	58	94	59	74	66	57	151	57	57
Y/Zr	.45	.42	.36	.36	.36	.36	.35	.38	.37	.34	.40	.37

Sample	CS026	CS027	CS028	CS029	CS030	CS031	CS032	CS035	CS036	CS037	CS038	CS039
SiO_2	46.53	47.14	47.36	46.39	46.60	47.67	47.31	46.94	46.88	46.91	46.69	47.28
Al_2O_3	13.84	13.68	14.20	13.86	13.63	12.70	13.76	13.24	15.14	13.94	12.61	13.75
TiO_2	0.99	0.98	1.05	1.22	1.09	1.78	1.30	1.53	0.86	1.08	1.50	1.15
FeO	11.20	11.15	11.28	12.45	11.60	14.80	13.00	14.27	9.93	11.13	14.27	11.93
Fe_2O_3	1.68	1.67	1.69	1.87	1.74	2.22	1.95	2.14	1.49	1.67	2.14	1.79
MgO	8.56	8.29	8.12	7.62	8.12	6.04	6.96	6.34	8.59	8.46	6.51	7.88
CaO	13.22	13.18	12.99	12.33	12.05	10.37	11.89	10.80	13.70	12.91	11.32	12.82
Na_2O	1.55	1.80	1.77	1.99	2.17	2.80	2.20	2.47	1.25	1.54	2.38	1.71
K_2O	0.19	0.15	0.17	0.19	0.12	0.34	0.24	0.28	0.40	0.47	0.31	0.21
MnO	0.18	0.20	0.19	0.22	0.20	0.23	0.20	0.22	0.16	0.20	0.25	0.20
P_2O_5	0.07	0.07	0.07	0.10	0.07	0.16	0.08	0.11	0.05	0.07	0.11	0.07
H_2O^+	2.05	1.77	1.52	2.02	2.72	1.44	1.72	2.20	1.64	1.97	2.29	1.38
Total	100.06	100.06	100.39	100.25	100.11	100.55	100.61	100.53	100.11	100.35	100.37	100.16
FFM	.6007	.6069	.6148	.6530	.6216	.7381	.6823	.7213	.5707	.6021	.7160	.6352
$Fe_2O_3^*$	12.45	12.39	12.54	13.84	12.86	16.47	14.41	15.82	11.07	12.40	15.88	13.29
Alk	1.74	1.95	1.94	2.18	2.29	3.14	2.44	2.75	1.65	2.01	2.69	1.92
% Pheno	1	1	4	n.d	<1	8	n.d	25	n.d	<1	14	7
A.I.	9	8	11	n.d	39	10	n.d	21	n.d	19	10	23
REE	n.d	n.d	*	*	n.d	n.d	n.d	n.d	n.d	n.d	*	n.d
Min chem.*		n.d	*	n.d	n.d	n.d	n.d	*	*	n.d	*	n.d
Trace elements (ppm)												
Ba	75	75	94	78	72	84	133	61	85	90	142	103
Cr	196	189	253	73	160	57	136	75	287	301	72	218
Cu	166	156	144	169	165	163	170	186	167	143	183	178
La	0	0	5	0	0	4	0	0	0	0	0	0
Ni	100	100	103	87	96	44	69	53	114	122	58	91
Nb	3	4	3	3	2	5	3	3	3	3	3	2
Pb	4	6	6	6	4	8	7	6	6	6	2	5
Rb	9	9	10	8	10	13	11	13	20	18	11	9
Sc	35	36	33	31	34	32	36	39	36	34	37	35
Sr	121	125	133	131	145	150	141	139	116	129	128	138
Th	4	0	0	0	0	0	1	2	1	0	2	0
U	1	0	0	0	0	0	0	0	0	0	2	0
V	243	261	249	291	264	353	314	363	236	266	364	280
Y	23	22	22	26	23	41	25	32	21	24	29	25
Zn	64	70	67	83	72	85	73	96	48	71	89	63
Zr	58	58	63	69	62	113	69	78	51	61	79	61
Y/Zr	.40	.38	.35	.38	.37	.36	.36	.41	.41	.39	.37	.41

Sample	CS040	CS041	CS042	CS043	CS044	CS046	CS047	CS048	CS049	CS050	CS051	CS052
SiO_2	46.86	47.31	47.04	46.93	46.60	47.41	47.31	47.22	46.43	47.85	47.28	46.99
Al_2O_3	13.91	13.66	14.62	13.05	20.39	13.86	13.78	14.10	14.73	12.72	13.20	14.12
TiO_2	1.42	1.16	1.05	1.37	0.73	1.13	1.13	0.97	1.90	1.75	1.32	1.04
FeO	12.80	12.07	11.20	12.93	7.87	11.93	12.00	10.67	14.13	15.47	12.80	11.13
Fe_2O_3	1.92	1.81	1.68	1.94	1.18	1.79	1.80	1.60	2.12	2.32	1.92	1.67
MgO	6.95	7.81	7.30	7.17	5.38	7.78	7.90	8.39	4.25	6.00	7.24	8.19
CaO	11.63	12.72	12.66	11.90	13.95	12.82	12.56	13.36	10.71	10.98	11.68	12.96
Na_2O	2.22	1.79	2.24	2.02	2.01	1.54	1.99	1.84	2.77	2.23	2.56	2.02
K_2O	0.46	0.23	0.27	0.41	0.15	0.17	0.13	0.17	0.19	0.11	0.19	0.11
MnO	0.22	0.20	0.20	0.20	0.13	0.20	0.19	0.19	0.23	0.25	0.24	0.19
P_2O_5	0.13	0.07	0.07	0.10	0.05	0.08	0.09	0.06	0.19	0.14	0.09	0.10
H_2O^+	2.24	1.47	1.73	2.33	1.73	1.46	1.46	2.03	2.72	0.79	1.72	1.79
Total	100.77	100.31	100.05	100.36	100.15	100.16	100.34	100.60	100.78	100.61	100.25	100.32
FFM	.6793	.6399	.6383	.6747	.6272	.6381	.6359	.5939	.7927	.7478	.6703	.6098
$Fe_2O_3^*$	14.19	13.41	12.47	14.40	8.86	13.27	13.31	11.85	15.71	17.16	14.26	12.39
Alk	2.68	2.02	2.51	2.43	2.16	1.71	2.12	2.01	2.96	2.34	2.75	2.13
% Pheno	4	10	12	0	20	n.d	n.d	n.d	1	<1	<1	9
A.I.	29	29	21	33	6	n.d	n.d	n.d	40	11	18	14
REE	n.d	n.d	n.d	n.d	n.d	n.d	n.d	n.d	n.d	*	n.d	*
Min chem.	n.d	n.d	n.d	*	*	n.d	n.d	n.d	n.d	n.d	n.d	n.d
Trace elements (ppm)												
Ba	171	99	119	132	40	96	109	99	14	62	121	61
Cr	62	197	144	113	96	148	156	262	34	36	106	206
Cu	143	171	171	185	119	176	191	141	123	164	196	159
La	0	0	0	5	0	0	0	0	0	0	9	0
Ni	66	86	84	80	58	87	89	99	28	40	66	108
Nb	4	3	2	5	3	3	4	2	7	4	5	2
Pb	2	6	6	4	5	6	5	2	4	8	6	5
Rb	14	12	12	14	9	7	5	8	10	7	8	5
Sc	29	40	33	38	28	36	37	39	36	38	35	34
Sr	146	137	148	139	167	148	149	139	153	142	145	127
Th	0	0	0	0	3	0	2	1	1	4	0	3
U	0	2	2	0	0	0	0	0	0	0	0	0
V	315	293	255	337	182	273	278	252	376	375	323	259
Y	28	24	21	29	18	23	21	22	47	37	29	25
Zn	86	68	68	82	45	69	63	62	100	85	80	71
Zr	82	61	58	75	45	59	60	54	124	90	71	58
Y/Zr	.34	.39	.36	.39	.40	.39	.35	.41	.38	.41	.41	.43

Sample	CS053	CS054	CS055	CS056	CS057	CS058	CS059	CS060	CS061	CS062	CS063	CS064
SiO_2	47.17	46.83	47.02	47.17	47.11	47.37	47.09	47.61	47.06	46.80	47.24	46.91
Al_2O_3	13.15	13.68	13.73	13.14	13.25	13.08	13.96	13.20	13.80	13.85	13.45	13.67
TiO_2	1.31	1.04	1.25	1.40	1.37	1.42	1.08	1.38	0.98	1.27	1.27	1.26
FeO	12.73	11.20	12.07	13.13	13.13	13.27	11.33	13.00	11.07	12.13	12.33	12.13
Fe_2O_3	1.91	1.68	1.81	1.97	1.97	1.99	1.70	1.95	1.66	1.82	1.85	1.82
MgO	7.46	8.40	8.04	7.39	7.25	6.93	8.46	7.39	8.28	7.61	7.41	7.79
CaO	11.91	13.08	12.63	11.95	12.27	11.92	13.02	11.91	13.16	12.74	12.17	12.70
Na_2O	2.32	2.09	2.14	2.48	2.35	2.27	1.83	2.22	1.87	2.17	2.14	1.99
K_2O	0.20	0.12	0.10	0.14	0.15	0.22	0.08	0.31	0.15	0.13	0.27	0.14
MnO	0.21	0.20	0.21	0.22	0.23	0.23	0.19	0.20	0.19	0.19	0.23	0.20
P_2O_5	0.10	0.07	0.09	0.10	0.09	0.10	0.08	0.10	0.08	0.09	0.08	0.08
H_2O^+	1.66	1.81	1.22	1.06	1.20	1.62	1.72	1.41	1.79	1.64	1.79	1.73
Total	100.14	100.18	100.30	100.15	100.38	100.41	100.56	100.69	100.09	100.44	100.23	100.41
FFM	.6624	.6053	.6332	.6714	.6756	.6877	.6063	.6692	.6059	.6470	.6568	.6417
$Fe_2O_3^*$	14.15	12.48	13.43	14.60	14.59	14.73	12.60	14.44	12.27	13.45	13.72	13.48
Alk	2.52	2.21	2.24	2.62	2.50	2.49	1.91	2.53	2.02	2.30	2.41	2.13
% Pheno	3	n.d	n.d	0	<1	1	<1	<1	n.d	n.d	3	n.d
A.I.	6	n.d	n.d	19	8	15	7	11	n.d	n.d	7	n.d
REE	n.d	n.d	n.d	n.d	*	*	*	*	n.d	n.d	*	n.d
Min chem.*		n.d	n.d	*	n.d	n.d	n.d	*	n.d	n.d	n.d	n.d
Trace elements (ppm)												
Ba	106	64	89	99	97	120	68	121	94	75	122	94
Cr	129	272	296	105	116	108	313	121	195	235	142	225
Cu	188	149	160	193	177	185	158	193	152	169	178	159
La	9	6	0	0	0	4	0	5	0	0	6	0
Ni	66	106	105	80	71	64	117	74	93	99	89	93
Nb	3	3	5	3	2	3	3	3	3	4	2	3
Pb	5	4	3	6	5	8	4	5	7	3	7	4
Rb	8	5	7	7	8	7	6	13	8	7	10	9
Sc	37	35	40	44	32	35	36	39	34	33	35	36
Sr	154	131	129	146	146	146	118	145	124	130	143	131
Th	0	4	0	1	3	2	0	0	4	2	0	0
U	2	2	0	0	2	0	0	1	0	0	0	0
V	292	246	299	332	305	313	256	331	245	288	295	276
Y	28	24	28	28	27	28	23	29	23	27	27	28
Zn	80	69	60	72	66	71	70	79	66	72	80	71
Zr	75	61	69	75	72	78	62	77	60	67	73	74
Y/Zr	.37	.39	.41	.37	.37	.36	.37	.38	.38	.40	.37	.38

Sample	CS065	CS066	CS067	CS068	CS069	CS070	CS071	CS072	CS073	CS074	CS080	CS081
SiO_2	46.64	46.64	47.33	47.77	47.65	47.21	46.82	46.89	52.99	47.08	45.46	46.86
Al_2O_3	13.86	14.08	13.35	12.93	15.54	16.17	13.96	13.84	13.22	13.43	12.78	14.35
TiO_2	1.06	1.12	1.33	1.45	1.11	1.00	1.06	1.10	1.19	1.31	2.45	1.02
FeO	11.13	11.33	13.07	14.20	11.27	10.44	11.13	11.40	10.87	12.80	15.50	10.96
Fe_2O_3	1.67	1.70	1.96	2.13	1.69	1.57	1.67	1.71	1.63	1.92	2.33	1.64
MgO	8.42	8.38	7.32	6.57	6.96	6.80	8.50	8.26	4.79	7.44	5.63	7.86
CaO	12.65	13.03	11.83	11.43	12.88	13.39	12.69	12.91	8.53	12.13	9.96	12.39
Na_2O	1.85	1.65	2.39	2.29	1.66	2.00	2.00	1.83	2.72	2.13	2.86	2.08
K_2O	0.22	0.19	0.17	0.19	0.95	0.17	0.21	0.40	0.29	0.18	0.11	0.13
MnO	0.20	0.18	0.23	0.23	0.18	0.21	0.22	0.20	0.20	0.20	0.20	0.21
P_2O_5	0.07	0.09	0.11	0.13	0.09	0.07	0.07	0.08	0.16	0.09	0.26	0.08
H_2O^+	2.49	1.73	1.49	1.07	1.10	1.25	1.86	1.96	2.87	1.58	2.54	2.95
Total	100.25	100.11	100.57	100.39	100.26	100.20	100.14	100.33	100.50	100.33	100.49	100.53
FFM	.6032	.6086	.6725	.7131	.6506	.5649	.6009	.6135	.7230	.6643	.7600	.6158
$Fe_2O_3^*$	12.35	12.56	14.54	15.80	12.52	11.61	12.38	12.67	12.07	14.19	17.23	12.18
Alk	2.07	1.84	2.56	2.48	1.78	2.13	2.20	1.97	4.04	2.31	3.31	2.25
% Pheno	<1	n.d	n.d	4	8	21	0	0	3	0	<1	2
A.I.	19	n.d	n.d	2	10	11	23	20	5	15	28	17
REE	n.d	n.d	n.d	*	n.d	n.d	n.d	n.d	n.d	n.d	*	n.d
Min chem.	n.d	n.d	n.d	n.d	*	*	n.d	n.d	n.d	n.d	n.d	n.d
Trace elements (ppm)												
Ba	48	81	121	116	86	69	75	90	281	84	85	81
Cr	312	306	86	55	159	159	297	324	50	92	118	136
Cu	146	151	199	199	174	167	150	151	118	165	75	152
La	0	6	8	0	0	0	5	0	5	0	5	4
Ni	111	118	67	57	80	78	122	106	37	77	63	101
Nb	4	4	3	4	4	3	3	4	7	3	5	1
Pb	2	7	5	3	10	4	6	0	6	4	9	5
Rb	9	10	8	8	6	7	8	9	45	8	14	6
Sc	36	37	37	37	35	31	35	38	27	37	31	41
Sr	126	122	145	139	143	143	130	134	136	130	174	129
Th	2	3	0	5	3	3	1	0	2	0	5	4
U	0	0	0	1	0	0	0	0	0	2	0	0
V	261	260	290	328	250	237	246	264	239	307	320	237
Y	24	25	27	33	25	20	25	26	41	30	47	24
Zn	63	68	82	82	50	57	64	73	84	77	133	80
Zr	60	65	77	89	68	57	62	63	156	73	158	61
Y/Zr	.40	.38	.35	.37	.37	.35	.40	.41	.26	.41	.30	.39

Sample	CS082	CS083	CS084	CS085	CS086	CS087	CS088	CS089	CS090	CS091
SiO_2	54.25	46.85	46.51	46.42	46.16	47.19	46.61	46.81	45.35	46.81
Al_2O_3	13.36	13.83	14.38	14.18	14.51	14.12	14.40	14.11	12.77	13.85
TiO_2	1.35	1.33	1.14	1.19	1.13	1.14	1.26	1.12	2.46	1.33
FeO	11.06	12.61	11.55	11.86	11.10	11.42	11.66	11.27	15.46	12.65
Fe_2O_3	1.66	1.89	1.73	1.78	1.66	1.71	1.75	1.69	2.32	1.90
MgO	4.43	7.19	7.75	7.80	7.68	8.14	7.93	8.03	5.64	7.23
CaO	8.65	12.03	12.29	12.46	12.13	12.49	12.32	12.76	9.94	11.98
Na_2O	2.69	2.34	2.06	1.86	2.22	2.13	2.21	2.13	2.84	2.43
K_2O	0.95	0.17	0.21	0.40	0.29	0.18	0.11	0.13	0.45	0.17
MnO	0.18	0.21	0.22	0.20	0.20	0.20	0.20	0.21	0.26	0.23
P_2O_5	0.14	0.11	0.09	0.09	0.08	0.07	0.10	0.08	0.26	0.10
H_2O^+	1.65	1.56	2.32	2.13	2.79	1.25	1.45	1.67	2.56	1.64
Total	100.38	100.13	100.26	100.37	99.93	100.04	100.00	100.01	100.29	100.32
FFM	.7417	.7459	.6315	.6362	.6243	.6173	.6284	.6174	.7590	.6680
$Fe_2O_3^*$	12.29	14.01	12.84	13.18	12.33	12.69	12.96	12.52	17.18	14.06
Alk	3.64	2.51	2.27	2.26	2.51	2.31	2.32	2.26	3.29	2.60
% Pheno	2	5	1	1	<1	<1	n.d	<1	n.d	n.d
A.I.	28	10	37	25	57	24	n.d	23	n.d	n.d
REE	n.d	n.d	n.d	n.d	n.d	n.d	n.d	n.d	n.d	n.d
Min chem.	n.d	n.d	n.d	n.d	n.d	n.d	n.d	n.d	n.d	n.d

Trace elements (ppm)

Ba	330	80	80	98	75	87	85	57	104	81
Cr	42	103	120	176	222	282	259	286	116	111
Cu	70	145	158	159	139	144	130	140	74	140
La	11	7	4	0	0	4	13	5	8	0
Ni	36	77	93	89	107	101	108	103	54	78
Nb	7	4	2	5	3	2	2	3	7	4
Pb	3	6	8	12	3	5	7	2	10	5
Rb	30	5	8	13	8	7	5	6	13	4
Sc	39	44	37	42	39	40	39	43	37	43
Sr	163	128	126	121	135	128	129	129	169	129
Th	6	5	6	4	2	2	3	4	6	9
U	2	0	0	0	1	0	0	0	0	0
V	262	278	239	273	278	259	273	255	323	281
Y	34	30	25	27	26	27	29	24	45	31
Zn	76	88	78	72	62	66	77	70	139	86
Zr	148	76	66	69	59	66	72	64	148	75
Y/Zr	.23	.39	.38	.39	.44	.41	.40	.37	.30	.41

Sample	IT02	IT03	IT04	IT05	IT06	IT07	IT08	IT09	IT10	IT11	IT12	IT13
SiO_2	48.96	52.82	52.90	50.67	46.31	46.45	51.93	51.62	50.64	50.71	52.05	52.10
Al_2O_3	15.44	13.96	14.95	14.63	15.21	14.71	14.87	14.30	14.26	13.68	14.19	14.10
TiO_2	0.72	1.06	0.93	1.12	0.88	0.97	0.93	1.27	0.98	1.09	1.05	0.97
FeO	9.24	10.88	9.35	10.14	10.28	10.85	9.39	10.26	10.21	11.67	10.65	10.09
Fe_2O_3	1.39	1.63	1.40	1.52	1.54	1.63	1.41	1.54	1.53	1.75	1.60	1.51
MgO	7.99	5.74	5.84	6.36	9.14	8.66	6.22	5.62	7.34	6.76	5.98	6.39
CaO	11.89	9.70	10.03	10.03	12.68	12.46	10.62	9.28	11.57	11.35	10.29	10.30
Na_2O	2.26	2.77	2.57	2.80	1.49	1.82	2.66	3.25	2.37	2.28	2.64	2.76
K2O	0.31	0.58	0.65	0.76	0.54	0.28	0.42	1.53	0.52	0.38	0.55	0.73
MnO	0.14	0.21	0.16	0.19	0.20	0.19	0.16	0.19	0.19	0.21	0.20	0.19
P_2O_5	0.06	0.10	0.10	0.16	0.07	0.07	0.12	0.25	0.09	0.09	0.11	0.11
H_2O	1.65	0.84	1.12	1.78	1.89	1.88	1.14	1.07	0.41	0.25	0.80	1.01
Total	100.05	100.29	100.00	100.16	100.23	99.97	99.87	100.18	100.11	100.22	100.11	100.26
FFM	.5709	.6855	.6480	.6471	.5639	.5904	.6345	.6774	.6153	.6650	.6720	.6448
Fe_2O_3*	10.27	12.09	10.39	11.27	11.42	12.06	10.43	11.40	11.35	12.97	11.84	11.21
Alk	2.57	3.35	3.22	3.56	2.03	2.10	3.08	4.78	2.89	2.66	3.19	3.49
% Pheno	7	28	9	n.d	1	4	1	3	<1	1	7	<1
A.I.	28	16	12	n.d	15	6	3	70	22	1	8	18
R.E.E.	n.d	*	n.d	n.d	*	n.d	n.d	n.d	*	n.d	n.d	n.d
Min chem.	n.d	n.d	n.d	n.d	*	n.d	*	*	*	n.d	n.d	n.d

Trace Elements (ppm)

Ba	78	244	239	428	82	75	261	595	257	173	260	256
Cr	296	45	131	186	387	264	137	147	245	207	103	141
Cu	101	145	113	121	137	140	112	126	114	136	122	121
La	0	19	13	14	0	0	11	21	11	6	11	11
Ni	93	50	54	56	143	56	26	50	73	46	43	56
Nb	2	2	2	5	2	3	5	4	3	2	5	3
Pb	4	8	8	8	4	5	7	9	10	8	6	7
Rb	13	14	16	14	15	9	1133	15	16	13	20	30
Sc	38	35	33	35	33	35	38	41	41	43	34	36
Sr	134	215	183	307	107	133	256	356	234	143	183	205
Th	0	4	10	6	4	3	0	6	3	4	7	6
U	0	0	0	1	2	0	00	0	2	0	2	0
V	193	265	203	235	223	219	214	258	241	270	228	213
Y	19	29	25	27	21	21	23	29	24	30	28	26
Zn	58	73	75	76	61	67	75	68	85	81	61	74
Zr	58	73	75	76	61	67	75	140	76	83	98	96
Y/Zr	.35	.30	.26	.23	.40	.37	.24	.21	.32	.36	.29	.27

Sample	IT15	IT16	IT17	IT18	IT19	IT20
SiO_2	51.00	47.09	51.93	56.20	50.90	52.34
Al_2O_3	12.88	14.22	14.25	12.91	12.85	14.26
TiO_2	2.26	0.99	0.94	1.51	2.25	1.05
FeO	13.98	11.20	9.88	11.55	13.99	10.57
Fe_2O_3	2.10	1.68	1.50	1.73	2.10	1.59
MgO	4.26	8.09	6.70	2.80	4.31	5.97
CaO	8.50	12.40	10.79	6.54	8.54	10.28
Na_2O	3.18	1.75	2.45	3.16	3.17	2.64
K_2O	1.37	0.52	0.52	1.84	1.37	0.55
MnO	0.25	0.11	0.20	0.17	0.23	0.20
P_2O_5	0.33	0.08	0.11	0.17	0.32	0.11
H_2O	0.00	1.81	0.90	1.48	0.00	0.83
Total	100.11	99.94	100.27	100.06	100.03	100.39
FFM	.7906	.6142	.6315	.8259	.7887	.6707
Fe_2O_3*	15.54	12.45	11.09	12.83	15.55	11.75
Alk	4.55	2.27	2.97	5.00	15.55	11.75
% Pheno	2	<1	2	17	3	5
A.I.	12	6	7	14	11	4
R.E.E.	*	*	n.d	n.d	n.d	n.d
Min chem.*		*	n.d	n.d	n.d	n.d

Trace Elements (ppm)

Ba	623	123	238	449	617	260
Cr	71	243	183	27	71	104
Cu	237	161	128	29	71	104
La	33	0	14	12	30	9
Ni	26	94	57	14	28	42
Nb	7	3	3	7	8	4
Pb	9	2	7	10	8	10
Rb	30	21	12	50	28	10
Sc	38	37	34	30	40	33
Sr	281	119	196	188	280	183
Th	5	5	0	11	4	4
U	0	0	0	3	0	0
V	393	253	222	284	390	222
Y	50	25	24	35	53	26
Zn	110	79	77	99	107	60
Zr	225	62	87	168	228	101
Y/Zr	.22	.40	.28	.21	.23	.26

Appendix V

Whole rock rare earth element analytical results

Explanation

PPM = Parts per million.

C.N. = Chondrite normalized values. Chondritic abundances are those of Nakamura (1974).

La = 0.33

Ce = 0.86

Pr = 0.12

Nd = 0.63

Sm = 0.20

Eu = 0.08

Gd = 0.28

Dy = 0.34

Ho = 0.08

Er = 0.23

Yb = 0.22

Lu = 0.03

Sample	CS006		CS007		CS009		CS015		CS016	
	PPM	C.N.	PPM	C.N.	PPM	C.N.	PPM	C.N.	PPM	C.N.
La	1.08	3.27	2.68	8.13	1.38	4.19	2.17	6.58	2.96	8.98
Ce	3.07	3.57	9.34	10.86	3.89	4.53	6.30	7.33	8.18	9.51
Pr	0.44	3.67	1.61	13.41	0.56	4.67	1.03	8.58	1.22	10.17
Nd	3.60	5.71	9.29	14.75	4.20	6.67	6.19	9.83	7.41	11.76
Sm	1.05	5.25	2.93	14.65	1.33	6.65	2.02	10.10	2.35	11.75
Eu	0.52	6.50	1.14	14.25	0.64	8.00	0.84	10.50	0.95	11.87
Gd	1.55	5.54	4.17	14.89	2.01	7.18	3.08	11.00	3.45	12.32
Dy	1.79	5.26	4.62	13.58	2.29	6.74	3.64	10.71	3.81	11.21
Ho	0.36	4.50	1.00	12.50	0.45	5.63	0.80	10.00	0.85	10.63
Er	1.06	4.61	2.87	12.48	1.38	6.00	2.44	10.61	2.45	10.65
Yb	1.04	4.73	2.67	12.14	1.31	5.95	2.24	10.18	2.34	10.64
Lu	0.15	5.00	0.37	12.33	0.20	6.67	0.30	10.00	0.33	11.00

Sample	CS019		CS022		CS023		CS024		CS028	
	PPM	C.N.	PPM	C.N.	PPM	C.N.	PPM	C.N.	PPM	C.N.
La	1.74	5.27	2.86	8.65	8.75	26.52	2.41	7.30	2.23	6.76
Ce	5.87	6.83	7.73	8.99	22.59	26.27	7.00	8.14	6.86	7.98
Pr	0.99	8.27	1.13	9.40	3.12	26.00	1.04	8.67	1.15	9.58
Nd	6.12	9.71	6.05	9.60	18.04	28.63	7.00	11.11	7.05	11.19
Sm	2.08	10.40	1.88	9.40	5.52	27.60	2.25	11.25	2.20	11.00
Eu	0.91	11.37	0.76	9.50	1.94	24.25	0.99	12.37	0.92	11.50
Gd	3.14	11.21	2.78	9.93	7.75	27.68	3.52	12.57	3.29	11.75
Dy	3.60	10.59	3.05	8.97	8.45	24.85	3.97	11.68	3.76	11.06
Ho	0.80	10.00	0.69	8.62	1.87	23.37	0.82	10.25	0.83	10.37
Er	2.30	10.00	2.00	8.70	5.41	23.52	2.47	10.74	2.49	10.83
Yb	2.22	10.09	1.84	8.36	5.14	23.36	2.38	10.82	2.27	10.32
Lu	0.30	10.00	0.27	9.00	0.69	23.00	0.36	12.00	0.31	10.33

Sample	CS029		CS038		CS050		CS052		CS057	
	PPM	C.N.	PPM	C.N.	PPM	C.N.	PPM	C.N.	PPM	C.N.
La	2.32	7.02	3.36	10.18	5.00	15.15	2.37	7.18	2.62	7.94
Ce	7.60	8.84	9.51	11.06	13.07	15.20	6.16	7.16	9.42	10.95
Pr	1.25	10.42	1.42	11.83	1.83	15.25	1.04	8.65	1.51	12.58
Nd	7.57	12.02	9.32	14.79	11.71	18.59	6.39	10.14	8.95	14.21
Sm	2.57	12.85	3.00	15.00	3.64	18.20	2.25	11.25	2.91	14.55
Eu	1.01	12.62	1.24	15.00	1.44	18.00	0.90	11.25	1.16	14.50
Gd	3.81	13.61	4.39	15.68	5.23	18.68	3.42	12.21	4.21	15.04
Dy	4.33	12.74	5.03	14.79	5.92	17.41	3.86	11.35	4.78	14.06
Ho	0.96	12.00	1.10	13.75	1.30	16.25	0.87	10.87	1.05	13.12
Er	2.82	12.26	3.24	14.09	3.77	16.39	2.54	10.65	2.99	13.00
Yb	2.69	12.23	2.99	13.59	3.50	5.91	2.40	10.91	2.86	13.00
Lu	0.37	12.33	0.40	13.33	0.47	15.67	0.35	11.67	0.39	13.00

Sample	CS058		CS059		CS060		CS063		CS068	
	PPM	C.N.	PPM	C.N.	PPM	C.N.	PPM	C.N.	PPM	C.N.
La	4.32	13.09	1.63	4.94	2.96	8.97	3.96	12.00	5.11	15.48
Ce	11.38	13.23	6.14	7.14	9.05	10.52	10.69	12.42	13.46	15.65
Pr	1.74	14.50	1.04	8.67	1.43	11.92	1.54	12.85	2.01	16.75
Nd	9.79	15.54	6.43	10.21	8.80	13.97	8.76	13.90	10.16	16.13
Sm	2.97	14.85	2.23	11.15	2.80	14.00	2.72	13.60	3.09	15.45
Eu	1.20	15.00	0.92	11.50	1.14	14.25	1.09	13.62	1.23	15.37
Gd	4.29	15.32	3.39	12.11	4.05	14.46	3.94	14.07	4.46	15.93
Dy	4.95	14.56	3.87	11.38	4.00	11.76	4.50	13.24	5.07	14.91
Ho	1.09	13.62	0.86	10.75	1.02	12.75	0.99	12.37	1.12	14.00
Er	3.26	14.17	2.50	10.87	3.01	13.09	2.90	12.61	3.25	14.13
Yb	2.92	13.27	2.43	11.05	2.80	12.73	2.67	12.14	3.00	13.64
Lu	0.40	13.33	0.34	11.33	0.38	12.67	0.36	12.00	0.41	13.67

Sample	CS080		IT003		IT006		IT015		IT017	
	PPM	C.N.	PPM	C.N.	PPM	C.N.	PPM	C.N.	PPM	C.N.
La	8.49	25.72	12.00	36.36	2.10	6.36	32.00	96.97	8.90	26.97
Ce	24.10	28.02	29.90	34.77	7.00	8.14	72.70	84.53	27.20	31.63
Pr	3.79	31.58	3.54	29.50	1.12	9.33	8.60	71.67	3.21	26.75
Nd	19.50	30.95	14.10	22.38	6.50	10.31	36.80	58.41	13.80	21.90
Sm	6.24	31.20	3.70	18.50	2.14	10.70	8.57	42.85	3.35	16.75
Eu	2.34	29.25	1.25	15.62	0.87	10.87	2.62	32.75	1.11	13.87
Gd	8.63	30.82	4.71	16.82	3.28	11.71	9.85	35.18	4.10	14.64
Dy	8.37	24.62	4.82	14.18	3.64	10.71	9.30	27.35	4.17	12.26
Ho	1.68	21.00	1.00	12.50	0.74	9.25	1.88	23.50	0.85	10.62
Er	4.69	20.39	3.15	13.70	2.20	9.57	5.46	23.74	2.51	10.91
Yb	4.42	20.09	2.80	12.73	2.09	9.50	5.12	23.27	2.35	10.68
Lu	0.66	22.00	0.46	15.33	0.33	11.00	0.80	26.67	0.36	12.00

Appendix VI

Mineral Chemistry

All mineral analyses were determined on a Cambridge Instuments Geoscan V electron probe microanalyser at the Grant Institute of Geology, University of Edinburgh, utilizing wavelength dispersive techniques. Standard operating conditions were 20 KV accelerating voltage, 30nA beam current and an integrated counting time of 40 seconds. Beam diameter was in the region of 2.5 microns. Standards comprised well characterized natural silicates and pure metals. Total iron was determined as FeO^{*}, and for pyroxene and spinel analyses , was subesquently partitioned between ferrous and ferric iron by the method of Finger (1972).

Locality identifiers CS and IT refer to cone-sheets and intrusive tholeiite sheets of part 1 whilst the identifier AG refers to rocks of part 2 of this study whose localities are shown on map 1

Spinels

Spinels

Locality	AG181B	AG175									
Sample	aIC	aIR	aC	aCc	aCR	bCC	bCR	aI	cC	bIC	bIR	dCC
SiO_2	-	0.02	0.06	0.12	0.81	-	0.01	-	0.26	-	0.03	0.01
Al_2O_3	21.31	24.02	11.26	21.27	21.07	25.73	27.13	27.92	9.65	22.80	23.85	8.53
Cr_2O_3	32.84	30.54	33.69	34.26	34.64	32.80	33.12	35.14	39.37	35.19	35.68	31.45
TiO_2	1.24	1.04	1.28	0.77	0.70	3.01	0.46	0.50	1.79	0.97	0.89	10.79
FeO	18.39	17.64	24.96	19.92	20.11	17.83	16.13	16.87	25.54	18.93	18.40	
Fe_2O_3	13.65	12.98	21.00	12.18	11.84	7.42	10.07	7.06	16.03	11.13	9.83	
MgO	11.00	11.50	5.36	9.78	10.46	13.32	12.96	12.68	5.44	11.02	11.44	
MnO	0.50	0.50	0.63	0.54	0.51	0.49	0.46	0.42	0.69	0.48	0.51	0.64
NiO	0.53	0.49	0.57	0.44	0.47	0.40	0.44	0.37	0.44	0.44	0.37	0.49
Total	99.46	98.73	98.81	99.28	100.61	101.00	100.78	100.96	99.21	100.96	101.00	93.28
FeO^*	30.71	29.34	43.84	30.86	30.78	24.52	25.19	23.22	40.01	28.92	27.22	41.37

Locality	AG175	AG245A				AG192		AG1				
Sample	dCR	aC	aIC	aIR	bI	aI	bI	aC	bC	cC	dC	eC
SiO_2	0.05	0.05	0.01	0.05	0.01	0.03	0.01	-	-	-	-	-
Al_2O_3	10.30	11.91	16.73	15.85	13.49	13.70	13.49	48.25	48.54	46.67	45.56	39.53
Cr_2O_3	34.29	41.53	40.70	39.10	37.70	38.82	37.70	15.91	14.90	16.13	16.84	23.09
TiO_2	2.33	1.39	1.28	3.15	2.74	3.30	2.74	0.19	0.28	0.31	0.29	0.44
FeO	25.79	23.58	21.20	22.58	25.54	25.61	25.54	8.22	8.08	8.28	8.29	9.25
Fe_2O_3	19.93	13.41	10.69	9.29	12.50	10.17	12.50	6.12	6.38	6.62	6.72	7.07
MgO	5.49	6.76	8.95	9.00	6.29	6.59	6.29	19.98	20.13	19.69	19.48	18.47
MnO	0.68	0.63	0.57	0.60	0.64	0.63	0.64	0.29	0.28	0.29	0.30	0.33
NiO	0.50	0.39	0.43	0.38	0.46	0.41	0.46	0.44	0.46	0.45	0.48	0.38
Total	99.36	99.65	100.56	99.95	99.37	99.26	99.37	99.40	99.05	98.44	97.96	98.56
FeO^*	43.75	35.61	30.80	30.99	36.80	34.75	36.80	13.71	13.82	14.23	14.32	15.58

Locality	AG1										AG173	AG181C
Sample	fC	gC	hTC	hT1	hT2	hT3	hT4	hT5	hTR	iC	aI	aI
SiO_2	-	-	-	-	-	-	-	-	0.02	-	0.02	0.07
Al_2O_3	47.87	45.63	47.04	49.14	49.01	49.28	49.32	48.80	48.02	48.52	17.94	29.75
Cr_2O_3	15.66	14.58	16.60	15.05	15.12	14.89	14.97	15.47	16.02	15.31	39.80	24.25
TiO_2	0.17	0.35	0.20	0.26	0.28	0.31	0.27	0.32	0.29	0.24	1.36	0.22
FeO	7.69	8.46	8.51	8.51	8.85	8.65	8.68	8.90	8.99	9.38	20.64	20.20
Fe_2O_3	6.48	8.34	5.95	5.85	5.64	5.72	6.03	5.92	5.77	6.23	10.48	15.55
MgO	20.14	19.22	19.53	19.94	19.75	19.89	19.94	19.78	19.55	19.40	9.53	10.54
MnO	0.25	0.31	0.28	0.28	0.29	0.28	0.31	0.28	0.30	0.30	0.56	0.47
NiO	0.46	0.44	0.47	0.44	0.47	0.45	0.43	0.50	0.46	0.44	0.44	0.49
Total	98.72	97.33	98.58	99.47	99.41	99.47	99.95	99.97	99.42	99.82	100.77	101.54
FeO^*	13.49	15.97	13.86	13.80	13.96	13.78	14.05	14.24	14.18	14.99	30.11	34.18

Spinels

Locality	AG297							AG291B		AG190B		
Sample	aI	bI	cI	dI	eI	fI	gI	aC	aI	aI	bI	cI
SiO_2	0.10	4.19	0.11	0.04	0.09	0.05	0.09	0.03	-	0.39	0.15	0.67
Al_2O_3	5.73	5.06	3.74	5.60	2.21	14.22	8.26	17.85	12.8	0.22	0.08	0.67
Cr_2O_3	17.36	4.21	1.19	17.43	0.71	23.34	20.12	29.10	32.24	0.21	0.09	0.12
TiO_2	1.99	0.95	7.60	2.40	1.02	0.67	2.35	0.59	2.59	53.13	51.15	50.58
FeO	30.77	36.49	35.79	33.23	31.61	28.38	30.72	22.47	24.08			
Fe_2O_3	40.76	45.78	48.41	39.55	63.32	29.16	34.20	21.36	20.44			
MgO	1.79	0.78	1.41	0.33	0.46	3.75	2.08	7.76	7.53	0.32	0.21	0.26
MnO	0.35	0.15	0.44	0.53	0.17	0.37	0.42	0.46	0.48	0.22	0.08	0.67
ZnO	0.13	0.02	0.26	0.18	0.10	0.06	0.14	0.13	0.08	0.39	0.15	0.67
Total	98.98	97.63	98.95	99.29	99.69	100.00	98.38	99.75	100.26	99.38	97.14	96.24
FeO^*	467.49	77.69	79.46	68.84	88.30	54.61	61.47	41.66	42.46	44.50	45.23	42.60

Locality	AG291B		AG240					AG287				AG291A
Sample	bI	bC	aI	bI	cI	dI	eI	aI	bI	cI	dI	aI
SiO_2	-	0.08	0.12	0.06	0.10	0.08	0.06	0.04	0.07	0.03	0.11	0.03
Al_2O_3	11.63	7.73	3.88	0.55	1.24	0.28	0.41	0.04	0.08	0.03	0.11	10.23
Cr_2O_3	25.93	23.92	10.91	0.54	1.70	0.39	0.08	0.13	0.63	0.19	0.03	29.86
TiO_2	3.37	1.64	2.40	44.17	4.69	44.03	49.98	52.85	42.02	50.69	48.28	2.99
FeO	25.08	27.78	32.26									28.09
Fe_2O_3	22.17	32.35	46.81									23.90
MgO	7.00	3.33	0.17	0.28	0.10	0.92	0.64	0.44	0.71	0.34	0.33	4.83
MnO	0.49	0.56	0.85	1.86	0.25	2.40	2.13	0.96	1.00	0.86	0.84	0.48
ZnO	0.11	0.18	0.13	0.02	0.08	0.03	-	-	0.02	0.05	0.01	0.13
Total	99.38	97.57	97.53	99.52	93.47	98.05	99.75	102.45	99.95	101.18	98.99	100.54
FeO^*	45.05	56.87	74.45	52.04	85.31	49.92	46.45	47.99	55.42	48.99	49.28	49.59

Locality	AG291A					AG249				AG261		
Sample	bI	cI	dI	eI	fI	aI	bI	cI	dI	aI	bI	cI
SiO_2	0.03	0.10	0.05	0.10	0.02	0.06	0.03	0.08	0.14	0.09	0.01	0.09
Al_2O_3	10.40	10.88	6.14	6.34	8.96	0.07	6.66	6.93	10.02	0.19	16.11	0.11
Cr_2O_3	30.07	29.88	22.90	23.44	27.58	0.47	20.47	22.11	25.76	0.15	37.88	0.25
TiO_2	2.72	2.58	2.41	2.34	2.06	52.32	3.95	4.12	2.74	44.08	1.66	45.28
FeO	27.16	27.07	28.60	28.61	28.48		29.70	29.95	27.85		20.48	
Fe_2O_3	23.75	23.25	35.63	35.28	28.66		34.99	32.39	27.29		14.70	
MgO	5.28	5.35	3.57	3.73	3.87	2.65	3.86	3.89	4.61	1.09	10.06	1.42
MnO	0.47	0.51	0.42	0.49	0.51	0.94	0.44	0.44	0.51	1.49	0.44	0.73
ZnO	0.10	0.07	0.22	0.05	0.08	0.03	0.17	0.14	0.09	0.06	0.06	-
Total	99.98	99.69	99.94	100.38	100.16	101.54	100.27	100.05	99.01	100.23	101.40	97.66
FeO^*	48.53	48.03	60.65	60.34	54.21	45.00	61.14	59.11	52.35	53.08	33.70	50.88

Spinels

Locality	AG248			AG266B			
Sample	aI	bI	cI	aI	bI	cI	dI
SiO_2	0.12	0.23	0.46	0.04	0.03	0.56	0.04
Al_2O_3	2.51	0.97	0.04	17.89	12.67	13.55	14.31
Cr_2O_3	0.40	0.56	-	39.38	37.19	36.50	37.13
TiO_2	0.78	0.78	51.49	0.86	3.77	2.32	1.72
FeO	31.92	31.92		22.27	23.14		
Fe_2O_3	63.69	65.50		10.18	17.56		
MgO	0.22	0.21	2.94	8.26	5.08	6.09	5.96
MnO	0.09	0.12	1.00	0.48	0.59	0.53	0.54
ZnO	0.11	0.05	0.05	0.04	0.05	0.10	0.10
Total	99.84	99.56	99.40	99.40	100.24	99.68	100.19
FeO^*	89.18	90.95	44.69	31.41	40.01	40.03	39.16

Locality	AG158					AG245		AG2				
Sample	aCC	aCR	bC	cCC	cCR	aI	aC	aCC	aCR	bC	cC	dC
SiO_2	-	-	-	-	-	-	5.25	-	-	-	0.15	-
Al_2O_3	45.47	47.42	43.18	45.03	43.63	25.00	7.31	50.78	50.84	51.64	46.01	49.60
Cr_2O_3	17.53	15.87	16.48	15.75	16.06	32.41	27.05	14.74	15.32	14.80	16.13	15.54
TiO_2	0.37	0.20	0.64	0.37	0.42	0.50	6.18	0.20	0.24	0.21	0.22	0.23
FeO	12.06	11.43	13.98	13.55	12.78	22.75	28.57	5.87	6.73	6.11	8.90	7.67
Fe_2O_3	5.73	5.22	8.10	7.62	8.30	7.68	12.16	4.05	3.49	3.72	7.17	5.39
MgO	17.63	18.06	16.17	16.66	16.78	10.44	10.02	21.92	21.49	22.03	19.64	20.94
MnO	0.14	0.09	0.15	0.13	0.12	0.35	0.48	0.04	0.05	0.04	0.05	0.06
ZnO	-	-	-	-	-	0.01	0.12	-	-	-	-	-
Total	98.93	98.29	98.70	99.11	98.09	99.14	97.14	97.60	98.16	98.57	98.31	99.43
FeO^*	17.14	16.12	21.25	20.43	20.28	28.68	39.53	9.45	9.93	9.44	15.35	12.49

Locality	AG2			AG181A							AG157	
Sample	eC	fC	gC	aIC	aIR	aC	bI	cI	dIC	dIR	aCC	aCR
SiO_2	-	-	-	0.04	0.71	0.16	0.08	0.08	0.03	0.06	0.06	0.03
Al_2O_3	48.90	49.14	51.65	27.21	28.46	14.29	31.55	27.35	24.73	25.76	49.68	49.34
Cr_2O_3	15.61	15.51	15.23	29.39	27.34	36.25	26.99	29.05	30.82	30.41	15.61	16.35
TiO_2	0.39	0.41	0.26	0.77	0.73	0.94	0.54	0.50	1.13	1.07	0.25	0.21
FeO	8.55	8.86	6.05	18.63	18.86	23.27	15.78	19.03	18.37	18.13	8.30	8.48
Fe_2O_3	5.57	5.37	3.74	12.14	10.32	16.55	10.64	12.62	12.66	11.94	4.85	4.65
MgO	20.47	20.19	22.12	11.73	11.88	7.09	13.77	11.19	11.64	11.87	20.53	20.37
MnO	0.20	0.17	0.16	0.39	0.35	0.56	0.33	0.36	0.41	0.38	0.12	0.22
ZnO	0.09	0.06	0.05	0.22	0.25	0.33	0.25	0.29	0.26	0.23	0.13	0.12
Total	99.60	99.71	99.26	100.52	98.90	99.44	99.93	100.47	100.05	99.85	99.53	99.77
FeO^*	13.56	13.71	9.39	29.60	28.18	38.14	25.37	30.39	29.72	28.85	12.64	12.66

Spinels

Locality	AG157				AG181A						AG241	
Sample	bCC	bCR	aI	bI	aIC	aIR	bI	aC	bCC	bCR	aI	bI
SiO_2	0.02	0.02	0.05	0.07	0.05	0.08	0.08	0.06	0.03	0.11	0.09	0.13
Al_2O_3	52.13	51.79	46.86	46.65	27.90	28.65	15.43	33.23	32.61	32.07	11.82	9.77
Cr_2O_3	14.26	14.92	15.94	15.98	31.29	29.98	35.60	28.79	28.49	28.66	23.40	24.30
TiO_2	0.23	0.20	0.48	0.51	0.65	0.65	0.41	0.45	0.47	0.49	1.83	1.83
FeO	7.21	7.35	9.89	9.53	17.16	16.82	23.29	14.29	14.32	14.71	28.23	31.51
Fe_2O_3	4.37	4.23	6.35	7.06	10.41	10.41	15.50	9.23	9.00	9.05	28.74	29.01
MgO	21.58	21.43	19.20	18.99	12.75	12.84	7.39	15.30	14.85	14.67	3.62	1.50
MnO	0.16	0.19	0.23	0.25	0.39	0.38	0.54	0.37	0.38	0.35	0.74	0.60
ZnO	0.06	0.07	0.14	0.12	0.26	0.27	0.43	0.26	0.24	0.23	0.39	0.36
Total	100.02	100.20	99.14	99.16	100.86	100.08	98.67	101.98	100.39	100.34	98.86	99.01
FeO^*	11.16	11.17	15.59	15.91	26.51	26.23	37.23	22.56	22.41	22.86	54.12	57.65

Spinels

Locality	AG181C		AG160				AG143F					AG119
Sample	bI	cI	aC	bC	aI	cC	aIC	aIR	aC	bC	cC	aC
SiO_2	0.02	0.08	0.05	0.23	0.01	0.06	0.03	0.04	0.02	0.03	1.34	3.22
Al_2O_3	15.81	21.18	15.92	15.36	36.65	16.72	9.94	13.21	10.50	11.27	15.92	13.69
Cr_2O_3	34.88	34.70	38.25	38.14	25.21	39.91	29.88	35.98	39.56	36.06	29.01	37.25
TiO_2	1.41	1.41	1.13	1.19	0.60	1.14	14.47	2.28	1.83	2.02	1.75	1.29
FeO	22.34	18.45	21.59	21.73	15.25	21.68		23.75	25.72	25.95	25.21	14.41
Fe_2O_3	17.07	12.62	13.51	13.84	7.47	11.08		16.21	15.28	17.46	17.82	7.98
MgO	8.16	11.38	8.35	8.47	14.71	8.55	8.05	7.41	5.31	5.27	7.32	7.74
MnO	0.59	0.54	0.62	0.57	0.39	0.59	0.61	0.60	0.67	0.63	0.57	0.56
NiO	0.47	0.48	0.44	0.42	0.42	0.40	0.42	0.44	0.43	0.43	0.45	0.41
Total	100.75	100.84	99.86	99.95	100.71	100.13	99.63	99.92	99.32	99.12	99.39	98.19
FeO^*	37.75	29.80	33.76	34.23	21.90	31.61	35.94	38.28	39.45	41.65	41.21	33.22

Locality	AG119		AG320									
Sample	aIC	aIR	aIC	bIC	dIC	eIR	eIC	fIC	gC	hC	iIC	jIC
SiO_2	-	-	0.02	0.03	0.07	0.18	0.74	0.07	0.08	0.13	0.05	0.05
Al_2O_3	39.04	38.71	17.89	17.84	17.87	18.23	16.68	17.92	16.17	16.37	16.27	17.76
Cr_2O_3	22.98	22.85	37.58	37.83	37.51	37.12	33.50	36.89	37.56	36.95	36.11	38.28
TiO_2	0.50	0.49	1.14	1.11	1.09	1.07	1.16	1.02	1.08	1.11	1.00	1.07
FeO	14.99	17.70	19.29	19.59	19.84	19.90	23.68	20.82	23.01	22.45	23.75	20.00
Fe_2O_3	8.26	12.49	12.81	12.34	12.48	12.08	11.76	13.04	13.29	13.94	13.83	12.50
MgO	15.56	15.08	10.20	10.03	9.89	9.90	7.52	9.29	7.62	8.09	6.96	9.87
MnO	0.34	0.36	0.45	0.37	0.42	0.37	0.50	0.41	0.49	0.47	0.45	0.43
NiO	0.41	0.46	0.20	0.21	0.23	0.20	0.18	0.16	0.20	0.20	0.21	0.20
Total	101.22	101.20	99.58	99.35	99.40	99.05	95.72	99.62	99.50	99.71	98.63	100.16
FeO^*	21.59	22.45	30.84	30.71	31.01	30.73	34.26	32.53	34.96	34.96	36.17	31.27

Locality	AG320											
Sample	kIC	kIR	aC	bC	cC	dCC	eCC	fCC	lIC	gTCC	gT	gTCR
SiO_2	0.08	0.29	1.84	0.10	0.52	0.16	0.07	0.11	0.01	0.02	0.08	0.10
Al_2O_3	19.38	18.99	16.35	16.67	17.15	15.90	15.66	16.14	17.64	15.72	15.48	15.82
Cr_2O_3	36.44	36.68	34.93	36.92	36.04	36.16	37.39	36.33	37.11	37.24	36.43	36.73
TiO_2	0.85	0.94	0.96	1.18	1.14	1.09	1.06	1.00	1.11	1.06	0.99	1.10
FeO	18.98	19.74	24.57	22.33	22.65	24.20	23.55	23.55	19.88	23.06	23.28	23.14
Fe_2O_3	12.42	11.55	11.13	13.44	12.34	13.70	13.80	13.38	12.82	13.41	14.68	13.31
MgO	10.50	10.09	7.83	8.22	8.21	6.78	7.15	6.97	9.70	7.23	7.14	7.24
MnO	0.35	0.41	0.50	0.46	0.44	0.48	0.49	0.48	0.43	0.49	0.44	0.48
NiO	0.18	0.22	0.20	0.22	0.22	0.18	0.24	0.19	0.18	0.16	0.22	0.19
Total	99.18	98.91	99.54	98.71	98.65	99.41	98.15	98.88	98.39	98.88	98.74	98.11
FeO^*	30.07	30.08	34.59	34.41	33.80	36.48	35.93	32.02	31.41	35.17	36.52	35.11

Spinels

Locality	AG152				AG178			AG277			AG295	
Sample	aC	bC	aI	bI	aC	aI	bC	aI	bI	aC	aI	aC
SiO_2	0.08	0.12	0.05	0.03	0.04	0.07	0.60	0.05	0.55	0.08	-	0.09
Al_2O_3	5.32	10.47	-	21.65	13.00	19.65	9.10	13.05	13.66	12.05	10.72	10.61
Cr_2O_3	25.58	35.56	0.23	34.53	33.36	35.15	30.13	36.19	35.40	37.43	31.92	34.89
TiO_2	4.00	2.32	54.02	0.68	2.90	0.92	1.72	4.05	1.62	1.53	2.32	1.78
FeO	31.13	28.33		17.70	25.28	18.52	29.57	24.69	23.49	23.24	26.95	26.96
Fe_2O_3	28.81	16.45		12.49	18.15	13.06	22.89	13.84	16.58	17.30	22.28	19.52
MgO	1.99	3.62	1.74	11.15	6.71	10.56	2.60	7.99	7.56	7.04	4.67	4.51
MnO	0.87	0.82	1.76	0.52	0.62	0.51	0.87	0.61	0.58	0.57	0.62	0.64
NiO	0.58	0.43	0.30	0.40	0.54	0.39	0.47	0.44	0.47	0.44	0.54	0.46
Total	97.86	98.12	101.39	99.15	100.60	98.83	97.95	100.91	99.91	99.68	100.02	99.46
FeO^*	57.04	43.12	43.29	28.99	51.58	30.25	50.14	37.18	38.34	38.83	46.98	44.48

Locality	AG244			AG186			AG255				AG254	
Sample	aC	aI	bI	aC	aI	bI	aI	bI	aC	bC	aI	aC
SiO_2	0.04	0.04	0.24	0.18	-	0.05	1.14	0.05	0.05	0.05	0.05	0.01
Al_2O_3	16.55	20.96	20.33	14.12	32.83	32.15	16.83	17.53	16.88	15.61	18.27	17.71
Cr_2O_3	39.65	37.06	37.85	37.26	28.68	29.84	38.04	38.56	37.15	37.64	41.15	40.94
TiO_2	1.46	0.99	1.05	1.48	0.40	0.60	1.88	1.29	1.34	1.06	0.85	1.14
FeO	23.09	17.47	17.84	22.99	16.98	16.94	22.92	21.02	24.32	24.54	18.19	19.09
Fe_2O_3	10.83	10.60	10.28	14.68	8.52	7.42	8.89	11.05	12.22	13.83	9.75	9.83
MgO	7.80	11.60	11.46	7.48	13.18	13.27	9.08	9.00	6.80	6.41	10.44	9.80
MnO	0.59	0.46	0.49	0.59	0.43	0.43	0.59	0.54	0.62	0.66	0.50	0.53
NiO	0.42	0.47	0.49	0.39	0.41	0.38	0.39	0.43	0.42	0.43	0.44	0.45
Total	100.43	99.65	100.03	99.17	101.43	101.08	99.76	99.47	99.80	100.23	99.64	99.50
FeO^*	32.86	27.03	27.11	36.21	24.68	23.62	30.91	30.99	35.34	36.97	27.69	28.77

Locality	AG5										181B	
Sample	aI	bI	cI	dI	aTC	aT	aT	aT	aT	aTR	ac	ac
SiO_2	-	-	0.04	-	0.01	-	0.09	0.03	-	-	0.05	0.05
Al_2O_3	28.76	28.37	26.76	16.37	33.78	34.74	34.26	35.64	34.83	34.46	19.74	19.74
Cr_2O_3	29.99	30.00	30.47	36.78	26.64	26.45	26.59	25.70	26.27	25.82	32.26	32.26
TiO_2	0.95	0.92	0.92	1.46	0.48	0.43	0.46	0.44	0.40	0.43	1.45	1.45
FeO	17.19	17.15	17.32	22.21	14.49	13.45	13.39	13.18	13.20	13.55	21.51	21.51
Fe_2O_3	10.46	10.47	9.83	13.55	8.48	8.08	7.75	7.69	8.08	8.50	14.17	14.17
MgO	12.77	12.62	11.98	8.11	14.40	15.25	15.11	15.48	15.34	15.00	8.83	8.83
MnO	0.43	0.44	0.45	0.56	0.38	0.37	0.36	0.34	0.35	0.36	0.52	0.52
NiO	0.46	0.53	0.46	0.45	0.51	0.48	0.50	0.51	0.46	0.45	0.52	0.52
Total	101.01	100.50	98.23	99.49	99.17	99.25	98.51	99.01	98.93	98.57	99.05	99.05
FeO^*	26.62	26.58	26.17	34.35	22.13	20.67	20.36	20.13	20.49	21.20	34.24	34.24

Spinels

Locality	AG320			AG2			AG244					
Sample	mITc	mIT	mITR	gC	hC	1I	1C	mC	nC	oC	pC	kI
SiO_2	0.03	0.03	0.42	0.10	0.07	-	0.18	0.26	0.94	0.13	0.06	0.13
Al_2O_3	17.49	17.46	17.86	50.03	49.24	50.21	15.74	15.06	21.42	8.96	11.43	19.79
Cr_2O_3	37.66	37.44	37.52	15.26	15.97	15.92	36.59	37.55	35.26	36.23	36.75	38.27
TiO_2	1.29	1.26	1.20	0.26	0.42	0.27	1.41	1.99	0.89	4.72	2.98	1.09
FeO	19.94	19.82	20.22	9.10	9.00	7.95	23.78	24.02	22.72	27.20	25.20	19.53
Fe_2O_3	12.45	12.85	11.55	5.01	5.10	4.58	12.37	12.23	8.14	13.48	14.37	9.68
MgO	9.80	9.86	10.01	20.12	20.13	20.76	6.94	7.39	8.89	5.74	6.31	10.38
MnO	0.40	0.43	0.41	0.19	0.19	0.16	0.60	0.56	0.49	0.59	0.57	0.46
NiO	0.21	0.22	0.26	0.30	0.31	0.29	0.27	0.32	0.22	0.28	0.30	0.25
Total	99.27	99.37	99.45	100.37	100.43	100.14	97.83	99.38	98.97	97.33	97.97	99.58
FeO^*	31.09	31.32	30.63	13.57	13.61	12.06	34.94	35.05	30.02	39.33	38.15	28.23

Locality	AG244	AG316				AG314			AG315			
Sample	1I	aC	bC	cC	dC	aIC	aIR	bI	aI	bIC	bIR	aI
SiO_2	0.12	0.11	0.32	0.59	0.21	0.07	0.39	1.25	0.15	0.05	0.19	0.11
Al_2O_3	14.98	6.44	5.22	5.21	7.15	6.08	8.33	7.86	10.66	8.64	9.77	14.14
Cr_2O_3	37.93	21.24	16.64	17.74	18.77	19.85	21.61	21.82	25.76	23.96	24.20	26.14
TiO_2	1.88	2.55	2.76	2.74	3.24	2.49	3.76	2.77	2.40	2.74	2.41	1.01
FeO	22.66	30.13	30.66	28.72	30.82	30.82	31.45	32.55	28.63	29.09	28.73	28.61
Fe_2O_3	12.93	35.50	40.00	41.47	35.90	37.32	28.49	30.14	26.43	29.85	28.62	24.92
MgO	8.18	2.45	2.02	2.01	2.59	1.86	2.30	2.20	3.93	3.56	3.73	3.41
MnO	0.50	0.60	0.56	0.54	0.58	0.56	0.61	0.59	0.47	0.45	0.50	0.79
NiO	0.31	0.40	0.43	0.49	0.37	0.48	0.38	0.44	-	-	-	0.21
Total	99.49	99.42	98.61	99.51	99.63	99.48	97.32	99.62	98.43	98.34	98.15	99.34
FeO^*	34.28	62.13	66.61	67.51	63.07	64.28	57.06	59.74	52.38	55.95	54.48	51.03

Locality	AG315	AG323				AG318					
Sample	bI	aC	aI	bI	cI	aI	aC	bC	cC	bI	cI
SiO_2	0.11	0.31	0.16	0.24	0.18	0.06	0.03	0.17	0.22	0.12	0.05
Al_2O_3	5.91	10.37	13.82	20.41	20.17	26.47	10.85	10.65	10.68	13.97	12.31
Cr_2O_3	16.52	32.04	33.25	36.60	35.99	33.58	37.62	35.85	34.18	33.24	33.81
TiO_2	2.06	1.95	2.63	0.60	0.78	0.47	1.91	2.27	1.95	5.80	5.00
FeO	30.88	26.11	23.49	21.51	20.06	16.47	24.85	26.28	25.28	29.57	29.71
Fe_2O_3	40.35	20.17	17.27	10.21	11.62	9.41	15.93	17.01	18.76	9.30	11.44
MgO	1.12	4.89	7.89	8.94	9.97	12.83	6.22	5.31	5.68	5.75	4.74
MnO	0.98	0.63	0.54	0.40	0.37	0.36	0.58	0.57	0.52	0.53	0.56
NiO	0.29	0.27	0.30	0.18	0.19	0.13	0.19	0.24	0.27	0.25	0.19
Total	98.22	96.74	99.35	99.09	99.33	99.78	98.18	98.35	97.54	98.53	97.81
FeO^*	67.21	44.28	39.04	30.71	30.42	24.90	39.14	41.61	42.16	37.94	40.00

Olivines

Olivines

Locality	AG245				AG158					AG2		
Sample	aC	aR	bC	bR	aC	bC	bR	cR	cC	aC	bC	bR
SiO_2	40.00	39.98	39.93	39.71	40.68	40.02	40.50	40.20	41.34	40.94	41.07	41.02
MgO	46.19	45.43	45.97	45.70	48.25	48.38	49.49	49.51	52.64	52.17	52.04	52.19
FeO	13.12	13.11	13.45	13.21	9.57	9.56	9.54	9.52	6.22	6.19	6.07	6.17
NiO	0.23	0.22	0.26	0.28	0.37	0.39	0.39	0.37	0.36	0.32	0.33	0.33
MnO	0.22	0.22	0.22	0.21	0.14	0.17	0.15	0.15	0.15	0.14	0.14	0.13
$Al2O_3$	0.05	0.05	0.07	0.05	0.07	0.04	0.04	0.04	0.03	0.03	0.10	0.03
CaO	0.06	0.10	0.05	0.07	0.07	0.03	0.04	0.06	0.08	0.10	0.05	0.08
Total	99.87	99.11	99.95	99.23	99.15	98.59	100.15	99.85	100.82	99.89	99.80	99.95
Fo	86.24	86.08	85.89	86.03	89.97	90.02	90.21	90.25	93.77	93.77	93.85	93.77
Fa	13.76	13.92	14.11	13.97	10.03	9.08	9.79	9.75	6.23	6.23	6.15	6.23

Locality	AG2	AG181A							AG157		
Sample	cR	bC	bR	cC	cR	dC	dR	eC	eR	aC	aR	bA
SiO_2	41.36	39.97	40.16	40.38	40.73	40.88	40.28	40.35	40.39	41.16	40.46	41.14
MgO	52.07	47.51	47.62	47.79	47.82	48.23	47.69	47.66	47.75	50.99	50.61	51.38
FeO	5.99	11.25	11.05	11.26	11.26	10.93	10.93	11.08	11.04	6.98	6.72	6.98
NiO	0.33	0.36	0.36	0.35	0.34	0.32	0.34	0.35	0.33	0.36	0.37	0.38
MnO	0.13	0.22	0.20	0.19	0.22	0.19	0.17	0.21	0.18	0.19	0.17	0.18
$Al2O_3$	0.02	0.03	0.04	0.03	0.05	0.02	0.04	0.06	0.06	0.04	0.44	0.02
CaO	0.07	0.02	0.05	0.04	0.06	0.01	0.04	0.03	0.06	0.09	0.09	0.11
Total	99.97	99.26	99.48	100.04	100.48	99.49	100.58	99.49	99.74	99.81	98.86	100.19
Fo	93.93	88.28	88.50	88.30	88.30	88.72	88.59	88.48	88.53	92.85	93.05	92.93
Fa	6.07	11.72	11.50	11.70	11.70	11.28	11.41	11.52	11.47	7.15	6.95	7.07

Locality	AG190B						AG241				AG297	
Sample	aC	bC	cC	dC	eC	fC	aC	bC	cC	dC	aC	bC
SiO_2	40.31	40.33	39.90	39.41	39.11	39.60	39.39	39.54	39.66	39.84	38.14	38.29
MgO	45.57	45.60	45.89	45.37	45.22	45.33	43.69	43.69	43.41	43.70	37.68	37.42
FeO	14.28	14.05	14.08	14.01	14.65	14.52	16.67	16.79	16.85	16.39	23.96	24.75
NiO	0.28	0.28	0.27	0.30	0.30	0.26	0.25	0.26	0.26	0.24	0.23	0.21
MnO	0.26	0.25	0.28	0.24	0.27	0.31	0.30	0.29	0.30	0.26	0.39	0.40
$Al2O_3$	0.03	0.03	0.03	0.03	0.03	0.08	0.03	0.03	0.03	0.03	0.03	0.05
CaO	0.02	0.03	0.02	-	0.02	0.05	0.03	0.02	0.04	0.04	0.04	0.03
Total	100.75	100.57	100.47	99.36	99.60	100.15	100.36	100.62	100.55	100.50	100.47	101.15
Fo	85.03	85.05	85.29	85.25	84.63	84.78	82.38	82.26	82.12	82.60	73.68	72.91
Fa	14.97	14.95	14.71	14.75	15.37	15.22	17.62	17.74	17.78	17.40	16.32	17.09

Olivines

Locality	AG266		AG316								AG314
Sample	bC	cC	aC	aC	bC	dC	cC	dC	eC	fC	gC	aC
SiO_2	40.46	40.49	40.49	39.98	39.16	38.96	39.29	39.43	39.69	39.08	39.87	38.43
MgO	45.98	46.53	46.00	43.01	43.41	42.77	43.39	43.23	43.74	43.53	42.37	40.00
FeO	12.76	12.89	12.86	17.39	17.53	17.24	17.04	17.35	17.03	17.08	16.74	21.60
NiO	0.27	0.28	0.28	0.25	0.29	0.32	0.28	0.26	0.26	0.28	0.25	0.17
MnO	0.20	0.23	0.23	0.30	0.29	0.28	0.29	0.28	0.26	0.29	0.29	0.32
Al_2O_3	0.03	0.03	0.05	0.12	0.03	0.02	0.01	0.03	0.04	0.03	0.10	0.04
CaO	0.04	0.06	0.05	0.05	0.03	0.03	0.03	0.10	0.09	0.13	0.42	0.04
Total	99.74	100.51	99.96	101.09	100.73	99.61	100.34	100.67	101.10	100.43	100.04	100.60
Fo	86.52	86.54	86.46	81.51	81.51	81.56	81.93	81.59	82.09	81.94	81.87	76.75
Fa	13.48	13.46	13.54	18.49	18.49	18.44	18.07	18.41	17.91	18.06	18.13	23.25

Locality	AG314		AG315				AG318					AG320
Sample	bC	cC	aC	bC	cC	dC	aC	bC	cC	dC	eC	aC
SiO_2	37.92	39.37	39.51	39.69	40.03	40.00	41.00	40.96	41.16	41.16	41.61	39.78
MgO	39.56	39.77	42.05	41.93	42.25	42.49	46.98	47.34	46.64	46.29	47.00	47.58
FeO	21.60	21.67	18.52	18.31	18.31	18.30	12.25	12.04	12.16	12.64	11.92	12.02
NiO	0.19	0.17	0.18	0.15	0.18	0.17	0.27	0.24	0.27	0.25	0.25	0.34
MnO	0.32	0.33	0.32	0.34	0.30	0.31	0.21	0.19	0.19	0.21	0.19	0.19
Al_2O_3	0.03	0.03	0.03	0.08	0.05	0.03	0.02	0.02	0.04	0.05	0.04	0.02
CaO	0.03	0.04	0.04	0.04	0.04	0.04	0.07	0.07	0.07	0.10	0.05	0.05
Total	99.64	99.40	100.64	100.53	101.15	101.34	100.78	100.85	100.52	100.69	101.06	99.98
Fo	76.55	76.58	80.18	80.32	80.42	80.53	87.22	87.51	87.25	86.73	87.52	87.57
Fa	23.45	23.42	19.82	19.68	19.58	19.47	12.78	12.49	12.75	13.27	13.48	13.43

Locality	AG320					AG2			AG244			AG323
Sample	bC	cC	dC	eC	fC	cC	dC	eC	gC	hC	iC	aC
SiO_2	39.63	40.67	39.65	39.86	39.24	41.07	40.95	40.99	39.89	40.30	40.12	40.91
MgO	47.73	47.66	47.87	47.58	47.97	51.72	51.79	51.39	46.44	47.02	46.63	46.05
FeO	11.64	11.73	11.71	12.02	11.84	5.87	5.98	5.74	11.89	11.71	12.05	13.01
NiO	0.30	0.28	0.30	0.30	0.33	0.36	0.33	0.34	0.37	0.38	0.36	0.30
MnO	0.19	0.18	0.17	0.20	0.19	0.11	0.12	0.13	0.20	0.20	0.19	0.22
Al_2O_3	0.02	0.02	0.03	0.03	0.02	0.03	0.07	0.05	0.06	0.09	0.07	0.03
CaO	0.03	0.06	0.06	0.07	0.06	0.09	0.12	0.08	0.08	0.05	0.08	0.06
Total	99.55	100.62	99.78	100.05	99.66	99.26	99.36	98.71	98.92	99.74	99.50	100.58
Fo	87.94	87.87	87.95	87.61	87.83	94.02	93.94	94.11	87.45	87.74	87.34	86.31
Fa	12.06	12.13	12.05	12.39	12.17	5.98	6.06	5.89	12.55	12.26	12.66	13.69

Olivines

Locality	AG186	AG244			AG255			AG254			
Sample	bR	aC	aR	bC	aC	aR	bC	aC	aR	bC	bR
SiO_2	40.70	40.40	40.44	40.51	40.32	40.29	40.48	40.79	39.90	39.99	40.26
MgO	48.99	47.45	47.19	47.40	46.96	47.12	46.81	48.48	47.13	48.01	48.42
FeO	10.05	12.11	11.89	11.88	12.00	11.71	12.02	9.92	9.79	9.99	9.67
NiO	0.33	0.38	0.37	0.39	0.31	0.34	0.34	0.41	0.42	0.40	0.44
MnO	0.15	0.22	0.20	0.19	0.20	0.22	0.22	0.17	0.15	0.18	0.14
Al_2O_3	0.05	0.06	0.05	0.05	0.02	0.04	0.02	0.01	0.16	0.02	0.02
CaO	0.04	0.07	0.09	0.08	0.03	0.09	0.05	0.06	0.25	0.08	0.06
Total	100.31	100.69	100.23	100.50	99.84	99.81	99.94	99.84	97.80	98.67	99.01
Fo	89.67	87.46	87.61	87.66	87.46	87.76	87.42	89.70	89.54	89.55	89.92
Fa	10.33	12.54	12.39	12.34	12.54	12.24	12.58	10.30	10.46	10.45	10.08

Locality	AG240					AG291						
Sample	aC	bC	cC	cR	dC	aC	aR	bC	bR	aG	bG	aC
SiO_2	38.45	38.89	37.44	36.76	37.90	40.54	40.15	40.26	41.20	40.86	40.72	40.07
MgO	38.22	39.94	36.17	35.87	37.49	46.13	46.31	45.89	45.54	46.21	46.51	45.03
FeO	23.62	20.43	25.18	24.75	24.72	12.40	13.03	12.62	12.46	12.80	12.83	14.01
NiO	0.16	0.20	0.13	0.15	0.14	0.29	0.35	0.29	0.31	0.32	0.37	0.36
MnO	0.38	0.43	0.44	0.41	0.42	0.22	0.23	0.22	0.24	0.20	0.24	0.22
Al_2O_3	0.03	0.05	0.06	1.05	0.05	0.11	0.05	0.01	0.61	0.07	0.05	0.02
CaO	0.03	0.05	0.07	0.07	0.02	0.03	0.07	0.03	0.07	0.06	0.15	0.04
Total	100.89	99.99	99.49	99.06	100.74	99.72	100.19	99.32	100.43	100.52	100.87	99.75
Fo	74.23	77.69	71.90	72.08	72.98	86.89	86.93	86.63	86.68	86.56	86.62	85.13
Fa	25.77	22.31	28.10	27.92	27.02	13.11	13.07	13.37	13.32	13.44	13.38	14.87

Locality	AG291	AG190C			AG249			AG261				
Sample	aR	aC	bC	cC	aC	bC	cC	aC	bC	cC	dC	eC
SiO_2	40.40	39.74	40.56	40.09	39.40	39.50	39.69	39.68	38.61	39.29	39.20	39.24
MgO	44.75	42.63	42.26	42.61	42.03	41.46	41.22	38.71	38.51	38.62	38.55	38.12
FeO	13.58	17.62	17.46	16.85	18.07	17.75	18.63	22.51	22.64	22.60	22.45	23.18
NiO	0.34	0.21	0.19	0.18	0.29	0.31	0.29	0.14	0.12	0.18	0.14	0.17
MnO	0.24	0.34	0.34	0.36	0.31	0.31	0.29	0.40	0.35	0.40	0.39	0.39
Al_2O_3	0.04	0.02	0.03	0.03	0.05	0.05	0.04	0.05	0.05	0.06	0.04	0.05
CaO	0.08	0.07	0.04	0.02	0.03	0.04	0.03	0.10	0.10	0.09	0.08	0.15
Total	99.43	100.63	100.88	100.14	100.18	99.42	100.19	101.59	100.38	101.24	100.85	101.30
Fo	85.44	81.18	81.17	81.85	80.55	79.77	79.77	75.40	75.26	75.29	75.37	74.55
Fa	14.56	18.82	18.83	18.15	9.45	20.23	20.23	24.60	24.74	24.71	24.63	25.45

Olivines

Locality	AG266		AG316								AG314	
Sample	bC	cC	aC	aC	bC	dC	cC	dC	eC	fC	gC	aC
SiO_2	40.46	40.49	40.49	39.98	39.16	38.96	39.29	39.43	39.69	39.08	39.87	38.43
MgO	45.98	46.53	46.00	43.01	43.41	42.77	43.39	43.23	43.74	43.53	42.37	40.00
FeO	12.76	12.89	12.86	17.39	17.53	17.24	17.04	17.35	17.03	17.08	16.74	21.60
NiO	0.27	0.28	0.28	0.25	0.29	0.32	0.28	0.26	0.26	0.28	0.25	0.17
MnO	0.20	0.23	0.23	0.30	0.29	0.28	0.29	0.28	0.26	0.29	0.29	0.32
Al_2O_3	0.03	0.03	0.05	0.12	0.03	0.02	0.01	0.03	0.04	0.03	0.10	0.04
CaO	0.04	0.06	0.05	0.05	0.03	0.03	0.03	0.10	0.09	0.13	0.42	0.04
Total	99.74	100.51	99.96	101.09	100.73	99.61	100.34	100.67	101.10	100.43	100.04	100.60
Fo	86.52	86.54	86.46	81.51	81.51	81.56	81.93	81.59	82.09	81.94	81.87	76.75
Fa	13.48	13.46	13.54	18.49	18.49	18.44	18.07	18.41	17.91	18.06	18.13	23.25

Locality	AG314		AG315				AG318					AG320
Sample	bC	cC	aC	bC	cC	dC	aC	bC	cC	dC	eC	aC
SiO_2	37.92	39.37	39.51	39.69	40.03	40.00	41.00	40.96	41.16	41.16	41.61	39.78
MgO	39.56	39.77	42.05	41.93	42.25	42.49	46.98	47.34	46.64	46.29	47.00	47.58
FeO	21.60	21.67	18.52	18.31	18.31	18.30	12.25	12.04	12.16	12.64	11.92	12.02
NiO	0.19	0.17	0.18	0.15	0.18	0.17	0.27	0.24	0.27	0.25	0.25	0.34
MnO	0.32	0.33	0.32	0.34	0.30	0.31	0.21	0.19	0.19	0.21	0.19	0.19
Al_2O_3	0.03	0.03	0.03	0.08	0.05	0.03	0.02	0.02	0.04	0.05	0.04	0.02
CaO	0.03	0.04	0.04	0.04	0.04	0.04	0.07	0.07	0.07	0.10	0.05	0.05
Total	99.64	99.40	100.64	100.53	101.15	101.34	100.78	100.85	100.52	100.69	101.06	99.98
Fo	76.55	76.58	80.18	80.32	80.42	80.53	87.22	87.51	87.25	86.73	87.52	87.57
Fa	23.45	23.42	19.82	19.68	19.58	19.47	12.78	12.49	12.75	13.27	13.48	13.43

Locality	AG320					AG2			AG244			AG323
Sample	bC	cC	dC	eC	fC	cC	dC	eC	gC	hC	iC	aC
SiO_2	39.63	40.67	39.65	39.86	39.24	41.07	40.95	40.99	39.89	40.30	40.12	40.91
MgO	47.73	47.66	47.87	47.58	47.97	51.72	51.79	51.39	46.44	47.02	46.63	46.05
FeO	11.64	11.73	11.71	12.02	11.84	5.87	5.98	5.74	11.89	11.71	12.05	13.01
NiO	0.30	0.28	0.30	0.30	0.33	0.36	0.33	0.34	0.37	0.38	0.36	0.30
MnO	0.19	0.18	0.17	0.20	0.19	0.11	0.12	0.13	0.20	0.20	0.19	0.22
Al_2O_3	0.02	0.02	0.03	0.03	0.02	0.03	0.07	0.05	0.06	0.09	0.07	0.03
CaO	0.03	0.06	0.06	0.07	0.06	0.09	0.12	0.08	0.08	0.05	0.08	0.06
Total	99.55	100.62	99.78	100.05	99.66	99.26	99.36	98.71	98.92	99.74	99.50	100.58
Fo	87.94	87.87	87.95	87.61	87.83	94.02	93.94	94.11	87.45	87.74	87.34	86.31
Fa	12.06	12.13	12.05	12.39	12.17	5.98	6.06	5.89	12.55	12.26	12.66	13.69

Olivines

Locality	AG297			AG1		AG173		AG152	AG291B		
Sample	bR	cC	cR	aC	bC	aC	bC	aC	aC	bC	bR
SiO_2	36.73	37.82	38.02	41.23	41.58	40.91	40.86	38.71	40.20	40.32	40.72
MgO	36.19	36.61	36.96	50.11	50.07	47.67	47.51	44.40	46.30	46.87	46.73
FeO	23.89	24.62	24.30	7.60	7.65	11.48	11.24	15.27	13.10	12.77	12.72
NiO	0.19	0.24	0.27	0.33	0.34	0.40	0.41	0.31	0.36	0.34	0.34
MnO	0.37	0.40	0.40	0.18	0.24	0.21	0.21	0.28	0.25	0.23	0.23
$Al2O_3$	0.04	0.05	0.07	0.02	0.02	0.03	0.01	0.05	0.03	0.05	0.05
CaO	0.03	0.04	0.03	0.10	0.07	0.05	0.04	0.07	0.04	0.02	0.07
Total	97.44	99.78	100.05	99.57	99.97	100.75	100.28	99.10	100.28	100.60	100.86
Fo	72.97	72.59	73.06	92.16	92.12	88.07	88.30	83.84	86.31	86.74	86.75
Fa	17.03	17.41	16.94	7.84	7.88	11.93	11.70	16.16	13.69	13.26	13.25

	AG181C		AG160		AG119				AG143F		AG152
Sample	aC	bC	aC	bC	aC	aR	bC	bR	aC	aR	bC
SiO_2	40.67	40.32	40.13	40.35	40.22	40.04	40.17	40.32	39.97	39.81	39.56
MgO	48.69	48.38	49.39	49.25	47.00	47.91	47.75	47.37	46.79	46.45	46.14
FeO	10.89	10.71	10.03	9.78	11.78	11.25	11.25	11.18	12.88	12.78	12.86
NiO	0.33	0.37	0.33	0.33	0.33	0.32	0.35	0.30	0.27	0.26	0.27
MnO	0.19	0.16	0.17	0.15	0.17	0.19	0.17	0.19	0.21	0.18	0.22
Al_2O_3	0.04	0.02	0.03	0.03	0.12	0.03	0.02	0.01	0.03	0.05	0.02
CaO	0.05	0.04	0.04	0.06	0.43	0.08	0.05	0.09	0.06	0.08	0.05
Total	100.86	100.00	100.12	99.87	100.05	99.82	99.76	99.46	100.21	99.53	99.12
Fo	88.84	88.86	89.78	89.98	87.68	87.88	88.33	88.31	86.61	86.63	86.49
Fa	11.16	11.14	10.22	10.02	12.32	12.12	11.67	11.69	13.39	13.37	13.51

Locality	AG152			AG178						AG181A		
Sample	bC	cC	cR	aC	aR	bC	cC	dC	eC	aC	aR	bC
SiO_2	39.29	39.08	39.89	39.62	39.64	39.34	39.84	39.77	39.98	40.84	40.35	40.26
MgO	45.44	44.93	44.80	46.09	45.91	46.32	46.86	46.84	46.89	48.04	45.57	47.90
FeO	14.14	14.57	13.97	12.08	13.54	12.97	12.17	12.14	12.15	11.19	10.80	11.22
NiO	0.31	0.34	0.35	0.34	0.36	0.34	0.32	0.35	0.33	0.41	0.36	0.36
MnO	0.26	0.23	0.23	0.19	0.24	0.24	0.19	0.20	0.20	0.22	0.17	0.18
Al_2O_3	0.08	0.05	0.05	0.02	0.05	0.07	0.03	0.04	0.02	0.04	0.38	0.03
CaO	0.09	0.08	0.09	0.03	0.07	0.09	0.04	0.04	0.03	0.04	0.78	0.02
Total	99.61	99.28	99.38	98.37	99.82	99.37	99.45	99.38	99.60	100.78	98.41	99.97
Fo	85.13	84.59	85.11	87.17	85.79	86.40	87.29	87.29	87.31	88.45	88.28	88.38
Fa	14.87	15.41	14.89	12.83	14.21	13.60	12.71	12.71	12.69	11.55	11.72	11.62

Olivines

Locality	AG181B						AG5				AG143P	
Sample	cC	cR	dC	dR	eC	fC	aC	bC	cC	dC	aC	aR
SiO_2	40.43	40.14	40.42	39.85	40.10	40.28	40.17	40.55	40.44	40.53	39.72	39.64
MgO	48.22	48.08	47.71	47.70	47.99	47.84	47.30	47.89	48.27	47.43	46.42	46.68
FeO	11.30	11.15	11.07	10.95	11.09	11.32	10.88	10.30	10.27	11.19	12.84	12.79
NiO	0.37	0.37	0.36	0.37	0.34	0.34	0.41	0.39	0.42	0.39	0.35	0.33
MnO	0.19	0.20	0.16	0.21	0.18	0.18	0.17	0.19	0.18	0.19	0.22	0.22
Al_2O_3	0.04	0.05	0.04	0.07	0.02	0.01	0.10	0.02	0.05	0.01	0.02	0.06
CaO	0.03	0.07	0.04	0.12	0.02	0.04	0.33	0.06	0.09	0.06	0.04	0.08
Total	100.58	100.06	99.80	99.27	99.74	99.99	99.36	99.40	99.72	99.80	99.61	99.80
Fo	88.39	88.51	88.48	88.59	88.51	88.28	88.57	89.24	89.33	88.29	86.54	86.68
Fa	11.61	11.49	11.52	11.41	11.49	11.72	11.43	10.76	10.67	11.71	13.46	13.32

Locality	AG175				AG245			AG192				AG143P
Sample	aC	bC	bR	cC	aC	aR	bC	aC	aR	bC	bR	bC
SiO_2	40.38	40.17	40.43	40.13	40.70	40.58	40.72	40.44	40.41	40.53	40.64	39.41
MgO	49.51	49.93	50.17	50.04	47.57	47.01	46.90	46.81	46.37	46.92	47.14	46.63
FeO	8.68	8.67	8.42	8.58	11.33	11.12	11.39	11.56	11.86	11.38	11.45	12.92
NiO	0.41	0.39	0.41	0.42	0.31	0.37	0.30	0.36	0.36	0.35	0.36	0.33
MnO	0.15	0.12	0.15	0.15	0.19	0.16	0.18	0.18	0.20	0.19	0.19	0.22
Al_2O_3	0.02	0.04	0.02	0.03	0.04	0.04	0.02	0.18	0.06	0.03	0.08	0.03
CaO	0.05	0.04	0.06	0.08	0.03	0.05	0.06	0.05	0.04	0.05	0.08	0.07
Total	99.20	99.39	99.66	99.43	100.19	99.33	99.57	99.58	99.30	99.45	99.93	99.61
Fo	91.04	91.14	91.37	91.20	88.19	88.28	88.01	87.83	87.46	88.04	87.99	86.52
Fa	8.96	8.86	8.63	8.80	11.81	11.72	11.99	12.17	12.54	11.96	12.01	13.48

Locality	AG295						AG277				AG186	
Sample	aC	bC	bR	cC	cR	dC	aC	aR	bC	cC	aC	aR
SiO_2	39.09	39.45	39.51	39.17	39.03	39.37	39.33	39.39	39.99	40.18	40.93	41.02
MgO	45.16	45.35	45.28	45.16	44.96	45.52	47.87	48.50	47.97	47.93	48.41	48.88
FeO	14.44	14.49	14.61	15.19	15.03	15.03	11.58	11.52	11.41	11.40	10.07	9.91
NiO	0.31	0.28	0.32	0.37	0.33	0.28	0.31	0.33	0.32	0.29	0.32	0.32
MnO	0.26	0.24	0.26	0.24	0.26	0.26	0.18	0.17	0.18	0.18	0.16	0.17
Al_2O_3	0.38	0.06	0.05	0.05	0.08	0.02	0.04	0.05	0.04	0.05	0.05	0.03
CaO	0.10	0.10	0.09	0.05	0.09	0.05	0.04	0.10	0.04	0.04	0.10	0.10
Total	99.74	99.97	100.12	100.23	99.78	100.53	99.35	100.06	99.95	100.07	100.04	100.43
Fo	84.79	84.82	84.66	84.10	84.18	84.36	88.04	88.23	88.24	88.21	89.53	89.58
Fa	15.21	15.18	15.34	15.90	15.82	15.64	11.96	11.77	11.76	11.79	10.47	10.42

Olivines

Locality	AG323				AG312	
Sample	bC	dC	eC	fC	aC	bC
SiO_2	40.79	40.78	40.60	40.32	39.10	39.64
MgO	46.34	47.27	46.25	46.35	42.53	43.38
FeO	12.85	12.48	12.27	12.72	17.09	15.72
NiO	0.28	0.23	0.25	0.26	0.17	0.16
MnO	0.21	0.24	0.18	0.23	0.25	0.28
Al_2O_3	0.03	-	0.04	0.03	0.05	0.05
CaO	0.04	0.06	0.09	0.07	0.05	0.04
Total	100.54	101.06	99.68	99.97	99.23	99.27
Fo	86.31	87.11	87.05	86.68	81.58	83.09
Fa	13.69	12.89	12.95	13.32	18.42	16.91

Feldspars

Feldspars

Locality	AG240					
Sample	aC	aR	bC	bR	cI	dI
SiO_2	47.71	47.48	46.72	47.59	46.85	47.89
Al_2O_3	33.66	33.87	34.26	34.49	34.02	33.89
FeO	0.51	0.44	0.49	0.48	0.51	0.50
MgO	0.02	0.01	0.02	0.02	-	0.03
CaO	17.36	17.46	18.44	18.07	18.05	17.91
Na_2O	1.50	1.49	1.00	1.24	1.23	1.46
K_2O	0.09	0.05	0.04	0.03	0.04	0.07
BaO	-	-	-	0.01	-	-
Total	100.25	100.80	100.97	101.93	100.70	101.75
An	86.00	86.39	90.90	88.82	88.79	86.79
Ab	13.44	13.34	8.89	11.03	10.96	12.79
Or	0.56	0.28	0.21	0.15	0.25	0.42

Locality	AG291B				AG291A				AG287			AG249
Sample	aI	bI	cI	dI	aI	bI	cI	dI	aI	bI	cI	aI
SiO_2	48.97	49.44	49.51	47.69	47.07	47.67	48.10	47.51	50.46	51.80	52.34	47.13
Al_2O_3	33.31	32.40	32.56	33.18	33.31	32.75	32.96	33.29	31.17	30.44	29.88	34.10
FeO	0.30	0.31	0.31	0.29	0.31	0.29	0.32	0.33	0.58	0.40	0.67	0.38
MgO	0.03	0.06	0.01	0.02	0.01	0.02	0.02	0.02	0.03	0.04	0.03	0.01
CaO	16.62	16.09	15.97	16.20	16.75	16.23	16.32	16.74	14.48	13.40	12.70	17.36
Na_2O	2.07	2.16	2.23	2.25	1.99	2.21	2.10	1.95	3.10	3.60	3.87	1.61
K_2O	0.04	0.05	0.04	0.05	0.02	0.02	0.02	0.02	0.17	0.26	0.19	0.04
BaO	-	-	-	-	0.02	-	-	-	-	-	0.01	-
Total	101.34	100.51	100.63	99.68	99.48	99.19	99.84	99.86	99.99	99.94	99.69	100.63
An	81.37	80.21	79.65	79.65	82.17	80.15	81.06	82.45	71.34	66.24	63.73	85.43
Ab	18.40	19.48	20.14	20.05	17.33	19.75	18.84	17.40	27.68	32.26	35.17	14.35
Or	0.23	0.31	0.21	0.30	0.10	0.10	0.10	0.15	0.98	1.50	1.10	0.22

Feldspars

Locality	AG266B				AG277			AG192				AG245
Sample	dR	aI	bI	cI	aI	bI	cI	aI	bI	cI	dI	aI
SiO_2	46.28	45.68	46.46	46.12	46.80	46.10	46.03	45.23	45.98	45.85	45.62	47.43
Al_2O_3	33.90	34.64	34.22	34.04	32.65	33.14	33.18	32.93	33.59	34.16	34.05	32.19
FeO	0.33	0.33	0.37	0.33	0.33	0.35	0.32	0.29	0.31	0.21	0.29	0.29
MgO	0.03	0.03	0.04	0.04	0.13	0.04	0.05	0.05	0.03	0.03	0.03	0.06
CaO	18.06	18.21	17.98	17.74	17.22	17.91	17.91	18.27	17.86	17.85	18.33	16.17
Na_2O	1.31	1.26	1.36	1.31	1.68	1.39	1.39	1.12	1.44	1.35	1.19	2.35
K_2O	0.05	0.07	0.03	0.07	0.07	0.05	0.03	0.06	0.04	0.02	0.04	0.05
BaO	0.02	-	-	-	0.05	0.02	0.02	-	-	-	-	-
Total	99.98	100.22	100.46	99.65	98.93	99.00	98.93	97.95	99.25	99.47	99.55	98.54
An	8.16	88.60	87.80	87.85	84.70	87.39	87.52	89.67	87.05	87.85	89.24	78.96
Ab	11.54	11.04	12.05	11.75	14.93	12.32	12.31	9.96	12.71	12.00	10.51	20.74
Or	0.30	0.37	0.15	0.40	0.37	0.29	0.17	0.37	0.24	0.15	0.25	0.30

Locality	AG245		AG143P				AG175				AG186	
Sample	bI	cI	aI	bI	cI	dI	aI	bI	cI	dI	aI	bI
SiO_2	48.41	49.07	47.04	46.60	46.53	48.09	47.93	47.95	47.57	46.49	46.32	48.18
Al_2O_3	31.61	31.88	32.94	33.24	33.20	32.32	32.75	32.69	32.63	33.31	34.05	32.93
FeO	0.33	0.30	0.32	0.31	0.34	0.29	0.23	0.26	0.24	0.20	0.19	0.20
MgO	0.03	0.05	0.02	0.07	0.02	0.04	0.03	0.09	0.06	0.02	0.04	0.05
CaO	15.40	15.39	17.37	17.38	17.85	16.47	16.88	17.01	16.65	17.44	17.87	16.42
Na_2O	2.75	2.89	1.66	1.62	1.47	2.24	1.98	1.97	2.08	1.65	1.42	2.14
K_2O	0.02	0.05	0.03	0.04	0.03	0.03	0.01	0.03	0.04	0.02	-	0.01
BaO	-	0.03	0.01	0.03	-	-	-	-	-	0.01	-	-
Total	98.55	99.66	99.39	99.29	99.44	99.48	99.81	100.00	99.27	99.14	99.89	99.93
An	75.51	74.43	85.08	85.39	86.89	80.12	82.40	82.52	81.34	85.25	87.39	80.83
Ab	24.37	25.30	14.75	14.39	12.94	19.71	17.55	17.33	18.42	14.63	12.61	19.21
Or	0.12	0.27	0.17	0.22	0.17	0.17	0.05	0.15	0.25	0.12	-	0.05

Feldspars

Locality	AG261						AG248					
Sample	aI	aC	aR	bI	bC	bR	aC	aR	aI	bC	bR	bI
SiO_2	45.10	46.72	49.50	46.36	46.78	46.17	52.04	53.21	53.08	52.76	53.25	51.87
Al_2O_3	33.92	33.18	31.19	33.29	32.93	32.97	29.72	28.77	28.77	28.94	27.40	30.04
FeO	0.60	0.61	0.78	0.60	0.66	0.59	0.41	0.58	0.61	0.53	0.36	0.60
MgO	0.04	0.03	0.07	0.07	0.04	0.08	0.03	0.04	0.04	0.04	0.10	0.04
CaO	18.29	17.59	15.34	17.64	17.28	17.47	13.39	12.29	12.44	12.63	10.94	13.81
Na_2O	1.10	1.62	2.76	1.53	1.70	1.51	3.81	4.39	4.14	4.19	4.87	3.84
K_2O	0.04	0.06	0.14	0.06	0.06	0.05	0.30	0.20	0.25	0.25	0.25	0.21
BaO	-	-	-	-	-	0.01	-	-	-	-	-	-
Total	99.04	99.81	99.78	99.55	99.45	98.85	99.70	99.48	99.33	99.34	97.17	100.41
An	89.97	85.40	74.84	86.20	84.60	86.27	64.89	73.36	61.47	61.55	54.60	65.71
Ab	9.79	14.26	24.37	13.48	15.03	13.46	33.40	25.86	37.06	36.99	43.95	33.09
Or	0.24	0.34	0.29	0.32	0.37	0.27	1.71	0.78	1.47	1.46	1.45	1.20

Locality	AG266B						AG241					
Sample	aC	bC	bR	cC	cR	dC	aI	bI	bC	bR	cI	dI
SiO_2	45.94	45.50	44.37	45.43	46.34	46.13	47.73	48.67	47.78	47.96	47.52	47.16
Al_2O_3	34.05	34.26	32.68	33.76	33.74	34.09	34.04	33.54	33.45	33.15	33.32	33.89
FeO	0.31	0.29	0.25	0.35	0.34	0.31	0.37	0.39	0.42	0.38	0.47	0.41
MgO	0.03	0.04	0.05	0.05	0.05	0.02	0.04	0.04	0.17	0.02	0.05	0.03
CaO	18.11	18.25	17.08	17.98	17.68	17.99	17.22	16.66	17.07	16.58	16.95	17.37
Na_2O	1.27	1.31	1.66	1.35	1.52	1.37	1.74	2.10	1.75	2.15	1.98	1.63
K_2O	0.03	0.05	0.02	0.03	0.06	0.09	0.05	0.04	0.04	0.05	0.03	0.03
BaO	0.02	-	-	0.01	-	-	-	0.02	-	-	-	-
Total	99.76	99.70	96.11	98.96	99.73	100.00	101.89	101.46	100.68	100.29	100.32	100.52
An	88.59	88.23	84.94	87.85	86.22	87.41	84.34	81.18	84.12	80.74	82.38	85.34
Ab	11.21	11.50	14.94	11.95	13.44	12.05	15.38	18.57	15.63	18.96	17.42	14.51
Or	0.20	0.27	0.12	0.20	0.34	0.54	0.28	0.25	0.25	0.30	0.20	0.15

Feldspars

Locality	AG181B			AG5								AG244
Sample	aI	bI	cI	aI	bI	cI	dI	eI	fI	gI	hI	aI
SiO_2	45.24	45.00	46.67	47.65	46.76	45.16	46.15	46.48	46.37	46.58	46.42	48.31
Al_2O_3	34.55	34.16	34.09	33.00	33.29	34.23	34.13	33.78	33.43	33.57	33.78	32.75
FeO	0.29	0.32	0.26	0.19	0.21	0.34	0.31	0.20	0.22	0.18	0.30	0.24
MgO	0.02	0.02	0.03	0.04	0.02	0.04	0.05	0.03	0.03	0.02	0.03	0.04
CaO	18.54	18.54	18.03	16.74	17.31	18.51	18.18	18.39	18.14	18.20	18.74	16.29
Na_2O	1.12	1.20	1.57	2.16	1.85	1.24	1.30	1.29	1.36	1.39	1.21	2.22
K_2O	0.02	0.01	0.01	0.04	0.02	0.01	0.03	0.02	0.02	0.02	0.01	0.01
BaO	0.01	-	-	-	-	-	-	0.03	-	0.01	0.02	-
Total	99.79	99.25	100.66	99.82	99.46	99.53	100.15	100.27	99.57	99.97	100.51	99.86
An	90.08	89.47	86.36	80.92	83.64	89.10	88.40	88.63	87.92	87.82	89.44	80.20
Ab	9.82	10.46	13.57	18.86	16.21	10.83	11.43	11.27	11.98	12.08	10.49	19.75
Or	0.10	0.07	0.07	0.22	0.15	0.07	0.17	0.10	0.10	0.10	0.07	0.05

Locality	AG244	AG186		AG297								
Sample	bI	aI	bI	aC	aR	bC	bR	aI	bI	cC	cR	cI
SiO_2	48.40	46.32	48.18	45.41	47.81	45.47	48.49	46.38	49.18	47.53	48.46	47.92
Al_2O_3	32.59	34.05	32.93	33.45	31.68	33.35	32.11	33.55	31.74	32.68	32.15	32.17
FeO	0.30	0.19	0.20	0.53	0.55	0.53	0.53	0.53	0.57	0.50	0.57	0.63
MgO	0.04	0.04	0.05	0.03	0.05	0.04	0.09	0.02	0.05	0.06	0.05	0.07
CaO	16.09	17.87	16.42	17.89	16.10	17.68	15.91	17.68	15.62	16.73	16.08	16.41
Na_2O	2.41	1.42	2.14	1.38	2.32	1.32	2.27	1.44	2.68	1.87	2.31	2.20
K_2O	0.04	-	0.01	0.07	0.12	0.08	0.12	0.08	0.16	0.11	0.11	0.11
BaO	-	-	-	0.01	0.02	-	-	0.02	0.01	0.03	0.01	-
Total	99.87	99.89	99.93	98.77	98.65	98.47	99.52	99.70	100.01	99.51	99.74	99.51
An	78.49	87.39	80.83	87.41	78.77	87.68	78.92	86.80	75.59	82.62	78.88	80.00
Ab	21.26	12.61	19.21	12.18	20.54	11.88	20.38	12.75	23.47	16.73	20.47	19.37
Or	0.25	-	0.05	0.41	0.69	0.44	0.70	0.45	0.94	0.65	0.65	0.63

Feldspars

Locality	AG249							AG190C				
Sample	bI	cI	dI	eI	fI	gI	hI	aI	bI	cI	dI	eI
SiO_2	50.75	45.71	46.47	46.02	46.19	46.13	46.22	47.66	50.08	47.10	47.88	47.98
Al_2O_3	29.74	33.26	33.41	33.16	33.15	32.86	33.44	32.50	31.53	31.80	31.91	32.28
FeO	0.37	0.42	0.28	0.42	0.40	0.40	0.34	0.57	0.56	0.60	0.61	0.56
MgO	0.02	0.01	0.02	0.03	0.01	0.03	0.03	0.03	0.06	0.04	0.06	0.06
CaO	13.64	17.61	17.52	17.67	17.18	17.54	17.41	16.40	15.47	16.04	16.16	16.36
Na_2O	3.72	1.48	1.61	1.51	1.64	1.54	1.56	2.22	2.81	2.23	2.34	2.25
K_2O	0.13	0.03	0.02	0.04	0.04	0.02	0.03	0.03	0.07	0.02	0.01	0.07
BaO-	-	-	-	-	-	-	-	0.02	-	-	-	-
Total	98.37	98.52	99.33	98.85	98.65	98.52	99.03	99.43	100.58	97.83	98.97	99.56
An	66.43	86.64	85.59	86.45	85.01	86.16	85.86	80.18	74.92	79.84	79.20	79.72
Ab	32.81	13.19	14.26	13.33	14.74	13.72	13.94	19.64	24.66	20.06	20.75	19.86
Or	0.76	0.17	0.15	0.22	0.25	0.12	0.20	0.17	0.42	0.10	0.05	0.42

Locality	AG190C		AG295			AG277		AG178B		AG152		AG119
Sample	bI	cI	aI	bI	cI	aI	bI	aI	bI	aI	bI	aI
SiO_2	48.22	47.30	46.76	46.52	47.03	46.27	46.11	46.77	48.09	50.20	48.91	45.07
Al_2O_3	31.63	32.48	33.52	33.40	32.74	34.12	34.12	33.40	32.03	31.77	31.54	34.84
FeO	0.57	0.59	0.41	0.47	0.47	0.39	0.39	0.23	0.47	0.55	0.52	0.29
MgO	0.05	0.07	0.06	0.05	0.02	0.06	0.07	0.03	0.04	0.06	0.06	0.04
CaO	15.75	16.44	17.65	17.53	17.10	18.13	18.27	16.66	15.88	14.77	15.70	18.79
Na_2O	2.58	2.30	1.70	1.77	1.86	1.29	1.27	2.18	2.56	3.15	2.65	0.88
K_2O	0.02	0.01	0.03	0.08	0.08	0.05	0.07	0.04	0.07	0.16	0.10	0.02
BaO	-	-	-	-	0.02	-	0.02	-	-	-	-	-
Total	98.82	99.19	100.13	99.82	99.32	100.31	100.32	99.31	99.14	100.66	99.48	99.93
An	77.06	79.77	85.03	84.17	83.19	88.35	88.46	80.67	77.05	71.50	76.15	92.11
Ab	22.82	20.18	14.80	15.40	16.37	11.35	11.15	19.08	22.53	27.58	23.26	7.77
Or	0.12	0.05	0.17	0.43	0.44	0.30	0.39	0.25	0.42	0.92	0.59	0.12

Feldspars

Locality	AG119				AG143F					AG160		AG181C
Sample	bI	cI	dI	eI	aC	aR	bR	bC	aI	aI	bI	aI
SiO_2	45.40	45.69	45.76	45.28	45.90	45.52	46.31	45.47	45.58	46.37	48.38	46.53
Al_2O_3	34.24	34.15	34.72	34.32	33.88	34.67	33.34	33.67	33.59	33.53	32.18	33.33
FeO	0.27	0.32	0.32	0.33	0.51	0.41	0.43	0.40	0.43	0.31	0.25	0.33
MgO	0.04	0.03	0.04	0.07	0.06	0.04	0.07	0.14	0.08	0.03	0.03	0.03
CaO	18.34	18.46	18.72	18.68	17.97	18.67	17.90	18.28	17.89	17.61	15.98	17.66
Na_2O	1.19	1.16	1.08	1.12	1.36	1.05	1.39	1.24	1.43	1.58	2.56	1.56
K_2O	0.06	0.05	0.04	0.03	0.05	0.04	0.05	0.04	0.05	0.01	0.02	0.01
BaO	0.01	0.01	0.01	0.02	0.03	-	-	0.01	-	0.01	-	-
Total	99.55	99.87	100.69	99.85	99.76	100.40	99.49	99.25	99.05	99.45	99.40	99.45
An	89.12	89.53	90.36	90.06	86.68	90.58	87.41	88.85	87.13	85.94	77.40	86.18
Ab	10.51	10.18	9.42	9.77	12.00	9.20	12.29	10.94	12.58	13.99	22.45	13.75
Or	0.37	0.29	0.22	0.17	0.32	0.22	0.30	0.21	0.29	0.07	0.15	0.07

Locality	AG181C		AG1			AG173		AG255		AG254		
Sample	bI	cI	aI	bI	cI	aI	bI	aI	bI	aI	bI	cI
SiO_2	46.11	45.53	46.71	46.06	47.01	46.45	46.39	46.41	47.34	47.93	47.68	46.62
Al_2O_3	33.88	34.00	33.92	33.58	33.27	33.81	34.06	33.28	32.77	32.38	32.76	33.36
FeO	0.30	0.28	0.16	0.15	0.13	0.19	0.14	0.25	0.26	0.23	0.18	0.15
MgO	0.19	0.01	0.03	0.03	0.04	0.04	0.03	0.03	0.03	0.17	0.08	0.04
CaO	18.03	18.29	17.66	17.91	17.34	17.75	17.86	17.10	17.01	16.25	16.08	17.19
Na_2O	1.32	1.28	1.43	1.38	1.63	1.54	1.41	1.93	1.82	2.31	2.46	1.76
K_2O	0.04	0.01	0.01	0.02	0.01	0.01	0.03	0.03	0.04	0.01	0.01	0.01
BaO	-	0.01	0.01	-	0.01	-	0.01	0.01	-	-	-	-
Total	99.87	99.41	99.93	99.13	99.44	99.79	99.93	99.04	99.27	99.28	99.20	99.13
An	88.10	88.67	87.16	87.64	85.36	86.39	87.34	82.94	83.62	79.49	78.27	84.30
Ab	11.68	11.25	12.79	12.24	14.57	13.54	12.51	16.89	16.33	20.46	21.66	15.65
Or	0.22	0.08	0.05	0.12	0.07	0.07	0.15	0.17	0.05	0.05	0.07	0.05

Feldspars

Locality	AG244			AG320								
Sample	cI	dI	eI	aI	bI	cI	dI	eI	fI	gI	hI	jI
SiO_2	47.97	48.01	48.39	46.21	45.73	46.13	45.92	45.01	46.02	45.57	46.30	46.40
Al_2O_3	33.36	33.41	33.24	34.68	34.29	34.17	34.24	34.21	34.58	34.78	34.64	34.17
FeO	0.55	0.34	0.33	0.27	0.34	0.37	0.28	0.34	0.41	0.28	0.38	0.29
MgO	0.20	0.08	0.05	0.06	0.17	0.21	0.06	0.14	0.44	0.06	0.18	0.05
CaO	15.86	16.09	15.72	17.49	17.67	17.41	17.24	17.14	17.35	17.85	17.40	17.08
Na_2O	2.36	2.51	2.47	1.59	1.64	1.58	1.71	1.79	1.58	1.55	1.65	1.88
K_2O	0.06	0.08	0.04	0.03	0.02	0.01	0.03	0.02	0.04	0.03	0.03	0.07
BaO	0.01	-	-	-	0.01	-	-	-	-	0.02	-	-
Total	100.37	100.52	100.24	100.33	99.87	99.88	99.48	98.65	100.42	100.14	100.58	99.94
An	78.50	77.61	77.69	85.72	85.48	84.65	84.65	83.99	85.69	86.23	85.20	83.00
Ab	21.15	21.89	22.06	14.11	14.37	14.14	15.17	15.89	14.08	13.57	14.60	16.58
Or	0.35	0.50	0.25	0.17	0.15	1.21	0.18	0.12	0.23	0.20	0.20	0.42

Locality	AG316						AG314					
Sample	aC	aR	aI	bC	bR	cC	aC	aR	bC	bR	aI	bI
SiO_2	48.08	49.45	48.18	48.09	50.24	48.15	46.88	47.38	46.53	46.77	46.80	46.80
Al_2O_3	32.14	31.26	31.81	32.02	30.88	32.07	33.41	32.97	33.73	32.72	33.33	33.08
FeO	0.37	0.35	0.35	0.34	0.33	0.39	0.51	0.46	0.51	0.50	0.44	0.56
MgO	0.06	0.06	0.07	0.05	0.10	0.08	0.06	0.07	0.07	0.06	0.06	0.06
CaO	16.23	15.06	15.43	15.65	14.27	15.69	17.55	17.26	18.11	17.23	17.49	17.10
Na_2O	2.46	3.17	2.81	2.55	3.44	2.69	1.44	1.70	1.18	1.70	1.56	1.76
K_2O	0.11	0.10	0.08	0.15	0.15	0.13	0.08	0.07	0.07	0.07	0.05	0.12
BaO	-	-	-	-	-	-	-	-	-	-	-	-
Total	99.45	99.45	98.23	98.85	99.41	99.20	99.93	99.91	100.20	99.05	99.73	99.48
An	78.02	71.97	74.84	76.57	69.00	75.76	86.65	84.50	89.12	84.50	85.81	83.68
Ab	21.37	27.45	24.67	22.59	30.14	23.51	12.90	15.08	10.48	15.11	13.89	15.63
Or	0.61	0.58	0.49	0.84	0.86	0.73	0.45	0.42	0.40	0.39	0.30	0.69

Feldspars

Locality	AG315				AG323							
Sample	aC	aR	bC	bR	aC	aR	bC	bR	cC	cR	dC	dR
SiO_2	48.02	49.07	47.12	48.34	47.15	49.12	46.56	46.47	47.04	48.51	47.27	47.65
Al_2O_3	32.92	31.84	33.11	32.39	33.61	32.46	33.78	34.18	33.13	33.36	33.92	32.51
FeO	0.47	0.59	0.50	0.49	0.33	0.39	0.37	0.50	0.34	0.40	0.36	0.26
MgO	0.04	0.09	0.05	0.09	0.08	0.06	0.06	0.27	0.08	0.07	0.11	0.15
CaO	16.73	15.84	17.40	16.51	17.51	16.13	18.01	17.60	17.28	16.06	17.21	15.96
Na_2O	1.80	2.52	1.69	2.07	1.62	2.46	1.30	1.36	1.75	2.40	1.59	2.76
K_2O	0.05	0.12	0.08	0.06	0.04	-	0.03	-	0.03	0.02	0.03	0.01
BaO												
Total	100.03	100.07	99.95	99.95	100.36	100.62	100.11	100.30	99.65	100.82	100.49	99.30
An	83.45	77.09	84.66	81.20	85.49	78.39	88.28	87.76	84.35	78.65	85.49	76.16
Ab	16.27	21.33	14.90	18.45	14.29	21.61	11.53	12.24	15.45	21.23	14.33	23.81
Or	0.28	1.58	0.44	0.35	0.22	-	0.19	-	0.20	0.12	0.18	0.03

Locality	AG312				AG318							
Sample	aR	aC	bC	bR	aC	aR	bC	bR	cC	cR	dC	dR
SiO_2	46.83	46.55	47.64	46.97	47.39	48.52	48.31	47.73	46.95	47.53	48.17	47.98
Al_2O_3	34.20	34.12	33.55	33.32	32.99	32.96	32.73	32.87	33.54	33.24	33.09	32.91
FeO	0.46	0.33	0.53	0.53	0.31	0.35	0.35	0.34	0.32	0.37	0.35	0.33
MgO	0.17	0.04	0.05	0.13	0.06	0.05	0.05	0.05	0.07	0.05	0.07	0.04
CaO	17.10	16.75	15.70	16.05	17.13	16.63	16.56	16.87	17.79	17.20	16.88	16.64
Na_2O	1.84	1.89	2.45	2.22	1.89	2.15	2.04	2.01	1.55	1.74	1.84	2.24
K_2O	0.02	0.02	0.03	0.06	0.04	0.01	-	0.01	0.03	0.03	0.04	-
BaO	-	-	0.02	0.01	-	-	-	-	-	-	-	-
Total	100.62	99.70	99.97	99.29	99.81	100.67	100.04	99.88	100.25	100.16	100.44	100.14
An	83.57	82.96	77.86	79.69	83.15	81.00	81.80	82.28	86.26	84.32	83.29	81.08
Ab	16.31	16.94	21.99	19.93	16.60	18.93	18.20	17.70	13.59	15.48	16.48	18.92
Or	0.12	0.10	0.15	0.38	0.25	0.07	-	0.02	0.15	0.02	0.23	-

Feldspars

Locality	AG157			AG181A			AG245A					AG158
Sample	a I	bI	cI	a I	bI	cI	aC	aR	a I	bC	bI	a I
SiO_2	45.93	46.31	55.56	45.78	45.42	45.16	46.90	46.50	46.73	47.72	46.00	46.82
Al_2O_3	34.10	33.94	27.54	34.67	33.86	34.50	32.73	33.05	32.82	31.23	33.36	33.05
FeO	0.13	0.22	0.12	0.26	0.21	0.17	0.40	0.48	0.29	0.57	0.41	0.28
MgO	0.03	0.03	0.03	0.01	0.03	-	0.01	0.07	0.03	0.39	0.06	0.05
CaO	17.72	17.62	9.99	18.37	18.13	18.13	17.32	17.68	17.61	16.80	18.12	17.56
Na_2O	1.43	1.39	5.75	1.09	1.28	1.20	1.77	1.61	1.68	2.31	1.35	1.63
K_2O	0.01	0.02	0.02	0.01	0.03	0.02	0.05	0.04	0.02	0.04	0.06	0.05
BaO	-	-	-	-	-	-	0.03	-	0.01	0.04	-	0.01
Total	99.35	99.53	99.01	100.19	98.96	99.18	99.21	99.43	99.18	99.10	99.36	99.45
An	87.17	87.34	48.88	90.19	88.55	89.25	84.13	85.69	86.50	79.93	87.81	85.32
Ab	12.78	12.51	50.97	9.73	11.27	10.65	15.57	14.09	13.18	19.86	11.85	14.35
Or	0.05	0.15	0.15	0.07	0.17	0.10	0.30	0.22	0.32	0.21	0.34	0.33

Locality	AG158		AG245				AG2			AG181A		
Sample	bI	cI	aC	aR	bC	bR	a I	bI	cI	a I	bI	cI
SiO_2	47.64	46.54	46.32	46.39	47.55	46.49	45.84	46.33	46.02	45.53	45.86	45.43
Al_2O_3	32.99	33.54	33.13	33.54	32.64	32.85	33.66	33.86	33.84	33.89	33.65	33.86
FeO	0.26	0.22	0.47	0.46	0.50	0.44	0.10	0.18	0.23	0.22	0.19	0.18
MgO	0.06	0.07	0.02	0.05	0.07	0.12	0.03	0.05	0.08	0.03	0.07	0.03
CaO	17.43	17.75	17.60	17.88	17.38	17.46	18.09	18.15	18.12	18.31	18.04	18.24
Na_2O	1.73	1.52	1.50	1.45	1.70	1.61	1.45	1.26	1.33	1.29	1.41	1.32
K_2O	0.03	0.04	0.03	0.04	0.07	0.06	0.02	0.02	0.02	0.02	0.02	0.02
BaO	-	-	-	0.01	-	-	0.01	-	-	-	0.02	-
Total	100.14	99.68	99.07	99.82	99.81	99.03	99.20	99.85	99.64	99.29	99.26	99.08
An	87.01	84.62	85.41	87.24	88.73	88.13	87.24	88.72	88.13	88.54	87.46	88.27
Ab	84.62	86.36	14.25	12.64	11.15	11.75	12.64	11.15	11.75	11.33	12.42	11.61
Or	0.20	0.25	0.34	0.12	0.12	0.12	0.02	0.13	0.12	0.12	0.12	0.12

Feldspars

Locality	AG190B										AG241	
Sample	aI	bI	cI	dI	eI	fI	aC	aR	gI	hI	aC	aR
SiO_2	46.91	47.40	46.52	45.69	46.36	47.64	47.03	47.57	46.44	46.72	47.96	48.24
Al_2O_3	33.53	35.61	32.75	33.15	33.78	33.23	33.75	32.65	33.46	34.05	32.91	33.17
FeO	0.46	0.45	0.40	0.45	0.47	0.46	0.46	0.52	0.45	0.49	0.35	0.48
MgO	0.06	0.03	0.06	0.03	0.04	0.10	0.08	0.03	0.05	0.03	0.09	0.06
CaO	17.47	18.17	17.11	17.51	17.72	16.97	17.46	16.72	17.66	17.81	16.64	16.83
Na_2O	1.86	1.53	1.75	1.49	1.42	1.90	1.63	2.13	1.63	1.44	2.18	1.98
K_2O	0.03	0.02	0.01	0.01	0.01	0.04	0.04	0.02	0.02	0.01	0.01	0.02
BaO	-	0.12	0.01	-	-	-	-	0.02	-	-	-	-
Total	100.32	103.23	98.61	98.33	99.80	100.34	100.45	99.66	99.71	100.55	100.14	100.78
An	83.70	86.71	84.35	86.61	87.24	82.29	85.37	81.18	85.55	87.21	80.76	82.36
Ab	16.11	13.17	15.58	13.29	12.69	16.79	14.39	18.72	14.30	12.72	19.17	17.51
Or	0.19	0.12	0.07	0.10	0.07	0.22	0.24	0.10	0.15	0.07	0.07	0.13

Locality	CS036											
Sample	PCl	PRl	PCm	PCn	PCo	PRo	PCp	PRp	PCq	PCr	PCs	PRs
SiO_2	45.66	49.33	45.69	45.35	45.24	45.34	45.48	46.76	46.03	45.87	46.08	46.22
Al_2O_3	33.37	30.78	33.63	33.39	33.56	33.53	33.67	32.38	33.26	33.30	33.15	32.97
FeO	0.42	0.71	0.42	0.49	0.42	0.42	0.41	0.43	0.44	0.42	0.43	0.44
MgO	0.23	0.27	0.25	0.22	0.20	0.20	0.20	0.27	0.23	0.24	0.25	0.24
CaO	18.23	15.48	18.07	18.42	18.41	18.30	18.47	17.34	17.86	18.15	17.83	17.67
Na_2O	1.42	3.08	1.45	1.33	1.24	1.33	1.30	1.94	1.51	1.42	1.58	1.72
K_2O	0.02	0.04	-	0.01	0.01	0.02	0.02	0.02	0.01	0.03	0.03	0.01
BaO	0.01	0.03	0.05	0.05	0.01	0.06	0.02	-	-	-	-	0.07
Total	99.38	99.78	99.58	99.29	99.12	99.22	99.58	99.17	99.42	99.47	99.39	99.39
An	87.53	73.33	87.30	88.38	89.05	88.31	88.62	83.08	86.50	87.50	86.04	85.95
Ab	12.37	26.43	12.68	11.56	10.89	11.60	11.27	16.79	13.42	12.36	13.79	14.99
Or	0.10	0.24	0.02	0.06	0.06	0.09	0.11	0.13	0.08	0.14	0.17	0.06

Feldspars

Locality	CS028				CS069							
Sample	PCe	PRe	PCf	PRf	Ga	Gb	Gc	PCa	PCb	PCc	PRc	PCd
SiO_2	51.90	52.53	46.70	47.56	46.77	52.26	50.53	45.98	46.45	46.75	51.62	47.76
Al_2O_3	28.48	28.80	32.52	30.88	32.81	29.27	31.18	33.61	32.84	33.48	29.06	32.27
FeO	0.79	0.80	0.60	0.70	0.56	0.84	0.70	0.49	0.52	0.49	1.57	0.52
MgO	0.13	0.14	0.14	0.18	0.20	0.13	0.25	0.18	0.19	0.18	0.43	0.23
CaO	12.72	12.89	17.09	15.78	17.17	12.93	14.91	17.93	17.52	17.52	12.98	16.77
Na_2O	4.27	4.34	1.86	2.47	1.80	4.36	3.20	1.42	1.77	1.70	4.26	2.21
K_2O	0.10	0.09	0.05	0.07	0.05	0.10	0.06	0.04	0.03	0.04	0.09	0.04
BaO	-	-	-	-	-	-	-	-	-	-	-	-
Total	98.45	99.66	98.98	97.68	99.39	99.94	100.86	99.65	99.34	100.18	100.15	99.84
An	61.87	61.83	83.30	77.56	83.79	61.74	71.73	87.28	84.35	84.83	62.38	80.53
Ab	37.57	37.63	16.41	22.00	15.94	37.70	27.90	12.50	15.46	14.93	37.06	19.25
Or	0.56	0.54	0.29	0.44	0.27	0.56	0.37	0.22	0.19	0.24	0.56	0.22

Locality	CS069											
Sample	PRd	PCe	PCf	PRf	PRe	PCg	PRg	PRh	PCh	PCi	PRi	PRa
SiO_2	52.55	46.51	46.15	45.37	51.10	47.16	49.70	50.04	46.62	46.83	46.86	50.83
Al_2O_3	28.44	33.36	34.00	34.01	30.15	32.83	30.75	30.67	33.22	33.63	33.08	30.06
FeO	0.93	0.54	0.53	0.53	0.81	0.53	0.66	0.69	0.51	0.50	0.54	0.73
MgO	0.13	0.18	0.16	0.14	0.17	0.20	0.22	0.20	0.19	0.20	0.16	0.19
CaO	12.42	17.80	18.03	17.92	14.05	17.06	14.83	14.66	17.57	17.87	17.33	14.10
Na_2O	4.69	1.60	1.41	1.40	3.70	1.93	3.19	3.46	1.69	1.66	1.78	3.83
K_2O	0.10	0.03	0.03	0.04	0.08	0.04	0.06	0.07	0.04	0.05	0.05	0.14
BaO	-	-	-	-	-	-	-	-	-	-	-	-
Total	99.32	100.04	100.34	99.42	100.10	99.79	99.46	99.82	99.87	100.75	99.82	99.91
An	59.07	85.77	87.39	87.39	67.38	82.76	71.71	69.76	84.92	85.33	84.07	66.52
Ab	40.38	14.01	12.41	12.39	32.16	16.99	27.92	29.83	14.84	14.35	15.67	32.71
Or	0.55	00.22	0.20	0.22	0.46	0.25	0.37	0.41	0.24	0.32	0.20	0.77

Feldspars

Locality	CS016					CS028						
Sample	Ga	Gb	PCa	PCb	PRb	Ga	Gb	Gc	Gd	Ge	Gf	Gh
SiO_2	54.90	50.98	45.49	45.89	45.63	50.29	49.33	50.73	50.67	50.28	50.51	49.80
Al_2O_3	27.50	28.50	33.71	33.45	33.48	31.03	30.55	30.61	29.56	29.60	30.58	29.80
FeO	0.92	0.75	0.46	0.49	0.48	0.82	0.75	0.82	0.88	0.88	0.74	0.90
MgO	0.10	0.15	0.15	0.16	0.17	0.53	0.24	0.26	0.17	0.15	0.26	0.26
CaO	10.60	12.92	18.13	17.83	19.78	15.58	15.37	15.33	14.04	13.86	14.43	14.18
Na_2O	5.41	3.91	1.26	1.43	1.33	3.12	2.98	3.40	3.54	3.64	3.31	3.59
K_2O	0.16	0.09	0.02	0.02	0.03	0.08	0.08	0.07	0.08	0.09	0.05	0.09
BaO	-	-	-	-	-	-	-	-	-	-	-	-
Total	99.65	97.36	99.22	99.27	99.12	101.49	99.33	101.27	98.99	98.55	99.91	98.69
An	51.51	64.22	87.80	87.17	88.01	73.09	73.66	71.06	68.36	67.39	70.44	68.22
Ab	47.59	35.18	12.07	12.68	11.79	26.47	25.88	28.54	31.18	32.05	29.26	31.25
Or	0.90	0.57	0.13	0.15	0.20	0.44	0.46	0.41	0.46	0.56	0.30	0.53

Locality	CS028											
Sample	Gi	Gj	Gk	Gl	Gm	PCa	PRa	PCb	PRb	PCc	PRc	PRd
SiO_2	48.95	49.30	51.67	51.92	52.07	45.91	47.26	46.12	46.60	51.54	51.77	49.05
Al_2O_3	30.96	30.90	29.32	29.14	29.21	33.36	32.73	33.05	32.39	29.57	29.19	30.38
FeO	0.64	0.76	0.76	0.79	0.78	0.40	0.52	0.55	0.51	0.79	0.81	0.67
MgO	0.28	0.26	0.14	0.14	0.14	0.20	0.26	0.11	0.22	0.12	0.14	0.24
CaO	15.49	15.35	13.42	13.60	13.41	18.02	17.32	17.50	17.03	13.43	13.12	15.28
Na_2O	2.69	2.92	3.89	3.98	4.10	1.28	1.81	1.59	1.92	3.94	4.13	2.91
K_2O	0.05	0.06	0.08	0.07	0.11	0.02	0.06	0.03	0.04	0.09	0.10	0.07
BaO	-	-	-	-	-	-	-	-	-	-	-	-
Total	99.11	99.58	99.33	99.71	99.86	99.21	99.98	98.98	98.74	99.54	99.32	98.63
An	75.83	74.14	65.28	65.07	63.97	88.43	83.75	85.67	82.89	64.90	63.35	74.04
Ab	23.85	25.52	34.25	34.49	35.40	11.42	15.89	14.13	16.89	34.53	36.08	25.55
Or	0.32	0.34	0.47	0.44	0.63	0.15	0.36	0.20	0.22	0.57	0.57	0.41

Feldspars

Locality	CS011									CS023		
Sample	PRa	PCa	PCb	PCc	PRc	Ga	Gb	PCd	PRd	Ga	Gb	Gc
SiO_2	47.91	46.32	46.49	45.56	50.11	54.01	50.24	45.76	49.00	62.98	53.07	56.10
Al_2O_3	33.48	33.86	34.37	33.65	30.73	28.16	30.72	33.94	31.91	22.82	27.59	26.64
FeO	0.36	0.36	0.37	0.41	0.64	0.94	0.67	0.37	0.60	0.01	0.65	0.44
MgO	0.24	0.23	0.22	0.24	0.27	0.13	0.25	0.21	0.25	0.01	0.11	0.07
CaO	17.47	18.15	18.12	17.96	15.03	11.49	14.81	18.04	15.62	4.03	11.56	9.14
Na_2O	1.51	1.23	1.13	1.31	3.12	4.96	3.23	1.29	2.66	9.42	4.35	6.22
K_2O	0.01	0.01	0.01	0.01	0.02	0.08	0.03	0.01	0.03	0.09	0.16	0.16
BaO	-	-	-	-	-	-	-	-	-	-	-	-
Total	100.99	100.32	100.70	99.13	99.92	99.77	99.96	99.62	100.07	99.36	97.49	98.76
An	86.43	89.01	89.86	88.30	72.59	5.85	71.59	88.48	76.29	19.01	58.90	44.42
Ab	13.55	10.94	10.13	11.68	27.29	43.67	28.24	11.47	23.56	80.50	40.10	54.68
Or	0.02	0.05	0.01	0.02	0.12	0.47	0.17	0.05	0.15	0.49	1.00	0.09

Locality	CS007					CS060			CS038			
Sample	Ga	Gb	Gc	Gd	PCa	PCa	Ga	Gb	PRa	PCa	PCb	Ga
SiO_2	50.85	53.14	53.90	51.20	50.52	47.45	51.40	52.64	53.84	52.15	49.27	53.86
Al_2O_3	29.32	27.78	27.23	29.62	29.81	32.26	29.26	29.12	26.72	24.16	30.62	26.82
FeO	1.16	0.67	0.97	1.05	0.71	0.57	1.12	1.16	0.49	2.70	0.68	1.07
MgO	0.35	0.22	0.11	0.23	0.25	0.20	0.29	0.24	0.08	1.36	0.21	0.13
CaO	14.07	11.84	10.99	13.79	13.86	16.83	13.75	13.19	9.79	11.75	14.53	10.39
Na_2O	3.58	3.34	5.25	3.82	3.60	1.50	3.77	3.12	5.64	4.38	3.05	4.87
K_2O	0.06	2.03	0.09	0.04	0.04	0.01	0.06	0.02	0.21	0.09	0.04	0.11
BaO	-	-	-	-	-	-	-	-	-	-	-	-
Total	98.85	99.02	98.54	99.75	98.80	98.81	99.65	99.49	96.77	96.59	98.40	97.23
An	68.24	58.30	53.37	66.45	67.83	86.13	66.58	69.93	48.34	59.37	72.30	53.77
Ab	31.44	29.79	46.11	33.30	31.92	13.87	33.07	29.91	50.42	40.08	27.45	45.58
Or	0.32	11.91	0.52	0.24	0.25	0.01	0.34	0.16	1.24	0.55	0.25	0.65

Feldspars

Locality	CS036											
Sample	Ga	Gb	Gc	Gd	PCa	PRa	Ge	Gf	Gh	PCb	PRb	PRc
SiO_2	50.11	56.28	50.95	49.66	46.04	49.75	51.48	57.34	53.84	45.67	45.78	50.46
Al_2O_3	29.93	26.05	28.73	29.74	33.32	30.63	30.16	25.64	27.48	33.11	33.32	30.01
FeO	0.78	0.75	0.91	0.90	0.43	0.73	0.80	0.85	1.08	0.50	0.42	0.80
MgO	0.25	0.06	0.20	0.33	0.20	0.30	0.30	0.08	0.12	0.22	0.21	0.23
CaO	14.56	9.59	13.52	14.77	17.72	15.17	14.46	8.96	11.41	17.89	18.00	14.38
Na_2O	3.50	5.93	4.14	3.40	1.41	2.30	2.96	5.93	5.10	1.29	1.34	3.50
K_2O	0.01	0.13	0.07	0.05	0.03	0.04	0.67	0.17	0.01	0.02	0.01	0.05
BaO	-	0.02	-	-	0.03	0.02	-	0.05	-	0.03	-	0.01
Total	99.23	98.90	98.59	98.91	99.19	99.70	100.88	99.09	99.23	98.77	99.10	99.50
An	69.48	46.82	64.10	70.39	87.30	73.49	70.17	45.06	54.96	88.31	88.10	69.22
Ab	30.20	52.40	35.53	29.34	12.55	26.28	25.97	53.94	44.48	11.56	11.84	30.50
Or	0.30	0.78	0.37	0.27	0.15	0.23	3.86	1.00	0.56	0.13	0.06	0.28

Locality	CS036											
Sample	PCc	PCd	Gi	PRe	PCe	PRf	PCf	PCg	PRg	PCh	PCi	PRi
SiO_2	45.63	48.79	50.26	48.30	46.34	45.63	45.61	50.12	51.81	45.98	45.90	48.18
Al_2O_3	33.29	31.08	29.84	31.22	32.94	33.41	33.47	30.06	28.77	33.10	33.13	31.32
FeO	0.42	0.60	0.83	0.63	0.41	0.51	0.45	0.88	1.06	0.46	0.42	0.57
MgO	0.19	0.33	0.26	0.30	0.23	0.21	0.20	0.31	0.20	0.23	0.02	0.31
CaO	17.90	15.79	14.28	16.04	17.62	17.92	18.14	14.67	13.25	17.86	17.70	16.27
Na_2O	1.34	2.64	3.48	2.54	1.54	1.34	1.30	3.16	4.20	1.46	1.43	2.42
K_2O	0.01	0.04	0.04	0.02	0.02	0.03	0.02	0.05	0.08	0.02	0.01	0.03
BaO	0.02	0.03	-	-	0.04	0.01	-	0.06	-	0.02	0.01	0.03
Total	98.83	99.34	99.04	99.09	99.16	99.09	99.21	99.34	99.42	99.14	98.83	99.18
An	88.07	76.61	69.23	77.64	86.27	87.98	88.41	71.72	63.29	87.02	87.22	78.63
Ab	11.89	23.19	30.56	22.25	13.65	11.88	11.49	28.00	36.28	12.89	12.71	21.20
Or	0.04	0.20	0.22	0.11	0.08	0.12	0.10	0.28	0.43	0.09	0.07	0.17

Feldspars

Locality	CS036	CS026									
Sample	PCj	PCa	PRa	Ga	Gb	PCb	PCc	Gc	PCd	PCe	PRe	PCf
SiO_2	46.37	45.78	46.38	52.42	52.71	49.36	49.47	52.16	46.56	46.28	49.65	46.34
Al_2O_3	32.53	33.87	33.69	29.44	28.81	31.26	31.34	29.55	33.28	33.69	30.78	33.60
FeO	0.46	0.41	0.43	0.90	0.95	0.68	0.74	0.94	0.43	0.46	0.62	0.47
MgO	0.23	0.21	0.20	0.17	0.14	0.29	0.27	0.18	0.24	0.22	0.28	0.21
CaO	17.24	18.22	17.97	13.30	12.76	15.61	15.51	13.52	17.71	17.96	15.31	17.97
Na_2O	1.68	1.35	1.55	4.08	4.36	3.01	3.04	3.89	1.65	1.55	2.95	1.55
K_2O	0.02	0.01	0.02	0.07	0.08	0.04	0.03	0.06	0.02	0.02	0.08	0.02
BaO	0.02	0.03	0.01	-	0.06	0.06	-	-	0.03	0.05	-	-
Total	98.60	99.90	100.29	100.45	99.94	100.36	100.45	100.38	99.94	100.26	99.73	100.20
An	84.88	88.15	86.39	64.07	61.51	73.98	73.72	65.53	85.47	86.44	73.84	86.41
Ab	15.00	11.79	13.48	35.54	38.03	25.81	26.12	34.12	14.42	13.45	25.70	13.51
Or	0.02	0.06	0.13	0.39	0.46	0.21	0.16	0.35	0.11	0.11	0.46	0.08

Locality	CS026	CS070					CS026		CS014			
Sample	Gd	PCa	PRa	PCb	PRb	Ga	Ga	Gb	PCa	PRa	Ga	Gb
SiO_2	55.06	46.04	48.82	46.36	49.81	56.63	49.52	49.19	49.32	52.33	52.52	53.28
Al_2O_3	27.83	33.29	30.89	33.16	30.45	26.06	31.16	31.32	31.09	28.64	28.60	28.26
FeO	0.89	0.47	0.58	0.51	0.61	0.60	0.77	0.71	0.65	0.92	0.98	0.92
MgO	0.11	0.19	0.29	0.19	0.29	0.07	0.30	0.34	0.28	0.13	0.15	0.13
CaO	10.85	17.86	15.49	17.76	14.98	9.15	15.64	15.70	15.52	12.63	12.48	12.05
Na_2O	5.44	1.62	3.06	1.70	3.32	6.39	2.92	2.87	2.94	4.59	4.66	4.92
K_2O	0.11	0.01	0.04	0.02	0.04	0.16	0.02	0.03	0.03	0.09	0.08	0.08
BaO	0.04	0.04	0.04	0.04	-	-	0.02	-	0.02	0.01	0.03	0.01
Total	100.40	99.54	99.26	99.77	99.55	99.12	100.39	100.20	99.90	99.41	99.57	99.72
An	52.12	85.87	73.53	85.14	71.23	43.78	74.68	75.07	74.35	60.04	59.41	57.28
Ab	47.26	14.06	26.25	14.74	28.57	55.31	25.22	24.78	25.51	39.46	40.16	42.29
Or	0.62	0.06	0.22	0.12	0.20	0.92	0.10	0.15	0.14	0.51	0.43	0.43

Feldspars

Locality	CS014				CS044							
Sample	Gc	PCa	PCb	PRb	PCa	PRa	PCb	PRb	Ga	PCc	Gb	PCd
SiO_2	53.02	46.53	46.47	49.61	46.75	47.05	46.01	48.98	51.38	46.07	53.34	45.19
Al_2O_3	29.04	33.04	33.11	30.83	33.34	32.61	33.38	31.04	29.51	33.38	28.36	34.02
FeO	1.04	0.49	0.54	0.69	0.53	0.59	0.50	0.63	0.78	0.53	0.89	0.50
MgO	0.18	0.21	0.23	0.23	0.17	0.21	0.19	0.25	0.17	0.18	0.13	0.15
CaO	12.54	17.56	17.51	15.06	17.53	17.25	18.03	15.56	13.48	17.96	12.21	18.41
Na_2O	4.83	1.74	1.80	3.24	1.27	2.05	1.60	2.95	3.95	1.55	4.66	1.29
K_2O	0.07	0.08	0.05	0.07	0.02	0.03	0.02	0.04	0.06	0.03	0.08	0.03
BaO	-	0.02	-	0.03	-	0.01	-	0.04	0.02	0.03	0.04	0.01
Total	100.78	99.70	99.73	99.82	99.65	99.82	99.77	99.56	99.40	99.76	99.80	99.63
An	58.67	84.43	84.05	71.72	88.26	82.17	86.06	74.32	65.16	86.35	58.87	88.58
Ab	40.92	15.12	15.67	27.91	11.61	17.68	13.81	25.45	34.51	13.50	40.69	11.27
Or	0.41	0.45	0.28	0.37	0.13	0.15	0.13	0.23	0.33	0.15	0.44	0.15

Locality	CS044								CS036			
Sample	Gc	Gd	Ge	Gf	Gg	Gh	PCe	PRe	Gi	Gj	PCk	PRk
SiO_2	51.44	52.00	50.16	49.72	50.68	51.14	45.51	48.80	59.36	52.71	45.42	54.27
Al_2O_3	29.68	28.94	30.37	30.59	29.71	29.67	33.67	31.25	26.85	28.67	33.83	27.48
FeO	0.79	0.87	0.67	0.67	0.78	0.73	0.46	0.66	0.40	0.97	0.48	0.87
MgO	0.19	0.17	0.25	0.22	0.20	0.18	0.16	0.26	0.18	0.15	0.21	0.09
CaO	13.87	13.19	14.68	15.13	14.10	13.94	18.22	15.77	9.11	12.45	18.34	11.28
Na_2O	3.83	4.22	3.43	3.28	3.59	3.79	1.41	2.81	2.02	4.77	1.27	5.56
K_2O	0.07	0.06	0.04	0.05	0.06	0.07	0.01	0.02	2.46	0.09	0.03	0.10
BaO	-	-	0.02	0.08	0.02	-	0.03	-	0.04	0.01	-	0.03
Total	99.92	99.50	99.67	99.80	99.22	99.61	99.50	99.61	100.43	99.89	99.59	99.75
An	66.45	63.13	70.12	71.65	68.22	66.77	87.64	75.49	58.09	58.78	88.74	52.55
Ab	33.17	36.52	29.64	28.09	31.45	32.84	12.30	24.36	23.24	40.74	11.12	46.90
Or	0.38	0.35	0.24	0.26	0.33	0.39	0.06	0.15	18.67	0.48	0.14	0.55

Feldspars

Locality	CS070											
Sample	Ga	Gb	Gc	PRa	Gd	Ge	Gf	PCb	PRb	Gh	Gi	PCc
SiO_2	51.49	50.20	63.08	49.85	52.32	50.27	49.93	46.14	46.71	56.22	51.32	46.45
Al_2O_3	29.48	29.90	22.93	30.51	28.31	30.07	30.34	33.43	32.90	26.44	29.36	32.92
FeO	0.80	0.76	0.45	0.66	0.88	1.10	0.72	0.45	0.49	0.67	0.75	0.49
MgO	0.15	0.18	0.02	0.28	0.14	0.18	0.25	0.20	0.22	0.07	0.16	0.21
CaO	13.41	14.25	4.98	14.80	12.54	14.33	14.54	17.80	17.30	9.47	13.57	17.46
Na_2O	4.15	3.69	6.96	3.41	4.80	3.62	3.51	1.67	1.96	5.51	4.12	1.81
K_2O	0.06	0.04	0.25	0.04	0.08	0.05	0.06	0.01	0.03	0.14	0.08	0.02
BaO	-	0.02	0.04	-	0.06	0.01	-	0.02	0.02	0.03	-	-
Total	99.60	99.11	98.76	99.60	99.21	99.74	99.41	99.78	99.66	98.62	99.42	99.41
An	63.90	67.92	27.84	70.38	58.81	68.46	69.39	85.41	88.83	48.32	64.26	84.06
Ab	35.77	31.84	70.47	29.38	40.72	31.29	30.30	14.53	17.00	50.87	35.32	15.80
Or	0.33	0.24	1.69	0.24	0.47	0.25	0.31	0.06	0.17	0.81	0.42	0.14

Locality	CS070										
Sample	PCd	PRd	Gj	Gk	Gl	PCe	PCf	PCg	PCh	PCi	Gm
SiO_2	45.93	49.40	52.21	52.54	52.45	45.75	46.14	45.45	46.24	45.57	50.61
Al_2O_3	33.73	30.36	28.74	28.66	28.80	33.44	33.22	33.45	32.88	33.80	30.16
FeO	0.48	0.68	0.91	0.84	0.87	0.51	0.49	0.50	0.50	0.49	0.76
MgO	0.20	0.29	0.15	0.14	0.16	0.17	0.20	0.19	0.21	0.19	0.21
CaO	18.17	14.90	12.74	12.57	12.70	18.16	17.70	18.18	17.57	18.32	14.33
Na_2O	1.51	3.32	4.63	4.52	4.67	1.52	1.64	1.41	1.78	1.34	3.69
K_2O	0.02	0.05	0.08	0.08	0.07	0.01	0.02	0.02	0.01	0.01	0.05
BaO	0.05	-	0.05	0.04	-	0.01	-	0.02	-	-	0.07
Total	100.12	99.02	9.60	99.46	99.81	99.61	99.43	99.24	99.22	99.76	99.95
An	86.84	71.10	60.08	60.31	59.79	86.76	85.55	87.61	84.49	88.22	68.06
Ab	13.07	28.65	39.50	39.25	39.81	13.17	14.36	12.28	15.48	11.74	31.66
Or	0.09	0.25	0.42	0.44	0.40	0.07	0.09	0.11	0.05	0.04	0.28

Feldspars

Locality	CS036											
Sample	PCt	PCu	PRu	Gk	Gl	Gm	Gn	PCv	PRv	PCw	PRw	PCx
SiO_2	46.26	46.48	48.67	49.61	55.21	49.00	51.96	45.56	47.95	45.95	48.67	45.47
Al_2O_3	32.77	33.08	31.13	29.96	26.82	31.07	28.48	33.56	31.80	33.32	31.21	33.70
FeO	0.44	0.40	0.71	0.81	0.53	0.75	0.98	0.43	0.58	0.41	0.74	0.45
MgO	0.24	0.24	0.35	0.31	0.23	0.33	0.18	0.21	0.31	0.23	0.35	0.21
CaO	17.76	17.51	15.93	14.90	10.51	15.70	12.69	18.24	16.43	18.11	16.07	18.43
Na_2O	1.75	1.74	2.81	3.40	2.06	2.95	4.62	1.40	2.49	1.51	2.70	1.33
K_2O	0.01	0.02	0.03	0.04	5.28	0.03	0.08	0.01	0.03	0.03	0.03	0.02
BaO	0.02	0.03	0.03	-	0.03	0.10	-	0.02	0.04	0.04	0.03	0.01
Total	99.30	99.53	99.71	99.08	100.70	99.90	99.07	99.45	99.67	99.63	99.85	99.66
An	84.83	84.66	75.68	70.59	51.21	74.50	60.00	87.74	78.33	86.76	76.55	88.34
Ab	15.10	15.20	24.16	29.17	18.17	25.34	39.54	12.22	21.50	13.07	23.29	11.56
Or	0.07	0.14	0.16	0.24	30.62	0.16	0.46	0.04	0.17	0.17	0.16	0.10

Locality	CS022		CS082			CS060			CS073		CS049	
Sample	Ga	Gb	PCa	PCb	Ga	Ga	Gb	Gc	Ga	Gb	PCa	Ga
SiO_2	49.36	49.13	53.82	59.48	54.92	55.08	53.69	52.62	55.77	53.43	50.70	53.09
Al_2O_3	32.07	32.15	28.06	24.48	27.79	26.94	28.39	29.80	27.58	28.04	29.78	27.93
FeO	0.53	0.52	0.92	0.09	1.07	0.79	1.08	0.90	0.71	0.90	0.70	0.84
MgO	0.32	0.29	0.14	0.16	0.19	0.10	0.15	0.19	0.10	0.15	0.14	0.13
CaO	15.65	15.59	11.57	7.42	11.84	10.32	12.32	13.68	11.17	11.86	13.53	11.48
Na_2O	2.63	2.63	4.92	6.92	4.91	5.70	4.64	3.85	5.23	4.62	3.70	4.86
K_2O	0.03	0.02	0.25	0.64	0.26	0.13	0.08	0.06	0.26	0.20	0.05	0.08
BaO	-	-	-	-	-	-	-	-	-	-	-	-
Total	100.59	100.34	99.69	100.01	100.98	99.06	100.35	101.10	100.83	99.19	98.60	98.42
An	76.58	76.52	55.68	35.84	56.30	49.66	59.21	66.01	53.31	57.93	66.70	56.33
Ab	23.27	23.36	42.89	60.47	42.22	49.61	40.32	33.64	45.20	40.88	33.03	56.33
Or	0.15	0.13	1.43	3.69	1.48	0.74	0.47	0.35	1.49	1.19	0.27	0.50

Feldspars

Locality	CS019											
Sample	Ga	PCa	PRa	PCb	PRb	PCc	PRc	PCd	PRd	PCa	PRa	PCb
SiO_2	48.57	45.70	50.13	45.83	45.88	46.94	61.68	45.26	49.10	46.87	45.97	47.09
Al_2O_3	30.94	32.93	29.99	33.03	33.15	31.74	22.55	32.92	30.52	33.44	33.39	32.38
FeO	0.88	0.53	1.07	0.48	0.50	0.54	0.44	0.56	0.79	0.48	0.49	0.87
MgO	0.30	0.21	0.30	0.19	0.19	0.21	0.10	0.19	0.29	0.19	0.19	0.44
CaO	15.60	17.78	14.98	17.71	17.47	16.28	4.01	17.41	15.14	17.90	17.67	17.14
Na_2O	2.89	1.67	3.29	1.55	1.64	1.94	9.47	2.23	3.01	1.64	1.78	1.90
K_2O	0.06	0.11	0.09	0.05	0.05	0.64	0.16	0.43	0.07	0.05	0.11	0.08
BaO	-	-	-	-	-	-	-	-	-	-	-	-
Total	99.26	98.97	99.91	98.86	98.91	98.33	98.42	99.02	98.95	100.59	99.63	99.92
An	74.64	84.87	71.17	86.06	85.18	79.18	18.80	79.25	73.21	85.49	84.05	82.91
Ab	25.02	14.46	28.30	13.62	14.53	17.10	80.31	18.39	26.35	14.19	15.30	16.60
Or	0.34	0.67	0.52	0.32	0.29	3.72	0.89	2.36	0.44	0.32	0.65	0.49

Locality	CS019	CS011									
Sample	PRb	Ga	Gb	Gc	PCa	PCb	PRc	PCd	PCd	PRe	PCf	PRf
SiO_2	54.28	50.42	48.72	50.18	44.88	49.24	54.64	49.54	45.54	45.36	44.90	44.89
Al_2O_3	27.75	30.19	31.15	29.97	33.67	30.41	27.40	30.77	33.54	34.06	33.89	33.20
FeO	0.93	0.81	0.80	0.88	0.39	0.65	0.72	0.85	0.40	0.47	0.37	0.39
MgO	0.15	0.15	0.28	0.16	0.19	0.24	0.09	0.20	0.22	0.17	0.18	0.19
CaO	11.29	14.03	15.56	13.95	18.20	14.78	10.92	14.26	17.76	18.06	18.31	17.80
Na_2O	5.24	3.64	2.76	3.41	1.10	3.14	5.39	3.37	1.30	1.10	1.04	1.24
K_2O	0.14	0.07	0.04	0.07	0.05	0.06	0.13	0.07	0.03	0.02	0.03	0.03
BaO	-	-	-	-	-	-	-	-	-	-	-	-
Total	99.85	99.33	99.35	98.66	98.51	98.56	99.37	99.10	98.80	99.26	98.74	97.76
An	53.94	67.79	75.55	69.03	89.84	71.95	52.38	69.75	88.10	89.93	90.54	87.73
Ab	45.28	31.81	24.28	30.57	9.87	27.71	46.83	29.85	11.70	9.92	9.29	12.06
Or	0.78	0.40	0.27	0.40	0.29	0.34	0.79	0.40	0.20	0.15	0.17	0.21

Feldspars

Locality	CS050						CS009				
Sample	PCc	PRc	PCb	PRb	Ga	Gb	PRa	PCb	PRb	Ga	Gb
SiO_2	49.26	51.22	50.78	52.53	51.24	51.03	46.13	47.51	52.38	51.66	49.63
Al_2O_3	31.29	30.75	29.22	29.82	27.80	28.90	34.60	34.03	30.30	29.48	30.46
FeO	0.67	0.74	0.72	0.74	1.02	0.80	0.40	0.46	0.80	1.44	0.74
MgO	0.14	0.17	0.18	0.18	0.17	0.16	0.22	0.23	0.19	0.54	0.19
CaO	14.62	14.00	12.81	13.00	11.72	12.51	17.81	17.46	13.34	12.42	13.85
Na_2O	3.02	3.51	3.85	3.94	4.58	4.09	1.22	1.46	3.66	3.97	3.37
K_2O	0.06	0.07	0.07	0.09	0.11	0.07	0.01	0.01	0.04	0.05	0.03
BaO	-	-	-	-	-	-	-	-	-	-	-
Total	99.07	100.45	97.64	100.29	96.63	97.56	100.40	101.15	100.72	99.55	98.27
An	72.55	68.54	64.47	64.27	58.19	62.55	88.88	86.87	66.66	63.14	69.28
Ab	27.12	31.08	35.12	35.23	41.17	37.03	11.04	13.10	33.08	36.54	30.54
Or	0.33	0.38	0.41	0.50	0.64	0.42	0.08	0.03	0.26	0.32	0.18

Locality	CS024				CS053			CS022				
Sample	PRa	PCa	PCb	Ga	PCa	Ga	Gb	PCa	PRa	PRb	PCb	PRc
SiO_2	47.22	46.55	46.00	50.48	50.93	53.55	52.69	48.22	48.52	56.03	51.49	50.54
Al_2O_3	33.49	33.85	33.93	30.80	31.23	28.95	30.09	32.99	31.81	28.14	29.09	30.89
FeO	0.42	0.44	0.49	0.92	0.80	0.91	0.93	0.62	0.52	0.64	0.70	0.74
MgO	0.26	0.25	0.15	0.37	0.12	0.16	0.22	0.17	0.28	0.13	0.17	0.19
CaO	17.39	17.68	17.95	14.71	14.36	12.03	13.29	16.45	15.89	10.84	12.71	14.20
Na_2O	1.62	1.51	1.27	3.10	3.50	4.75	4.04	2.14	2.38	5.53	4.34	3.46
K_2O	0.01	0.07	0.01	0.04	0.04	0.20	0.06	0.02	0.02	0.06	0.09	0.05
BaO	-	-	-	-	-	-	-	-	-	-	-	-
Total	100.41	100.35	99.81	100.42	100.98	100.56	101.33	100.60	99.43	101.36	98.58	100.06
An	85.54	86.20	88.57	72.24	69.25	57.65	64.27	80.89	78.58	51.81	61.49	69.16
Ab	14.38	13.40	11.38	27.53	30.52	41.17	35.35	19.00	21.29	47.86	38.00	30.54
Or	0.08	0.40	0.05	0.23	0.23	1.16	0.38	0.01	0.12	0.33	0.51	0.30

Feldspars

Locality	CS011			IT10
Sample	PRc	PCf	PRf	PCc
SiO_2	44.89	46.01	56.63	51.65
Al_2O_3	33.20	33.36	26.64	29.39
FeO	0.39	0.45	0.78	0.72
MgO	0.19	0.22	0.06	0.07
CaO	17.80	17.52	9.52	13.06
Na_2O	1.24	1.46	6.17	4.03
K_2O	0.03	0.04	0.16	0.16
BaO	-	-	-	-
Total	97.76	99.09	100.02	99.08
An	87.73	86.70	45.60	63.57
Ab	12.06	13.08	53.48	35.54
Or	0.21	0.22	0.92	0.89

Locality	IT15					IT16						
Sample	PCa	PRa	PCb	PRb	Ga	PCa	PRa	PCb	PRB	Ga	Gb	PCc
SiO_2	55.18	56.85	53.21	50.96	56.56	45.17	52.95	48.29	53.76	52.26	51.93	45.85
Al_2O_3	27.62	23.36	28.40	28.55	26.57	33.44	28.35	31.80	27.95	28.48	28.95	33.18
FeO	0.76	0.53	0.37	2.22	0.64	0.50	1.04	0.43	0.88	1.03	0.90	0.51
MgO	0.19	0.04	0.06	0.64	0.04	0.17	0.19	0.17	0.16	0.22	0.19	0.19
CaO	10.56	8.99	11.63	11.60	9.31	17.99	12.17	16.35	11.76	12.67	13.03	17.56
Na_2O	5.41	6.43	4.99	4.16	6.29	1.15	4.61	2.19	4.95	4.31	4.34	1.47
K_2O	0.36	0.26	0.23	0.37	0.41	0.01	0.09	0.02	0.08	0.08	0.07	0.01
BaO	0.02	-	0.02	0.01	0.04	-	-	-	-	-	-	-
Total	100.10	99.46	99.21	98.51	99.84	98.44	99.39	99.25	99.56	99.04	99.40	98.76
An	50.82	42.91	55.56	59.29	43.95	89.55	59.03	80.37	56.47	61.63	62.15	86.81
Ab	47.14	55.60	43.15	38.46	53.78	10.37	40.48	19.51	43.06	37.93	37.44	13.12
Or	2.04	1.48	1.29	2.25	2.27	0.07	0.49	0.12	0.47	0.44	0.41	0.07

Feldspars

Locality	IT18	IT10						IT08				
Sample	PCa	PCa	PRa	PCb	PRb	Ga	Gb	PCa	PRa	PCb	PRb	Ga
SiO_2	52.98	49.89	54.15	46.94	47.40	54.14	51.65	50.10	49.28	51.15	50.40	54.61
Al_2O_3	28.32	30.95	28.15	31.99	32.27	27.26	29.39	31.25	31.80	29.15	30.78	27.69
FeO	0.74	0.62	0.85	0.57	0.55	0.61	0.72	0.54	0.59	0.71	0.63	0.91
MgO	0.21	0.14	0.19	0.20	0.09	0.05	0.07	0.26	0.24	0.37	0.24	0.15
CaO	11.64	14.94	11.31	16.39	16.05	10.71	13.06	15.35	15.82	13.35	14.48	11.14
Na_2O	4.73	2.89	5.08	1.54	2.28	4.12	4.03	2.81	2.56	3.67	3.17	5.07
K_2O	0.28	0.10	0.14	0.07	0.09	0.17	0.16	0.09	0.09	0.16	0.12	0.24
BaO	-	-	-	-	-	-	-	-	-	-	-	-
Total	98.89	99.52	99.87	97.69	98.72	97.06	99.08	100.39	100.38	98.56	99.83	99.81
An	56.68	73.67	54.71	85.07	79.13	58.29	63.57	74.73	77.00	66.13	71.07	54.09
Ab	41.69	25.75	44.49	14.49	20.32	40.61	35.54	24.77	22.45	32.92	28.20	44.51
Or	1.63	0.58	0.80	0.44	0.55	1.10	0.89	0.50	0.55	0.95	0.73	1.40

Locality	IT08	IT09						IT06				
Sample	Gb	PCa	PRa	PCb	PRb	Ga	PCc	PRa	PCa	PCb	PRb	Ga
SiO_2	52.46	49.26	57.62	50.32	55.56	54.31	52.15	52.36	51.10	45.97	45.29	48.58
Al_2O_3	28.94	31.59	25.52	30.92	27.44	27.74	28.74	29.37	29.93	34.34	33.84	31.86
FeO	0.82	0.62	1.38	0.68	1.06	1.01	0.73	0.69	0.91	0.37	0.39	0.73
MgO	0.22	0.21	0.39	0.18	0.15	0.17	0.21	0.16	0.23	0.22	0.23	0.31
CaO	12.64	15.09	9.18	14.46	10.62	11.04	12.46	12.74	13.44	18.06	17.77	15.83
Na_2O	4.26	2.73	6.17	3.24	5.31	5.06	4.27	4.13	3.77	1.22	1.30	2.45
K_2O	0.22	0.14	0.39	0.18	0.35	0.38	0.24	0.05	0.03	0.01	0.01	0.03
BaO	-	-	0.03	-	-	-	0.01	-	-	-	-	-
Total	99.55	99.63	100.68	99.99	100.49	99.71	98.81	99.51	99.41	100.19	98.84	99.78
An	61.35	74.70	44.10	70.43	51.44	53.45	60.85	62.83	66.20	89.09	88.23	78.01
Ab	37.41	24.44	53.70	28.53	46.58	44.34	37.74	36.89	33.63	10.86	11.20	21.84
Or	1.24	0.86	2.20	1.04	1.98	2.21	1.41	0.28	0.17	0.05	0.07	0.15

Pyroxenes

Pyroxenes

Locality	AG287			AG291A			AG190C				AG249	
Sample	d	e	f	a	b	c	a	b	c	d	a	b
SiO_2	54.68	52.34	53.26	52.02	52.51	56.68	52.50	55.71	52.96	54.16	53.13	56.49
Al_2O_3	1.24	2.06	1.26	2.36	2.96	0.58	2.83	0.95	2.52	1.32	2.41	1.13
Cr_2O_3	0.11	0.19	0.32	0.52	0.85	0.03	1.09	0.11	0.94	0.09	0.42	0.08
TiO_2	0.21	0.41	0.15	0.89	0.64	0.21	0.34	0.38	0.57	0.62	0.37	0.19
FeO	12.84	7.20	6.53	1.67	3.51	7.42	4.30	11.44	4.65	11.09	4.81	11.98
Fe_2O_3	1.76	0.93	0.36	2.61	0.71	2.46	0.70	0.65	1.62	0.49	2.41	1.42
MgO	27.34	15.57	15.19	16.11	15.73	31.56	17.51	30.07	17.52	28.87	17.47	27.70
CaO	2.14	20.59	22.36	22.88	23.14	0.71	20.36	1.04	19.20	1.71	17.91	2.11
Na_2O	0.20	0.29	0.29	0.68	0.44	0.09	0.29	0.06	0.34	0.06	0.30	0.05
MnO	0.31	0.25	0.21	0.13	0.13	0.22	0.15	0.30	0.18	0.27	0.18	0.36
Total	100.83	99.83	99.93	99.87	100.62	99.96	100.07	100.71	100.50	98.68	99.41	101.51
FeO^*	14.43	8.07	6.85	4.02	4.13	9.60	4.91	12.01	6.14	11.53	6.81	13.08
Ca	4.14	42.24	45.63	47.13	47.88	1.37	41.82	1.97	39.62	3.35	37.57	4.14
Mg	73.61	44.40	43.11	46.19	45.24	83.99	50.05	79.73	50.24	78.65	50.96	75.31
Fe	22.25	13.36	11.27	6.68	6.88	14.64	8.13	18.31	10.14	18.00	11.48	20.55

Locality	AG249					AG248				AG261		
Sample	c	d	e	f	g	a	b	c	d	a	b	c
SiO_2	52.68	54.43	53.50	52.84	54.38	53.07	52.85	52.71	51.77	51.76	54.07	53.44
Al_2O_3	2.39	1.33	1.15	2.19	1.11	1.09	1.44	1.97	1.88	2.37	1.58	1.55
Cr_2O_3	0.52	0.09	0.09	0.29	0.09	0.01	0.01	0.30	0.35	0.40	0.15	0.09
TiO_2	0.30	0.45	0.28	0.35	0.18	0.24	0.31	0.27	0.27	0.84	0.59	0.68
FeO	6.83	12.94	11.79	7.72	12.05	17.91	16.96	7.65	7.21	7.10	13.15	12.83
Fe_2O_3	0.43	0.67	1.44	1.06	0.96	1.16	1.52	1.35	1.92	0.84	0.96	1.52
MgO	16.89	27.97	27.53	18.05	27.81	23.94	24.27	17.05	15.79	16.96	27.36	27.16
CaO	19.24	1.58	2.19	17.35	2.26	1.86	1.96	18.50	19.52	18.42	2.05	2.05
Na_2O	0.31	0.06	0.03	0.25	0.06	0.04	0.06	0.27	0.32	0.31	0.06	0.05
MnO	0.23	0.37	0.39	0.22	0.37	0.48	0.46	0.28	0.28	0.26	0.36	0.35
Total	99.32	99.89	98.39	100.32	99.27	99.80	99.84	100.35	99.31	99.26	100.33	99.72
FeO^*	7.20	13.53	13.09	8.64	12.91	18.99	18.31	8.84	8.96	7.86	13.99	14.19
Ca	39.63	3.09	4.31	35.14	4.43	3.71	3.87	37.46	40.05	38.10	4.00	4.02
Mg	48.41	75.76	75.06	50.85	75.38	66.10	67.05	48.08	45.12	48.80	74.18	73.79
Fe	11.96	21.15	20.63	14.01	20.19	30.19	29.07	14.47	14.83	13.10	21.82	22.18

Pyroxenes

Locality	AG277		AG178	AG152			AG119		AG143F			AG160
Sample	b	c	a	a	b	c	a	b	a	b	c	a
SiO_2	51.29	51.73	48.83	50.96	50.85	53.32	51.57	52.11	51.41	51.70	51.48	51.29
Al_2O_3	3.19	2.84	4.38	3.31	3.66	2.61	3.22	2.85	3.24	3.01	3.06	3.19
Cr_2O_3	1.47	1.28	0.92	1.18	1.20	0.95	1.20	1.28	1.32	1.21	1.20	1.09
TiO_2	0.60	0.64	2.35	0.53	0.48	0.39	0.38	0.56	0.54	0.53	0.59	1.82
FeO	1.80	1.97	1.75	2.89	2.64	2.52	2.19	2.77	3.74	3.33	3.06	2.49
Fe_2O_3	2.56	12.02	2.71	1.92	2.02	1.91	2.11	1.68	0.70	1.36	1.30	1.02
MgO	17.33	16.64	15.66	16.87	16.87	17.43	17.72	18.32	16.46	17.15	16.69	16.83
CaO	21.62	22.94	22.26	21.18	21.34	21.32	20.98	20.27	21.62	21.19	21.86	21.94
Na_2O	0.60	0.64	0.47	0.24	0.22	0.20	0.25	0.26	0.21	0.22	0.23	0.47
MnO	0.18	0.16	0.14	0.19	0.17	0.16	0.19	0.20	0.20	0.21	0.19	0.16
Total	100.64	100.06	99.47	99.27	99.45	100.81	99.81	100.30	99.44	99.91	99.66	100.30
FeO^*	4.10	3.77	4.15	4.60	4.44	4.37	4.09	4.30	4.34	4.56	4.25	3.42
Ca	44.06	46.68	46.96	43.75	44.10	43.43	42.83	41.13	45.00	43.48	45.04	45.59
Mg	49.09	47.10	45.95	48.49	48.49	49.37	50.31	51.74	47.63	48.91	47.81	48.62
Fe	6.85	6.22	7.09	7.76	7.41	7.20	6.85	7.12	7.37	7.61	7.15	5.79

Locality	AG160				AG240					AG287		
Sample	b	c	d	e	a	b	c	d	e	a	b	c
SiO_2	51.66	50.63	51.69	51.71	53.11	50.92	52.31	52.15	51.93	50.77	53.53	54.73
Al_2O_3	3.30	3.15	3.31	3.22	1.19	2.54	1.13	2.49	3.05	3.13	0.97	1.09
Cr_2O_3	1.41	1.16	1.40	1.33	-	-	-	0.15	0.80	0.09	0.04	0.11
TiO_2	0.45	1.78	0.45	0.44	0.44	0.90	0.51	0.46	0.37	0.68	0.23	0.24
FeO	1.87	2.34	1.70	1.87	16.17	7.01	15.49	4.79	4.43	7.18	18.99	15.07
Fe_2O_3	1.72	1.30	1.75	1.72	0.57	1.92	1.48	2.03	1.21	1.86	0.14	1.31
MgO	17.78	16.96	16.95	17.47	25.16	15.27	25.00	15.85	16.50	14.33	23.55	25.47
CaO	21.26	21.25	22.10	21.70	1.80	20.16	1.80	21.94	21.33	19.54	2.02	2.67
Na_2O	0.26	0.47	0.39	0.27	0.04	0.29	0.05	0.30	0.23	0.33	0.05	0.06
MnO	0.16	0.15	0.15	0.14	0.37	0.27	0.39	0.21	0.16	0.25	0.42	0.34
Total	99.87	99.19	99.89	99.87	98.85	99.28	98.16	100.37	100.01	98.13	99.94	101.09
FeO^*	3.40	3.52	3.29	3.42	16.70	8.76	16.81	6.61	5.54	8.93	19.12	15.93
Ca	43.62	44.78	45.66	44.49	3.58	41.61	3.61	44.48	43.77	41.91	4.05	5.25
Mg	50.68	49.15	48.76	49.82	69.81	43.82	69.54	44.69	47.11	42.71	65.47	69.74
Fe	5.70	6.07	5.58	5.70	26.60	14.57	26.85	10.83	9.12	15.38	30.48	25.01

Pyroxenes

Locality	AG181A		AG245A			AG181A						AG190B
Sample	a	b	a	b	c	a	b	c	d	e	f	a
SiO_2	51.31	50.11	52.16	51.91	51.74	51.56	51.98	49.63	50.95	50.87	50.85	52.08
Al_2O_3	3.46	3.99	2.80	2.84	3.16	3.48	2.90	3.31	3.48	3.81	3.79	2.67
Cr_2O_3	1.31	1.26	0.67	0.71	1.26	1.31	1.06	1.22	1.22	1.40	1.40	1.10
TiO_2	0.93	1.10	0.79	1.18	0.53	0.99	0.61	0.95	0.93	0.76	1.00	0.29
FeO	3.13	1.75	3.99	3.64	3.78	1.46	2.80	0.90	2.54	2.44	2.67	2.90
Fe_2O_3	0.58	2.14	0.58	0.92	0.85	2.50	0.77	0.92	1.57	1.30	0.99	0.79
MgO	15.92	16.31	15.99	17.56	16.81	16.97	17.12	16.34	16.63	15.76	15.92	17.26
CaO	21.99	22.51	20.59	21.80	20.85	22.15	22.74	21.92	21.60	22.59	22.45	21.60
Na_2O	0.37	0.37	0.27	0.31	0.31	0.44	0.32	0.39	0.39	0.40	0.38	0.23
MnO	0.09	0.10	0.16	0.16	0.16	0.14	0.14	0.11	0.10	0.11	0.11	0.12
Total	99.09	99.64	98.00	101.03	99.45	101.00	100.44	95.69	99.41	99.44	99.56	99.04
FeO^*	3.65	3.67	4.49	4.45	4.53	3.72	3.50	3.66	3.92	3.61	3.57	3.62
Ca	46.19	47.20	42.31	44.67	43.32	45.23	47.08	45.95	45.11	47.63	47.31	44.52
Mg	47.68	46.62	50.21	47.96	49.08	48.64	47.08	47.87	48.34	46.24	46.67	49.48
Fe	6.13	6.18	7.48	7.37	7.60	6.14	5.84	6.19	6.55	6.13	6.03	6.00

Locality	AG190B				AG241					AG245
Sample	b	c	d	e	a	b	c	d	e	a
SiO_2	51.64	52.33	49.35	52.20	52.13	50.96	51.65	51.32	51.50	53.04
Al_2O_3	3.03	2.42	3.71	2.28	2.54	2.49	2.83	3.14	3.29	2.77
Cr_2O_3	1.32	0.66	0.18	0.47	0.76	0.76	0.99	1.19	0.82	1.13
TiO_2	0.32	0.39	0.69	0.52	0.59	0.76	0.29	0.33	0.49	0.34
FeO	2.41	2.91	2.16	3.74	4.91	3.09	4.31	3.15	3.71	3.34
Fe_2O_3	1.52	1.65	3.52	1.23	2.68	2.56	1.63	1.80	1.95	0.64
MgO	16.94	17.49	17.34	18.03	19.77	16.27	16.67	15.78	15.93	18.39
CaO	22.01	21.60	19.96	20.25	16.48	21.52	20.42	22.44	21.90	20.56
Na_2O	0.24	0.22	0.18	0.20	0.29	0.38	0.36	0.32	0.36	0.25
MnO	0.10	0.12	0.14	0.13	0.23	0.18	0.17	0.14	0.17	0.10
Total	99.53	99.79	97.23	99.05	100.38	98.97	99.32	99.61	100.12	100.56
FeO^*	3.78	4.14	5.33	4.83	7.33	5.39	5.75	4.76	5.48	3.91
Ca	45.30	43.87	41.28	41.15	33.04	44.38	42.37	46.57	45.19	41.75
Mg	48.49	49.38	49.85	50.98	55.12	46.65	48.07	45.53	45.72	51.91
Fe	6.21	6.75	8.87	7.87	11.83	8.97	9.56	7.95	9.09	6.34

Pyroxenes

Locality	AG297					
Sample	a	b	c	d	e	f
SiO_2	52.62	51.48	51.35	54.28	54.07	54.17
Al_2O_3	1.78	2.29	2.82	1.09	1.09	1.19
Cr_2O_3	0.27	0.22	0.79	0.08	0.08	0.08
TiO_2	0.46	0.58	0.52	0.36	0.34	0.38
FeO	12.76	7.63	4.88	14.87	13.97	15.92
Fe_2O_3	0.77	1.91	3.47	1.02	1.53	0.22
MgO	20.63	16.67	16.18	25.28	25.81	26.47
CaO	10.13	18.32	20.76	1.90	2.15	1.25
Na_2O	0.12	0.22	0.28	0.02	0.01	0.02
MnO	0.27	0.22	0.23	0.31	0.30	0.33
Total	99.81	99.54	101.28	99.21	100.45	100.03
FeO^*	13.41	9.34	8.00	15.81	15.03	16.11
Ca	20.44	37.44	41.79	3.81	4.29	2.43
Mg	58.00	47.34	45.31	70.82	71.79	72.35
Fe	21.56	15.22	12.91	25.37	23.91	25.22

Locality	AG297			AG291B							AG192
Sample	g	h	i	a	b	c	d	e	f	g	a
SiO_2	54.13	51.98	51.87	50.74	51.10	54.03	55.58	48.68	51.63	54.89	50.29
Al_2O_3	1.22	2.32	2.35	2.86	2.72	1.48	3.69	5.76	2.66	1.45	2.62
Cr_2O_3	0.11	0.24	0.26	0.84	1.05	0.47	0.40	1.23	0.81	0.30	0.94
TiO_2	0.32	0.73	0.52	0.88	0.77	0.52	1.15	1.47	0.36	0.40	1.27
FeO	14.85	8.22	6.76	1.58	1.79	6.65	6.47	1.03	0.98	6.62	1.95
Fe_2O_3	1.19	0.48	1.01	2.70	3.01	2.70	1.18	4.32	3.41	2.43	2.11
MgO	25.96	15.79	14.88	16.02	16.53	31.77	28.32	16.31	17.07	32.56	16.99
CaO	1.99	19.45	21.65	22.74	22.13	1.09	3.33	18.63	22.29	0.74	20.95
Na_2O	0.03	0.26	0.27	0.44	0.44	0.03	0.66	1.17	0.42	0.02	0.45
MnO	0.32	0.22	0.19	0.13	0.13	0.23	0.19	0.13	0.15	0.27	0.11
Total	100.12	99.69	99.76	98.93	99.67	98.92	100.97	98.73	99.78	9.68	97.68
FeO^*	15.92	8.63	7.69	4.00	4.48	9.10	7.55	4.92	4.03	8.80	3.83
Ca	3.90	40.25	44.65	47.12	45.42	2.09	6.81	41.18	45.23	1.40	43.97
Mg	71.11	45.45	42.68	46.19	47.18	84.06	80.80	50.14	48.15	85.29	49.61
Fe	24.99	14.30	12.67	6.69	7.40	13.85	12.39	8.68	6.62	13.32	6.42

Pyroxenes

Locality	AG245	AG192		AG245	AG143P				AG244		AG186	
Sample	b	b	c	c	a	b	c	d	a	b	a	b
SiO_2	52.18	51.78	51.08	52.43	52.49	52.58	52.05	52.42	51.61	51.65	52.75	52.39
Al_2O_3	2.76	2.38	2.73	2.95	2.51	2.48	2.71	3.12	3.45	3.32	2.85	3.13
Cr_2O_3	1.19	0.89	0.92	1.24	1.00	0.96	0.92	1.19	1.26	1.27	1.16	1.25
TiO_2	0.35	0.83	1.46	0.32	1.14	1.13	1.35	0.74	0.32	0.36	0.60	0.71
FeO	2.75	2.97	2.83	3.00	4.28	4.25	3.94	4.15	2.51	2.77	3.36	3.22
Fe_2O_3	1.28	0.98	1.71	1.00	0.49	0.51	0.73	0.32	1.02	0.99	0.12	0.22
MgO	17.88	17.78	18.00	17.89	17.84	17.66	17.38	17.02	17.09	17.02	18.00	17.55
CaO	20.79	20.33	19.78	20.88	20.17	20.52	20.73	21.15	21.81	21.59	20.80	21.07
Na_2O	0.29	0.40	0.44	0.27	0.36	0.36	0.38	0.34	0.21	0.26	0.31	0.36
MnO	0.09	0.09	0.09	0.09	0.19	0.19	0.21	0.19	0.09	0.09	0.08	0.09
Total	99.56	98.43	99.04	100.07	100.47	100.64	100.40	100.64	99.37	99.32	100.03	99.99
FeO^*	3.90	3.85	4.35	3.86	4.71	4.71	4.58	4.43	3.42	3.65	3.42	3.52
Ca	42.61	42.25	40.97	42.71	41.32	41.96	42.59	43.67	45.14	44.81	42.79	43.70
Mg	50.97	51.36	51.86	50.94	50.84	50.21	49.68	48.86	49.19	49.13	51.51	50.61
Fe	6.42	6.39	7.17	6.34	7.83	7.83	7.73	7.47	5.68	6.06	5.71	5.69

Locality	AG186				AG244			AG295				AG277
Sample	c	d	e	f	a	b	c	a	b	c	d	a
SiO_2	51.42	51.60	51.51	51.75	51.70	51.62	51.98	51.54	52.04	52.03	52.64	51.88
Al_2O_3	3.37	3.30	2.97	2.72	3.14	2.77	3.61	2.82	2.42	2.64	2.46	2.78
Cr_2O_3	1.49	1.40	1.18	1.19	1.27	1.15	1.42	1.15	0.86	0.99	1.03	1.07
TiO_2	0.71	0.73	0.93	0.56	0.39	0.82	0.36	0.59	0.97	0.54	0.44	0.61
FeO	2.39	2.41	1.93	2.15	2.97	3.06	2.63	3.45	4.54	3.60	4.16	2.46
Fe_2O_3	1.28	1.09	1.64	1.35	1.01	1.45	0.85	1.88	2.02	1.75	1.69	1.68
MgO	17.08	16.89	17.18	17.25	17.26	17.57	17.11	16.98	19.27	17.97	18.65	17.52
CaO	21.53	21.67	21.75	21.61	21.19	20.38	21.98	20.57	17.62	19.80	19.01	21.55
Na_2O	0.33	0.39	0.40	0.35	0.24	0.38	0.22	0.40	0.30	0.32	0.29	0.23
MnO	0.17	0.16	0.15	0.16	0.18	0.21	0.17	0.23	0.25	0.22	0.24	0.20
Total	99.17	99.64	99.64	99.09	99.35	99.41	100.33	99.61	100.29	99.86	100.61	99.98
FeO^*	3.52	3.38	3.38	3.37	3.88	4.36	3.38	5.12	6.32	5.16	5.67	3.96
Ca0	44.69	44.94	44.93	44.69	43.81	42.14	45.27	42.55	35.57	40.39	38.37	43.83
Mg	49.34	49.34	49.33	49.61	49.63	50.52	49.02	48.82	54.07	51.04	52.36	49.59
Fe	5.97	5.72	5.72	5.70	6.56	7.34	5.71	8.63	10.36	8.57	9.27	6.58

Pyroxenes

Locality	261	266B		AG312			AG323					
Sample	d	a	b	a	b	c	a	b	c	d	e	f
SiO_2	52.39	52.43	52.60	52.51	52.09	52.38	53.31	54.06	50.92	50.89	53.11	52.74
Al_2O_3	2.86	2.90	2.75	2.59	2.50	2.57	2.47	2.48	3.33	2.89	2.66	2.77
Cr_2O_3	0.76	0.92	1.00	0.44	0.53	0.50	1.03	1.03	0.71	0.42	1.17	1.03
TiO_2	0.52	0.46	0.51	0.23	0.19	0.21	0.31	0.43	1.78	1.23	0.41	0.94
FeO	4.89	3.49	2.67	4.87	4.04	4.17	3.89	4.02	3.97	0.73	3.92	3.87
Fe_2O_3	0.85	0.51	1.37	0.63	1.12	1.30	0.07	0.31	0.31	4.06	0.10	0.11
MgO	16.90	16.62	16.68	17.17	16.08	15.97	17.69	17.16	16.13	19.79	17.40	16.62
CaO	20.76	21.77	22.46	20.39	21.81	22.21	21.23	21.94	21.74	18.99	21.05	22.00
Na_2O	0.29	0.41	0.43	0.27	0.35	0.34	0.27	0.35	0.38	0.32	0.33	0.40
MnO	0.16	0.17	0.16	0.14	0.17	0.15	0.15	0.17	0.14	0.14	0.13	0.15
Total	100.38	99.68	100.63	99.24	98.88	99.80	100.42	101.94	99.41	99.46	100.28	100.63
FeO^*	5.62	3.96	3.90	5.42	5.06	5.35	3.93	4.12	4.25	4.36	4.00	3.95
Ca	42.54	45.26	45.99	41.95	45.21	45.35	43.31	45.64	37.93	37.93	43.42	45.51
Mg	48.19	48.07	47.51	49.14	46.35	45.86	50.18	41.73	55.02	55.02	49.95	47.84
Fe	9.26	6.67	6.50	8.91	8.44	8.79	6.51	7.23	7.05	7.05	6.63	6.65

Locality	AG318				AG316							
Sample	a	b	c	d	a	b	c	d	e	f	g	h
SiO_2	55.82	52.88	53.06	53.04	54.84	51.57	55.80	55.13	54.60	55.23	54.52	51.27
Al_2O_3	2.98	3.25	3.06	2.70	1.11	2.56	1.21	1.71	1.59	1.51	1.58	3.17
Cr_2O_3	1.09	1.33	1.14	0.99	0.26	0.48	0.14	0.68	0.52	0.48	0.45	1.02
TiO_2	0.92	0.54	0.65	0.85	0.44	0.98	0.28	0.20	0.17	0.18	0.20	0.39
FeO	4.17	3.93	3.94	3.87	9.79	3.64	9.59	8.80	8.77	9.99	9.43	3.70
Fe_2O_3	0.27	0.52	0.56	0.41	1.47	2.15	1.50	2.18	2.03	1.11	1.64	2.45
MgO	17.70	17.11	18.40	17.52	30.54	16.42	31.27	30.07	29.96	30.54	29.95	17.27
CaO	20.54	20.95	20.02	20.45	1.08	21.47	0.92	2.35	2.10	1.05	1.60	19.42
Na_2O	0.38	0.32			0.02	0.42	0.04	0.09	0.09	0.03	0.05	0.46
MnO	0.17	0.14	0.12	0.12	0.25	0.18	0.27	0.25	0.25	0.26	0.24	0.15
Total	100.04	100.97	100.95	99.95	99.80	99.87	101.70	101.46	100.08	100.38	99.66	99.28
FeO^*	4.40	4.07	4.41	4.22	11.12	5.55	10.91	10.77	10.59	10.98	10.92	5.90
Ca	42.18	43.62	40.73	40.09	2.05	44.02	1.71	4.44	4.02	2.02	3.08	40.32
Mg	49.71	49.57	52.05	52.88	80.98	46.82	81.85	79.27	79.74	81.19	80.18	49.85
Fe	8.11	6.81	7.22	7.03	16.97	9.16	16.44	16.29	16.24	16.79	16.74	9.83

Pyroxenes

Locality	AG316					AG314						
Sample	i	j	k	l	m	a	b	c	d	e	f	g
SiO_2	50.18	52.25	53.55	54.20	51.77	53.98	54.39	55.24	54.98	54.91	52.21	51.73
Al_2O_3	4.47	2.83	2.74	2.07	2.70	1.16	1.13	0.97	1.13	1.03	2.33	2.71
Cr_2O_3	0.69	0.74	0.50	0.49	0.80	0.04	0.05	0.04	0.06	0.04	0.15	0.40
TiO_2	1.04	0.49	0.33	0.19	0.63	0.41	0.51	0.35	0.40	0.34	0.89	0.74
FeO	1.94	4.85	7.98	9.15	2.82	12.67	13.72	13.40	13.26	12.99	5.46	6.36
Fe_2O_3	4.87	2.42	2.22	2.08	2.62	1.01	0.71	0.22	0.55	0.46	0.79	1.27
MgO	17.33	20.54	25.64	30.40	16.40	28.17	27.72	28.79	28.62	27.99	15.78	16.36
CaO	18.98	15.39	7.53	0.95	22.02	1.29	1.51	1.02	1.12	1.41	22.08	19.87
Na_2O	0.78	0.33	0.17	0.03	0.44	0.05	0.02	0.01	0.02	0.02	0.26	0.29
MnO	0.17	0.19	0.21	0.27	0.17	0.24	0.31	0.28	0.28	0.31	0.15	0.19
Total	100.45	100.03	100.87	99.83	100.37	99.00	100.07	100.32	100.09	99.50	100.02	99.44
FeO^*	6.31	7.04	9.95	11.01	5.17	13.55	14.37	13.60	13.75	13.42	6.17	7.50
Ca	39.44	31.01	14.72	1.82	44.95	2.51	2.92	4.14	2.17	2.75	45.69	40.84
Mg	50.08	57.59	69.79	81.28	46.56	76.47	74.86	75.01	76.74	76.28	44.83	46.81
Fe	10.48	11.40	15.49	16.90	8.49	21.02	22.22	20.85	21.09	20.97	10.08	12.35

Locality	AG314		AG315								
Sample	h	i	a	b	c	d	e	f	g	h	i
SiO_2	52.96	52.03	53.48	56.88	56.02	51.94	52.63	55.68	53.56	51.68	55.51
Al_2O_3	2.19	2.05	2.00	1.65	1.33	2.36	2.56	1.15	4.57	3.36	1.38
Cr_2O_3	0.31	0.21	0.31	-	0.14	0.37	0.68	0.09	0.13	1.11	0.14
TiO_2	0.58	0.65	0.50	0.07	0.19	0.84	0.46	0.25	0.30	0.31	0.28
FeO	6.73	6.14	6.12	4.72	11.33	5.47	5.66	11.23	4.69	5.04	10.21
Fe_2O_3	0.12	1.22	0.51	1.69	0.69	1.27	0.87	0.55	1.78	1.35	0.46
MgO	16.14	16.71	18.12	2.50	29.01	15.88	16.52	30.22	21.16	15.74	26.84
CaO	21.03	19.96	19.12	11.06	1.65	21.19	20.62	0.98	10.96	20.97	4.83
Na_2O	0.26	0.24	0.28	0.22	0.04	0.38	0.35	0.02	0.70	0.41	0.07
MnO	0.18	0.18	0.16	0.18	0.29	0.17	0.19	0.32	0.28	0.21	0.27
Total	100.50	99.39	100.60	98.97	100.69	99.87	100.54	100.49	98.13	100.18	99.99
FeO^*	6.83	7.24	6.58	5.29	11.86	6.61	6.45	11.76	5.11	6.23	10.58
Ca	42.98	40.74	38.56	23.73	3.18	43.63	45.79	1.87	24.57	43.76	9.52
Mg	45.84	47.41	50.83	67.13	78.38	45.51	43.91	80.13	65.98	45.72	73.76
Fe	11.18	11.85	10.61	9.14	18.44	10.86	10.30	18.00	9.45	10.52	16.72

Pyroxenes

Locality	CS036					CS070						
Sample	a	b	c	d	e	a	b	c	d	e	f	g
SiO_2	49.25	48.63	49.23	51.70	49.43	50.51	48.62	49.03	49.21	48.99	48.98	49.47
Al_2O_3	4.54	5.44	4.90	2.27	5.51	1.31	3.67	1.98	2.74	3.31	5.48	4.50
Cr_2O_3	-	0.09	0.04	0.24	0.21	0.03	-	0.03	-	0.01	0.19	0.33
TiO_2	0.95	1.25	0.99	0.08	0.96	0.61	1.23	0.84	1.11	1.14	0.98	1.02
FeO^*	9.60	8.93	9.00	8.24	7.12	15.62	12.06	17.61	14.20	12.94	6.75	7.12
MgO	14.17	14.50	14.61	18.23	15.41	12.97	12.46	9.72	11.14	12.57	14.89	15.34
CaO	20.27	20.30	20.40	17.38	21.06	17.07	20.40	18.88	20.04	19.50	21.26	20.99
Na_2O	0.35	0.31	0.31	0.18	0.28	0.29	0.45	0.39	0.40	0.45	0.29	0.29
MnO	0.22	0.21	0.21	0.24	0.19	0.49	0.25	0.51	0.36	0.36	0.18	0.19
Total	99.33	99.67	99.69	99.38	100.16	98.90	99.14	98.98	99.19	99.26	98.99	99.26
Ca	42.56	42.63	42.56	36.08	43.69	35.83	43.10	29.05	42.77	36.93	44.89	44.46
Mg	41.36	42.36	42.40	50.68	44.48	37.82	36.61	40.56	33.06	41.19	43.73	43.68
Fe	16.68	15.01	15.04	13.24	11.83	26.35	20.29	30.39	24.17	21.88	11.38	11.86

Locality	CS070		
Sample	h	i	j
SiO_2	49.11	49.36	48.85
Al_2O_3	5.17	4.36	3.76
Cr_2O_3	0.31	0.12	0.20
TiO_2	0.92	0.85	1.05
FeO^*	7.49	8.69	12.02
MgO	14.82	15.00	13.64
CaO	20.89	20.10	19.11
Na_2O	0.32	0.34	0.46
MnO	0.17	0.22	0.25
Total	99.20	99.03	99.15
Ca	44.02	41.95	40.12
Mg	43.43	43.55	39.87
Fe	12.55	14.50	20.01

Pyroxenes

Locality	CS026						CS014					
Sample	a	b	c	d	e	f	a	b	c	d	e	f
SiO_2	49.51	49.27	49.24	50.21	48.43	48.83	51.01	50.97	48.99	51.47	52.06	51.49
Al_2O_3	4.44	5.01	4.33	2.06	6.14	5.66	1.71	1.46	3.54	2.06	2.05	2.05
Cr_2O_3	0.07	0.18	0.07	-	0.17	0.21	0.01	0.02	0.01	-	0.01	-
TiO_2	0.86	0.81	0.94	0.86	1.08	1.01	0.74	0.63	1.19	0.58	0.49	0.56
FeO^*	8.46	8.10	9.15	14.33	7.71	7.85	12.62	14.24	12.48	9.37	7.81	9.62
MgO	14.10	14.12	14.32	12.76	13.73	14.34	14.11	13.36	12.59	15.63	16.61	15.80
CaO	21.61	21.52	20.75	18.75	21.82	21.30	19.02	18.16	20.28	20.13	20.57	19.71
Na_2O	0.31	0.32	0.34	0.30	0.31	0.29	0.31	0.29	0.42	0.30	0.26	0.28
MnO	0.19	0.16	0.22	0.38	0.16	0.17	0.39	0.46	0.31	0.24	0.22	0.28
Total	99.54	99.48	99.36	99.64	99.56	99.66	99.91	99.58	99.80	99.79	100.07	99.79
Ca	45.05	45.21	43.23	39.05	46.37	44.84	38.95	37.66	42.43	40.77	41.18	39.91
Mg	40.85	41.23	41.53	37.02	40.59	42.00	40.21	38.53	36.69	44.07	46.24	44.46
Fe	14.10	13.56	15.24	23.93	13.04	13.16	20.84	23.81	20.88	15.16	12.58	15.63

Locality	CS014							CS036				
Sample	a	b	c	d	e	f	g	f	g	h	i	j
SiO_2	49.78	52.01	51.88	49.30	50.46	52.24	51.97	49.12	49.36	51.08	51.61	48.63
Al_2O_3	3.82	2.14	2.22	3.77	4.03	2.12	2.07	4.47	5.69	2.72	3.13	6.34
Cr_2O_3	-	0.02	0.01	0.03	0.13	0.09	0.02	0.01	0.22	0.16	0.12	0.51
TiO_2	0.81	0.47	0.48	1.01	0.66	0.39	0.47	0.98	0.94	0.51	0.46	0.91
FeO^*	8.99	7.77	7.56	11.15	6.52	6.54	7.47	8.50	6.58	7.90	6.79	6.37
MgO	14.53	16.58	16.54	13.39	15.92	17.60	16.49	14.18	15.24	17.52	17.10	15.38
CaO	21.02	20.48	20.65	20.36	21.51	20.20	20.68	21.42	21.66	18.84	20.36	21.09
Na_2O	0.34	0.21	0.20	0.42	0.26	0.18	0.25	0.31	0.28	0.17	0.18	0.24
MnO	0.20	0.22	0.22	0.26	0.14	0.17	0.22	0.18	0.12	0.25	0.19	0.15
Total	99.48	99.89	99.76	99.69	99.62	99.53	99.64	99.16	100.08	99.13	99.96	99.61
Ca	43.45	41.11	41.52	42.50	44.03	40.45	41.66	44.70	45.04	37.99	41.03	44.32
Mg	41.76	46.33	46.28	38.90	45.31	49.00	46.22	41.14	44.09	49.16	47.94	44.96
Fe	14.79	12.56	12.20	18.60	10.66	10.55	12.12	14.16	10.87	12.85	11.03	10.72

Pyroxenes

Locality	CS036					CS044						
Sample	k	l	m	n	o	a	b	c	d	e	f	g
SiO_2	48.54	48.03	48.356	48.58	47.99	49.29	49.75	50.22	49.71	48.39	50.12	49.75
Al_2O_3	6.00	6.04	4.83	6.36	3.36	3.88	4.10	4.06	3.83	3.86	4.04	3.80
Cr_2O_3	0.29	0.39	0.07	0.24	0.02	-	0.02	0.04	0.03	0.01	0.10	0.01
TiO_2	0.94	1.09	0.93	0.91	1.19	0.93	0.89	0.76	0.89	1.19	0.70	0.94
FeO^*	6.83	6.37	8.96	6.41	15.08	10.44	8.35	7.89	9.02	11.69	7.78	9.63
MgO	15.14	15.22	14.63	15.19	11.70	13.76	14.87	15.09	14.59	12.96	15.44	14.55
CaO	21.37	21.14	20.69	21.31	18.69	20.44	21.10	21.48	20.82	20.38	20.70	20.63
Na_2O	0.28	0.27	0.29	0.27	0.40	0.38	0.32	0.32	0.34	0.41	0.30	0.35
MnO	0.16	0.14	0.23	0.14	0.41	0.25	0.19	0.19	0.19	0.20	0.19	0.22
Total	99.55	98.69	99.18	99.41	98.88	99.36	99.59	100.05	99.42	99.14	99.36	99.88
Ca	44.61	44.60	42.23	44.80	39.64	42.67	43.56	44.03	43.11	42.69	42.77	42.49
Mg	43.99	44.65	42.89	44.43	34.75	39.94	42.69	43.05	42.03	37.78	44.37	41.67
Fe	11.40	10.75	14.88	10.77	25.61	17.39	13.75	12.92	14.86	19.53	12.86	15.84

Locality	CS044		CS026								
Sample	h	i	g	h	i	j	k	l	m	n	o
SiO_2	49.78	49.36	51.05	49.16	49.81	49.60	48.20	49.38	48.63	48.99	49.01
Al_2O_3	4.42	4.13	1.94	3.42	4.04	4.17	6.34	3.24	5.90	3.61	3.48
Cr_2O_3	0.17	0.01	-	-	0.06	0.06	0.28	0.01	0.15	0.03	0.02
TiO_2	0.90	0.95	0.61	1.06	0.77	0.86	1.29	1.05	1.00	0.98	1.04
FeO^*	7.65	9.59	12.18	12.87	9.49	9.02	7.82	13.68	7.71	12.23	12.99
MgO	15.18	14.88	14.78	12.85	14.49	14.54	13.91	12.57	14.05	12.99	12.44
CaO	21.14	19.95	18.70	19.44	20.64	20.62	21.34	19.18	21.77	19.79	19.72
Na_2O	0.32	0.35	0.29	0.41	0.31	0.31	0.29	0.37	0.33	0.38	0.42
MnO	0.21	0.24	0.34	0.31	0.21	0.21	0.16	0.34	0.17	0.25	0.31
Total	99.76	99.45	99.89	99.52	99.83	99.38	99.63	99.81	99.71	99.26	99.43
Ca	43.80	41.29	38.13	40.84	42.69	42.89	45.48	40.28	45.87	41.57	41.61
Mg	43.35	42.84	41.92	37.55	41.66	42.07	41.22	36.73	41.19	37.98	36.51
Fe	12.85	15.87	19.95	21.61	15.65	15.04	13.30	22.99	12.94	20.45	21.88

Pyroxenes

Locality	CS028										
Sample	a	b	c	d	e	f	g	h	i	j	k
SiO_2	49.25	51.84	49.17	50.01	49.57	48.10	51.05	49.43	49.49	49.50	49.42
Al_2O_3	4.91	2.33	4.03	4.04	4.53	3.63	3.47	5.49	5.05	4.73	5.08
Cr_2O_3	0.04	-	0.01	0.04	0.02	0.01	0.38	0.27	0.09	0.06	0.14
TiO_2	1.06	0.50	0.98	0.76	0.84	1.32	0.53	0.90	0.98	0.91	0.87
FeO	6.16	5.87	6.96	4.44	4.44	9.64	4.36	4.56	5.60	5.51	4.86
Fe_2O_3	3.52	3.24	4.70	4.79	3.98	5.22	2.49	2.27	2.82	3.55	2.86
MgO	14.37	16.39	13.63	14.97	14.61	11.38	17.31	15.12	14.98	15.03	15.12
CaO	21.32	20.14	20.50	21.00	21.70	20.28	19.38	20.87	20.19	19.76	20.73
Na_2O	0.66	0.26	0.37	0.47	0.33	0.48	0.26	0.31	0.34	0.45	0.27
MnO	0.19	0.23	0.26	0.21	0.18	0.35	0.17	0.15	0.20	0.21	0.17
Total	101.48	100.79	100.61	100.73	100.20	100.41	99.40	99.31	99.75	99.71	99.51
FeO^*	9.20	8.86	11.32	8.84	8.10	14.51	6.63	6.64	8.19	8.78	7.48
Ca	43.81	40.24	42.25	42.93	44.74	42.47	39.73	44.19	42.41	41.43	43.41
Mg	41.07	45.54	39.08	42.57	41.91	33.16	49.33	44.56	43.78	43.84	44.04
Fe	15.12	14.22	18.67	14.50	13.35	24.37	10.94	11.25	13.81	14.73	12.55

Locality	CS011							CS016		
Sample	a	b	c	d	e	f	g	a	b	c
SiO_2	50.49	50.53	51.90	50.29	51.60	50.26	51.37	52.36	51.86	50.17
Al_2O_3	4.08	4.42	2.50	4.47	2.15	4.37	2.06	1.93	2.02	4.20
Cr_2O_3	0.12	0.45	0.02	0.07	0.09	0.04	0.01	-	0.05	0.09
TiO_2	0.55	0.58	0.34	0.65	0.33	0.72	0.45	0.41	0.36	0.67
FeO	3.83	4.17	5.16	4.63	4.19	5.33	7.72	6.59	4.50	4.30
Fe_2O_3	3.12	2.14	2.31	2.84	2.61	2.69	2.63	2.18	2.84	2.97
MgO	16.10	15.86	16.89	15.44	17.28	15.34	15.70	16.83	17.64	15.85
CaO	20.99	21.07	19.92	20.92	19.85	20.63	18.97	19.45	19.57	20.65
Na_2O	0.28	0.28	0.28	0.33	0.28	0.30	0.31	0.24	0.22	0.28
MnO	0.15	0.17	0.18	0.17	0.17	0.19	0.26	0.23	0.19	0.17
Total	99.70	99.68	99.49	99.80	98.53	99.87	99.50	100.22	99.20	99.34
FeO^*	6.70	6.13	7.27	7.24	6.58	7.80	10.13	8.59	7.10	7.01
Ca	43.06	43.84	40.45	43.39	40.39	42.80	38.76	39.08	39.31	42.75
Mg	45.95	45.89	47.70	44.58	48.86	44.25	44.60	47.03	49.24	45.60
Fe	10.99	10.27	11.85	12.03	10.75	12.95	16.64	13.89	11.45	11.65

Pyroxenes

Locality	CS019					CS069						
Sample	a	b	c	d	e	a	b	c	d	e	f	g
SiO_2	48.77	49.39	47.63	49.04	48.95	49.85	51.45	50.71	49.94	49.65	52.15	49.85
Al_2O_3	4.05	2.42	6.46	3.72	3.72	2.75	3.36	3.78	3.59	3.17	2.09	2.96
Cr_2O_3	0.05	0.02	0.13	0.02	0.03	-	0.07	0.07	0.02	0.02	0.01	0.01
TiO_2	1.03	0.96	1.28	0.96	1.01	0.99	0.54	0.73	0.87	1.02	0.49	0.96
FeO	5.30	14.64	5.46	9.95	7.93	9.87	6.24	45.43	6.84	9.71	6.71	10.25
Fe_2O_3	5.92	2.73	3.49	4.07	4.07	2.90	1.82	2.62	3.36	3.43	2.21	3.33
MgO	13.57	10.98	13.07	13.40	13.22	12.59	16.92	15.32	14.09	13.21	15.99	13.35
CaO	19.94	17.98	21.48	18.11	20.02	20.09	18.85	20.92	20.75	18.98	20.20	18.63
Na_2O	0.82	0.43	0.33	0.42	0.41	0.43	0.26	0.33	0.35	0.48	0.30	0.44
MnO	0.25	0.51	0.18	0.38	0.26	0.34	0.21	0.17	0.22	0.36	0.24	0.37
Total	99.44	100.07	99.52	100.07	99.61	99.80	99.71	100.08	100.03	100.02	100.89	100.13
FeO^*	10.78	17.21	8.66	13.74	11.70	12.56	7.89	7.83	9.92	12.90	8.75	13.36
Ca	42.01	38.17	45.76	37.90	41.92	42.10	38.70	43.14	42.93	39.75	40.83	38.77
Mg	39.78	32.43	38.76	38.97	38.48	36.70	48.27	43.92	40.58	38.52	44.96	38.87
Fe	18.21	29.40	15.48	23.13	19.60	21.20	24.86	12.94	16.49	21.73	14.21	2.36

Locality	CS011		CS23			CS007				CS060		
Sample	a	b	a	b	c	a	b	c	d	a	b	c
SiO_2	49.81	50.65	50.31	50.36	50.96	47.74	48.29	48.46	48.49	48.35	48.57	48.71
Al_2O_3	4.18	4.82	2.11	1.11	1.75	6.03	6.36	5.47	6.07	6.27	5.83	5.49
Cr_2O_3	0.01	0.36	0.01	0.02	1.00	0.08	0.07	0.08	0.11	0.09	0.14	0.11
TiO_2	0.94	0.67	0.80	0.60	0.60	1.39	1.71	1.46	1.39	1.29	1.29	1.09
FeO^*	9.61	6.30	13.59	16.66	12.36	8.46	9.26	10.84	8.90	9.69	8.65	8.77
MgO	14.45	15.78	14.40	12.45	15.05	14.04	13.17	13.45	13.79	14.46	14.47	14.10
CaO	20.73	21.10	17.27	17.08	17.72	20.63	21.54	20.18	20.65	19.24	20.18	20.86
Na_2O	0.35	0.28	0.29	0.22	0.28	0.34	0.36	0.38	0.38	0.33	0.32	0.29
MnO	0.22	0.14	0.41	0.54	0.38	0.17	0.17	0.23	0.18	0.23	0.18	0.17
Total	100.29	100.10	99.19	99.04	99.14	98.90	100.93	100.55	99.96	99.95	99.64	99.59
Ca	42.73	43.88	35.83	35.70	36.46	43.99	45.61	42.45	44.01	40.85	42.76	43.97
Mg	41.44	45.68	41.51	36.21	43.03	41.62	38.81	39.36	40.87	42.71	42.60	41.34
Fe	15.83	10.44	22.66	28.09	20.51	14.38	15.58	18.19	15.11	16.45	14.64	14.69

Pyroxenes

Locality	CS038			CS050		CS009			CS024		CS053	
Sample	a	b	c	a	b	a	b	c	a	b	a	b
SiO_2	49.84	49.52	50.61	51.31	49.52	49.09	49.61	51.37	47.87	48.90	48.86	50.19
Al_2O_3	4.18	4.02	2.73	2.59	4.07	4.42	4.14	2.25	4.55	3.80	5.15	4.48
Cr_2O_3	0.02	0.03	0.01	0.09	0.04	0.21	0.06	0.13	0.03	0.01	0.05	0.10
TiO_2	1.05	0.95	0.98	0.46	0.99	0.46	0.56	0.32	1.39	0.98	1.04	0.71
FeO^*	11.45	11.66	15.08	7.68	10.25	5.82	6.61	5.79	12.68	14.48	9.23	8.88
MgO	12.86	13.68	12.32	15.05	13.94	14.84	15.02	16.87	12.30	12.25	14.80	15.77
CaO	20.07	18.74	18.08	20.33	19.48	21.27	20.72	20.17	20.26	18.45	20.05	19.15
Na_2O	0.39	0.37	0.34	0.31	0.32	0.24	0.27	0.20	0.39	0.38	0.34	0.33
MnO	0.27	0.28	0.43	0.18	0.24	0.12	0.14	0.14	0.28	0.38	0.21	0.22
Total	100.14	99.24	100.58	97.99	98.84	96.48	97.12	97.24	99.73	99.64	99.72	99.82
Ca	42.62	39.82	38.20	42.90	41.38	45.70	44.18	41.79	42.67	39.19	41.74	39.76
Mg	37.99	40.40	36.22	44.15	41.23	44.33	44.55	48.61	36.03	36.18	42.89	45.49
Fe	19.39	19.78	25.59	12.94	17.39	9.97	11.27	9.60	21.30	24.63	15.37	14.75

Locality	CS022			CS060	
Sample	a	b	c	d	e
SiO_2	50.03	48.65	50.83	52.11	50.97
Al_2O_3	5.53	3.43	4.00	3.08	4.28
Cr_2O_3	0.50	0.02	0.03	0.03	0.04
TiO_2	0.80	1.14	0.71	0.65	0.85
FeO^*	6.02	13.60	8.20	8.79	9.10
MgO	15.36	12.27	14.78	16.21	14.52
CaO	21.38	18.67	21.15	19.88	21.20
Na_2O	0.27	0.41	0.30	0.27	0.34
MnO	0.13	0.39	0.20	0.23	0.19
Total	100.00	98.59	100.20	101.24	101.49
Ca	44.97	40.00	43.84	40.18	43.58
Mg	44.97	36.58	42.59	45.59	41.49
Fe	10.07	32.42	13.57	14.23	14.93

Pyroxenes

Locality	IT08		IT09				IT06		IT16			IT15
Sample	a	b	a	b	c	d	a	b	a	b	c	a
SiO_2	51.53	51.77	50.29	51.36	50.47	51.57	49.62	51.81	48.47	49.61	48.73	49.67
Al_2O_3	3.16	2.99	2.82	2.92	3.14	3.12	4.15	1.95	3.83	4.40	3.96	3.55
Cr_2O_3	0.12	0.12	0.32	0.59	0.64	0.54	0.22	0.04	0.02	0.08	0.01	0.13
TiO_2	0.61	0.54	0.57	0.54	0.64	0.54	0.79	0.46	1.14	0.78	0.95	1.24
FeO^*	8.44	8.65	7.18	6.93	6.87	6.96	8.39	9.86	14.22	8.02	12.66	11.26
MgO	16.33	17.10	16.03	16.13	16.47	16.33	14.76	16.33	11.87	14.80	12.86	14.47
CaO	18.69	17.81	19.76	20.09	20.08	20.32	20.81	18.48	18.87	20.82	19.20	18.44
Na_2O	0.24	0.25	0.31	0.31	0.57	0.35	0.28	0.22	0.46	0.30	0.43	0.62
MnO	0.22	0.23	0.19	0.18	0.19	0.17	0.19	0.28	0.33	0.18	0.29	0.29
Total	99.35	99.47	97.46	99.05	98.98	99.92	99.22	99.45	99.20	98.98	99.08	99.67
Ca	38.81	36.71	41.35	41.76	41.40	41.83	43.30	37.61	40.39	43.55	40.69	38.73
Mg	47.16	49.01	46.60	46.66	47.22	46.72	42.73	46.26	35.31	43.04	37.90	42.32
Fe	14.03	14.28	12.05	11.57	11.38	11.45	19.97	16.13	24.30	13.41	21.41	18.95